ARTICLE IN PRESS Available online http://jopr.mpob.gov.my/category/article-in-press/

Journal of Oil Palm Research

Vol. 38 (3) · September 2026

REVIEW ARTICLE

eISSN 2811-4701
9772811470006

MPOB

JOURNAL OF OIL PALM RESEARCH (formerly known as ELAEIS)

JOURNAL OF OIL PALM RESEARCH (JOPR), an international refereed journal, carries full-length original research papers, short communications and scientific review papers on various aspects of oil palm and palm oil. JOPR is published four times per year, i.e. March, June, September and December.

Impact Factor:
1.0
data from 2025 *Journal Citation Report®* Science Edition
– A Clarivate Analytics product.

For more information on JOPR, please write to:

Editor-in-Chief
Journal of Oil Palm Research
Malaysian Palm Oil Board
6, Persiaran Institusi, Bandar Baru Bangi
43000 Kajang, Selangor, Malaysia

Tel: *+603-8769 4400*
E-mail: *jopr.admin@mpob.gov.my*
Website: *jopr.mpob.gov.my*

MPOB

MPOB Press
Malaysian Palm Oil Board
6, Persiaran Institusi, Bandar Baru Bangi
43000 Kajang, Selangor, Malaysia
Tel: +603-8769 4400 | Fax: +603-8925 9446
E-mail: *jopr.admin@mpob.gov.my*

JOURNAL OF OIL PALM RESEARCH

Vol. 38 (3) September 2026

CONTENTS

Cover picture:

1. Empty fruit bunches are generated as a valuable biomass resource.
2. Measuring height increment in oil palm under field conditions.

Journal of Oil Palm Research Vol. 38 (3) September 2026 p. 391–407
DOI: https://doi.org/10.21894/jopr.2025.0027

SUSTAINABLE INNOVATIONS IN PALM OIL EXTRACTION: A COMPREHENSIVE OVERVIEW OF GREEN TECHNOLOGIES

NICKY RAHMANA PUTRA[1*]; YUSTISIA YUSTISIA[2]; R. BAMBANG HERYANTO[2]; NI WAYAN TRISNAWATI[3]; DAMASUS RIYANTO[4]; NYOMAN NGURAH ARYA[5] and BRAMANTYO AIRLANGGA[6*]

ABSTRACT

This review critically examines recent advancements in green extraction methods for palm oil production, emphasising their potential to improve sustainability, extraction efficiency and product quality. Innovative green technologies, including supercritical carbon dioxide ($SCCO_2$) extraction, ultrasound-assisted extraction (UAE), microwave-assisted extraction (MAE) and deep eutectic solvents (DES), provide eco-friendly alternatives that maintain or even enhance oil yield and quality. Notably, $SCCO_2$ extraction produces high-purity oils rich in bioactive compounds, while UAE and MAE demonstrate significant energy efficiency and superior preservation of nutrients. DES, an emerging solvent, enhances extraction processes with a lower environmental impact. Comparative analysis reveals that these methods not only reduce environmental risks but also improve product safety and quality. The review concludes by highlighting the need for further optimisation of these techniques, positioning them as essential for the future of sustainable and responsible palm oil production.

Keywords: eco-friendly, green extraction, palm oil.

Received: 9 September 2024**; Accepted:** 14 March 2025**; Published online:** 5 June 2025.

INTRODUCTION

Palm oil is one of the most widely produced and consumed vegetable oils globally, playing a crucial role in the food, cosmetic, and biofuel industries (Anggoro et al., 2024; Mah et al., 2024; Yusof et al., 2023). Its extensive use and economic significance, particularly in countries like Malaysia and Indonesia, have made palm oil a vital agricultural commodity (Khairuddin et al., 2021; Shaari et al., 2021; Zainal Abidin et al., 2024). However, the traditional methods of extracting palm oil, such as mechanical pressing and solvent extraction, have become less favorable due to their inefficiency in recovering valuable bioactive compounds and their inability to meet increasing demands for high-quality oil (Irianto et al., 2024; Nikolova et al., 2024). These conventional techniques often result in lower extraction yields and are unable to preserve the nutritional and functional properties of sensitive compounds, which limits the potential for producing value-added products (Ayoib et al., 2020; Phan-Tai & Brunner, 2023; Promraksa et al., 2020; Zain et al., 2020).

[1] Faculty of Engineering Technology and Science, Higher College of Technology (HCT), Ruwais, Abu Dhabi 22401, United Arab Emirates.

[2] Research Center for Food Crops, National Research and Innovation Agency (BRIN), Jl. Raya Jakarta-Bogor KM. 46, Cibinong, Bogor 16911, Indonesia.

[3] Research Center for Agroindustry, National Research and Innovation Agency (BRIN), Jl. Raya Jakarta-Bogor KM. 46, Cibinong, Bogor 16911, Indonesia.

[4] Institute of Agriculture (Intan), Yogyakarta 55284, Indonesia.

[5] Research Center for Behavioral and Circular Economics, National Research and Innovation Agency (BRIN), Jakarta 12710, Indonesia.

[6] Department of Chemical Engineering, Institut Teknologi Sepuluh Nopember, Surabaya 60111, Indonesia.

* *Corresponding author e-mail: nickyrahman1309@gmail.com; bramantyo.airlangga@its.ac.id*

As global awareness of sustainability and environmental responsibility grows, there is increasing pressure on the palm oil industry to adopt more sustainable practices. This has led to the development and adoption of green extraction technologies that aim to reduce the environmental impact of palm oil production while maintaining or even enhancing the efficiency and quality of the extraction process (Chan et al., 2018; Iftikhar et al., 2017; Mulia et al., 2018; Valasques et al., 2018). Green extraction methods such as supercritical carbon dioxide ($SCCO_2$) extraction, ultrasound-assisted extraction (UAE), microwave-assisted extraction (MAE) and deep eutectic solvents (DES) are at the forefront of this shift, offering innovative solutions that align with global sustainability goals.

Green extraction methods such as MAE, UAE and $SCCO_2$ offer promising alternatives to conventional extraction processes by minimising environmental impacts and enhancing extraction efficiency (Irianto et al., 2024; Rizkiyah et al., 2023). MAE operates by utilising microwave energy to rapidly heat both the solvent and sample, leading to faster extraction and better preservation of heat-sensitive compounds (Alvi et al., 2022; Siddique et al., 2022). It is particularly noted for its energy efficiency, as the process allows for precise control of temperature and extraction time. Similarly, the UAE uses ultrasonic waves to create cavitation, which improves mass transfer and cell disruption, making it highly effective at extracting bioactive compounds while preserving their integrity due to the mild conditions (Liu et al., 2022; Yusoff et al., 2022). Both MAE and UAE are recognised for reducing solvent use and energy consumption, contributing to more sustainable extraction practices in industries such as palm oil production (Rani et al., 2021).

$SCCO_2$ extraction, on the other hand, operates by using carbon dioxide (CO_2) in its supercritical state, where it exhibits both gas-like diffusivity and liquid-like solvation power (Ahangari et al., 2021; Arumugham et al., 2021). This method is particularly valuable for producing high-purity oils without the need for toxic organic solvents. $SCCO_2$ has been extensively utilised in palm oil extraction, offering a cleaner and more selective method that produces high-quality oils while minimising environmental impact. Additionally, emerging solvents like DES are offering biodegradable and non-toxic alternatives, further enhancing the sustainability of extraction methods (Guía-García et al., 2022; Saravanakumar et al., 2023). DES, composed of renewable organic salts and hydrogen bond donors, represents a new frontier in green extraction technologies, offering efficiency and environmental benefits in line with sustainable development goals. Together, these green extraction methods hold great potential for transforming industrial extraction practices, making them more environmentally friendly and resource-efficient (Chew et al., 2024).

This review aims to provide a comprehensive analysis of these green extraction methods, comparing their efficiency, yield and impact on the quality of palm oil against conventional methods. By examining the advantages and challenges associated with each technology, this review seeks to highlight the potential of green extraction methods to revolutionise the palm oil industry, making it more sustainable and aligned with global environmental standards. As the industry continues to evolve, the adoption of these green technologies is not only a response to environmental concerns but also a strategic move towards producing higher quality, safer and more sustainable palm oil products.

MAE FOR PALM OIL EXTRACTION

MAE has garnered attention as a green and efficient technology for palm oil extraction, providing significant advantages in terms of energy savings, extraction efficiency and preservation of bioactive compounds (Kamaruddin et al., 2023; Li et al., 2023). In comparison to traditional methods, MAE utilises microwave energy to heat the extraction solvent and sample simultaneously, leading to rapid temperature increases that break down cell structures and enhance mass transfer as shown in *Figure 1*. By applying controlled microwave radiation, MAE can optimise the extraction of palm oil and its bioactive components, such as antioxidants and fatty acids, with reduced energy consumption and environmental impact (Kostas et al., 2017; Mandal et al., 2007; Tambun et al., 2021). This review examines key studies on MAE for palm oil extraction, focusing on how different process parameters (solvent selection, temperature, time and microwave power) affect extraction yield and product quality (Chemat et al., 2020).

One of the critical parameters in MAE is the selection of solvents, which plays a crucial role in determining extraction efficiency and the quality of the extracted compounds. Several studies have demonstrated the use of DES as a green alternative to conventional organic solvents. For instance, Han and Hadi (2024), and Ng and Nu'man (2021) employed DES composed of choline chloride and amino acid (ChCl-AA) with 30% water to extract ferulic acid, an antioxidant, from palm oil by-products. At an extraction temperature of 60°C and times ranging from 6–15 min, these studies achieved significant yields of ferulic acid with high radical scavenging activity. The use of DES not only enhances the sustainability of the extraction process

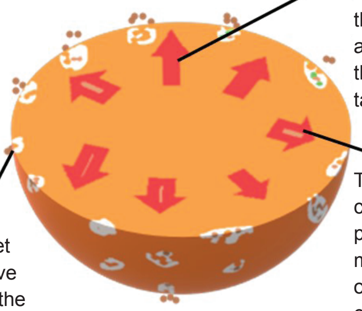

Figure 1. Mechanism of microwave-assisted extraction (MAE) for palm oil recovery.

but also allows for selective extraction of bioactive compounds, providing added value beyond palm oil production.

Temperature is another crucial factor in MAE, as it affects both the extraction kinetics and the stability of bioactive compounds. Nuchdang et al. (2022) studied the extraction of palm oil using isopropanol as a solvent at 150°C, resulting in an oil yield of 11.70%. While higher temperatures can accelerate extraction rates, they can also lead to the degradation of sensitive compounds. Therefore, it is important to balance the temperature to optimise yield without compromising the quality of the extracted oil. Zamanhuri et al. (2021, 2022) explored the use of microwave extraction at different power levels (100 and 300 W) and extraction times (30 min), resulting in a 64.00% crude palm oil (CPO) yield and high palmitic acid content. These studies highlight the need to carefully optimise microwave power and temperature to achieve maximum extraction efficiency while preserving the integrity of bioactive compounds.

Extraction time is also a significant parameter in MAE. Shorter extraction times can enhance energy efficiency and reduce operational costs, making the process more sustainable. For example, Phatthiya et al. (2024) combined microwave-assisted pyrolysis with $SCCO_2$ extraction to achieve an oil yield of 63.09%–67.72% within a relatively short time. This process produced oils enriched with valuable fatty acids, such as dodecanoic and octadecanoic acids, demonstrating that integrating MAE with other extraction technologies can further improve yields and product quality. Similarly, Rashid et al. (2023) applied a microwave-assisted enzyme aqueous (MAEA) extraction method with a 4 hr incubation period, achieving a 39.48% oil yield along with high squalene content. This extended extraction time allowed the enzymes to break down the cell walls more effectively, enhancing the recovery of both oil and bioactive compounds.

The power of the microwave itself is a critical parameter, as it directly influences the rate of heating and the efficiency of cell disruption. Higher microwave power increases the energy delivered to the sample, accelerating the extraction process. However, excessive power can cause localised overheating, potentially leading to the degradation of sensitive compounds. For instance, Kanjanapongkul (2021) found that combining ohmic heating with microwave pretreatment resulted in a 47% CPO yield with lower free fatty acid (FFA) content and reduced energy consumption. This combination of technologies highlights the potential of using lower microwave power in conjunction with other thermal methods to balance efficiency and product quality. Additionally, Ong et al. (2021) demonstrated that microwave pretreatment improved the yield of palm oil from oil palm decanter cake (OPDC) when followed by Soxhlet extraction, showing that careful adjustment of microwave power can significantly enhance extraction outcomes.

The process parameters in MAE (solvent selection, temperature, time and microwave power) are critical in determining the success of palm oil extraction. By optimising these parameters, MAE can enhance oil yields, improve the recovery of bioactive compounds, and minimise energy consumption, making it a highly sustainable extraction method. The reviewed studies show that integrating MAE with other green technologies, such as enzyme-assisted extraction or $SCCO_2$ extraction, can further improve the efficiency and sustainability of the process. As the demand for greener extraction methods grows, MAE is well-positioned to play a key role in the future of palm oil extraction, offering an environmentally-friendly alternative to traditional extraction methods while maintaining high-quality outputs.

Table 1 provides comprehensive summary of recent studies on MAE techniques applied to palm oil recovery, highlighting the diversity of extraction conditions, yields and outcomes. The reviewed research spans from enzymatic-assisted MAE and DES applications to advanced integrations with ohmic heating and $SCCO_2$ processes. The yield of palm oil and bioactive compounds varies widely depending on extraction parameters such as temperature, solvent type and microwave intensity. Notably, several studies demonstrated improved oil yield and quality, as well as enhanced recovery of valuable compounds like ferulic acid and squalene. In addition, various outcomes such as energy efficiency, antioxidant activity and compositional enrichment were reported, underscoring the potential of MAE as a green and scalable technology for palm oil processing.

UAE FOR PALM OIL EXTRACTION

UAE has emerged as an effective and environmentally friendly method for extracting valuable compounds from palm oil and its by-products. The studies summarised in *Table 2* demonstrate the versatility and effectiveness of UAE in enhancing extraction yields, reducing processing times and improving the quality of extracted products. This technique relies on ultrasonic waves to create cavitation bubbles in the extraction medium, which collapse and generate localised high temperatures and pressures as shown in *Figure 2*.

TABLE 1. OVERVIEW OF STUDIES ON MAE FOR PALM OIL EXTRACTION, DETAILING EXTRACTION CONDITIONS, YIELDS AND OUTCOMES

Authors	Extraction condition	Yield	Outcome
Han and Hadi (2024)	Deep eutectic solvent (ChCl-AA with 30% water) and microwave at 60°C for 6 min	Not specified for oil; 40.3 mg/g ferulic acid	Ferulic acid from unsterilised fruitlets showed higher radical scavenging activity; sterilisation did not significantly affect ferulic acid content.
Phatthiya et al. (2024)	High-intensity microwave-assisted pyrolysis, followed by $SCCO_2$ extraction	63.09%–67.72% for $SCCO_2$-oil extract	$SCCO_2$ oil enriched with acids such as dodecanoic, n-hexadecanoic, and octadecanoic acids; the production cost of bio-phenol was estimated.
Bauwens and Purcaro (2024)	Microwave-assisted saponification for MOAH analysis	Not specified	Reduced variability in MOAH quantification; improved internal standard partitioning, significant reduction in uncertainty.
Rashid et al. (2023)	MAEA extraction (2% mixed enzyme, pH 8, 4 hr incubation)	39.48% oil yield, 961.77 mg/100 g squalene	MAEA significantly increased oil yield and squalene content; suitable for producing squalene-rich virgin palm oil.
Nuchdang et al. (2022)	MAE with isopropanol at 150°C	11.70% oil yield	MAE comparable to Soxhlet extraction; moderate energy consumption; yielded aromatic and phenolic compounds.
Zamanhuri et al. (2022)	Microwave extraction (300 W, 30 min, 80 g mesocarp loading)	Not specified	Second-order kinetic model represented extraction; effective in reducing POME production and increasing extraction efficiency.
Kanjanapongkul (2021)	Ohmic and microwave heating pretreatment	47% CPO yield	Combined ohmic-microwave pretreatment produced lower FFA content, higher yield, and lower energy consumption than single processes.
Ong et al. (2021)	Microwave pre-treatment followed by Soxhlet extraction	3.289 g of palm oil from OPDC	Microwave pre-treatment improved extraction yield and altered physicochemical properties; RSM helped optimise parameters.
Zamanhuri et al. (2021)	Microwave-assisted extraction at 100 W, 64% yield for CPO, 300 W for PFA distillate	64% CPO yield, high palmitic acid content in distillate	Efficient cell structure breakdown, high-quality CPO; optimal conditions identified for PFA extraction.
Ng and Nu'man (2021)	Microwave-assisted DES extraction (ChCl-AA, 30% water, 60°C, 9–15 min)	0.609–1.123 mg/g ferulic acid	Effective extraction of ferulic acid with good antioxidant properties; optimised DES composition.
Nomanbhay et al. (2018)	MAE with enzymatic hydrolysis	Not specified	Enhanced phenolic compound extraction yield; significant time reduction compared to conventional methods.

Note: MOAH - mineral oil aromatic hydrocarbons; RSM - response surface methodology; FFA - free fatty acid; PFA - palm fatty acid; POME - palm oil mill effluent; CPO - crude palm oil; MAEA - microwave-assisted enzyme aqueous; MAE - microwave-assisted extraction; DES - deep eutectic solvents; OPDC - oil palm decanter cake.

TABLE 2. OVERVIEW OF STUDIES ON UAE FOR PALM OIL EXTRACTION, HIGHLIGHTING EXTRACTION CONDITIONS, YIELDS AND OUTCOMES

Authors	Extraction condition	Yield	Outcome
Ben-Youssef et al. (2017)	Ultrasound extraction with n-hexane and 2-MeTHF	7.24%–5.97% lipid yield from date palm seeds	Ultrasound and microwave extraction significantly reduced extraction time (30 min vs. 8 hr) and increased lipid yield compared to maceration (about 6% vs. 4%).
Ngadi and Rusli (2014)	UAE is using sodium hydroxide solution	Not specified for lignin	Ultrasound extraction was more efficient than conventional heating, resulting in higher lignin yield, lower reaction temperature and shorter reaction time.
Martínez-Girón et al. (2024)	Ultrasound-assisted emulsion with sunflower oil at 480 W for 5 min	Carotenoid content: 67.61 µg/g	Stable emulsion with provitamin A activity, chemically and physically stable for 35 days; potential as a bio functional food additive.
Ordoñez-Santos et al. (2015)	UAE at 1,528 W/m2, 35°C, 30 min	163.47 mg/100 g total carotenoids	UAE optimised using RSM; higher carotenoid yield compared to maceration; validated model showed good consistency.
Zain et al. (2020)	UAE at 25°C, 0.5 hr, 4:1 methanol-water ratio	TPC: 335.30 mg QCE/g, TFC: 60.67 mg QCE/g	Optimised extraction conditions resulted in high polyphenolic and flavonoid content with strong free radical scavenging activity.
Ordoñez-Santos et al. (2019)	UAE at 48°C, 28 min, 0.0037 g/mL solid-solvent ratio	151.50 mg/100 g carotenoids	UAE yielded 33.6% more carotenoids than maceration; optimised using RSM and validated experimentally.
Putra et al. (2022)	UAE with 70% methanol	Not specified	UAE was less effective compared to Soxhlet extraction for polyphenol and flavonoid yield; antioxidant activity measured was promising but inconclusive.
Cypriano et al. (2008)	UAE with 1:1 HCl-H_2O_2 for 60 min	~100% extraction of Cu and Pb	UAE effectively extracted trace metals, showing good correlation with conventional methods; suitable for oil quality assessment.

Note: QCE - quercetin equivalents; TPC - total phenolic content; TFC - total flavonoid content; UAE - ultrasound-assisted extraction; RSM - response surface methodology; Cu - copper; Pb - leads; HCl - hydrogen acid; H_2O_2 - hydrogen peroxide.

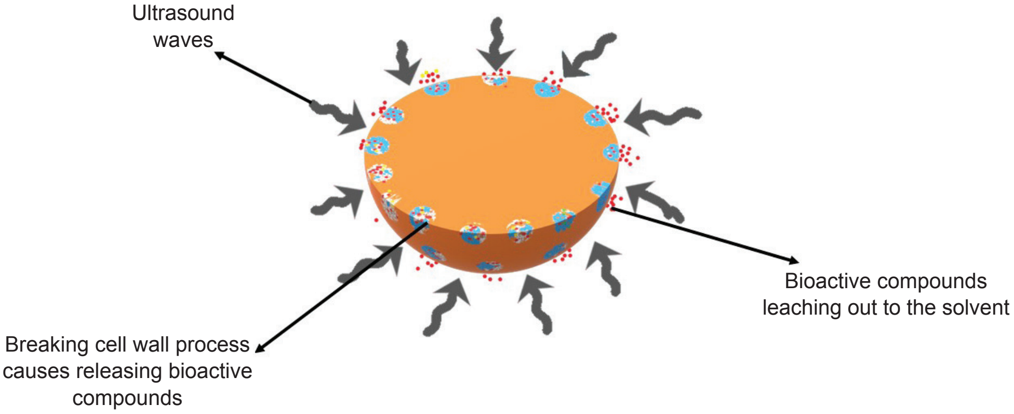

Figure 2. Mechanism of ultrasound-assisted extraction (UAE) for palm oil recovery.

These conditions break down cell walls, improving mass transfer and extraction efficiency. In comparison to traditional extraction methods, UAE offers advantages such as shorter extraction times, lower energy consumption and enhanced yields of bioactive compounds like lipids, carotenoids and polyphenols (Kumar et al., 2021; Liu et al., 2022; Wen et al., 2018). The effectiveness of UAE, however, depends heavily on optimising key process parameters such as solvent selection, temperature, extraction time and ultrasonic power, each of which plays a crucial role in determining the yield and quality of the extracted materials (Esclapez et al., 2011).

Solvent choice is a critical factor in the UAE, influencing the extraction efficiency and the solubility of target compounds. For instance, Ben-Youssef et al. (2017) demonstrated that using a combination of n-hexane and 2-methyltetrahydrofuran (2-MeTHF) significantly improved lipid yield from date palm seeds, achieving a higher extraction rate and faster processing times than traditional maceration. The ability to tailor solvent selection for specific applications shows the UAE's versatility in improving extraction outcomes across various matrices. Similarly, studies that focused on bioactive compounds like carotenoids have shown that solvent composition and concentration directly affect the recovery of high-value extracts, especially when combined with optimised temperatures to preserve sensitive compounds.

Temperature is another critical factor in the UAE, particularly for heat-sensitive compounds like carotenoids. Ordoñez-Santos et al. (2015, 2019) explored the optimisation of UAE conditions using Response Surface Methodology (RSM), revealing that relatively low temperatures (35°C–48°C) were sufficient to extract high yields of carotenoids from palm oil by-products, outperforming traditional extraction methods. These results highlight the UAE's ability to balance efficient extraction with the preservation of delicate bioactive compounds, ensuring high-quality outputs. Moreover, the moderate temperatures used in the UAE help to retain the nutritional and functional properties of the extracted compounds, further emphasising their potential in producing health-beneficial oils and additives.

Extraction time also plays a key role in the UAE's efficiency. Shorter extraction times not only reduce energy consumption but also make UAE a more commercially viable technique for large-scale applications. Zain et al. (2020) demonstrated the effectiveness of UAE in extracting polyphenols and flavonoids from palm oil by-products within just 30 min, achieving high levels of antioxidant activity. These results illustrate the UAE's ability to quickly and efficiently extract bioactive compounds with minimal energy input, making it an attractive option for industries aiming to reduce their carbon footprint while maintaining high-quality outputs. The reduction in processing time without compromising yield is a significant advantage of UAE over conventional extraction methods, which often require hours of operation.

Ultrasonic power is another essential parameter that directly influences the cavitation process, impacting the breakdown of plant cells and the release of compounds. Higher ultrasonic power can enhance extraction efficiency by creating more intense cavitation effects, but it must be carefully controlled to prevent degradation of sensitive compounds. Martínez-Girón et al. (2024) used high ultrasonic power (480 W) to successfully form stable carotenoid emulsions, showing that UAE can be effectively applied not only for extraction but also for the formulation of bio functional products. This highlights the UAE's broader applications beyond extraction, such as in the development of nutraceuticals and food additives, further expanding its industrial relevance.

The UAE offers numerous advantages for palm oil extraction, including shorter processing times, lower energy consumption and higher yields of valuable bioactive compounds. The success of the UAE depends on optimising key parameters like solvent selection, temperature, extraction time and ultrasonic power, each of which influences the overall efficiency and quality of the extraction. By fine-tuning these parameters, UAE can be adapted to extract a wide range of compounds, from lipids to polyphenols, while maintaining the integrity of heat-sensitive bioactive. Given its environmental benefits and industrial scalability, the UAE represents a promising green technology for the future of palm oil extraction, offering an efficient and sustainable alternative to traditional methods.

$SCCO_2$ FOR PALM OIL EXTRACTION

$SCCO_2$ extraction has become a preferred green technology for palm oil extraction due to its efficiency and ability to operate under mild conditions, preserving the quality of the extracted oils and bioactive compounds. By using CO_2 in its supercritical state, which combines the properties of both liquids and gases, $SCCO_2$ can effectively dissolve and extract oils while minimising the use of harmful organic solvents as shown in *Figure 3*. This makes it a highly sustainable method, particularly for industries focused on producing high-quality palm oil rich in valuable compounds such as carotenoids, tocopherols and fatty acids. The performance of $SCCO_2$ extraction is greatly influenced by process parameters like solvent modifiers, temperature, pressure and particle size, all of which play a crucial role in determining extraction yields and outcomes.

One critical factor in improving $SCCO_2$ extraction efficiency is the use of solvent modifiers. Studies such as Barbi et al. (2020) and Krishnaiah et al. (2012) demonstrated that adding ethanol as a co-solvent significantly enhances the recovery of bioactive compounds like fatty acids and tocopherols. Ethanol, being a polar solvent, increases the solubility of certain compounds that are not easily extracted by pure $SCCO_2$, resulting in higher yields and improved oil quality. These findings highlight the importance of combining $SCCO_2$ with appropriate solvent modifiers to maximise extraction efficiency and target specific compounds that add value to palm oil products.

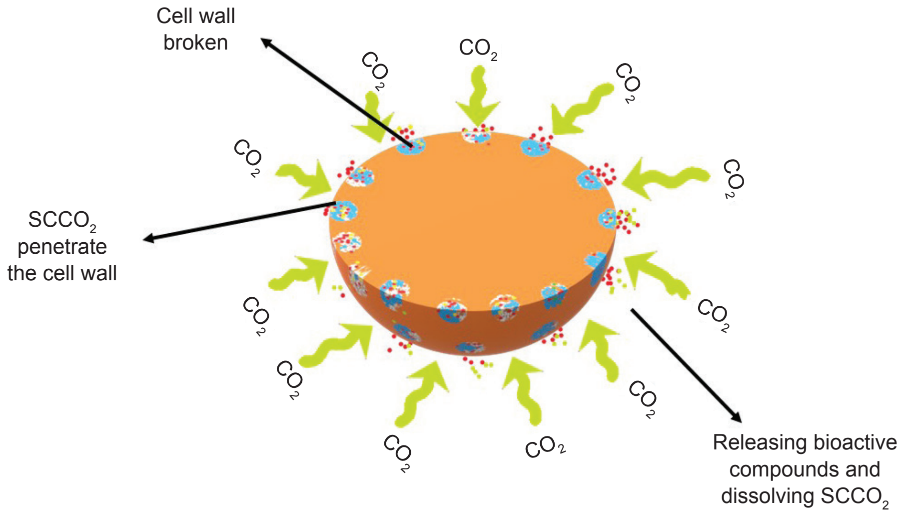

Figure 3. Mechanism of supercritical carbon dioxide ($SCCO_2$) for palm oil recovery.

Temperature and pressure are equally important in $SCCO_2$ extraction as they directly influence the solubility of oils and bioactive compounds. Studies by Norhuda and Omar (2009) and Zaidul et al. (2007) showed that higher pressures and temperatures lead to increased extraction yields and alter the composition of the extracted oils. For example, higher pressures tend to extract longer-chain fatty acids more efficiently, contributing to oil products that are richer in specific bioactive compounds. Optimising these parameters is key to improving the overall efficiency of the extraction process while ensuring that the quality of the oil is maintained or enhanced, particularly when dealing with heat-sensitive compounds like carotenoids and tocopherols.

$SCCO_2$ extraction is particularly valued for its ability to recover high-value compounds, such as carotenoids, tocopherols and squalene, which have significant applications in food, cosmetics and pharmaceuticals. Puah et al. (2006, 2007, 2011) demonstrated that $SCCO_2$ can extract palm oil components rich in carotenoids and vitamin E under mild conditions, producing high-quality oils suitable for commercial applications. Similarly, Al-Darmaki (2012) showed that a thermal gradient during extraction significantly improved the recovery of squalene, a compound with high antioxidant properties. These studies emphasised the potential of $SCCO_2$ for producing functional palm oil products enriched with bioactive compounds, which adds significant value to the oil beyond its basic nutritional properties.

Particle size and extraction duration also significantly impact the efficiency of $SCCO_2$ extraction. Rahman et al. (2012) found that smaller particle size increased oil yield, as smaller particles provide a larger surface area for mass transfer. Additionally, studies like Hossain et al. (2016) showed that adjusting the extraction time can maximise oil recovery while preserving the nutrient quality of the oil. This is particularly important in producing de-oiled palm kernel cake (PKC), which can be used for human and animal consumption. Optimising these physical parameters ensures that $SCCO_2$ extraction not only improves oil yields but also maintains the integrity of both the oil and the remaining by-products, making the process more versatile and sustainable.

In conclusion, $SCCO_2$ extraction presents numerous advantages for palm oil extraction, particularly in its ability to enhance oil yields while preserving bioactive compounds under environmental-friendly conditions. The use of co-solvents, temperature, pressure, particle size and extraction time all play a significant role in optimising the process for specific applications, whether in food, pharmaceuticals or cosmetics. The growing body of research shows that $SCCO_2$ is an efficient and sustainable alternative to conventional extraction methods, with potential for further refinement through the continued exploration of solvent modifiers and the integration of alternative supercritical fluids like subcritical propane. This positions $SCCO_2$ extraction as a key technology in the sustainable production of palm oil and its high-value derivatives.

DES FOR PALM OIL EXTRACTION

DES have gained significant attention as a promising class of green solvents for palm oil extraction and processing due to their low toxicity, biodegradability and sustainability. Formed by mixing a hydrogen bond acceptor and a hydrogen bond donor, DES results in a eutectic mixture with a much lower melting point than its individual components, enhancing their effectiveness in various extraction processes. This section discusses recent advancements in DES applications for extracting valuable bioactive compounds from palm oil and its by-products, demonstrating their potential for revolutionising the industry.

DES have been particularly effective in extracting bioactive compounds from palm biomass. For instance, Ng and Hadi (2022) demonstrated the ability of choline chloride-based DES to selectively extract ferulic acid, a potent antioxidant, from oil palm pressed fibre. This extraction method proved to be a more sustainable alternative to traditional solvents, which are often harmful to the environment. Further, Ng et al. (2024) highlighted the economic and environmental advantages of DES by showcasing their recyclability, allowing for repeated use without significant loss of efficiency. This ability to recycle DES makes them highly suitable for large-scale applications in the palm oil industry, where both sustainability and cost-effectiveness are critical considerations.

The integration of DES with other green technologies has further enhanced the efficiency of palm oil extraction. Zain et al. (2020) integrated choline chloride-based DES with macroporous resin to produce enriched oil palm flavonoids, which have applications in natural wound healing. This combination not only improved the yield and purity of the extracted flavonoids but also maintained their bioactivity, which is often compromised under conventional extraction conditions. Similarly, Yaakob et al. (2024) combined DES with MAE to extract lignin from oil palm empty fruit bunches (EFB). This synergistic approach significantly reduced processing time while improving extraction yields (achieved a 57.12% yield), demonstrating the potential of combining DES with other green technologies to enhance the efficiency of lignocellulosic biomass processing.

Understanding the physicochemical properties of DES is essential for optimising their use in extraction processes. Zain et al. (2021) characterised the solubility, viscosity and thermal stability of choline chloride-based DES, providing valuable insights that are crucial for achieving high extraction efficiency and selectivity. Similarly, Hadi et al. (2015) investigated the performance of DES in extracting tocols (vitamin E compounds) from CPO. Their findings revealed that DES could effectively extract these bioactive compounds while preserving their bioactivity, making DES suitable for producing high-quality palm oil derivatives with enhanced nutritional properties.

DES have also proven to be effective in extracting specific compounds from palm oil and its by-products. Mulia et al. (2018) demonstrated the selective extraction of palmitic acid, a widely used saturated fatty acid, using betaine-based DES. Rizki et al. (2022) further explored the use of natural DES for extracting tocotrienols and tocopherols (vitamin E isomers) from CPO, achieving high extraction yields while maintaining the stability and functionality of these compounds. The highest vitamin E concentration and extraction efficiency were 4,439 mg/kg and 74.98%, respectively. Additionally, Manurung et al. (2020) showed that menthol-based DES could efficiently extract carotenoids, important antioxidants and pigments, from CPO, offering a sustainable method for producing carotenoid-rich palm oil products.

Beyond extraction, DES have been employed in the fractionation and pretreatment of palm oil biomass. Yong and Wu (2024) explored the fractionation of oil palm fronds using ethanol-assisted DES, focusing on enhancing enzymatic saccharification and lignin extraction. The inclusion of ethanol in the DES system significantly improved the fractionation process, resulting in higher yields of fermentable sugars and more efficient lignin recovery (Ethanol-assisted DESs able to preserve 60%–84% of β-O-4 linkages in lignin). These findings suggest that DES could play a crucial role in improving the pretreatment of palm oil biomass for various downstream applications, including biofuel production.

Table 3 presents an overview of studies employing $SCCO_2$ extraction for palm oil recovery, emphasising the influence of extraction conditions, yields and outcomes. These studies reflect the versatility and efficiency of $SCCO_2$ as a green extraction technique, with operating parameters such as temperature, pressure, co-solvent use (e.g., ethanol) and extraction duration playing critical roles in oil yield and quality. The reported oil yields vary considerably, ranging from 0.18% to 70.00%, often influenced by matrix type, particle size and the presence of high-value bioactives like tocopherols, carotenoids and squalene. Notably, several works demonstrated the ability of $SCCO_2$ to enhance the extraction of nutritionally important fractions and separate fatty acids selectively. Furthermore, innovations such as the use of subcritical propane, ethanol-modified $SCCO_2$ and thermodynamic modelling (e.g., Peng-Robinson EOS) have advanced process optimisation, improving both oil recovery and quality. Collectively, these findings underline $SCCO_2$ extraction as a promising and tunable method for valorising palm-based biomass into high-value oil products.

COMPARATIVE ANALYSIS OF GREEN EXTRACTION METHODS

Efficiency and Yield

In the quest for more sustainable and environmentally friendly methods of palm oil extraction, several green technologies have been developed and evaluated. This section compares

TABLE 3. OVERVIEW OF STUDIES ON $SCCO_2$ FOR PALM OIL EXTRACTION, HIGHLIGHTING EXTRACTION CONDITIONS, YIELDS AND OUTCOMES

Authors	Extraction condition	Yield	Outcome
Barbi et al. (2020)	$SCCO_2$ (333.15 K, 20 MPa) and pressurised ethanol	3.6% ($SCCO_2$), 20.4% ($SCCO_2$ + EtOH), 47.8% (PLE)	PLE showed the highest recovery of oil. $SCCO_2$ + EtOH increased recovery compared to pure $SCCO_2$. The oil was rich in unsaturated fatty acids and bioactive compounds, suitable for food and pharmaceuticals.
Norhuda and Omar (2009)	$SCCO_2$ at 50°C–70°C and 27.6–48.3 MPa	Not specified	The overall mass transfer coefficient increased with temperature and pressure, indicating improved extraction efficiency under higher temperature and pressure.
Al-Darmaki et al. (2012)	$SCCO_2$ with isothermal and temperature gradient (313–353 K, 10–20 MPa)	Squalene increased from 2%–16% in the top product	High squalene recovery (95%) and concentration achieved. The thermal gradient along the column enhanced squalene recovery.
Hossain et al. (2016)	$SCCO_2$ (44.6 MPa, 60°C, 50 min)	49.2% oil yield	$SCCO_2$ maintained nutrient compositions in deoiled PKC, which is suitable for human and animal consumption. Significant reduction in anti-nutrient compositions was observed.
Norulaini et al. (2004)	$SCCO_2$ at 80°C and 27.6–48.3 MPa for 30–60 min	28.2%–44.75% oil yield depending on pressure	The solubility of oil increased with pressure, and fatty acid composition varied across different fractions.
Zaidul et al. (2007)	$SCCO_2$ (313.2–353.2 K, 20.7–48.3 MPa)	49 g oil/100 g palm kernel at 48.3 MPa and 353.2 K	Higher pressure resulted in the extraction of longer chain fatty acids. A kinetic mass transfer model was developed to estimate CO_2 usage for a given yield.
Puah et al. (2011)	$SCCO_2$ (14–30 MPa, 40°C–80°C)	0.1751–6.60 mg/g CO_2	Solubility of palm oil components in $SCCO_2$ was influenced by acylglycerols and FFAs. Optimal solubility was at 60°C and 30 MPa.
Hong et al. (2010)	$SCCO_2$ with Peng-Robinson EOS (333.2–373.2 K, 8.5–35 MPa)	Not specified	PR-EOS with Wong-Sandler mixing rule effectively predicted vapor-liquid equilibria of palm oil and $SCCO_2$.
Promraksa et al. (2020)	$SCCO_2$ for palm oil and α-tocopherol extraction	Not specified	Axial dispersion played a significant role in constant extraction-rate periods. Extraction of α-tocopherol confirmed the role of axial dispersion.
Puah et al. (2006)	$SCCO_2$ (14–30 MPa, 40°C)	>1,000 ppm carotenoids, 350 ppm vitamin E	$SCCO_2$ produced carotenoids-rich palm olein with a lower cloud point, comparable to commercial olein.
Phan-Tai and Brunner, (2023)	Subcritical propane (50 bar, 120 min)	70% oil yield	Compressed propane effectively extracted oil enriched in carotenes and tocochromanols. Subcritical propane was a viable alternative to $SCCO_2$ for simultaneous recovery of valuable compounds.
Norulaini et al. (2004)	$SCCO_2$ (80°C, 27.6–48.3 MPa, 30–60 min)	37.5%–44.75% oil yield	Oil yield increased with pressure, and fatty acid composition varied across different fractions. $SCCO_2$ was effective for separating lauric and oleic acids.
Krishnaiah et al. (2012)	$SCCO_2$ (19.8 MPa, 51°C) with ethanol	Not specified	$SCCO_2$ with ethanol effectively extracted tocopherols, tocotrienols and fatty acids. Oil quality improved with increasing ethanol content.
Rahman et al. (2012)	$SCCO_2$ (27.57–41.36 MPa, 40°C–70°C) with different particle sizes	9.26 g oil/100 g sample	Smaller particle sizes increased oil yield. $SCCO_2$ was effective in extracting residual oil, producing defatted PKC.

Note: PLE - pressurised liquid extraction; FFA - free fatty acid; PKC - palm kernel cake; $SCCO_2$ - supercritical carbon dioxide; CO_2 - carbon dioxide; EtOH - ethanol.

the efficiency and yield of various green extraction methods, such as $SCCO_2$ extraction, UAE, MAE and DES, based on data from recent studies.

$SCCO_2$ extraction has gained popularity due to its ability to operate without toxic solvents while maintaining high extraction efficiency. For example, Barbi et al. (2020) demonstrated that $SCCO_2$, when combined with ethanol as a co-solvent, could significantly enhance oil recovery from *Maximiliana maripa* pulp. The study reported a yield of 20.4% with $SCCO_2$ + ethanol, compared to only 3.6% with pure $SCCO_2$. This method was found to be particularly effective in extracting unsaturated fatty acids and bioactive compounds, which are valuable for food and pharmaceutical applications. Similarly, Zaidul et al. (2007) found that $SCCO_2$ extraction at higher pressures (48.3 MPa) resulted in a substantial yield of 49 g oil/100 g palm kernel, demonstrating the method's potential for high-yield extractions when optimised for pressure and temperature.

UAE is another method that has shown promise in enhancing the extraction yield of palm oil and its derivatives. The efficiency of UAE is primarily attributed to the cavitation effect, which enhances the penetration of solvents into plant materials, thereby increasing the extraction rate. For instance, studies like those by Othman et al. (2017) showed that UAE could achieve up to 83.0% removal of phenol from wastewater using a palm oil-based solvent, highlighting its effectiveness in both extraction yield and environmental impact. Although direct comparisons of palm oil yield using UAE are less common, its ability to enhance the extraction of valuable compounds from palm oil waste products suggests significant potential for further development.

MAE is recognised for its rapid heating and efficient energy transfer, which can lead to reduced extraction times and improved yields. Studies such as those by Han and Hadi (2024) on the MAE of ferulic acid from palm fruitlets have shown that MAE can maintain high bioactivity in the extracted compounds while achieving considerable yields. MAE's ability to efficiently break down plant cell walls enhances the extraction of oils and other valuable compounds, making it a competitive method in terms of yield and efficiency, particularly for compounds that are sensitive to conventional heating methods.

DES have emerged as a green alternative to conventional organic solvents, offering a non-toxic, biodegradable and cost-effective solution for biomass pretreatment. Studies like those by Loow et al. (2017) and Jablonský et al. (2018) have shown that DES, when combined with other methods such as UAE or $SCCO_2$, can significantly enhance the extraction yield of specific components like xylose and phenolic compounds from lignocellulosic biomass. For example, Loow et al. (2017) reported a 25.0% increase in xylose recovery when using DES in conjunction with an inorganic salt, compared to using the salt alone. This highlights DES's potential in improving extraction efficiency, especially when integrated into multi-step extraction processes.

When comparing these green extraction methods, $SCCO_2$ stands out for its ability to achieve high yields, particularly when combined with co-solvents like ethanol. However, this method requires high-pressure equipment, which can be cost-prohibitive for some applications. UAE and MAE offer lower-cost alternatives with good efficiency, particularly for extracting heat-sensitive compounds and enhancing yields from waste materials. DES, while still emerging, shows great promise in improving the efficiency of existing extraction processes and reducing the environmental footprint. Overall, the choice of extraction method depends on the specific application, the desired compounds, and the available resources. Each method has its strengths, with $SCCO_2$ being ideal for high-value oil extraction, UAE and MAE offering quick and efficient alternatives for various compounds, and DES providing a versatile and green solution for enhancing extraction processes. The integration of these methods into a comprehensive extraction strategy can potentially maximise both efficiency and yield while minimising environmental impact.

Comparison of Extraction Yields with Conventional Methods

Conventional methods such as mechanical pressing and solvent extraction have traditionally dominated the palm oil extraction industry. Mechanical pressing, commonly used in small to medium-scale operations, typically achieves an oil yield of about 20.0%–25.0% (Cheng et al., 2021). While this method is cost-effective and straightforward, it is not particularly efficient, often leaving a significant amount of oil in the palm kernel or fruit pulp. On the other hand, solvent extraction using hexane could achieve higher yields, often up to 45.0%–50.0% (Ong et al., 2021). However, the use of hexane poses serious environmental and health risks due to its toxicity and flammability, along with the significant energy required for solvent recovery and the potential for solvent residues in the final product. These drawbacks make solvent extraction less desirable from a sustainability perspective.

In contrast, green extraction methods offer promising alternatives that can match or exceed the yields of conventional methods while mitigating their environmental impacts. For example, $SCCO_2$ extraction has demonstrated yields comparable to or higher than those of solvent extraction, particularly when co-solvents like ethanol are used. Study by

Barbi et al. (2020) showed that $SCCO_2$ with ethanol achieved a yield of 20.4% from *Maximiliana maripa* pulp, which, while slightly lower than conventional solvent extraction, is notable for its significantly reduced environmental impact. Zaidul et al. (2007) reported an even higher yield of 49 g oil/100 g of palm kernel using $SCCO_2$ under optimal pressure conditions, matching or surpassing yields from traditional solvent methods.

UAE, though less extensively studied for palm oil yield specifically, has shown effectiveness in enhancing extraction processes for other valuable compounds, suggesting its potential for high oil yields. For instance, Othman et al. (2017) demonstrated an 83.0% removal of phenol from wastewater using a palm oil-based solvent, highlighting UAE's efficiency in extracting compounds from complex matrices. Similarly, MAE is recognised for its rapid, energy-efficient process, which can yield comparable results to solvent extraction while significantly reducing processing time. Han and Hadi (2024) reported successful extraction of ferulic acid from palm fruitlets using MAE, retaining high bioactivity and suggesting that MAE could also enhance palm oil extraction yields with proper optimisation.

DES, an emerging technology, has shown great promise in improving extraction efficiency. Loow et al. (2017) observed a 25.0% increase in xylose recovery using DES combined with inorganic salts, compared to conventional methods. Although direct comparisons with palm oil extraction are limited, these efficiency gains suggest that DES could potentially match or exceed conventional solvent extraction yields when optimised for palm oil.

In summary, while conventional methods such as solvent extraction offer high yields, their environmental and health-related drawbacks are significant. Green extraction methods, although sometimes yielding slightly lower percentages, offer substantial advantages in terms of sustainability, safety and process efficiency. $SCCO_2$ extraction stands out for achieving high yields comparable to solvent extraction without the need for toxic chemicals. UAE and MAE provide rapid, energy-efficient alternatives well-suited for extracting high-value compounds from palm oil and its by-products. DES shows great promise as a green solvent that could further enhance yields with minimal environmental impact. As these green technologies continue to advance and be optimised, they are poised to become the preferred methods for sustainable palm oil extraction, aligning industry practices with global sustainability goals.

Table 4 provides comparative analysis of green extraction methods employed in palm oil extraction, highlighting the efficiency, yields, benefits and limitations of each technique. The reviewed methods include $SCCO_2$, UAE, MAE and DES, each offering distinct advantages for enhancing extraction performance. $SCCO_2$ is noted for its high efficiency, especially when combined

TABLE 4. COMPARATIVE ANALYSIS OF GREEN EXTRACTION METHODS FOR PALM OIL EXTRACTION

Extraction method	Key studies	Efficiency	Yield	Advantages	Challenges
$SCCO_2$	Barbi et al. (2020); Zaidul et al. (2007)	High efficiency, especially with co-solvents like ethanol. High pressure improves mass transfer and extraction rates.	3.6% yield with pure $SCCO_2$. 20.4% yield with $SCCO_2$ + ethanol. 49 g oil/100 g palm kernel at high pressure.	Solvent-free, environmental-friendly. High yield for unsaturated fatty acids and bioactive compounds.	Requires high-pressure equipment, increasing cost. Optimisation is needed for specific applications.
UAE	Ali et al. (2023); Anggoro et al. (2024); Zain et al. (2020)	Cavitation effect enhances solvent penetration, improving extraction rate.	83.0% phenol removal from wastewater using palm oil-based solvent.	Low cost, efficient for waste treatment. Enhances the extraction of valuable compounds from waste products.	Limited direct studies on palm oil yield. Optimisation needed for large-scale applications.
MAE	Han and Hadi (2024); Yaakob et al. (2024)	Rapid heating and efficient energy transfer, reducing extraction time.	High bioactivity retention in extracted compounds.	Fast, energy-efficient. Suitable for heat-sensitive compounds.	Requires specialised equipment. Potential for uneven heating at larger scales.
DES	Jablonský et al. (2018); Loow et al. (2017)	Improves delignification and biomass pretreatment, especially when combined with other methods.	25.0% increase in xylose recovery with DES + inorganic salt.	Non-toxic, biodegradable and cost-effective. Enhances extraction when integrated with other methods.	Emerging technology, require further optimisation. Scalability and consistency need evaluation.

Note: $SCCO_2$ - supercritical carbon dioxide; UAE - ultrasound-assisted extraction; MAE - microwave-assisted extraction; DES - deep eutectic solvents with co-solvents like ethanol, delivering high-quality oil rich in unsaturated fatty acids but requiring high-pressure systems and cost-intensive optimisation. UAE demonstrates outstanding potential in wastewater valorisation through phenol removal, promoting sustainability but suffers from limited direct studies on palm oil. MAE offers rapid, energy-efficient extraction with excellent bioactivity retention, making it ideal for heat-sensitive compounds; however, its scalability and need for precise thermal control remain challenges. DES, as an emerging and environmentally benign technique, has shown promise in improving delignification and biomass pretreatment, although it still requires optimisation and validation for consistency at scale. Overall, the table underscores the complementary roles of these methods in advancing sustainable palm oil extraction technologies.

CONCLUSION

The transition to green extraction methods in the palm oil industry marks a critical advancement towards sustainability by addressing both environmental concerns and the demand for higher-quality products. While conventional methods like mechanical pressing and solvent extraction have been reliable in terms of yield, they are becoming less favored due to their environmental and health-related drawbacks, inefficiency in preserving bioactive compounds, and substantial waste generation. In contrast, green extraction technologies not only meet but often surpass conventional techniques in terms of efficiency, yield, and product quality, while significantly minimising environmental impact.

$SCCO_2$ extraction has proven particularly effective in achieving high yields and maintaining the nutritional integrity of palm oil, especially when used with co-solvents like ethanol to improve extraction efficiency. Technologies like UAE and MAE offer rapid, energy-efficient processes that preserve bioactive compounds, making them ideal for high-quality palm oil derivatives. The emerging application of DES demonstrates substantial potential by improving extraction efficiency with minimal environmental harm, although more research is needed to further optimise its performance.

Despite these promising developments, challenges remain in scaling up these green technologies for widespread industrial application. Future studies should focus on refining process parameters, reducing energy consumption further, and improving the cost-effectiveness of these methods. In addition, more research is needed to assess the long-term economic viability and the potential of combining green extraction techniques to maximise extraction yields and product quality. As these technologies continue to evolve, they are expected to become the industry standard, contributing significantly to the mitigation of environmental impacts while maintaining the high standards of palm oil products. Therefore, further exploration into the integration of these methods with circular economy models and renewable energy sources could unlock even greater potential in creating a fully sustainable palm oil production system.

ACKNOWLEDGEMENT

The authors would like to acknowledge the National Research and Innovation Agency (BRIN) and Institut Teknologi Sepuluh Nopember for supporting this work.

REFERENCES

Ahangari, H., King, J. W., Ehsani, A., & Yousefi, M. (2021). Supercritical fluid extraction of seed oils – A short review of current trends. *Trends in Food Science & Technology, 111*, 249–260. https://doi.org/10.1016/j.tifs.2021.02.066

Al-Darmaki, N. I. K. (2012). *Extraction and enrichment of minor lipid components of palm fatty acid distillate using supercritical carbon dioxide* [Ph.D Dissertation]. University of Birmingham.

Alvi, T., Asif, Z., & Khan, M. K. I. (2022). Clean label extraction of bioactive compounds from food waste through microwave-assisted extraction technique – A review. *Food Bioscience, 46*, 101580. https://doi.org/10.1016/j.fbio.2022.101580

Anggoro, D. D., Prasetyaningrum, A., Udaibah, W., Imtinan, A. B., Nabilah, F., & Monde, B. U. L. (2024). Effect of ultrasound-advanced oxidation processes for pretreatment of oil palm mesocarp fiber for cellulose extraction. *International Journal of Renewable Energy Development, 13*(3), 532–538. https://doi.org/10.61435/ijred.2024.60027

Arumugham, T., Rambabu, K., Hasan, S. W., Show, P. L., Rinklebe, J., & Banat, F. (2021). Supercritical carbon dioxide extraction of plant phytochemicals for biological and environmental applications – A review. *Chemosphere, 271*, 129525. https://doi.org/10.1016/j.chemosphere.2020.129525

Ayoib, A., Hashim, U., & Gopinath, S. C. B. (2020). Automated, high-throughput DNA extraction protocol for disposable label free, microfluidics integrating DNA biosensor for oil palm pathogen, *Ganoderma boninense*. *Process Biochemistry, 92*, 447–456. https://doi.org/10.1016/j.procbio.2020.02.003

Barbi, R. C. T., De Souza, A. R. C., De Melo, A. M., Teixeira, G. L., Corazza, M. L., & Ribani, R. H. (2020). Fatty acid profile and lipid quality of *Maximiliana maripa* oil obtained by supercritical CO_2 and pressurized ethanol. *The Journal of Supercritical Fluids*, *165*, 104979. https://doi.org/10.1016/j.supflu.2020.104979

Bauwens, G., & Purcaro, G. (2024). Improved microwave-assisted saponification to reduce the variability of MOAH determination in edible oils. *Analytica Chimica Acta*, *1312*, 342788. https://doi.org/10.1016/j.aca.2024.342788

Ben-Youssef, S., Fakhfakh, J., Breil, C., Abert-Vian, M., Chemat, F., & Allouche, N. (2017). Green extraction procedures of lipids from Tunisian date palm seeds. *Industrial Crops and Products, 108*, 520–525. https://doi.org/10.1016/j.indcrop.2017.07.010

Chan, Y. H., Yusup, S., Quitain, A. T., Chai, Y. H., Uemura, Y., & Loh, S. K. (2018). Extraction of palm kernel shell derived pyrolysis oil by supercritical carbon dioxide: Evaluation and modeling of phenol solubility. *Biomass and Bioenergy, 116*, 106–112. https://doi.org/10.1016/j.biombioe.2018.06.009

Chemat, F., Vian, M. A., Fabiano-Tixier, A., Nutrizio, M., Jambrak, A. R., Munekata, P. E. S., Lorenzo, J. M., Barba, F. J., Binello, A., & Cravotto, G. (2020). A review of sustainable and intensified techniques for extraction of food and natural products. *Green Chemistry*, *22*(8), 2325–2353. https://doi.org/10.1039/c9gc03878g

Cheng, Y. W., Chong, C. C., Lam, M. K., Ayoub, M., Cheng, C. K., Lim, J. W., Yusup, S., Tang, Y., & Bai, J. (2021). Holistic process evaluation of non-conventional palm oil mill effluent (POME) treatment technologies: A conceptual and comparative review. *Journal of Hazardous Materials*, *409*, 124964. https://doi.org/10.1016/j.jhazmat.2020.124964

Chew, S. C., How, Y. H., Hasan, Z. A. B. A. & Chu, C. C. (2024). Recovery of bioactive compounds from oil palm waste using green extraction techniques and its applications. *International Journal of Food Science & Technology, 59*(11), 8101–8113. https://doi.org/10.1111/ijfs.17572

Cypriano, J. C., Matos, M. A. C., & Matos, R. C. (2008). Ultrasound-assisted treatment of palm oil samples for the determination of copper and lead by stripping chronopotentiometry. *Microchemical Journal, 90*(1), 26–30. https://doi.org/10.1016/j.microc.2008.03.001

Esclapez, M., García-Pérez, J. V., Mulet, A., & Cárcel, J. A. (2011). Ultrasound-assisted extraction of natural products. *Food Engineering Reviews.*, *3*, 108–120. https://doi.org/10.1007/s12393-011-9036-6

Guía-García, J. L., Charles-Rodríguez, A. V., Reyes-Valdés, M. H., Ramírez-Godina, F., Robledo-Olivo, A., García-Osuna, H. T., Cerqueira, M. A., & Flores-López, M. L. (2022). Micro and nanoencapsulation of bioactive compounds for agri-food applications: A review. *Industrial Crops and Products, 186*, 115198. https://doi.org/10.1016/j.indcrop.2022.115198

Hadi, N. A., Ng, M. H., Choo, Y. M., Hashim, M. A., & Jayakumar, N. S. (2015). Performance of choline-based deep eutectic solvents in the extraction of tocols from crude palm oil. *Journal of the American Oil Chemists Society*, *92*(11–12), 1709–1716. https://doi.org/10.1007/s11746-015-2720-6

Han, N. M., & Hadi, N. A. (2024). Consolidation of deep eutectic solvents with microwave for the extraction of ferulic acid from the fruitlets of oil palm. *Journal of Oil Palm Research, 36*(1), 115–127. https://doi.org/10.21894/jopr.2023.0022

Hong, S. -A., Kim, J. -D., Kim, J., Kang, J. W., & Kang, I. -J. (2010). Phase equilibria of palm oil, palm kernel oil, and oleic acid + supercritical carbon dioxide and modeling using Peng-Robinson EOS. *Journal of Industrial and Engineering Chemistry*, *16*(5), 859–865. https://doi.org/10.1016/j.jiec.2010.03.009

Hossain, M. S., Norulaini, N. N., Naim, A. A., Zulkhairi, A. M., Bennama, M. M., & Omar, A. M. (2016). Utilization of the supercritical carbon dioxide extraction technology for the production of deoiled palm kernel cake. *Journal of CO_2 Utilization*, *16*, 121–129. https://doi.org/10.1016/j.jcou.2016.06.010

Iftikhar, N., Tan, H., & Zhao, Y. (2017). Enrichment of β-carotene from palm oil using supercritical carbon dioxide pretreatment-solvent extraction technique. *LWT – Food Science and Technology, 83*, 262–266. https://doi.org/10.1016/j.lwt.2017.05.026

Irianto, I., Naryaningsih, A., Trisnawati, N. W., Astuti, A., Komariyah, K., Qomariyah, L., Chaidir, C., Saputri, A., Wulandari, R., Rizkiyah, D. N., & Putra, N. R. (2024). From sea to solution: A review of green extraction approaches for unlocking the potential of brown algae. *South African Journal of Chemical Engineering*, *48*, 1–21. https://doi.org/10.1016/j.sajce.2024.01.001

Jablonský, M., Škulcová, A., Malvis, A., & Šima, J. (2018). Extraction of value-added components from food industry based and agro-forest biowastes by deep eutectic solvents. *Journal of Biotechnology*, *282*, 46–66. https://doi.org/10.1016/j.jbiotec.2018.06.349

Kamaruddin, M. S. H., Chong, G. H., Daud, N. M., Putra, N. R., Salleh, L. M., & Suleiman, N. (2023). Bioactivities and green advanced extraction technologies of ginger oleoresin extracts: A review. *Food Research International*, *164*, 112283. https://doi.org/10.1016/j.foodres.2022.112283

Kanjanapongkul, K. (2021). Single and combined effects of ohmic and microwave heating on crude palm oil quality and stability. *Agriculture and Natural Resources*, *55*(2), 177–186. https://li01.tci-thaijo.org/index.php/anres/article/view/251027

Khairuddin, N. S. K., Yeoh, C. B., Sulaiman, N., Bustamam, F. K. A., Muhamad, H., & Sahid, I. (2021). Determination of metsulfuron methyl in crude palm oil using liquid chromatography triple quadrupole mass spectrometer. *Malaysian Journal of Analytical Sciences, 25*(2), 352–362.

Kostas, E. T., Beneroso, D., & Robinson, J. P. (2017). The application of microwave heating in bioenergy: A review on the microwave pre-treatment and upgrading technologies for biomass. *Renewable and Sustainable Energy Reviews, 77*, 12–27. https://doi.org/10.1016/j.rser.2017.03.135

Krishnaiah, D., Bono, A., Sarbatly, R., & Fadhilah, S. (2012). Supercritical fluid extraction of palm kernel oil from palm kernel. *American Journal of Food Technology*, *7*(3), 168–172. https://doi.org/10.3923/ajft.2012.168.172

Kumar, K., Srivastav, S., & Sharanagat, V. S. (2021). Ultrasound assisted extraction (UAE) of bioactive compounds from fruit and vegetable processing by-products: A review. *Ultrasonics sonochemistry, 70*, 105325. https://doi.org/10.1016/j.ultsonch.2020.105325

Li, Q., Putra, N. R., Rizkiyah, D. N., Aziz, A. H. A., Irianto, I., & Qomariyah, L. (2023). Orange pomace and peel extraction processes towards sustainable utilization: A short review. *Molecules, 28*(8), 3550. https://doi.org/10.3390/molecules28083550

Liu, Y., Liu, X., Cui, Y., & Yuan, W. (2022). Ultrasound for microalgal cell disruption and product extraction: A review. *Ultrasonics Sonochemistry, 87*, 106054. https://doi.org/10.1016/j.ultsonch.2022.106054

Loow, Y. L., New, E. K., Yang, G. H., Ang, L. Y., Foo, L. Y. W., & Wu, T. Y. (2017). Potential use of deep eutectic solvents to facilitate lignocellulosic biomass utilization and conversion. *Cellulose*, *24*(9), 3591–3618. https://doi.org/10.1007/s10570-017-1358-y

Mah, S. H., Sundrasegaran, S., & Lau, H. L. N. (2024). Topical nanoemulsion hydrogel formulated from supercritical fluid extracted palm-pressed fiber oil and virgin coconut oil with antioxidant and antibacterial effects. *Journal of Oleo Science*, *73*(4), 489–502. https://doi.org/10.5650/jos.ess23197

Mandal, V., Mohan, Y., & Hemalatha, S. (2007). Microwave assisted extraction – An innovative and promising extraction tool for medicinal plant research. *Pharmacognosy Review*, *1*(1), 7–18.

Manurung, R., & Siregar, A. G. A. (2020). Performance of menthol based deep eutectic solvents in the extraction of carotenoids from crude palm oil. *International Journal of GEOMATE*, *19*(74), 131–137. https://doi.org/10.21660/2020.74.96998

Martínez-Girón, J., Cafarella, C., Rigano, F., Giuffrida, D., Mondello, L., Baena, Y., Osorio, C., & Ordoñez-Santos, L. E. (2024). Peach palm fruit (*Bactris gasipaes*) peel: A source of provitamin a carotenoids to develop emulsion-based delivery systems. *ACS Omega*, *9*(26), 28738–28753. https://doi.org/10.1021/acsomega.4c03095

Mulia, K., Adam, D., Zahrina, I., & Krisanti, E. A. (2018). Green extraction of palmitic acid from palm oil using betaine-based natural deep eutectic solvents. *International Journal of Technology, 9*(2), 335–344. https://doi.org/10.14716/ijtech.v9i2.1008

Ng, M. H., & Hadi, N. A. (2022). Extraction of ferulic acid from oil palm pressed fiber by a choline chloride based deep eutectic solvent. *Journal of the American Oil Chemists Society*, *99*(5), 443–453. https://doi.org/10.1002/aocs.12577

Ng, M. H., & Nu'man, A. H. (2021). Investigation on the use of deep eutectic solvent with microwave assistance for the extraction of ferulic acid from palm pressed fibre. *Current Research in Green and Sustainable Chemistry*, *4*, 100155. https://doi.org/10.1016/j.crgsc.2021.100155

Ng, W. L., Er, Z. X., Chandrakumar, D., Loy, A. C. M., Vongsvivut, J., & Bhattacharya, S. (2024). Sustainable route of ethylene carbonate production via CO_2 carboxylation: Process development, process integration, and economic analysis. *ACS Sustainable Chemistry & Engineering*, *12*(51), 18320–18334. https://doi.org/10.1021/acssuschemeng.4c06519

Ngadi, N., & Rusli, N. S. (2014). Ultrasound-assisted extraction of lignin from oil palm frond. *Jurnal Teknologi (Sciences and Engineering)*, *67*(4), 67–70. https://doi.org/10.11113/jt.v67.2801

Nomanbhay, S., Uskenbayeva, S. A., & Ong, M. Y. (2018). On increase of the efficiency of extracting phenolic compounds from palm oil mill effluent. *Journal of Chemical Technology and Metallurgy, 53*(1), 101–111.

Norhuda, I., & Omar, A. M. (2009). Mass transfer of palm kernel oil under supercritical conditions. *World Academy of Science, Engineering and Technology*, *49*, 169–172.

Norulaini, N. A. N., Zaidul, I. M., Anuar, O., & Omar, A. M. (2004). Supercritical enhancement for separation of lauric acid and oleic acid in palm kernel oil (PKO). *Separation and Purification Technology*, *39*(3), 133–138. https://doi.org/10.1016/s1383-5866(03)00129-1

Nuchdang, S., Phruetthinan, N., Paleeleam, P., Domrongpokkaphan, V., Chuetor, S., Chirathivat, P., & Phalakornkule, C. (2022). Soxhlet, microwave-assisted, and room temperature liquid extraction of oil and bioactive compounds from palm kernel cake using isopropanol as solvent. *Industrial Crops and Products, 176*. 114379. https://doi.org/10.1016/j.indcrop.2021.114379

Ong, T. H., Hamzah, M. H., & Che Man, H. (2021). Optimization of palm oil extraction from decanter cake using soxhlet extraction and effects of microwaves pre-treatment on extraction yield and physicochemical properties of palm oil. *Food Research, 5*(S1), 25–32. https://doi.org/10.26656/fr.2017.5(s1).008

Ordoñez-Santos, L. E., Martínez-Girón, J., & Rodríguez-Rodríguez, D. X. (2019). Extraction of total carotenoids from peach palm fruit (*Bactris gasipaes*) peel by means of ultrasound application and vegetable oil. *DYNA (Colombia), 86*(209), 91–96. https://doi.org/10.15446/dyna.v86n209.74840

Ordoñez-Santos, L. E., Pinzón-Zarate, L. X., & González-Salcedo, L. O. (2015). Optimization of ultrasonic-assisted extraction of total carotenoids from peach palm fruit (*Bactris gasipaes*) by-products with sunflower oil using response surface methodology. *Ultrasonics Sonochemistry, 27*, 560–566. https://doi.org/10.1016/j.ultsonch.2015.04.010

Othman, N., Noah, N. F. M., Shu, L. Y., Ooi, Z.-Y., Jusoh, N., Idroas, M., & Goto, M. (2017). Easy removing of phenol from wastewater using vegetable oil-based organic solvent in emulsion liquid membrane process. *Chinese Journal of Chemical Engineering, 25*(1), 45–52. https://doi.org/10.1016/j.cjche.2016.06.002

Phan-Tai, H., & Brunner, G. (2023). Extraction of oil, carotenes and tocochromanols from oil palm (*Elaeis guineensis*) fruit with subcritical propane. *Grasas Y Aceites, 74*(1), e496. https://doi.org/10.3989/gya.0896211

Phatthiya, A., Jumrat, S., Punvichai, T., Karrila, S., Chotikhun, A., & Pianroj, Y. (2024). High-intensity microwave-assisted pyrolysis liquid subjected to supercritical fluid extraction with carbon dioxide (case study: Bio-phenol). *Chemical Engineering & Technology, 47*(1), 128–134. https://doi.org/10.1002/ceat.202300090

Promraksa, A., Siripatana, C., Rakmak, N., & Chusri, N. (2020). Modeling of supercritical CO_2 extraction of palm oil and tocopherols based on volumetric axial dispersion. *The Journal of Supercritical Fluids, 166,* 105021. https://doi.org/10.1016/j.supflu.2020.105021

Puah, C. W., Choo, Y. M., Ma, A. N., & Chuah, C. H. (2006). Very long chain fatty acid methyl esters in transesterified palm oil. *Lipids*, *41*, 305–308. https://doi.org/10.1007/s11745-006-5102-x

Puah, C. W., Choo, Y. M., Ma, A. N., & Chuah, C. H. (2007). Solubility of tocopherol and tocotrienols from palm oil in supercritical carbon dioxide. *Journal of Food Lipids*, *14*(4), 377–385. https://doi.org/10.1111/j.1745-4522.2007.00093.x

Puah, C. W., Choo, Y. M., Ma, A. N., & Chuah, C. H. (2011). Solubility of palm oil components in supercritical carbon dioxide. *International Journal of Food Engineering*, *7*(4), 1–9. https://doi.org/10.2202/1556-3758.2186

Putra, L. S., Sukweenadhi, J., Nathania, C., Wibowo, E. S., Buschle-Diller, G., & Marianti Purwanto, M. G. (2022). Comparative study of polyphenolic compound extraction from empty palm fruit bunches and sugarcane pulp. *Heliyon, 8*(2). e08951. https://doi.org/10.1016/j.heliyon.2022.e08951

Rahman, N. N. A., Al-Rawi, S. S., Ibrahim, A. H., Nama, M. M. B., & Kadir, M. O. A. (2012). Supercritical carbon dioxide extraction of the residual oil from palm kernel cake. *Journal of Food Engineering*, *108*(1), 166–170. https://doi.org/10.1016/j.jfoodeng.2011.06.033

Rani, H., Sharma, S., & Bala, M. (2021). Technologies for extraction of oil from oilseeds and other plant sources in retrospect and prospects: A review. *Journal of Food Process Engineering*, *44*(11), e13851. https://doi.org/10.1111/jfpe.13851

Rashid, S. N. A. A., Leong, H., Cheng, K., Yaakob, H., & Latiff, N. A. (2023). Squalene rich virgin palm oil by microwave-assisted enzyme aqueous extraction from palm mesocarp. *Biocatalysis and Agricultural Biotechnology, 47*. 102568. https://doi.org/10.1016/j.bcab.2022.102568

Rizki, I. F., Panjaitan, F. R., Mulyono, M. E., & Bajra, B. D. (2022). The utilization of natural deep eutectic solvent composition in tocotrienol and tocopherol extraction from crude palm oil and its acylglycerol products. *Journal of Food Composition and Analysis*, *114*, 104818. https://doi.org/10.1016/j.jfca.2022.104818

Rizkiyah, D. N., Putra, N. R., Yunus, M. A. C., Veza, I., Irianto, I., Aziz, A. H. A., Rahayuningsih, S., Yuniarti, E., & Ikhwani, I. (2023). Insight into green extraction for roselle as a source of natural red pigments: A review. *Molecules*, *28*(3), 1336. https://doi.org/10.3390/molecules28031336

Saravanakumar, A., Sudha, M., Chen, W.-H., Pradeshwaran, V., Ashokkumar, V., & Selvarajoo, A. (2023). Biomethane production as a green energy source from anaerobic digestion of municipal solid waste: A state-of-the-art review. *Biocatalysis and Agricultural Biotechnology, 53,* 102866. https://doi.org/10.1016/j.bcab.2023.102866

Shaari, A., Yunus, R., Raman, I. A., Omar, D., Shahar, M. K., Biak, D. R. A., Kania, D., & Aulia, A. (2021). Field efficacy of palm oil-based nanoemulsion insecticides against *Aedes aegypti* in Malaysia. *Acta Tropica*, *224*, 106107. https://doi.org/10.1016/j.actatropica.2021.106107

Siddique, I. J., Salema, A. A., Antunes, E., & Vinu, R. (2022). Technical challenges in scaling up the microwave technology for biomass processing. *Renewable and Sustainable Energy Reviews, 153,* 111767. https://doi.org/10.1016/j.rser.2021.111767

Tambun, R., Alexander, V., & Ginting, Y. (2021). Performance comparison of maceration method, soxhletation method, and microwave-assisted extraction in extracting active compounds from soursop leaves (*Annona muricata*): A review. *IOP Conference Series: Materials Science and Engineering*, *1122*(1), 012095. https://doi.org/10.1088/1757-899x/1122/1/012095

Valasques, G. S., Dos Santos, A. M. P., Da Silva, D. G., Alves, J. P. S., & Bezerra, M. A. (2018). Use of constrained mixture design in the optimization of a method based on extraction induced by emulsion breaking for the determination of Ca, Mg, Mn, Fe and Zn from palm oil by flame atomic absorption spectrometry. *Journal of the Brazilian Chemical Society, 29*(10)*,* 2189–2196. https://doi.org/10.21577/0103-5053.20180095

Wen, C., Zhang, J., Zhang, H., Dzah, C. S., Zandile, M., Duan, Y., Ma, H., & Luo, X. (2018). Advances in ultrasound assisted extraction of bioactive compounds from cash crops – A review. *Ultrasonics Sonochemistry*, *48*, 538–549. https://doi.org/10.1016/j.ultsonch.2018.07.018

Yaakob, M. N. A., Salim, N., Mustapha, S. N. H., Misnon, I. I., Rahim, M. H. A., & Roslan, R. (2024). Efficient lignin extraction from oil palm empty fruit bunches using guanidine-based deep eutectic solvents under microwave assistance. *Industrial Crops and Products, 218,* 118968. https://doi.org/10.1016/j.indcrop.2024.118968

Yong, K. J., & Wu, T. Y. (2024). Fractionation of oil palm fronds using ethanol-assisted deep eutectic solvent: Influence of ethanol concentration on enhancing enzymatic saccharification and lignin β-O-4 content. *Environmental Research*, *250*, 118366. https://doi.org/10.1016/j.envres.2024.118366

Yusof, M. A. B. M., Chan, Y. J., Chong, C. H., & Chew, C. L. (2023). Effects of operational processes and equipment in palm oil mills on characteristics of raw palm oil mill effluent (POME): A comparative study of four mills. *Cleaner Waste Systems, 5*, 100101. https://doi.org/10.1016/j.clwas.2023.100101

Yusoff, I. M., Taher, Z. M., Rahmat, Z., & Chua, L. S. (2022). A review of ultrasound-assisted extraction for plant bioactive compounds: Phenolics, flavonoids, thymols, saponins and proteins. *Food Research International, 157*, 111268. https://doi.org/10.1016/j.foodres.2022.111268

Zaidul, I. S. M., Nik Norulaini, N. A., Mohd Omar, A. K., & Smith Jr, R. L. (2007). Supercritical carbon dioxide ($SCCO_2$) extraction of palm kernel oil from palm kernel. *Journal of Food Engineering, 79*(3), 1007–1014. https://doi.org/10.1016/j.jfoodeng.2006.03.021

Zain, M. S. C., Jakariah, N. A., Yeoh, J. X., Lee, S. Y., & Shaari, K. (2020). Ultrasound-assisted extraction of polyphenolic contents and acid hydrolysis of flavonoid glycosides from oil palm (*Elaeis guineensis* Jacq.) leaf: Optimization and correlation with free radical scavenging activity. *Processes, 8*(12), 1540. https://doi.org/10.3390/pr8121540

Zain, N. F. M., Paramasivam, M., Tan, J. S., Lim, V., & Lee, C. K. (2021). Response surface methodology optimization of polyhydroxyalkanoate production by *Burkholderia cepacia* BPT1213 using waste glycerol from palm oil-based biodiesel production. *Biotechnology Progress, 37*(1), e3077. https://doi.org/10.1002/btpr.3077

Zainal Abidin, N. H., Othman, A. H., Wan Ibrahim, W. N., Mohammad Tahirudin, N. S., Mohamad Hanapi, N. S., & Mat Hadzir, N. (2024). Enriched silica from oil palm biomass for magnetic solid phase extraction of organochlorine pesticide: Characterization and method development. *Malaysian Journal of Analytical Sciences, 28*(2), 277–289. https://mjas.analis.com.my/mjas/v28_n2/html/28_2_4.html

Zamanhuri, N. A., Rahman, N. A., & Bakar, N. F. A. (2021). Effect of microwave power and extraction time on crude palm oil quality using microwave-assisted extraction process. *International Journal of Renewable Energy Development, 10*(3), 495–505. https://doi.org/10.14710/ijred.2021.35402

Zamanhuri, N. A., Rahman, N. A., & Bakar, N. F. A. (2022). Extraction of palm fatty acids from sterilized oil palm mesocarp by microwave technique: Optimization and kinetics. *Materials Today Proceedings, 63*, S166–S173. https://doi.org/10.1016/j.matpr.2022.02.127

Journal of Oil Palm Research Vol. 38 (3) September 2026 p. 408–432
DOI: https://doi.org/10.21894/jopr.2025.0036

BIOGENIC SILICA FROM OIL PALM BIOMASS: A REVIEW ON THE POTENTIAL, EXTRACTION METHODS AND PROPERTIES

HOERUDIN HOERUDIN[1]; TATANG HIDAYAT[1]; ATON YULIANTO[1]*; SITI AGUSTINA[1]; FAJRIYAN[1]; KARNADI[1]; ABDUL MAJID[1]; AHMAD SUHENDRA[1]; EDDY SAPTO HARTANTO[1] and ACHMAD KAMIL[1]

ABSTRACT

The oil palm industry has witnessed significant growth and has emerged as one of the world's largest vegetable oil sectors. However, this rapid expansion in production is accompanied by a notable increase in waste generation. While mills are utilising some oil palm biomass, a large portion still goes untapped and underexplored. There is increasing interest in leveraging various types of oil palm biomass as alternative, renewable, and economically viable resources to generate biogenic silica, a valuable material with diverse applications. This approach not only adds value to the biomass but also addresses environmental concerns. This article represents one of the first in-depth reviews of the recent technological advancements in leveraging oil palm biomass for the high-value synthesis of biogenic silica. It explores various aspects, covering the potential extraction methods (including those reported as green techniques, positioning them as a promising alternative to conventional approaches), as well as the properties and relevant applications of biogenic silica derived from oil palm biomass. The findings from this thorough review are expected to provide valuable insights for future research in the efficient production and sustainable utilisation of this bio-based material. Such support has the potential to enhance the sustainability of the oil palm industry.

Keywords: characteristics, oil palm, silica, synthesis, valorisation.

Received: 28 October 2024**; Accepted:** 17 April 2025**; Published online:** 22 July 2025.

INTRODUCTION

Global palm oil production has undergone significant expansion in the past 20 years. Between 2000 and 2023, palm oil output increased more than three times, rising from 22.23 to 79.46 million tonnes (*Figure 1*). During this period, roughly 80%–85% of the global supply has been sourced from only two nations, Indonesia and Malaysia (Food and Agriculture Organisation of the United Nations, Statistics Division [FAOSTAT], 2023; United States Department of Agriculture [USDA], 2023). The forecast for the marketing year (MY) 2023/2024 predicts a 2% increase in global palm oil production, totalling 79.60 million tonnes. Moreover, worldwide palm oil consumption is anticipated to rise by more than 3% in MY 2023/2024, approaching 78.00 million tonnes (Ates & Bukowski, 2023).

The expansion of the oil palm business, encompassing plantations and mills, results in substantial oil palm biomass production, hence creating the difficulty of excessive waste accumulation. Oil palm biomass consists of agricultural waste generated by the oil palm industry during pruning, replanting and milling operations (Nabila et al., 2023; Nur 'Aisyah Ar-Raudhoh et al., 2024; Onoja et al., 2019). An oil palm plantation may produce a significant quantity of biomass or total dry matter (TDM), with an annual yield of approximately 55 t/ha (Jafri et al., 2021). The production of oil palm agro-industrial biomass waste in Indonesia is expected to continue increasing. By 2030, oil palm biomass production is projected to reach roughly 419 million tonnes (Hambali & Rivai, 2017).

[1] Research Center for Agroindustry, Research Organization for Agriculture and Food, National Research and Innovation Agency, Soekarno Science and Technology Area, Jl. Raya Jakarta-Bogor KM 46, Cibinong 16911, Indonesia.

* *Corresponding author e-mail: aton001@brin.go.id*

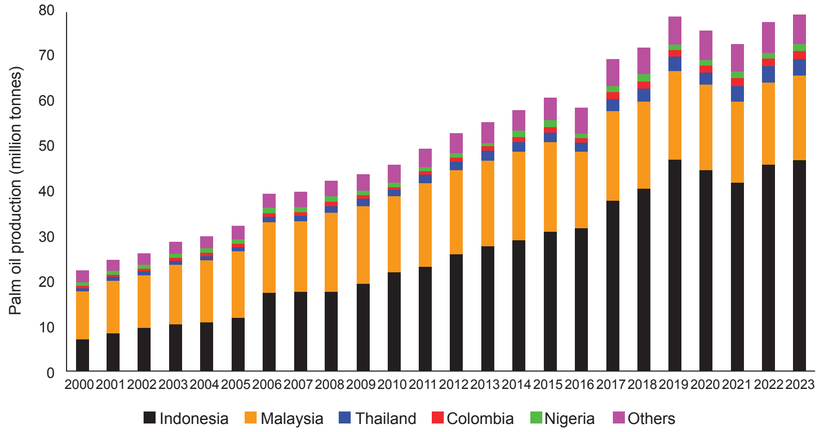

Source: FAOSTAT (2023); USDA (2023).

Figure 1. Global production and the top five producers of palm oil from 2000 to 2023.

Oil palm biomass has been utilised partially across different applications, each employing specific types of biomass and conversion techniques. Its applications range from basic uses like mulch and organic fertilisers (Khairuddin et al., 2018) to more advanced value-added products such as biochar, bio-oil (Abdullah et al., 2017) and adsorbents (Jahi et al., 2020). Traditional uses, such as combustion for energy, are prevalent (Nabila et al., 2023); however, these methods often need more efficiency and sustainability. Advanced and emerging conversion techniques, like pyrolysis, thermochemical processes, nanocomposites, enzymatic saccharification and fermentation, offer pathways to produce higher-value products such as biochar, biofuels, biosugar and bioplastics (Nabila et al., 2023; Norrrahim et al., 2022), which can enhance economic returns and environmental benefits. Nonetheless, the adoption of these technologies are still limited due to factors like high initial investment costs, technological complexity, cost-effectiveness, price competition and lack of infrastructure. As a result, significant quantities of oil palm biomass continue to be underutilised or wasted. This indicates that more innovative uses are warranted, especially in high-value applications, to maximise its economic and environmental potential.

Study on the valorisation of oil palm biomass is consistently advancing. Oil palms (*Elaeis guineensis* Jacq.) are recognised as silica accumulators (Greenshields et al., 2023; Munevar & Romero, 2015). This indicates that oil palm biomass may possess a substantial quantity of siliceous material. Consequently, oil palm biomass has been the subject of many previous studies as a potentially viable, renewable and cost-effective source to produce biogenic silica. Faizul et al. (2014), extracted high-purity silica (>90.00%) from palm ash (PA) using an eco-friendly citric acid leaching method. Khan et al. (2015) produced silica nanoparticles (20–80 nm) with a surface area of 326 m^2/g from palm oil fuel ash (POFA), showcasing their suitability for nanomaterial applications. Utama et al. (2019) further advanced silica extraction techniques by utilising sol-gel processes combined with mechanical fragmentation and CO_2 impregnation, producing precipitated silica with high purity and specific surface areas ranging from 50–140 m^2/g, which are ideal for catalyst and adsorption applications. More recently, Imoisili et al. (2020a, 2020b) synthesised amorphous mesoporous silica from palm kernel shell ash (PKSA) using sol-gel methods, achieving silica yields up to 96.83% with a specific surface area of 438 m^2/g, emphasising the material's applicability in drug delivery, energy storage and lightweight composites. Osman et al. (2021) explored the application of oil palm frond-derived silica nanomaterials for phenol removal from wastewater, achieving 68.00% removal efficiency and further underlining the potential of biogenic silica in environmental remediation. Additionally, Novita and Idris (2022) demonstrated the effectiveness of silica gel derived from PKSA as a moisture absorber in pharmaceutical packaging, achieving 85.65% moisture absorption efficiency and thus expanding the industrial utility of oil palm biomass. These studies confirm the potential of oil palm biomass as a sustainable and valuable source of silica for diverse industrial applications.

Grand View Research (2023) reported that the global silica market, encompassing precipitated silica, fumed silica, silica gels, silica sols and silica fumes, was valued at RM49.12 billion in 2022, with an anticipated Compound Annual Growth Rate (CAGR) of 9.90% from 2023 to 2030. Commercial synthetic amorphous silica (SAS) is often derived from mineral-based precursors. The SAS production process comprises two energy-intensive stages: i) High-temperature fusion for melting silica sand and soda ash,

ii) high-temperature digestion for dissolving sodium silicate. These energy-intensive processes can be significantly expensive (Utama et al., 2018). The traditional technique also produces byproducts, including CO_2 and significant volumes of wastewater, that are detrimental to the environment. As a result, there is an increasing research interest focused on generating amorphous silica from renewable and economical sources using energy-efficient techniques. These initiatives are progressively acknowledged as sustainable methods to reutilise byproducts and reduce ecological harm (Samat et al., 2021). The significant quantity of oil palm biomass presents a viable and sustainable opportunity for silica extraction from this byproduct.

Although substantial research and reviews have explored the production of biogenic silica from various agricultural residues, such as rice husks (Chun & Lee, 2020; Dizaji et al., 2019; Hossain et al., 2018; Steven et al., 2021) and crop wastes (Kouadri et al., 2023; Razak et al., 2022; Sarkar et al., 2021; Setiawan & Chiang, 2021; Yadav et al., 2022), the unique potential of oil palm biomass as a significant renewable source of silica remains underexplored. Existing studies primarily focus on individual aspects of silica extraction from oil palm biomass. However, a comprehensive review that synthesises these findings and evaluates the specific properties and relevant applications of biogenic silica derived from oil palm biomass is notably lacking. Furthermore, there is limited discussion on sustainable and environmentally-friendly extraction methods tailored specifically for this biomass. Addressing these gaps will highlight oil palm biomass as a valuable contributor to sustainable material production and, hence, the circular economy.

This review aims to critically analyse the potential of oil palm biomass as a sustainable source of biogenic silica by exploring advanced extraction techniques, focusing on environmentally-friendly approaches, assessing the unique properties of the resulting biogenic silica and identifying opportunities for advancing its utilisation in various industrial applications. Several key research questions addressed include identifying the types of oil palm biomass most suitable for sustainable biogenic silica production; examining recent advancements and current challenges in silica extraction methods for oil palm biomass and strategies to address these sustainably; evaluating the unique physical, chemical and functional properties of biogenic silica derived from oil palm biomass; investigating its potential applications in high-value industrial sectors; and highlighting significant research gaps and future directions in this field.

BIOGENIC SILICA IN OIL PALM BIOMASS

Biogenic Silica in Oil Palm Trees

Silicon (Si) is vital in numerous ecological and biogeochemical processes. In biogeochemistry, Si is commonly referred to as silica (SiO_2), as it is invariably associated with oxygen (O) in ecosystems (Tréguer et al., 2021). Si, following oxygen, is the second most prevalent element in the Earth's crust, comprising approximately 28.00% of its composition (Tubaña & Heckman, 2015). Plants absorb soluble Si as orthosilicic acid (H_4SiO_4) from the soil solution and translocate it to the roots and aerial structures. Si is ultimately incorporated into plant tissues as hydrated amorphous biogenic silica structures referred to as phytoliths ($SiO_2.nH_2O$) (Haynes, 2017; Puppe et al., 2021). Si has been noted to confer various beneficial effects on plants, including increased resistance to biotic stresses (such as pest infestations and fungal diseases) and abiotic stresses (such as drought, low temperatures and metal toxicity), optimised nutrient availability, enhanced photosynthesis, improved plant growth and elevated productivity (Debona et al., 2017; Dhakate et al., 2022; Pereira et al., 2024).

Published data regarding the concentrations of Si or SiO_2 in various regions of an oil palm are typically few. Duangpan et al. (2022) examined the concentration and distribution of Si in oil palm seedlings. Si buildup in oil palm seedlings was detected in all tissues, with the highest average concentration in the leaf (0.66%), followed by the root (0.45%) and stem (0.17%). Greenshields et al. (2023) evaluated Si concentrations in several mature oil palm components taken from smallholder plantings in Indonesia. Their study also quantified the quantity of (i) accumulated Si in the total above-ground biomass of a mature oil palm tree and in one hectare of an oil palm plantation, (ii) Si storage in pruned palm fronds, and the Si transferred during fruit bunch harvest. Leaflets exhibited an average Si content of at least 1.00%. Conversely, rachises, frond bases, fruit-bunch stalks, fruit pulp and kernels exhibited mean Si contents below 0.50%. Leaflets in senescent fronds exhibited markedly elevated Si concentrations (>3.50%) compared to frond No. 17 (1.30%–1.70%) and frond No. 9 (about 1.10%). The findings aligned with those presented by Von Der Lühe et al. (2023), demonstrating that a dead leaf possessed double the quantity of Si relative to a mature leaf. Comparable results were noted in the research conducted by Munevar and Romero (2015), who evaluated Si contents in the leaves of oil palm trees beyond eight years of age, collected from 17 estates in Colombia. The study revealed a gradual increase in Si concentrations in oil palm leaves, from roughly 1.30% in leaf No. 1 to almost 4.00% in leaf No. 25. The results indicate that Si accumulates as the oil palm leaves age and presumably functions as a non-mobile element within the plant. Comparable Si behaviour was also documented in cereal crops (Ma & Yamaji, 2006).

Figure 2 illustrates the distribution and quantity of accumulated silica in different sections of oil palm biomass, as observed in the plantations and mills. In that graphic and the next discussion, published data on Si storage in oil palm biomass were transformed into SiO_2 storage. In plantations, oil palm fronds (OPF) and oil palm trunk (OPT) constitute the primary biomass produced during pruning and replanting operations. OPF are considered a significant source of SiO_2 in plantations (Von Der Lühe et al., 2023). The study conducted by Greenshields et al. (2023) revealed that SiO_2 accumulation in a senescing OPF (0.13 kg SiO_2) exceeded that in frond No. 9 (0.04 kg SiO_2) and frond No. 17 (0.06 kg SiO_2). This study indicated that SiO_2 deposition in OPF generally escalates with the frond's age. In a smallholder oil palm plantation, around 14–16 fronds are clipped each year. Greenshields et al. (2023) estimated that SiO_2 storage in the annually pruned OPF ranged from roughly 237 to 280 kg/ha.

The core part of an oil palm stem is claimed to possess silica-accumulating tissues. SiO_2

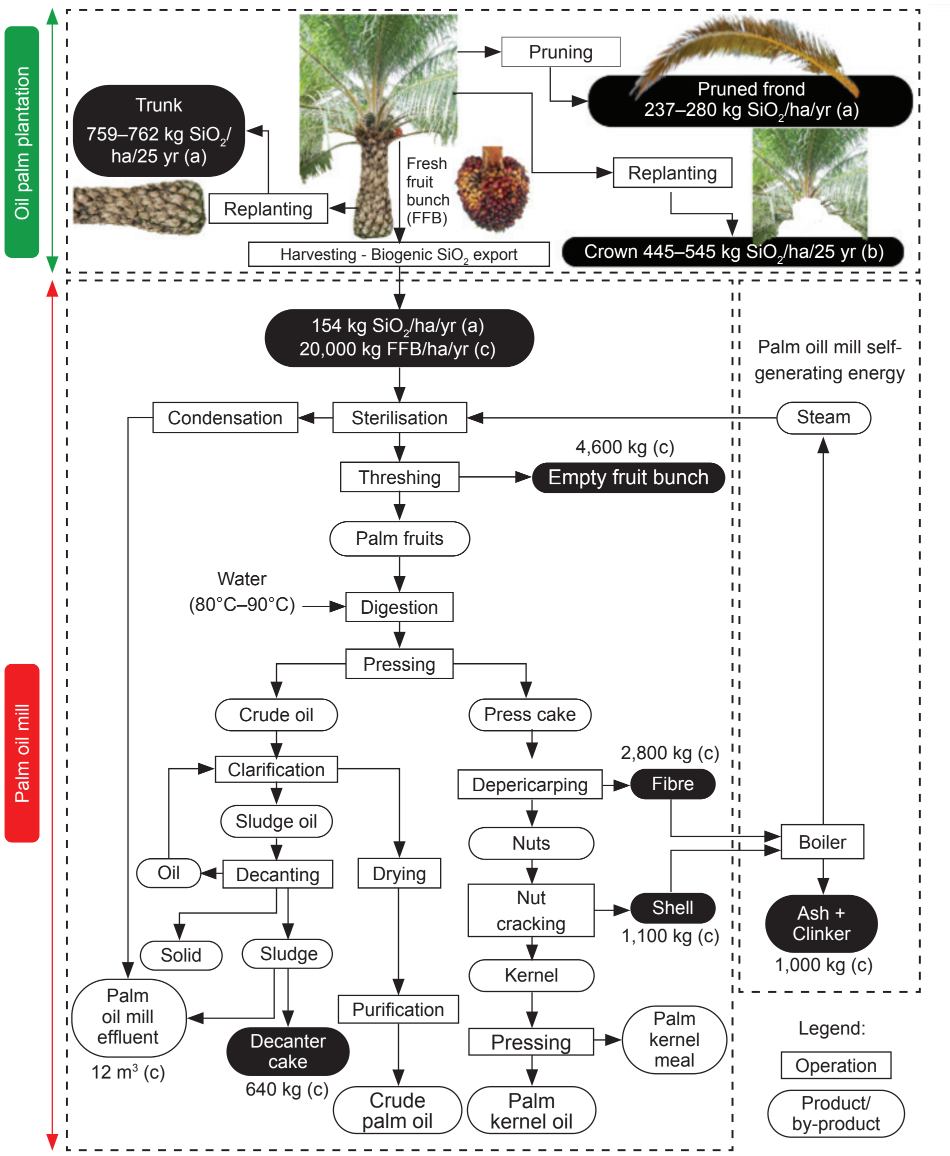

Note: (a) - Converted from Greenshields et al. (2023); (b) - Converted and calculated from Greenshields et al. (2023) and PASPI-Monitor (2021); (c) - Calculated from Chavalparit et al. (2006).

Source: Abdullah and Sulaiman, (2013); Nabila et al. (2023).

Figure 2. Schematic diagram of palm oil production and the potential availability of oil palm silica and silica-containing biomass.

accumulation in the OPT may transpire either within the vascular system or within the cell walls (Greenshields et al., 2023). The lower, middle and higher segments of the OPT demonstrated an increasing trend in SiO_2 concentrations of 1.02%, 1.69% and 4.52%, respectively (Pratiwi et al., 2018). Greenshields et al. (2023) reported that a mature oil palm stem could acquire roughly 5.36 kg of SiO_2. The extraction of OPT from plantations before replanting may lead to a significant export of SiO_2, estimated at a minimum of 759–762 kg SiO_2/ha, assuming a planting density of 142 oil palms/ha in a smallholder plantation. Nonetheless, this considerable SiO_2 outflow may occur at periods of 25–30 years, aligning with oil palm replanting cycles (*Figure 2*).

A mature oil palm tree is typically maintained with 40–48 fronds (PASPI-Monitor, 2021). Considering an average SiO_2 storage of 0.08 kg/frond and a planting density of 142 trees/ha (Greenshields et al., 2023), an oil palm crown may sequester around 445–545 kg SiO_2/ha. The accumulated SiO_2 may be exported before replanting cycles, which generally take place every 25–30 years. Based on its dimensions and mass, an oil palm fruit bunch might contain about 0.04–0.15 kg of SiO_2. An oil palm tree is predicted to acquire approximately 8,000–11,000 kg of SiO_2 in its aerial components, including fruit bunches. Based on this computation, roughly 1,178–1,459 kg of SiO_2 may be deposited in the aerial components of 1 ha in a smallholder oil palm plantation, as noted by Greenshields et al. (2023). In this instance, OPT could be the principal source of the estimated SiO_2 storage in the aerial components of an individual oil palm tree. Nevertheless, the SiO_2 contained in the trunks of oil palm trees may only be extracted for subsequent use after a period of 25–30 years, particularly during the replanting phase. Consequently, the SiO_2 reserves in plantations with optimal availability for consistent short-term use are expected to derive from the clipped fronds of oil palm trees. The calculations indicate that a fully developed oil palm tree can absorb an equivalent amount of SiO_2 as rice, which is capable of absorbing 500 kg of Si/ha (Makabe et al., 2009), equal to 1,069 kg of SiO_2/ha, and is acknowledged as a Si-accumulator (Qurrohman et al., 2023). This suggests the possible categorisation of oil palm as a Si-accumulating plant.

Figure 2 shows exports of fruit bunch harvest and SiO_2 storage from oil palm plantations to palm oil mills. Each year, a mature oil palm tree in a smallholder plantation may produce 12–14 fruit bunches, resulting in an accumulation of approximately 0.51–2.10 kg of SiO_2. A small-scale oil palm plantation, with a planting density of 142 trees/ha and a fruit bunch production of 9–20 t/ha of dry biomass (Greenshields et al., 2023), was predicted to store around 68–154 kg of SiO_2/ha annually within its fruit bunches. In other words, approximately 5.00%–10.00% of SiO_2 stored in the aerial components of a 1 ha oil palm plantation is conveyed to a palm oil mill via the harvesting of fruit bunches.

Biogenic Silica in Palm Oil Mill By-Products

At palm oil mills, fresh fruit bunches (FFB) are processed to yield crude palm oil as the principal product, alongside palm kernel oil, contingent upon the availability of suitable processing equipment (*Figure 2*). The production of palm oil encompasses several processes: Sterilisation, threshing, digesting, pressing, clarification, purification, drying, depericarping and cracking. During these operations, numerous intermediate products and significant amounts of trash are produced. Approximately 70.00% of the processed FFB in palm oil mills generates substantial waste, including empty fruit bunch (EFB), mesocarp fibre (MF), palm kernel shell (PKS), palm oil mill effluent (POME), palm oil mill sludge (POMS), palm oil decanter cake (PODC), palm kernel meal (PKM), POFA and palm oil clinker (POC). The burning of MF and PKS as boiler fuel in palm oil mills produces biogenic waste in the form of unburned ash. This ash has been identified by various terms in the literature, including PA (Faizul et al., 2014), POFA (Hoerudin et al., 2024; Khan et al., 2015; Liew et al., 2017), palm oil mill fly ash (POMFA) (Aman et al., 2017), oil palm boiler ash (OPBA) (Bukit et al., 2022) and oil palm mill boiler ash (OPMBA) (Adha & Warsiki, 2023). Within the scope of this review, the term "boiler ash" (BA) is employed to characterise the ash, as delineated by Zarina et al. (2013). BA comprises porous, flaky and irregular stones, referred to as POC (Karim et al., 2017). For each tonne of FFB processed in conventional palm oil mills, the projected by-product or trash creation is as follows: 23.00% of EFB, 14.00% of MF, 5.50% of PKS, 3.20% of oil palm decanter cake (OPDC), 5.00% of BA, and 0.6 m^3 of POME (Chavalparit et al., 2006). A 1 ha of mature oil palm plantation with an FFB productivity of 20.00 t would yield approximately 4.60 t of EFB, 2.80 t of MF, 1.10 t of PKS, 0.64 t of OPDC, 1.00 t of BA and 2 m^3 of POME (*Figure 2*).

Each type of oil palm mill waste possesses distinct physico-chemical characteristics. This analysis examines palm oil mill waste with notable SiO_2 concentrations, as recorded in the existing literature (*Table 1*). This attention is essential for assessing the prospective opportunity for recovering silica from these palm oil mill by products.

TABLE 1. MINERAL COMPOSITION OF UNTREATED PALM OIL MILL WASTE BY TYPE AND GEOGRAPHICAL ORIGIN

Type of waste	Country	Mineral composition (wt %)											Reference
		SiO_2	K_2O	CaO	Al_2O_3	MgO	Fe_2O_3	P_2O_5	Na_2O	Cl	SO_3	Others	
PKS	Nigeria	13.65	6.48	13.21	9.18	6.54	1.81	4.37	1.71	n.a	0.84	n.a	Imoisili et al. (2020b)
PKSA	Nigeria	56.76	9.19	12.57	8.58	5.45	0.91	4.21	1. 62	n.a	0.71	n.a	Imoisili et al. (2020b)
EFBA	Malaysia	9.50	35.20	39.20	n.a	n.a	2.60	4.20	n.a	2.50	2.10	n.a	Rahmat et al. (2021)
EFBA	Thailand	12.12	55.48	9.65	0.26	1.90	n.a	3.58	0.09	6.84	1.66	n.a	Madhiyanon et al. (2013)
BA	Indonesia	52.41	14.47	7.64	5.10	4.54	4.18	n.a	n.a	n.a	n.a	n.a	Adha and Warsiki (2023)
BA	Malaysia	45.50	23.30	12.80	5.40	3.20	3.26	5.38	n.a	n.a	n.a	n.a	Pa et al. (2016)
BA	Malaysia	55.00	5.40	5.50	5.40	3.50	4.70	3.40	n.a	n.a	n.a	1.10	Khan et al. (2015)
BA	Thailand	50.57	8.45	15.92	1.03	4.73	2.56	6.53	n.a	n.a	n.a	10.21	Kongnoo et al. (2017)
BA	Nigeria	53.52	3.08	4.62	11.40	3.28	12.68	n.a	1.56	n.a	n.a	1.26	Oyejobi et al. (2015)
BA	Bangladesh	63.60	6.90	7.60	1.60	3.90	1.40	n.a	0.10	n.a	n.a	n.a	Tessema et al. (2023)
OPDC	Malaysia	22.10	16.30	26.00	4.08	n.a	10.30	4.76	n.a	n.a	5.77	10.69	Rahim et al. (2023)
OPDCA	Malaysia	32.10	12.60	26.10	5.53	n.a	4.08	6.66	n.a	n.a	3.16	9.77	Rahim et al. (2023)
POC	Malaysia	63.90	10.20	6.93	3.89	3.37	3.30	2.12	n.a	n.a	n.a	n.a	Khan et al. (2015)

Note: n.a - data not available; PKS - palm kernel shell; PKSA - palm kernel shell ash; EFBA - empty fruit bunch ash; POC - palm oil clinker; BA - boiler ash; OPDC - oil palm decanter cake; OPDCA - oil palm decanter cake ash.

Published literature indicates that palm oil mill wastes exhibit different concentrations of SiO_2 according to their type. The POC generated concurrently with BA by the identical procedure exhibited the highest SiO_2 concentration, surpassing 45.00%, followed by OPDC at 22.10% and PKS at 13.65% (*Table 1*). The SiO_2 concentration in PKSA incinerated at 750°C for 3 hr increased significantly by roughly 43.00%, attaining 56.76% (Imoisili et al., 2020b). The incineration procedure at 600°C for 5 hr increased the SiO_2 content in oil palm decanter cake ash (OPDCA) by approximately 10.00%, resulting in a concentration of 32.10% (Rahim et al., 2023). According to the literature assessment, the SiO_2 concentration data for (raw) EFB and MF are inadequately recorded. *Table 1* shows that the SiO_2 concentration in empty fruit bunch ash (EFBA) was analogous to that of PKS. Consequently, the SiO_2 concentration in EFB is probably inferior to that in PKS. The existing literature indicates that SiO_2 concentration does not vary widely within the same type of waste, regardless of geographical location. Nonetheless, a considerable variance exists in the composition of K_2O and CaO in BA sourced from various places. This variety may be ascribed to genetic disparities among plants, cultivation sites, agricultural practices, and/or processing conditions in palm oil mills. BA, including POC, is a highly promising source of SiO_2 derived from palm oil processing waste, owing to its comparatively elevated SiO_2 concentration, ease of subsequent processing, and abundant availability.

EXTRACTION OF BIOGENIC SILICA

Most industrial silica comes from natural sources, such as quartz, found in nearly all mineral rocks. These rocks are heated to produce sodium silicate as a silica precursor, but this process requires extremely high temperatures (1,300°C), making it energy-intensive and a significant source of greenhouse gas emissions (Zulfiqar et al., 2015). Silica can also be synthesised from toxic and costly alkyl orthosilicate precursors like tetraethyl orthosilicate (TEOS), which pose health risks and are impractical economically and environmentally (September et al., 2023; Tessema et al., 2023). To address these issues, agricultural wastes, such as rice husk, corn cob, sugarcane bagasse and palm oil wastes (e.g., BA, EFBA, PKS, PKSA, OPDC, OPDCA), have been explored as low-cost, silica-rich alternatives. Silica extraction from biomass is eco-friendly, reduces energy consumption, and achieves comparable quality to conventional methods (September et al., 2023).

Biomass can be converted into bioproducts via biochemical or thermochemical methods. Thermochemical conversion, which decomposes biomass using heat, is particularly suitable for extracting biogenic silica from palm oil solid waste. This waste contains cellulose, hemicellulose, lignin and metal components (e.g., calcium, potassium and iron), which influence silica properties during high-temperature treatments. Pre-treatment processes are often needed to remove these impurities, facilitating extraction and improving yield and product quality (Norsuraya et al., 2016; Nzereogu et al., 2023; Teixeira et al., 2021).

Extraction Methods

The extraction of biogenic silica from agricultural biomass, such as oil palm biomass, generally follows two stages: i) Raw material pre-treatment and ii) extraction process. Raw material pre-treatment is typically carried out before the biogenic silica extraction process. The selection of pre-treatment and extraction methods for biogenic silica production is pivotal in balancing efficiency, cost and environmental considerations. Several considerations in selecting pre-treatment and biogenic silica extraction methods are summarised in *Table 2*.

Commonly employed pre-treatment methods include acid leaching and combustion, each with distinct advantages and disadvantages. Acid leaching is effective in removing metal impurities, significantly enhancing silica yield and purity (Nzereogu et al., 2023; Pa et al., 2016; Rahmat et al., 2021). However, the use of strong acids, such as hydrochloric, sulfuric and nitric acids, raises concerns regarding environmental safety, human health and waste disposal. Although effective, these drawbacks necessitate the exploration of greener alternatives, such as organic acids, which offer a more sustainable approach.

Combustion, on the other hand, is a simpler method that effectively decomposes organic components like cellulose, hemicellulose and lignin, facilitating further silica extraction. Despite its simplicity, combustion alone may not fully remove metal impurities, limiting silica purity. Additionally, its high energy requirements introduce economic and environmental concerns, particularly in large-scale operations. Combining combustion with acid leaching can overcome these limitations, leveraging the strengths of both methods to produce high-purity silica. However, this approach inherits the complexity and resource demands of both processes, making it suitable only for applications where exceptional purity is paramount.

Green extraction methods have emerged as a promising alternative to conventional processes by utilising organic acids and lower energy inputs, thereby mitigating environmental impacts (Aharipour et al., 2022; Hoerudin et al., 2024; Pa et al., 2016; Rahim et al., 2023; September et al., 2023; Tessema et al., 2023; Utama et al., 2019). These methods are environmentally-friendly and effective in removing impurities, but face challenges in scalability and cost-effectiveness due to the relatively high expense of organic acids. Process optimisation is required to ensure they achieve comparable efficiency to conventional methods.

The sol-gel and calcination methods for biogenic silica extraction are closely aligned with the chemical and physical properties of biogenic silica derived from agricultural biomass waste. Biomass such as PKS and EFB contains silica predominantly in amorphous form, embedded within organic matrices of cellulose, hemicellulose, lignin and metal oxides. Both methods offer distinct mechanisms for silica isolation and purification.

The sol-gel method employs chemical dissolution and precipitation processes to extract high-purity silica. Initially, silica in the biomass is solubilised using an alkaline solution such as NaOH to form soluble sodium silicate [Equation (1)] (Norsuraya et al., 2016; Tessema et al., 2023). To recover pure biogenic silica, an acid, such as HCl or organic acids (e.g., citric acid), is added to reduce the pH to below 10, precipitating silica gel [Equation (2); Tessema et al., 2023]. The resulting silica gel is aged, washed, and dried to obtain amorphous silica. The sol-gel process maintains the amorphous nature of biogenic silica due to its low processing temperature, preventing the formation of crystalline silica (Hoerudin et al., 2024; Imoisili et al., 2020a, 2020b; Rahim et al., 2023; Utama et al., 2019). This method produces fine particle sizes, high surface area and tailored morphologies.

$$SiO_2\ (s) + 2NaOH\ (aq) \rightarrow Na_2SiO_3\ (aq) + H_2O \qquad (1)$$

$$Na_2SiO_3\ (aq) + 2HCl\ (aq) \rightarrow SiO_2\ (gel) + 2NaCl\ (aq) + H_2O \qquad (2)$$

Calcination, in contrast, is a thermal decomposition method that exploits the thermal stability of silica compared to organic components. The organic matrix (cellulose, hemicellulose and lignin) is decomposed at specific temperature ranges: Hemicellulose (220°C–300°C), cellulose (300°C–340°C) and lignin (300°C–900°C) (Bakar et al., 2016; El-Sayed et al., 2024). During calcination at 600°C–800°C, the organic material combusts completely, leaving behind amorphous silica [Equation (3)]. Maintaining temperatures below 900°C is critical to avoid crystallisation into cristobalite or tridymite, which reduces silica's reactivity and industrial suitability (Nelson et al., 2023; Nzereogu et al., 2023).

TABLE 2. ADVANTAGES AND DISADVANTAGES OF PRE-TREATMENT AND EXTRACTION METHODS FOR PRODUCING BIOGENIC SILICA

Criteria	Considerations	Advantages	Disadvantages	Reference
Pre-treatment method	Required to remove impurities and improve the yield/quality of extracted silica.	Improves purity and extraction efficiency.	May add additional processing steps and costs.	Nelson et al. (2023); Pa et al. (2016); Rahmat et al. (2021)
• Acid leaching	Effectively removes metal impurities; commonly uses HCl, H_2SO_4, or H_3PO_4; risk of environmental and health hazards.	Significant removal of metal oxides and impurities; proven high leaching efficiency.	Use of strong acids poses health and environmental risks; and disposal challenges.	Bakar et al. (2016); Rahmat et al. (2021); Setiawan and Chiang (2021)
• Combustion	Decomposes organic components (cellulose, hemicellulose, lignin); simplifies raw material processing.	Simplifies treatment and eliminates organic matrix components.	Requires high energy input for combustion; may not fully remove metal impurities.	Imoisili et al. (2020b); Rahim et al. (2023)
• Combination of combustion and acid leaching	Combines impurity removal with decomposition of organic matrix; increases silica purity and yield.	High silica purity due to the combined benefits of both processes.	Combines the complexities of both methods; increases time and cost.	Nelson et al. (2023); Osman and Sapawe (2020); Rahmat et al. (2021)
Extraction method	Used to extract silica efficiently from palm oil waste through chemical or thermal processes.	Facilitates silica extraction from biomass with high efficiency.	The selection of appropriate methods depends on the raw material type; initial pre-treatments may be necessary.	Adha and Warsiki (2023); Hoerudin et al. (2024)
• Sol-gel method	Uses alkaline solution to dissolve silica, followed by precipitation with acid; produces high-purity silica.	Produces high-purity biogenic silica through precise chemical processing.	Involves chemical reagents, requiring precise pH control; extended processing time for precipitation.	Hoerudin et al. (2024); Tessema et al. (2023)
• Calcination	Thermally decomposes organic matter; produces amorphous silica below 800°C; higher temperatures (>900°C) risk crystalline silica formation.	Simple, cost-effective thermal method; produces amorphous silica efficiently.	High temperatures (above 900°C) risk the formation of crystalline silica; an energy-intensive process.	Bakar et al. (2016); Samat et al. (2021)
Green extraction methods	An environmentally-friendly approach with reduced toxicity and lower temperatures; organic acids like citric acid are effective.	Lower environmental impact; effective in removing impurities.	Requires optimisation to match conventional methods' efficiency; organic acids can be costly.	Pa et al. (2016); September et al. (2023)

Note: HCl - hydrochloric acid; H_2SO_4 - Sulfuric acid; H_3PO_4 - phosporic acid.

$$\text{Biomass} \rightarrow \text{Thermal treatment} \rightarrow SiO_2 \text{ (amorphous)} + CO_2 + H_2O \quad (3)$$

Several pre-treatment/processing routes have been developed for extracting biogenic silica from oil palm solid waste (*Figure 3*). Each route is tailored to specific raw materials and production goals, with the choice of method depending on the desired purity, cost and environmental impact as described previously (*Table 2*).

Extraction Yield of Biogenic Silica

A summary of published works on the extraction yields and purity of biogenic silica from oil palm solid wastes is presented in *Table 3*, highlighting the comparison between conventional and green extraction methods, sol-gel extraction and calcination methods and the effects of different processing routes. The comparison between conventional and green extraction methods reveals that green extraction approaches, such as citric acid pre-treatment, offer a more sustainable alternative while improving silica yields in certain cases. For example, Samat et al. (2021) demonstrated that using 1 M citric acid as a pre-treatment for PKS and EFB improved the silica yield to 4.35% and 0.95%, respectively. This yield is notably higher compared to conventional extraction with 1 M HCl followed by calcination at 800°C, which resulted in lower yields of 1.49% for PKS and 0.80% for EFB (Samat et al., 2018). The significant weight loss during calcination in the conventional methods limits the overall yield, whereas citric acid leaching mitigates this issue. However, despite the modest yield improvement, green methods are preferred for their reduced environmental impact and sustainability.

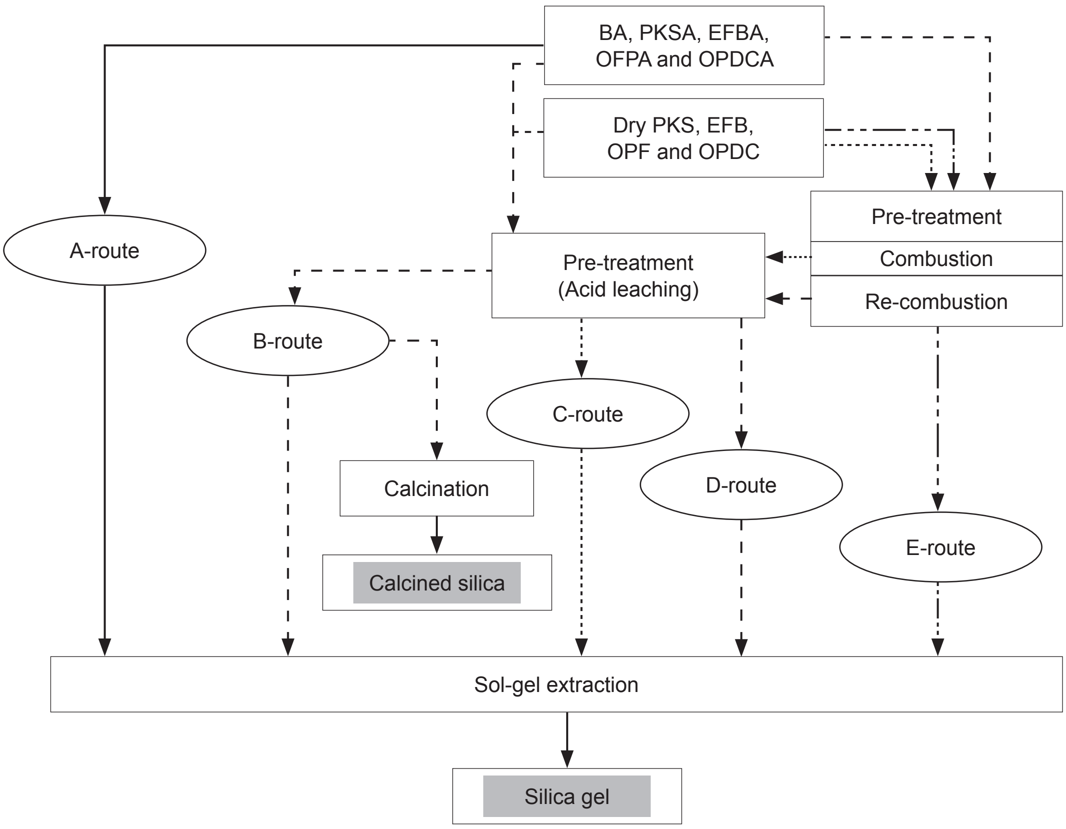

Note: A-route: Extraction without pre-treatment, typically applied to combusted raw materials like BA, followed by the sol-gel extraction process (Utama et al., 2018, 2019).
B-route: Acid leaching pre-treatment, suitable for both combusted (BA) and dry raw materials (PKS, EFB, OPF and OPDC), followed by the sol-gel extraction process for ash raw materials (Adha & Warsiki, 2023) or calcination for dry raw materials (Samat et al., 2021).
C-route: Combustion followed by acid leaching, used for dry raw materials like EFB OPF, followed by the sol-gel extraction process (Osman & Sapawe, 2020; Rahmat et al., 2021).
D-route: Combusted ash undergoes re-combustion before extraction with the sol-gel extraction process (Hoerudin et al., 2024; Nelson et al., 2023).
E-route: Combustion of dry raw materials without acid leaching, followed by the sol-gel extraction process (Imoisili et al., 2020a, 2020b; Rahim et al., 2023).

Figure 3. Pre-treatment routes and extraction methods for producing biogenic silica from oil palm solid waste.

TABLE 3. EXTRACTION YIELD AND SIO_2 CONCENTRATION OF BIOGENIC SILICA FROM OIL PALM BIOMASS

Type of biomass	Methods (Pre-treatments and extraction)	Route/type of silica	Results (yield and silica purity)	Reference
Conventional Extraction				
BA	Acid leaching pre-treatment (1.2 M HCl, 24 hr), alkaline extraction (4–8 M NaOH, 30–90 min), and precipitation (1 M HCl).	B/Silica gel	Silica yield was 41.17%** and silica purity were 79.20% under optimal extraction conditions.	Adha and Warsiki (2023)
EFBA	Re-carbonised (600°C–800°C) and acid leaching (1% HCl) pre-treatment, alkaline extraction (NaOH), precipitation (1 M HCl+3 M NH_4OH), and calcination (550°C, 3 hr).	D/Calcined silica	Silica yield ranged from 14.70%–17.30%** and silica purity was 59.85% after re-carbonisation at 800°C.	Nelson et al. (2023)
PKS	Acid leaching pre-treatment (1 M HCl) and calcination (400°C–800°C, 6 hr).	B/Calcined silica	Weight loss was 98.51% (~silica yield was 1.49%*) during calcination at 800°C.	Samat et al. (2018)
EFB	Acid leaching pre-treatment (1 M HCl) and calcination (400°C–800°C, 6 hr).	B/Calcined silica	Weight loss was 99.20% (~silica yield was 0.8%*) during calcination at 800°C.	Samat et al. (2018)
	Combustion (600°C–800°C, 2 hr) and acid leaching (5 N H_2SO_4, 30 min) pre-treatment.	C/Ash	Burning at 600°C–800°C increased the silica purity from 9.50%–45.60% after leaching.	Rahmat et al. (2021)
Green Extraction				
BA	Acid leaching pre-treatment (1.00%–6.00% citric acid) and calcination (800°C, 30 min).	B/Ash	Silica purity was 92.00% at a citric acid leaching concentration of ≥3.00%.	Pa et al. (2016)
	Alkaline extraction (1.5 N NaOH, 60 min, ratio sample to NaOH 0.23 g/cm^3, temperature 75°C–100°C, stirring speed 500–1,200 rpm), precipitation (10.00% H_2SO_4), and ageing (18 hr).	A/Silica gel	60.42% of silica in the sample can be extracted, and silica purity was 95.33% under the optimum extraction conditions.	Utama et al. (2018)
	Alkaline extraction (1.4 N NaOH, 50 min, 105°C, sample-to-NaOH ratio 0.23 g/cm^3, stirring speed 1,065 rpm) and precipitation using CO_2 impregnation and mechanical fragmentation.	A/Silica gel	Silica purity was 96.90% under the optimum precipitation conditions.	Utama et al. (2018)
	Re-ashing (600°C, 2 hr) and acid leaching (6.00% citric acid, 600°C, 1.5 hr) pre-treatment, alkaline extraction (6.00%–10.00% NaOH, 100°C, 1.5 hr), and precipitation (3.00% HCl, pH 7), ageing (18 hr).	D/Silica gel	Silica purity was 94.68% under optimal extraction conditions.	Hoerudin et al. (2024)
PKS	Combustion pre-treatment (750°C, 3 hr), alkaline extraction (2 N NaOH, 2 hr), precipitation (2 N HCl, pH 7.5–8.5), and ageing (24 hr).	E/Silica xerogel	Silica yield was 56.65%** and silica purity were 96.83%.	Imoisili et al. (2020b)
	Combustion pre-treatment (750°C, 3 hr), alkaline extraction (3 N NaOH, 2 hr), precipitation (3 N HCl), and ageing (24 hr). Refluxed silica xerogel (3 M HCl, 70°C, 4 hr), dissolved with 3 M NaOH, and silica precipitation (H_2SO_4, pH 7.5).	E/Silica nanoparticles	Silica nanoparticle yield was 54.35%** and nano silica purity was 96.59%.	Imoisili et al. (2020a)
	Acid leaching pre-treatment (1 M citric acid, 2 hr) and calcination (400°C–800°C, 6 hr).	B/Calcined silica	Weight loss was 95.65% (~silica yield was 4.35%*) during calcination at 800°C.	Samat et al. (2021)
EFB	Acid leaching pre-treatment (1 M citric acid, 2 hr) and calcination (400°C–800°C, 6 hr).	B/Calcined silica	Weight loss was 99.05% (~silica yield was 0.95%*) during calcination at 800°C.	Samat et al. (2021)
OPF	Combustion (600°C, 3 hr) and acid leaching (3.00% citric acid, 70°C, 1 hr) pre-treatment, alkaline extraction (2 M NaOH, 1 hr), precipitation (1 M H_2SO_4, pH 7), and ageing (18 hr).	C/Silica gel	1 kg of OPF produced 34.7 g of ash (3.50%); after leaching, it produced 18.7 g of leached ash (53.90%), with a silica yield of 12.8 g (1.28%* from the OPF; 36.89%** from the ash).	Osman and Sapawe (2020)
OPDC	Combustion pre-treatment (600°C–900°C, 5 hr), alkaline extraction (5 M NaOH, 100°C, 1 hr) and precipitation (2.5 M H_2SO_4, pH 6–7).	E/Silica gel	Silica purity ranged from 32.10%–75.96%.	Rahim et al. (2023)
	Acid leaching pre-treatment (1 M citric acid, 2 hr) and calcination (400°C–800°C, 6 hr).	B/Calcined silica	Weight loss 83.95% (~silica yield 16.05%*) under calcination at 800°C.	Samat et al. (2021)

Note: * - Silica yield from dry raw material; ** - Silica yield from ash raw material; n.a. - Not available; BA - boiler ash; EFBA - empty fruit bunch ash; PKS - palm kernel shell; EFB - empty fruit bunch; OPF - oil palm fronds; OPDC - oil palm decanter cake..

Among the extraction techniques, the sol-gel methods have shown considerable advantages over calcination routes regarding silica purity. For instance, Utama et al. (2018) can convert silica in samples by 60.38%–60.42% with a SiO_2 purity of 95.33% using the sol-gel method on BA. Further refinement, such as CO_2 impregnation during gelation, increased the SiO_2 purity to 96.90% (Utama et al., 2019). In contrast, the calcination method, although simpler, tends to produce lower purity silica due to incomplete removal of impurities (Pa et al., 2016), where BA treated with ≥3.00% citric acid and calcined at 800°C resulted in a silica product with 92.00% SiO_2 purity. These findings suggest that while calcination is effective for bulk processing, sol-gel methods are more suitable for applications requiring high-purity silica, such as in catalysts, electronics and pharmaceutical industries.

The comparison across different types of oil palm solid waste raw materials also highlights significant variations in yield and purity. BA emerges as the most promising biomass due to its high silica yield and purity without requiring pre-treatment. Direct extraction using the sol-gel method can convert silica in samples by 60.38%–60.42% (Utama et al., 2018). In contrast, OPF and EFB exhibited lower yields. For instance, OPF subjected to combustion at 600°C and subsequent citric acid leaching achieved a silica yield of only 1.28% when calculated from raw materials or 36.89% when calculated from ash (Osman & Sapawe, 2020). On the other hand, OPDC demonstrated significant potential, achieving a silica yield of 16.05% with a purity of 75.96% (Rahim et al., 2023; Samat et al., 2021). This result suggests that OPDC, due to its lower weight loss during calcination, is suitable for bulk silica production with balanced yield and purity.

The choice of extraction route also strongly influences both the silica yield and purity. For example, Imoisili et al. (2020b) optimised the process for PKS by using combustion at 750°C for 3 hr followed by alkaline extraction and precipitation, which resulted in a significantly high yield of 56.65% and SiO_2 purity of 96.83%. A subsequent modification to the process, involving refluxing with 3 M HCl and re-extraction with 3 M NaOH, enabled the production of silica nanoparticles with a yield of 54.35% (Imoisili et al., 2020a). These findings underscore the effectiveness of alkaline extraction and sol-gel methods in producing high-purity silica or advanced materials like silica nanoparticles, which are critical for high-value applications in nanotechnology.

From the comparative analysis, BA stands out as the most favourable source of biogenic silica, offering both high yield and significant SiO_2 purity without requiring intensive pre-treatment. However, for applications demanding high-purity silica (e.g., electronics, pharmaceuticals and speciality catalysts), processes such as alkaline extraction or sol-gel methods are preferred. In contrast, for bulk silica production where cost-effectiveness is essential, calcination remains a viable option, particularly for raw materials like OPDC and PKS, which demonstrate balanced yield and purity. In terms of applications, the choice of silica purity and particle size determines its suitability for specific uses. High-purity silica (>95.00%) obtained via sol-gel methods is ideal for high-value applications, such as nanocomposites and catalysts. Silica produced through calcination with moderate purity is suitable for bulk applications like fillers in rubber composites and as a raw material in construction materials. Moreover, the production of silica nanoparticles, as demonstrated by Imoisili et al. (2020a), opens opportunities in advanced technologies requiring materials with enhanced surface area and reactivity.

The comparative review highlights the importance of selecting appropriate extraction routes based on the desired silica yield, purity and intended application. Green extraction methods offer environmental benefits and sustainable processing. Sol-gel techniques remain superior for applications requiring high-purity silica, such as electronics, pharmaceuticals and speciality catalysts. Among the raw materials, BA demonstrates the greatest potential for silica production, offering high yields and significant purity without requiring intensive pre-treatment.

PROPERTIES OF BIOGENIC SILICA FROM OIL PALM BIOMASS

Chemical Composition

Table 4 shows the chemical composition of biogenic silica extracted from oil palm biomass. The SiO_2 concentration is influenced by various factors, including the type of biomass (BA, EFB, PKS, OPF, OPDC), pre-treatment route and extraction methods. According to Adha and Warsiki (2023), biogenic silica from BA processed through the B-route had a SiO_2 concentration of 79.20%. This SiO_2 concentration was relatively low because various impurities could not be removed, such as Al_2O_3 (8.20%), Na_2O (6.20%) and K_2O (1.50%). Rahmat et al. (2021) conducted a pre-treatment using the C-route method to increase SiO_2 concentrations in ash and silica from EFB. In their study, the structure of the silica ash observed was crystalline following combustion and acid leaching pre-treatment involving sulfuric acid. Although acid leaching led to an increase in SiO_2 concentration in EFBA, it was unable to eliminate metal oxide impurities, such as CaO (17.80%), K_2O (16.40%), SO_3 (3.50%) and Fe_2O_3 (3.30%). Nelson et al. (2023) performed a multi-step process to produce biogenic silica from EFBA. This involved re-combustion of EFBA, an acid leaching pre-treatment using HCl (D-route), followed by sol-gel extraction using NaOH and gelation through the co-precipitation method. The resulting SiO_2 concentration increased to 58.95% and the silica structure exhibited an amorphous nature. Despite these improvements, the concentration of other metal oxides as impurities remained notably high.

Pa et al. (2016) utilised organic acid, specifically citric acid, as an alternative chemical to replace the strong acids (HCl and H_2SO_4) in the leaching process of BA. The use of citric acid as a leaching pre-treatment agent (B-route) has been demonstrated to be effective, resulting in a significant increase in SiO_2 concentration to 92.0%. However, the subsequent calcination at 800°C for a short period (30 min) was unsuccessful in converting the crystalline structure to an amorphous form.

Biogenic silica has been extracted from OPDC involving a pre-treatment through combustion at 600°C for 5 hr (E-route), followed by sol-gel extraction. This process resulted in biogenic silica with a SiO_2 concentration of 76.95% (Rahim et al., 2023). The remaining impurity components include K_2O (11.60%), Al_2O_3 (7.80%), P_2O_5 (1.71%), SO_3 (0.99%), Fe_2O_3 (0.21%) and CaO (0.18%). Similarly, the extraction of biogenic silica from PKS involved a comparable pre-treatment to OPDC, followed by sol-gel extraction. In this case, the resulting SiO_2 concentration was notably higher at 96.83%, with remaining impurities present in relatively low concentrations (Imoisili et al., 2020b).

Biogenic silica with relatively high SiO_2 concentrations, ranging from 95.33% to 96.90%, was obtained by simple extraction of BA without pre-treatment (A-route) (Utama et al., 2018, 2019). This was achieved by optimising the sol-gel extraction conditions (extraction temperature and stirring speed) (Utama et al., 2019) or modifying the sol-gel method through CO_2 impregnation during the gelation process (Utama et al., 2019). The remaining metal oxide impurities in both studies were Na_2O (1.59%–2.50%), K_2O (1.29%), Al_2O_3 (0.39%–0.46%) and SO_3 (0.48%). The SiO_2 concentrations of BA-derived biogenic silica were higher than those of the biogenic silica from sugarcane bagasse ash, 91.58% (Affandi et al., 2009). Additionally, they were comparable to that of the commercial silica, 95.37% (Setyawan et al., 2021), but lower than those of rice husk ash-derived biogenic silica, 99.25%–99.61% (Fernandes et al., 2017).

TABLE 4. CHEMICAL COMPOSITION OF TREATED ASH AND BIOGENIC SILICA FROM OIL PALM BIOMASS

Type of biomass	Route/type of silica	SiO_2 (%)	Na_2O (%)	Al_2O_3 (%)	Cl (%)	K_2O (%)	P_2O_5 (%)	CaO (%)	Fe_2O_3 (%)	SO_3 (%)	MgO (%)	MnO (%)	TiO_2 (%)	ZnO (%)	Others (%)	Reference
Conventional extraction																
BA	B/Silica gel	79.20	6.20	8.20	3.40	1.50	0.60	0.20	0.20	0.40	n.a	n.a	0.001	0.001	n.a	Adha and Warsiki (2023)
EFBA	D/Calcined silica	59.85	0.56	1.97	n.a	11.66	6.28	7.34	1.55	n.a	8.62	0.44	0.150	n.a	n.a	Nelson et al. (2023)
EFB	C/Ash	45.60	n.a	n.a	0.00	16.40	0.00	17.80	3.30	3.50	n.a	n.a	n.a	n.a	n.a	Rahmat et al. (2021)
Green extraction																
BA	A/Silica gel	95.33	2.50	0.39	n.a	1.29	n.a	n.a	n.a	0.48	n.a	n.a	n.a	n.a	n.a	Utama et al. (2018)
	A/Silica gel	96.90	1.59	0.46	n.a	1.29	n.a	n.a	n.a	n.a	n.a	n.a	n.a	n.a	n.a	Utama et al. (2018)
	C/Ash	92.00	n.a	0.00	n.a	3.58	0.00	1.22	2.13	n.a	n.a	n.a	n.a	n.a	n.a	Pa et al. (2016)
	D/Silica gel	94.64	0.17	2.63	0.22	0.22	0.53	0.68	0.26	0.16	0.46	n.a	n.a	n.a	0.03	Hoerudin et al. (2024)
PKS	E/Silica xerogel	96.83	0.97	0.00	n.a	1.43	0.00	0.43	0.17	0.00	0.17	n.a	n.a	n.a	n.a	Imoisili et al. (2020b)
OPDC	E/Silica gel	76.95	n.a	7.80	n.a	11.60	1.71	0.18	0.21	0.99	n.a	n.a	n.a	n.a	0.76	Rahim et al. (2023)
Commercial silica	-	95.37	2.47	0.63	0.07	0.01	n.a	0.02	0.06	n.a	0.06	0.00	n.a	n.a	0.04	Setyawan et al. (2021)

Note: n.a - not available; BA - boiler ash; EFBA - empty fruit bunch ash; EFB - empty fruit bunch; PKS - palm kernel shell; OPDC - oil palm decanter cake.

Crystallinity and Amorphicity

Crystallinity refers to the proportion of crystalline substances within a blend of both crystalline and non-crystalline materials. Conversely, amorphicity exhibits an inverse relationship with the crystallinity of materials. The extent of crystallinity plays a crucial role in pozzolanic activity, as only amorphous materials actively participate in the pozzolanic reaction (Karim et al., 2017). X-ray diffraction (XRD) serves as a characterisation technique employed to ascertain the presence of crystalline compounds. The method is particularly useful for crystal structure analysis due to the distinct patterns associated with each compound. By referencing the known diffraction pattern of an element in this analysis, it becomes possible to identify the specific compound.

Table 5 shows XRD 2θ values for treated ash derived from EFB and BA, as well as biogenic silica extracted from BA, EFB, PKS and OPDC. The 2θ values are presented for both before and after undergoing a leaching or extraction process, employing both conventional and green extraction methods. The raw materials derived from palm oil solid waste exhibit a crystalline nature before undergoing the extraction process. According to Rahmat et al. (2021), EFBA retained its crystalline nature when subjected only to leaching without subsequent extraction (*Figure 4a*). Similarly, Faizul et al. (2013) reported that BA maintained a crystalline structure even after undergoing pre-treatment and subsequent calcination at a temperature of 800°C for a short time (30 min). Nelson et al. (2023) asserted that the transformation of crystalline silica into its amorphous counterpart could be achieved through a thermochemical process. Additionally, Samat et al. (2018, 2021) reported that amorphous silica from EFB, PKS and OPDC could be produced by extraction involving calcination at a temperature of 800°C for 6 hr.

In general, amorphous silica is characterised by a broad hump at diffraction angles 2θ between 15.0° and 35.0°. The XRD pattern of biogenic silica obtained from palm oil solid waste through the sol-gel method exhibits a pronounced absence of sharp peaks, indicating the amorphous structure of the resulting product. For example, the XRD pattern of biogenic silica extracted from EFBA by the sol-gel method showed a 2θ value of 31.8°, confirming the amorphous nature of the silica (Nelson et al., 2023). The amorphous structure of biogenic silica extracted from PKS was identified with an XRD 2θ value of 22.5°, as shown in *Figure 4b* (Imoisili et al., 2020b). Biogenic silica extracted from OPDC by the sol-gel method exhibited a broad diffraction peak at a 2θ value of 22.0°, indicating the transformation of crystals into an amorphous form due to alkali treatment (Rahim et al., 2023). The results align with XRD patterns observed for amorphous biogenic silica obtained from other sources such as rice husk ash (Hoerudin et al., 2022), corn cob ash (Velmurugan et al., 2015), sugarcane bagasse ash (Chindaprasirt & Rattanasak, 2020) and commercial amorphous silica (Setyawan et al., 2021).

Depending on its applications, amorphous silica is usually preferred over crystalline silica due to its random and irregular atomic structure and patterns, which enhance its reactivity. It is widely acknowledged that chemical treatment induces structural phase transformation in biogenic silica. In addition, amorphous silica is generally considered safe and non-toxic, in contrast to crystalline silica, which can be toxic and may lead to the development of silicosis, as highlighted by Rovani et al. (2018). A study by Erawati et al. (2024) investigated the preparation, characterisation and cytotoxicity of calcium silicate derived from amorphous SiO_2 extracted from black, red and white rice husks. The results demonstrated that all three calcium silicate samples were non-toxic, with mean cell viability ranging from 78.72%–123.51%, as per ISO 10993-5 standards. This confirms the biocompatibility of the materials. This expands the opportunities for the broader utilisation of biogenic silica derived from oil palm biomass in various fields.

Functional Groups

Fourier transform infrared spectroscopy (FTIR) is a well-known vibrational spectroscopy technique based on the observation of molecular vibrations that absorb infrared radiation. This method offers insights into the molecular structure of materials and functional groups within compounds (Tessema et al., 2023). Nelson et al. (2023) reported that the FTIR spectra of biogenic silica extracted from EFBA exhibited vibration bands corresponding to Si-OH, O-Si-O, and Si-O-Si functional groups. According to Okoronkwo et al. (2013), the band at wavenumbers 463–475 cm^{-1} was associated with bending vibrations of the O-Si-O network, while 791–807 cm^{-1} corresponded to symmetric stretching vibrations of Si-O-Si. The band at wavenumbers 1,071–1,090 cm^{-1} represented the siloxane group or the asymmetric Si-O-Si stretching vibration. This reveals the bond structure of Si and O atoms towards smaller particle sizes. Meanwhile, the broad bands at 1,633–1,645 cm^{-1} and 3,350–3,750 cm^{-1} were caused by O-H bending and stretching vibrations of the Si-OH silanol groups and due to the adsorption of H_2O molecules on the silica surface (Imoisili et al., 2020a).

The infrared (IR) spectra of biogenic silica obtained from palm oil solid waste (BA, EFB, PKS, OPF, OPDC) using the conventional and green

TABLE 5. XRD PATTERN OF ASH AND BIOGENIC SILICA FROM OIL PALM BIOMASS

Type of biomass	Methods (pre-treatments and extraction)	Route	Before leaching/extraction			After leaching/extraction			Reference
			Metal oxide	Structure	2θ value (°)	Metal oxide	Structure	2θ value (°)	
Conventional extraction									
EFB	Combustion (600°C–800°C, 2 hr) and acid leaching (5 N H_2SO_4, 30 min) pre-treatment	C	SiO_2	Hexagonal	26.74	SiO_2	Rhombohedral	20.93	Rahmat et al. (2021)
					39.38			29.18	
			CaO	n.a	29.76			31.10	
			K_2O	n.a	25.78			32.87	
			P_2O_5	n.a	29.55	K_2O	Hexagonal	40.61	
			Fe_2O_3	n.a	40.32	SO_3	Orthorhombic	32.34 40.36 43.83 47.99	
EFBA	Re-carbonised (600°C–800°C) and acid leaching (1% HCl) pre-treatment, alkaline extraction (NaOH), precipitation (1 M HCl + 3 M NH_4OH), and calcination (550°C, 3 hr)	D	SiO_2, $KAlSiO_4$, $CaCO_3$	Quartz	30.00	SiO_2	Amorphous	31.80	Nelson et al. (2023)
Green Extraction									
BA	Acid leaching pre-treatment (1%–6% citric acid) and calcination (800°C, 30 min)	B	SiO_2, $KAlSiO_4$, C	Quartz	n.a n.a n.a	SiO_2, C	n.a n.a	n.a n.a	Pa et al. (2016)
	Alkaline extraction (1.4 N NaOH, 50 min, 105°C, sample-to-NaOH ratio 0.23 g/cm³, stirring speed 1,065 rpm) and precipitation using CO_2 impregnation and mechanical fragmentation	A	n.a	n.a	n.a	SiO_2	Amorphous	23.00	Utama et al. (2019)
	Re-ashing (600°C, 2 hr) and acid leaching (6% citric acid, 600°C, 1.5 hr) pre-treatment, alkaline extraction (6%–10% NaOH, 100°C, 1.5 hr) and precipitation (3% HCl, pH 7), ageing (18 hr)	D	SiO_2	Quartz	26.70	SiO_2	Amorphous	22.50	Hoerudin et al. (2024)
PKS	Combustion pre-treatment (750°C, 3 hr), alkaline extraction (2 N NaOH, 2 hr), precipitation (2 N HCl, pH 7.5–8.5) and ageing (24 hr)	E	SiO_2	Quartz	24.00 43.00	SiO_2	Amorphous	22.50	Imoisili et al. (2020b)
	Combustion pre-treatment (750°C, 3 hr), alkaline extraction (3 N NaOH, 2 hr), precipitation (3 N HCl) and ageing (24 hr). Refluxed silica xerogel (3 M HCl, 70°C, 4 hr), dissolved with 3 M NaOH and silica precipitation (H_2SO_4, pH 7.5)	E	SiO_2	Quartz	20.00 26.00 40.00 47.00 55.00	SiO_2	Amorphous	22.50	Imoisili et al. (2020a)
			$CaCO_3$	Calcite	22.00 44.00 47.00 55.00				
OPDC	Combustion pre-treatment (600°C–900°C, 5 hr), alkaline extraction (5 M NaOH, 100°C, 1 hr) and precipitation (2.5 M H_2SO_4, pH 6–7)	E	SiO_2	Quartz	21.00 28.00 29.00	SiO_2	Amorphous	22.00	Rahim et al. (2023)

Note: n.a - not available; EFB - empty fruit bunch; EFBA - empty fruit bunch ash; BA - boiler ash; PKS - palm kernel shell; OPDC - oil palm decanter cake; SiO_2 - silicon dioxide; K_2O - potassium oxide.

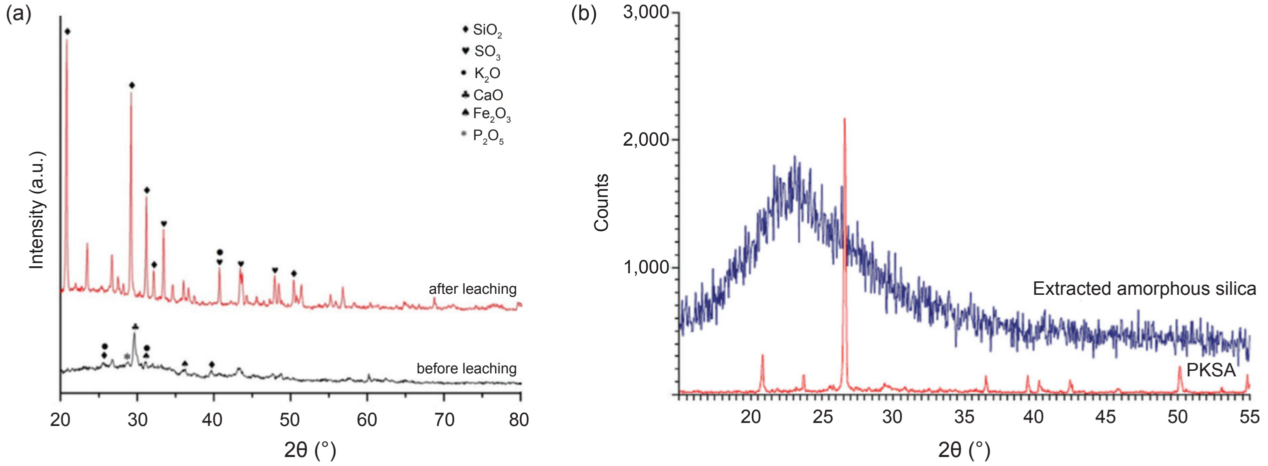

Source: Imoisili et al. (2020b); Rahmat et al. (2021).

Figure 4. XRD pattern, (a) EFBA before and after leaching and (b) amorphous silica.

extraction methods are presented in *Table 6*. The functional groups in biogenic silica derived from solid palm oil waste exhibit some variation. This is likely due to differences in raw materials (BA, EFB, PKS, OPF and OPDC), pre-treatment route and extraction methods employed. The evident variations in the IR spectra are particularly pronounced in the extraction of biogenic silica using the sol-gel method (silica-gel), a process that typically involves NaOH as a solvent (Imoisili et al., 2020a, 2020b; Nelson et al., 2023; Osman & Sapawe, 2020; Rahim et al., 2023; Utama et al., 2018, 2019) and the calcination method (calcined silica), especially when conducted at high temperatures for an extended period, e.g., 800ºC for 6 hr. These specific calcination conditions have been considered optimal for biogenic silica production from EFB, PKS and OPDC (Samat et al., 2018, 2021).

In the studies by Samat et al. (2018, 2021), the calcined silica showed no detectable infrared spectrum in the range of 3,350–3,750 cm^{-1}. In contrast, this range was observed in silica gel, appearing as broad bands in the IR spectrum. The difference is evident in the IR spectra of biogenic silica from PKS processed using the sol-gel and calcination method (*Figure 5*).

According to Usman et al. (2015), the bands at 1,450–3,450 cm^{-1} were undetected, indicating the absence of all traces of water molecules and polar functional groups during the calcination process at high temperatures. Similarly, the IR spectrum at wavenumbers 447–473 cm^{-1} is generally undetected in calcined silica from EFB, PKS and OPDC. Geetha et al. (2016) observed that no band was detected at 447–473 cm^{-1}, indicating the loss of all traces of original organic compounds found in plants during the calcination at high temperatures. However, in the calcination process of BA carried out by Faizul et al. (2013) using the B-route pre-treatment, an IR spectrum at a wavenumber of 3,445 cm^{-1} was still observed. This may be due to the relatively short calcination time of 30 min at 800°C. The short duration of the calcination process may not have permitted the complete combustion of organic compounds, resulting in the persistence of certain functional groups, as indicated by the observed IR spectrum.

Surface Properties

Available data on the surface properties of biogenic silica extracted from oil palm biomass have been limited. *Table 7* shows the surface properties of biogenic silica extracted from various oil palm biomass sources using different extraction and pre-treatment methods. These properties vary depending on factors such as the biomass type (BA, EFB, EFBA, PKS and OPDC), pre-treatment route and extraction method. A multi-stage process for producing biogenic silica from EFBA, involving re-ashing, acid leaching pre-treatment with hydrochloric acid (conventional extraction/ D-route), followed by sol-gel extraction with sodium hydroxide and gelation through a co-precipitation method, resulted in a low Brunauer-Emmett-Teller (BET) surface area of 0.38 m^2/g and a very high average pore size of 23.9 μm (Nelson et al., 2023). This relatively low surface area might be due to the relatively brief combustion period, leading to lower surface porosity. In contrast, biogenic silica extracted from EFB using citric acid leaching pre-treatment (green extraction/ B-route), followed by calcination at 800°C produced a higher BET surface area of 15.10 m^2/g (Samat et al., 2021). This discrepancy may be due to the incomplete removal of impurities (such as alkali metals) in the biogenic silica from EFBA, attributed to eutectic reactions occurring during the re-ashing process.

TABLE 6. THE IR SPECTRA OF ASH AND BIOGENIC SILICA FROM OIL PALM BIOMASS

Type of biomass	Methods (Pre-treatments and extraction)	Route/Type of silica	Wavenumber (cm^{-1})	Type of bond	Reference
Conventional extraction					
EFBA	Re-carbonised (600°C–800°C) and acid leaching (1% HCl) pre-treatment, alkaline extraction (NaOH), precipitation (1 M HCl + 3 M NH_4OH) and calcination (550°C, 3 hr)	D/Calcined silica	619 1,151	Symmetric stretching of the Si-O-Si bond Asymmetric stretching of the Si-O-Si bond	Nelson et al. (2023)
EFB	Acid leaching pre-treatment (1 M HCl) and calcination (400°C–800°C, 6 hr)	B/Calcined silica	447 792 1,076	Si-O bending vibration of the O-Si-O bond Symmetric stretching of the Si-O-Si bond Asymmetric stretching of the Si-O-Si bond	Samat et al. (2018)
PKS	Acid leaching pre-treatment (1 M HCl) and calcination (400°C–800°C, 6 hr)	B/Calcined silica	474 788 1,035	Si-O bending vibration of the O-Si-O bond Symmetric stretching of the Si-O-Si bond Asymmetric stretching of the Si-O-Si bond	Samat et al. (2018)
Green extraction					
BA	Acid leaching pre-treatment (1%–6% citric acid) and calcination (800°C, 30 min)	B/Ash	460 796 1,099 1,625 3,445	Si-O bending vibration of the O-Si-O bond Symmetric stretching of the Si-O-Si bond Asymmetric stretching of Si-O-Si, vibration of the Si-O bond Stretching vibration of the O-H bond in silanol (Si-OH) and adsorbed water molecules Stretching vibration of the O-H bond in silanol (Si-OH) and adsorbed water molecules	Faizul et al. (2013)
	Alkaline extraction (1.4 N NaOH, 50 min, 105°C, sample-to-NaOH ratio 0.23 g/cm^3, stirring speed 1,065 rpm) and precipitation using CO_2 impregnation and mechanical fragmentation	A/Silica gel	471–473 800 1,107 1,639–1,641 3,452–3,458	Si-O bending vibrations of the O-Si-O bond Symmetric stretching of the Si-O-Si bond Asymmetric stretching of the Si-O-Si bond Bending vibrations of water molecules Stretching vibration of the O-H bond in silanol (Si-OH) and adsorbed water molecules	Utama et al. (2018; 2019)
	Re-ashing (600°C, 2 hr) and acid leaching (6% citric acid, 600°C, 1.5 hr) pre-treatment, alkaline extraction (6%–10% NaOH, 100°C, 1.5 hr) and precipitation (3% HCl, pH 7), ageing (18 hr)	D/Silica gel	467 791 1,081 1,635 3,450	Si-O bending vibration of the O-Si-O bond Symmetric stretching of the Si-O-Si bond Asymmetric stretching of the Si-O-Si bond Bending vibration of the O-H bond in silanol groups Stretching vibration of the O-H bond in silanol (Si-OH)	Hoerudin et al. (2024)

TABLE 6. THE IR SPECTRA OF ASH AND BIOGENIC SILICA FROM OIL PALM BIOMASS (continued)

Type of biomass	Methods (Pre-treatments and extraction)	Route/Type of silica	Wavenumber (cm^{-1})	Type of bond	Reference
PKS	Combustion pre-treatment (750°C, 3 hr), alkaline extraction (3 N NaOH, 2 hr), precipitation (3 N HCl) and ageing (24 hr). Refluxed silica xerogel (3 M HCl, 70°C, 4 hr), dissolved with 3 M NaOH and silica precipitation (H_2SO_4, pH 7.5)	E/Silica xerogel/ nanoparticle	469 611 777 805 1,073 1,077 1,640 3,395 3,691 3,750	Si-O bending vibration of the O-Si-O bond Symmetric stretching of the Si-O-Si bond Asymmetric stretching of Si-O-Si, vibration of the Si-O bond Bending vibration of the O-H bond in silanol (Si-OH) Stretching vibration of the O-H bond in silanol (Si-OH) and adsorbed water molecules	Imoisili et al. (2020a, 2020b)
	Acid leaching pre-treatment (1 M citric acid, 2 hr) and calcination (400°C–800°C, 6 hr)	B/Calcined silica	794 880 1,046 1,417	Symmetric stretching of the Si-O-Si bond Si-C bond Asymmetric stretching of Si-O-Si, vibration of the Si-O bond In-plane C=H bond	Samat et al. (2021)
EFB	Acid leaching pre-treatment (1 M citric acid, 2 hr) and calcination (400°C–800°C, 6 hr)	B/Calcined silica	790 1,045 1,070	Symmetric stretching of the Si-O-Si bond Asymmetric stretching of Si-O-Si, vibration of the Si-O bond Asymmetric stretching of Si-O-Si, vibration of the Si-O bond	Samat et al. (2021)
OPDC	Combustion pre-treatment (600°C–900°C, 5 hr), alkaline extraction (5 M NaOH, 100°C, 1 hr) and precipitation (2.5 M H_2SO_4, pH 6–7)	E/Silica gel	462 1,074 1,645 3,473	Si-O bending vibration of the O-Si-O bond Asymmetric stretching of the Si-O-Si bond Stretching of the C=O bond Stretching vibration of the O-H bond in silanol (Si-OH) and adsorbed water molecules	Rahim et al. (2023)
	Acid leaching pre-treatment (1 M citric acid, 2 hr) and calcination (400°C–800°C, 6 hr)	B/Calcined silica	779 880 1,026 1,409	Symmetric stretching of the Si-O-Si bond Si-C bond Asymmetric stretching of Si-O-Si, vibration of the Si-O bond In-plane C=H bond	Samat et al. (2021)
OPF	Combustion (600°C, 3 hr) and acid leaching (3% citric acid, 70°C, 1 hr) pre-treatment, alkaline extraction (2 M NaOH, 1 hr), precipitation (1 M H_2SO_4, pH 7) and ageing (18 hr)	C/Silica gel	610 1,040–1,100 1,600–1,640 3,350–3,390	Symmetric stretching of the Si-O-Si bond Asymmetric stretching of the Si-O-Si bond Si-OH bond Stretching vibration of the O-H bond in silanol (Si-OH) and adsorbed water molecules	Osman and Sapawe (2020)

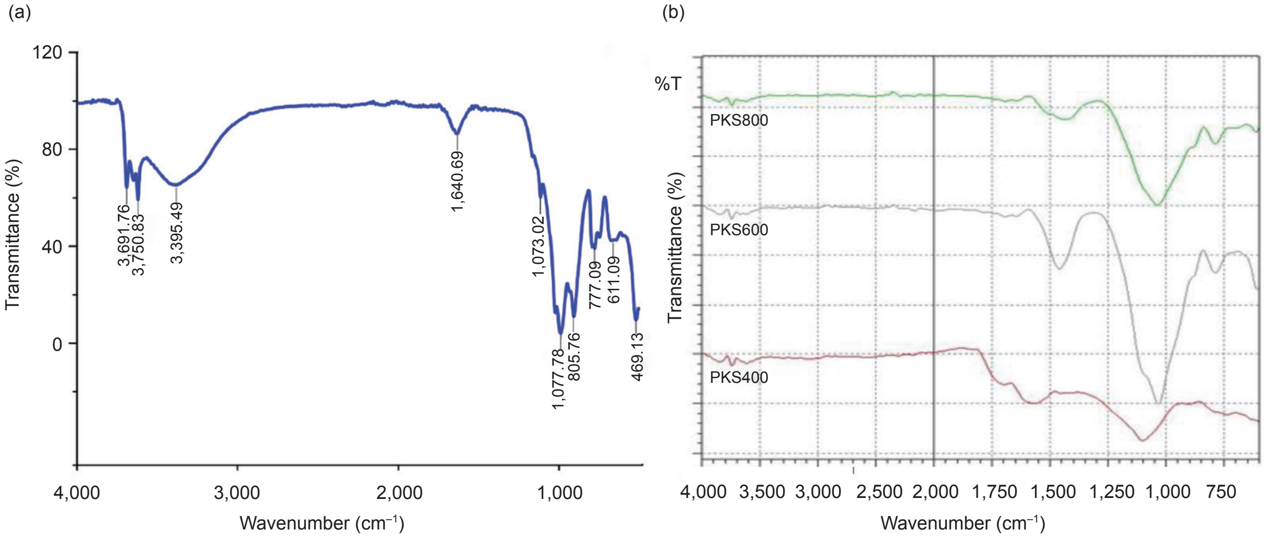

Source: Imoisili et al. (2020a); Samat et al. (2018).

Figure 5. Fourier transform infrared spectroscopy (FTIR) spectra of biogenic silica, from palm kernel shell (PKS) processed by (a) the sol-gel and (b) the calcination method.

TABLE 7. SURFACE PROPERTIES OF BIOGENIC SILICA FROM OIL PALM BIOMASS

Type of biomass	Methods (pre-treatments and extraction)	Route/type of silica	BET surface area (m^2/g)	Pore size (nm)	Particle size (nm)	Reference
Conventional extraction						
EFBA	Re-carbonised (600°C–800°C) and acid leaching (1% HCl) pre-treatment, alkaline extraction (NaOH), precipitation (1 M HCl + 3 M NH_4OH) and calcination (550°C, 3 hr)	D/Calcined silica	0.38	23.90	n.a	Nelson et al. (2023)
Green extraction						
BA	Alkaline extraction (1.4 N NaOH, 50 min, 105°C, sample-to-NaOH ratio 0.23 g/cm³, stirring speed 1,065 rpm) and precipitation using CO_2 impregnation and mechanical fragmentation	A/Silica gel	138.00	n.a	58.96	Utama et al. (2019)
	Re-ashing (600°C, 2 hr) and acid leaching (6% citric acid, 600°C, 1.5 hr) pre-treatment, alkaline extraction (6%–10% NaOH, 100°C, 1.5 hr) and precipitation (3% HCl, pH 7), ageing (18 hr)	D/Silica gel	390.80	n.a	n.a	Hoerudin et al. (2024)
PKS	Combustion pre-treatment (750°C, 3 hr), alkaline extraction (3 N NaOH, 2 hr), precipitation (3 N HCl), and ageing (24 hr). Refluxed silica xerogel (3 M HCl, 70°C, 4 hr), dissolved with 3 M NaOH and silica precipitation (H_2SO_4, pH 7.5)	E/Nanoparticles	438.00	2.20–6.30	n.a	Imoisili et al. (2020a)
	Acid leaching pre-treatment (1 M citric acid, 2 hr) and calcination (400°C–800°C, 6 hr)	B/Calcined silica	20.08	n.a	n.a	Samat et al. (2021)
EFB	Acid leaching pre-treatment (1 M citric acid, 2 hr) and calcination (400°C–800°C, 6 hr)	B/Calcined silica	15.10	n.a	n.a	Samat et al. (2021)
OPDC	Acid leaching pre-treatment (1 M citric acid, 2 hr) and calcination (400°C–800°C, 6 hr)	B/Calcined silica	9.49	n.a	n.a	Samat et al. (2021)

Note: EFBA - empty fruit bunch ash; BA - boiler ash; PKS - palm kernel shell; EFB - empty fruit bunch; OPDC - oil palm decanter cake.

Metal impurities present during the combustion process may lead to the formation of crystalline silica, causing a notable reduction in surface area. Similarly, extracting biogenic silica from OPDC and PKS with the same treatment applied to EFB yielded higher BET surface areas than EFBA, at 9.49 and 20.08 m^2/g, respectively (Samat et al., 2021).

Utama et al. (2019) reported that a relatively high BET surface area of 138 m^2/g for biogenic silica was achieved from BA using the A-route (green extraction) process. The extraction process developed used 1.4 N NaOH, while the gelation process employed CO_2 impregnation and mechanical fragmentation. The surface area of biogenic silica from BA was further enhanced with the D-route process, as demonstrated by Hoerudin et al. (2024). The high surface area from the D-route, particularly, suggests improved silica purity and porosity due to re-combustion and strong leaching with NaOH, making it suitable for applications requiring high surface reactivity.

A significant increase in the surface area of biogenic silica was achieved from PKS through the E-route, which involves combustion pre-treatment at 750°C for 3 hr, followed by the sol-gel method to obtain biogenic silica. By continuing the process with refluxing the previously produced silica with 3 M HCl for 4 hr and re-extracting it with 3 M NaOH, silica nanoparticles were produced with a BET surface area of 438 m^2/g and a pore size distribution ranging from 2.2 to 6.3 Nm (Imoisili et al., 2020a).

Biogenic silica from each biomass type has distinct surface properties based on extraction methods, pre-treatment routes and combustion conditions. The significant differences in BET surface area and particle sizes across different routes imply that selecting an appropriate pre-treatment and extraction method is crucial. The extraction route and biomass type substantially impact the surface properties of biogenic silica. High BET surface areas and fine particle sizes obtained through specific pre-treatment and extraction routes open up opportunities for high-performance applications.

Real-world applications of biogenic silica from oil palm biomass remain scarce, if not unavailable. Most recent applications are largely confined to laboratory-scale research. Moreover, studies investigating the use of biogenic silica generated from different oil palm biomasses for the same type of application within a single study have not yet been reported, highlighting the limited scope of existing research.

Nonetheless, biogenic silica shows considerable potential for sustainable use in medical, pharmaceutical, healthcare and food industries, particularly due to the desirable properties of amorphous silica, including its non-toxic nature, high porosity and superior adsorption capacity. For example, biogenic silica derived from oil palm biomass holds significant promise for sustainable applications in biomedical fields, as demonstrated in the study by Sreekantan et al. (2020). This study explored the synthesis of a sustainable super-hydrophobic coating composed of silica from POFA and polydimethylsiloxane (PDMS), intended for biomedical applications. The silica was extracted from POFA through a series of thermal and chemical treatments, resulting in a silica solution (SS) that was incorporated into a PDMS-based super-hydrophobic coating. The coating, applied to a glass substrate via spray coating, exhibited a remarkable water contact angle of 151°, confirming its superior hydrophobicity. Biocompatibility and cytotoxicity assessments using fibroblast cell lines (L929 and V79) revealed that the toxicity of the coating was concentration-dependent, with concentrations exceeding 12.5 mg/mL leading to cell toxicity. The study's findings validate the potential of POFA-derived silica for biomedical applications, particularly as a material for super-hydrophobic coatings that require biocompatibility and cytotoxicity control. This innovative application highlights the value of oil palm biomass as a sustainable source of biogenic silica, paving the way for further advancements in environmentally-friendly and functional materials for biomedical use.

Novita and Idris (2022) demonstrated the successful synthesis of silica gel from PKSA as a moisture absorber for pharmaceutical bottle packaging. Their study revealed that PKSA, containing 55.20% SiO_2, could be processed into silica gel with a yield of 34.00%, achieving an 85.65% moisture absorption efficiency over a two-week period. These findings highlight the potential of PKSA-derived silica gel for pharmaceutical applications while also emphasising the importance of reducing impurities to enhance its performance and viability for broader use.

Biogenic silica derived from oil palm biomass has demonstrated significant potential in environmental remediation, particularly as an adsorbent for wastewater treatment, where silica with a high BET surface area is essential. Osman et al. (2021) explored the synthesis of silica nanomaterials from OPF using the sol-gel method and achieved a notable phenol removal efficiency of 68.00% from aqueous solutions under optimised conditions. The biogenic silica nanomaterials displayed an adsorption capacity of 34 mg/g, with structural properties comparable to those of commercially available silica.

These findings highlight the diverse applications of biogenic silica from oil palm biomass and emphasise the need to optimise extraction processes to improve its purity, surface characteristics and amorphicity. Overcoming challenges related to cost-effectiveness, impurity removal and scalability will be critical to advancing the transition from laboratory-scale research to industrial-scale applications.

CONCLUSION

This review highlights the significant potential of palm oil solid waste as an alternative, renewable, and cost-effective source to produce biogenic silica. This review underscores the importance of tailoring extraction routes to specific types of palm oil solid waste to maximise yield and production efficiency while minimising sustainability issues. Among the different types of oil palm solid waste, BA demonstrates superior yield performance and economic viability. This is attributed to the fact that BA stands out for not requiring combustion pre-treatment, and its abundant availability further contributes to its profitability. However, its effective utilisation requires addressing several challenges, particularly in extraction methodologies and scalability for industrial applications. Emerging green methods, such as using organic acids (e.g., citric acid) as leaching agents and optimised sol-gel techniques, show promise in reducing environmental impacts while improving biogenic silica yield and purity. These methods offer a viable pathway for sustainable extraction but need further refinement to minimise costs and scale up for industrial use. The properties of biogenic silica extracted from solid oil palm biomass exhibit similarities with those of biogenic silica obtained from other agricultural waste sources and closely resemble the characteristics of commercial silica. Producing amorphous silica with high BET surface areas and controlled particle sizes is critical for advanced applications. This requires fine-tuning of pre-treatment and extraction parameters, including benign and cheap leaching agents and an optimised gelation process.

Several aspects merit attention in future research endeavours aimed at achieving low-cost input materials, producing pure silica products and maintaining environmental friendliness. The following considerations are crucial: (i) Exploration of untapped palm oil solid waste by investigating other types of palm oil solid waste/byproducts, such as OPDC, clinkers and other potential sources, that may yield high silica concentration but have not been extensively studied, (ii) scaling up green extraction techniques, such as organic acid leaching and CO_2-assisted sol-gel processes, while exploring alternative eco-friendly reagents and energy-efficient pre-treatment and extraction technologies, such as microwave-assisted heating, to reduce operational costs, bridge the gap between laboratory and industrial applications, and enhance process sustainability, (iii) comprehensive life cycle analyses of green extraction methods to identify the most sustainable and economically viable approaches, (iv) functionalisation of biogenic silica for specific applications, which require advanced characterisation and functional testing to tailor silica properties to target industries, (v) integration of biogenic silica production units directly within palm oil mills that will reduce transportation costs associated with BA and harness surplus steam from the mill's boiler, which can significantly lower energy requirements, ultimately optimising biogenic silica production costs and (vi) development of integrated processing systems that combine silica extraction with the recovery of other valuable byproducts, such as lignin, cellulose and alkali metals, to improve overall process efficiency and economic viability.

A multidisciplinary approach is essential to unlock the full potential of oil palm biomass as a biogenic silica source, encompassing advancements in green technologies, industrial collaboration and sustainability assessments. By addressing these challenges, oil palm biomass can transition from an underutilised byproduct to a critical component of the global circular economy, providing a sustainable and eco-friendly alternative for silica production in various applications. Eventually, this can contribute to the development of sustainable oil palm industries.

ACKNOWLEDGEMENT

The authors acknowledge the Indonesian Palm Oil Plantations Fund Management Agency (BPDPKS) for their support through the oil palm research grant No. PRJ-04/DPKS/DIT.IV/2023. Gratitude is extended to Mulyana Hadipernata, Head of the Research Center for Agroindustry, for his invaluable guidance and input in developing this manuscript. Special thanks are also given to Sulhan Iskandar for generously providing the oil palm photographs with courtesy.

REFERENCES

Abdullah, N., & Sulaiman, F. (2013). The oil palm wastes in Malaysia. In M. D. Matovic (Ed.), *Biomass now – Sustainable growth and* *use* (pp. 75–100), InTech eBooks. https://doi.org/10.5772/55302

Abdullah, N., Sulaiman, F., & Safana, A. A. (2017). Bio-oil and biochar derived from the pyrolysis of palm kernel shell for briquette. *Sains Malaysiana*, *46*(12), 2441–2445. https://doi.org/10.17576/jsm-2017-4612-20

Adha, F. F., & Warsiki, E. (2023). Silica synthesis from oil palm mill boiler ash under different concentration of NaOH and extraction time. *IOP Conference Series: Earth and Environmental Science*, *1187*(1), 012012. https://doi.org/10.1088/1755-1315/1187/1/012012

Affandi, S., Setyawan, H., Winardi, S., Purwanto, A., & Balgis, R. (2009). A facile method for production of high-purity silica xerogels from bagasse ash. *Advanced Powder Technology*, *20*(5), 468–472. https://doi.org/10.1016/j.apt.2009.03.008

Aharipour, N., Nemati, A., & Malek Khachatourian, A. (2022). Green synthesis of silica extracted from rice husk ash. *Advanced Ceramics Progress, 8(4)*, 15–20.

Aman, Utama, P. S., & Saputra, E. (2017). High purity silica from palm oil mill fly ash for catalyst ZSM-5 zeolite synthesis. *Applied Science and Technology, 1*(1), 267–272.

Ates, A. M., & Bukowski, M. (2023). *Oil Crops Outlook: May 2023* (OCS-23e). United States Department of Agriculture, Economic Research Service. https://ers.usda.gov/sites/default/files/_laserfiche/outlooks/106531/OCS-23e.pdf?v=60711

Bakar, R. A., Yahya, R., & Gan, S. N. (2016). Production of high purity amorphous silica from rice husk. *Procedia Chemistry*, *19*, 189–195. https://doi.org/10.1016/j.proche.2016.03.092

Bukit, B. F., Frida, E., Humaidi, S., Sinuhaji, P., & Bukit, N. (2022). Optimization of palm oil boiler ash biomass waste as a source of silica with various preparation methods. *Journal of Ecological Engineering*, *23*(8), 192–198. https://doi.org/10.12911/22998993/150694

Chavalparit, O., Rulkens, W. H., Mol, A. P. J., & Khaodhair, S. (2006). Options for environmental sustainability of the crude palm oil industry in Thailand through enhancement of industrial ecosystems. *Environment Development and Sustainability, 8*(2), 271–287. https://doi.org/10.1007/s10668-005-9018-z

Chindaprasirt, P., & Rattanasak, U. (2020). Eco-production of silica from sugarcane bagasse ash for use as a photochromic pigment filler. *Scientific Reports*, *10*(1), 9890. https://doi.org/10.1038/s41598-020-66885-y

Chun, J., & Lee, J. H. (2020). Recent progress on the development of engineered silica particles derived from rice husk. *Sustainability*, *12*(24), 10683. https://doi.org/10.3390/su122410683

Debona, D., Rodrigues, F. A., & Datnoff, L. E. (2017). Silicon's role in abiotic and biotic plant stresses. *Annual Review of Phytopathology*, *55*(1), 85–107. https://doi.org/10.1146/annurev-phyto-080516-035312

Dhakate, P., Kandhol, N., Raturi, G., Ray, P., Bhardwaj, A., Srivastava, A., Kaushal, L., Singh, A., Pandey, S., Chauhan, D. K., Dubey, N. K., Sharma, S., Singh, V. P., Sahi, S., Grillo, R., Peralta-Videa, J., Deshmukh, R., & Tripathi, D. K. (2022). Silicon nanoforms in crop improvement and stress management. *Chemosphere*, *305*, 135165. https://doi.org/10.1016/j.chemosphere.2022.135165

Dizaji, H. B., Zeng, T., Hartmann, I., Enke, D., Schliermann, T., Lenz, V., & Bidabadi, M. (2019). Generation of high quality biogenic silica by combustion of rice husk and rice straw combined with pre- and post-treatment strategies – A review. *Applied Sciences*, *9*(6), 1083. https://doi.org/10.3390/app9061083

Duangpan, S., Tongchu, Y., Hussain, T., Eksomtramage, T., & Onthong, J. (2022). Beneficial effects of silicon fertilizer on growth and physiological responses in oil palm. *Agronomy*, *12*(2), 413. https://doi.org/10.3390/agronomy12020413

El-Sayed, S. A., Khass, T. M., & Mostafa, M. E. (2024). Thermal degradation behaviour and chemical kinetic characteristics of biomass pyrolysis using TG/DTG/DTA techniques. *Biomass Conversion and Biorefinery*, *14*(15), 17779–17803. https://doi.org/10.1007/s13399-023-03926-2

Erawati, J., Bachtiar, E. W., Indrani, D. J., & Hoerudin, H. (2024). Preparation, characterization and *in vitro* cytotoxicity assay of calcium silicate derived SiO_2 rice husk. *Research Journal of Pharmacy and Technology*, *17*(9), 4552–4558. https://doi.org/10.52711/0974-360x.2024.00703

Faizul, C. P., Abdullah, C., & Fazlul, B. (2013). Extraction of silica from palm ash via citric acid leaching treatment. *Advances in Environmental Biology*, *7*(12), 3690–3695.

Faizul, C. P., Abdullah, C., Fazlul, B., & Noorina, H. J. (2014). Extraction of silica from palm ash using organic acid leaching treatment. *Key Engineering Materials*, *594-595*, 329–333. https://doi.org/10.4028/www.scientific.net/kem.594-595.329

Food and Agriculture Organization of the United Nations, Statistics Division (FAOSTAT). (2023). *Crops and livestock products*. https://www.fao.org/faostat/en/#data/QCL

Fernandes, I. J., Calheiro, D., Sánchez, F. A. L., Camacho, A. L. D., De Campos Rocha, T. L. A., Moraes, C. A. M., & De Sousa, V. C. (2017). Characterization of silica produced from rice husk ash: Comparison of purification and processing methods. *Materials Research*, *20*, 512–518. https://doi.org/10.1590/1980-5373-mr-2016-1043

Geetha, D., Ananthiand, A., & Ramesh, P. (2016). Preparation and characterisation of silica material from rice husk ash - An economical viable method. *Research and Reviews: Journal of Pure and Applied Physics*, *4*(3): 20–26.

Grand View Research. (2023). *Silica market size, share, and trends analysis report by application (construction, agrochemicals, rubber, oral care, food and feed, others) by region, and segment forecasts, 2023–2030*. https://www.grandviewresearch.com/industry-analysis/silica-market#

Greenshields, B., Von Der Lühe, B., Schwarz, F., Hughes, H. J., Tjoa, A., Kotowska, M., Brambach, F., & Sauer, D. (2023). Estimating oil-palm Si storage, Si return to soils, and Si losses through harvest in smallholder oil-palm plantations of Sumatra, Indonesia. *Biogeosciences*, *20*(7), 1259–1276. https://doi.org/10.5194/bg-20-1259-2023

Hambali, E., & Rivai, M. (2017). The potential of palm oil waste biomass in Indonesia in 2020 and 2030. *IOP Conference Series: Earth and Environmental Science*, *65*, 012050. https://doi.org/10.1088/1755-1315/65/1/012050

Haynes, R. J. (2017). The nature of biogenic Si and its potential role in Si supply in agricultural soils. *Agriculture Ecosystems & Environment*, *245*, 100–111. https://doi.org/10.1016/j.agee.2017.04.021

Hoerudin, N., Hidayat, T., Yuliani, S., & Wahyuningsih, K. (2024). Extraction yield and properties of biogenic silica from palm oil fuel ash: Effect of re-ashing pretreatment and solvent concentration. *IOP Conference Series: Earth and Environmental Science*, *1354*(1), 012012. https://doi.org/10.1088/1755-1315/1354/1/012012

Hoerudin, N., Setyawan, N., Suismono, N., Purwaningsih, H., & Apriliani, N. (2022). Morphology, extraction yield, and properties of biogenic silica nanoparticles from indonesian rice husk as influenced by solvent type and aging time. *IOP Conference Series: Earth and Environmental Science*, *1024*(1), 012076. https://doi.org/10.1088/1755-1315/1024/1/012076

Hossain, S. K. S., Mathur, L., & Roy, P. K. (2018). Rice husk/rice husk ash as an alternative source of silica in ceramics: A review. *Journal of Asian Ceramic Societies*, *6*(4), 299–313. https://doi.org/10.1080/21870764.2018.1539210

Imoisili, P. E., Ukoba, K. O., & Jen, T. C. (2020a). Green technology extraction and characterisation of silica nanoparticles from palm kernel shell ash via sol-gel. *Journal of Materials Research and Technology*, *9*(1), 307–313. https://doi.org/10.1016/j.jmrt.2019.10.059

Imoisili, P. E., Ukoba, K. O., & Jen, T. C. (2020b). Synthesis and characterization of amorphous mesoporous silica from palm kernel shell ash. *Boletín de la Sociedad Española de Cerámica y Vidrio*, *59*(4), 159–164. https://doi.org/10.1016/j.bsecv.2019.09.006

Jafri, N. H. S., Jimat, D. N., Azmin, N. F. M., Sulaiman, S., & Nor, Y. A. (2021). The potential of biomass waste in Malaysian palm oil industry: A case study of Boustead Plantation Berhad. *IOP Conference Series: Materials Science and Engineering*, *1192*(1), 012028. https://doi.org/10.1088/1757-899x/1192/1/012028

Jahi, N., Othaman, R., Lazim, A. M., & Ramli, S. (2020). Empty fruit bunch cellulose based sorbent for oil sorption in palm oil mill effluent. *Sains Malaysiana*, *49*(9), 2323–2333.

Karim, M. R., Hashim, H., Razak, H. A., & Yusoff, S. (2017). Characterization of palm oil clinker powder for utilization in cement-based applications. *Construction and Building Materials*, *135*, 21–29. https://doi.org/10.1016/j.conbuildmat.2016.12.158

Khairuddin, M., Md Isa, I., Abd, Z., & Abdul-Hamid, H. (2018). Influence of treated palm oil mill effluent sludge on maize (*Zea mays*) growth performance and gas exchange. *Sains Malaysiana*, *47*(5), 961–969. https://doi.org/10.17576/jsm-2018-4705-11

Khan, M. I., Azizli, K., Sufian, S., Man, Z., & Khan, A. S. (2015). Simultaneous preparation of nano silica and iron oxide from palm oil fuel ash and thermokinetics of template removal. *RSC Advances*, *5*(27), 20788–20799. https://doi.org/10.1039/c4ra15922e

Kongnoo, A., Tontisirin, S., Worathanakul, P., & Phalakornkule, C. (2017). Surface characteristics and CO_2 adsorption capacities of acid-activated zeolite 13X prepared from palm oil mill fly ash. *Fuel*, *193*, 385–394. https://doi.org/10.1016/j.fuel.2016.12.087

Kouadri, I., Seghir, B. B., Hemmami, H., Zeghoud, S., Allag, N., Rebiai, A., Amor, I. B., Chala, A., & Belkhalfa, H. (2023). Extraction of silica from different sources of agricultural waste. *Asian Journal of Research in Chemistry*, 97–101. https://doi.org/10.52711/0974-4150.2023.00016

Liew, W. L., Muda, K., Kassim, M. A., Affam, A. C., & Loh, S. K. (2017). Agro-industrial waste sustainable management – A potential source of economic benefits to palm oil mills in Malaysia. *Journal of Urban and Environmental Engineering*, 108–118. https://doi.org/10.4090/juee.2017.v11n1.108118

Ma, J. F., & Yamaji, N. (2006). Silicon uptake and accumulation in higher plants. *Trends in Plant Science*, *11*(8), 392–397. https://doi.org/10.1016/j.tplants.2006.06.007

Madhiyanon, T., Sathitruangsak, P., Sungworagarn, S., Fukuda, S., & Tia, S. (2013). Ash and deposit characteristics from oil-palm empty-fruit-bunch (EFB) firing with kaolin additive in a pilot-scale grate-fired combustor. *Fuel Processing Technology*, *115*, 182–191. https://doi.org/10.1016/j.fuproc.2013.05.018

Makabe, S., Kakuda, K., Sasaki, Y., Ando, T., Fujii, H., & Ando, H. (2009). Relationship between mineral composition or soil texture and available silicon in alluvial paddy soils on the Shounai Plain, Japan. *Soil Science & Plant Nutrition*, *55*(2), 300–308. https://doi.org/10.1111/j.1747-0765.2008.00352.x

Munevar, M. F., & Romero, F. A. (2015). Soil and plant silicon status in oil palm crops in Colombia. *Experimental Agriculture*, *51*(3), 382–392. https://doi.org/10.1017/s0014479714000374

Nabila, R., Hidayat, W., Haryanto, A., Hasanudin, U., Iryani, D. A., Lee, S., Kim, S., Kim, S., Chun, D., Choi, H., Im, H., Lim, J., Kim, K., Jun, D., Moon, J., & Yoo, J. (2023). Oil palm biomass in Indonesia: Thermochemical upgrading and its utilization. *Renewable and Sustainable Energy Reviews*, *176*, 113193. https://doi.org/10.1016/j.rser.2023.113193

Nelson, E. S., Iyuke, S., Daramola, M. O., & Okewale, A. (2023). Extraction and characterization of silica from empty palm fruit bunch (EPFB) ash. *Processes*, *11*(6), 1684. https://doi.org/10.3390/pr11061684

Norrahim, M. N. F., Farid, M. A. A., Lawal, A. A., Yasim-Anuar, T. A. T., Samsudin, M. H., & Zulkifli, A. A. (2022). Emerging technologies for value-added use of oil palm biomass. *Environmental Science Advances*, *1*(3), 259–275. https://doi.org/10.1039/d2va00029f

Norsuraya, S., Fazlena, H., & Norhasyimi, R. (2016). Sugarcane bagasse as a renewable source of silica to synthesize Santa Barbara Amorphous-15 (SBA-15). *Procedia Engineering*, *148*, 839–846. https://doi.org/10.1016/j.proeng.2016.06.627

Novita, L., & Idris, I. (2022). Effectiveness of silica gel from palm kernel shell ash as a moisture absorber of bottle packaging medicine. *IOP Conference Series: Earth and Environmental Science*, *1041*(1), 012044. https://doi.org/10.1088/1755-1315/1041/1/012044

Nur 'Aisyah Ar-Raudhoh, M. T., Muhamad Haziq, M. F., Zafirah, Z. A., Siti Nur Liyana, M., & Nahrul Hayawin, Z. (2024). Comparative studies on cure characteristics and mechanical properties of oil palm biomass filled natural rubber composites. *Journal of Oil Palm Research*, *36*(1), 128–139. https://doi.org/10.21894/jopr.2023.0009

Nzereogu, P., Omah, A., Ezema, F., Iwuoha, E., & Nwanya, A. (2023). Silica extraction from rice husk: Comprehensive review and applications. *Hybrid Advances*, *4*, 100111. https://doi.org/10.1016/j.hybadv.2023.100111

Okoronkwo, E. A., Imoisili, P. E., & Olusunle, S. O. O. (2013). Extraction and characterization of amorphous silica from corn cob ash by sol-gel method. *Chemistry and Materials Research*, *3*(4), 68–72.

Onoja, E., Chandren, S., Razak, F. I. A., Mahat, N. A., & Wahab, R. A. (2018). Oil palm (*Elaeis guineensis*) biomass in Malaysia: The present and future prospects. *Waste and Biomass Valorization*, *10*(8), 2099–2117. https://doi.org/10.1007/s12649-018-0258-1

Osman, N. S., & Sapawe, N. (2020). High purity and amorphous silica (SiO_2) prepared from oil palm frond (OPF) through sol-gel method. *Materials Today Proceedings*, *31*, 228–231. https://doi.org/10.1016/j.matpr.2020.05.299

Osman, N. S., Ismail, M. L., & Sapawe, N. (2021). Synthesis of oil palm frond (OPF) based silica nanomaterial via sol-gel method with enhanced phenol removal. *Journal of Chemical Engineering and Industrial Biotechnology*, *7*(2), 20–26. https://doi.org/10.15282/jceib.v7i2.6917

Oyejobi, D. O., Abdulkadir, T. S., & Ahmed, A. T. (2015). A study of partial replacement of cement with palm oil fuel ash in concrete production. *Journal of Agricultural Technology*, *12*(4), 619–631.

Pa, F. C., Chik, A., & Bari, M. F. (2016). Palm ash as an alternative source for silica production. *MATEC Web of Conferences*, *78*, 01062. https://doi.org/10.1051/matecconf/20167801062

PASPI-Monitor. (2021). Oil palm plantation: An integral part of soil and water conservation. *Palm Oil Journal*, *2*(26), 439–443.

Pereira, S., Monteiro, A., Moutinho-Pereira, J., & Dinis, L. (2024). Silicon, an emergent strategy to lighten the effects of (A)biotic stresses on crops: A review. *Journal of Agronomy and Crop Science*, *210*(6). https://doi.org/10.1111/jac.12762

Pratiwi, W., Sugiharto, A., & Sugesty, S. (2018). The effect of pulping process variable and elemental chlorine free bleaching on the quality of oil palm trunk pulp. *Jurnal Selulosa*, *8*(02), 85–94. https://doi.org/10.25269/jsel.v8i02.218

Puppe, D., Kaczorek, D., Schaller, J., Barkusky, D., & Sommer, M. (2021). Crop straw recycling prevents anthropogenic desilication of agricultural soil-plant systems in the temperate zone – Results from a long-term field experiment in NE Germany. *Geoderma*, *403*, 115187. https://doi.org/10.1016/j.geoderma.2021.115187

Qurrohman, B. F. T., Suriadikusumah, A., Joy, B., & Sudirja, R. (2023). Spatial distribution of status silicon availability for plant and its effect to rice yield. *Sains Tanah - Journal of Soil Science and Agroclimatology*, *20*(1), 10. https://doi.org/10.20961/stjssa.v20i1.65862

Rahim, N. A., Harun, N. Y., Saeed, A. A. H., & Bilad, M. R. (2023). Green route synthesis of amorphous silica from oil palm decanter cake: From literature review to experiments. *Indonesian Journal of Science and Technology*, *8*(2), 141–156. https://doi.org/10.17509/ijost.v8i2.53724

Rahmat, F., Fen, Y. W., Anuar, M. F., Omar, N. A. S., Zaid, M. H. M., Matori, K. A., & Khaidir, R. E. M. (2021). Synthesis and characterization of ZnO-SIO_2 composite using oil palm empty fruit bunch as a potential silica source. *Molecules*, *26*(4), 1061. https://doi.org/10.3390/molecules26041061

Razak, N. A. A., Othman, N. H., Shayuti, M. S. M., Jumahat, A., Sapiai, N., & Lau, W. J. (2022). Agricultural and industrial waste-derived mesoporous silica nanoparticles: A review on chemical synthesis route. *Journal of Environmental Chemical Engineering*, *10*(2), 107322. https://doi.org/10.1016/j.jece.2022.107322

Rovani, S., Santos, J. J., Corio, P., & Fungaro, D. A. (2018). Highly pure silica nanoparticles with high adsorption capacity obtained from sugarcane waste ash. *ACS Omega*, *3*(3), 2618–2627. https://doi.org/10.1021/acsomega.8b00092

Samat, N. A. S. A., Jaman, U. Z. K., Saree, S., Mahmod, D. S. A., & Lai, J. C. H. (2021). Characteristics of calcined palm oil pastes for biosilica extraction as a function of calcination temperatures. *Journal of Applied Research and Technology*, *19*(1), 23–34. https://doi.org/10.22201/icat.24486736e.2021.19.1.1489

Samat, N. A. S. A., Zulkafly, S. A., Jaman, U. Z. K., Zauzi, N. S. A., Rahman, M. R., & Baini, R. (2018). Characteristics analysis of bio-based silica extracted from Sarawak palm oil waste. *International Journal of Engineering & Technology*, *7*(3.18), 94–96. https://doi.org/10.14419/ijet.v7i3.18.16685

Sarkar, J., Mridha, D., Sarkar, J., Orasugh, J. T., Gangopadhyay, B., Chattopadhyay, D., Roychowdhury, T., & Acharya, K. (2021). Synthesis of nanosilica from agricultural wastes and its multifaceted applications: A review. *Biocatalysis and Agricultural Biotechnology*, *37*, 102175. https://doi.org/10.1016/j.bcab.2021.102175

September, L. A., Kheswa, N., Seroka, N. S., & Khotseng, L. (2023). Green synthesis of silica and silicon from agricultural residue sugarcane bagasse ash – A mini review. *RSC Advances*, *13*(2), 1370–1380. https://doi.org/10.1039/d2ra07490g

Setiawan, W. K., & Chiang, K. (2021). Crop residues as potential sustainable precursors for developing silica materials: A review. *Waste* *and Biomass Valorization*, *12*(5), 2207–2236. https://doi.org/10.1007/s12649-020-01126-x

Setyawan, N., Hoerudin, N., & Yuliani, S. (2021). Synthesis of silica from rice husk by sol-gel method. *IOP Conference Series: Earth and Environmental Science*, *733*(1), 012149. https://doi.org/10.1088/1755-1315/733/1/012149

Sreekantan, S., Hassan, M., Murthe, S. S., & Seeni, A. (2020). Biocompatibility and cytotoxicity study of polydimethylsiloxane (PDMS) and palm oil fuel ash (POFA) sustainable super-hydrophobic coating for biomedical applications. *Polymers*, *12*(12), 3034. https://doi.org/10.3390/polym12123034

Steven, S., Restiawaty, E., & Bindar, Y. (2021). Routes for energy and bio-silica production from rice husk: A comprehensive review and emerging prospect. *Renewable and Sustainable Energy Reviews*, *149*, 111329. https://doi.org/10.1016/j.rser.2021.111329

Teixeira, L. B., De Moraes, E. G., Shinhe, G. P., Falk, G., & De Oliveira, A. P. N. (2021). Obtaining biogenic silica from sugarcane bagasse and leaf ash. *Waste and Biomass Valorization*, *12*(6), 3205–3221. https://doi.org/10.1007/s12649-020-01230-y

Tessema, B., Gonfa, G., Hailegiorgis, S. M., & Prabhu, S. V. (2023). An overview of current and prognostic trends on synthesis, characterization, and applications of biobased silica. *Advances in Materials Science and Engineering*, *2023*, 1–23. https://doi.org/10.1155/2023/4865273

Tréguer, P. J., Sutton, J. N., Brzezinski, M., Charette, M. A., Devries, T., Dutkiewicz, S., Ehlert, C., Hawkings, J., Leynaert, A., Liu, S. M., Monferrer, N. L., López-Acosta, M., Maldonado, M., Rahman, S., Ran, L., & Rouxel, O. (2021). Reviews and syntheses: The biogeochemical cycle of silicon in the modern ocean. *Biogeosciences*, *18*(4), 1269–1289. https://doi.org/10.5194/bg-18-1269-2021

Tubaña, B. S., & Heckman, J. R. (2015). Silicon in soils and plants. In F. A. Rodrigues, & L. E. Datnoff, (Eds.), *Silicon and plant diseases* (pp. 7–51). Springer. https://doi.org/10.1007/978-3-319-22930-0_2

United States Department of Agriculture (2023). *Palm Oil Explorer*. Foreign Agricultural Service USDA. Retrieved November 4, 2024 from https://ipad.fas.usda.gov/cropexplorer/cropview/commodityView.aspx?cropid=4243000

Usman, A. R., Abduljabbar, A., Vithanage, M., Ok, Y. S., Ahmad, M., Ahmad, M., Elfaki, J., Abdulazeem, S. S., & Al-Wabel, M. I. (2015). Biochar production from date palm waste: Charring temperature induced changes in composition and surface chemistry. *Journal of Analytical and Applied Pyrolysis*, *115*, 392–400. https://doi.org/10.1016/j.jaap.2015.08.016

Utama, P. S., Yamsaensung, R., & Sangwichien, C. (2018). Silica gel derived from palm oil mill fly ash. *Songklanakarin Journal of Science and Technology*, *40*, 121–126.

Utama, P. S., Yamsaengsung, R., & Sangwichien, C. (2019). Production and characterization of precipitated silica from palm oil mill fly ash using CO_2 impregnation and mechanical fragmentation. *Brazilian Journal of Chemical Engineering*, *36*(1), 523–530. https://doi.org/10.1590/0104-6632.20190361s20170458

Velmurugan, P., Shim, J., Lee, K., Cho, M., Lim, S., Seo, S., Cho, K., Bang, K., & Oh, B. (2015). Extraction, characterization, and catalytic potential of amorphous silica from corn cobs by sol-gel method. *Journal of Industrial and Engineering Chemistry*, *29*, 298–303. https://doi.org/10.1016/j.jiec.2015.04.009

Von Der Lühe, B., Bezler, K., Hughes, H. J., Greenshields, B., Tjoa, A., & Sauer, D. (2023). Oil-palm and rainforest phytoliths dissolve at different rates-with implications for silicon cycling after transformation of rainforest into oil-palm plantation. *Silicon*, *15*(3), 1347–1354. https://doi.org/10.1007/s12633-022-02066-y

Yadav, M., Dwibedi, V., Sharma, S., & George, N. (2022). Biogenic silica nanoparticles from agro-waste: Properties, mechanism of extraction and applications in environmental sustainability. *Journal of Environmental Chemical Engineering*, *10*(6), 108550. https://doi.org/10.1016/j.jece.2022.108550

Zarina, Y., Al Bakri, A. M. M., Kamarudin, H., Khairul Nizar, I., & Rafiza, A. R. (2013). Review on the various ash from palm oil waste as geopolymer material. *Reviews on Advanced Materials Science*, *34*, 37–43.

Zulfiqar, U., Subhani, T., & Husain, S. W. (2015). Towards tunable size of silica particles from rice husk. *Journal of Non-Crystalline Solids*, *429*, 61–69. https://doi.org/10.1016/j.jnoncrysol.2015.08.037

Journal of Oil Palm Research Vol. 38 (3) September 2026 p. 433–445
DOI: https://doi.org/10.21894/jopr.2025.0038

LOWERING THE COSTS OF BIO-HYDROGEN PRODUCTION FROM EMPTY FRUIT BUNCH (EFB) WITH SOLAR GASIFICATION – TECHNO-ECONOMIC AND THERMODYNAMIC ANALYSIS

ZHAO CHEN[1] and ZAIDI MOHD RIPIN[1*]

ABSTRACT

Hydrogen production from empty fruit bunches (EFBs) is proposed here using a gasification system powered by solar energy and biomass, generating bio-hydrogen through combined steam methane reforming, along with electricity using an organic Rankine cycle. For EFB input of 1,286 kg/hr, the hourly production is 28.5 kW of electricity and 36 kg of hydrogen. The overall design efficiency is 60.37%, and the equivalent energetic efficiency is 46.33%. Finally, an economic analysis is conducted, showing an 8-year payback period. The system's environmental friendliness is highlighted by the hydrogen production cost, which is as low as USD1.21/kg. Although the carbon dioxide (CO_2) emissions in this study are relatively high, the CO_2 from EFB does not increase the environmental concentration. Importantly, the hydrogen yield from EFB is relatively high at 23.83 H_2 g/kg feed.

Keywords: bio-fuels, bio-hydrogen, empty fruit bunches, energy system, exergy and energy analysis.

Received: 3 September 2024; **Accepted:** 8 May 2025; **Published online:** 23 July 2025.

INTRODUCTION

Malaysia is the second largest producer of palm oil (Yeng et al., 2024) utilising less than 17% of its total land area, supplies 47% of the world's palm oil (Abbasi et al., 2023). In 2022, just in one year, over a million tonnes of empty fruit bunches (EFBs) were discarded in Nigeria (Obada et al., 2023), and around 88 million tonnes in Malaysia (Rajakal et al., 2024). Under unfavourable decomposition conditions, EFB releases greenhouse gases such as nitrous oxide and methane, equivalent to emitting 0.23 t of carbon dioxide (CO_2)/t of EFB (Vela Garcia, 2021). Thus, just in Malaysia and Nigeria, EFB disposal annually results in approximately 20.47 million tonnes of CO_2 emissions, causing environmental pollution and resource wastage. The EFB can be looked at as a renewable energy source and can help to overcome the current reliance on fossil fuels (Song et al., 2022) which is clearly incompatible with the future requirements for green energy (Fan et al., 2024).

Hydrogen is a clean energy source that falls within the category of green energy sources (Yuksel et al., 2022). Two main sources of green hydrogen are water electrolysis and biomass gasification (Castro et al., 2022). The former requires renewable electricity to provide the necessary energy, while the latter offers a higher conversion efficiency and lower costs compared to traditional hydrogen production methods (Safarian et al., 2019). Biomass pyrolysis and biomass gasification are two primary methods for producing hydrogen from biomass, with the latter considered at present the most efficient and economically viable method (Nguyen et al., 2024). Hydrogen can be produced from EFB and other palm oil waste through various thermochemical and biochemical processes (Ruya et al., 2020). Additionally, other researchers have produced value-added fuels from

[1] School of Mechanical Engineering, Engineering Campus, Universiti Sains Malaysia, 14300 Nibong Tebal, Penang, Malaysia.

* *Corresponding author e-mail: mezaidi@usm.my*

the palm oil waste including methanol (Im-orb et al., 2020), bio-methanol and bio-dimethyl ether (Im-orb & Arpornwichanop, 2022), methane and electricity (Saritpongteeraka et al., 2022). It is clear that bio-hydrogen production from EFB is viable. Additionally, none of the models for solar biomass gasification mentioned above have considered EFB as the feedstock for gasification.

The use of solar energy can be divided into two main groups. They are solar photovoltaic and solar thermal energy. The process of solar thermal technology involves gathering sunlight and storing its energy as heat. A solar collector is the primary component of a solar thermal system. Generally speaking, a solar collector is a device that uses a specially coated and reinforced glass tubing to capture sunlight (Nirmala et al., 2022). Many researchers have explored the use of solar energy to convert various types of biomasses into energy, including yellow grease (Naveen et al., 2021), rice husks, beech wood and plastic waste (Naveen et al., 2023). Among all hydrogen production technologies, the cost of hydrogen produced via electrolysis is the highest. The cost of solar-powered electrolysis ranges from USD3.34 to USD17.30/kg, while wind-powered electrolysis ranges from USD3.56 to USD10.82/kg (Parkinson et al., 2019). In contrast, biomass-based hydrogen production costs range from USD1.48 to USD3.00/kg (Al-Qahtani et al., 2021), whereas hydrogen production from geothermal energy is the cheapest among green methods, ranging from USD1.08 to USD4.38/kg (Farhana et al., 2024). To address this cost disparity, this article proposes a solar-assisted EFB gasification system for hydrogen production, aiming to reduce the cost of biomass-based hydrogen production to a level comparable with coal-based hydrogen production.

Solar gasification involves the use of a hyperbolic reflector, which can produce temperatures of above 1,000°C (D. Xu, et al., 2023), which is adequate for biomass gasification temperature of 600°C–1,000°C (Abanades et al., 2021). Direct normal irradiation (DNI) is a key parameter for solar gasification. Studies on biomass solar gasification have achieved gasification temperatures under different DNI levels, including 850°C at 766 W/m^2 (Assareh et al., 2023), 800°C at 850 W/m^2 (Anvari et al., 2019), 1,073°C at 800 W/m^2 (Wang et al., 2019) and 877°C at 751 W/m^2 (Bai et al., 2019).

Even though the gasification temperatures reported above are high, the values of DNI reported above are higher than the mean value of DNI for Malaysia which is 600 W/m^2 (Mohammad et al., 2020). It is important that the representative value of DNI is used in the study of solar gasification in order to arrive at a realistic cost for bio-hydrogen production.

Table 1 compares the hydrogen production from EFB and related poly-generation systems in this study with those reported by other researchers. Although several studies have investigated EFB gasification for hydrogen production, most focus primarily on technical performance and lack comprehensive economic and thermodynamic analysis. Many studies only construct basic models without detailing energy sources, and few consider the combustion of EFB and palm oil shell (POS) as inputs. Detailed assessments of hydrogen production, as well as strategic and environmental analysis, are also rare. Furthermore, few studies examine the scalability and economic feasibility of these systems for practical industrial applications. This study fills these gaps by integrating techno-economic and thermodynamic analysis, offering a more comprehensive perspective on EFB-based hydrogen production.

In *Table 1*, abbreviations are used to streamline references to key areas of analysis: En stands for energy (focusing on the energy efficiency and output of systems); Ex represents exergy (evaluating the quality and utilisation of energy within the system); Ec denotes economic (assessing cost-effectiveness and financial viability); Env refers to environmental considerations (emphasising the system's impact on ecological sustainability) and SCWG stands for supercritical water gasification.

This study proposed a combined approach of solar energy gasification and biomass combustion gasification. Malaysia, in particular, has abundant solar energy due to its geographical location (Mohammad et al., 2020). To reduce the cost of hydrogen production or provide a low-cost alternative to coal gasification for hydrogen production, this article introduces a novel solar biomass EFB gasification system integrated with an organic rankine cycle (ORC) system for the production of hydrogen and electricity. Thermodynamic analysis of the system is first conducted to perform an exergy loss analysis. This is followed by an economic feasibility study by calculating the payback period of the system and its environmental costs by assessing the hydrogen output and CO_2 equivalent emissions.

MATERIALS AND METHODS

System Description

The solar gasification unit (SG), biomass combustion (BC), steam methane reforming (SMR) and ORC are the four main components of the unique design system, as shown in *Figure 1*.

In order to convert EFB biomass into syngas, the SG or BC units need solar energy as a heat source. Hydrogen is created in the SMR when steam reacts with syngas methane and carbon monoxide. Heat for the SMR is produced by burning unreacted

TABLE 1. THE COMPARISON OF EFB HYDROGEN PRODUCTION SYSTEM STUDIES

Source	Pro	System	Analysis				References
			En	Ex	Ec	Env	
Palm tree residues	H_2	Gasification	√	√			Kayişoğlu and Demirtaş (2023)
BC-EFB	H_2	SMR	√	√			Ruya et al. (2020)
EFB	H_2	SCWG					Vargas-Mira et al. (2019)
EFB	H_2	SMR					Sinaga et al. (2020)
EFB	H_2	SMR			√		Rahmi et al. (2019)
EFB	H_2	SMR	√	√			Laguna et al. (2018)
SG-BC	H_2	SMR	√	√	√	√	This study

Note: EFB - empty fruit bunch; BC - biomass combustion; SG - solar gasification; SMR - steam methane reforming; SCWG - supercritical water gasification; En - energy; Ex - exergy; Ec - economic; Env - environmental considerations.

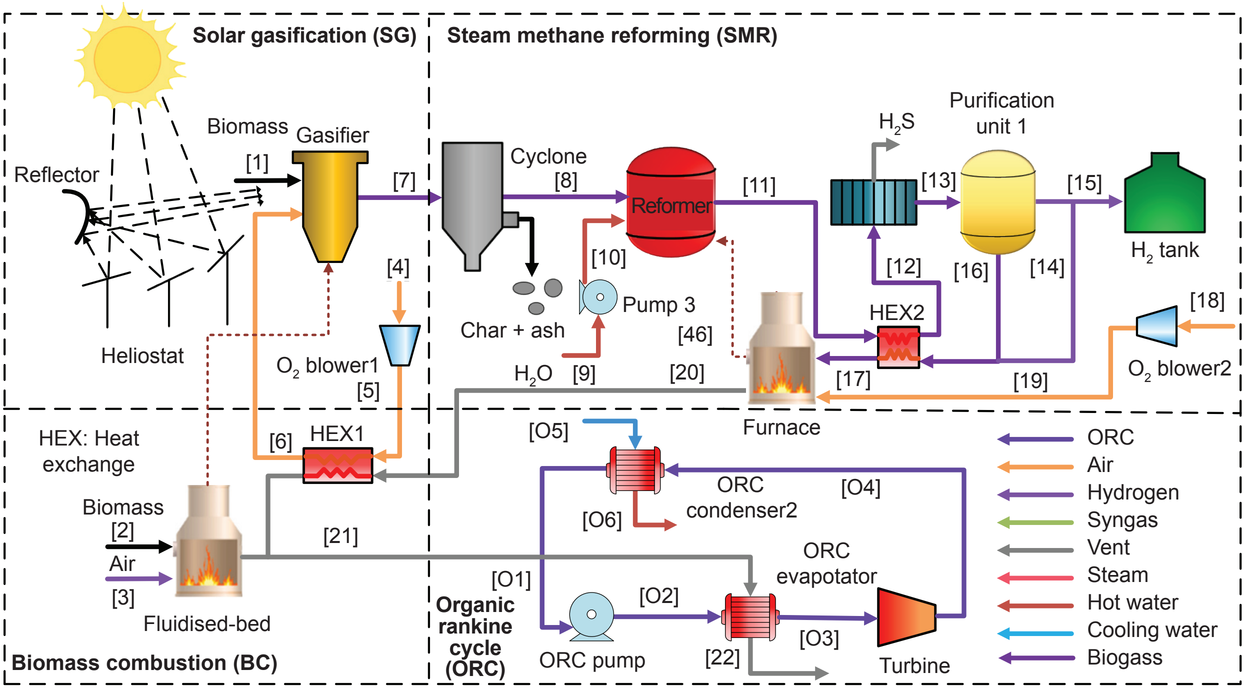

Figure 1. Integrated flowchart of the system.

carbon monoxide, methane and some unextracted hydrogen in a furnace. The ORC receives the leftover heat in order to generate power. After production, the hydrogen is stored for sale. The establishment of the entire model is based on the following assumptions: The reaction in the gasifier reduction zone achieves complete conversion with a 100% carbon conversion rate, where the biomass and the gasification agent are thoroughly mixed upon contact at a constant temperature (Zaman & Ghosh, 2021). The pyrolysis process of biomass is completed rapidly, and the volatile matter is evenly mixed with the gasification agent. Tar production is disregarded, as tar is considered an inert substance (Vikram et al., 2022). Nitrogen makes up 79% of the air and oxygen makes up 21%. The system operates in a steady state. The surrounding air is 25°C in temperature and 1 atm in pressure.

Analysis Methods

The specific proximate and elemental analysis parameters of the EFB (Ruya et al., 2020) are used in this study as listed in *Table 1*, and the lower heating value (LHV) is 19.06 MJ/kg (Huang et al., 2020). The mass input rate of EFB can be found in *Table 2*.

SG unit and BC. SG is the process of directly collecting and heating EFB using solar energy. The solar gasification system consists of two main components: The solar collection section and the biomass gasification section. The solar collection subsystem, including parabolic mirrors and a dish collector, concentrates solar radiation to generate high-temperature thermal energy. This energy, focused on the gasifier's opening, drives the gasification of EFB, converting biomass into combustible gas. The high-temperature thermal energy provides the necessary conditions for the gasification reaction of EFB at elevated temperatures. The directly acquired solar energy and absorbed solar energy are calculated using the formulas as shown in Equation (1) and (2) (Bai et al., 2019):

$$Q_{solar} = DNI \times A_{heliostat} * \eta_{heliostat} \quad (1)$$

$$Q_{solar,\ absorb} = Q_{solar} \times \eta_{attenuation} \times \eta_{reflectance} \times \eta_{receiver} \quad (2)$$

During the gasification process, the energy balance can be represented by the following equation as shown in Equation (3):

$$\sum_{i=p} (n_i(h^0_{T_a,i} + C_{p,i}(T_G - T_a))) = \sum_{i=r} (n_i (h^0_{T_a,i} + C_{p,i} (T_i - T_a))) + Q_{solar,\ absorb} + Q_{in} - Q_{inout} \quad (3)$$

The total enthalpy of the products is on the left side, and the first term on the right side is the enthalpy of the reactants. The last three terms represent the changes in heat. For detailed specifics, please refer to reference (Wang et al., 2019). The gasification temperature range for EFB is 750°C–1,000°C (Im-orb et al., 2020), and this study utilises a temperature of 800°C.

Given the intermittent nature of solar energy, this study adopts the combustion of EFB as an alternative gasification method. Under certain assumptions, the combustion products include only carbon dioxide (CO_2), carbon monoxide (CO), hydrogen gas (H_2), water (H_2O), methane (CH_4), nitrogen gas (N_2), oxygen gas (O_2) and the emissions of harmful gases from the exhaust were not considered (Muhtadin et al., 2020).

The SMR Process. During the SMR process, the primary reactions are as follows Equation (4) and (5). The specific mass and energy balance equations are shown in Equation (6) to (8). For the SMR process, where the temperature range is 700°C–900°C, this study sets it at 800°C. Additionally, the CH_4 conversion rate is set to 90% (Kumar et al., 2024).

$$CH_4 + H_2O \leftrightarrow CO + 3H_2 \quad (4)$$

$$CO + H_2O \leftrightarrow CO_2 + H_2 \quad (5)$$

$$\frac{dc_i}{dt} = R_i \quad (6)$$

$$V_r C_p \frac{dT}{dt} = Q + Q_{ext} + \frac{dp}{dt} Vr \quad (7)$$

$$Q = -V_r \sum_j H_j r_j \quad (8)$$

where, c_i represents the molar flow rate of the species, V_r represents the volume of the reactor, C_p is the molar heat capacity of the species, H_j is the heat of the reaction and r_j is the reaction rate.

The ORC Process. To create the thermodynamic model of ORC, it is necessary to consider two governing equations: One for mass conservation and one for energy conservation. The mass balance, concentration balance and energy balance equations (Kholghi et al., 2019) can be expressed as follows [Equation (9) and (10)]. The symbol " represents the mass flow.

$$\sum_{in} (\dot{m}x)_{in} = \sum_{out} (\dot{m}x)_{out} \quad (9)$$

$$\sum \dot{Q} + \sum_{in} (\dot{m}h)_{in} = \sum_{out} (\dot{m}h)_{out} + \sum \dot{W} \quad (10)$$

Exergy. One important metric in this study that is impacted by thermodynamic irreversibility is exergy reduction (Talbi & Agnew, 2000). The total exergy consists of four components: Physical, chemical, kinetic and potential exergy. However, the latter two types of exergy can be neglected in the calculations, so only physical and chemical exergies need to be considered (Ahmadi et al., 2013). A system's total heat release, computed as Equation (11), is the result of adding the system's chemical and physical heat releases while ignoring the other heat release (Misra et al., 2006).

$$\dot{E} = m(ex_{ph} + ex_{ch}) \quad (11)$$

The mole flow is represented by the letter "m". The quantities h and s stand for specific enthalpy and entropy, respectively. Chemical exergy can be calculated using standard chemical exergy (Farooqui et al., 2019). Potential and kinetic exergy are not taken into consideration while discussing the idea of chemical exergy (Oh et al., 2023). Equation designated as Equation (11) are used in the computation of exergy. Previous studies have shown that in the ORC system, the chemical exergy is very minimal and only the physical exergy has to be estimated (Cantone, 2019).

Several components are included within the system, such as fuel, product and exergy destruction. For the calculation of exergy efficiency (η) and exergy destruction ($\dot{E}_{D,\ i}$) for each component, Equation (12) is employed.

$$\dot{E}_{D,\ i} = \sum \dot{E}_{in,\ i} - \sum \dot{E}_{out,\ i} \quad (12)$$

The efficiency formulae for the system are listed below in Equation (13). The exergy calculation formula for biomass EFB is shown in Equation (14) (Huang et al., 2020). The system all design parameters are in *Table 2*.

$$\eta = \frac{LHV_{H2} \times \dot{m}_{H2} + W_{e,\,orc}}{\dot{E}_{bio}} \quad (13)$$

$$E_{x_{Bio}} = \dot{m}_{Bio} LHV_{Bio} (2.0144 + 0.0342 \frac{w_H}{w_C} - 1.2536 \frac{w_O}{w_C}) \quad (14)$$

Environment. In this article, the reduction of greenhouse gas (GHG) emissions serves as the primary environmental evaluation index. The bio-hydrogen process involved in phosphoric acid fuel cell (PAFC) operation primarily emits CO and CO_2, with CO being converted into equivalent CO_2 for calculation purposes (U.S. Environmental Protection Agency, 2024). The penalty cost associated with CO_2 emissions is USD24/t (You et al., 2020). This penalty cost is considered an environmental expense and will be incorporated into the overall system cost (Wu et al., 2023).

Economic Valuation. A technique used in the economic analysis of the hybrid system involves the categorisation of the costs presented in *Table 3*. The economics of the system over its lifespan were assessed using net present values (NPV). The NPV included in this study are total project cost, total overnight cost, total as-spent cost, bare erected cost, engineering, procurement and construction cost (Abbasi et al., 2023). *Table 4* provides a summary of the parameters used to evaluate the economic analysis.

RESULTS AND DISCUSSION

Exergy Performance

The material and energy balance data show that, during the SG operation, the process's total input exergy is 2,556.81 kW (*Figure 2*). This comprises 1,070.71 kW from BC and solar exergy, and 1,470.10 kW from EFB. At 500.38 kW, or 36.54% of the total exergy loss, the gasification process shows the largest exergy loss. With an exergy loss of 420.23 kW, the cyclone comes next, making up 30.69% of the overall loss. At 177.9 kW, or 12.75% of the total exergy loss, the furnace exhibits the third-highest exergy loss. The ORC uses furnace waste heat while burning biomass, which raises the ORC's exergy loss from 82 to 305 kW. Within the ORC, the gasification, cyclone and ORC have the most exergy losses (31.42%, 26.39% and 19.15%, respectively).

TABLE 2. MAIN OPERATING PARAMETERS AND SYSTEM CONDITIONS

Parameter	Value	Unit
Ambient temperature	25	°C
DNI	600	w/m^2
Solar collection efficiency	44.00	%
Reflectance efficiency	90.00	%
Attenuation efficiency	90.70	%
Combustion efficiency	57.00	%
Heat exchanger efficiency	80.00	%
Pump efficiency	95.00	%
Land area	4,727	m^2
Fluidised bed surfance	10	m^2
EFB gasification	548	kg/hr
EFB combustion	925	kg/hr
Pressure	1	Atm
Gasification temperature	800	°C
Steam to feed ratio	6	
CH_4 conversion	74.00	%
Oxygen to feed ratio	0.25	
SMR operating temperature	800	°C
Chilled water inlet and outlet	7/15	°C
DHW water inlet and outlet	25/60	°C
Voltage	0.67	V
Current density	125	mA/cm^2
Proximate analysis (V:FC:A:M)	69:18.5:7:5.5	
Elemental analysis (C:H:O:N:S)	42.33:5.28:50.85:1.46:0.08	
LHV	19.06	MJ/kg

Note: DNI - direct normal irradiation; DHW - domestic hot water; LHV - lower heating value; EFB - empty fruit bunches; CH_4 - methane; SMR - steam methane reforming.

TABLE 3. ORIGINAL EQUIPMENT COST AND COST CONVERSION

Component	Equation	Unit of parameter	Reference
Land cost	88 × Area	A (m^2)	Seo et al. (2022)
Heliostat	75 × Area	A (m^2)	Seo et al. (2022)
Gasifier	$1{,}600 \times (\dot{m}_{Biomass})^{0.67}$	kg/s	Habibollahzade et al. (2019)
Tower height	USD3M/86.5m	m	Bai et al. (2019)
Fluidised bed	USD4.51M/1,748m^2	Surfance (m^2)	Stenberg et al. (2020)
Absorber	$52.84 \times \dot{W}_{Absorber}$	$\dot{W}_{Absorber}$ (kW)	Cormos (2014)
H_2 tank	$4.28 \times m_{H2}$	m_{H2} (Kg)	Le et al. (2017)
Reformer	$76.29 \times \dot{W}_{Reformer}$	$\dot{W}_{Reformer}$ (kW)	Cormos (2014)
Furance	$1{,}479 \times (\dot{Q}_{Furance})^{0.75}$	$\dot{Q}_{Furance}$ (kW)	Wu et al. (2023)
Purification	$1{,}785 \times \dot{Q}_{Puri}$	$\dot{Q}_{Puri}$ (kW)	Wu et al. (2023)
Blower	$91{,}562 \times (\dot{W}_{Blower}/445)^{0.67}$	$\dot{W}_{Blower}$ (kW)	Sammes et al. (2004)
Pump	$16{,}800 \times (\dot{W}_{Pump}/200)^{0.67}$	$\dot{W}_{Pump}$ (kW)	Whitaker (1998)
Heat exchange	$235 \times (\dot{Q}_{HEX})^{0.75}$	$\dot{Q}_{HEX}$ (kW)	M. Xu et al. (2023)
ORC condenser	$597 \times (\dot{Q}_{Con})^{0.68}$	$\dot{Q}_{Con}$ (kW)	Desai and Bandyopadhyay (2015)
Turbine	$3{,}143.7 + 217.423 \times (\dot{V}_{Tur})^{0.68}$	$\dot{V}_{Tur}$ (1/sec)	Astolfi (2015)
ORC pump	$200 \times (\dot{W}_{Pump})^{0.65}$	$\dot{W}_{Pump}$	Zhang et al. (2019)
ORC evaporator	$209.14 \times (A_{Eva})^{0.85}$	A_{Eva}	Zhang et al. (2019)

Note: H_2 - hydrogen; ORC - organic rankine cycle.

TABLE 4. ESSENTIAL ECONOMIC FACTORS AND PRESUMPTIONS

Component	Equation	Unit
Interest (discount) rate (i)	4.35	%
Owner's cost	5.00	%
Construction	2	yr
Insurance cost	1.00	%
Contingency	0.02	%
OPEX		
O_2 prices	0.02	USD/kg
Hydrogen prices	2.5	USD/kg
CO_2 prices	0.024	USD/kg
EFB prices	0.00	USD/Nm^3
Depreciation cost of equipment	1.00	%
Cost of installation	5.00	%
Economic		
Average inflation rate	2.00	%
System lifetime	20	yr
SG (annual plant operating hours)	3,000	hr/yr
EFB (combustion Annual plant operating hours)	5,000	hr/yr
Payback time	8	yr

Note: O_2 - oxygen; CO_2 - carbon dioxide; EFB - empty fruit bunch; SG - solar gasification.

Economic Performance

Figure 3 presents a detailed study of the NPV parameters for the system, using an EFB cost of USD0.00/t (Reeb et al., 2014), an electricity price of USD0.15/kWh (GlobalPetrolPrices.com, 2023), and a hydrogen price of USD2.50/kg (Ríos et al., 2024). Given that EFB is the primary energy input and hydrogen makes up the bulk of the energy output relative to electricity, the analysis focuses on how changes in the prices of EFB and hydrogen affect the net present value. With a hydrogen selling price of around USD2.10/kg and an EFB purchasing price of USD0.00/t, the system can pay for itself in eight years under current market circumstances. The payback period is still within eight years despite market fluctuations, where the price of EFB climbs to USD15.00/t and the price of hydrogen sold increases to about USD2.60/kg, as shown by the junction locations of the vertical lines in *Figure 3*'s subplots.

Figure 4 presents a sensitivity analysis of the NPV in the eighth year with respect to the prices of EFB, hydrogen and electricity. In this figure, deep blue represents lower or even negative NPV values, indicating that the project may not be profitable under these price combinations. In contrast, red indicates higher NPV values, suggesting greater profitability under favourable conditions. It can be observed that in the eighth year, there are numerous scenarios where NPV > 0, showing that various combinations of EFB and product prices result in profitability. This demonstrates a degree of economic resilience within the project.

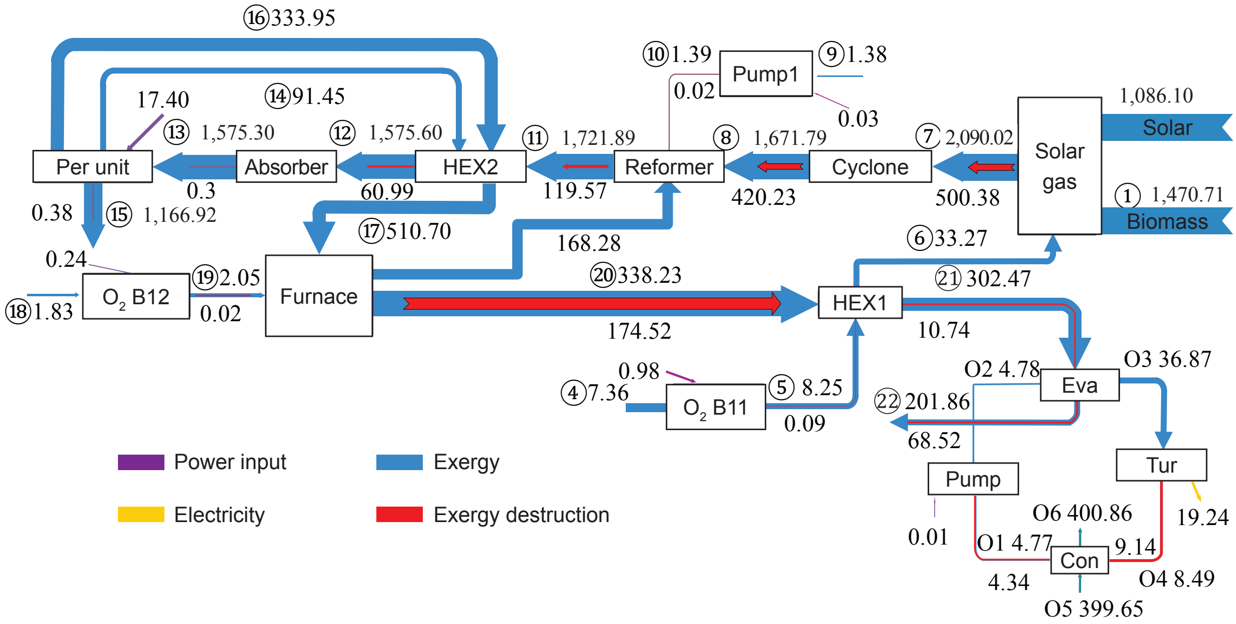

Figure 2. Sankey diagram of exergy flow.

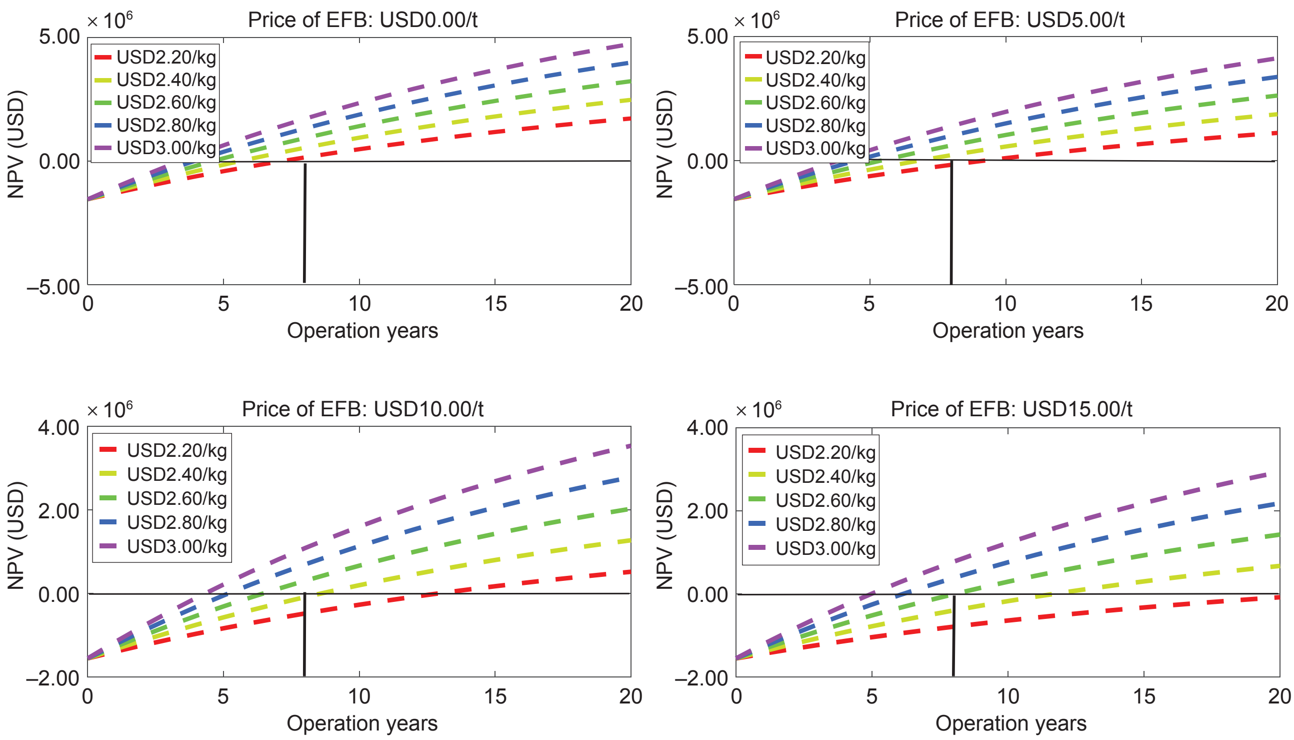

Figure 3. Net present values (NPV) analysis.

Environment Analysis

Table 5 shows that the hydrogen production efficiency of EFB is higher than that of general biomass and fossil fuels (Al-Qahtani et al., 2021), reaching 23.83 H_2 g/kg feed. However, its CO_2 emissions are lower than those of general biomass gasification, which are 32.84 kg CO_2/kg H_2, but higher than those of fossil fuels, at 25.65 kg CO_2/kg H_2, as well as hydrogen production via wind and solar-powered electrolysis (Parkinson et al., 2019). The reason is that EFB is not only gasified to produce hydrogen but also burned for heating when there is no sunlight. However, the CO_2 emitted from biomass is considered not to increase the atmospheric CO_2 concentration (Kemper, 2015), making it environmental-friendly.

TABLE 5. COMPARED WITH OTHER TECHNO-ECONOMIC STUDIES

Technologies	H_2 yield (H_2 g/kg feed)	CO_2 emission (kg CO_2/kg H_2)
Fossil-based SMR	297.00	9.26
Coal gasification	118.00	22.00
Biomass gasification	27.00	32.84
Electrolysis wind	-	1.34
Electrolysis solar	-	4.47
This study	23.83	25.65

Note: H_2 - hydrogen gas; CO_2 - carbon dioxide; SMR - steam methane reforming

Influences of DNI in Work Conditions

The DNI ranges from 500 to 50 W/m², based on real measurements in Seri Iskandar and other cities (Mohammad et al., 2020). *Figure 5* illustrates the system's energy inputs and outputs. From January to July, the system's hydrogen and electricity output meet the expected results. However, excess solar thermal energy occurs when the DNI surpasses the design parameter of 600 W/m² due to capacity limitations. From August to December, due to the rainy season, the DNI is below the design standard, resulting in reduced output. The variation in DNI throughout the year is attributed to seasonal changes in Malaysia: January to July (dry season) contribute nearly 63% of the total DNI, while August-December (rainy season) contribute 37%.

Compare Comparison and System Efficiency

Figure 6 compares the hydrogen production costs of various technologies. The average hydrogen cost from this study is significantly lower than that of other technologies, reaching the levels of coal (USD0.86–USD1.89/kg) and geothermal (USD1.08–USD4.38/kg), indicating that the system is more cost-effective. Specifically, the hydrogen cost in this study is around USD1.21–USD1.42/kg, which on average is lower than all other listed technologies, including solar, biomass, wind, grid, geothermal, nuclear, natural gas and coal (Farhana et al., 2024). This demonstrates the substantial economic advantage of the system evaluated in this research.

The overall energy and exergy efficiencies of the developed system are compared with other solar and biomass-based energy systems found in the literature. As shown in *Table 6*, the present system achieves higher energy and exergy efficiencies compared to biomass-based systems that produce electricity as the useful output energy and exergy efficiencies of 60.37% and 46.33%, respectively, by utilising waste heat for additional energy production.

Other studies have developed multigeneration systems that utilise both solar and biomass energy resources, but they did not consider EFB biomass for producing these commodities, nor did they evaluate the systems from the perspectives of exergy efficiency and economic analysis simultaneously. Therefore, the present study provides important results associated with the use of EFB biomass in combination with solar energy.

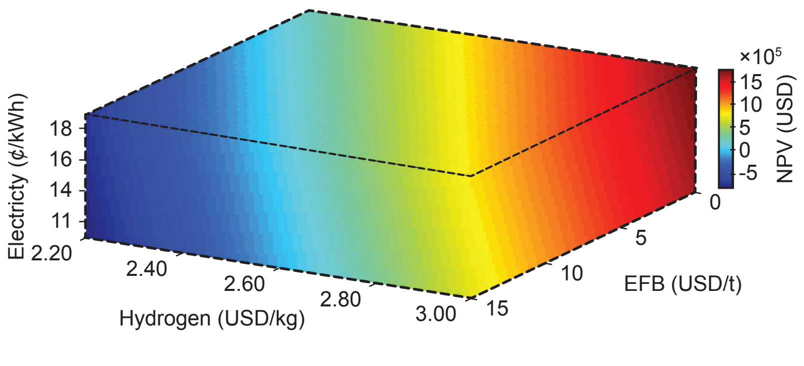

Figure 4. Sensitivity analysis of net present value (NPV) on empty fruit bunch (EFB) price and productions in the eighth year.

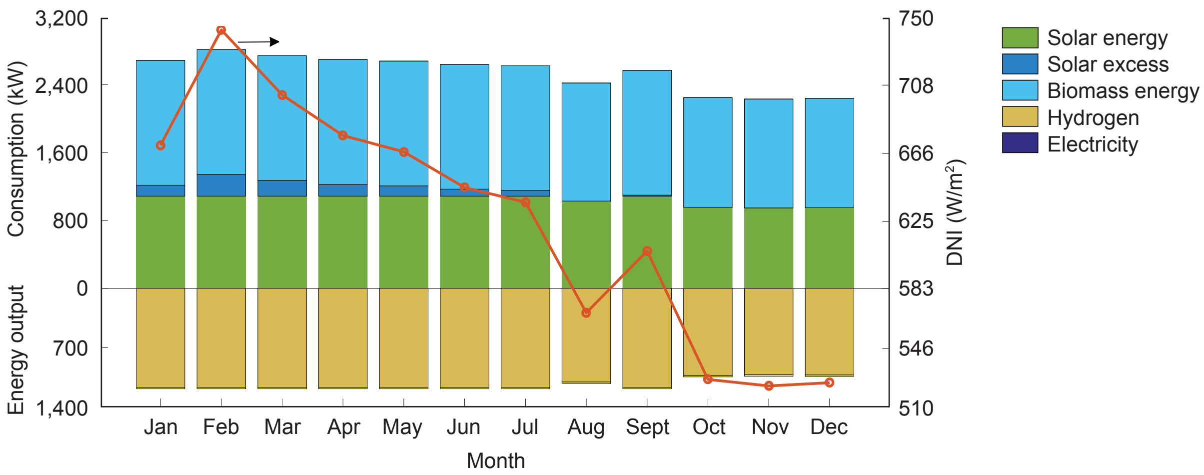

Figure 5. Input and output variations with direct normal irradiation (DNI) in months.

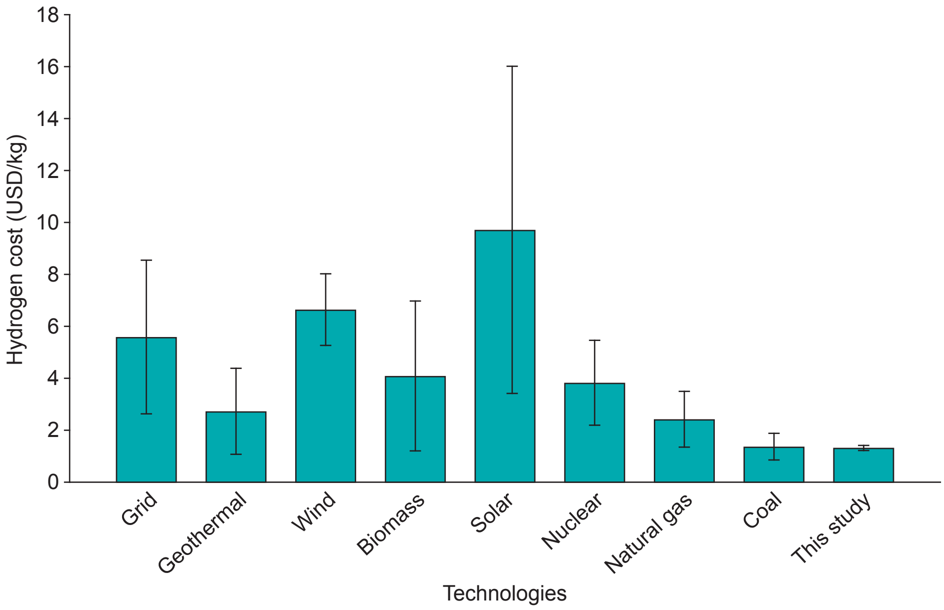

Figure 6. Comparison chart of the hydrogen cost of production from various sources.

TABLE 6. COMPARISON OF THE STUDY WITH OTHER SYSTEMS

Input	Output	Energy efficiency	Exergy efficiency	Reference
Oil palm shell	Hydrogren	19	22	Cohce et al. (2011)
Oil palm shell and EFB	Hydrogren	47.5–49.0	9.0–30.0	Ruya et al. (2020)
Solar and beech, charcoal, sewage sludge and fluff	Hydrogen	14.14–27.29	10.43–27.29	Kalinci et al. (2013)
Solar and coal	Electricity, hydrogen	49.84	4.97	Xue et al. (2023)
This study	Hydrogen electricity	60.37	46.33	This study

CONCLUSION

This study developed an innovative energy system that uses EFB biomass to produce hydrogen and electricity. The overall energy efficiency of the system is evaluated at 60.37%, with an exergy efficiency of 46.33%. A comparison of CO_2 equivalent emissions with other biomass-based hydrogen production systems shows that this system emits 25.65 kg CO_2/kg H_2, which is lower than typical biomass systems. Additionally, economic analysis reveals that the system can achieve a payback period of eight years and demonstrates economic resilience. The study further highlights the system's environmental sustainability and economic viability, particularly given its relatively low hydrogen production cost, ranging from USD1.21 to USD1.42/kg, which brings the cost of biomass-based hydrogen production on par with that of coal gasification.

ACKNOWLEDGEMENT

The authors sincerely thank to Universiti Sains Malaysia for the support and help.

REFERENCES

Abanades, S., Rodat, S., & Boujjat, H. (2021). Solar thermochemical green fuels production: A review of biomass pyro-gasification, solar reactor concepts and modelling methods. *Energies*, *14*(5), 1494. https://doi.org/10.3390/en14051494

Abbasi, I. A., Ashari, H., & Yusuf, I. (2023). System dynamics modelling: Integrating empty fruit bunch biomass logistics to reduce GHG emissions. *Resources*, *12*(4), 53. https://doi.org/10.3390/resources12040053

Ahmadi, P., Dincer, I., & Rosen, M. A. (2013). Development and assessment of an integrated biomass-based multi-generation energy system. *Energy, 56*, 155–166. https://doi.org/10.1016/j.energy.2013.04.024

Al-Qahtani, A., Parkinson, B., Hellgardt, K., Shah, N., & Guillen-Gosalbez, G. (2021). Uncovering the true cost of hydrogen production routes using life cycle monetisation. *Applied Energy*, *281*, 115958. https://doi.org/10.1016/j.apenergy.2020.115958

Anvari, S., Khalilarya, S., & Zare, V. (2019). Power generation enhancement in a biomass-based combined cycle using solar energy: Thermodynamic and environmental analysis. *Applied Thermal Engineering*, *153*, 128–141. https://doi.org/10.1016/j.applthermaleng.2019.02.112

Assareh, E., Agarwal, N., Paul, M. C., Ahmadi, P., Ghodrat, M., & Lee, M. (2023). Investigation and development of a novel solar-biomass integrated energy system for clean electricity and liquid hydrogen production. *Thermal Science and Engineering Progress*, *42*, 101925. https://doi.org/10.1016/j.tsep.2023.101925

Astolfi, M. (2015). Techno-economic optimization of low temperature CSP systems based on ORC with screw expanders. *Energy Procedia*, *69*, 1100–1112. https://doi.org/10.1016/j.egypro.2015.03.220

Bai, Z., Liu, Q., Gong, L., & Lei, J. (2019). Investigation of a solar-biomass gasification system with the production of methanol and electricity: Thermodynamic, economic and off-design operation. *Applied Energy*, *243*, 91–101. https://doi.org/10.1016/j.apenergy.2019.03.132

Cantone, D. (2019). *Energy, exergy and exergo-economic analysis of an ORC biomass cogeneration system integrated with an hybrid solar thermal solution*. (Doctoral dissertation) Politecnico di Torino.

Castro, J., Leaver, J., & Pang, S. (2022). Simulation and techno-economic assessment of hydrogen production from biomass gasification-based processes: A review. *Energies*, *15*(22), 8455. https://doi.org/10.3390/en15228455

Cohce, M. K., Dincer, I., & Rosen, M. A. (2011). Energy and exergy analyses of a biomass-based hydrogen production system. *Bioresource Technology, 102*(18), 8466–8474. https://doi.org/10.1016/j.biortech.2011.06.020

Cormos, C. C. (2014). Economic evaluations of coal-based combustion and gasification power plants with post-combustion CO_2 capture using calcium looping cycle. *Energy*, *78*, 665–673. https://doi.org/10.1016/j.energy.2014.10.054

Desai, N. B., & Bandyopadhyay, S. (2015). Optimization of concentrating solar thermal power plant based on parabolic trough collector. *Journal of Cleaner Production*, *89*, 262–271. https://doi.org/10.1016/j.jclepro.2014.10.097

Fan, R., Li, Z. Q., Zhang, H. M., & Tao, W. Q. (2024). Analysis of a combined heating and power system based on high-temperature proton exchange membrane fuel cell and steam methane reforming: From energy, exergy and economic point of views. *Applied Thermal Engineering, 247*, 123075. https://doi.org/10.1016/j.applthermaleng.2024.123075

Farhana, K., Mahamude, A. S. F., & Kadirgama, K. (2024). Comparing hydrogen fuel cost of production from various sources – A competitive analysis. *Energy Conversion and Management, 302*, 118088. https://doi.org/10.1016/j.enconman.2024.118088

Farooqui, A., Di Tomaso, F., Bose, A., Ferrero, D., Llorca, J., & Santarelli, M. (2019). Techno-economic and exergy analysis of polygeneration plant for power and DME production with the integration of chemical looping CO_2/H_2O splitting. *Energy Conversion and Management, 186*, 200–219. https://doi.org/10.1016/j.enconman.2019.02.043

GlobalPetrolPrices.com (2023). *Electricity prices around the world*. Retrieved December, 2023, from https://www.globalpetrolprices.com/electricity_prices/

Habibollahzade, A., Gholamian, E., & Behzadi, A. (2019). Multi-objective optimization and comparative performance analysis of hybrid biomass-based solid oxide fuel cell/solid oxide electrolyzer cell/gas turbine using different gasification agents. *Applied Energy, 233-234*, 985–1002. https://doi.org/10.1016/j.apenergy.2018.10.075

Huang, W., Zheng, D., Chen, X., Shi, L., Dai, X., Chen, Y., & Jing, X. (2020). Standard thermodynamic properties for the energy grade evaluation of fossil fuels and renewable fuels. *Renewable Energy*, *147*, 2160–2170. https://doi.org/10.1016/j.renene.2019.09.127

Im-orb, K., & Arpornwichanop, A. (2022). Comparative techno-economic assessment of bio-methanol and bio-DME production from oil palm residue. *Energy Conversion and Management, 258*, 115511. https://doi.org/10.1016/j.enconman.2022.115511

Im-orb, K., Phan, A. N., & Arpornwichanop, A. (2020). Bio-methanol production from oil palm residues: A thermodynamic analysis. *Energy Conversion and Management, 226*, 113493. https://doi.org/10.1016/j.enconman.2020.113493

Kalinci, Y., Hepbasli, A., & Dincer, I. (2013). Performance assessment of hydrogen production from a solar-assisted biomass gasification system. *International Journal of Hydrogen Energy, 38*(14), 6120–6129. https://doi.org/10.1016/j.ijhydene.2013.01.109

Kayi̇şoğlu, B., & Demi̇rtaş, G. (2023). Energy and exergy analysis of palm tree pruning residues gasification. *Journal of Agricultural Sciences*, *29*(1), 122–129. https://doi.org/10.15832/ankutbd.818623

Kemper, J. (2015). Biomass and carbon dioxide capture and storage: A review. *International Journal of Greenhouse Gas Control*, *40*, 401–430. https://doi.org/10.1016/j.ijggc.2015.06.012

Kholghi, S. A., & Mahmoudi, S. M. S. (2019). Energy and exergy analysis of a modified absorption cycle: A comparative study. *Sustainable Energy Technologies and Assessments*, *32*, 19–28. https://doi.org/10.1016/j.seta.2019.01.002

Kumar, R., Kumar, A., & Pal, A. (2024). Simulation modelling of hydrogen production from steam reforming of methane and biogas. *Fuel*, *362*, 130742. https://doi.org/10.1016/j.fuel.2023.130742

Laguna, L., Castro, M., Cassiani, D., Leon-Pulido, J., & Gonzalez-Delgado, A. (2018). Computer-Aided exergy evaluation of direct empty fruit bunches (EFB) gasification and PSA technology for hydrogen production. *Indian Journal of Science and Technology*, *11*(14), 1–8. https://doi.org/10.17485/ijst/2018/v11i14/121767

Le Duigou, A., Bader, A. G., Lanoix, J. C., & Nadau, L. (2017). Relevance and costs of large scale underground hydrogen storage in France. *International Journal of Hydrogen Energy*, *42*(36), 22987–23003. https://doi.org/10.1016/j.ijhydene.2017.06.239

Misra, R. D., Sahoo, P. K., & Gupta, A. (2006). Thermoeconomic evaluation and optimization of an aqua-ammonia vapour-absorption refrigeration system. *International Journal of Refrigeration*, *29*(1), 47–59. https://doi.org/10.1016/j.ijrefrig.2005.05.015

Mohammad, S. T., Al-Kayiem, H. H., Aurybi, M. A., & Khlief, A. K. (2020). Measurement of global and direct normal solar energy radiation in Seri Iskandar and comparison with other cities of Malaysia. *Case Studies in Thermal Engineering*, *18*, 100591. https://doi.org/10.1016/j.csite.2020.100591

Muhtadin, M., Erdiwansyah, E., Mahidin, M., Faisal, M., Mahyudin, M., Hamdani, H., Khairil, K., & Mel, M. (2020). Investigation of biomass combustion and conceptual design of the fluidized-bed. *Journal of Advanced Research in Fluid Mechanics and Thermal Sciences, 74*(1), 81–97. https://doi.org/10.37934/arfmts.74.1.8197

Naveen, S., Aravind, S., Yamini, B., Vasudhareni, R., Gopinath, K. P., Arun, J., & Pugazhendhi, A. (2023). A review on solar energy intensified biomass valorization and value-added products production: Practicability, challenges, techno economic and lifecycle assessment. *Journal of Cleaner Production*, *405*, 137028. https://doi.org/10.1016/j.jclepro.2023.137028

Naveen, S., Gopinath, K. P., Malolan, R., Jayaraman, R. S., Aakriti, K., & Arun, J. (2021). A solar reactor for bio-diesel production from Pongamia oil: Studies on transesterfication process parameters and energy efficiency. *Chinese Journal of Chemical Engineering*, *40*, 218–224. https://doi.org/10.1016/j.cjche.2020.10.010

Nirmala, N., Subathra, M., Shyam, S., Dawn, S. S., Gopinath, K. P., & Arun, J. (2022). Hydrothermal gasification of biomass for hydrogen production: Advances, challenges, and prospects. *Innovations in Thermochemical*

Technologies for Biofuel Processing, 259–273. https://doi.org/10.1016/B978-0-323-85586-0.00011-1

Nguyen, V. G., Nguyen-Thi, T. X., Nguyen, P. Q. P., Tran, V. D., Ağbulut, Ü., Nguyen, L. H., Balasubramanian, D., Tarelko, W., Bandh, S. A., & Pham, N. D. K. (2024). Recent advances in hydrogen production from biomass waste with a focus on pyrolysis and gasification. *International Journal of Hydrogen Energy*, *54*, 127–160. https://doi.org/10.1016/j.ijhydene.2023.05.049

Obada, D. O., Kekung, M. O., Levonyan, T., & Norval, G. W. (2023). Palm oil mill derived empty palm fruit bunches as a feed stock for renewable energy applications in Nigeria: A review. *Bioresource Technology Reports*, *24*, 101666. https://doi.org/10.1016/j.biteb.2023.101666

Oh, S., Kim, T., Kim, S., & Kang, S. (2023). Energetic, exergetic, economic, and exergoeconomic analysis of a phosphoric acid fuel cell-organic rankine cycle hybrid system. *Energy Conversion and Management*, *284*, 116993. https://doi.org/10.1016/j.enconman.2023.116993

Parkinson, B., Balcombe, P., Speirs, J. F., Hawkes, A. D., & Hellgardt, K. (2019). Levelized cost of CO_2 mitigation from hydrogen production routes. *Energy & Environmental Science*, *12*(1), 19–40. https://doi.org/10.1039/c8ee02079e

Rahmi, M. S., Taufiq, B. N., Indah, R., Syahputri, K., Mangara, M. T., & Wandika, A. S. (2019). Economic feasibility analysis of hydrogen production from raw materials of oil palm empty fruit bunches. *Journal of Physics Conference Series*, *1230*(1), 012052. https://doi.org/10.1088/1742-6596/1230/1/012052

Rajakal, J. P., Ng, F. Y., Zulkifli, A., How, B. S., Sunarso, J., Ng, D. K., & Andiappan, V. (2024). Analysis of current state, gaps, and opportunities for technologies in the Malaysian oil palm estates and palm oil mills towards net-zero emissions. *Heliyon*, *10*(10), e30768. https://doi.org/10.1016/j.heliyon.2024.e30768

Reeb, C. W., Hays, T., Venditti, R. A., Gonzalez, R., & Kelley, S. (2014). Supply chain analysis, delivered cost, and life cycle assessment of oil palm empty fruit bunch biomass for green chemical production in Malaysia. *BioResources*, *9*(3), 5385–5416. https://doi.org/10.15376/biores.9.3.5385-5416

Ruya, P. M., Lim, S. S., Purwadi, R., & Zunita, M. (2020). Sustainable hydrogen production from oil palm derived wastes through autothermal operation of supercritical water gasification system. *Energy*, *208*, 118280. https://doi.org/10.1016/j.energy.2020.118280

Ríos, C., Molina, P., De León, C. M., & Brey, J. J. (2024). Simulation of the optimal plant size to produce renewable hydrogen based on the available electricity. *International Journal of Hydrogen Energy*, *52*, 1325–1337. https://doi.org/10.1016/j.ijhydene.2023.08.306

Safarian, S., Unnþórsson, R., & Richter, C. (2019). A review of biomass gasification modelling. *Renewable and Sustainable Energy Reviews*, *110*, 378–391. https://doi.org/10.1016/j.rser.2019.05.003

Sammes, N., Bove, R., & Stahl, K. (2004). Phosphoric acid fuel cells: Fundamentals and applications. *Current Opinion in Solid State and Materials Science*, *8*(5), 372–378. https://doi.org/10.1016/j.cossms.2005.01.001

Saritpongteeraka, K., Natisupacheevin, K., Tan, C., Rehman, S., Charnnok, B., Vaurs, L. P., Leu, S., & Chaiprapat, S. (2022). Comparative assessment between hydrothermal treatment and anaerobic digestion as fuel pretreatment for industrial conversion of oil palm empty fruit bunch to methane and electricity – A preparation study to full scale. *Fuel*, *310*, 122479. https://doi.org/10.1016/j.fuel.2021.122479

Seo, S. B., Go, E. S., Ling, J. L. J., & Lee, S. H. (2022). Techno-economic assessment of a solar-assisted biomass gasification process. *Renewable Energy*, *193*, 23–31. https://doi.org/10.1016/j.renene.2022.05.033

Sinaga, F. T. H., Napitupulu, F. H., & Nur, T. B. (2020). Hydrogen gas production simulation utilizing empty fruit bunch of oil palm pyrolysis unit by steam methane reforming process. *Journal of Physics Conference Series*, *1566*(1), 012125. https://doi.org/10.1088/1742-6596/1566/1/012125

Song, H., Liu, Y., Bian, H., Shen, M., & Lin, X. (2022). Energy, environment, and economic analyses on a novel hydrogen production method by electrified steam methane reforming with renewable energy accommodation. *Energy Conversion and Management, 258*, 115513. https://doi.org/10.1016/j.enconman.2022.115513

Stenberg, V., Spallina, V., Mattisson, T., & Rydén, M. (2020). Techno-economic analysis of H_2 production processes using fluidized bed heat exchangers with steam reforming - Part 1: Oxygen carrier aided combustion. *International Journal of Hydrogen Energy*, *45*(11), 6059–6081. https://doi.org/10.1016/j.ijhydene.2019.10.202

Talbi, M. M., & Agnew, B. (2000). Exergy analysis: An absorption refrigerator using lithium bromide and water as the working fluids. *Applied Thermal Engineering*, *20*(7), 619–630. https://doi.org/10.1016/S1359-4311(99)00052-6

U.S. Environmental Protection Agency (2024). *Sources of greenhouse gas emissions*. Retrieved July 5, 2024, from https://www.epa.gov/ghgemissions/sources-greenhouse-gas-emissions

Vargas-Mira, A., Zuluaga-García, C., & González-Delgado, Á. D. (2019). A technical and environmental evaluation of six routes for industrial hydrogen production from empty palm fruit bunches. *ACS Omega*, *4*(13), 15457–15470. https://doi.org/10.1021/acsomega.9b01683

Vela García, F. N. (2021). *Biojet fuel production via alternative thermochemical routes: Thermoeconomic, life cycle and flight performance analysis*. [Doctoral dissertation]. Universidad Politécnica de Madrid.

Vikram, S., Rosha, P., Kumar, S., & Mahajani, S. (2022). Thermodynamic analysis and parametric optimization of steam-CO_2 based biomass gasification system using Aspen PLUS. *Energy*, *241*, 122854. https://doi.org/10.1016/j.energy.2021.122854

Wang, J., Ma, C., & Wu, J. (2019). Thermodynamic analysis of a combined cooling, heating and power system based on solar thermal biomass gasification. *Applied Energy*, *247*, 102–115. https://doi.org/10.1016/j.apenergy.2019.04.039

Whitaker, R. (1998). Investment in volume building: The virtuous cycle in PAFC. *Journal of Power Sources*, *71*(1-2), 71–74. https://doi.org/10.1016/S0378-7753(97)02769-9

Wu, Z., Xu, G., Zhang, W., Xue, X., & Chen, H. (2023). Thermodynamic and economic analysis of a new methanol steam reforming system integrated with CO_2 heat pump and cryogenic separation system. *Energy*, *283*, 128501. https://doi.org/10.1016/j.energy.2023.128501

Xu, M., Li, S., Jin, Z., Jiang, W., & Du, K. (2023). The influence of NH_3-H_2O-LiBr ternary working fluid on the performance and solution circulation in ammonia absorption refrigeration system. *Applied Thermal Engineering*, *234*, 121297. https://doi.org/10.1016/j.applthermaleng.2023.121297

Xu, D., Gu, X., & Dai, Y. (2023). Concentrating solar assisted biomass-to-fuel conversion through gasification: A review. *Frontiers in Energy Research*, *10*, 1029477. https://doi.org/10.3389/fenrg.2022.1029477

Xue, X., Han, W., Liu, C., Li, J., Jin, H., & Wang, X. (2023). Proposal and evaluation of a hydrogen and electricity cogeneration system based on thermochemical complementary utilization of coal and solar energy. *Energy Conversion and Management*, *291*, 117266. https://doi.org/10.1016/j.enconman.2023.117266

Yeng, F. F., Zainuddin, Z. M., & Pheng, H. S. (2024). Optimizing palm oil biomass supply chain logistics through multi-objective location-routing model. *Malaysian Journal of Fundamental and Applied Sciences*, *20*(2), 247–265. https://doi.org/10.11113/mjfas.v20n2.3085

You, H., Han, J., Liu, Y., Chen, C., & Ge, Y. (2020). 4E analysis and multi-objective optimization of a micro poly-generation system based on SOFC/MGT/MED and organic steam ejector refrigerator. *Energy*, *206*, 118122. https://doi.org/10.1016/j.energy.2020.118122

Yuksel, Y. E., Ozturk, M., & Dincer, I. (2022). Design and analysis of a new solar hydrogen plant for power, methane, ammonia and urea generation. *International Journal of Hydrogen Energy*, *47*(45), 19422–19445. https://doi.org/10.1016/j.ijhydene.2021.12.162

Zaman, S. A., & Ghosh, S. (2021). A generic input-output approach in developing and optimizing an Aspen plus steam-gasification model for biomass. *Bioresource Technology*, *337*, 125412. https://doi.org/10.1016/j.biortech.2021.125412

Zhang, X., Zeng, R., Mu, K., Liu, X., Sun, X., & Li, H. (2019). Exergetic and exergoeconomic evaluation of co-firing biomass gas with natural gas in CCHP system integrated with ground source heat pump. *Energy Conversion and Management*, *180*, 622–640. https://doi.org/10.1016/j.enconman.2018.11.009

Journal of Oil Palm Research Vol. 38 (3) September 2026 p. 446–460
DOI: https://doi.org/10.21894/jopr.2025.0041

PREDICTION OF OIL PALM BUNCHES PRODUCTION USING ARTIFICIAL NEURAL NETWORK

EMANUELLY CANABRAVA MAGALHÃES[1]*; CARLOS ALBERTO ARAÚJO JÚNIOR[2]; HELIO GARCIA LEITE[1]; GIANMARCO GOYCOCHEA CASAS[1]; JULIANA MACHADO LISBOA[3]; CARLOS HENRIQUE GARCIA[3] and RODRIGO RABE SALES BICALHO[3]

ABSTRACT

The study aimed to evaluate the ability of Artificial Neural Networks (ANN) to estimate the current monthly production of oil palm bunches using variables from the forest inventory, climatic elements, water deficit, soil and those related to the registration and management of plantations. The ANN estimated current production with a correlation above 0.6 and an average percentage relative error of around 13.0%, with the variables that gave the greatest contribution to modelling being those related to management, soil, genetic material and the accounting of mature bunches. Climatic variables were not as important, however, due to the influence of the climatic element on oil palm productivity, it is necessary to keep them in the modelling. The ANN demonstrated that it is capable of modelling oil palm production, characterised by high variability, opening opportunities for future studies, combining and using new variables to improve the accuracy of estimates using this tool.

Keywords: artificial intelligence, modelling, oil palm.

Received: 12 August 2024**; Accepted:** 26 May 2025**; Published online:** 13 August 2025.

INTRODUCTION

Brazil has the potential to become one of the world's largest producers of palm oil due to its vast availability of land and favourable climatic conditions. However, current production is still much lower than the world's leading producers and cannot meet the growing domestic demand (Murphy et al., 2021; Organização Internacional do Trabalho [OIT], 2022). In 2022, Brazil produced around 570,000 t of palm oil, ranking 10th globally. This represents just 0.70% of the world's total production (U.S. Department of Agriculture [USDA], 2022). The oil palm cultivated area in Brazil has expanded rapidly in recent years, and it is expected to continue to grow. The Brazilian Palm Oil Producer Association (ABRAPALMA), estimates that the palm oil area in Pará is 535,493 ha, with 226,834 ha planted with oil palm (Drost et al., 2021).

The consumption of palm oil in Brazil has been growing steadily since 2008. In 2023, Brazil is expected to consume about 930,000 t of palm oil, an increase of 15,000 t from the previous year. This growth is being driven by a number of factors, including the increasing popularity of processed foods that contain palm oil, the growing middle class in Brazil, and the expansion of the palm oil industry in the country (Statista, 2023).

To meet increasing demand, it's crucial to optimise production by efficiently utilising available resources. Achieving this optimisation hinges on a deeper understanding of the factors influencing

[1] Federal University of Viçosa,
P. H. Rolfs Avenue, Campus UFV,
Viçosa/MG, 36.570-900, Brazil.

[2] Federal University of Minas Gerais,
Universitária Avenue, Universitário,
Institute of Agricultural Sciences,
Montes Claros/MG, 39.404-547, Brazil.

[3] Agropalma S.A., Road PA 150 s/n Km 74 left,
Tailândia/PA, 68.695-000, Brazil.

* *Corresponding author e-mail: emanuellymagalhaes1@gmail.com*

species growth and development, enabling informed decision-making. Consequently, it's imperative for forest managers to employ computational tools capable of modelling production based on production-related variables, aiding in problem-solving (Briassoulis, 2020).

Artificial intelligence (AI), which includes machine learning, deep learning and computer vision, is being actively promoted to improve industrial efficiency and sustainability while minimising environmental impact. Its applications in precision agriculture, production mapping, land use monitoring and remote sensing, which use satellite imagery, unmanned aerial vehicles (UAVs) and ground sensors, are enabling advances in palm oil management, such as yield forecasting, disease detection and land use classification (Akhtar et al., 2023).

AI has been shown to be very effective in accurately classifying the maturity of oil palm fruit bunches, leading to significant improvements in harvesting efficiency. The potential benefits of using this AI technology include increased harvesting efficiency and productivity, as well as improved quality control and reduced waste (Harsawardana et al., 2020). AI can more accurately and efficiently estimate oil palm yield by using vegetation and moisture indices extracted from satellite imagery, outperforming traditional methods (Watson-Hernández et al., 2022). AI can reliably forecast the anthesis stages of oil palm flowers, helping oil palm planters improve assisted pollination operations and overall productivity in oil palm plantations (Yousefi et al., 2021). Additionally, AI can predict future yield functions in oil palm plantations using Bayesian networks, with a study showing that AI can accurately forecast these future yield functions (Chapman et al., 2018). Furthermore, Ashrafian et al. (2023) explored another application, investigating the use of AI to predict the strength of agroecological lightweight concrete with palm oil by-products.

Among AI techniques, Artificial Neural Networks (ANN) have gained prominence in modelling forest products, with a series of studies focusing on species such as eucalyptus, pine and teak, primarily aimed at estimating height and wood volume (Binoti, 2010; Binoti et al., 2015; Gorgens et al., 2009; Loureiro, 2016). The widespread application of ANN in forest species, combined with robust results and consistent performance, has led to increasing acceptance in both the scientific community and the industry. These techniques have been used to optimise processes, enhance decision-making, and increase the efficiency of natural resource use. Thus, the expansion of ANN for modelling agricultural crops emerges as a promising alternative, offering opportunities to improve productivity and promote sustainable practices in the agricultural sector. This approach not only enhances the prediction of outcomes but also contributes to adaptation to environmental variables and effective management of crops.

ANN can accurately forecast the duration of palm oil production processes. This predictive capability has the potential to help palm oil mills optimise their production efficiency and reduce operational costs (Adizue et al., 2020). ANN have also been used to predict oil palm yield using meteorological variables and have been shown to be able to accurately predict oil palm yield (Kartika et al., 2016).

AI is a promising technology that has the potential to significantly improve palm oil management. By improving efficiency, sustainability and yield, AI can help the palm oil industry to meet the growing demand for palm oil while minimising its environmental impact. This method could be used by oil palm farmers and plantation managers to improve the yield and productivity of their crops.

Most studies on palm oil have been conducted in other countries, and there is no development of studies in Brazil. Therefore, it is important to conduct national-scale research to model the growth and development of the crop using AI tools. In this sense, the objective of this study was to predict the production of palm oil bunches using inventory and climatic variables through ANN.

MATERIALS AND METHODS

Localisation of the Study Area

The study area was a 103,000 ha property owned by Agropalma in the state of Pará, Brazil. It is in the northern region of the country, as shown in *Figure 1*.

Approximately 39,000 ha of the property are used for commercial seed plantations of the *tenera* variety of *Elaeis guineensis* (Jacq.). The remaining 64,000 ha are occupied by forest reserves and other infrastructure areas (Agropalma, 2019).

The predominant soil type in the region is Argissolo Amarelo Distrófico, which is variable in depth, acidic, well-drained and has a medium to clayey texture. In some areas, there is also Gleissolo Háplico dystrophic, which is shallow, acidic, hydromorphic, greyish in colour and sandy in texture (Rodrigues et al., 2005; Santos et al., 2018).

The climate in the Tailândia region is of the Am type, which is tropical monsoon. This means that the driest month has less than 60 mm of rainfall. The other three regions (Tomé-Açu, Acará and Moju) have an Af climate, which is tropical with no dry season. For both climate types, the average temperature of the coldest month of the year is above 18ºC (Alvares et al., 2013).

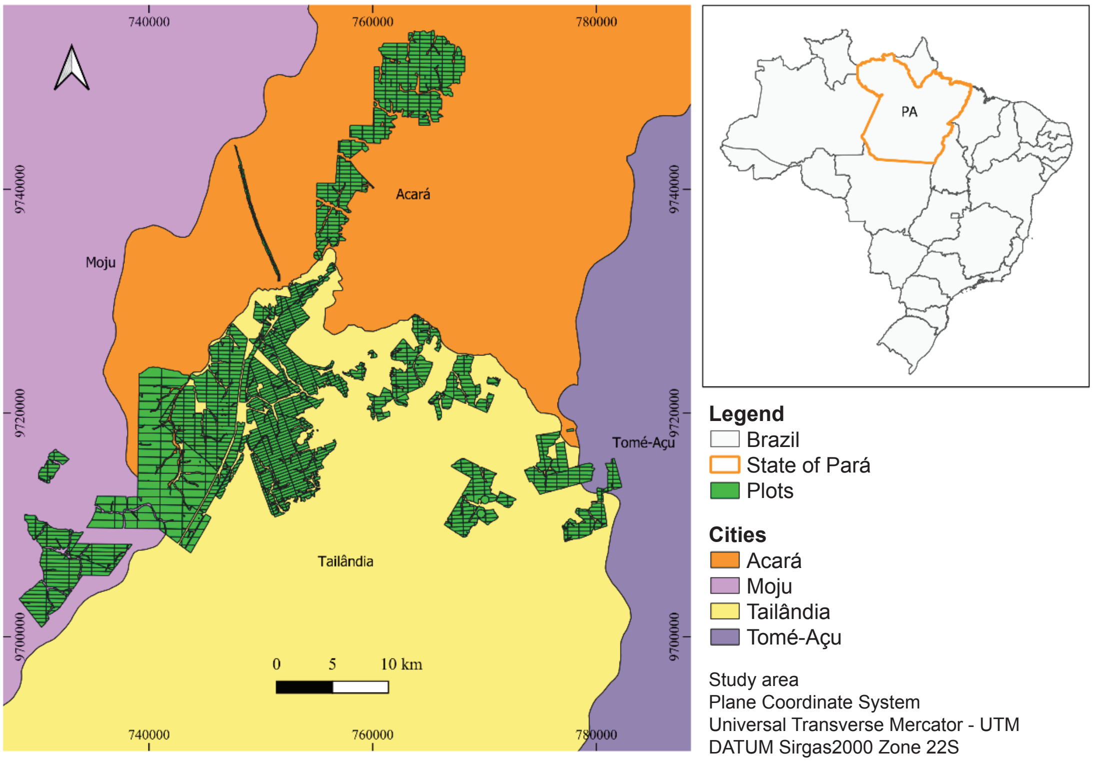

Figure 1. Location of the study area.

Characterisation of the Plantations and Organisation of the Database

Palm oil plantations were stratified by planting years and distributed across the A, B, C, D, E, F, G and H farms. Plantings were established on plots of varying sizes, ranging from 2 to 118 ha. Different genetic materials were used, with Deli X Lamé being the most common variety. Planting was also carried out with different spacings between plants, with a standard density of 143 plants/ha.

Forest inventories were conducted monthly, sampling 25–40 plants/plot. Inflorescences in anthesis (before fertilisation) and fecund (already fertilised), green bunches and mature bunches were quantified.

Four meteorological stations were installed at the A, C, D and F farms to collect monthly climate data, including temperature, precipitation, solar radiation and relative humidity. Additionally, the monthly water deficit was calculated.

To build the dataset, the forestry company provided historical monthly data from 2014 to 2022, including information from the forest inventory, total bunch production/plot, meteorological station records and general plantation records. This data was linked and checked, errors were corrected, rows without values for all attributes were deleted and outliers in bunch production, number of inflorescences in anthesis, fecund, green and mature bunches were removed. With the checked dataset, qualitative and quantitative variables were pre-defined for use in modelling the production of palm oil bunches.

Oil Palm Bunch Yield Prediction

The ANN with default configuration were applied to predict the production of oil palm bunches. An ANN consists of three layers: The input layer, where the information is received, the output layer, responsible for generating the outputs/responses and the hidden layer that connects both previous layers (*Figure 2*).

The prediction of the current monthly production of oil palm bunches was based on the values of climatic variables recorded in the months prior to the prediction month. This approach was taken because climatic variables for the current month were not yet available at the time of sampling, and previous climatic conditions have an impact on current bunch production.

Table 1 presents the minimum, mean, maximum, standard deviation (SD) and coefficient of variation (CV%) of the quantitative variables used in the study. These variables include the number of bunches/ha, the weight of bunches and the yield of oil/bunch. Qualitative variables encompass eight farms, 26 strata based on planting years, 19 genetic materials and seven soil classes.

TABLE 1. DESCRIPTIVE ANALYSIS OF QUANTITATIVE VARIABLES FOR PREDICTING THE YIELD OF PALM OIL BUNCHES

Quantitative variables	Acronym	Unit	Min	Mean	Max	SD	CV (%)
Anthesis inflorescences	AntHa	no/ha	0.00	4.32	102.96	7.91	182.90
Inflorescences in fecund	FecHa	no/ha	0.00	3.42	205.29	7.26	211.91
Green bunches	GBHa	no/ha	5.24	566.22	1,836.12	324.36	57.29
Mature bunches	MBHa	no/ha	1.79	96.63	1,024.00	95.92	99.26
Average bunch weight	BWCa	kg	2.02	14.81	84.06	5.79	39.11
Sampling percentage	%samp	%	0.50	1.06	14.63	0.77	72.69
Age	-	yr	4.00	15.33	33.00	8.08	52.69
Average temperature of the previous month	Temp1	°C	25.62	26.89	28.19	0.70	2.59
Precipitation of the previous month	PP1	mm	0.40	194.76	670.61	173.36	89.01
Water deficit of the previous month	Def1	mm	0.00	41.29	168.16	50.70	122.78
Relative humidity of the previous month	Humid1	%	67.91	84.8	92.86	5.74	6.77
Insolation of the previous month	Insol1	W/m^2	116.54	157.59	205.44	19.35	12.28
Monthly bunch production	ProdHa	t/ha	1.00	2.26	21.57	1.44	63.66

Note: SD - standard deviation; CV% - coefficient of variation.

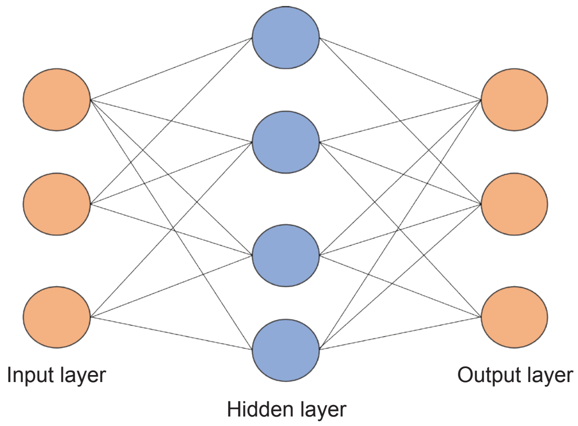

Figure 2. Structure of an artificial neural networks (ANN).

The prediction of the current monthly production of oil palm bunches relied on a comprehensive set of variables. These included general plot registration details such as farm, planting year, genetic material and soil. Also factored in were current month inventory metrics (AntHa, FecHa, GBHa, MBHa, BWCa), climatic conditions, and water deficit from the previous month (Temp1, PP1, Def1, Humid1, Insol1), as well as harvest month, age and sampling percentage, totalling 73 variables. These variables were input into an ANN trained to forecast bunches/ha production.

The output variable was the current monthly production of oil palm bunches/ha (ProdHa) at the plot level. To achieve this, we employed Neuroforest 4.0 software (Binoti, 2012).

The ANN models were configured using standard settings provided by the software: Eight neurons in the hidden layer, a sigmoid activation function, resilient propagation as the training algorithm, a stopping criterion of 3,000 epochs and a data split of 70% for training and 30% for validation.

Using these ANN models, we estimated bunches per hectare production for individual plots. Subsequently, we calculated total bunches production in tonnes across various levels: Total t/plot/yr and respective harvest month (level 1); total t/yr and harvest month (level 2); total t/harvest month (level 3); and total t/yr of harvest (level 4), without specific plot breakdown, representing aggregate data. This process enabled assessment of the correlation between observed and estimated values, and determination of the average relative percentage error at each level.

Model Performance

After processing, statistical metrics were calculated to evaluate the performance of the artificial neural network defined for this study, considering both the training and validation phases, following the methods described by Campos and Leite (2017). Additionally, graphical representations were generated to visualise the results, including scatter plots illustrating the distribution of relative percentage errors, the relationship between estimated and observed values and histograms showing the frequency of relative percentage errors. These metrics include Linear correlation between predicted and observed values [Equation (1)], bias [Equation (2)], square root of the mean squared percentage error [Equation (3)], mean relative percentage error [Equation (4)], percentage bias [Equation (5)] and variance [Equation (6)].

$$r_{y\hat{y}} = \frac{\sum_{i=1}^{n}(Y_i - \overline{Y}) \cdot (\hat{Y}_i - \overline{\hat{Y}})}{\sqrt{\sum_{i=1}^{n}(Y_i - \overline{Y})^2 \cdot \sum_{i=1}^{n}(\hat{Y}_i - \overline{\hat{Y}})^2}} \quad (1)$$

$$bias = \frac{1}{n}\sum_{i=1}^{n}(Y_i - \hat{Y}_i) \quad (2)$$

$$RMSE\% = \frac{\sqrt{\frac{\sum_{i=1}^{n}(Y_i - \hat{Y}_i)^2}{n}}}{\overline{Y}} \cdot 100 \quad (3)$$

$$\overline{ER}\% = \frac{1}{n}\sum_{i=1}^{n}\frac{(\hat{Y}_i - Y_i) \cdot 100}{Y_i} \quad (4)$$

$$bias\% = \frac{bias}{\overline{Y}} \cdot 100 \quad (5)$$

$$Var = \frac{\sum[\text{bias} - (Y_i - \hat{Y}_i)]^2}{n-1} \quad (6)$$

where, Y_i is the observed value, $\hat{Y}_i$ is the estimated value, $\overline{Y}$ is the average of the observed values, $\overline{\hat{Y}}$ is the average of the estimated values and n is the total number of observations.

Identification of the Most Influential Variables in the Modelling Process

To understand the relationship between the input and output variables used in the study, a correlation matrix was generated. The correlation coefficient was used to measure the strength of the relationship between two variables, where a correlation coefficient of 1 indicated a perfect positive relationship, –1 indicated a perfect negative relationship and 0 indicated no relationship.

The correlation matrix was generated using the psych package (Revelle, 2023) in the R software (R Core Team, 2020). This package produced a correlation matrix with histograms of the distribution of each variable on the diagonal, correlations in the upper part of the diagonal and graphs illustrating the relationships between variables in the lower part.

Additionally, the Garson algorithm (Garson, 1991) was employed to assess the importance of each input variable in the model. This algorithm utilised the absolute values of weights between neurons in the input and hidden layers, as well as between the hidden and output layers, to quantify variable importance (Casas et al., 2022; Freitas et al., 2020).

A neural network, configured identically to the one used in the previous study, was trained using all available qualitative and quantitative variables. The weights derived from this training were then applied in the Garson algorithm. This process was executed using the R software and the Neuralnet package (Fritsch et al., 2019).

Additional Modelling Tests

Following the identification of variables most closely associated with bunch production per hectare, two additional modelling tests were conducted. These tests involved removing specific inventory and climatic elements from the dataset. The modified models were subsequently compared against the original model, and statistical analyses were performed to compute the correlation between observed and estimated values, as well as the mean relative percentage error.

RESULTS AND DISCUSSION

Prediction of Palm Oil Bunch Production

The ANN exhibited similar error statistics in both the training and validation phases, with a mean relative percentage error of approximately 13%, root mean squared error (RMSE) around 40%, bias close to zero and variance around one, representing the prediction variability. However, when evaluating the correlation between observed and estimated values, there is a difference, with a correlation above 0.74 for training and 0.67 for validation (*Table 2*).

The scatter plots of the mean relative percentage error show that most of the errors range between –100% and 100%, particularly for productions between 1 and 5 t/ha. However, for lower production levels, some points begin to deviate from the overall trend, resulting in errors exceeding 100% (*Figure 3b* and *3e*). The distribution of relative percentage errors is better visualised when grouped into classes (*Figure 3c* and *3f*). Consequently, classes were defined ranging from –100 to 100%, encompassing slightly over 80% of the errors falling between –40% and 60%, both in the training and validation datasets (*Figure 3*).

The concentration of the largest error ranges in lower bunch yields per hectare may be related to inadequate agricultural management practices, water stress and soil quality. These variables can significantly impact the productivity of oil palm plantations, resulting in inaccurate predictions. Understanding these factors is fundamental to

TABLE 2. STATISTICS CALCULATED TO ASSESS THE ACCURACY OF THE ARTIFICIAL NEURAL NETWORKS (ANN) IN THE TRAINING AND VALIDATION PHASES

Data splitting	Bias	Bias%	RMSE%	Var	$\overline{ER}$%	$r_{y\hat{y}}$
Training	0.000001	0.000060	42.29	0.92	12.62	0.74
Validation	-0.009437	-0.420264	47.86	1.15	13.36	0.67

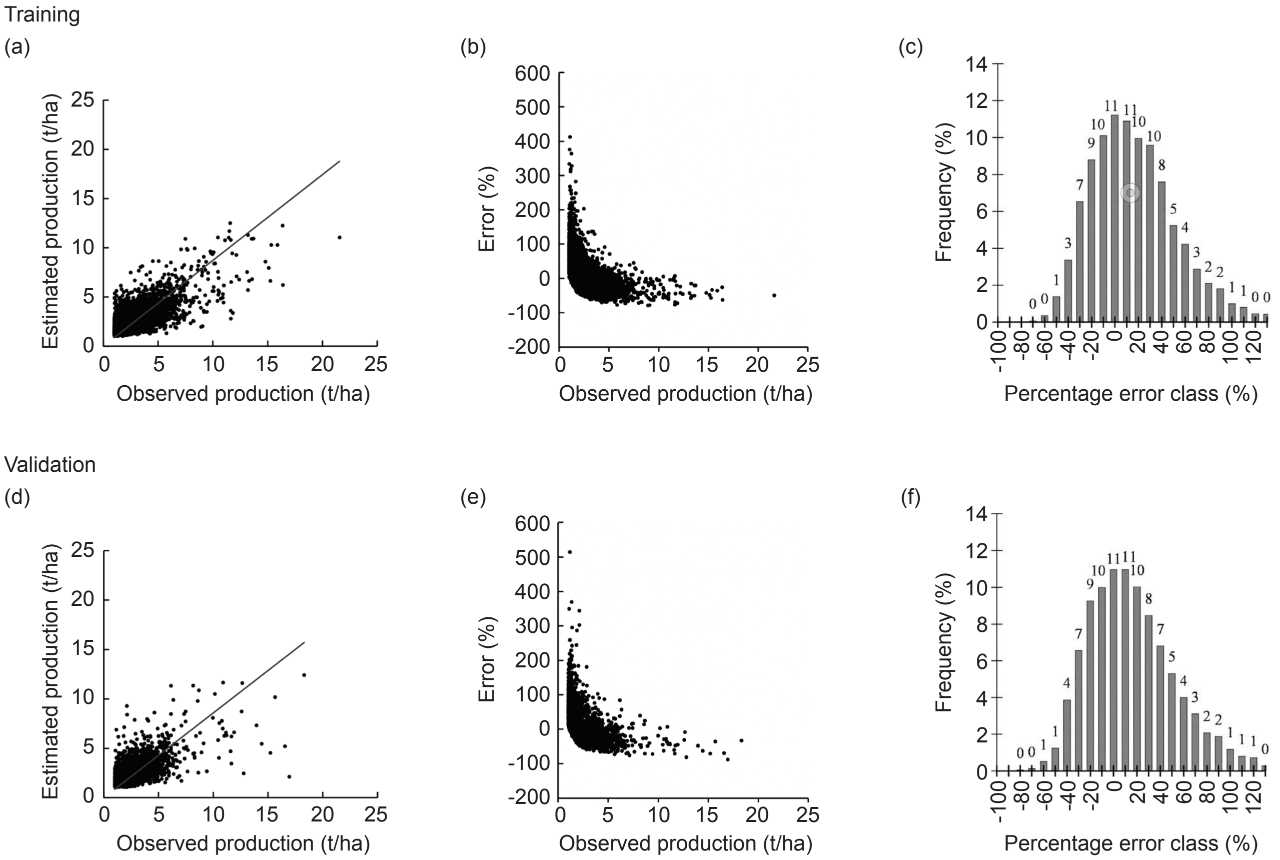

Figure 3. Relationships between (a, d) estimated and observed productions, (b, e) relative percentage errors and observed productions and (c, f) percentage of cases per class of relative percentage error in bunch production estimates.

identifying the limitations of the model, allowing for the analysis of the specific conditions affecting production in different contexts. Additionally, developing mitigation strategies, such as implementing more appropriate management practices, monitoring and improving soil fertility, can help enhance the accuracy of the predictions.

The behaviour of percentage errors concerning qualitative variables reveals the presence of outliers in most categories of each variable. For instance, the planting years 2001, 2009, 2010 and 2012, characterised by the largest planting areas, exhibited a significant number of outliers, meaning errors exceeding 100%. A similar pattern was observed for the farms; larger farms generated outliers, while smaller ones like B and H did not. Genetic materials such as Deli Lamé and Deli Yangambi, commonly found in most plantations, exhibited errors that deviated from the general trend, whereas the less represented Deli X Dami variety displayed errors ranging between 80% and 200% (*Figure 4*).

Regarding soil types, it is evident that the Argissolo (pad1, pad2, pad3, pad4 and pad5), which is predominant in the region, accounted for errors exceeding 100%. For both genetic materials and soil types, there is no consistent error in the behaviour pattern, implying the influence of other factors on these variables (*Figure 4*).

When evaluating the residual percentage dispersion in relation to quantitative variables, the sampling percentage deserves special attention, as it shows the highest errors at lower percentages, specifically between 0% and 1%. Inventory-related variables such as the number of anthesis, fecundation and mature bunches follow a similar pattern, with the ANN displaying greater errors at lower values. When conducting monthly inventories, in many cases, there is a minimal identification of bunches and inflorescences, or sometimes their presence is not even confirmed. However, this does not imply zero production for that month since production is quantified at a specific time. These minimal or null values do not directly represent the actual tonne of bunches delivered to the factory in the current month. Consequently, when relating these variables to the bunch production for the current month, the ANN tends to make more errors because it cannot establish a clear relationship. As for climatic variables, there is no distinct trend (*Figure 5*).

Evaluating the performance of estimates at different levels, there is an increase in correlation and a decrease in percentage errors as the estimates are assessed more broadly. This demonstrates the high accuracy of the ANN in estimating the total production for each month (1.90% error) as well

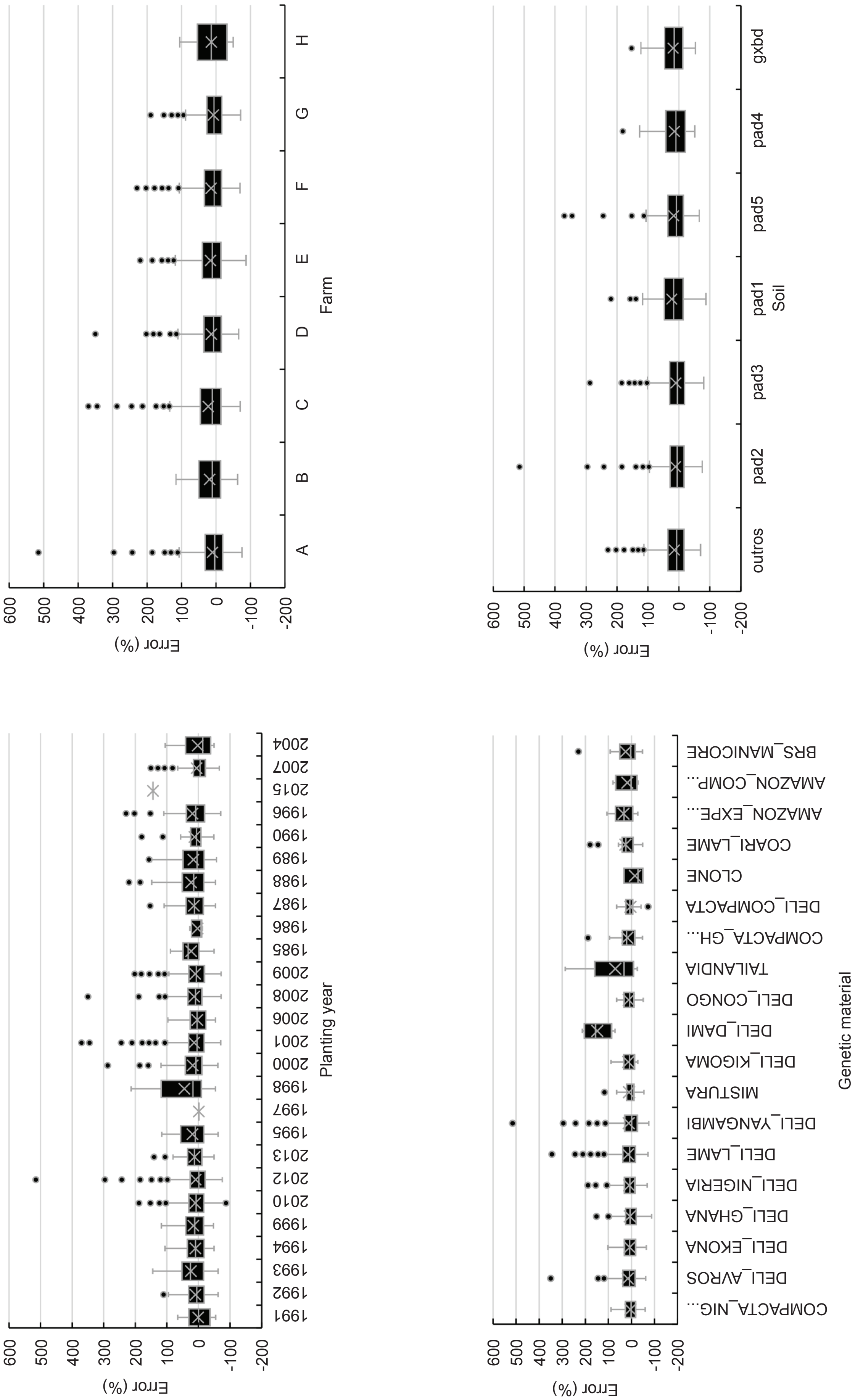

Figure 4. Scatterplot of relative percentage errors assessed by qualitative variable in the validation phase of the artificial neural networks (ANN).

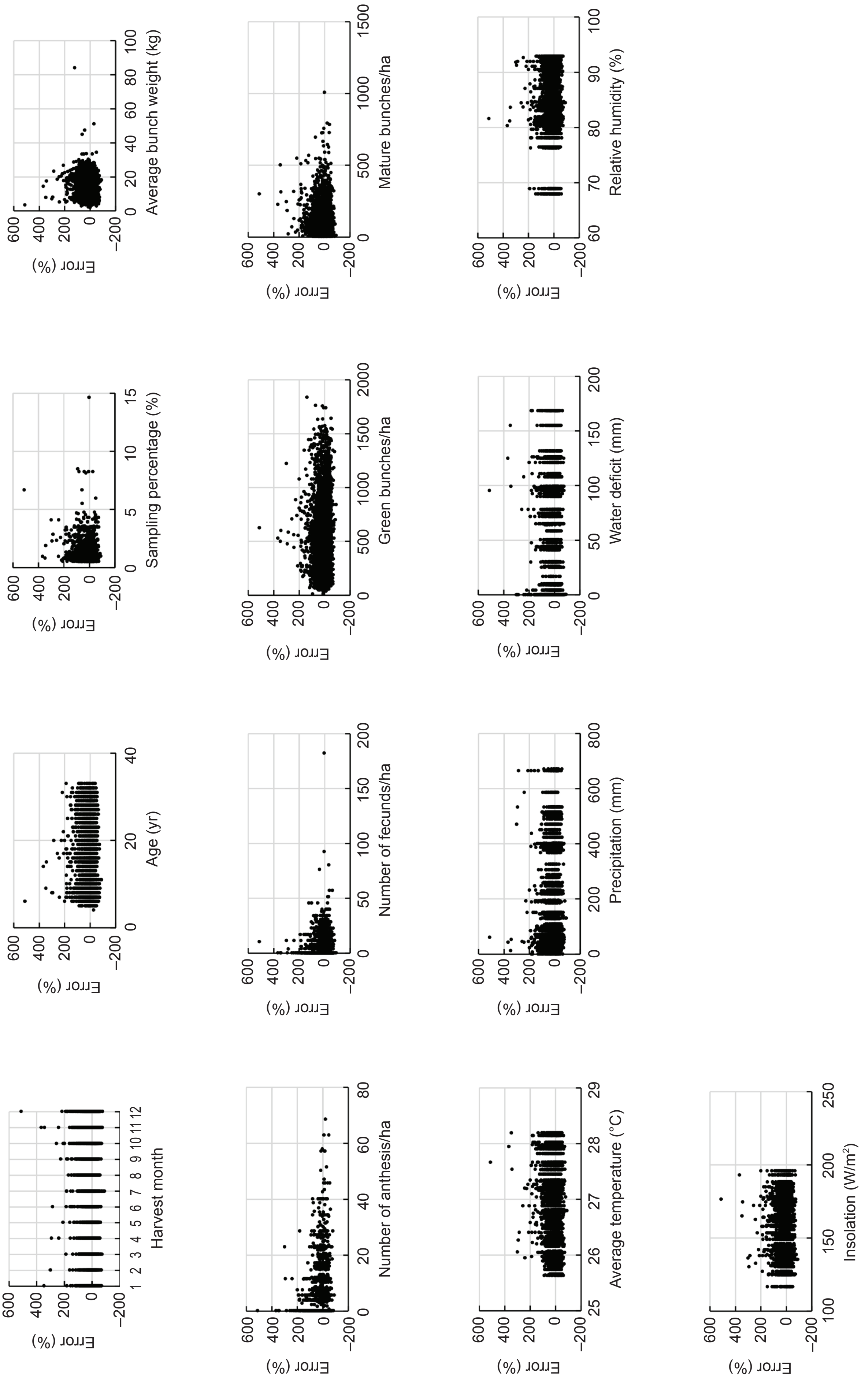

Figure 5. Scatterplot of relative percentage errors assessed by the quantitative variable in the validation phase of the artificial neural networks (ANN).

TABLE 3. ANALYSIS OF ESTIMATED TOTAL BUNCH PRODUCTION BY HARVEST YEAR AND MONTH

Total bunch production (t)	Level	Stratification	$r_{y\hat{y}}$	ER%
Harvest year and month	1	Plot	0.75228	13.30%
Harvest year and month	2	General	0.99103	6.30%
Harvest month	3	General	0.99725	1.90%
Harvest year	4	General	0.99615	1.50%

as for each harvest year (1.50% error). Considering that one of the objectives is to obtain more reliable monthly bunch production estimates, the analysis at level 3 confirms the effectiveness of the modelling using ANN (*Table 3*).

Modelling at the parcel level is influenced by the sampling database, an operational procedure where the plot undergoes management and represents the main interfering factor in the estimation of precision (Khan et al., 2021; Nain et al., 2022). The lower precision of parcel level estimates is due to high variability, which becomes evident when analysing variables such as anthesis, fecundation, green bunches, mature bunches, sampling percentage and bunch production values over the years.

The data collection process for inventory is a significant challenge in the field due to the difficulty in visualising bunches and inflorescences, especially in the case of larger plants, leading to counting errors. This results in reduced reliability in the data collected in the field for consolidation and processing in the office. This issue has been discussed in a study by Chapman et al. (2018), which associated lower accuracy in fresh fruit bunches (FFB) yield estimates with errors in database records. Reducing the impact of sampling errors on modelling depends on changes in the planning of operational procedures, such as applying higher sampling percentages in areas with high heterogeneity (Soares et al., 2011). This enables the ANN to gain a deeper understanding of production variability and the factors that influence it.

Most Influential Variables in the Modelling

Based on a correlation coefficient threshold of 0.2 bunch yield/ha (ProdHa) has the strongest relationship with the following variables: Harvest month (Month), sampling percentage (%samp), mature bunches (MBHa), average temperature (Temp1), water deficit (Def1), precipitation (PP1) and relative humidity (Humid1) (*Figure 6*).

The Garson algorithm determines that the variables with the greatest contribution to the modelling are planting year, genetic material, soil, farm (qualitative), anthesis and fecundation inflorescences, mature bunches, average bunch weight and sampling percentage (quantitative).

The behaviour of the estimates in each additional modelling test is represented in *Table 4*, which summarises the variables used (marked with an X), the calculated correlation and mean relative error statistics. It is observed that the two new tests, Test 1 and Test 2, which excluded some input variables from modelling, exhibit similar performance to Test 0, which utilises all input variables, demonstrating that certain variables, such as climatic variables, did not exert a significant influence on the model's performance.

TABLE 4. INPUT VARIABLES USED IN EACH TEST AND THEIR RESPECTIVE MODELING STATISTICS (CORRELATION, MEAN RELATIVE PERCENTAGE ERROR) FOR TRAINING (T) AND VALIDATION (V)

Variables		Test 0	Test 1	Test 2
Planting year		X	X	X
Farm		X	X	X
Genetic material		X	X	X
Soil		X	X	X
Month		X	X	X
Age		X		
%samp		X	X	X
AntHa		X		
FecHa		X		
GBHa		X		
MBHa		X	X	X
BWCa		X		
Temp1		X	X	
PP1		X		
Def1		X	X	
Humid1		X		
Insol1		X	X	
$r_{y\hat{y}}$	T	0.74	0.71	0.71
	V	0.67	0.67	0.62
ER%	T	12.62	13.38	13.68
	V	13.36	14.66	15.92

Both the Garson algorithm and the conducted tests indicated that climatic variables did not exert a significant influence on the estimates. Test 2, which excluded all climatic variables, obtained statistically similar results to the other

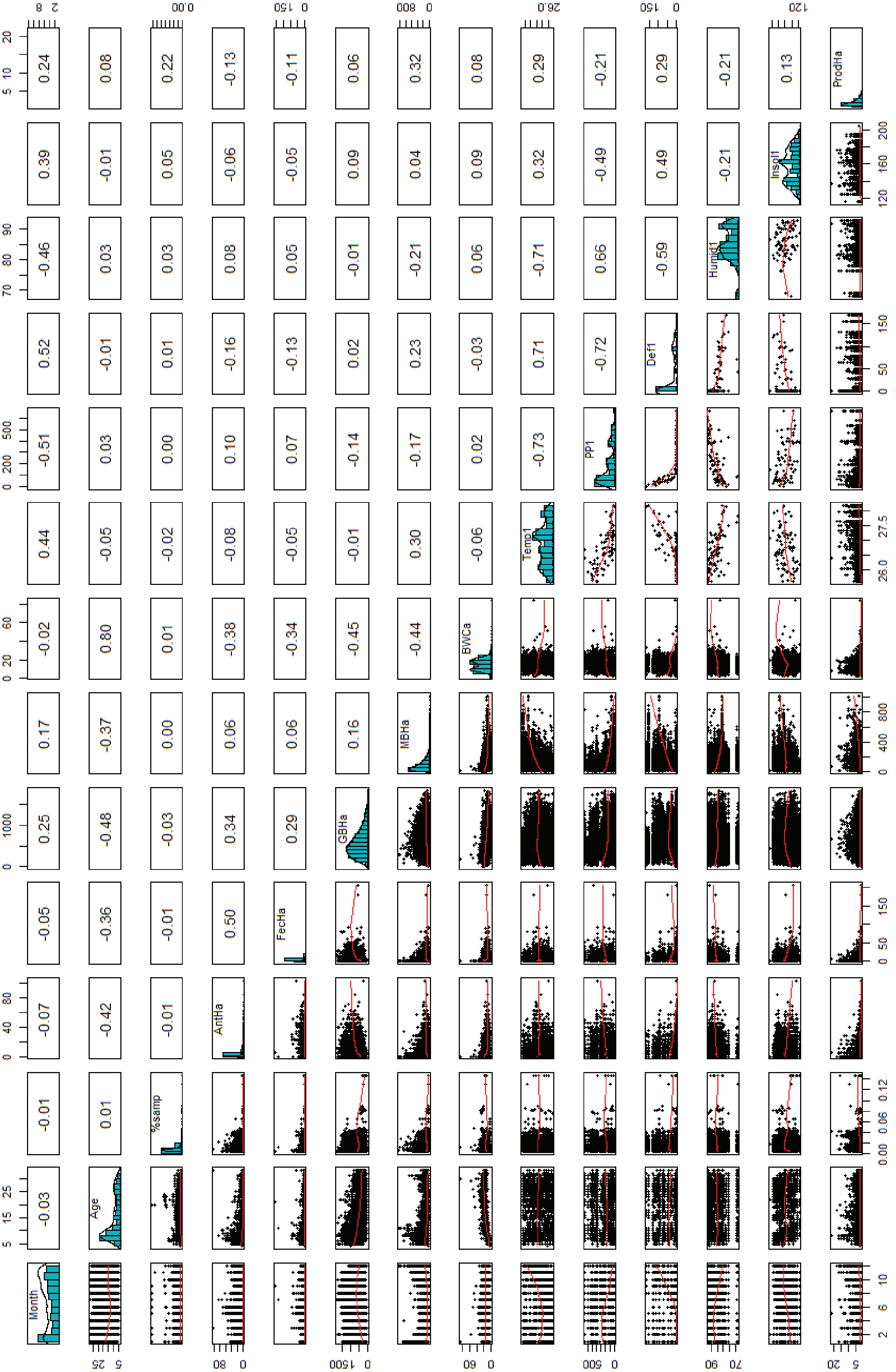

Figure 6. Pearson correlation among the quantitative variables used in the modelling.

tests (*Table 4*). This result may suggest that the climatic variation between months was not significant enough to affect the ANN learning or that the quality of the climatic database was suboptimal. This is because meteorological stations experienced technical issues during certain periods, reducing the reliability of the collected variables. Therefore, it is essential to invest in equipment and techniques to enhance the quality of available climatic data (Hoffmann et al., 2014, 2017; Kartika et al., 2016). Additionally, using the climatic factor from only the month preceding the prediction month was not sufficient to express the climate's influence on oil palm bunch production. The development of inflorescences occurs 32 months after seed germination, and during this period, the climatic influence accumulates (Adam et al., 2005). It would be valuable in future studies to apply climatic variables with lags and cumulative periods of up to 32 months before the prediction month.

The influence of climatic variables on the productivity of oil palm plantations is complex, as different ranges of climate conditions can have varying effects. While adequate levels of rainfall can promote healthy growth, excessive or insufficient precipitation may cause stress, leading to negative impacts on productivity. This duality highlights the need for more sophisticated approaches in analyses that consider the variability of crop responses to climate change. Understanding these nuances is crucial for optimising oil palm production under changing climatic conditions (Fleiss et al., 2022).

Maintaining the collection and use of climatic variables is crucial for oil palm modelling studies, given the climate's influence on the crop development. In the case of random events, the inclusion of variables such as temperature, solar radiation, precipitation, or water deficit becomes indispensable. Water deficit, for instance, is the primary limiting factor for bunch production as it delays floral initiation, increases abortion rates and consequently reduces fruit production (Corley & Tinker, 2016; Monzon et al., 2022; Murugesan et al., 2017; Pirker et al., 2016; Rhebergen et al., 2016). A similar effect is observed during periods of high precipitation, which has a negative correlation with FFB production and oil production in the bunch. Excessive rainfall during inflorescence development leads to flower abortion and subsequently lower bunch and oil production, affecting the industrial extraction rate (Silva, 2006).

Oil palm is a crop that requires specific climatic conditions, and if not met, it results in low annual yields. The Amazon region, where this study is conducted, is characterised by annual average temperatures between 24°C and 28°C, water deficit below 200 mm, relative humidity between 75% and 90%, precipitation exceeding 100 mm, and high levels of solar radiation (1,600 hr/yr), conditions favourable for oil palm establishment in the region. However, constant climate change tends to alter normal conditions and consequently, crop yields.

Using strata such as planting years and farms in modelling provides specific information about plantation management and reflects environmental changes directly affecting these strata. These strata generally exhibit a pattern of production peaks throughout the harvest year, which occurs in January, November and December, coinciding with peaks in average temperature and insolation. These climatic factors, along with precipitation, significantly influence oil palm productivity (Corley & Tinker, 2016; Hoffmann et al., 2014; Monzon et al., 2022). Monzon et al. (2022) assessed the variation in oil palm productivity in terms of space (plantation strata) and time (year and month) in the Indonesian region. In their study, monthly bunch yield peaks differed in the four regions evaluated, occurring at the beginning (January), middle (May-August), or end of the year (November). These yields were closely associated with water stress. Thus, the monthly bunch production of oil palm depends on specific aspects of the region and the local climatic behaviour.

The importance of categorical variables such as soil type and genetic material aligns with research conducted outside Brazil, as discussed in the review by Nain et al. (2022). They categorised variables into three categories: Environment, phenotype and genotype. They highlighted genotype as a widely used factor with soil and fertilisation as the second most addressed environmental factor in the studies, second only to climate.

Among the inventory variables, the identification and counting of mature bunches are essential for modelling due to their direct relationship with oil palm yield (Monzon et al., 2022). After harvesting the bunches, they must be processed as quickly as possible to avoid high acidity in the extracted oil and consequently, a loss of final product quality (Corley & Tinker, 2016; Muller et al., 2006; Teles, 2014). Typically, the classification of fresh fruit bunch is done manually based on the subjective judgment of the responsible person, influenced by the palm tree's height, fruit position and direction of sunlight. Additionally, the number of fruits found on the ground is observed to confirm bunch maturity. This method is not very efficient as it cannot capture the internal quality of the fruit, resulting in a high error rate that directly affects the prediction of palm oil yield (Alfatni et al., 2020, 2018; Ishak et al., 2019; Makky & Cherie, 2021). Therefore, the use of alternative and accurate methods for classifying mature bunches is crucial for estimating the t of bunches/planted area, such as image-based classification.

Study Limitations

The developed prediction model relies heavily on the quality and quantity of available historical data. The lack of accurate data related to climatic conditions, management practices and soil characteristics may compromise the model's effectiveness, resulting in less reliable predictions. This dependence on historical data is a significant limitation, as the absence of comprehensive information may lead to either underestimation or overestimation of production.

Another point to highlight is the complexity of the environmental factors influencing oil palm production. The interaction between these factors is intricate, and the model may not fully capture these interactions. Consequently, the predictions generated may not adequately reflect the dynamics of the cultivation system, limiting the accuracy of the estimates.

Furthermore, the generalisation of the model to different regions or cultivation conditions may be limited. Although the study has shown satisfactory results, local factors, such as microclimatic variations and specific agricultural practices, present high variability, which may affect the model's applicability in different contexts.

CONCLUSION

This study demonstrated that ANN are effective in estimating the current monthly production of oil palm bunches. By integrating variables from forest inventory, climatic elements, water deficit, soil characteristics and plantation management records, the methodology proved to be efficient and achieved the proposed objective of accurately predicting production. These findings highlight the practical potential of ANN as a reliable tool for inventory and production planning in oil palm crops. For future work, it is recommended to adopt advanced techniques that ensure proper data treatment, particularly concerning outliers and missing information. Incorporating lagged climatic variables over extended periods is an excellent strategy for improving model performance, as oil palm productivity is highly influenced by climatic factors. Additionally, incorporating data related to soil fertilisation and management practices is crucial for a more comprehensive modelling approach. In the context of Brazil, where the study was conducted and which has significant potential for oil palm expansion, this study represents a significant advancement in the development of management techniques for oil palm plantations. Moreover, it opens up opportunities for other researchers to explore more advanced investigations in the sector, testing and incorporating new variables that could explain variations in palm productivity, thereby contributing to the robustness and applicability of the model.

ACKNOWLEDGEMENT

The present work was carried out with support from the Coordenação de Aperfeiçoamento de Pessoal de Nível Superior – Brasil (CAPES) – Financing Code 001 and the company Agropalma, which provided the production data for the crop under study.

REFERENCES

Adam, H., Jouannic, S., Escoute, J., Duval, Y., Verdeil, J. L., & Tregear, J. W. (2005). Reproductive developmental complexity in the African oil palm (*Elaeis guineensis*, Arecaceae). *American Journal of Botany, 92*(11), 1836–1852. https://doi.org/10.3732/ajb.92.11.1836

Adizue, U. L., Nwanya, S. C., & Ozor, P. A. (2020). Artificial neural network application to a process time planning problem for palm oil production. *Engineering and Applied Science Research, 47*(2), 161–169. https://ph01.tci-thaijo.org/index.php/easr/article/view/211130

Agropalma. (2019). *Relatório de sustentabilidade* [Sustainability report]. Helikonia.

Akhtar, M. N., Ansari, E., Alhady, S. S. N., & Abu Bakar, E. (2023). Leveraging on advanced remote sensing- and artificial intelligence-based technologies to manage palm oil plantation for current global scenario: A review. *Agriculture, 13*(2), 504. https://doi.org/10.3390/agriculture13020504

Alfatni, M. S. M., Mohamed Shariff, A. R., Bejo, S. K., Ben Saaed, O. M., & Mustapha, A. (2018). Real-time oil palm FFB ripeness grading system based on ANN, KNN and SVM classifiers. *IOP Conference Series: Earth and Environmental Science, 169*, 012067. https://doi.org/10.1088/1755-1315/169/1/012067

Alfatni, M. S. M., Mohamed Shariff, A. R., Ben Saaed, O. M., Albhbah, A. M., & Mustapha, A. (2020). Colour feature extraction techniques for real time system of oil palm fresh fruit bunch maturity grading. *IOP Conference Series: Earth and Environmental Science, 540*(1), 012092. https://doi.org/10.1088/1755-1315/540/1/012092

Alvares, C. A., Stape, J. L., Sentelhas, P. C., Gonçalves, J. M., & Sparovek, G. (2013). Köppen's climate classification map for Brazil. *Meteorologische Zeitschrift, 22*(6), 711–728. https://doi.org/10.1127/0941-2948/2013/0507

Ashrafian, A., Panahi, E., Salehi, S., Karoglou, M., & Asteris, P. G. (2023). Mapping the strength of agro-ecological lightweight concrete containing oil palm by-product using artificial intelligence techniques. *Structures, 48*, 1209–1229. https://doi.org/10.1016/j.istruc.2022.12.108

Binoti, M. L. M. S. (2010). *Redes neurais artificiais para prognose da produção de povoamentos não desbastados de eucalipto* [Artificial neural networks for prognosis of yield of non-thinned stands of eucalyptus] [Master's thesis, Universidade Federal de Viçosa]. Locus UFV. https://locus.ufv.br/items/2b074c84-4944-4a3a-b168-ad7c2b8c44d8

Binoti, M. L. M. S. (2012). *Emprego de redes neurais artificiais em mensuração e manejo florestal* [Use of artificial neural networks in measurement and forest management] [Doctoral dissertation, Universidade Federal de Viçosa]. Locus UFV. https://locus.ufv.br/items/519f5745-92dd-4d2c-8e2b-187d7c9a5736

Binoti, M. L. M. S., Leite, H. G., Binoti, D. H. B., & Gleriani, J. M. (2015). *Prognose em nível de povoamento de clones de eucalipto empregando redes neurais artificiais* [Stand-level growth prediction of eucalyptus clones using artificial neural networks]. *Cerne, 21*(1), 97–105. https://doi.org/10.1590/01047760201521011153

Briassoulis, H. (2020). *Analysis of land use change: Theoretical and modelling approaches* (2nd ed.). WVU Research Repository.

Campos, J. C. C., & Leite, H. G. (2017). *Forest measurement: Questions and answers* (5th ed.). UFV.

Casas, G. G., Fardin, L. P., Silva, S., Oliveira Neto, R. R., Binoti, D. H. B., Leite, R. V., Domiciano, C. A. R., Sousa Lopes, L. S., Cruz, J. P., Reis, T. L., & Leite, H. G. (2022). Improving yield projections from early ages in eucalypt plantations with the Clutter model and artificial neural networks. *Pertanika Journal of Science & Technology, 30*(2), 1257–1272. https://doi.org/10.47836/pjst.30.2.22

Chapman, R., Cook, S., Donough, C., Lim, Y. L., Vun Vui Ho, P., Lo, K. W., & Oberthür, T. (2018). Using Bayesian networks to predict future yield functions with data from commercial oil palm plantations: A proof of concept analysis. *Computers and Electronics in Agriculture, 151*, 338–348. https://doi.org/10.1016/j.compag.2018.06.006

Corley, R. H. V., & Tinker, P. B. (2016). *The oil palm* (5th ed.). BlackWell Science.

Drost, S., Rijk, G., & Piotrowski, M. (2021). *Palm oil production in Brazilian Amazon threatens NDPE commitments*. Chain Reaction Research.

Fleiss, S., McClean, C. J., King, H., & Hill, J. K. (2022). Limited impacts of climatic conditions on commercial oil palm yields in Malaysian plantations. *CABI Agriculture and Bioscience, 3*(59), 1–18. https://doi.org/10.1186/s43170-022-00127-1

Freitas, E. C. S. de, Paiva, H. N., Neves, J. C. L., Marcatti, G. E., & Leite, H. G. (2020). Modeling of eucalyptus productivity with artificial neural networks. *Industrial Crops and Products, 146*, 112149. https://doi.org/10.1016/j.indcrop.2020.112149

Fritsch, S., Guenther, F., & Wright, M. N. (2019). *neuralnet: Training of neural networks* [R package]. https://CRAN.R-project.org/package=neuralnet

Garson, G. D. (1991). Interpreting neural network connection weights. *AI Expert, 6*(4), 46–51.

Gorgens, E. B., Leite, H. G., Santos, H. N., & Gleriani, J. M. (2009). *Estimação do volume de árvores utilizando redes neurais artificiais* [Estimation of tree volume using artificial neural networks]. *Revista Árvore, 33*(6), 1141–1147.

Harsawardana, Rahutomo, R., Mahesworo, B., Cenggoro, T. W., Budiarto, A., Suparyanto, T., Atmaja, D. B. S., Samoedro, B., & Pardamean, B. (2020). AI-based ripeness grading for oil palm fresh fruit bunch in smart crane grabber. *IOP Conference Series: Earth and Environmental Science, 426*(1), 012147. https://doi.org/10.1088/1755-1315/426/1/012147

Hoffmann, M. P., Donough, C. R., Cook, S. E., Fisher, M. J., Lim, C. H., Lim, Y. L., Cock, J., Kam, S. P., Mohanaraj, S. N., Indrasuara, K., Tittinutchanon, P., & Oberthür, T. (2017). Yield gap analysis in oil palm: Framework development and application in commercial operations in Southeast Asia. *Agricultural Systems, 151*, 12–19. https://doi.org/10.1016/j.agsy.2016.11.005

Hoffmann, M. P., Vera, A. C., Van Wijk, M. T., Giller, K. E., Oberthür, T., Donough, C., & Whitbread, A. M. (2014). Simulating potential growth and yield of oil palm (*Elaeis guineensis*) with PALMSIM: Model description, evaluation and application. *Agricultural Systems, 131*, 1–10. https://doi.org/10.1016/j.agsy.2014.07.006

Ishak, H., Shiddiq, M., Fitra, R. H., & Yasmin, N. Z. (2019). Ripeness level classification of oil palm fresh fruit bunch using laser induced luorescence imaging. *Journal of Aceh Physics Society, 8*(3), 84–89. https://doi.org/10.24815/jacps.v8i3.14139

Kartika, N. D., Astika, I. W., & Santosa, E. (2016). Oil palm yield forecasting based on weather variables using artificial neural network. *Indonesian Journal of Electrical Engineering and Computer Science*, *3*(3), 626–633. https://doi.org/10.11591/ijeecs.v3.i3.pp626-633

Khan, N., Kamaruddin, M. A., Sheikh, U. U., Yusup, Y., & Bakht, M. P. (2021). Oil palm and machine learning: Reviewing one decade of ideas, innovations, applications, and gaps. *Agriculture, 11*(9), 832. https://doi.org/10.3390/agriculture11090832

Loureiro, G. H. (2016). *Redes neurais artificiais e modelos de regressão para estimação de variáveis dendrométricas em* Pinus taeda *L: Análise comparativa* [Artificial neural networks and regression models for estimating dendrometric variables in *Pinus taeda* L: A comparative analysis] [Doctoral dissertation, Universidade Federal do Paraná]. Acervo Digital da UFPR. https://acervodigital.ufpr.br/xmlui/handle/1884/52605

Makky, M., & Cherie, D. (2021). Pre-harvest oil palm FFB nondestructive evaluation technique using thermal-imaging device. *IOP Conference Series: Earth and Environmental Science, 757*(1), 012003. https://doi.org/10.1088/1755-1315/757/1/012003

Monzon, J. P., Jabloun, M., Cock, J., Caliman, J. P., Couëdel, A., Donough, C. R., Vui, P. H. V., Lim, Y. L., Mathews, J., Oberthür, T., Prabowo, N. E., Edreira, J. I. R., Sidhu, M., Slingerland, M. A., & Sugianto, H. (2022). Influence of weather and endogenous cycles on spatiotemporal yield variation in oil palm. *Agricultural and Forest Meteorology, 314*, 108789. https://doi.org/10.1016/j.agrformet.2021.108789

Muller, A. A., Furlan, J. J., & Filho, P. C. (2006). *A Embrapa Amazônia Oriental e o agronegócio do dendê no Pará* [Eastern Amazônia Embrapa and the oil palm agribusiness in Pará]. Embrapa Amazônia Oriental.

Murphy, D. J., Goggin, K., & Paterson, R. R. M. (2021). Oil palm in the 2020s and beyond: Challenges and solutions. *CABI Agriculture and Bioscience*, *2*(1), 1–22. https://doi.org/10.1186/s43170-021-00058-3

Murugesan, P., Aswathy, G. M., Kumar, K. S., Masilamani, P., Kumar, V., & Ravi, V. (2017). Oil palm (*Elaeis guineensis*) genetic resources for abiotic stress tolerance: A review. *Indian Journal of Agricultural Sciences, 87*(5), 571–579. https://doi.org/10.56093/ijas.v87i5.70087

Nain, F. N. M., Malim, N. H. A. H., Abdullah, R., Rahim, M. F. A., Mokhtar, M. A. A., & Fauzi, N. S. M. (2022). A review of an artificial intelligence framework for identifying the most effective palm oil prediction. *Algorithms*, *15*(6), 218. https://doi.org/10.3390/a15060218

Organização Internacional do Trabalho. (2022). *Cadeia produtiva do óleo de palma – Avanços e desafios rumo à promoção do trabalho decente: Análise situacional* [Palm oil value chain – Advances and challenges toward promoting decent work: Situational analysis].

Pirker, J., Mosnier, A., Kraxner, F., Havlík, P., & Obersteiner, M. (2016). What are the limits to oil palm expansion? *Global Environmental Change, 40*, 73–81. https://doi.org/10.1016/j.gloenvcha.2016.06.007

R Core Team. (2020). *R: A language and environment for statistical computing* [Computer software]. R Foundation for Statistical Computing. https://www.R-project.org/

Revelle, W. (2023). *psych: Procedures for psychological, psychometric, and personality research* [R package]. https://CRAN.R-project.org/package=psych

Rhebergen, T., Fairhurst, T., Zingore, S., Fisher, M., Oberthür, T., & Whitbread, A. (2016). Climate, soil and land-use based land suitability evaluation for oil palm production in Ghana. *European Journal of Agronomy, 81*, 1–14. https://doi.org/10.1016/j.eja.2016.08.004

Rodrigues, T. E., Silva, J. M. L., Silva, B. N. R., Valente, M. A., Gama, J. R. N. F., Santos, E. S., Rollim, P. A. M., & Ponte, F. C. (2005). *Caracterização e classificação dos solos do município de Tailândia, Estado do Pará* [Characterization and classification of soils in the municipality of Tailândia, Pará State]. Embrapa Amazônia Oriental.

Santos, H. G., Jacomine, P. K. T., Anjos, L. H. C., Oliveira, V. A., Lumbreras, J. F., Coelho, M. R., Almeida, J. A., Araújo Filho, J. C., Oliveira, J. B., & Cunha, T. J. F. (2018). *Sistema brasileiro de classificação de solos* [Brazilian soil classification system]. Embrapa Solos.

Silva, J. S. O. (2006). *Produtividade de óleo de palma na cultura do dendê na Amazônia Oriental: Influência do clima e do material genético* [Palm oil productivity in oil palm cultivation in the Eastern Amazon: Influence of climate and genetic material] [Master's thesis, Universidade Federal de Viçosa]. Locus UFV. https://locus.ufv.br/items/3e35e31c-f023-41e4-bdae-684b01c15074

Soares, C. P. B., Paula Neto, F., & Souza, A. L. (2011). *Dendrometria e inventário florestal* [Forest mensuration and inventory] (2nd ed.). Universidade Federal de Viçosa.

Statista. (2023). *Brazil: Palm oil consumption 2008–2023*. https://www.statista.com/statistics/876584/palm-oil-consumption-brazil/

Teles, D. A. A. (2014). *Características físicas e rendimento mensal em óleo de cachos de duas cultivares de dendezeiro cultivadas, sob irrigação, no Cerrado do Distrito Federal* [Physical characteristics and monthly oil yield of bunches from two oil palm cultivars grown under irrigation in the Cerrado of the Federal District] [Master's thesis, Universidade de Brasília]. Alice (Repositório de Informação Tecnológica da Embrapa). https://www.alice.cnptia.embrapa.br/handle/doc/1033176

U.S. Department of Agriculture. (2022). *Brazil palm oil: Potential and pitfalls* (Commodity Intelligence Report). Foreign Agricultural Service. https://ipad.fas.usda.gov/highlights/2022/12/Brazil_Palm_Oil/

Watson-Hernández, F., Gómez-Calderón, N., & Silva, R. P. (2022). Oil palm yield estimation based on vegetation and humidity indices generated from satellite images and machine learning techniques. *AgriEngineering, 4*(1), 279–291. https://doi.org/10.3390/agriengineering4010019

Yousefi, M. D. B., Mohd Rafie, A. S., Abd Aziz, S., Azrad, S., Mohd Masri, M. M., Shahi, A., & Marzuki, O. F. (2021). Classification of oil palm female inflorescences anthesis stages using machine learning approaches. *Information Processing in Agriculture, 8*(4), 537–549. https://doi.org/10.1016/j.inpa.2020.11.007

Journal of Oil Palm Research Vol. 38 (3) September 2026 p. 461–471
DOI: https://doi.org/10.21894/jopr.2025.0025

GENETIC ANALYSIS OF HEIGHT INCREMENT (HINC) IN ELMINA-ULU REMIS OIL PALM USING SNP MARKERS

CHEAH TEAD WENG[1]*; SENG TZER YING[1]; GOH HUA LEK[2] and JOSHUA MATHEWS[3]

ABSTRACT

Dwarf or short palm is considered one of the desired traits in oil palm breeding, offering advantages of extending the economic viability and harvesting. This study aimed to identify single nucleotide polymorphism (SNP) markers associated with height increment (Hinc) for future breeding improvement programmes. A total of 537 SNPs and 107 Elmina x Ulu Remis (ELxUR) hybrid palm crosses were used in the marker-trait association study, with phenotypic data collected at age 8 and 16. Eight significant SNPs were detected associated with Hinc on chromosome 1, 2, 3, 4 and 10. Candidate gene identification within these significant SNPs was performed using the palm genome sequence and bioinformatics tools, revealing 13 potential candidate genes and transcription factors linked to phytohormone biosynthesis, signalling and plant growth. This study provides a groundwork for implementing marker-assisted breeding for the height trait within the ELxUR oil palm breeding materials.

Keywords: *Elaeis guineensis*, marker-trait association, single nucleotide polymorphism, slow height increment.

Received: 13 June 2024**; Accepted:** 13 February 2025**; Published online:** 17 April 2025.

INTRODUCTION

Oil palm (*Elaeis guineensis* Jacq.) stands as the foremost commodity crop in Malaysia's agricultural sector. Over the years, efforts to improve yields have been made without compromising on breeding standards for the industry's sustainability. Harvesting ripe bunches from old and taller palm trees is one of the challenges faced by the industry. The breeding of short palms is considered a desirable trait because of its potential to benefit oil palm operational management and ease harvesting, which in turn prolongs the economic lifespan of planted palms and the land use of the plantation.

[1] IOI Palm Biotech Sdn. Bhd., IOI Resort City, 62502 Putrajaya, Malaysia.

[2] IOI Group Pamol Plantations Sdn. Bhd., P. O. Box 1, 86007 Kluang, Johor, Malaysia.

[3] IOI Research Centre, 2 km Gemencheh-Batang Melaka Road, 73200 Gemencheh, Negeri Sembilan, Malaysia.

* *Corresponding author e-mail: twcheah@ioigroup.com*

Dwarf oil palms are known to occur in several 'populations' such as derivatives of the Dumpy E206 palm, palms prospected at Pobe in Ivory Coast by CIRAD (formerly IRHO), the La Me type (a good DxP bred by CIRAD at their La Me breeding station in Ivory Coast). Additionally, Malaysian Palm Oil Board (MPOB) extensive germplasm collection, particularly population 12 from their Nigerian collection was famous for the short trait (Rajanaidu et al., 2017). In Malaysia, the Nigerian Prospection Material (NPM) of the MPOB is known to contain palms of dwarf stature (Rajanaidu & Jalani, 1994). Genetic variability in the NPM population is still high, giving ample scope for further selection (Noh et al., 2014).

The oil palm's annual trunk height increment (Hinc) primarily occurs through the continuous and annual production of new fronds. These fronds, or nodes, are arranged in a spiral pattern of eight whorls, with the spacing between them, known as internodes determining the overall height of the palm (Corley & Gray, 1976). These variations in frond production and internode spacing contribute to the observable height discrepancies among palms, a factor of particular significance for individuals engaged in harvesting activities. Palm height (HT) serves as a fundamental metric in assessing the growth and development of oil palms. While height measurements can be taken at any stage of growth, the bulk of recorded data stems from what is known as 'vegetative measurements' (VM). These VM encapsulate a range of assessments focused on the palm's vegetative features and growth dynamics, providing valuable insights into its overall performance. Reducing the height of oil palm trees has consistently been a significant consideration for both oil palm breeders and growers. This focus aims to minimise the expenses associated with harvesting from tall palms, particularly after reaching the age of 25 years. Several researches have shown that the height of oil palm is heritable (Lee et al., 2015; Teh et al., 2020).

Polygenic or quantitative inheritance occurs when a trait is controlled by more than one gene. Usually, the traits are polygenic inheritance when there is a wide variation of a trait. Height is a polygenic trait, controlled not by a single gene, but rather, by multiple genes that each make a small contribution to the overall expression of the trait. When there are large numbers of genes involved, it becomes hard to distinguish the effect of each gene, and even harder to identify the gene variants (alleles) that are inherited according to Mendelian inheritance rules. Circumstantial evidence in various molecular publications suggests that HT is under polygenic control, as quantitative trait loci were identified (Babu et al., 2019; Pootakham et al., 2015; Seng et al., 2016; Ting et al., 2023). Despite height being one of the most heritable and easily measured traits in oil palm, mapping alleles explaining natural variation in oil HT remains a formidable challenge. The height character in general not only dependent on expression of the regulating genes, as well as environmental factors that impact the expression pattern, highlighting the complex interplay between gene expression and the environment in determining the phenotype.

The advancements in single nucleotide polymorphism (SNP) marker technology and its successful application in identifying height-related traits in crops such as soybean (Yang et al., 2023), wheat (Chen et al., 2017; B. Cheng et al., 2023), coffee (Da Silva et al., 2024) and barley (Bai et al., 2021), suggest its potential for improving crop breeding programs. In the present study, the Elmina x Ulu Remis (ELxUR) populations were genotyped with 600 height-related SNP markers by AgriSeq™ Targeted Genotyping-by-Sequencing (GBS) Solutions (Thermo Fisher Scientific) to identify significant SNP markers associated with Hinc. The information gathered from the present study is expected to develop a marker-assisted identification of dwarf palms, which may aid future oil palm breeding programmes. This marker-assisted selection may be applied at an early stage of palm growth, especially at pre-nursery level to identify short palms before commercial planting of palms in the field.

MATERIALS AND METHODS

Plant Materials and DNA Extraction

Three crosses were developed from the Deli Dumpy palm E206 Elmina (0.175/964) and Ulu Remis *tenera* (0.151/2,626), denoted as ELxUR, as part of the breeding effort. These crosses included one T-sibling (SDP2) and two T-self crosses (SDP1 and SDP3), utilising two parental palms (PKg494/188/1,876 and PKg494/188/1,880). The objective of the cross breeding was to establish progenies of the F_2 cross with segregation for Hinc trait for molecular markers analysis. The trial was designed in a Complete Randomised Design (CRD), with a total of 192 palms planted in June 2002 at field PM02B of Pamol Timur Estate at a density of 136 palms ha^{-1}. However, out of the total 192 palms planted initially, only 107 ELxUR palms were available for sampling from the experimental plot. An additional 13 palms were randomly selected to serve as duplicates. Hence, a total of 120 palms were genotyped in this study.

The number of palms evaluated in each cross is shown in *Table 1*. Leaves were collected from mature palms, cleaned, punched into small pieces and kept at 4°C. The leaves samples were sent to Thermo Fisher Scientific in the USA for DNA isolation. DNA was extracted using MagMAX™ CORE Nucleic Acid Purification Kit (Plant Module).

TABLE 1. NUMBER OF PALMS EVALUATED IN EACH CROSS

Programme code	Cross	Total
SDP1	Selfed	29
SDP2	Sib-crossing	39
SDP3	Selfed	39

Phenotypic Data

The height of the palm is measured from the base of the trunk, or ground level to the base of frond number 41 (Corley & Tinker, 2016). Corley et al. (1971) suggested that height measurements should be conducted once palms have attained stable growth. Height measurements are typically taken a few years after the canopy has closed. This timing ensures that the measurement reflects the height of a palm when it is in middle age and encompasses the period during which competition for light between neighbouring palms gradually intensifies. In this study, two sets of height data (palm age eight and 16) were available to be used for the marker-trait association study.

HT was measured from the ground level to the base of the leaf 41. Hinc was calculated using the following Equation (1):

$$HT/yr\left(\frac{\text{Height increase}}{\text{yr}}\right)=\frac{\text{(Height in yr t)}}{\text{(t-2)}}, \quad (1)$$

where, t is the age of the palm expressed in years, from the date of planting to the moment of a given measurement (Corley & Tinker, 2016). The latter deduction is to take into account that the growth of the trunk was not fully exposed in the initial two years after planting but only growth in the girth of the palm to produce the bole.

SNP Panel Design

The SNPs utilised in this study were primarily identified through a combination of gene differential expression analysis, QTL associated with stem Hinc trait, and candidate gene approach. The SNP marker mining process involved sourcing these SNPs from both the Oil Palm Genome Projects (OPGP) as well as publicly available SNPs related to oil palm height.

Those SNPs sourced from OPGP were filtered based on five selected origins [Eg-Deli-59 (Deli Dumpy Serdang), Eg-Deli-Ulu (IOI Ulu Remis), Eg-Ekona, Eg-Nigeria and Eg-Angola]. A total of 727 SNPs were shortlisted for AgriSeq™ Targeted GBS SNP panel design, including 21 SNPs compiled from four publications (Babu et al., 2019; Ong et al., 2018; Teh et al., 2020; Yaakub et al., 2020). The selected SNPs passed through AgriSeq's design quality control process. The primer designs were *in-silico* checked for specificity and sensitivity of the target regions using the oil palm reference genome (accession: GCF_000442705.1) and OPGP's oil palm reference genome (data not published). After that, the SNPs were submitted for the SNP panel design. Finally, 600 SNPs were selected to constitute the custom SNP panel.

GBS and SNP Calling

The GBS was done by Thermo Fisher Scientific (USA) using AgriSeq™ Targeted GBS Solutions. The AgriSeq™ Targeted GBS procedure includes target region PCR amplification, amplicon sequencing and sequence alignment for variant calling. Details on the AgriSeq™ genotyping workflow are available in the report by Carrasco et al. (2018). Only SNPs with call rates >90% were retained for subsequent analysis.

Marker-trait Association Study

The marker-trait association study was performed using PLINK v1.90 (Purcell et al., 2007). For enhanced accuracy of the genetic data, quality control measures excluded subjects with an SNP call rate below 90%. SNPs with a minor allele frequency (MAF) below 1% or a Hardy-Weinberg equilibrium (HWE) *p*-value below 10^{-6} were also removed from the dataset. The principal component analysis (PCA) and the marker-trait association analysis were performed in PLINK. The two input files (ped and map) for PLINK were converted from Hapmap files using Trait Analysis by Association, Evolution and Linkage (TASSEL) software version 5.2.85 (Bradbury et al., 2007). Marker-trait associations were performed using linear regression, with Hinc phenotypes as the dependent variable and principal components as covariates. The linear option in PLINK performs a linear regression analysis with each SNP as a predictor.

Identifying the Potential Candidate Genes for Hinc

The significant Hinc SNP positions were mapped to the oil palm whole genome sequence EG5.1 (http://genomsawit.mpob.gov.my/genomsawit/) and OPGP's oil palm reference genome (unpublished data) using SNP flanking sequences to define the boundaries for gene mining. Sequence similarity analysis (BLAST) was employed with the SNP-containing sequences as the query against the predicted oil palm gene model database (Chan et al., 2017; Ting et al., 2023) and OPGP Reference Gene Annotation (data not published). Candidate genes and transcription factors related to Hinc and stem height were identified through a comprehensive review of their biological functions, as documented in the literature and public databases, including http://palmxplore.mpob.gov.my/palmXplore/palmxplore_res and https://www.uniprot.org/. The search focused on biological activities, including the biosynthesis and signalling of phytohormones, DELLA genes, transcription factors and cell morphogenesis, which can contribute to dwarfism during the growth and development of plants (Ting et al., 2023).

RESULTS AND DISCUSSION

Hinc Data

Height data measurements were conducted at eight and 16 years after planting. Two sets of height data were utilised in this study to identify SNPs consistently associated with Hinc at eight (Hinc8) and 16 (Hinc16) years. The three ELxUR crosses (SDP 1, SDP 2 and SDP 3) exhibited mean Hinc of 16.42 and 35.58 cm/yr for Hinc8 and Hinc16, respectively. For Hinc8, the recorded Hinc ranged from a maximum of 25.00 to a minimum of 8.33 cm/yr. Similarly, at Hinc16, the maximum and minimum Hinc were 50.86 and 19.86 cm/yr, respectively (*Table 2*). The coefficients of variation (CV) calculated for the Hinc8 and Hinc16 datasets were 18.94% and 14.87%, respectively. These values indicate that the ELxUR germplasm exhibits relatively narrow genetic variation in Hinc when compared to previous studies by Ong et al. (2018) and Ting et al. (2023), which reported CVs of up to 32.5% and 26.9%, respectively. Analysis of variance (ANOVA) indicated significant differences in Hinc among the crosses at both Hinc8 and Hinc16 ($p < 0.05$).

SNP Data

Genomic DNA from 120 individuals palms was used to prepare AgriSeq HTS libraries. The libraries were genotyped using the Ion 540 Chef kit and Ion 540 Chip, generating approximately 80 million reads. Overall, the results achieved a 95.1% call rate, indicating that all 107 samples attained above-average coverage. The call rate for a given SNP is defined as the proportion of individuals in the study for which the corresponding SNP information is not missing (Reed et al., 2015). The distribution of raw reads across the sequenced portion of the genome was notably uniform, achieving an average base coverage uniformity of 95.8% with a mean depth of 335X. Approximately 96.2% of on-target reads were successfully aligned to the unique locations on the reference genome.

The genotyped SNP data was first scrutinised by comparing the genotype calls of 13 duplicate samples to verify the precision of genotyping results. An average of 97.9% of the SNPs exhibited identical genotype calls, with 1.8% missing data in either one or both of the duplicated samples. A minimal discrepancy in genotype calls (0.3%) was observed among the 13 duplicate samples. These genotyping results show reproducible genotypes.

A total of 600 SNP markers were genotyped, of which 537 SNP markers had a call rate exceeding 90.0%. The low call rate observed in some markers may be attributed to factors such as low DNA concentration, suboptimal primer and probe design, or issues during sequencing. A total of 537 SNP markers were genotyped, of which 216 SNPs (40.2%) were polymorphic and 321 SNPs (59.8%) were monomorphic. Of the 216 polymorphic SNPs, 193 (89.4%) were polymorphic in the SDP1 cross, and 192 (88.9%) were polymorphic in the SDP3 cross. As expected, all SNPs were detected as polymorphic in the SDP2 cross, which involved the sib-crossing of two palms (PKg494/188/1,876 and PKg494/188/1,880). Most of the polymorphic SNPs detected were transitions (A/G or C/T) (61.6%) while 38.4% were transversion SNPs. The most frequently observed variation was A/G, accounting for 31.5%, while the least common type of change was C/G, representing only 4.6% of the total polymorphisms (*Table 3*).

Although the genotyped SNPs were selected by different approaches, the transition: transversion ratio is 1.60, which was similar to earlier reported for oil palm by Pootakham et al. (2013, 2015) and Ting et al. (2014) at 1.77, 1.67 and 1.55, respectively. The 63 remaining SNPs, with less than 90.0% call rate, were excluded from this study to improve the accuracy of the genetic information.

TABLE 2. DESCRIPTIVE PARAMETERS OF HEIGHT INCREMENT (HINC) IN EACH CROSS OF ELxUR AT PALM AGE EIGHT AND 16

Item	Height increment (cm)							
	Year 8 (Hinc8)				Year 16 (Hinc16)			
	SDP1	SDP2	SDP3	Overall	SDP1	SDP2	SDP3	Overall
N	29	39	39	107	29	39	39	107
Mean	15.28	16.12	17.57	16.42	32.69	34.89	38.44	35.58
Std. Deviation	3.11	2.79	3.09	3.11	5.85	4.61	4.06	5.29
Minimum	11.33	9.33	8.33	8.33	19.86	24.79	28.57	19.86
Maximum	23.33	21.83	25.00	25.00	50.86	44.79	46.29	50.86
CV (%)	20.35	17.31	17.59	18.94	17.90	13.21	10.56	14.87

Note: N - number of palms; CV - coefficient of variation.

TABLE 3. SUMMARY OF SNPS USED FOR GBS

Total number of SNP	600			
Call rate >90%	537		89.5%	
Call rate <90%	63		10.5%	
Total number of monomorphic SNP	321		59.8%	
Total number of polymorphic SNP	216		40.2%	
Programme code	**Monomorphic**		**Polymorphic**	
SDP1	23	10.6%	193	89.4%
SDP2	0	0.0%	216	100.0%
SDP3	24	11.1%	192	88.9%
Transition				
A/G	68		31.5%	
C/T	65		30.1%	
Transversion				
A/T	27		12.5%	
T/G	24		11.1%	
A/C	22		10.2%	
C/G	10		4.6%	

Marker-trait Association Study

A total of 587 SNP markers with a minor allele frequency (MAF) higher than >5% were used to estimate the genetic relationship and mapping of marker-trait associations (MTAs) related to Hinc. The study included three crosses derived from ELxUR comprising 107 palms along with the two sets of phenotypic data (palm age eight and 16) for height. Prior to analysis, quality control (QC) was carried out to eliminate samples with a missing genotype rate exceeding 10%. Following the quality control (QC) steps, a total of 107 palm samples and 537 SNP markers remained for further analysis.

The association analysis of trait-marker data resulted in the identification of 22 SNP markers linked to Hinc8 (using PC1) on five chromosomes in ELxUR. Among the 22 SNP markers, nine were located on chromosomes 4 and 3, respectively. Two SNP markers at chromosome 2 and one SNP marker mapped to chromosomes 1 and 10. Only markers with $P \leq 0.05$ will be considered as significantly associated with Hinc. By using the palm height phenotypic data at age 16 (Hinc16) with the PC1 as the covariate, 69 SNP markers were detected linked with Hinc16. Interestingly, all 22 SNP markers associated with the Hinc8 were also found in the 69 SNP significant markers list. Most of the SNP markers are located on chromosomes 4 and 10. However, redundant markers were identified and removed from further analysis. Reducing redundant SNPs based on similar genotype calls at the same genomic region can help streamline the genetic analysis. Consequently, pattern comparison and analysis resulted in the retention of only eight SNPs following the deduplication process (*Table 4*).

Remarkably, two out of 21 SNP markers compiled from previous publications were found to be linked to Hinc in ELxUR too. Specifically, two markers (SNPM00563 and SNPM03201) from Yaakub et al. (2020) were named M011 and M013 in this study, respectively. These two significant markers were associated with Hinc and petiole cross-section (SNPM0563) and rachis length (SNPM03201) located at chromosome 2 (Yaakub et al., 2020). Interestingly, SNPM03201 associated with rachis length in Yaakub et al. (2020) study was linked with Hinc in this study. However, the palm material [backcross of T128 (0.151/128)] used in the Yaakub et al. (2020) study does not have the common bloodline as shown in this study which is Elmina (0.175/964) and Ulu Remis (0.151/2,626). It suggests some of the SNP markers might be able to transfer between the palms of different origin. However, 10 selected SNP markers from Teh et al. (2020) which were associated with trunk height and frond length in *Dumpy* AVROS *pisifera* (DAV) x *Gunung Melayu dura* (GM) cross did not show any significant association with Hinc in this study.

Compiling the findings from various studies (Bhagya et al., 2020; Billotte et al., 2010; Lee et al., 2015; Ong et al., 2018; Pootakham et al., 2015; Teh et al., 2020; Ting et al., 2023; Yaakub et al., 2020), QTLs for HT, Hinc and rachis length were identified across nearly all chromosomes, except chromosome 3 in various genetic backgrounds. In this study, there were three SNP markers (M020, M024 and M270) identified significantly associated with Hinc located in chromosome 3 (*Table 4*). Contrastingly, in Ting et al. (2023) study, major QTL effects on HT and Hinc were detected on chromosomes 6 and 8 of the Nigerian *tenera* (T128). Meanwhile, it was reported that the major QTL for HT and frond length were co-located on chromosomes 11 (Bhagya et al., 2020; Teh et al., 2020), 10, 14 and 15 (Pootakham et al., 2015). In summary, height regulation is likely dependent on genetic background, and it is necessary to correct Hinc data across different studies due to observations made in varying environments. It is challenging to compare one study to another because of environmental influences.

Potential Candidate Genes Identification

The physical positions of the SNP markers were acquired from the Genomsawit website of the MPOB Oil Palm Genome Programme (MPOB-OPGP) (http://genomsawit.mpob.gov.my) and OPGP's oil palm reference genome (data not published). These positions, along with the SNP flanking regions, can help to specify the boundaries for gene mining.

The BLAST results of eight significant SNPs identified 13 candidate genes associated with Hinc in oil palm. There were four phytohormone-related candidate genes located in chromosome 3 associated with three SNP markers (*Table 5*). The shortlisted phytohormones-related candidate gene, *gibberellin 3-beta-dioxygenase 1* (*GA3ox1*) was located in between markers M020 and M024. *GA3ox1* is an enzyme involved in the biosynthesis of *gibberellins* (*GAs*), catalysing the conversion of inactive GA precursors into active forms. *GAs* are plant hormones crucial for various aspects of plant growth and development (Mitchum et al., 2006; Yamaguchi et al., 1998). J. Cheng et al. (2023) demonstrated by gene editing of *GA3-oxidase*, an alternative semi-dwarfing gene in barley that combines an optimal reduction in plant height without restricting coleoptile emergence and subsequent seedling growth. Remarkably, two auxin signalling genes, protein kinase *PINOID 2* and auxin (Aux)-responsive protein *indole-3-acetic-acid-inducible 8* (*IAA8*) were identified on the same chromosome. *PINOID* is a protein kinase found in plants, particularly in *Arabidopsis thaliana*, and it plays a crucial role in the regulation of polar auxin transport and regulation of auxin signalling (Morita & Kyozuka, 2007; Zourelidou et al., 2014). *PINOID phosphorylates* and regulates the activity of *PIN* proteins. *PIN* proteins are integral to polar auxin transport, which determines the direction of auxin flow within plant tissues. This transport is essential for processes such as organ development, tropisms and embryogenesis. The constitutive expression of *PINOID* results in a phenotype in both shoots and roots resembling that of auxin-insensitive plants. This suggests that *PINOID*, encoding a serine-threonine protein kinase, functions as a negative regulator of auxin signalling, leading toward stature (Christensen et al., 2000). Meanwhile, auxin-response protein *IAA8* is well-known for its role as an early responder to auxin, engaging in auxin signalling by interacting with auxin response factor (*ARF*) protein and functioning as transcriptional repressors (Lavy & Estelle, 2016; Li et al., 2016; Luo et al., 2018). In Song and Xu (2013) study, overexpression of *OsIAA4* in rice leads to less sensitivity to exogenous auxin, dwarfism and more tiller angles in comparison with wild-type plants. Meanwhile, there is another auxin-response protein identified at chromosome 2 is associated with marker M013.

The gene *indole-3-pyruvate monooxygenase YUCCA6* was also identified on Chromosome 3 which is associated with marker M270. *YUCCA6* is part of the *YUCCA* family of enzymes, which are responsible for the conversion of *indole-3-pyruvate* to *indole-3-acetic acid* (*IAA*), a major form of auxin

TABLE 4. ALLELE POSITION AND VARIANT ALLELE OF MARKERS ASSOCIATED WITH HIGH INCREMENT (HINC) ON OIL PALM CHROMOSOME

Marker ID	EG5.1 chromosome	Physical position (bp)	Ref_ allele	Var_ allele	*p*-value (Hinc8)	*p*-value (Hinc16)
M346	1	34,012,126	G	T	0.013	0.0001
M011	2	3,522,890	A	C	0.018	0.000000565
M013	2	4,297,558	G	A	0.004	0.00000994
M020	3	1,307,898	A	G	0.007	0.001
M024	3	2,014,780	A	G	0.002	0.006
M270	3	13,279,910	T	C	0.006	0.001
M180	4	54,707,398	T	C	0.004	0.0002
M379	10	26,037,658	C	T	0.0025	0.021

Note: bp - base pair.

in plants. This conversion is a key step in the biosynthesis of auxin (Kim et al., 2007; Won et al., 2011).

Furthermore, *BAM1* encodes a leucine-rich repeat receptor-like serine/threonine-protein kinase (*LRR-RLKs*) located on chromosome 4 and associated with marker M180. *LRR-RLK*s are known to participate in cellular differentiation and various developmental processes. They play crucial roles in root development, shoot development and xylem differentiation (Soltabayeva et al., 2022). *LRR-RLKs* also influence hormone signalling pathways, including brassinosteroid (BR) and GA signalling pathways (Clouse, 2011). Previous studies have suggested this gene has the potential to influence oil palm rachis length (Yaakub et al., 2020).

The gene repressor of GA1-3-like 1 (*RGL1*) is linked to marker M346 on chromosome 1. It is a key component in the GA signalling pathway in plants. *RGL1* is a member of the *DELLA* family of proteins, which act as negative regulators in the GA signalling pathway. GA are plant hormones that play a crucial role in various aspects of plant growth and development, including seed germination, stem elongation and flowering (Swain & Olszewski, 1996; Wen & Chang, 2002). The GA-deficient mutant *ga1-3* is a non-germinating, extreme dwarf that flowers late and produces male-sterile flowers in *Arabidopsis* (Tyler et al., 2004).

Some of the transcription factors involved in growth and development were shortlisted, e.g., *grf1-interacting factor 1* (*GIF1*) and *ethylene-responsive transcription factors* (*ERFs*). *GIF1* is known to interact with *growth-regulating factor 1* (*GRF1*), which is a transcription factor involved in the regulation of plant growth and development. The interaction between *GIF1* and *GRF1* suggests a role in modulating gene expression related to growth processes (Lu et al., 2020). *ERFs* are plant transcription factors essential for regulating gene expression in response to ethylene, a plant hormone pivotal in numerous physiological processes such as growth, development and stress responses (Müller & Munné-Bosch, 2015). The identification of candidate genes associated with eight significant SNPs on chromosomes 1, 2, 3, 4 and 10 has been achieved through mining. These genes exhibit potential effects on Hinc in oil palms, and this is supported by their known roles in influencing comparable traits in other crop species. Although the candidate genes identified were interesting, it's essential to note that their participation and impact in regulating the Hinc in oil palm remain speculative. Further studies and research are needed to support the prediction.

CONCLUSION

Our study marks an important advance in understanding the genetic basis of Hinc in oil palm, with findings that hold substantial promise for improving oil palm breeding and agricultural productivity. By identifying eight SNPs associated with Hinc in the ELxUR oil palm population, we have developed genetic markers that enable marker-assisted selection (MAS) for height traits. This allows breeders to target specific height-related traits early in the growth cycle, even at the pre-nursery stage, which facilitates the selection of shorter palms for commercial planting, optimising land use and potentially reducing harvest costs over the lifespan of the crop.

Figure 1. Progenies of ELxUR hybrid palm crosses at the field, where a significant difference in palm height (HT) was observed.

TABLE 5. BLAST RESULTS TO THE OIL PALM GENOME IDENTIFIED 13 CANDIDATE GENES WITHIN THE 8 SIGNIFICANT SNPS AFFECTING THE HEIGHT INCREMENT (HINC) IN IOI ELxUR CROSSES

Marker ID	EG5.1 chromosome	Physical position (bp)	Nearby gene	Candidate gene position	SNP position relative to the candidate gene	Candidate gene annotation
M346	1	34,012,126	p5.00_sc00027_p0005	33,423,370...33,426,263	-588kb	*Della protein rgl1*
			p5.00_sc00027_p0020	338,05,511...33,811,810	-206kb	*GRF1-interacting factor 1*
M011	2	3,522,890	p5.00_sc00263_p0032	3,624,681...3,677,297	+101kb	*Phospholipase A*
			p5.00_sc00263_p0023	3,815,313...3,815,789	+292kb	*Ethylene-responsive transcription factor*
M013	2	4,297,558	p5.00_sc00051_p0113	4,610,179...4,614,551	+312kb	*Auxin-responsive protein IAA25*
M020	3	1,307,898	O24648 l G3OX_PEA	1,614,924...1,616,002	+307kb	*Gibberellin 3-beta-dioxygenase 1*
			p5.00_sc00220_p0033	710,029...711,493	-597kb	*Protein kinase PINOID 2*
M024	3	2,014,780	O24648 l G3OX_PEA	1,614,924...1,616,002	-400kb	*Gibberellin 3-beta-dioxygenase 1*
M270	3	13,279,910	p5.00_sc00001_p0431	13,988,128...13,993,162	+708kb	*Auxin-responsive protein IAA8*
			p5.00_sc00001_p0389	13,044,638..13,047,562	-235kb	*Indole-3-pyruvate monooxygenase YUCCA6*
M180	4	54,707,398	Q8VZG8 l Y4885_ARATH	55,216,179...55,494,670	+508kb	*Leucine-rich repeat receptor-like serine/threonine-protein kinase*
M379	10	26,037,658	p5.00_sc00004_p0377	26,034,509...26,038,761	-3kb	*Protein TITF 6b*
			p5.00_sc00004_p0376	26,021,267...26,031,321	-16kb	*TPR repeat-containing thioredoxin*
			p5.00_sc00004_p0332	25,218,092...25,244,739	-819kb	*Hydroxyproline-rich glycoprotein*

Note: bp - base pair; SNP - single nucleotide polymorphism.

These SNPs are located within genomic regions harbouring genes that have known functions related to plant growth and development, particularly in influencing height. The discovery of these candidate genes provides valuable insights into the molecular mechanisms underlying Hinc in oil palm. These genes may regulate key pathways and processes involved in plant growth, such as phytohormone signalling, cell elongation and morphogenesis. Understanding their roles in Hinc can potentially lead to the development of targeted breeding strategies aimed at enhancing this trait in oil palm populations.

Moving forward, further investigations are warranted to delve deeper into the roles and functions of these candidate genes. Additional studies, including functional genomics experiments, expression analyses and genetic mapping studies, can provide a more comprehensive understanding of how these genes contribute to Hinc in oil palms. Ultimately, this knowledge will empower breeders to make informed decisions and implement targeted breeding strategies to improve Hinc and overall productivity in oil palm cultivation.

In summary, the findings from this study establish a solid foundation for the development of improved oil palm varieties, enabling the selection of shorter palms that align with industry needs and promoting more sustainable and economically viable oil palm production systems.

ACKNOWLEDGEMENT

The authors express their sincere appreciation to IOI Plantation Berhad senior management and Plantation Director for their generous funding and permission to publish this article. The authors would like to express their gratitude to all members of the research team for their invaluable contributions throughout every phase of this study. The authors would like to thank Dr. Rajinder Singh and Dr. Ting Ngoot Chin from MPOB for their valuable advice.

REFERENCES

Babu, B. K., Mathur, R. K., Ravichandran, G., & Venu, M. V. B. (2019). Genome-wide association study (GWAS) for stem height increment in oil palm (*Elaeis guineensis*) germplasm using SNP markers. *Tree Genetics & Genomes*, *15*, 40. https://doi.org/10.1007/s11295-019-1349-2

Bai, Y., Zhao, X., Yao, X., Yao, Y., An, L., Li, X., Wang, Y., Gao, X., Jia, Y., Guan, L., Li, M., Wu, K., & Wang, Z. (2021). Genome wide association study of plant height and tiller number in hulless barley. *PLoS ONE*, *16*(12), e0260723. https://doi.org/10.1371/journal.pone.0260723

Bhagya, H. P., Babu, B. K., Gangadharappa, P. M., Naika, M. B. N., Satish, D., & Mathur, R. K. (2020). Identification of QTLs in oil palm (*Elaeis guineensis* Jacq.) using SSR markers through association mapping. *Journal of Genetics*, *99*, 19. https://doi.org/10.1007/s12041-020-1180-4

Billotte, N., Jourjon, M. F., Marseillac, N., Berger, A., Flori, A., Asmady, H., Adon, B., Singh, R., Nouy, B., Potier, F., Cheah, S. C., Rohde, W., Ritter, E., Courtois, B., Charrier, A., & Mangin, B. (2010). QTL detection by multi-parent linkage mapping in oil palm (*Elaeis guineensis* Jacq.). *Theoretical and Applied Genetics*, *120*(8), 1673–1687. https://doi.org/10.1007/s00122-010-1284-y

Bradbury, P. J., Zhang, Z., Kroon, D. E., Casstevens, T. M., Ramdoss, Y., & Buckler, E. S. (2007). TASSEL: Software for association mapping of complex traits in diverse samples. *Bioinformatics*, *23*(19), 2633–2635. https://doi.org/10.1093/bioinformatics/btm308

Carrasco, C., Wall, J., Burrell, A., Gujjula, K. R., Suren, H., Siddavatam, P., & Adams, C. (2018). A customisable high-throughput genotyping technology that permits fast, easy, and inexpensive alteration of marker content [Poster]. *Thermo Fisher Scientific*. https://assets.thermofisher.com/TFS-Assets/GSD/posters/genotyping-marker-content-alteration-poster.pdf

Chan, K., Tatarinova, T. V., Rosli, R., Amiruddin, N., Azizi, N., Halim, M. A. A., Sanusi, N. S. N. M., Jayanthi, N., Ponomarenko, P., Triska, M., Solovyev, V., Firdaus-Raih, M., Sambanthamurthi, R., Murphy, D., & Low, E. L. (2017). Evidence-based gene models for structural and functional annotations of the oil palm genome. *Biology Direct*, *12*(1). https://doi.org/10.1186/s13062-017-0191-4

Chen, G. F., Wu, R. G., Li, D. M., Yu, H. X., Deng, Z., & Tian, J. C. (2017). Genomewide association study for seeding emergence and tiller number using SNP markers in an elite winter wheat population. *Journal of Genetics*, *96*(1), 177–186. https://doi.org/10.1007/s12041-016-0731-1

Cheng, B., Gao, X., Luo, Y., Ding, Y., Chen, T., Cao, N., Xu, J., Xin, Z., & Zhang, L. (2023). Utilization of wheat 55K SNP array for QTL mapping of plant height and flag leaf in a RIL population. *Cereal Research Communications*, *52*, 1273–1286. https://doi.org/10.1007/s42976-023-00475-2

Cheng, J., Hill, C., Han, Y., He, T., Ye, X., Shabala, S., Guo, G., Zhou, M., Wang, K., & Li, C. (2023). New semi-dwarfing alleles with increased coleoptile length by gene editing of gibberellin 3-oxidase 1 using CRISPR-Cas9 in barley *(Hordeum vulgare* L.). *Plant Biotechnology Journal*, *21*(4), 806–818. https://doi.org/10.1111/pbi.13998

Christensen, S. K., Dagenais, N., Chory, J., & Weigel, D. (2000). Regulation of Auxin response by the protein kinase PINOID. *Cell*, *100*(4), 469–478. https://doi.org/10.1016/s0092-8674(00)80682-0

Clouse, S. D. (2011). Brassinosteroid signal transduction: From receptor kinase activation to transcriptional networks regulating plant development. *The Plant Cell*, *23*(4), 1219–1230. https://doi.org/10.1105/tpc.111.084475

Corley, R. H. V., & Gray, B. S. (1976). Growth and morphology. In R. H. V. Corley, J. J. Hardon, & B. J. Wood (Eds.), *Oil palm research* (pp. 7–21). Elsevier.

Corley, R. H. V., Hardon, J. J., & Tan, G. Y. (1971). Analysis of growth of the oil palm (*Elaeis guineensis* Jacq.) I. Estimation of growth parameters and application in breeding. *Euphytica*, *20*, 307–315. https://doi.org/10.1007/bf00056093

Corley, R. H. V., & Tinker, P. B. (2016). *The oil palm* (5th ed.). Wiley.

Da Silva, R. A., Caixeta, E. T., De Faria Silva, L., Sousa, T. V., Barreiros, P. R. R. M., De Oliveira, A. C. B., Pereira, A. A., Barreto, C. A. V., & Nascimento, M. (2024). Identification of SNP markers and candidate genes associated with major agronomic traits in *Coffea arabica*. *Plants*, *13*(13), 1876. https://doi.org/10.3390/plants13131876

Kim, J. I., Sharkhuu, A., Jin, J. B., Li, P., Jeong, J. C., Baek, D., Lee, S. Y., Blakeslee, J. J., Murphy, A. S., Bohnert, H. J., Hasegawa, P. M., Yun, D.-J., & Bressan, R. A. (2007). Yucca6, a dominant mutation in *Arabidopsis*, affects auxin accumulation and auxin-related phenotypes. *Plant Physiology*, *145*(3), 722–735. https://doi.org/10.1104/pp.107.104935

Lavy, M., & Estelle, M. (2016). Mechanisms of auxin signaling. *Development*, *143*(18), 3226–3229. https://doi.org/10.1242/dev.131870

Lee, M., Xia, J. H., Zou, Z., Ye, J., Rahmadsyah, N., Alfiko, Y., Jin, J., Lieando, J. V., Purnamasari, M. I., Lim, C. H., Suwanto, A., Wong, L., Chua, N., &

Yue, G. H. (2015). A consensus linkage map of oil palm and a major QTL for stem height. *Scientific Reports*, *5*, 8232. https://doi.org/10.1038/srep08232

Li, S.-B., Xie, Z., Hu, C., & Zhang, J. (2016). A review of auxin response factors (ARFs) in plants. *Frontiers in Plant Science*, *7*, 47. https://doi.org/10.3389/fpls.2016.00047

Lu, Y., Meng, Y., Zeng, J., Luo, Y., Feng, Z., Bian, L., & Gao, S. (2020). Coordination between GROWTH-REGULATING FACTOR1 and GRF-INTERACTING FACTOR1 plays a key role in regulating leaf growth in rice. *BMC Plant Biology*, *20*, 200. https://doi.org/10.1186/s12870-020-02417-0

Luo, J., Zhou, J.-J., & Zhang, J.-Z. (2018). Aux/IAA Gene family in plants: Molecular structure, regulation, and function. *International Journal of Molecular Sciences*, *19*(1), 259. https://doi.org/10.3390/ijms19010259

Mitchum, M. G., Yamaguchi, S., Hanada, A., Kuwahara, A., Yoshioka, Y., Kato, T., Tabata, S., Kamiya, Y., & Sun, T.-P. (2006). Distinct and overlapping roles of two gibberellin 3-oxidases in *Arabidopsis* development. *The Plant Journal*, *45*(5), 804–818. https://doi.org/10.1111/j.1365-313x.2005.02642.x

Morita, Y., & Kyozuka, J. (2007). Characterization of OsPID, the rice ortholog of PINOID, and its possible involvement in the control of polar auxin transport. *Plant and Cell Physiology*, *48*(3), 540–549. https://doi.org/10.1093/pcp/pcm024

Müller, M., & Munné-Bosch, S. (2015). Ethylene response factors: A key regulatory hub in hormone and stress signaling. *Plant Physiology*, *169*(1), 32–41. https://doi.org/10.1104/pp.15.00677

Noh, A., Rafii, M., Din, A. M., Kushairi, A., Norziha, A., Rajanaidu, N., Latif, M., & Malek, M. (2014). Variability and performance evaluation of introgressed Nigerian *dura* x Deli *dura* oil palm progenies. *Genetics and Molecular Research*, *13*(2), 2426–2437. https://doi.org/10.4238/2014.april.3.15

Ong, P. W., Maizura, I., Marhalil, M., Rajanaidu, N., Abdullah, N. A. P., Rafii, M. Y., Ooi, L. C. L., Low, E. T. L., & Singh, R. (2018). Association of SNP markers with height increment in MPOB-Angolan natural oil palm populations. *Journal of Oil Palm Research*, *30*(1), 61–70. https://doi.org/10.21894/jopr.2018.0003

Pootakham, W., Jomchai, N., Ruang-Areerate, P., Shearman, J. R., Sonthirod, C., Sangsrakru, D., Tragoonrung, S., & Tangphatsornruang, S. (2015). Genome-wide SNP discovery and identification of QTL associated with agronomic traits in oil palm using genotyping-by-sequencing (GBS). *Genomics*, *105*(5–6), 288–295. https://doi.org/10.1016/j.ygeno.2015.02.002

Pootakham, W., Uthaipaisanwong, P., Sangsrakru, D., Yoocha, T., Tragoonrung, S., & Tangphatsornruang, S. (2013). Development and characterization of single-nucleotide polymorphism markers from 454 transcriptome sequences in oil palm (*Elaeis guineensis*). *Plant Breeding*, *132*(6), 711–717. https://doi.org/10.1111/pbr.12095

Purcell, S., Neale, B., Todd-Brown, K., Thomas, L., Ferreira, M. A., Bender, D., Maller, J., Sklar, P., De Bakker, P. I., Daly, M. J., & Sham, P. C. (2007). PLINK: A tool set for whole-genome association and population-based linkage analyses. *The American Journal of Human Genetics*, *81*(3), 559–575. https://doi.org/10.1086/519795

Rajanaidu, N., & Jalani, B. S. (1994, 13 September). *Oil palm genetic resources – Collection, evaluation, utilisation and conservation* [Paper presentation]. Colloquium Oil Palm Genetic Resources, Malaysia.

Rajanaidu, N., Kushairi, A., & Mohd Din, A. (2017). *Monograph: Oil palm genetic resources*. Malaysian Palm Oil Board.

Reed, E., Nunez, S., Kulp, D., Qian, J., Reilly, M. P., & Foulkes, A. S. (2015). A guide to genome-wide association analysis and post-analytic interrogation. *Statistics in Medicine, 34*(28), 3769–3792. https://doi.org/10.1002/sim.6605

Seng, T.-Y., Ritter, E., Saad, S. H. M., Leao, L.-J., Singh, R. S. H., Zaman, F. Q., Tan, S., Alwee, S. S. R. S., & Rao, V. (2016). QTLs for oil yield components in an elite oil palm (*Elaeis guineensis*) cross. *Euphytica*, *212*, 399–425. https://doi.org/10.1007/s10681-016-1771-6

Soltabayeva, A., Dauletova, N., Serik, S., Sandybek, M., Omondi, J. O., Kurmanbayeva, A., & Srivastava, S. (2022). Receptor-like kinases (LRR-RLKs) in response of plants to biotic and abiotic stresses. *Plants*, *11*(19), 2660. https://doi.org/10.3390/plants11192660

Song, Y., & Xu, Z. (2013). Ectopic overexpression of an AUXIN/INDOLE-3-ACETIC ACID (AUX/IAA) gene OSIAA4 in rice induces morphological changes and reduces responsiveness to Auxin. *International Journal of Molecular Sciences*, *14*(7), 13645–13656. https://doi.org/10.3390/ijms140713645

Swain, S. M., & Olszewski, N. E. (1996). Genetic analysis of gibberellin signal transduction. *Plant Physiology*, *112*(1), 11–17. https://doi.org/10.1104/pp.112.1.11

Teh, C. -K., Ong, A. -L., Mayes, S., Massawe, F., & Appleton, D. R. (2020). Major QTLs for trunk height and correlated agronomic traits provide insights into multiple trait integration in oil palm breeding. *Genes*, *11*(7), 826. https://doi.org/10.3390/genes11070826

Ting, N., Chan, P., Buntjer, J., Ordway, J. M., Wischmeyer, C., Ooi, L. C., Low, E. T. L., Marjuni, M., Sambanthamurthi, R., & Singh, R. (2023). High-resolution genetic linkage map and height-related QTLs in an oil palm (*Elaeis guineensis*) family planted across multiple sites. *Physiology and Molecular Biology of Plants*, *29*(9), 1301–1318. https://doi.org/10.1007/s12298-023-01360-2

Ting, N., Jansen, J., Mayes, S., Massawe, F., Sambanthamurthi, R., Ooi, L. C.-L., Chin, C. W., Arulandoo, X., Seng, T., Alwee, S. S. R. S., Ithnin, M., & Singh, R. (2014). High density SNP and SSR-based genetic maps of two independent oil palm hybrids. *BMC Genomics*, *15*, 309. https://doi.org/10.1186/1471-2164-15-309

Tyler, L., Thomas, S. G., Hu, J., Dill, A., Alonso, J. M., Ecker, J. R., & Sun, T. (2004). DELLA proteins and gibberellin-regulated seed germination and floral development in *Arabidopsis*. *Plant Physiology*, *135*(2), 1008–1019. https://doi.org/10.1104/pp.104.039578

Wen, C., & Chang, C. (2002). *Arabidopsis* RGL1 encodes a negative regulator of gibberellin responses. *The Plant Cell*, *14*(1), 87–100. https://doi.org/10.1105/tpc.010325

Won, C., Shen, X., Mashiguchi, K., Zheng, Z., Dai, X., Cheng, Y., Kasahara, H., Kamiya, Y., Chory, J., & Zhao, Y. (2011). Conversion of tryptophan to indole-3-acetic acid by tryptophan aminotransferases of arabidopsis and YUCCAs in *arabidopsis*. *Proceedings of the National Academy of Sciences*, *108*(45), 18518–18523. https://doi.org/10.1073/pnas.1108436108

Yaakub, Z., Kamaruddin, K., Singh, R., Mustafa, S., Marjuni, M., Ting, N., Amiruddin, M. D., Leslie, L. E., Cheng-Li, O. L., Sritharan, K., Nookiah, R., Jansen, J., & Abdullah, M. O. (2020). An integrated linkage map of interspecific backcross 2 (BC2) populations reveals QTLs associated with fatty acid composition and vegetative parameters influencing compactness in oil palm. *BMC Plant Biology*, *20*, 356. https://doi.org/10.1186/s12870-020-02563-5

Yamaguchi, S., Smith, M. W., Brown, R. G. S., Kamiya, Y., & Sun, T. (1998). Phytochrome regulation and differential expression of gibberellin 3β-hydroxylase genes in germinating *Arabidopsis* seeds. *The Plant Cell*, *10*(12), 2115–2126. https://doi.org/10.1105/tpc.10.12.2115

Yang, Q., Zhang, J., Shi, X., Chen, L., Qin, J., Zhang, M., Yang, C., Song, Q., & Yan, L. (2023). Development of SNP marker panels for genotyping by target sequencing (GBTS) and its application in soybean. *Molecular Breeding*, *43*, 26. https://doi.org/10.1007/s11032-023-01372-6

Zourelidou, M., Absmanner, B., Weller, B., Barbosa, I. C., Willige, B. C., Fastner, A., Streit, V., Port, S. A., Colcombet, J., De La Fuente Van Bentem, S., Hirt, H., Kuster, B., Schulze, W. X., Hammes, U. Z., & Schwechheimer, C. (2014). Auxin efflux by PIN-FORMED proteins is activated by two different protein kinases, D6 PROTEIN KINASE and PINOID. *eLife*, *3*. https://doi.org/10.7554/elife.02860

Journal of Oil Palm Research Vol. 38 (3) September 2026 p. 472–482
DOI: https://doi.org/10.21894/jopr.2025.0034

CYTOTOXIC AND ANTI-ACNE ACTIVITY OF SUGAR FATTY ACID ESTERS (SFAE) FROM CPO AND PALM OIL HYDROLYSATE

TUTI WUKIRSARI[1]*; ADE ANDRIANI[2]; OBIE FAROBIE[3]; SRI HANDAYANI[1] and SUMI HUDIYONO[1]

ABSTRACT

This study aimed to determine the potential of sugar fatty acid esters (SFAE) derived from crude palm oil (CPO) and palm oil hydrolysates as cytotoxic and anti-acne agents. The influence of structural variations among different saccharides on the SFAE properties was also investigated. Three types of saccharides were tested in this study; D-mannitol (a sugar alcohol), D-mannose (an aldose) and D-fructose (a ketose). SFAEs were prepared enzymatically by reacting fatty acids and saccharides using the low-cost liquid lipase Eversa® Transform 2.0 at 5% (w/w) concentration. Thin layer chromatography (TLC) analysis, Fourier transform infrared spectroscopy (FTIR) and nuclear magnetic resonance (NMR) spectra, emulsification properties, conversion rate and degree of esterification indicated the formation of SFAE. Some SFAE exhibited strong cytotoxic and antibacterial activities. SFAE of palmitic acid-mannitol and SFAE of stearic acid-fructose showed the highest cytotoxic activity against MCF-7 cells, with an IC_{50} value of 29 ppm. The SFAE of palm oil hydrolysate exhibited stronger cytotoxic activity than the SFAE of CPO hydrolysate. Additionally, the SFAE from CPO hydrolysate and D-mannitol exhibited the strongest antibacterial activity, achieving 100% inhibition against Cutibacterium acnes *at 0.9 mg/mL. These findings highlight the potential of SFAE as a promising raw materials for the development of health and cosmetic products.*

Keywords: CPO and palm oil hydrolysate, cytotoxic and anti-acne activities, enzymatic esterification, Eversa® Transform 2.0, sugar fatty acid ester.

Received: 25 July 2024**; Accepted:** 21 April 2025**; Published online:** 16 July 2025.

INTRODUCTION

Indonesia and Malaysia are the two largest palm oil producers in the world, accounting for most of global production (U.S. Department of Agriculture, 2024). These two countries dominate the market because of their favourable climates for palm oil cultivation and large-scale plantations. However, by the end of 2022, the European Union issued a new regulation on deforestation-free products that tightened the rules for importing crude palm oil (CPO) into its territory. Therefore, downstreaming palm oil and CPO into derivative products (oleochemicals) is crucial in increasing their sales value and benefits. The most common oleochemical products were fatty acid hydrolysates, glycerin, soap noodles and oleic acid. Oleochemical products in the form of sugar fatty acid esters (SFAE) have not been widely studied. One of the companies operating in this field is Ryoto™ Sugar Ester, which is based in Japan. The main application of sucrose-fatty acid esters from Ryoto™ is as an emulsifier in the food sector.

The application of SFAE as an emulsifier in the food industry showed that these compounds are safe for consumption (Sardar et al., 2024). The emulsification properties of SFAE have also been applied to the pharmaceutical, detergent and cosmetics industries (Qi et al., 2024). The non-ionic surfactant SFAE has also been used to produce niosomes for quercetin encapsulation (Elmowafy

[1] Department of Chemistry, Faculty of Mathematics and Sciences, Universitas Indonesia, Depok, West Java 16424, Indonesia.

[2] Research Centre for Biotechnology, National Research and Innovation Agency, Jl. Raya Bogor, Cibinong, Bogor, West Java 16911, Indonesia.

[3] Department of Mechanical and Biosystem Engineering, Faculty of Agricultural Engineering and Technology, IPB University (Bogor Agricultural University), IPB Dramaga Campus, Bogor, West Java 16680, Indonesia.

* *Corresponding author e-mail: tutiwukirsari@sci.ui.ac.id*

et al., 2020). Niosome-encapsulated quercetin showed a higher hepatoprotective activity than free quercetin. Emulsification properties have also been reported to be associated with biological activities, such as antibacterial (Falk, 2019; Pirog et al., 2019) and anticancer (Chiewpattanakul et al., 2010; Walvekar et al., 2022). Emulsifiers or surfactants can damage the membranes of both microbes and cancer cells. The cytotoxic activity of SFAE has been described by Teng et al. (2021), Snoch et al. (2021), Chen et al. (2023) and Wang et al. (2024), while the antimicrobial activity of SFAE has been reported by Matin et al. (2020, 2022), Teng et al. (2021), and Yang et al. (2024). The role of SFAE in suppressing inflammation caused by acne bacteria was even reported by a US patent in 2005 (Pauly & Grisoni, 2005). However, study on the bioactivity comparison of SFAE from CPO hydrolysate and palm oil hydrolysate for anticancer and anti-acne has never been reported. Study into developing SFAE as a safe active compound is expected to be an alternative to anticancer and anti-acne medication. Anticancer and anti-acne medicines with minimal side effects are urgently needed because recent research by Vitiello et al. (2024) even shows that anticancer drugs can change the ocular surface of cancer chemotherapy patients. Wiśniewska et al. (2023) mentioned that salicylic acid, a well-known anti-acne cosmetic ingredient, causes several side effects such as hyperpigmentation, allergic reaction and swelling.

SFAE can be prepared either chemically or enzymatically. The chemical synthesis of SFAE has been described using a base-catalysed transesterification reaction between triglycerides or fatty acid methyl esters and sugars (Teng et al., 2021). In contrast, lipases have been widely reported for the enzymatic synthesis of SFAE. Surprisingly, proteases also exhibited the ability to catalyse the formation of SFAE (Bernal et al., 2018). Commercially available lipases that are widely used for the synthesis of SFAE include immobilised lipase B derived from *Candida antarctica* (Chen et al., 2023; Hollenbach et al., 2020; Nieto et al., 2021; Shin et al., 2019; Snoch et al., 2021) and immobilised lipase derived from *C. rugosa* (El-Baz et al., 2021). Ferdjani and Selaimia (2024) prepared SFAE using lipase from maize seed. The utilisation of lipase Eversa® Transform 2.0 as a catalyst for synthesising SFAE has never been studied. Eversa® Transform 2.0 is a low-cost liquid lipase for biodiesel production (Chang et al., 2021; Farobie et al., 2021). Monteiro et al. (2024) reported the utilisation of Eversa® Transform 2.0 to produce fatty ester for biolubricants. This study prepared several SFAEs from CPO and palm oil hydrolysates using Eversa® Transform 2.0 lipase as the catalyst. Commercially available pure palmitic acid, stearic acid and oleic acid were also employed to prepare SFAE as a comparison. Three types of saccharides were used in this study, namely, D-mannitol (a sugar alcohol), D-mannose (an aldose) and D-fructose (a ketose), to better understand the relationship between the structural moiety, chemical reactivity and bioactivity. The feasibility of SFAE application in the health and cosmetics sector was explored by screening the synthesised SFAE for anticancer (cytotoxic) activity against MCF-7 cells and antimicrobial activity against *Cutibacterium acnes*. The MCF-7 cell line is a model for studying breast cancer, whereas *C. acnes* is associated with *Acne vulgaris*. Cancer is among the top ten causes of death worldwide, and breast cancer is among the top five deadly cancers (Sung et al., 2021).

MATERIALS AND METHODS

Fifteen SFAEs were included in this study. Fatty acids were obtained by the hydrolysis of CPO and palm oil. The palm oil was purchased from a local supermarket. Commercially pure (≥ 98.0%) palmitic acid (Merck, Germany), stearic acid (Pudak Scientific, Indonesia) and oleic acid were used in this study. D-Mannitol and D-fructose were obtained from Sigma-Aldrich (USA) and D-mannose from HiMedia (India). The commercial lipase Eversa® Transform 2.0 from Novozyme (Denmark) was used as the catalyst in this study. Thin layer chromatography (TLC) analysis was conducted on TLC aluminium sheets coated with silica gel 60 F_{254} using 2′, 7′-dichlorofluorescein (Sigma-Aldrich) as the staining agent. All chemicals were used without further purification.

Hydrolysis of CPO and Palm Oil

The CPO and palm oil were hydrolysed separately under alkaline conditions. CPO and palm oil were separately mixed with a 1M NaOH solution in alcohol. The reaction mixture was refluxed for 1 hr and monitored using TLC. A solution of 1M HCl was added to the reaction mixture to neutralise the product. The product was extracted twice using *n*-hexane, dried using anhydrous Na_2SO_4 and concentrated to obtain CPO and palm oil hydrolysates. The fatty acid composition of CPO and palm oil was analysed using GC-MS. The acid and iodine numbers were also measured using the standard titrimetric method.

Synthesis of SFAE

Prior to the reaction, the reactants were dissolved in a suitable solvent. Fatty acids were dissolved separately in *n*-hexane, whereas the saccharides were dissolved in a small amount of water. Fatty acids were obtained by the hydrolysis of CPO, hydrolysis of palm oil and commercially available fatty acids. Saccharides solution was added to the fatty acid solution followed by 5% weight-in-weight (w/w) lipase Eversa® Transform 2.0. The mole ratio of saccharide to fatty acid was 1:6. The mixture was incubated at 40°C for 48 hr and stirred at 500 rpm. The reaction mixture was heated at 100°C to deactivate the enzyme and stop the reaction. The product was separated from the reaction mixture by centrifugation. The product was washed with water to separate the enzyme and hexane to remove unreacted fatty acid. The amount of unreacted fatty acid was measured by acid-base titration using NaOH solution in alcohol. Conversion rate and degree of esterification were calculated by using the Equation (1) and (2):

$$\text{Conversion rate} = \frac{\text{Mole of initial fatty acid} - \text{Mole of unreacted fatty acid}}{\text{mole of initial fatty acid}} \times 100\% \quad (1)$$

$$\text{Degree of esterification} = \frac{\text{Mole of initial fatty acid} - \text{Mole of unreacted fatty acid}}{\text{Mole of saccharide}} \quad (2)$$

All SFAE was analysed by using Fourier transform infrared spectroscopy (FTIR) and only a representative of SFAE was analysed by using nuclear magnetic resonance (NMR) to confirm the formation of SFAE. FTIR spectra were analysed on potassium bromide (KBr) using a Shimadzu 2450 Prestige (Shimadzu Corp., Japan). ^{1}H-NMR and ^{13}C-NMR spectra were recorded in CD_3OD (Merck, Germany) on a Bruker Avance Neo 500 (500 MHz) spectrophotometer (Bruker Biospin, Germany).

Emulsification Properties

The emulsification properties of SFAE were evaluated by adding 50 mg of SFAE to a water-oil mixture. A water-in-oil (w/o) emulsion was prepared by mixing 0.3 mL of water and 1 mL of oil, while a mixture of 0.3 mL of oil and 1 mL of water was used as a model for an oil-in-water (o/w) emulsion. The mixture containing SFAE was vortexed. The stability of the emulsions was observed for 24 hr. Phase separation was used as the parameter for emulsion stability. A light microscope and water-soluble dye (methylene blue) were used to facilitate observation of the emulsion. The emulsification properties of the starting material (saccharides and fatty acids) were also observed. A mixture of water and oil without a sample was used as the negative control.

Cytotoxic Activity Against MCF-7

MCF-7 cell suspension was added to 96-well plates at 5,000 cells/100 µL of medium. Dulbecco's Modified Eagle Medium (DMEM) supplemented with 10% fetal bovine serum was used as the medium. The medium was enriched with 100 U/mL of penicillin and 100 µg/mL of streptomycin to prevent microbial contamination. The cells were incubated for 24 hr at 37°C before the addition of a series concentration of SFAE samples in dimethyl sulfoxide (DMSO). The final concentration of DMSO in the medium was 1% volume-in-volume (v/v). Therefore, 1% DMSO was used as the negative control. After 48 hr of incubation, 10 µL 3-(4,5-dimethylthiazol-2-yl)-2,5-diphenyl-2H-tetrazolium bromide (MTT) (5 mg/mL) was added to each well. The plates were then incubated for another 4 hr. Ethanol was added to dissolve the formazan, and the sample absorption was read at 595 nm. The experiment was conducted in triplicate.

Antimicrobial Activity Against *C. acnes*

Antibacterial activity against *C. acnes* was determined using the broth dilution method in reinforced clostridial medium (RCM). A 250 mL *C. acnes* suspension was mixed with 5 mL RCM media and a 250 mL sample at room temperature. The DMSO was used as the SFAE solvent and the negative control. A 1,000 ppm salicylic acid was used as a positive control (the final concentration was 45 ppm). Antibacterial activity was determined by measuring optical density at 600 nm (OD600). The experiment was conducted in duplicate.

RESULTS AND DISCUSSION

Fatty Acid Composition of CPO and Palm Oil

The fatty acid composition of palm oil and CPO was analysed using GC-MS (*Table 1*). CPO and palm oil showed similar fatty acid compositions. Oleic acid and palmitic acid were the major fatty acid constituents of CPO and palm oil, respectively. However, the oleic acid content of palm oil was slightly higher than that of CPO. Moreover, unsaturated medium-chain fatty acids (C8 and C10) were only detected in CPO but not in palm oil. Chompoo et al. (2019) reported that the degumming process during the conversion of CPO to palm oil increased the total amount of unsaturated fatty acids and reduced the total amount of saturated fatty acids.

Hydrolysates of CPO and Palm Oil

Hydrolysis of both CPO and palm oil was conducted under alkaline conditions. Acidic conditions were avoided to prevent changes in the C=C configuration of the unsaturated fatty acids in CPO and palm oil. The hydrolysate of CPO had a lower R_f value (R_f = 0.57, hexane-ethyl acetate 3:1) on TLC than the starting material (R_f = 0.86, hexane-ethyl acetate 3:1), indicating the conversion of triglycerides to fatty acids. The TLC analysis of palm oil and its hydrolysate also showed a similar trend. The CPO hydrolysate was an orange solid, whereas the palm oil hydrolysate was a pale-yellow solid. Izuddin et al. (2022) stated that CPO is rich in β-carotene. Thus, the orange colour of CPO hydrolysate exhibited that the β-carotene could not be separated from the fatty acids. However, the presence of β-carotene in CPO hydrolysates did not interfere with the SFAE synthesis through the esterification reactions due to the absence of hydroxyl and carboxyl groups in its structure.

The formation of fatty acids from the hydrolysis of CPO and palm oil was also demonstrated by a significant increase in the acid number after hydrolysis (*Table 2*). However, the iodine numbers before and after hydrolysis were within similar ranges. It can be concluded that hydrolysis under alkaline conditions did not influence the unsaturated fatty acid content in CPO and palm oil. The electron-rich nature of the C=C bond is not reactive towards the nucleophilic property of the hydroxide anion from the alkaline hydrolysis reaction. The difference in chemical composition between CPO and palm oil hydrolysates affected the acid and iodine number values. CPO hydrolysate contained fatty acids and other nonpolar compounds (Goon et al., 2019) that cannot be separated during hydrolysis.

Synthesis of SFAE

The enzymatic reaction for preparing SFAE was conducted at 40°C according to Chang et al. (2021) and Farobie et al. (2021). Farobie et al. (2021) stated that 40°C was the optimum temperature for enzymatic esterification using Eversa® Transform 2.0 lipase. The esterification reaction in this research was carried out in an organic phase with as little water as possible to promote the esterification and prevent the hydrolysis of the product. The water was used only to dissolve the sugar. The amount of water was calculated depending on the solubility of each saccharide. Therefore, molecular sieves were not used in the present study. Water adsorption by the molecular sieve separated the sugar from the reaction mixture. The esterification reaction catalysed by lipase occurs at the interface between the organic phase and water (Khan et al., 2017). Under hydrophobic conditions, the subdomain covering the lipase active site shifted, and the active site was accessible to the substrate. Hexane, which has a log *P*-value of 3.5, was chosen as the hydrophobic solvent in this study. Kumar et al. (2016) stated that solvents with log *P*-values above 2 did not interfere with the essential water in enzymes. Thus, hexane did not influence the active conformation of lipase.

The formation of SFAE was indicated by the appearance of a white layer between the water and hexane layers (*Figure 1*). The SFAE obtained in this research was sparingly insoluble in water or hexane at room temperature. The solubility test of sucrose fatty acid esters in water conducted by Nagai et al. (2017) showed that nine out of ten samples precipitated in water. Sucrose-lauric acid ester was the only sucrose ester that formed a transparent homogeneous solution (Nagai et al., 2017). The orange colour of the hexane layer in the SFAE of CPO hydrolysate (*Figure 1a*) denoted the presence of β-carotene. The β-carotene and SFAE of CPO hydrolysate can be separated easily at this stage.

TABLE 1. FATTY ACID COMPOSITION OF CRUDE PALM OIL (CPO) AND PALM OIL SAMPLES

Fatty acids	Percentage (%)	
	CPO	Palm oil
Caprylic acid (C8:0)	0.02	-
Capric acid (C10:0)	0.02	-
Lauric acid (C12:0)	0.18	0.21
Myristic acid (C14:0)	0.94	0.93
Palmitic acid (C16:0)	39.60	36.00
Stearic acid (C18:0)	4.59	4.08
Oleic acid (C18:1; 9c)	40.60	44.20

TABLE 2. ACID NUMBER AND IODINE NUMBER BEFORE AND AFTER HYDROLYSIS OF CRUDE PALM OIL (CPO) AND PALM OIL SAMPLES

Quality parameter	CPO		Palm oil	
	Before	After	Before	After
Acid number (mg NaOH/g sample)	28.6	204.8	5.3	183.1
Iodine number (mg I/g sample)	54.7	n.d	58.4	51.5

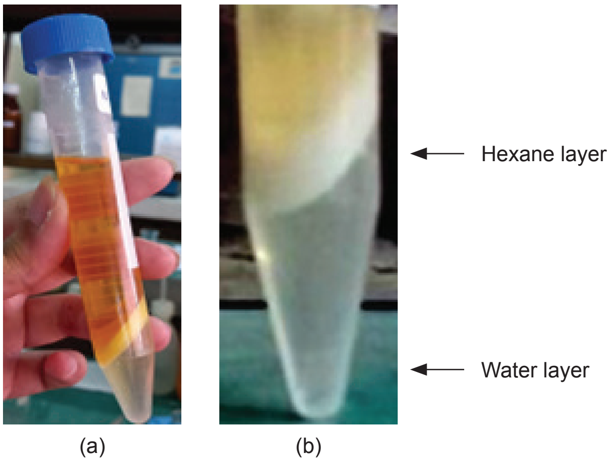

Figure 1. Formation of sugar fatty acid ester (SFAE) from (a) crude plam oil (CPO) and (b) palm oil hydrolysate.

Conversion Rate and Degree of Esterification

The esterification between carboxylic acids and alcohols is a reversible reaction. This study used an excessive amount of fatty acids to shift the equilibrium towards the formation of SFAE. The amount of reacted fatty acids was used to calculate the conversion rate and the degree of esterification (*Table 3*). The conversion rate and degree of esterification vary for each SFAE. In general, the Eversa® Transform 2.0 lipase used in this study preferred oleic acid, followed by stearic acid and palmitic acid. Depending on the source, lipases exhibit selectivity toward certain fatty acids (Halldorsson et al., 2004).

TABLE 3. CONVERSION RATE AND DEGREE OF ESTERIFICATION DURING THE SYNTHESIS OF SFAE

Sample's name	Conversion rate (%)	Degree of esterification
SFAE palmitic acid-mannitol	11.70	0.8
SFAE palmitic acid-mannose	21.40	1.3
SFAE palmitic acid-fructose	27.30	1.6
SFAE stearic acid-mannitol	30.30	1.8
SFAE stearic acid-mannose	20.60	1.2
SFAE stearic acid-fructose	13.90	0.8
SFAE oleic acid-mannitol	39.73	2.4
SFAE oleic acid-mannose	19.11	1.1
SFAE oleic acid-fructose	20.67	1.2
SFAE CPO-mannitol	74.80	4.4
SFAE CPO-mannose	58.10	2.0
SFAE CPO-fructose	61.00	3.7
SFAE palm oil-mannitol	22.40	1.3
SFAE palm oil-mannose	34.30	1.4
SFAE palm oil-fructose	21.80	2.0

Note: SFAE - sugar fatty acid esters; CPO - crude palm oil.

Most of the SFAE obtained in this study had a low degree of esterification. Zheng et al. (2015) reported that the products of enzymatic esterification commonly had a low degree of substitution. Lipase enzymes are more selective towards primary hydroxyl groups because of their low steric hindrance (Zago et al., 2021). Based on their structures, D-mannitol and D-fructose have two primary hydroxyl groups, whereas D-mannose only has one. Therefore, the degree of esterification of D-mannitol and D-fructose SFAE should be higher than that of D-mannose. SFAE of CPO hydrolysate, SFAE of oleic acid and SFAE of stearic acid showed the highest degree of esterification in D-mannitol. The hydroxyl groups of D-mannitol were assumed to be more reactive than those of D-fructose because D-mannitol does not form furanose or pyranose structures in solution. Meanwhile, the SFAE of palm oil hydrolysate and the SFAE of palmitic acid exhibited different behaviours, with D-fructose possessing the highest degree of esterification. Although the fatty acid compositions of CPO hydrolysate and palm oil hydrolysate were similar, the SFAE of CPO hydrolysate displayed a higher degree of esterification than SFAE-palm oil. The non-fatty acid components of the CPO hydrolysate may promote lipase activation. Sterol, vitamin E, dolichol and polyprenol are components of CPO (Goon et al., 2019) that may be responsible for lipase activation. Study by Delome et al. (2011) proved that the presence of surfactant can increase the activity of lipase by changing the three-dimensional structure of the enzyme and improving the accessibility of the substrate to the active site.

FTIR and NMR Spectra of SFAE

The formation of SFAE was confirmed by using FTIR and NMR spectra. The representative data of the FTIR spectra can be seen in *Figure 2*. The FTIR spectrum of the fatty acid (palmitic acid) showed a typical very broad hydroxyl peak at 3,400–2,500 cm^{-1} and a sharp carbonyl peak absorption of carboxylic acid at 1,703 cm^{-1}. On the other hand, the hydroxyl group of the D-fructose and D-mannitol appeared as a broad peak at 3,400–3,000 cm^{-1}. The absence of a very broad hydroxyl peak of the carboxylic group in the SFAE indicated the formation of an ester group between fatty acid (palmitic acid) and saccharides. Moreover, the shifting of the carbonyl peak to a higher frequency (1,734 cm^{-1}) also proved the presence of an ester group of SFAE.

The ^{13}C-NMR spectrum (*Figure 3a*) of SFAE palmitic acid-fructose exhibited the presence of carbonyl groups of esters at 175 and 176 ppm. The formation of an ester between palmitic acid and fructose can also be seen from the ^{1}H-NMR spectrum (*Figure 3b*). Based on the peak integral value, it can be concluded that the degree of esterification of SFAE palmitic acid-fructose was more than one. The number of protons from the palmitoyl was about twice the number of protons from the D-fructose. However, the peak of fructose's acidic protons (the hydroxyl groups) cannot be seen clearly because the acidic protons are able to exchange with deuterated methanol as the analysis solvent. This data was suitable with the degree of esterification of SFAE palmitic acid-fructose.

Emulsification Properties of SFAE

The surfactant properties of the starting materials (fatty acids and saccharides) and SFAE obtained in this study were examined by emulsification test in w/o and o/w systems. Emulsion stability was determined based on visual observation. The saccharides could not stabilise both w/o and o/w mixture. The o/w mixture with the addition of fatty acids gave a milky system that underwent phase separation after 15 min. The milky system consisting of a w/o system and fatty acids was stable for up to 30 min. Fameau et al. (2012) described that the fatty acids can reduce the surface tension.

The addition of SFAE prolonged the phase separation of the w/o and o/w system. All SFAE were more suitable for w/o emulsions than o/w emulsion systems. The phase separation was not

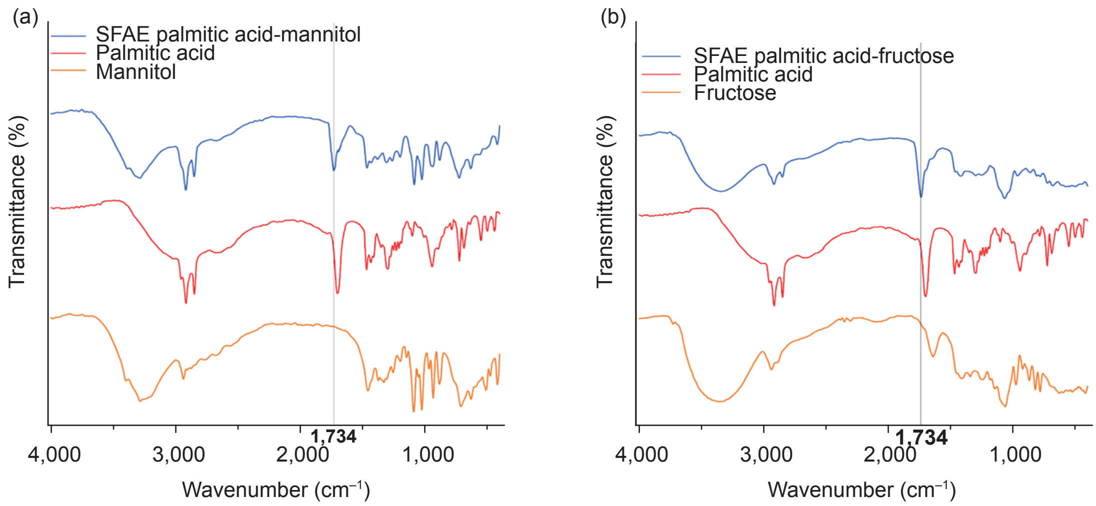

Figure 2. *Fourier transform infrared spectroscopy (FTIR) spectra of (a) sugar fatty acid ester (SFAE) palmitic acid-fructose and (b) SFAE palmitic acid-mannitol compared to its starting material.*

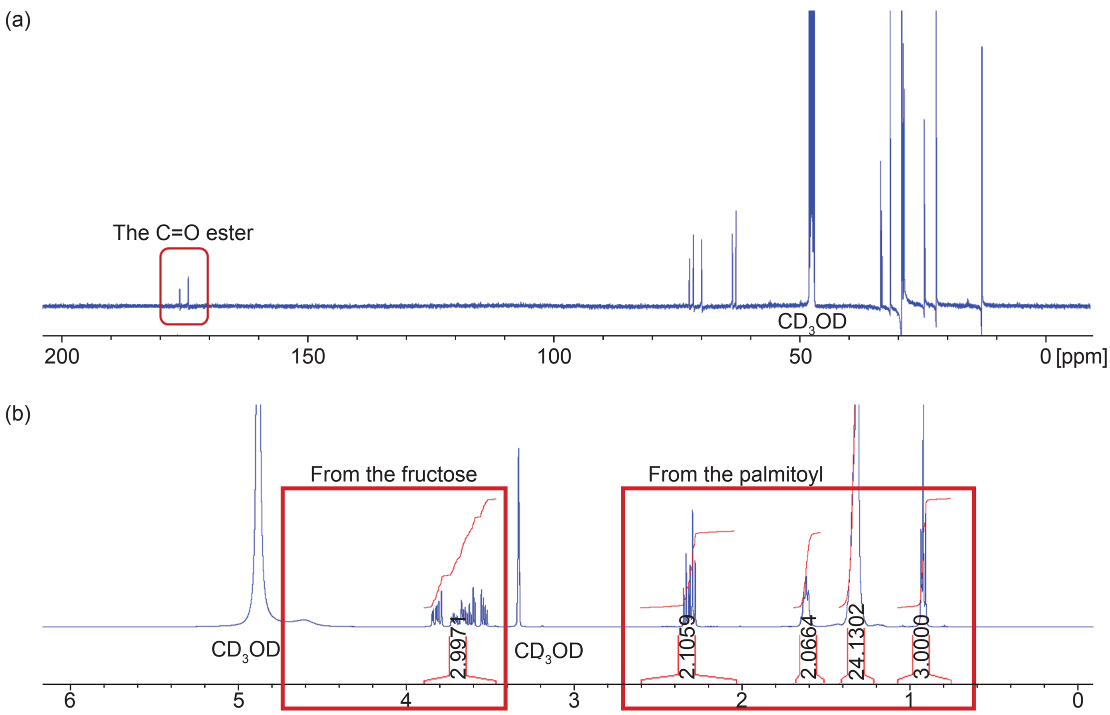

Figure 3. *(a) ^{13}C-NMR and (b) ^{1}H-NMR spectrum of sugar fatty acid ester (SFAE) palmitic acid-fructose.*

observed on the w/o emulsion system containing SFAE after 24 hr. On the other hand, phase separation of the o/w system was noticed after 4 hr. SFAE possesses emulsifying properties because of the polar residues from sugar and nonpolar residues from fatty acids (Teng et al., 2021). Representative data are presented in *Figure 4a* and *4b*. *Figure 4c* shows the microscopic observation of the w/o emulsion. Blue indicates the water phase.

Cytotoxic Activity Against MCF-7

The cytotoxic activity of SFAE was determined using an MTT assay based on mitochondrial enzyme activity in viable MCF-7 breast cancer cells (Perinelli et al., 2016). The cytotoxic activity of SFAE varied, with IC_{50} values between 29 and 200 ppm (*Table 4*). The SFAE of saturated fatty acids (palmitic and stearic acid) was more cytotoxic than the SFAE of oleic acid. These data are consistent with our previous research on the cytotoxicity of lipoamide derivatives. Lipoamides from saturated fatty acids exhibited the lowest IC_{50} value compared to lipoamides from unsaturated fatty acids (Wukirsari et al., 2024). The presence of the C=C bond is disadvantageous for cytotoxicity.

The cytotoxicity SFAE of D-mannose was lower than the SFAE of D-fructose and D-mannitol. The hydrophilic part SFAE of D-mannose (a pyranose ring) is bigger than D-fructose (a furanose ring) and D-mannitol (a linear chain). Among the SFAEs of D-fructose and D-mannitol synthesised from the same fatty acids, in general, the cytotoxic activity was inversely proportional to the degree of esterification. The SFAE of CPO hydrolysate with a higher degree of esterification also possessed lower cytotoxicity than the SFAE of palm oil hydrolysate. It seemed that the large size of SFAEs was unfavourable for SFAE-cell membrane interaction. According to Bunchongprasert and Shao (2020), the bulky size of the hydrophilic parts of fatty acid ester increased the intermolecular interactions of micelles and limited the SFAE interactions with the phospholipid bilayer membrane of cancer cells. The disruption of cell membrane integrity is important for the cytotoxic activity of SFAE (Bunchongprasert & Shao, 2020). Okabe et al. (1999) stated that SFAE inhibited cancer cell proliferation by suppressing the secretion of TNF-α.

TABLE 4. CYTOTOXIC ACTIVITY OS SUGAR-FATTY ACID ESTERS (SFAE) AGAINST MCF-7 CELL LINE

Sample's name	IC_{50} (ppm)
SFAE palmitic acid-mannitol	29.5 ± 3.6
SFAE palmitic acid-mannose	95.9 ± 5.4
SFAE palmitic acid-fructose	78.4 ± 6.0
SFAE stearic acid-mannitol	54.3 ± 2.2
SFAE stearic acid-mannose	104.4 ± 7.2
SFAE stearic acid-fructose	29.7 ± 2.0
SFAE oleic acid-mannitol	127.4 ± 3.6
SFAE oleic acid-mannose	>200
SFAE oleic acid-fructose	125.2 ± 1.1
SFAE CPO-mannitol	131.0 ± 28.0
SFAE CPO-mannose	107.0 ± 11.0
SFAE CPO-fructose	66.0 ± 5.5
SFAE palm oil-mannitol	65.5 ± 1.0
SFAE palm oil-mannose	102.8 ± 3.0
SFAE palm oil-fructose	65.5 ± 1.0

Note: SFAE - sugar fatty acid esters; CPO - crude palm oil.

Antimicrobial Activity Against *C. acnes*

Using the broth dilution method, SFAE applications in the cosmetic sector were investigated by determining their antibacterial activity against the acne-causing bacterium *C. acnes*. The assay was conducted at a 0.9 mg/mL concentration for all samples. Bacterial growth was directly proportional to the optical density value. Therefore, samples with lower optical densities displayed higher antimicrobial activity. CPO hydrolysate, palm oil hydrolysate and SFAE showed antibacterial activity against *C. acnes* (*Table 5*). The sugar moiety of SFAE

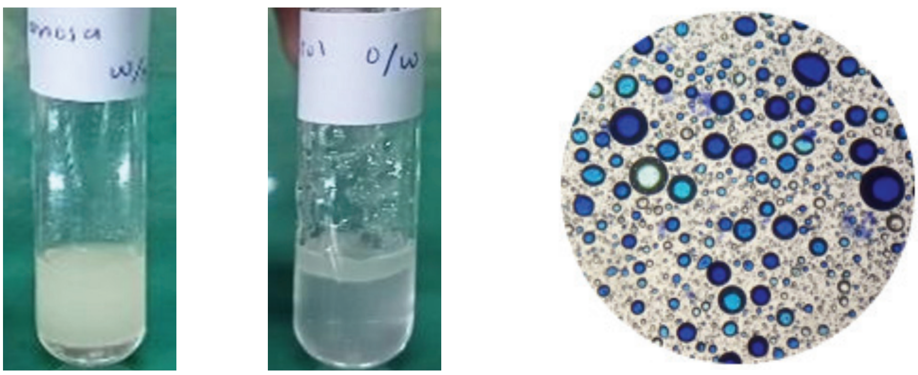

(a) (b) (c)

Figure 4. Emulsification of sugar fatty acid ester (SFAE) properties in the (a) w/o and (b) o/w emulsion systems. (c) Observation of the w/o emulsion under a microscope; the blue colour indicates water dyed with methylene blue.

exhibited variable effects on antibacterial activity against *C. acnes*. Based on its cell wall composition, *C. acnes* is classified as a Gram-positive bacteria (Mayslich et al., 2021). Zhao et al. (2015) mentioned that Gram-positive bacteria were more sensitive towards SFAE than Gram-negative bacteria. Many researchers have also reported the antibacterial activity of fatty acids against *Propionibacterium acnes* (*C. acnes*) (Casillas-Vargas et al., 2021; Desbois & Lawlor, 2013; Kim et al., 2021). Several mechanisms for the antibacterial activity of fatty acids have been reported. Unsaturated fatty acids have been reported to prevent bacterial growth by interfering with DNA replication, cell wall formation and protein synthesis (Desbois & Lawlor, 2013). The disruption of bacterial cell membrane permeability by SFAE has been proposed by Zhao et al. (2015). Zhao et al. (2015) observed the leakage of bacterial cell components such as protein and reducing sugars after being treated with SFAE. Disruption of the microbe membrane is associated with the emulsification properties of SFAE (Falk, 2019; Pirog et al., 2019). The emulsification properties are influenced by the degree of esterification of SFAE and its HLB value (Chen et al., 2023). Therefore, the CPO and palm oil hydrolysate and also SFAE are promising candidate as active ingredient in anti-acne agents. The addition of SFAE as an ingredient in anti-acne products will provide dual benefits, i.e., as an antibacterial and emulsifier agent. The strong antimicrobial activity of SFAE was also stated by Yang et al. (2024).

TABLE 5. ANTIMICROBIAL ACTIVITY AGAINST *Cutibacterium acnes*

Sample's name	Inhibition (%)
CPO hydrolysate	86 ± 17
SFAE CPO-mannitol	100 ± 0
SFAE CPO-mannose	23
SFAE CPO-fructose	35 ± 12
Palm oil hydrolysate	100 ± 0
SFAE palm oil-mannitol	35 ± 9
SFAE palm oil-mannose	39 ± 9
SFAE palm oil-fructose	81 ± 6
Salicylic acid (45 mg/mL)	25 ± 1.7

Note: SFAE - sugar fatty acid esters; CPO - crude palm oil.

CONCLUSION

In this study, SFAE were synthesised through enzymatic esterification using the lipase enzyme Eversa® Transform 2.0. The potent cytotoxic effect was attributed to the saturated fatty constituents (acyl group) of the SFAE and SFAE having a low degree of esterification. SFAE of palmitic acid-mannitol and SFAE of stearic acid-fructose showed the highest cytotoxic activity against MCF-7 breast cancer cells, with an IC_{50} value of 29 ppm. The SFAE of palm oil hydrolysate with a lower degree of esterification exhibited stronger cytotoxic activity than the SFAE of CPO hydrolysate. In contrast, SFAE from CPO hydrolysate and D-mannitol showed the strongest antibacterial activity achieving 100% inhibition against *C. acnes* at 0.9 mg/mL.

ACKNOWLEDGEMENT

This study was financially supported by the Research Grant Faculty of Mathematics and Natural Sciences, Universitas Indonesia (PKS-034/UN2.F3.D/PPM.00.02/2023). We would also like to thank AERG 23 (Alisya Rahmah, Angelia Sabrina Lexthariana, Novella Dhindha Pangestika, Olan Maulana and Zahrotun Nisa) for the support.

REFERENCES

Bernal, C., Poveda-Jaramillo, J. C., & Mesa, M. (2018). Raising the enzymatic performance of lipase and protease in the synthesis of sugar fatty acid esters, by combined ionic exchange -hydrophobic immobilisation process on aminopropyl silica support. *Chemical Engineering Journal*, *334*, 760–767. https://doi.org/10.1016/j.cej.2017.10.082

Bunchongprasert, K., & Shao, J. (2020). Effect of fatty acid ester structure on cytotoxicity of self-emulsified nanoemulsion and transport of nanoemulsion droplets. *Colloids and Surfaces B: Biointerfaces*, *194*, 111220. https://doi.org/10.1016/j.colsurfb.2020.111220

Casillas-Vargas, G., Ocasio-Malavé, C., Medina, S., Morales-Guzmán, C., Del Valle, R. G., Carballeira, N. M., & Sanabria-Ríos, D. J. (2021). Antibacterial fatty acids: An update of possible mechanisms of action and implications in the development of the next-generation of antibacterial agents. *Progress in Lipid Research*, *82*, 101093. https://doi.org/10.1016/j.plipres.2021.101093

Chang, M. Y., Chan, E., & Song, C. P. (2021). Biodiesel production catalysed by low-cost liquid enzyme Eversa® Transform 2.0: Effect of free fatty acid content on lipase methanol tolerance and kinetic model. *Fuel*, *283*, 119266. https://doi.org/10.1016/j.fuel.2020.119266

Chen, J-Q., Hai, Y-W., Qing, C., Liang, M-Y., Banwell, M. G., & Lan, P. (2023). The synthesis of certain fatty acid ester derivatives of trehalose and an investigation of their emulsifying properties and bioactivities. *LWT – Food Science and Technology, 187*, 115369. https://doi.org/10.1016/j.lwt.2023.115369

Chiewpattanakul, P., Phonnok, S., Durand, A., Marie, E., & Thanomsub, B. W. (2010). Bioproduction and anticancer activity of biosurfactant produced by the dematiaceous fungus *Exophiala dermatitidis* SK80. *Journal of Microbiology and Biotechnology*, *20*(12), 1664–1671.

Chompoo, M., Damrongwattanakool, N., & Raviyan, P. (2019). Effect of chemical degumming process on physicochemical properties of red palm oil. *Songklanakarin Journal of Science & Technology, 41*(3), 513–521.

Delome, V., Dhouib, R., Canaan, S., Fotiadu, F., Carrière, F., & Cavalier, J.-F. (2011). Effect of surfactant on lipase structure, activity, and inhibition. *Pharmaceutical Research, 28*, 1831–1842. https://doi.org/10.1007/s11095-010-0362-9

Desbois, A. P., & Lawlor, K. C. (2013). Antibacterial activity of long-chain polyunsaturated fatty acids against *Propionibacterium acnes* and *Staphylococcus aureus*. *Marine Drugs*, *11*(11), 4544–4557. https://doi.org/10.3390/md11114544

El-Baz, H. A., Elazzazy, A. M., Saleh, T. S., Dourou, M., Mahyoub, J. A., Baeshen, M. N., Madian, H. R., & Aggelis, G. (2021). Enzymatic synthesis of glucose fatty acid esters using SCOs as acyl group-donors and their biological activities. *Applied Sciences*, *11*(6), 2700. https://doi.org/10.3390/app11062700

Elmowafy, E., El-Derany, M. O., Biondo, F., Tiboni, M., Casettari, L., & Soliman, M. E. (2020). Quercetin loaded monolaurate sugar esters-based niosomes: Sustained release and mutual antioxidant-hepatoprotective interplay. *Pharmaceutics*, *12*(2), 143. https://doi.org/10.3390/pharmaceutics12020143

Falk, N. A. (2019). Surfactants as antimicrobials: A brief overview of microbial interfacial chemistry and surfactant antimicrobial activity. *Journal of Surfactants and Detergents, 22*(5), 1119–1127. https://doi.org/10.1002/jsde.12293

Fameau, A.-L., Ventureira, J., Novales, B., & Douliez, J.-P. (2012). Foaming and emulsifying properties of fatty acids neutralized by tetrabutylammonium hydroxide. *Colloids and Surfaces A: Physicochemical and Engineering Aspects, 403,* 87–95. https://doi.org/10.1016/j.colsurfa.2012.03.059

Farobie, O., Jannah, Q. R., & Hartulistiyoso, E. (2021). Biodiesel production from crude palm oil under different free fatty acid content using Eversa® Transform 2.0 enzyme. *International Journal of Renewable Energy Research, 11*(4), 1590–1596. https://doi.org/10.20508/ijrer.v11i4.12338.g8366

Ferdjani, S., & Selaimia, O. (2024). Synthesis of sugar esters using maize seed lipase as a biocatalyst. *Hungarian Journal of Industry and Chemistry, 52*(1), 9–14. https://doi.org/10.33927/hjic-2024-02

Goon, D. E., Kadir, S. H. S. A., Latip, N. A., Rahim, S. A., & Mazlan, M. (2019). Palm oil in lipid-based formulations and drug delivery systems. *Biomolecules, 9*(2), 64. https://doi.org/10.3390/biom9020064

Halldorsson, A., Kristinsson, B., & Haraldsson, G. G. (2004). Lipase selectivity toward fatty acids commonly found in fish oil. *European Journal of Lipid Science and Technology, 106*(2), 79–87. https://doi.org/10.1002/ejlt.200300867

Hollenbach, R., Ochsenreither, K., & Syldatk, C. (2020). Enzymatic synthesis of glucose monodecanoate in a hydrophobic deep eutectic solvent. *International Journal of Molecular Sciences*, *21*(12), 1–11. https://doi.org/10.3390/ijms21124342

Izuddin, W. I., Loh, T. C., Akit, H., Nayan, N., Noor, A. M., & Foo, H. L. (2022). Influence of dietary palm oils, palm kernel oil and soybean oil in laying hens on production performance, egg quality, serum biochemicals and hepatic expression of beta-carotene, retinol and alpha-tocopherol genes. *Animals*, *12*(22), 3156. https://doi.org/10.3390/ani12223156

Khan, F. I., Lan, D., Durrani, R., Huan, W., Zhao, Z., & Wang, Y. (2017). The lid domain in lipases: Structural and functional determinant of enzymatic properties. *Frontiers in Bioengineering and Biotechnology, 5*, 16. https://doi.org/10.3389/fbioe.2017.00016

Kim, Y. G., Lee, J. H., & Lee, J. (2021). Antibiofilm activities of fatty acids including myristoleic acid against *Cutibacterium acnes* via reduced cell hydrophobicity. *Phytomedicine*, *91*, 153710. https://doi.org/10.1016/j.phymed.2021.153710

Kumar, A., Dhar, K., Kanwar, S. S., & Arora, P. K. (2016). Lipase catalysis in organic solvents: Advantages and applications. *Biological Procedures Online, 18*, 2. https://doi.org/10.1186/s12575-016-0033-2

Matin, M. M., Bhuiyan, M. M. H., Kibria, S. M., & Hasan, M. S. (2022). Synthesis, pass predication of antimicrobial activity and pharmacokinetic properties of hexanoyl galactopyranosides and experimental evaluation of their action against four human pathogenic bacteria and four fungal strains. *Pharmaceutical Chemistry Journal*, *56*, 627–637. https://doi.org/10.1007/s11094-022-02687-y

Matin, M. M., Hasan, M. S., Uzzaman, M., Bhuiyan, M. M. H., Kibria, S. M., Hossain, M. E., & Roshid, M. H. O. (2020). Synthesis, spectroscopic characterisation, molecular docking, and ADMET studies of mannopyranoside esters as antimicrobial agents. *Journal of Molecular Structure*, *1222*, 128821. https://doi.org/10.1016/j.molstruc.2020.128821

Mayslich, C., Grange, P. A., & Dupin, N. (2021). *Cutibacterium acnes* as an opportunistic pathogen: An update of its virulence-associated factors. *Microorganisms*, *9*(2), 303. https://doi.org/10.3390/microorganisms9020303

Monteiro, R. R. C., de Mela Neta, M. M. F., Rocha, W. S., Soares, J. B., de Luna, F. M. T., Fernandez-Lafuente, R., & Vieira, R. S. (2024). Optimizing the enzymatic production of biolubricants by the Taguchi method: Esterification of the free fatty acids from castor oil with 2-ethyl-1-hexanol catalyzed by Eversa Transform 2.0. *Enzyme and Microbial Technologu, 175,* 110409. https://doi.org/10.1016/j.enzmictec.2024.110409

Nagai, Y., Kawano, S., Motoda, K., Tomida, M., Tatebe, C., Sato, K., & Akiyama, H. (2017). Solubility testing of sucrose esters of fatty acids in international food additive specifications. *Biological and Pharmaceutical Buletin*, *40*(3), 284–289. https://doi.org/10.1248/bpb.b16-00738

Nieto, S., Villa, R., Donaire, A., & Lozano, P. (2021). Ultrasound-assisted enzymatic synthesis of xylitol fatty acid esters in solvent-free conditions. *Ultrasonics Sonochemistry*, *75*, 105606. https://doi.org/10.1016/j.ultsonch.2021.105606

Okabe, S., Suganuma, M., Tada, Y., Ochiai, Y., Sueoka, E., Kohya, H., Shibata, A., Takahashi, M., Mizutani, M., Matsuzaki, T., & Fujiki, H. (1999). Disaccharide esters screened for inhibition of tumor necrosis factor-α release are new anti-cancer agents. *Japanese Journal of Cancer Research*, *90*(6), 669–676. https://doi.org/10.1111/j.1349-7006.1999.tb00799.x

Pauly, G., & Grisoni, P. (2005). *Use of sugar esters in cosmetic and/or pharmaceutical preparations*. (U.S. Patent No. 2005/0220726 A1). U.S. Patent Application Publication.

Perinelli, D. R., Casettari, L., Cespi, M., Fini, F., Man, D. K. W., Giorgioni, G., Canala, S., Lam, J. K. W., Bonacucina, G., & Palmieri, G. F. (2016). Chemical-physical properties and cytotoxicity of *N*-decanoyl amino acid-based surfactants: Effect of polar heads. *Colloids and Surfaces A: Physicochemical and Engineering Aspects*, *492*, 38–46. https://doi.org/10.1016/j.colsurfa.2015.12.009

Pirog, T. P., Lutsay, D. A., Kliuchka, L. V., & Beregova, K. A. (2019). Antimicrobial activity of surfactants of microbial origin. *Biotechnologia Acta*, *12*(1), 30–57. https://doi.org/10.15407/biotech12.01.039

Qi, Y., Chen, M., Jin, T., Chong, W., Zhang, Z., Nian, B., & Hu, Y. (2024). Computer-aided engineering of lipase solvent tolerance enhanced their applications in sugar esters industry: State of the art. *Trends in Food Science and Technology, 144*, 104323. https://doi.org/10.1016/j.tifs.2023.104323

Sardar, N. R., Akabari, S. H., Bhatt, H. G., & Modi, R. B. (2024). Role of sucrose ester for enhancing the food quality and safety: A review. *Asian Journal of Food Research and Nutrition 3*(3), 425–430. https://journalajfrn.com/index.php/AJFRN/article/view/144

Shin, D. W., Mai, N. L., Bae, S. W., & Koo, Y. M. (2019). Enhanced lipase-catalysed synthesis of sugar fatty acid esters using supersaturated sugar solution in ionic liquids. *Enzyme and Microbial Technology*, *126*, 18–23. https://doi.org/10.1016/j.enzmictec.2019.03.004

Snoch, W., Wnuk, D., Witko, T., Staroń, J., Bojarski, A. J., Jarek, E., Plou, F. J., & Guzik, M. (2021). In search of effective anticancer agents-novel sugar esters based on polyhydroxyalkanoate monomers. *International Journal of Molecular Sciences*, *22*(13), 7238. https://doi.org/10.3390/ijms22137238

Sung, H., Ferlay, J., Siegel, R. L., Laversanne, M., Soerjomataram, I., Jemal, A., & Bray, F. (2021). Global cancer statistics 2020: GLOBOCAN estimates of incidence and mortality worldwide for 36 cancers in 185 countries. *CA: A Cancer Journal for Clinicians, 71(3)*, 209–249. https://doi.org/10.3322/caac.21660.

Teng, Y., Stewart, S. G., Hai, Y. W., Li, X., Banwell, M. G. & Lan, P. (2021). Sucrose fatty acid esters:

Synthesis, emulsifying capacities, biological activities and structure-property profiles. *Critical Reviews in Food Science and Nutrition, 61*(19), 3297–3317. https://doi.org/10.1080/10408398.2020.1798346

U.S. Department of Agriculture. (2024, October 7). *Palm oil production: Top producing countries*. https://fas.usda.gov/data/production/commodity/4243000

Vitiello, L., Lixi, F., Coco, G., & Giannaccare, G. (2024). Ocular surface side effect of novel anticancer drugs. *Cancer*, *16*(2), 344. https://doi.org/10.3390/cancers16020344

Walvekar, S., Yasaswi, S., Shetty, K., & Yadav, K. S. (2022). Applications of surfactin and other biosurfactants in anticancer activity. In *Green sustainable process for chemical and environmental engineering and science* (pp. 223–234). Elsevier. https://doi.org/10.1016/B978-0-323-85146-6.00024-3

Wang, Y., Wang, Z., Sun, Y., Zhu, M., Jiang, Y., Bai, H., Yang, B., & Kuang, H. (2024). Isovaleryl sucrose esters from *Atractylodes japonica* and their cytotoxic activity. *Molecules*, *29*(13), 3069. https://doi.org/10.3390/molecules29133069

Wiśniewska, J., Klasik-Ciszewska, S., & Duda-Grychtoł, K. (2023). Salicylic acid and its use in cosmetology. *Aesthetic Cosmetology and Medicine*, *12*(3), 91–95. https://doi.org/10.52336/acm.2023.011

Wukirsari, T., Nadiroh, N., Kembara, T. F., Gunawan, M. I. A., Priosoeryanto, B. P., Handayani, S., & Hudiyono, S. (2024). The effect of fatty alkanolamide structure on cytotoxic and antimicrobial activity. *Egyptian Journal of Chemistry*, *67*(9), 289–295. https://doi.org/10.21608/ejchem.2023.212786.8007

Yang, J., Huang, D., Wang, X., Liu, Q., & Guo, R. (2024). Research progress of eco-friendly sugar-based surfactants. *Academic Journal of Science and Technology, 10*(2), 70–77. https://doi.org/10.54097/002vp898

Zago, E., Joly, N., Chaveriat, L., Lequart, V., & Martin, P. (2021). Enzymatic synthesis of amphiphilic carbohydrate esters: Influence of physicochemical and biochemical parameters. *Biotechnology Reports, 30*, e00631. https://doi.org/10.1016/j.btre.2021.e00631

Zhao, L., Zhang, H., Hao, T., & Li, S. (2015). *In vitro* antibacterial activities and mechanism of sugar fatty acid esters against five food-related bacteria. *Food Chemistry, 187*, 370–377. https://doi.org/10.1016/j.foodchem.2015.04.108

Zheng, Y., Zheng, M., Ma, Z., Xin, B., Guo, R., & Xu, X. (2015). Sugar fatty acid esters. *Polar Lipids*, 215–243. https://doi.org/10.1016/b978-1-63067-044-3.50012-1

Journal of Oil Palm Research Vol. 38 (3) September 2026 p. 483–493
DOI: https://doi.org/10.21894/jopr.2025.0028

GENETIC PERFORMANCE OF 3-WAY (MPOB-NIGERIA × DELI) *Dura* × *Pisifera* OIL PALM CROSSES

NOR AZWANI, A B[1*]; ZULKIFLI YAAKUB[1]; NORAZIYAH ABD AZIZ SHAMSUDIN[2]; MARHALIL MARJUNI[1] and FADILA AHMAD MALIKE[1]

ABSTRACT

The AVROS and Yangambi populations represent the primary paternal lineages utilised in global oil palm seed production and breeding programmes. This study assessed the progeny performance of two 3-way crosses, Cross I (MPOB-Nigeria × Deli) Dura × *AVROS* Pisifera *and Cross II (MPOB-Nigeria × Deli)* Dura × *Yangambi* Pisifera *with emphasis on bunch yield, bunch quality components and vegetative traits. All genotypes were cultivated using a Randomised Complete Block Design (RCBD) in 2011. Analysis of variance (ANOVA) revealed highly significant variations between genotypes for most traits of bunch yield, bunch quality components, and vegetative traits, indicating the impact of their genetic background on these variables. PKG115 from Cross II produced the highest fresh fruit bunches (FFB) at 264.46 kg palm^{-1} yr^{-1} and oil yield (OY) at 62.67 kg palm^{-1} yr^{-1}, whereas PKG144 from Cross I obtained an exceptional oil to bunch (O/B) of 29.35%. The broad-sense heritability (h_b^2) for leaflet length (LL) was estimated at 61.17%, indicating greater genetic variance than the other traits. Due to its excellent FFB yields, high mesocarp to fruit ratio (M/F) and OY, with low shell to fruit ratio (S/F), PKG115 has been recognised as a potential parental material for upcoming oil palm breeding programmes.*

Keywords: AVROS, oil yield, 3-way cross, Yangambi.

Received: 12 December 2023; **Accepted:** 7 April 2025; **Published online:** 5 June 2025.

INTRODUCTION

Palm oil dominates the global vegetable oil market, representing more than 60% of worldwide oil-bearing crop exports (Organisation for Economic Co-operation and Development [OECD] & Food and Agriculture Organization of the United Nations [FAO], 2022). In 2021, approximately one-third of the global oil and fat production (241.36 million tonnes) originated from major palm oil-producing countries: Indonesia (42.00 million tonnes), Malaysia (18.15 million tonnes) and Thailand (3.38 million tonnes) (Oil World, 2021; U.S. Department of Agriculture, 2024). Considering the expanding world population and rising standards of living, the demand for palm oil is estimated to increase to at least 240 million tonnes by 2050 (Corley, 2009; Srisawasdi et al., 2023). Palm oil has been used in a variety of high-end manufacturing processes, especially in the chemical, pharmaceutical and food sectors. Additionally, it is frequently used as a primary raw material in biodiesel manufacturing due to its relatively cheaper cost compared to other oil crops (Mukherjee & Sovacool, 2014).

For several decades, the Deli *Dura* × AVROS *Pisifera* (D×P) hybrid has been the predominant commercial planting material in Malaysia and globally (Kushairi et al., 1999), although some seed producers also develop Deli *Dura* × Yangambi *Pisifera* hybrids (Kushairi et al., 2011).

[1] Malaysian Palm Oil Board,
6, Persiaran Institusi, Bandar Baru Bangi,
43000 Kajang, Selangor, Malaysia.

[2] Department of Biological Sciences and Biotechnology,
Faculty of Science and Technology,
Universiti Kebangsaan Malaysia,
43600 Bangi, Selangor, Malaysia.

* *Corresponding author e-mail: nor.azwani@mpob.gov.my*

However, the development of these D×P planting materials in the global oil palm industry remains heavily dependent on a limited genetic pool. The Deli populations in Malaysia trace their origins to only four Bogor palms, while the AVROS and Yangambi *Pisifera*s were derived from the "Djongo" palms of the Eala Botanical Garden in Zaire (currently Democratic Republic of the Congo). The limited genetic base of the current planting materials poses a significant challenge for further yield improvements. To address this issue, the Malaysian Palm Oil Board (MPOB), together with members from the industry, has gathered 1,467 oil palm accessions from the wild populations since the 1970s. This was done to achieve substantial improvement of the oil palm's genetic diversity. MPOB currently owns the biggest collection of oil palm germplasm in the world (Martin et al., 2022; Okwuagwu et al., 2011; Rajanaidu, 1994). The collection of *Elaeis guineensis* and *E. oleifera* germplasm was brought into Malaysia for cultivation and evaluation at the MPOB Research Station Kluang. Results of continued germplasm evaluation have been implemented into the ongoing process of improving the breeding stock (Rajanaidu et al., 2000; Yaakub et al., 2023) and developing superior D×P planting materials (Arolu et al., 2017; Fadila et al., 2024).

Genes from new germplasm sources were introgressed into the existing Deli and AVROS populations to improve the breeding stock. Noh et al. (2014) reported significant genetic variability among 12 introgressed Nigeria *Dura* × Deli *Dura* oil palm progenies, highlighting adequate potential for further breeding and selection. The progenies had demonstrated exceptional performance, producing high fresh fruit bunches (FFB) yields of up to 212 kg palm^{-1} yr^{-1} and oil to bunch (O/B) of up to 19%. Similarly, progenies from MPOB-Zaire *Tenera* × AVROS *Pisifera* and MPOB-Nigeria *Tenera* × AVROS *Pisifera* demonstrated strong potential as new *Pisifera* pollen sources for commercial D×P seed production. The top-performing progenies from these crosses achieved high oil yields (OY) of 36.15 and 35.47 kg palm^{-1} yr^{-1}, respectively (Nor Azwani et al., 2020).

These introgressed progenies served as the foundation for initiating 3-way and 4-way crosses at MPOB, with the goal of leveraging heterosis, where hybrids outperform their parents. Consequently, the primary objective of this study was to evaluate 18 3-way *Dura* (D×D) × *Pisifera* (P) progenies, derived from two 3-way crosses: Cross I (MPOB-Nigeria × Deli) *Dura* × AVROS *Pisifera* and Cross II (MPOB-Nigeria × Deli) *Dura* × Yangambi *Pisifera* with emphasis on yield, bunch quality and vegetative characteristics. The parental lines of superior progenies can be utilised in the development of commercial D×P seed production and breeding programmes to mitigate the yield stagnation observed in the oil palm sector over the past two decades.

MATERIALS AND METHODS

Planting Materials

Eight genotypes (progenies) from Cross I, and 10 from Cross II were planted in a triangular planting arrangement, spaced 9 m apart, utilising a Randomised Complete Block Design (RCBD) (*Table 1*). The *Pisifera* was an AVROS descendant of BM119 from the Oil Palm Research Station, Banting, Selangor, Malaysia, while the Yangambi was from FELDA Agricultural Services Sdn. Bhd. (FASSB). The genotypes were planted in Trial 0.529 at MPOB Research Station Hulu Paka, Terengganu, Malaysia, in 2011. The mean annual rainfall from 2016–2021 was 3,458.33 mm yr^{-1}, ranging from 2,934.00–3,811.00 mm yr^{-1}. Fertiliser was provided every three months for each palm, at a rate of 3 kg palm^{-1} yr^{-1}. Each genotype is represented by four replications.

Data Collection

The yield performance of each genotype was recorded for each palm at intervals of two rounds each month. The FFB yield is the sum of bunch weight, whereas the average bunch weight (ABW) is the ratio of FFB to bunch number (BNO). Each palm weight and number were recorded at every harvesting cycle, from 36 months after field planting, and data for four consecutive years (2017–2020) were used for analysis. To evaluate the oil extraction and bunch quality components, the bunch analysis method established by Blaak et al. (1963) and modified by Rao et al. (1983) was implemented. Three to five bunches were sampled from each palm from 2016 to 2021. Ripe bunches with one to 10 loose fruits were randomly collected at least three months after the previous palm to eliminate seasonal change (Rao, 1987). One round of vegetative measurement was applied in 2019, at eight years following field planting, as suggested by Corley and Breure (1981).

Statistical Analysis

The data on bunch yield, bunch quality components, and vegetative characters were analysed using the Statistical Analytical System (SAS version 9.4). The analysis of variance (ANOVA) for all traits was conducted. The means of the data obtained were subjected to analysis of variance using a general linear model (PROC GLM) due to some missing and uneven distribution of

TABLE 1. LIST OF *Tenera* (D×P) GENOTYPES

No.	Cross-type	Genotype code	MPOB-Nigeria × Deli *Dura* code	Female parent (A)	Male parent (B)	Pedigree
1	Cross I	PKG116	D1	0.318/1,165	0.395/419	0.318/1,165 × 0.395/419
2		PKG124	D2	0.318/1,052	0.395/419	0.318/1,052 × 0.395/419
3		PKG136	D3	0.318/4	0.395/384	0.318/4 × 0.395/384
4		PKG144	D3	0.318/4	0.395/419	0.318/4 × 0.395/419
5		PKG153	D4	0.318/572	0.395/384	0.318/572 × 0.395/384
6		PKG163	D5	0.318/618	0.395/419	0.318/618 × 0.395/419
7		PKG169	D6	0.318/403	0.395/419	0.318/403 × 0.395/419
8		PKG164	D6	0.318/403	0.395/384	0.318/403 × 0.395/384
9	Cross II	PKG100	D7	0.318/583	0.395/176	0.318/583 × 0.395/176
10		PKG102	D1	0.318/1,165	0.395/148	0.318/1,165 × 0.395/148
11		PKG110	D2	0.318/1,052	0.395/176	0.318/1,052 × 0.395/176
12		PKG111	D1	0.318/1,165	0.395/176	0.318/1,165 × 0.395/176
13		PKG115	D8	0.318/2	0.395/148	0.318/2 × 0.395/148
14		PKG126	D9	0.318/1,018	0.395/176	0.318/1,018 × 0.395/176
15		PKG141	D3	0.318/4	0.395/176	0.318/4 × 0.395/176
16		PKG142	D8	0.318/2	0.395/176	0.318/2 × 0.395/176
17		PKG166	D6	0.318/403	0.395/176	0.318/403 × 0.395/176
18		PKG151	D10	0.318/673	0.395/148	0.318/673 × 0.395/148
19	SC	PK 5193		0.212/3	0.174/247	0.212/3 × 0.174/247

Note: Cross I - (MPOB-Nigeria × Deli) *Dura* × AVROS *Pisifera*; Cross II - (MPOB-Nigeria × Deli) *Dura* × Yangambi *Pisifera*; SC - Standard cross Deli *Dura* × AVROS *Pisifera*.

the progeny's palms (Arolu et al., 2016). Duncan's new multiple range test (DMRT) was used for the comparison between the genotype means while the least significant difference (LSD) analysis was used to compare the means between crosses. Broad-sense heritability (h_b^2) statistics were estimated for each character, using variance components. The variance analysis for the estimation of h_b^2 was processed from the variance component procedure (PROC VARCOMP) using the formula in Equation (1):

$$h_b^2 = \frac{\sigma_g^2}{\sigma_g^2 + \sigma_e^2} \quad (1)$$

where, σ_g^2 is the genotype variance and σ_e^2 is the error variance. The 18 three-way *Dura* (D×D) × *Pisifera* (P) genotypes were used to calculate the h_b^2 from the $2h_b^2$ (Falconer & Mackay, 1996).

RESULTS AND DISCUSSION

Agro-morphological Variabilities in Bunch Yield

The ANOVA revealed no significant differences in the FFB, BNO and ABW between the two crosses (*Table 2*), while there were significant differences in FFB and ABW ($p < 0.01$) among the genotypes, but not in BNO. For bunch yield traits, the coefficient of variation (CV) for FFB was the highest for both cross-type (25.57%) and genotype (23.58%). In contrast, the CV values for ABW were the lowest, which were 19.52% (cross-type) and 17.32% (genotype). The observed variability in the genotypes was related to the nature of these traits as the yield and yield component traits are quantitatively regulated by polygenes (Ithnin et al., 2021). A wide genetic variation among genotypes is critical for oil palm breeding and selection because it could enhance breeding efficiency and selection gains (Nor Azwani et al., 2020).

Among genotypes, PK115 from Cross II recorded the highest FFB mean yield (264.46 kg palm^{-1} yr^{-1}), followed by PKG136 from Cross I (204.13 kg palm^{-1} yr^{-1}), with yields 69.31% and 30.69% higher than the standard cross (SC), respectively (*Table 3*). The outstanding FFB yield is not surprising as the MPOB-Nigeria genotype had successfully produced over 200 kg palm^{-1} yr^{-1} through its use as a *Pisifera* parent crossed with Deli *Dura* in the PS1.1 planting material (Mohd Din et al., 2023). PKG115's high FFB yields is likely associated to its high ABW of 15.57 kg bunch^{-1} while PKG126 from Cross II exhibited the lowest

FFB yield (159.23 kg palm^{-1} yr^{-1}), attributed to its low ABW (11.21 kg bunch^{-1}) despite having a moderate BNO (14.21 bunches palm^{-1} yr^{-1}). These results are in contrast with the observations by Arolu et al. (2016) and Myint et al. (2019), where the BNO of their genotypes was suggested to affect their FFB yields. Although a high BNO is necessary for a high FFB, the most important component for an even higher yield is the ABW (Kushairi et al., 2001). The significance of ABW in determining FFB yields was possibly due to an earlier selection pressure for high BNO, which resulted in the consistently high BNO of varied ABW displayed in the current planting materials.

TABLE 2. ANOVA RESULTS FOR BUNCH YIELD COMPONENTS BASED ON THE CROSS-TYPES AND GENOTYPES

Source of variance	df	FFB	BNO	ABW
Cross-type	1	2,277.96^{ns}	8.89^{ns}	0.16^{ns}
Error	214	2,331.83	10.93	6.56
Total	215	501,290.11	2,347.63	1,403.56
CV (%)		25.57	22.66	19.52
Genotype	17	6,393.81**	15.81^{ns}	22.48**
Error	198	1,982.81	10.50	5.16
Total	215	501,290.11	2,347.63	1,403.56
CV (%)		23.58	22.21	17.32

Note: ** and ns - significant at $P \leq 0.01$ and not significant, respectively; df - degrees of freedom; FFB - fresh fruit bunches; BNO - bunch number; ABW - average bunch weight; CV - coefficient of variation.

TABLE 3. COMPARISON OF THE BUNCH YIELD COMPONENTS MEANS AMONG CROSSES AND GENOTYPES

No.	Cross-type	Genotype code	FFB (kg palm^{-1} yr^{-1})	BNO (No. palm^{-1} yr^{-1})	ABW (kg bunch^{-1})
1	Cross I	PKG116	179.52^{ab}	13.83	13.04^{b-f}
2		PKG124	167.35^{ab}	14.17	11.95d^{ef}
3		PKG136	204.13^{b}	15.31	13.75^{a-e}
4		PKG144	199.27^{ab}	16.27	12.38^{def}
5		PKG153	171.58^{ab}	13.08	13.40^{b-f}
6		PKG163	191.08^{ab}	14.92	12.85^{c-f}
7		PKG169	176.52^{ab}	14.56	12.27^{def}
8		PKG164	192.29^{ab}	12.77	15.04^{ab}
	Cross I mean		185.22	14.36	13.09
9	Cross II	PKG100	198.88^{ab}	15.19	13.24^{b-f}
10		PKG102	190.06^{ab}	14.19	14.12^{a-d}
11		PKG110	188.17^{ab}	16.02	12.10^{def}
12		PKG111	162.38^{ab}	14.10	11.56^{ef}
13		PKG115	**264.46^{a}**	16.73	**15.57^{a}**
14		PKG126	**159.23^{ab}**	14.21	**11.21^{f}**
15		PKG141	182.33^{ab}	15.69	11.69^{ef}
16		PKG142	197.15^{ab}	13.35	14.91^{abc}
17		PKG166	177.77^{ab}	15.10	11.88^{ef}
18		PKG151	197.13^{ab}	13.15	15.13^{ab}
	Cross II mean		191.75	14.77	13.14
19	SC	PK5193	156.20	9.74	15.68
	Cross mean		188.85	14.59	13.12
LSD 0.05 (Cross I vs. Cross II)			13.03 ns	0.89 ns	0.69 ns

Note: Cross I - (MPOB-Nigeria × Deli) *Dura* × AVROS *Pisifera;* Cross II - (MPOB-Nigeria × Deli) *Dura* × Yangambi *Pisifera;* SC- Standard cross Deli *Dura* × AVROS *Pisifera*. FFB - fresh fruit bunches; BNO - bunch number; ABW - average bunch weight. Means with the same superscript letters are not significantly different at $p \leq 0.05$ based on Duncan's new multiple range test (DMRT). Figures in bold within the mean column are minimum and maximum values.

Agro-morphological Variabilities in Bunch Quality Component Traits

There were no significant differences in all of the bunch quality component traits observed between the cross-types, except for the O/B ratio (*Table 4*). However, a comparison among genotypes revealed that all bunch quality component traits were highly significant, except for fruit to bunch ratio (F/B), which was significant. The kernel yield (KY) had the highest CV values of 41.52% for cross-type and 39.76% for genotype, demonstrating substantial variation. On the other hand, traits like oil to dry matter (O/DM) and mesocarp to fruit (M/F) showed much lower variability, suggesting these traits are more stable across the crosses and genotypes. The genetic variation in oil palm populations is useful for conservation and breeding programmes to develop new improved varieties with desirable traits. These results correspond with Nor Azwani et al. (2022), who reported high genetic variability in bunch quality traits in MPOB-Nigeria *Dura* × AVROS *Pisifera* genotypes.

In addition, the LSD test indicated that Cross I produced a better O/B ratio than Cross II, with half of the genotypes exceeding an O/B of 28% (*Table 5*). The results revealed that PKG144 from Cross I achieved the highest O/B of 29.35%, which is 5.54% higher than the SC. The excellent O/B may be attributed to the AVROS, which are recognised for their high oil-to-bunch ratios (Amiruddin et al., 2020; Lee & Yeow, 1985). The results obtained were comparable to PS1.1 materials, which produce an O/B of about 28% (Mohd Din et al., 2023). Besides displaying the highest O/B, PKG144 also produced the highest M/F although it exhibited the lowest kernel to fruit (K/F), kernel to bunch (K/B), and shell to fruit (S/F). On the other hand, PKG126 produced the highest K/B and thickest S/F among the Cross II genotypes, with corresponding lowest M/F, O/DM, and O/B values. Both mesocarp and shell traits have an impact on all oil palm breeding and selection programmes (Swaray et al., 2020). The selection process usually prioritises a high M/F ratio instead of an S/F ratio to produce high yielding planting materials.

The oil component in these O/DM, O/B and OY traits refers to the mesocarp oil. Thus, the oil output for each bunch is significantly affected by the fruit's mesocarp composition, which leads to oil yield production (Corley & Tinker, 2016; Gawankar et al., 2022). PKG115 from Cross II recorded the highest oil yield (OY), making it highly valuable for oil production. Furthermore, its high M/F and F/B ratios added to its productivity. About 95% of OY is from the mesocarp (M/F), which determines the O/B and consequently affects the OY (Corley, 2003; Gawankar et al., 2022). Since the OY is a composite character, it is highly dependent on other components such as FFB, M/F, S/F and O/B. From these findings, the OY observed from PKG115 was likely attributed to its high FFB yield and M/F.

Agro-morphological Variabilities in Vegetative Characters

Significant differences in the vegetative traits were observed only for the petiole cross-section (PCS), leaflet length (LL), and leaf width (LW) between the cross-type (*Table 6*). In addition, there was a significant influence of the genotype on all vegetative characters, suggesting variation among the genotypes. The PCS exhibited the highest CV of 23.15% among cross-types and 22.64% among genotypes, whereas the leaf number (LN) trait recorded the lowest CV of 6.92% among cross-types and 6.34% among genotypes. Arolu et al. (2017) also observed a substantial influence of the

TABLE 4. ANOVA RESULT FOR BUNCH QUALITY COMPONENTS BASED ON CROSS-TYPES AND GENOTYPES

Source of variance	df	M/F	K/F	S/F	O/DM	F/B	O/B	K/B	OY	KY
Cross-type	1	0.31^{ns}	5.13^{ns}	2.91^{ns}	4.88^{ns}	0.50^{ns}	84.90*	2.82^{ns}	80.60^{ns}	13.89^{ns}
Error	214	22.40	5.04	8.50	4.67	24.82	11.25	2.63	149.73	9.90
Total	215	4,793.53	1,082.91	1,821.64	1,004.10	5,312.70	2,492.68	566.16	3,2123.78	2,133.35
CV (%)		5.75	28.73	29.32	2.72	7.83	12.44	34.92	27.63	41.52
Genotype	17	76.85**	16.49**	29.21**	12.46**	42.46*	29.21**	8.53**	462.29**	19.73**
Error	198	17.61	4.05	6.69	4.00	23.19	10.08	2.13	122.55	9.08
Total	215	4,793.53	1,082.91	1,821.64	1,004.10	5,312.70	2,492.68	566.16	32,123.78	2,133.35
CV (%)		5.10	25.77	26.01	2.52	7.57	11.78	31.39	25.00	39.76

Note: *, **, and ns - significant at $P \leq 0.05$, $P \leq 0.01$ and not significant, respectively; df - degrees of freedom; M/F - mesocarp to fruit ratio; K/F - kernel to fruit ratio; S/F - shell to fruit ratio; O/DM - oil to dry mesocarp ratio; F/B - fruit to bunch ratio; O/B - oil to bunch ratio; K/B - kernel to bunch ratio; OY - oil yield; KY - kernel yield; CV - coefficient of variation.

TABLE 5. COMPARISON OF BUNCH QUALITY COMPONENT MEANS AMONG CROSS-TYPES AND GENOTYPES

No.	Cross-type	Genotype code	M/F (%)	K/F (%)	S/F (%)	O/DM (%)	F/B (%)	O/B (%)	K/B (%)	OY (kg palm^{-1} yr^{-1})	KY (kg palm^{-1} yr^{-1})
1	Cross I	PKG116	79.16^{fg}	9.63^{ab}	11.21^{abc}	79.00^{abc}	65.75^{a}	26.87^{abc}	5.94^{a}	41.28^{b-e}	9.02^{abc}
2		PKG124	82.13^{b-f}	7.87^{b-f}	10.01^{b-e}	**80.70^{a}**	64.37^{ab}	28.46^{ab}	4.62^{a-e}	45.14^{bcd}	7.33^{a-d}
3		PKG136	84.08^{a-e}	6.47^{f}	9.45^{c-f}	79.19^{abc}	62.93^{ab}	27.84^{ab}	3.84^{de}	47.63^{bcd}	6.50^{bcd}
4		PKG144	**86.43^{a}**	**6.41^{f}**	**7.16^{f}**	80.54^{a}	62.25^{ab}	**29.35^{a}**	**3.55^{e}**	51.02^{b}	6.28^{bcd}
5		PKG153	81.56^{c-f}	7.53^{c-f}	10.91^{abc}	79.80^{ab}	**66.36^{a}**	28.32^{ab}	4.61^{a-e}	42.61^{b-e}	6.90^{a-d}
6		PKG163	80.59^{efg}	8.21^{a-f}	11.21^{abc}	77.67^{cd}	62.68^{ab}	25.51^{bc}	4.89^{a-e}	41.37^{b-e}	8.13^{a-d}
7		PKG169	85.05^{abc}	6.56^{ef}	8.40^{def}	80.19^{a}	63.28^{ab}	28.10^{ab}	3.62^{e}	45.43^{bcd}	5.84^{cd}
8		PKG164	79.32^{f-g}	8.44^{ae}	12.24^{ab}	80.48^{a}	61.93^{ab}	26.88^{abc}	5.08^{a-d}	45.28^{bcd}	8.37^{a-d}
	Cross I mean		82.29	7.64	10.07	79.70	63.69	27.67^{A}	4.52	44.97	7.30
9	Cross II	PKG100	81.37^{c-f}	7.73^{c-f}	10.91^{abc}	79.47^{abc}	**59.87^{b}**	24.55^{cd}	4.41^{b-e}	39.62^{cde}	7.09^{a-d}
10		PKG102	82.13^{b-f}	8.65^{abc}	9.23^{c-f}	80.03^{ab}	64.05^{ab}	27.66^{ab}	5.12^{a-d}	44.34^{bcd}	8.18^{a-d}
11		PKG110	80.98^{d-g}	8.43a-e	10.59^{a-d}	80.15^{ab}	66.10^{a}	27.97^{ab}	5.27^{abc}	49.13^{bc}	9.21^{ab}
12		PKG111	80.67^{efg}	8.50^{a-d}	10.83^{a-d}	79.93^{ab}	65.39^{a}	26.98^{abc}	5.39^{ab}	37.41^{de}	7.56^{a-d}
13		PKG115	85.93^{ab}	6.48^{f}	7.59^{ef}	79.70^{ab}	63.00^{ab}	26.85^{abc}	3.73^{de}	**62.67^{a}**	8.81^{abc}
14		PKG126	**77.43^{g}**	9.66^{ab}	**12.91^{a}**	**76.91^{d}**	64.37^{ab}	**22.56^{d}**	**5.96^{a}**	**33.11^{e}**	9.08^{abc}
15		PKG141	84.87^{a-d}	6.99^{c-f}	8.14^{ef}	80.09^{ab}	59.95^{b}	26.95^{abc}	3.77^{de}	40.32^{b-e}	**5.67^{d}**
16		PKG142	84.56^{a-e}	6.56^{ef}	8.88^{c-f}	78.24^{bcd}	64.65^{a}	26.28^{abc}	3.98^{cde}	43.05^{b-e}	6.58^{bcd}
17		PKG166	83.64^{a-e}	6.71^{def}	9.65^{cde}	80.08^{ab}	63.48^{ab}	27.41^{abc}	3.91^{cde}	42.86^{b-e}	6.14^{cd}
18		PKG151	80.55^{efg}	**9.78^{a}**	9.67^{cde}	79.33^{abc}	65.11^{a}	26.83^{abc}	5.95^{a}	44.89^{bcd}	**9.77^{a}**
	Cross II mean		82.21	7.95	9.84	79.39	63.60	26.40^{B}	4.75	43.74	7.81
19	SC	PK5193	82.79	7.86	9.35	79.41	64.2	27.81	4.77	35.65	5.92
	Cross mean		82.25	7.81	9.94	79.53	63.64	26.96	4.65	44.29	7.58
LSD 0.05 (Cross I vs. Cross II)			1.28 ns	0.61 ns	0.79 ns	0.59 ns	1.34 ns	0.91 *	0.44 ns	3.30 ns	0.85 ns

Note: Cross I - (MPOB-Nigeria × Deli) *Dura* × AVROS *Pisifera*; Cross II - (MPOB-Nigeria × Deli) *Dura* × Yangambi *Pisifera*; SC - Standard cross Deli Dura × AVROS *Pisifera*; M/F - mesocarp to fruit ratio; K/F - kernel to fruit ratio; S/F - shell to fruit ratio; O/DM - oil to dry mesocarp ratio; F/B - fruit to bunch ratio; O/B - oil to bunch ratio; K/B - kernel to bunch ratio; OY - oil yield; KY - kernel yield. Means with the same small letter are not significantly different at $p \leq 0.05$ based on Duncan's new multiple range test (DMRT). Figures in bold within the mean column are minimum and maximum values.

TABLE 6. ANOVA RESULT FOR VEGETATIVE TRAITS BASED ON CROSS-TYPES AND GENOTYPES

Source of variance	df	FP	PCS	RL	LL	LW	LN	HTI	LA	LAI	DIA
Cross-Type	1	16.38^{ns}	232.55*	0.44^{ns}	958.14**	1.47*	25.06^{ns}	0.02^{ns}	1.91^{ns}	0.67^{ns}	0.01^{ns}
Error	214	5.18	55.32	0.25	99.38	0.33	141.34	0.01	3.04	1.06	0.01
Total	215	1,124.37	12,070.22	54.73	22,225.61	72.84	30,270.87	1.28	651.98	228.47	1.16
CV (%)		8.97	23.15	8.75	10.93	10.50	6.92	19.22	17.70	17.70	11.44
Genotype	17	14.98**	94.04*	0.99**	458.29**	0.85**	397.84**	0.01**	8.23**	2.88**	0.01**
Error	198	4.39	52.89	0.19	72.90	0.29	118.73	0.01	2.59	0.91	0.00
Total	215	1,124.37	12,070.22	54.73	22,225.61	72.84	30,270.87	1.28	651.98	228.47	1.16
CV (%)		8.26	22.64	7.59	9.36	9.87	6.34	18.50	16.33	16.33	10.92

Note: *, **, and ns - significant at $P \leq 0.05$, $P \leq 0.01$ and not significant, respectively; df - degrees of freedom, FP - frond production; PCS - petiole cross section; RL- rachis length; LL -leaflet length; LW - leaflet width; LN - leaflet number; HTI - height increment; LA - leaf area; LAI - leaf area index; DIA - trunk diameter.

high genetic variability on the vegetative traits in their D×P progenies. According to Swaray et al. (2020), vegetative traits should also be considered in selecting better performing materials.

The LSD results suggested that Cross I performed slightly higher in LL, while Cross II produced better in PCS and LW when compared to Cross I (*Table 7*). PKG163 from Cross I displayed the largest leaf length (LL) of 102.87 cm, while PKG110 of Cross II recorded the shortest LL of 81.19 cm. Broader leaves may indicate a better photosynthesis potential, as wider leaves typically capture more sunlight. PKG110 had the widest leaves (6.27 cm), whereas PKG163 had the narrowest (5.19 cm). Additionally, selecting palms with smaller PCS and shorter rachis length (RL) is advantageous, as it enables increased planting density each hectare and better land utilisation. PKG111 from Cross II was observed to have the lowest PCS at 25.61 cm^2 combined with low RL at 5.45 m, which were 19.31% and 5.22% lower than the SC, respectively. Breeding for compactness is one of the main objectives in the oil palm industry, where height increment (HTI) and rachis length (RL) are crucial traits. These traits may enhance production and profitability for each hectare on the currently limited land (Norziha et al., 2020). For the genotypes in this study, HTI varied from 0.32 m yr^{-1} (PKG153) to 0.45 m yr^{-1} (PKG110), compared to the dwarfed PS1.1 materials, which display a height increment of 0.20–0.45 m yr^{-1} (Mohd Din et al., 2023). Frond production, which plays a key role in photosynthesis and yield improvements, ranged from 23.75 fronds yr^{-1} (PKG 116) to 27.25 fronds yr^{-1} (PKG166).

The highest number of leaves (LN) was observed in PKG144, with an average of 181.50 leaves, which could contribute to an overall higher photosynthetic capacity. In contrast, PKG111 recorded the lowest number of leaves (161.08 leaves). For leaf area (LA), the results ranged from 8.51 m² (PKG111) to 11.54 m² (PKG151). PKG151 also gained the highest value in leaf area index (LAI, 6.83), suggesting it possesses a more efficient canopy area for light interception and nutrient use.

Heritability Estimates

Heritability estimates ranged from very low (<30%), to medium (30%–60%), to high (over 60%) (Johnson et al., 1955). Broad-sense heritability estimates for bunch yields revealed that h_b^2 values varied from low (for BNO) to moderate (for FFB and ABW) (*Table 8*). This could be due to the wide genetic variability among the genotypes studied, affecting the genetic contribution to these traits. Sritharan et al. (2017) reported moderate (30.20%) to high (82.50%) h_b^2 in two-way and multi-way crosses of D×P oil palm progenies. On the other hand, the h_b^2 for yield and its components were low in the Deli *Dura* x MPOB-NGA *Pisifera* population (Arolu et al., 2017). Low h_b^2 is due to the high environmental sensitivity of these yield traits (Corley & Tinker, 2016). Poor female inflorescence production, water stress, climate change, or inadequate fertiliser input in oil palm may reduce productivity. In this study, low to medium range h_b^2 values were obtained for bunch quality components, with the highest heritability estimate obtained for S/F (43.87%) while the lowest was for F/B (12.98%). High h_b^2 had been reported for bunch quality components such as mesocarp and oil content (Kushairi & Rajanaidu, 2000). For vegetative traits, the highest broad-sense heritability estimate was observed for LL (61.17%), suggesting higher genetic variation in this trait than the other traits. The observations in this study suggested that the expression of most traits was greatly influenced by environmental factors.

TABLE 7. COMPARISON OF VEGETATIVE TRAITS MEANS AMONG CROSS-TYPES AND GENOTYPES

No.	Cross-type	Genotype code	FP (frond yr^{-1})	PCS (cm^2)	RL (m)	LL (cm)	LW (cm)	LN (No.)	HTI (m yr^{-1})	LA (m^2)	LAI	DIA (m)
1		PKG116	**23.75**^{g}	33.39^{a}	5.66^{def}	92.23$^{c\text{-}f}$	5.43^{bcd}	166.75^{cde}	0.40^{abc}	9.52$^{b\text{-}e}$	5.63$^{b\text{-}e}$	0.62^{abc}
2		PKG124	24.92$^{d\text{-}g}$	30.46^{abc}	5.48^{ef}	88.49$^{d\text{-}i}$	5.25^{cd}	168.25$^{b\text{-}e}$	0.37^{cd}	9.03^{cde}	5.34^{cde}	0.59^{c}
3		PKG136	26.25$^{a\text{-}d}$	34.13^{a}	5.70$^{b\text{-}f}$	93.05$^{b\text{-}e}$	5.46^{bcd}	171.50$^{a\text{-}d}$	0.40$^{a\text{-}d}$	9.91$^{b\text{-}e}$	5.87$^{b\text{-}e}$	0.66^{ab}
4	Cross I	PKG144	26.25$^{a\text{-}d}$	32.41^{ab}	5.67$^{c\text{-}f}$	92.10$^{c\text{-}f}$	5.29^{bcd}	178.50^{ab}	0.44^{abc}	9.87$^{b\text{-}e}$	5.85$^{b\text{-}e}$	0.62^{abc}
5		PKG153	24.08^{fg}	32.74^{ab}	6.07^{ab}	94.42^{bcd}	5.39^{bcd}	164.50^{de}	**0.32**^{d}	9.51$^{b\text{-}e}$	5.63$^{b\text{-}e}$	0.66^{ab}
6		PKG163	25.08$^{c\text{-}g}$	35.12^{a}	6.07^{abc}	**102.87**^{a}	**5.19**^{d}	172.58$^{a\text{-}d}$	0.38^{bcd}	10.66^{ab}	6.31^{ab}	0.64^{abc}
7		PKG169	25.92$^{a\text{-}f}$	34.08^{a}	5.88$^{a\text{-}e}$	94.03^{bcd}	5.46^{bcd}	172.58$^{a\text{-}d}$	0.37^{cd}	10.10$^{a\text{-}d}$	5.98$^{a\text{-}d}$	0.66^{ab}
8		PKG164	24.25$^{d\text{-}g}$	33.96^{a}	5.94$^{a\text{-}d}$	91.55$^{c\text{-}g}$	5.79^{b}	**181.50**^{a}	0.45^{ab}	11.00^{ab}	6.52^{ab}	0.60^{bc}
	Cross I mean		25.06	33.28^{A}	5.81	93.59^{A}	5.41^{B}	172.26	0.39	9.95	5.89	0.63
9		PKG100	24.42$^{d\text{-}g}$	29.63^{abc}	5.60^{def}	84.16^{ghi}	5.57^{bcd}	164.58$^{\text{-}de}$	0.41^{abc}	8.80^{de}	5.21^{de}	**0.58**^{c}
10		PKG102	27.17^{ab}	30.73^{abc}	6.10^{ab}	92.73^{cde}	5.19^{d}	176.58^{abc}	0.41^{abc}	9.74$^{b\text{-}e}$	5.76$^{b\text{-}e}$	0.69^{a}
11		PKG110	27.00^{abc}	33.93^{a}	5.57^{def}	**81.19**^{i}	**6.27**^{a}	175.67^{abc}	**0.45**^{a}	10.24$^{a\text{-}d}$	5.06$^{a\text{-}d}$	0.64^{abc}
12		PKG111	25.50$^{a\text{-}g}$	**25.61**^{c}	5.45^{f}	84.36f-i	5.50^{bcd}	**161.08**^{e}	0.44^{abc}	**8.51**^{e}	**5.04**^{e}	0.64^{abc}
13	Cross II	PKG115	24.58$^{d\text{-}g}$	**36.09**^{a}	6.08^{ab}	99.36^{abc}	5.22^{d}	175.00$^{a\text{-}d}$	0.41^{abc}	10.41^{abc}	5.16^{abc}	**0.69**^{a}
14		PKG126	26.17$^{a\text{-}e}$	26.19^{bc}	**5.30**^{f}	85.31$^{f\text{-}i}$	5.66^{bcd}	165.17^{de}	0.41^{abc}	9.08^{cde}	5.37^{cde}	0.66^{ab}
15		PKG141	25.25$^{b\text{-}g}$	31.78^{abc}	5.46^{f}	89.52$^{d\text{-}h}$	5.40^{bcd}	172.50$^{a\text{-}d}$	0.41^{abc}	9.51$^{b\text{-}e}$	5.63$^{b\text{-}e}$	0.62^{abc}
16		PKG142	24.17^{efg}	34.28^{a}	5.90$^{a\text{-}d}$	93.84^{bcd}	5.77^{bcd}	174.92$^{a\text{-}d}$	0.39$^{a\text{-}d}$	10.83^{ab}	6.42^{ab}	0.64^{abc}
17		PKG166	**27.25**^{a}	31.73^{abc}	5.46^{f}	82.27^{hi}	5.53^{bcd}	171.00$^{a\text{-}e}$	0.38^{bcd}	8.95^{cde}	5.30^{cde}	0.66^{ab}
18		PKG151	24.67$^{d\text{-}g}$	32.55^{ab}	**6.28**^{a}	100.82^{ab}	5.63^{bcd}	179.25^{a}	0.38^{bcd}	**11.54**^{a}	**6.83**^{a}	0.66^{ab}
	Cross II mean		25.62	31.20^{B}	5.72	89.35^{B}	5.57^{A}	171.58	0.41	9.76	5.78	0.65
19	SC	PK5193	24.73	31.74	5.75	88.12	5.68	178.07	0.43	10.28	6.09	0.59
	Cross Mean		25.37	32.12	5.76	91.24	5.50	171.88	0.40	9.85	5.83	0.64
LSD 0.05 (Cross I vs. Cross II)			0.61 ns	2.00 *	0.14 ns	2.69 *	0.16 *	3.21 ns	0.02 ns	0.47 ns	0.28 ns	0.02 ns

Note: Cross I - (MPOB-Nigeria × Deli) *Dura* × AVROS *Pisifera*; Cross II - (MPOB-Nigeria × Deli) *Dura* × Yangambi *Pisifera*; SC - Standard cross Deli *Dura* × AVROS *Pisifera*; FP - frond production; PCS - petiole cross-section; RL - rachis length; LL - leaflet length; LW -leaflet width; LN - leaflet number; HTI - height increment; LA - leaf area; LAI - leaf area index; DIA - trunk diameter. Means with the same small letter are not significantly different at $p \leq 0.05$ based on Duncan's new multiple range test (DMRT). Figures in bold within the mean column are minimum and maximum values.

TABLE 8. VARIANCE COMPONENTS AND HERITABILITY ESTIMATES

Category	Traits	σ^2_g	σ^2_e	Total	Heritability (%)
Yield	FFB	367.58	1,982.80	2,350.38	31.28
	BNO	0.44	10.50	10.94	8.04
	ABW	1.44	5.16	6.60	43.64
Bunch quality	M/F	4.94	17.61	22.55	43.81
	K/F	1.04	4.05	5.09	40.86
	S/F	1.88	6.69	8.57	43.87
	O/DM	0.70	4.00	4.70	29.79
	F/B	1.61	23.19	24.80	12.98
	O/B	1.59	10.08	11.67	27.25
	K/B	0.53	2.13	2.66	39.85
	OY	28.31	122.55	150.86	37.53
	KY	0.89	9.08	9.97	17.85
Vegetative	FP	0.88	4.39	5.27	33.40
	PCS	3.43	52.89	56.32	12.18
	RL	0.07	0.19	0.26	53.85
	LL	32.12	72.90	105.02	61.17
	LW	0.05	0.29	0.34	29.41
	LN	23.26	118.73	141.99	32.76
	HTI	0.00	0.01	0.01	0.00
	LA	0.47	2.59	3.06	30.72
	LAI	0.16	0.91	1.07	29.91
	DIA	0.00	0.00	0.00	0.00

Note: σ^2_g - variance of genotype; σ^2_e- variance of error; FFB - fresh fruit bunches; BNO - bunch number; ABW - average bunch weight; M/F - mesocarp to fruit ratio; K/F - kernel to fruit ratio; S/F - shell to fruit ratio; O/DM - oil to dry mesocarp ratio; F/B - fruit to bunch ratio; O/B - oil to bunch ratio; K/B - kernel to bunch ratio; OY - oil yield; KY - kernel yield; FP - frond production; PCS - petiole cross-section; RL - rachis length; LL - leaflet length; LW - leaflet width; LN - leaflet number; HTI - height increment; LA - leaf area; LAI - leaf area index; DIA - trunk diameter.

CONCLUSION

Generally, the genotype factor was highly significant for all traits, suggesting adequate genetic variation for effective selection within this breeding population. The broad-sense heritability estimates were low for most of the traits, suggesting a greater influence on these traits by the environment. PKG115 from Cross II has been identified to possess a good combination of traits, such as its high FFB yields of 264.46 kg palm^{-1} yr^{-1} or 39.14 t ha^{-1}. The high yield was combined with promising bunch quality components such as high M/F and OY, and a low S/F. From the *Dura* side, the Nigerian germplasm could also incorporate other interesting traits for future breeding programmes, apart from its good FFB yield. The female (0.318/2 of MPOB-NGA x Deli *Dura*) and male (0.395/148 of Yangambi *Pisifera*) parents of PKG115 can be used in the development of commercial D×P seed production and breeding programmes as the mother palm and pollen source, which may help to address the yield stagnation observed in the oil palm sector in recent decades.

ACKNOWLEDGEMENT

The authors would like to thank the Director-General of MPOB for permission to publish this article. Special thanks to the Breeding and Genetics Group of MPOB for their assistance in the laboratory and fieldwork.

REFERENCES

Amiruddin, M. D., Abu Bakar, N. A., Ahmad Malike, F., Mustaffa, S., Abdullah, N., Marjuni, M., Mohammad, M. M., Hassan, M. Y., Kushairi, A., & Nookiah, R. (2020). Wild and advanced resources of *Elaeis guineensis* and *Elaeis oleifera*. In M. Ithnin & A. Kushairi (Eds.), *The oil palm genome* (pp. 9–23). Springer. https://doi.org/10.1007/978-3-030-22549-0_2

Arolu, I. W., Rafii, M. Y., Marjuni, M., Hanafi, M. M., Sulaiman, Z., Rahim, H. A., Kolapo, O. K., Abidin, M. I. Z., Amiruddin, M. D., Din, A. K., & Nookiah, R. (2016). Genetic variability analysis and selection of *pisifera* palms for commercial production of high yielding and dwarf oil palm planting materials. *Industrial Crops and Products*, *90*, 135–141. https://doi.org/10.1016/j.indcrop.2016.06.006

Arolu, I. W., Rafii, M. Y., Marjuni, M., Hanafi, M. M., Sulaiman, Z., Rahim, H. A., Abidin, M. I. Z., Amiruddin, M. D., Din, A. K., & Nookiah, R. (2017). Breeding of high yielding and dwarf oil palm planting materials using Deli *dura* × Nigerian *pisifera* population. *Euphytica*, *213*, 154. https://doi.org/10.1007/s10681-017-1943-z

Blaak, G., Sparnaaij, L. D., & Menendez, T. (1963). Breeding and inheritance in the oil palm (*Elaeis guineensis* Jacq.). Part II: Methods of bunch quality analysis. *Journal of the West African Institute for Oil Palm Research*, *4*, 146–155.

Corley, R. H. V. (2003). Oil palm: A major tropical crop. *Burotrop Bulletin*, *19*, 5–8.

Corley, R. H. V. (2009). How much palm oil do we need? *Environmental Science & Policy*, *12*(2), 134–139. https://doi.org/10.1016/j.envsci.2008.10.011

Corley, R. H. V., & Breure, C. J. (1981). *Measurements in oil palm experiments* (Internal report, p. 21). Unilever Plantations Group.

Corley, R. H. V., & Tinker, P. B. (2016). The classification and morphology of the oil palm. In *The oil palm* (5th ed., pp. 30–48). John Wiley & Sons.

Fadila, A. M., Noraziyah, A. A. S., Mohd Din, A., Marhalil, M., & Zulkifli, Y. (2024). Development of new high-yielding planting material based on performance of 38 oil palm (*Elaeis guineensis* Jacq.) *Dura* × *Pisifera* families. *Euphytica, 220*, 73. https://doi.org/10.1007/s10681-024-03333-2

Falconer, D. S., & Mackay, T. F. C. (1996). *Introduction to quantitative genetics* (4th ed.). Addison Wesley Longman.

Gawankar, M. S., Sumitha, S., Maheswarappa, H. P., Mathur, R. K., Haldankar, P. M., & Debaje, P. P. (2022). Evaluation of *tenera* oil palm hybrids in Western Costal Region of India. *Indian Journal of Horticulture*, *79*(4), 410–414. https://doi.org/10.5958/0974-0112.2022.00057.3

Ithnin, M., Vu, W. T., Shin, M., Suryawanshi, V., Sherbina, K., Zolkafli, S. H., Serdari, N. M., Amiruddin, M. D., Abdullah, N., Mustaffa, S., Marjuni, M., Nookiah, R., Kushairi, A., Marjoram, P., Nuzhdin, S. V., Chang, P. L., & Singh, R. (2021). Genomic diversity and genome-wide association analysis related to yield and fatty acid composition of wild American oil palm. *Plant Science*, *304*, 110731. https://doi.org/10.1016/j.plantsci.2020.110731

Johnson, H. W., Robinson, H. F., & Comstock, R. E. (1955). Estimates of genetic and environmental variability in soybeans. *Agronomy Journal*, *47*(7), 314–318. https://doi.org/10.2134/agronj1955.00021962004700070009x

Kushairi, A., & Rajanaidu, N. (2000). Breeding populations, seed production and nursery management. In Y. Basiron, B. S. Jalani, & K. W. Chan (Eds.), *Advances in oil palm research* (Vol. 1, pp. 39–96). Malaysian Palm Oil Board.

Kushairi, A., Mohd Din, A., & Rajanaidu, N. (2011). Oil palm breeding and seed production. In W. Mohd Basri, Y. M. Choo, & K. W. Chan (Eds.), *Further advances in oil palm research (2000–2010)* (pp. 47–101). Malaysian Palm Oil Board.

Kushairi, A., Rajanaidu, N., & Jalani, B. S. (2001). Response of oil palm progenies to different fertilizer rates. *Journal of Oil Palm Research*, *13*(1), 84–96.

Kushairi, A., Rajanaidu, N., Jalani, B. S., Rafii, M. Y., & Mohd Din, A. (1999). PORIM oil palm planting materials. *PORIM Bulletin, 38*, 1–13.

Lee, C. H., & Yeow, K. H. (1985). Progress in breeding and selection for seed production at HMPB Oil Palm Research Station. *The Planter, 61*(706), 18–31.

Martin, J. J. J., Yarra, R., Wei, L., & Cao, H. (2022). Oil palm breeding in the modern Era: Challenges and opportunities. *Plants*, *11*(11), 1395. https://doi.org/10.3390/plants11111395

Mohd Din, A., Marhalil, M., Fadila, A. M., Nor Azwani, A. B., Zulkifli, Y., Norziha, A., & Suzana, M. (2023). Oil palm breeding and seed production. In G. K. A. Parveez & I. Zainab (Eds.), *Advances in oil palm research* (Vol. 1, pp. 29–56). Malaysian Palm Oil Board.

Mukherjee, I., & Sovacool, B. K. (2014). Palm oil-based biofuels and sustainability in Southeast Asia: A review of Indonesia, Malaysia, and Thailand. *Renewable and Sustainable Energy Reviews*, *37*, 1–12. https://doi.org/10.1016/j.rser.2014.05.001

Myint, K. A., Amiruddin, M. D., Rafii, M. Y., Samad, M. Y. A., Ramlee, S. I., Yaakub, Z., & Oladosu, Y. (2019). Genetic diversity and selection criteria of MPOB-Senegal oil palm (*Elaeis guineensis* Jacq.)

germplasm by quantitative traits. *Industrial Crops and Products*, *139*, 111558. https://doi.org/10.1016/j.indcrop.2019.111558

Noh, A., Rafii, M., Din, A. M., Kushairi, A., Norziha, A., Rajanaidu, N., Latif, M., & Malek, M. (2014). Variability and performance evaluation of introgressed Nigerian *dura* x Deli *dura* oil palm progenies. *Genetics and Molecular Research*, *13*(2), 2426–2437. https://doi.org/10.4238/2014.april.3.15

Norziha, A., Fadila, A. M., Marhalil, M., Zulkifli, Y., Mohd Din, A., Rajanaidu, N., Ong-Abdullah, M., & Kushairi, A. (2020). MPOB oil palm (*Elaeis guineensis* Jacq.) germplasms linked to compact trait for high density planting. *Journal of Oil Palm Research*, *32*(3), 394–405.

Nor Azwani, A. B., Fadila, A. M., Din, M. A., Rajanaidu, N., Norziha, A., Suzana, M., Marhalil, M., Zulkifli, Y., & Kushairi, A. (2020). Potential oil palm genetic materials derived from introgression of germplasm (MPOB-Nigeria, MPOB-Zaire, and MPOB-Cameroon accessions) to advanced (AVROS) breeding population. *Journal of Oil Palm Research*, *32*(4), 569–581.

Nor Azwani, A. B., Malike, F. A., Amiruddin, M. D., & Abdullah, M. O. (2022). Genetic variability and performance of MPOB-Nigeria *dura* × AVROS *pisifera* planting materials. *Journal of Oil Palm Research*, *5*(1), 26–38.

Oil World. (2021). *Oil world monthly* (No. 50, Vol. 64). ISTA Mielke GmbH.

Okwuagwu, C., Ataga, C., Okoye, M., & Okolo, E. (2011). Germplasm collection of highland palms of Afikpo in Eastern Nigeria. *Bayero Journal of Pure and Applied Sciences*, *4*(1). https://doi.org/10.4314/bajopas.v4i1.25

Organisation for Economic Co-operation and Development (OECD), & Food and Agriculture Organization of the United Nations (FAO). (2022). *OECD-FAO agricultural outlook 2022-2031*. OECD Publishing.

Rajanaidu, N. (1994). *PORIM oil palm genebank: Collection, evaluation, utilization and conservation of oil palm genetic resources*. Palm Oil Research Institute of Malaysia.

Rajanaidu, N., Kushairi, A., Rafii, M., Mohd Din, A., Maizura, I., & Jalani, B. S. (2000). Oil palm breeding and genetic resources. In Y. Basiron, B. S. Jalani, & K. W. Chan (Eds.), *Advances in oil palm research* (Vol. 1, pp. 171–237). Malaysian Palm Oil Board.

Rao, V. (1987). Important traits in oil palm selection. In *Proceedings of the colloquium on breeding and selection for clonal oil palms* (pp. 21–33). Palm Oil Research Institute of Malaysia.

Rao, V., Soh, A. C., Corley, R. H. V., & Lee, C. H. (1983). A critical re-examination of the method of bunch quality analysis in oil palm breeding. *PORIM Occasional Paper, 9*, 1–28.

Srisawasdi, W., Tsusaka, T. W., & Cortes, J. R. (2023). Palm oil trade and production toward achieving sustainable development goals: A global panel regression analysis. *ABAC Journal*, *43*(3), 98–111.

Sritharan, K., Subramaniam, M., Arulandoo, X., & Yusop, M. R. (2017). Yield and bunch quality component comparison between two-way crosses and multi-way crosses of DxP oil palm progenies. *Sains Malaysiana*, *46*(9), 1587–1595. https://doi.org/10.17576/jsm-2017-4609-30

Swaray, S., Amiruddin, M. D., Rafii, M. Y., Jamian, S., Ismail, M. F., Jalloh, M., Marjuni, M., Mohamad, M. M., & Yusuff, O. (2020). Influence of parental *Dura* and *Pisifera* genetic origins on oil palm fruit set ratio and yield components in their D×P progenies. *Agronomy*, *10*(11), 1793. https://doi.org/10.3390/agronomy10111793

U.S. Department of Agriculture. (2024). *Palm oil 2021 world production*. https://ipad.fas.usda.gov/cropexplorer/cropview/commodityView.aspx?cropid=4243000&sel_year=2021&rankby=Production

Yaakub, Z., Marjuni, M., Mustaffa, S., Tun Mohd Salim, W. N. S., Mohd Nasir, F., Abdullah, N., Amiruddin, M. D., Nookiah, R., Din, A. K., & Ong-Abdullah, M. (2023). Phenotypic variability of *Elaeis oleifera* germplasm revealed by principal component and cluster analyses. *Journal of Oil Palm Research*, *35*(4), 582–595. https://doi.org/10.21894/jopr.2022.0054

Journal of Oil Palm Research Vol. 38 (3) September 2026 p. 494–508
DOI: https://doi.org/10.21894/jopr.2025.0049

BIOSYNTHESIS OF SILVER NANOPARTICLES USING PALM OIL MILL EFFLUENT (POME) EXTRACT

ABDULRAHMAN SANI ALIERO[1,2]; NURLIYANA AHMAD ZAWAWI[1*]; NIK AHMAD NIZAM NIK MALEK[1,3]; MUHAMMAD HARIZ ASRAF[1]; IQBAL JALALULDIN[4]; MOHD FIRDAUS ABDUL WAHAB[1] and MUSTAPHA ISAH[1]

ABSTRACT

Silver nanoparticles (AgNP) possess broad biocidal activities, making them ideal for antibacterial, antiviral and anti-inflammatory formulations. A green synthesis method using palm oil mill effluent (POME) extract as both a stabilising and reducing agent was developed, eliminating the need for hazardous chemicals, with a 1.5 mM $AgNO_3$ solution used as the precursor for the synthesis. Preliminary profiling of POME extract was performed, including quantification of total phenolic, flavonoid and tannin contents. The synthesis was optimised using one factor at a time (OFAT) approach and characterised with vis-spectroscopy, Fourier transform infrared (FTIR) and dynamic light scattering (DLS). Liquid chromatography-mass spectrometry (LC-MS) was used to identify organic compounds containing hydroxyl, carbonyl and amine groups as possible reducing agents. Under optimised conditions of 6 mL extract and 1.5 mM $AgNO_3$ incubated at room temperature for 14 hr, AgNP exhibited a surface plasmon resonance (SPR) peak at 440 nm. FTIR spectra revealed significant hydroxyl and carboxyl groups essential for reducing Ag^+ to Ag^0. The synthesised POME-AgNP were crystalline, spherical in shape and 21 nm average size, with a low polydispersity index (PdI = 0.295) indicating monodispersity. A zeta potential of –19.3 mV demonstrated good stability against agglomeration and oxidation. Overall, the green AgNP synthesis method using POME extract proved successful, offering a sustainable alternative to conventional chemical and physical methods.

Keywords: bioactive compounds, biosynthesis, LC-MS, POME, silver nanoparticles.

Received: 26 April 2024**; Accepted:** 6 June 2025**; Published online:** 23 September 2025.

INTRODUCTION

Nanotechnology offers a transformative approach to advancing technology across various disciplines, including science, medicine and engineering. Among nanomaterials, metallic nanoparticles and their composites are broadly explored for various applications due to their exceptional properties. These include enhanced mechanical and thermal stability, a high surface-to-volume ratio and an abundance of reactive sites on their surfaces, making them highly desirable for a wide range of applications (Alvarez et al., 2018; Haleem et al., 2023; Liu et al., 2023; Savolainen et al., 2010). With growing awareness of the environmental impact of traditional manufacturing processes, there is an increasing demand for sustainable and eco-friendly methods for nanoparticle synthesis and application. Green synthesis addresses this need by offering a range of techniques that minimise the use of hazardous chemicals, reduce energy consumption and promote the use of renewable

[1] Department of Biosciences, Faculty of Science, Universiti Teknologi Malaysia, 81300 Johor, Malaysia.

[2] Department of Animal and Environmental Biology, Kebbi State University of Science and Technology, 1144 Aliero, Nigeria.

[3] Centre for Sustainable Nanomaterials (CSNano), Ibnu Sina Institute for Scientific and Industrial Research (ISI-SIR), Universiti Teknologi Malaysia, 81300 Johor, Malaysia.

[4] Department of Chemistry, Faculty of Science, Universiti Teknologi Malaysia, 81300 Johor, Malaysia.

* *Corresponding author e-mail: nurliyana@utm.my*

resources. This approach has the potential to revolutionise various sectors and provide sustainable solutions to pressing global challenges (Barabadi et al., 2021; Vankudoth et al., 2022).

In the energy sector, metallic nanoparticles offer significant opportunities, such as the use of nanomaterials in solar cells to enhance light absorption and improve energy conversion efficiency, leading to cleaner and more efficient energy sources (Dastafkan et al., 2015; Dolatabadi et al., 2022). In medicine, it enables the production of biocompatible nanoparticles for drug delivery, diagnostics and therapeutics, reducing toxicity and enhancing efficacy (Kumari et al., 2021a; Wasilewska et al., 2023). For environmental remediation, green-synthesised nanoparticles can be applied in water purification, pollutant detection and the cleanup of contaminated sites (Zahoor et al., 2021). Additionally, in agriculture, green nanotechnology contributes to crop improvement, pest control and nutrient delivery systems (Acharya & Pal, 2020).

Among emerging metallic nanomaterials, silver nanoparticles (AgNP) have gained significant interest due to their outstanding physicochemical properties (De Matteis et al., 2023). Their unique surface chemistry, composition, morphology, shape, size distribution and reactivity in solution make them highly desirable for a range of applications, including as antioxidants, anticancer agents, antimicrobials, larvicides and in the degradation of dyes for water treatment (Jaast & Grewal, 2021; Mondal et al., 2024). Typical method used to synthesise AgNP mainly uses chemical agents that are hazardous and toxic, which adversely affect our environment (Iravani et al., 2014). Other than toxic side effects, chemical methods commonly use volatile chemical reactants that are very hazardous to the environment. The reducing agents such as sodium borohydrate and hydrazine derivatives, are highly noxious, causing air pollution. Other examples include volatile solvents like aromatic amines and thiols that have high vapour pressure (Zhang et al., 2021). The presence of chemical substances on the surface of AgNP can compromise their effectiveness and hinder their biocompatibility as such in future medical applications. Thus, there is a pressing need to adopt environmentally friendly techniques that harness the power of renewable resources to ensure the sustainable use of AgNP (Wasilewska et al., 2023). Recently, there has been a growing demand for safe, eco-friendly and non-toxic approaches to synthesise AgNP of various sizes and morphology while minimising toxicity (Abdullah et al., 2021).

In the green synthesis method of AgNP, biological sources such as bacteria, fungi, algae and plants have previously been reported as advantageous to mediate the reduction of silver ions (Ag^+) to AgNP. The use of bacteria, fungi, and algae has been reported previously by Aziz et al. (2015), Murugesan et al. (2017) and Uzair et al. (2020) but has encountered challenges in achieving good control over the size distribution, shape and crystallinity of the nanoparticles (Mukherji et al., 2019). Moreover, the steps are time-consuming, and require substantial aseptic conditions and maintenance, limiting their suitability for industrial applications (Yahya & Alharbi, 2023).

In contrast, plant-mediated synthesis of AgNP is comparatively simpler and more cost-efficient. Various phytochemicals from various plant species and plant parts including leaves, vegetables, oilseed, barks, roots and fruits aid the reduction process of metal ions. Notably, fruit peels such as banana (Cheong et al., 2022; Teo et al., 2023), citrus (Khane et al., 2022; Nahar et al., 2021) and dragon fruit (Phongtongpasuk & Poadang, 2016) have demonstrated the ability to produce biocompatible AgNP. These plants produce biomolecules such as steroids, sapogenins, tannins, terpenoids, polyols, alkaloids, polysaccharides, flavonoids, phenolics, proteins, amino acids, enzymes and vitamins that function as strong chelating, reducing and stabilising agents for the AgNP synthesis (Asmat-Campos et al., 2020; Githala & Trivedi, 2023).

Recently, there has been a pressing need to exploit agro-industrial biowaste for materials synthesis to mitigate environmental pollution and promote sustainability. Exploiting agro-industrial waste to produce profitable high-value products facilitates the implementation of a circular economy, which in turn helps reduce the amount of waste generated. Among such agro-industrial waste is palm oil mill effluent (POME), which is a by-product generated during oil extraction from fresh fruit bunches (FFB) in palm oil mill industries. It is estimated that about 3 t of POME are produced for every tonnes of crude palm oil, with Malaysia alone processing over 90 million tonnes of FFB annually (Mahmod et al., 2023; Tang et al., 2024). Managing POME poses a significant challenge for the palm oil milling industry due to its high concentration of pollutants and other harmful substances, which can adversely affect aquatic life. The brown colour of POME was known to have high levels of phenolic compounds, fatty acids, polyphenols and proteins (Chantho et al., 2016).

To the best of our knowledge, the utilisation of POME in mediating AgNP formation has been relatively unexplored until now, unlike its role in forming other metallic nanoparticles such as gold nanoparticles (AuNP), in which hydroxyl and carbonyl functional groups served as reducing and capping agents. This study aims to identify compounds containing hydroxyl and carboxyl functional groups present in POME extract that are involved in the biosynthesis of AgNP without the addition of external surfactant or capping agent. Synthesis parameters were optimised using one factor at a time (OFAT) approach. The successful synthesis was confirmed using various analytical techniques including vis-spectroscopy, Fourier transform infrared (FTIR) spectroscopy and dynamic light scattering (DLS).

MATERIALS AND METHODS

POME Collection and Extraction

Raw POME was obtained from the Maokil Palm Oil Mill in Labis, Johor, Malaysia, and was dried at 60°C for 24 hr using a glass container. Subsequently, the raw material was scraped, ground to powder and sieved (Gan et al., 2012). The 2% POME powder was dissolved in 100 mL of deionised (DI) water, stirred for 15 min at 90°C and filtered using Whatman filter paper to obtain pure POME extract. The extracted POME was kept in a refrigerator at 4°C for further analysis. The schematic process of extraction is shown in *Figure 1*. The extract was used to quantify total phenolic, flavonoid and tannin content and synthesise AgNP. For liquid chromatography-mass spectroscopy (LC-MS) analysis, 2 g of POME powder was added to 100 mL of methanol and stirred overnight and the prepared sample was submitted for analysis.

Profiling of Organic Compounds in POME Extract using LC-MS

Water extract of POME was characterised using an LC-MS instrument from Hewlett Packard (Agilent Technologies, Germany) to examine the chromatographic profiles of organic compounds in POME extract. The chromatographic system consists of a normal phase. The mobile phase comprises 0.1% formic acid (v/v) (A), while the aqueous organic phase contains 0.1% formic acid (v/v) (B). The analysis was conducted using C18 column (150.0 × 2.1 mm), with a vacuum pump flow velocity of 1 mL/min and temperature of 40°C. The eluent gradient was set from 10.0%–30.0% B in 20 min, followed by 30.0% B in 20–30 min, with a 0.8 mL/min flow rate. Positive ion mode of electrospray ionisation-mass spectrometry (ESI-MS) was used to monitor the eluent, scanning from m/z 110–810. An electrospray ionisation (ESI) was performed at 3.5 kV with an optimum collision energy of 60.0%. At a flow rate of 12 L/min and a capillary temperature of 350°C, high-purity nitrogen was used as the dry gas, while nitrogen was used as the nebuliser at 40/inch^2. The compounds from POME extract that could potentially act as reducing and stabilising agents in the biosynthesis of AgNP were chosen using the available reference library (Metlin_Metabolites_AM_PCDL.cdb). The compounds exhibiting the best match percentage with a database score above 70.0%, along with hydroxyl and carboxyl functional were recorded.

Total Phenolic Compound (TPC)

The TPC of aqueous POME is to assess the concentration of phenolic compounds in a sample (Baba & Malik, 2015). A 1.00 mL of POME extract sample, standard calibration solutions containing different concentrations of gallic acid (0.00, 0.02, 0.04, 0.06, 0.08, 1.00 and 1.20 mg/mL), 0.50 mL of Folin-Ciocalteu (FC) reagent and 5.00 mL of DI water were mixed and centrifuged in a 15.00 mL tube for 5 min. Subsequently, 1.50 mL of 20% Na_2CO_3 was added, and the final volume was adjusted to 10 mL with DI water. The absorbance was recorded after 30 min of incubation at 40°C using a visible spectrophotometer at 750 nm. These analyses were conducted in triplicate and

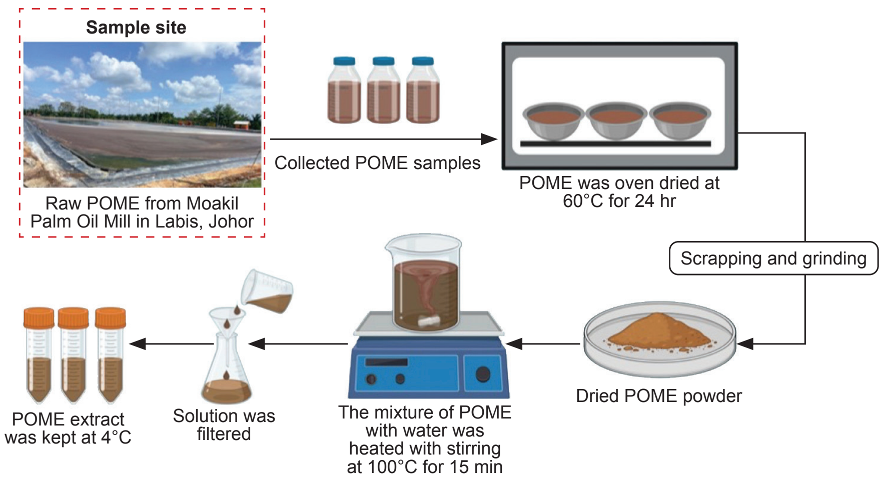

Figure 1. Schematic process of extraction using palm oil mill effluent (POME).

linear regression depicts the correlation coefficient, $r^2 > 0.95$. The total phenolic contents were estimated as gallic acid equivalents (mg GAE/g).

Total Flavonoid Content (TFC)

The assessment of the TFC of aqueous POME was conducted as described by Chantiratikul et al. (2009). Quercetin standard concentrations (0.0, 0.2, 0.4, 0.6, 0.8, 1.0 and 1.2 mg/mL) were used to make a standard calibration curve. The sample (1.0 mL) was placed in a 15.0 mL centrifuge tube, followed by 4.0 mL DI water. Subsequently, 0.3 mL of 5% sodium nitrate was added to the solution and allowed to stand for 5 min before adding 0.3 mL of 10% aluminium chloride solution and 2.0 mL of 1 M sodium hydroxide. Subsequently, the mixture was adjusted to 10.0 mL with DI water. Finally, the absorbance was measured using a Jenway 7200 visible spectrophotometer at 510 nm. TFC was measured as quercetin equivalent (mg QE/g). All measurements were performed at least three times.

Total Tannin Content (TTC)

The TTC of POME was spectrophotometrically determined by FC phenol reagent assay to determine the total tannin contents according to (Haile & Kang, 2019). POME (1.0 mL) extract was mixed with 7.5 mL DI water in a falcon tube, followed by the addition of 0.5 mL of FC phenol reagent and 1.0 mL of Na_2CO_3. DI (1.0 mL) water was added to achieve a total volume of 10.0 mL. The mixture was vortexed and shaken vigorously using a vortex mixer, and the homogeneous mixture was wrapped with aluminium foil and kept at room temperature for 30 min. Standard solutions of tannic acid (0.0, 0.2, 0.4, 0.6, 0.8, 1.0 and 1.2 mg/mL) were prepared, and the absorbance was measured at 760 nm using a visible spectrophotometer. TTC in POME was expressed as mg of tannic acid equivalents (mg TAE/g).

Optimising AgNP Synthesis Parameters using OFAT

POME-AgNP were synthesised by incubating POME extract with silver nitrate ($AgNO_3$) solutions at different temperatures. The results will provide an overview of the ideal conditions for synthesising AgNP under optimised conditions. OFAT was then employed to explore optimal levels of operating conditions that positively influenced AgNP formation. The study focuses on the effect of four variables, such as the volume of POME extract, $AgNO_3$, temperature and pH of the extract. For each 15 mL test tube, 10 mL of $AgNO_3$ at 1.0 mM concentration was used. The tubes were incubated for 24 hr at specific temperatures (30°C, 40°C, 50°C, 60°C, 70°C and 80°C) and contained different volumes (0.2, 0.4, 0.6, 0.8 and 10.0 mL) of plant extract at specific pH levels (4, 5, 6, 7, 8, 9 and 10). The pH of the experiment was adjusted to 4, 5, 6, 8, 9 and 10 using 0.1 M HCl and 0.1 M NaOH. The absorbance, indicating surface plasmon resonance (SPR), was measured using a vis-spectrophotometer across a wavelength range of 350–750 nm. Detailed information on the experimental setup is provided in *Table 1*.

Characterisation of POME-AgNP

The confirmation of biosynthesised POME-AgNP formation was determined using vis-spectroscopy (Jenway 7200). The SPR was examined from 350 to 750 wavelength (nm). The surface functional group of biomolecules was investigated using FTIR (Nicolet IS5 IR, Thermo Scientific, US) spectroscopy in the range of 400–4,000 cm^{-1}. The size distribution and zeta potential of POME-AgNP were analysed using a Zetasizer Ver. 7.11 (Malvern DLS, UK) through DLS. To prevent aggregation, the samples were diluted before analysing particle size distribution and zeta potential at 25°C.

RESULTS AND DISCUSSION

Organic Compounds Identification in POME Extract

LC-MS analysis revealed that major organic compounds of POME extract contain alkaloids, phospholipids, fatty acids, sphingolipids, saponins, 1,2-aminoalcohols and ketones. Among the organic compounds identified include

TABLE 1. THE DESIGN STUDY OF DIFFERENT SYNTHESIS PARAMETERS OF AgNP USING POME

Parameter	Volume of POME (mL)	$AgNO_3$ (mM)	Temperature (°C)	Extract pH
Volume of extract	0.2, 0.4, 0.6, 0.8, 10.0	1.0	30	7
Extract pH	0.6	1.0	30	4, 5, 6, 7,8, 9, 10
$AgNO_3$	0.6	0.5, 1.0, 1.5, 2.0, 2.5, 3.0	30	7
Temperature	0.6	1.0	30, 40, 50, 60, 70, 80	7

Note: POME - palm oil mill effluent; $AgNO_3$ - silver nitrate.

anhalamine, hebevinoside VII, aminopentol, camptothecin, safingol, stearic acid, palmitic acid and myristone as shown in *Table 2*. These constituents could potentially act as reducing agents in the biosynthesis of AgNP. It is deduced that the AgNP may be capped and stabilised by hydroxyl (OH), carboxyl (–COOH) and amine ($–NH_2$) functional groups from POME, such as alkaloid through the interaction of amine group, or fatty acids and phospholipids through OH and carboxy (C=O), or amine (N–H). Gan et al. (2012) reported similar findings and deduced the capping and stabilisation involvement of OH, C=O, and H-H functional groups from proteins and polyphenols.

The classes of organic compounds portrayed in this study was also found present in numerous plant extracts as depicted in *Table 3*. Their potential to serve as reducing and stabilising agents in AgNP synthesis not only relate with OH, $N–H_2$, and C=O but also possible interaction with C=C, C–H, –COOH, C–O–C, $–COCH_3$, –COO and NH_2 (*Table 3*). Stearic acid, one of the compounds identified in POME extract belongs to the saturated long-chain fatty acids group. It plays a crucial role in the biosynthesis of AgNP by forming a long hydrocarbon chain that attached to the surface of AgNP, creating a protective layer. This layer could effectively prevent aggregation and reaction with other substances. Grizzo et al. (2023) have demonstrated that stearic acid enhances the formation of AgNP on graphene and improves the surface wetting of the nanoparticles when combined in a composite with polylactic acid (PLA). Similarly, it also increased the atomic concentration of AgNP within the composite, emphasising its role in promoting nanoparticle formation (Grizzo et al., 2023). On the other hand camptothecin, an alkaloid identified in POME is not commonly found in the effluent, which primarily consists of degradable organic matter such as water, unrecovered oil, free fatty acids (FFA), starches, proteins and non-toxic plant tissues. This compound likely originates from microorganisms that are present in POME aeration ponds during the aerobic digestion process (Mohammad et al., 2021).

Total Phenolic, Flavonoids and Tannin Contents

In this study, total phenolic, flavonoids and tannin contents of POME were quantified using three different assays, namely, TPC, TFC and TTC. Results in *Figure 2* showed that flavonoids content was the highest compared to tannins and phenolics. Quantitatively, the concentrations of phenols, flavonoids and tannins in 2 g of dried POME were 75 ± 4.10, 102 ± 3.60 and 83 ± 1.89 mg/g as depicted in *Figure 2*.

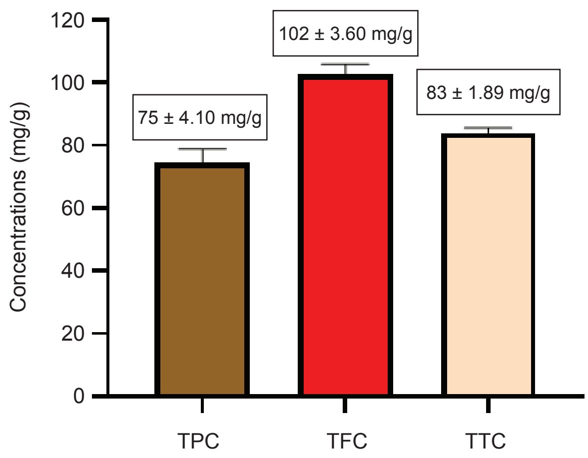

Figure 2. Total phenolic (TPC), flavonoid (TFC) and tannin content (TTC) of aqueous palm oil mill effluent (POME).

The increased flavonoid content is likely due to a higher concentration of organic compounds belonging to the flavonoid groups in POME. Among the identified organic compounds in POME are palmitic acid, stearic acid, anhalamine, hebevinoside VII and aminopentol. These compounds are potential agents that play a role in both reducing and stabilising the nanoparticles during the green synthesis of AgNP (Asmat-Campos et al., 2020).

Screening Process of Synthesis Parameters using OFAT Approach

The production of AgNP is affected by several factors, such as the volume of extract, $AgNO_3$ concentration, temperature and pH, which can be adjusted to control the size, shape, morphology, efficacy and applicability of the nanoparticles. The absorption peak spectrum for AgNP formation ranges from 410 to 500 nm (Dhaka et al., 2023). In this study, the visible spectrum between 400 and 500 nm was used to verify the formation of AgNP and assess the effects of different factors such as volume of extract, temperature, pH and $AgNO_3$ concentration on the POME-AgNP synthesis.

Effect of Extract Volume

The organic compounds within the extract are crucial for the synthesis of AgNP. Therefore, varying volumes of POME extract were investigated to achieve a stable synthesis of POME-AgNP. It was observed that increasing the extract volume from 0.2 to 0.6 mL corresponded to an increase in the absorption band intensity, as depicted in *Figure 3a*. This enhances the participation of organic compounds in the reduction and stabilisation of the synthesised AgNP. However, the increase of the extract volume above 0.6 mL led to shifts in

TABLE 2. SELECTED ORGANIC COMPOUNDS IDENTIFIED USING LC-MS ANALYSIS

Compound	Rt	Molecular formula	Mass	Class	Functional groups	Structural molecules
Anhalamine	6.649	$C_{11}H_{15}N_{03}$	209.1050	Alkaloid	OH and NH	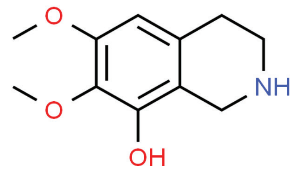
Camptothecin	14.153	$C_{20}H_{16}N_2O_4$	348.1098	Alkaloid	–COO and OH	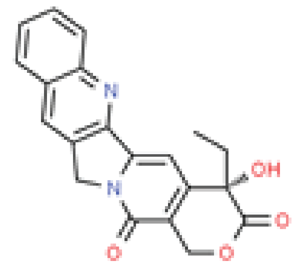
Hebevinoside VII	8.780	$C_{45}H_{72}O_{14}$	836.4956	Saponins	–OH, C–O–C and –$COCH_3$	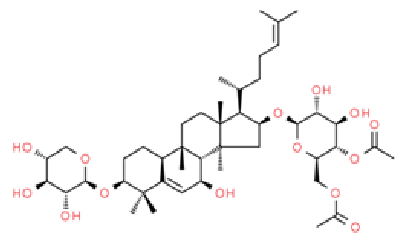
1-Oleoyl-2-palmitoyl-sn-glycero-3-PC	7.142	C_{45} H_{74} NO_8P	787.5150	Phospholipids	–COOH, –COOR and –$N^+(CH_3)_3$	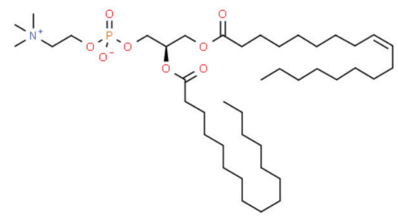
Phosphatidylethanolamine (40:8)	8.643	$C_{45}H_{74}O_{14}$	787.5146	Phospholipids	–PO_4, OH, NH_2 and –COOH	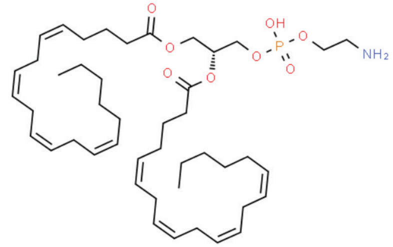

TABLE 2. SELECTED ORGANIC COMPOUNDS IDENTIFIED USING LC-MS ANALYSIS (continued)

Compound	Rt	Molecular formula	Mass	Class	Functional groups	Structural molecules
C_{16} Sphinganine	12.037	$C_{16}H_{35}NO_2$	273.2661	Sphingolipids	–OH and $–NH_2$	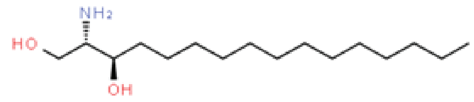
Safingol	12.633	$C_{18}H_{39}NO_2$	301.2970	Sphingolipids	–OH and $–NH_2$	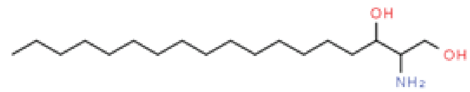
2-hydroxyphytanic acid	11.635	$C_{20}H_{40}O_3$	328.2968	Fatty Acids	–COOH and –OH	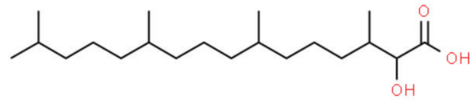
Palmitic acid	12.037	$C_{16}H_{32}O_2$	256.2396	Fatty Acids	–COOH	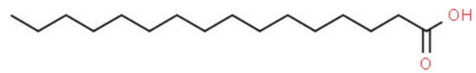
Stearic acid	12.633	$C_{18}H_{36}O_2$	284.2705	Fatty acids	–COOH	
Aminopentol	12.153	$C_{22}H_{12}O_3$	192.0791	1,2-aminoalcohols	–OH and $–NH_2$	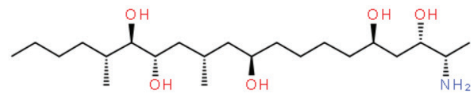
Myristone	12.124	$C_{14}H_{28}O$	212.2138	Ketone	–CHO and C=O	

Note: OH - hydroxy; –OH - hydroxyl; NH - secondary amine; –COO - carboxylate; C–O–C - ether; –COOH - carboxylic acid; –CHO - aldehyde; $–NH_2$ - primary amine; $–PO_4$ - phosphate; $–COCH_3$ - acetyl; COOR - ester; $N^+(CH_3)_3$ - quaternary ammonium.

TABLE 3. PLANTS SOURCE AND PHYTOCHEMICALS INVOLVED IN GREEN SYNTHESIS OF AgNPS WITH DIFFERENT FUNCTIONAL GROUPS

Source of extract	AgNPs-based	Plant parts	Functional groups	Reference
Mussaenda frondose leaf extract	Chitosan/Gelatin@Ag nanocomposites film	Leaves	$–CO–NH_2$	Ediyilyam et al. (2021)
Dioscorea altissima (dunguey)	AgNPs incorporated nanofilm	Tuber	OH-group of starch	Silva et al. (2021)
Pomegranate and citrus fruit peel	AgNPs on cellulose wrapper	Fruit peel	OH in phenols and flavonoids groups	Gopalakrishnan et al. (2023)
Azadirachta indica leaf extract	AgNPs@microcrystalline cellulose	Leaves	OH functionality	Pandian et al. (2023)
Ficus carica extract	AgNPs into Chitosan	Leaves	OH group	Goh et al. (2023)
Banana waste peduncles	AgNPs/Degussa	Fruit peel	Phenolic OH	El-Desouky et al. (2021)
PVA starch	Cassava starch/polyvinyl alcohol@ AgNPs film	Vegetable	OH group	Srikhao et al. (2021)
Pea hull waste	Carboxymethyl cellulose nanocrystals@AgNPs	Vegetable waste	OH and SO_3H groups	He et al. (2021)
Hardwood bleached kraft pulp	Cellulose-AgNP composite sheets	Wood pulp	OH group of cellulose chain	Li et al. (2023)
Bagasse raw material	Alginate/oxidised nanocellulose-AgNPs	Plant waste material	H-bonding	Abutalib and Rajeh (2021)
Fresh leaves of tulasi, mint and aloe vera	AgNPs@cellulosic network	Leaves	NH_2 and OH groups	Kumari et al. (2021b)
Corn cobs	AgNPs with poly (lactic acid)/ nanocellulose nano-films	Corn cobs	Polyphenols, OH and NH groups	Ng et al. (2021)

Note: CO - carbonyl; NH_2 - primary amine; OH - hydroxyl; PVA - polyviyl alcohol; SO_3H - sulfonic acid; NH - secondary amine; AgNP - silver nanoparticles.

the absorption intensity and increased noise in the spectrum, which could be due to a high concentration of reducing agent leading to agglomeration. Therefore, the optimal volume of POME extract for AgNP synthesis is 0.6 mL. Vadakkan et al. (2024) reported that an increase in concentration enhances the synthesis of AgNP until the synthesis reaches the threshold level, however, beyond which particle accumulation occurs. When nanoparticles aggregate, they may lose their essential features and economic value. Hence, it is crucial to maintain an optimal concentration.

Effect of Temperature

Figure 3b illustrates the variation in the absorption spectrum of AgNP synthesised using POME extract at different reaction temperatures. The spectrum shows that the optimal temperature is 50°C. Moreover, at 60°C, 70°C and 80°C, there is an increase in activation energy, which results in AgNP agglomeration. Chemical reactions are facilitated by temperature, as it provides the activation energy required to initiate the fastest reaction. Additionally, temperature also increases the likelihood of reactants colliding, thus increasing the chances of them converting into the desired product (Lotfy et al., 2021).

Effect of pH

AgNP synthesis is significantly influenced by the pH range of the solution as it enhances the ability of phytochemicals to bind with Ag^+, this facilitates their reducing and capping potentials (Azarbani & Shiravand, 2020). In this study, the synthesis of AgNP using POME at its natural pH of 4.5 showed no absorbance peak, indicating the absence of AgNP formation. To achieve optimal synthesis conditions, the pH of the POME extract was adjusted. As shown in *Figure 3c*, the optimal pH for synthesising AgNP is pH 7. At this pH, the reduced concentration of H^+ ions increases the surface charge of the particles, facilitating AgNP formation. In contrast, synthesis at pH levels of 4 and 5 showed no SPR absorbance peak, suggesting that acidic conditions are unfavourable for AgNP synthesis. Supporting these findings, Hamouda et al. (2019) reported that the optimal pH for AgNP formation using *Oscillatoria limnetica* was 6.7, with synthesis being completely inhibited at pH 4.7 and 5.7.

Effect of $AgNO_3$ Concentration

In this study, various concentrations of $AgNO_3$ (ranging from 0.5 to 3.0 mM) were examined to determine the optimal concentration for AgNP formation with POME extract at ambient temperature. The absorption spectrum of the POME-AgNP showed that increasing the $AgNO_3$ concentration up to 1.5 mM led to higher absorption band intensity. However, at concentrations between 1.5 and 3.0 mM as shown in *Figure 3d*, there was a decrease in the absorption spectrum, likely due to nanoparticle aggregation. Therefore, a concentration of 1.5 mM $AgNO_3$ was identified as the optimal condition for the green synthesis of AgNP.

Characterisation of POME-AgNP

FTIR spectroscopy. The involvement of surface functional groups in the biosynthesis of POME-AgNP was examined using FTIR analysis. *Figure 4* displays a comparative analysis of the FTIR spectrum for raw POME powder and POME-AgNP. The absorption peaks in the FTIR spectrum of POME-AgNP showed reduced intensity at 3,761 and 1,744 cm^{-1}, which indicates C=O stretching vibrations of the carbonyl group present in the raw POME. This can be attributed to the involvement of compounds with carbonyl functional groups in the synthesis of POME-AgNP, which aligns with previous studies on gold nanoparticles synthesised using POME (Gan et al., 2012). The significant absorption bands observed in the range of 3,400–2,900 cm^{-1} are associated with phenolic compounds in the biosynthesised AgNP. The presence of carbonyl groups, indicated by the C=O stretching vibration at 1,700 cm^{-1}, suggests the presence of aromatic structural vibrations in flavonoids and glucosides. Thus, the FTIR results imply that the organic compounds in POME contain functional groups responsible for the reduction and stabilisation of POME-AgNP.

The differences in band and peak intensity showed the structural changes and the change in the extent of hydrogen bonding. These might be due to the oxidisation of phytochemicals in POME. In Indian propolis extract, flavonoids contribute to AgNP synthesis by reducing Ag^+ to Ag^0 (Rashid et al., 2019). In the process, flavonoids undergo oxidation, which results in the formation of diketone and unsaturated carbonyl groups. It is possible that the carbonyl and hydroxyl functional groups found in POME can serve not only as reducing agents by giving electrons to convert Ag^+ to Ag^0 during AgNP synthesis but also as capping agents through electrostatic interactions to keep the synthesised AgNP stable. This suggests that these active functional groups play a dual role in the synthesis and stabilisation of AgNP (Chi et al., 2022).

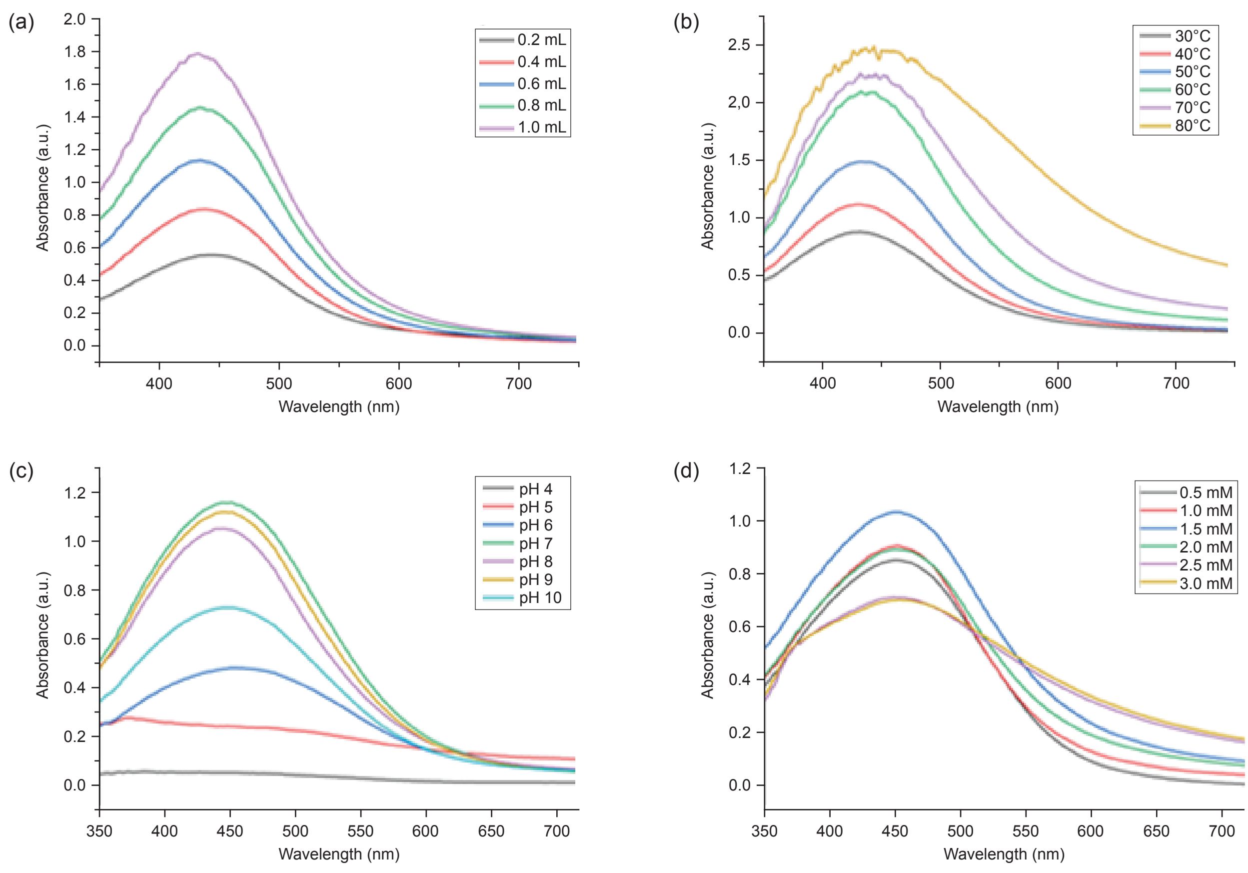

Figure 3. Visible spectra of POME-AgNP: (a) Volume, (b) temperature, (c) pH values and (d) $AgNO_3$ concentrations of palm oil mill effluent (POME) extract.

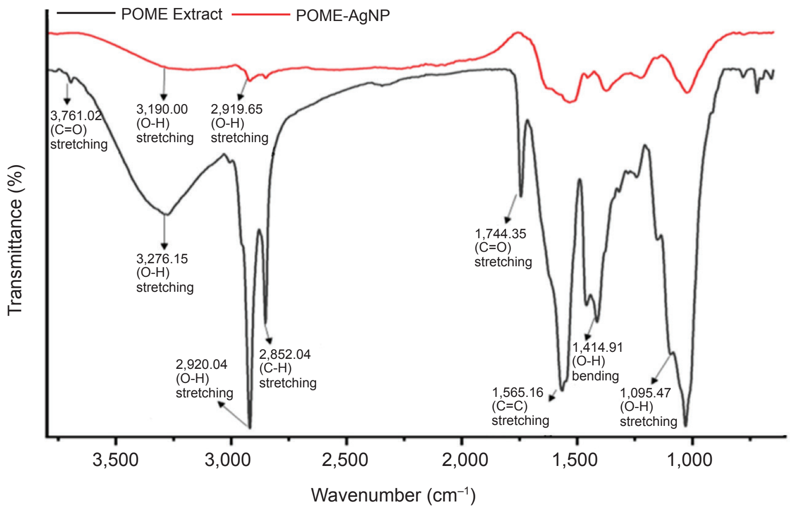

Figure 4. Fourier Transform Infrared (FTIR) spectra of raw palm oil mill effluent (POME) extract and POME-AgNP.

DLS analysis. DLS determines the time-dependent light intensity variations caused by particle Brownian motion and measures the hydrodynamic diameter of the nanoparticles (Yusof et al., 2020). The DLS allows the quantitative measurement of size distribution as well as the dispersion (polydispersion or monodispersion) of nanomaterials in a colloidal system (John et al., 2020). *Figure 5a* shows the average hydrodynamic particle sizes of 21.18 nm with a polydisperse index (PdI) of 0.259. A value of PdI less than 0.5 indicates the mono dispersion of nanoparticles (Agnihotri et al., 2014). In addition, the AgNP stability was evaluated by measuring the zeta potential magnitude. *Figure 5b* shows the zeta-potential value of –19.3 mV for the POME-AgNP colloidal solution. The charge surface (-) obtained is due to the macromolecules in the raw POME adhering to the AgNP surface which indicates repulsion between the particles, preventing their aggregation. According to Tavakol et al. (2017), suspended particles with a negative surface charge are likely to repel each other and less likely to aggregate (electrostatically stable). In this work, a zeta potential of –19.3 mV indicates that the POME-AgNP are considerably stable. Thus, AgNP with zeta potential of < –25 mV or > 25 mV have significant stability (Vadakkan et al., 2024).

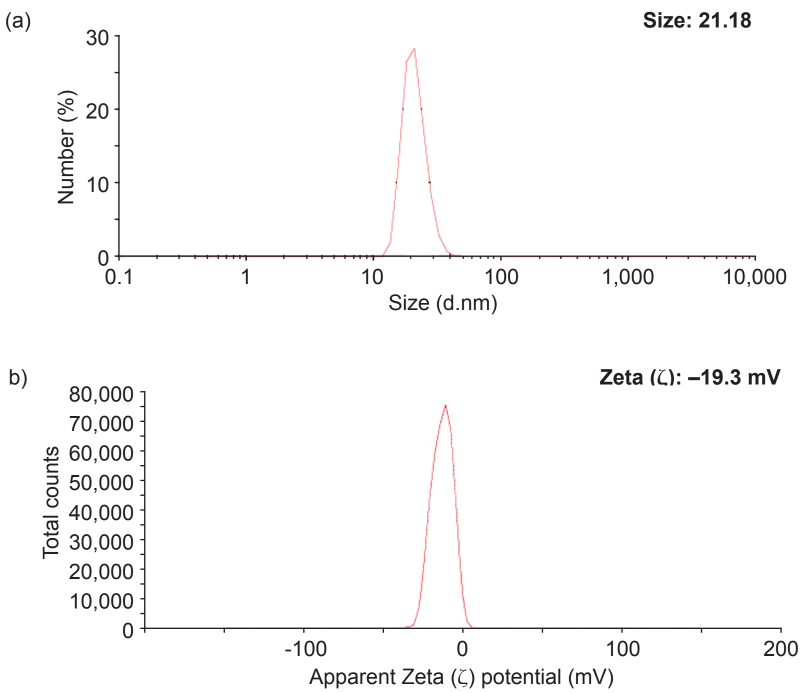

Figure 5. DLS analysis showing the (a) size distribution and (b) zeta (ζ) potential.

CONCLUSION

This study presents the novel approach to the biosynthesis of AgNP using POME. Utilising agro-industrial waste such as POME for AgNP synthesis is both sustainable and advantageous, as it helps reduce environmental pollution while providing antimicrobial properties. The LC-MS analysis identified several compounds, including stearic acid, palmitic acid, anhalamine, phosphatidylethanolamine (40:8), hebevinocide VII, aminopentol, safingol, camptothecin and myristone, which likely play roles in the reduction, capping and stabilisation of Ag^+ ions during AgNP formation. The optimal conditions for synthesising POME-AgNP synthesis were established using the OFAT approach and the physicochemical properties of the resulting POME-AgNP were comprehensively evaluated. Future research should focus on identifying and isolating individual compounds and assess their effectiveness to elucidate their roles, thereby improving our understanding of the biosynthetic process, especially considering the increasing demands for solutions in various health applications.

ACKNOWLEDGEMENT

The authors would like to thank the Maokil Palm Oil Mill in Labis, Johor, Malaysia, for providing access to obtained raw POME for this experiment. We also extend our gratitude to the Department of Bioscience, Faculty of Science, for their support and resources throughout this study. Additionally, we are grateful to Tetfund Nigeria for the financial assistance provided to the first author.

REFERENCES

Abdullah, H. S. T. S. H., Asseri, S. N. A. R. M., Mohamad, W. N. K. W., Kan, S., Azmi, A. A., Julius, F. S. Y., & Chia, P. W. (2021). Green synthesis, characterization and applications of silver nanoparticle mediated by the aqueous extract of red onion peel. *Environmental Pollution*, *271*, 116295. https://doi.org/10.1016/j.envpol.2020.116295

Abutalib, M. M., & Rajeh, A. (2021). Enhanced structural, electrical, mechanical properties and antibacterial activity of Cs/PEO doped mixed nanoparticles (Ag/TiO_2) for food packaging applications. *Polymer Testing*, *93*, 107013. https://doi.org/10.1016/j.polymertesting.2020.107013

Acharya, A., & Pal, P. K. (2020). Agriculture nanotechnology: Translating research outcome to field applications by influencing environmental sustainability. *NanoImpact*, *19*, 100232. https://doi.org/10.1016/j.impact.2020.100232

Agnihotri, S., Mukherji, S., & Mukherji, S. (2014). Size-controlled silver nanoparticles synthesized over the range 5–100 nm using the same protocol and their antibacterial efficacy. *RSC Advances*, *4*(8), 3974–3983. https://doi.org/10.1039/c3ra44507k

Alvarez, P. J. J., Chan, C. K., Elimelech, M., Halas, N. J., & Villagrán, D. (2018). Emerging opportunities for nanotechnology to enhance water security. *Nature Nanotechnology*, *13*(8), 634–641. https://doi.org/10.1038/s41565-018-0203-2

Asmat-Campos, D., Abreu, A. C., Romero-Cano, M. S., Urquiaga-Zavaleta, J., Contreras-Cáceres, R., Delfín-Narciso, D., Juárez-Cortijo, L., Nazario-Naveda, R., Rengifo-Penadillos, R., & Fernández, I. (2020). Unraveling the active biomolecules responsible for the sustainable synthesis of nanoscale silver particles through nuclear magnetic resonance metabolomics. *ACS Sustainable Chemistry & Engineering*, *8*(48), 17816–17827. https://doi.org/10.1021/acssuschemeng.0c06903

Azarbani, F., & Shiravand, S. (2020). Green synthesis of silver nanoparticles by *Ferulago macrocarpa* flowers extract and their antibacterial, antifungal and toxic effects. *Green Chemistry Letters and Reviews*, *13*(1), 41–49. https://doi.org/10.1080/17518253.2020.1726504

Aziz, N., Faraz, M., Pandey, R., Shakir, M., Fatma, T., Varma, A., Barman, I., & Prasad, R. (2015). Facile algae-derived route to biogenic silver nanoparticles: Synthesis, antibacterial, and photocatalytic properties. *Langmuir*, *31*(42), 11605–11612. https://doi.org/10.1021/acs.langmuir.5b03081

Baba, S. A., & Malik, S. A. (2015). Determination of total phenolic and flavonoid content, antimicrobial and antioxidant activity of a root extract of *Arisaema jacquemontii* Blume. *Journal of Taibah University for Science*, *9*(4), 449–454. https://doi.org/10.1016/j.jtusci.2014.11.001

Barabadi, H., Mojab, F., Vahidi, H., Marashi, B., Talank, N., Hosseini, O., & Saravanan, M. (2021). Green synthesis, characterization, antibacterial and biofilm inhibitory activity of silver nanoparticles compared to commercial silver nanoparticles. *Inorganic Chemistry Communications*, *129*, 108647. https://doi.org/10.1016/j.inoche.2021.108647

Chantho, P., Musikavong, C., & Suttinun, O. (2016). Removal of phenolic compounds from palm oil mill effluent by thermophilic *Bacillus thermoleovorans* strain A2 and their effect on anaerobic digestion. *International Biodeterioration & Biodegradation*, *115*, 293–301. https://doi.org/10.1016/j.ibiod.2016.09.010

Chantiratikul, P., Meechai, P., & Nakbanpotec, W. (2009). Antioxidant activities and phenolic contents of extracts from *Salvinia molesta* and *Eichornia crassipes*. *Research Journal of Biological Sciences*, *4*(10), 1113–1117.

Cheong, W. Y., Amran, S. I., Hussin, H., & Ahmad Zawawi, N. (2022). Silver nanoparticles synthesis using banana peels extract and its *in silico* evaluation for antibacterial activity against *Escherichia coli*. *Journal of Materials in Life Sciences*, *1*(1), 37–44.

Chi, N. T. L., Narayanan, M., Chinnathambi, A., Govindasamy, C., Subramani, B., Brindhadevi, K., Pimpimon, T., & Pikulkaew, S. (2022). Fabrication, characterization, anti-inflammatory, and anti-diabetic activity of silver nanoparticles synthesized from *Azadirachta indica* kernel aqueous extract. *Environmental Research*, *208*, 112684. https://doi.org/10.1016/j.envres.2022.112684

Dastafkan, K., Khajeh, M., Bohlooli, M., Ghaffari-Moghaddam, M., & Sheibani, N. (2015). Mechanism and behavior of silver nanoparticles in aqueous medium as adsorbent. *Talanta*, *144*, 1377–1386. https://doi.org/10.1016/j.talanta.2015.03.065

De Matteis, V., Cascione, M., Costa, D., Martano, S., Manno, D., Cannavale, A., Mazzotta, S., Paladini, F., Martino, M., & Rinaldi, R. (2023). Aloe vera silver nanoparticles addition in chitosan films: Improvement of physicochemical properties for eco-friendly food packaging material. *Journal of Materials Research and Technology*, *24*, 1015–1033. https://doi.org/10.1016/j.jmrt.2023.03.025

Dhaka, A., Mali, S. C., Sharma, S., & Trivedi, R. (2023). A review on biological synthesis of silver nanoparticles and their potential applications. *Results in Chemistry*, *6*, 101108. https://doi.org/10.1016/j.rechem.2023.101108

Dolatabadi, M., Naidu, H., & Ahmadzadeh, S. (2022). Adsorption characteristics in the removal of chlorpyrifos from groundwater using magnetic graphene oxide and carboxy methyl cellulose composite. *Separation and Purification Technology*, *300*, 121919. https://doi.org/10.1016/j.seppur.2022.121919

Ediyilyam, S., George, B., Shankar, S. S., Dennise, T. T., Wacławek, S., Cerník, M., & Padil, V. V. T. (2021). Chitosan/gelatin/silver nanoparticles composites films for biodegradable food packaging applications. *Polymers*, *13*(11), 1680. https://doi.org/10.3390/polym13111680

El-Desouky, N., Shoueir, K. R., El-Mehasseb, I., & El-Kemary, M. (2021). Bio-inspired green manufacturing of plasmonic silver nanoparticles/degussa using banana waste peduncles: Photocatalytic, antimicrobial, and cytotoxicity evaluation. *Journal of Materials Research and Technology*, *10*, 671–686. https://doi.org/10.1016/j.jmrt.2020.12.035

Gan, P. P., Ng, S. H., Huang, Y., & Li, S. F. Y. (2012). Green synthesis of gold nanoparticles using palm oil mill effluent (POME): A low-cost and eco-friendly viable approach. *Bioresource Technology*, *113*, 132–135. https://doi.org/10.1016/j.biortech.2012.01.015

Githala, C. K., & Trivedi, R. (2023). Review on synthesis method, biomolecules involved, size affecting factors and potential applications of silver nanoparticles. *Biocatalysis and Agricultural Biotechnology*, *54*, 102912. https://doi.org/10.1016/j.bcab.2023.102912

Goh, H. T., Cheok, C. Y., & Yeap, S. P. (2023). Green synthesis of silver nanoparticles using banana peel extract and application on banana preservation. *Food Frontiers*, *4*(1), 283–288. https://doi.org/10.1002/fft2.206

Gopalakrishnan, K., Chandel, M., Gupta, V., Kaur, K., Patel, A., Kaur, K., Kishore, A., Prabhakar, P. K., Singh, A., Prasad, J. S., Bodana, V., Saxena, V., Shanmugam, V., & Sharma, A. (2023). Valorisation of fruit peel bioactive into green synthesized silver nanoparticles to modify cellulose wrapper for shelf-life extension of packaged bread. *Food Research International*, *164*, 112321. https://doi.org/10.1016/j.foodres.2022.112321

Grizzo, A., Santos, D. M. D., Da Costa, V. P., Lopes, R. G., Inada, N. M., Correa, D. S., & Campana-Filho, S. P. (2023). Multifunctional bilayer membranes composed of poly(lactic acid), beta-chitin whiskers and silver nanoparticles for wound dressing applications. *International Journal of Biological Macromolecules*, *251*, 126314. https://doi.org/10.1016/j.ijbiomac.2023.126314

Haile, M., & Kang, W. H. (2019). Antioxidant activity, total polyphenol, flavonoid and tannin contents of fermented green coffee beans with selected yeasts. *Fermentation*, *5*(1), 29. https://doi.org/10.3390/fermentation5010029

Haleem, A., Javaid, M., Singh, R. P., Rab, S., & Suman, R. (2023). Applications of nanotechnology in medical field: A brief review. *Global Health Journal*, *7*(2), 70–77. https://doi.org/10.1016/j.glohj.2023.02.008

Hamouda, R. A., Hussein, M. H., Abo-Elmagd, R. A., & Bawazir, S. S. (2019). Synthesis and biological characterization of silver nanoparticles derived from the cyanobacterium *Oscillatoria limnetica*. *Scientific Reports*, *9*(1), 13071. https://doi.org/10.1038/s41598-019-49444-y

Harish Pandian, J., Senthilkumar, K., Venkata Ratnam, M., Naveenkumar, M., & Samraj, S. (2023). *Azadirachta indica* leaf extract mediated silver nanoparticles impregnated nano composite film (AgNP/MCC/starch/whey protein) for food packaging applications. *Environmental Research*, *216*, 114641. https://doi.org/10.1016/j.envres.2022.114641

He, Y., Li, H., Fei, X., & Peng, L. (2021). Carboxymethyl cellulose/cellulose nanocrystals immobilized silver nanoparticles as an effective coating to improve barrier and antibacterial properties of paper for food packaging applications. *Carbohydrate Polymers*, *252*, 117156. https://doi.org/10.1016/j.carbpol.2020.117156

Iravani, S., Korbekandi, H., Mirmohammadi, S. V., & Zolfaghari, B. (2014). Synthesis of silver nanoparticles: Chemical, physical and biological methods. *Research in Pharmaceutical Science*, *9*(6), 385–406.

Jaast, S., & Grewal, A. (2021). Green synthesis of silver nanoparticles, characterization and evaluation of their photocatalytic dye degradation activity. *Current Research in Green and Sustainable Chemistry*, *4*, 100195. https://doi.org/10.1016/j.crgsc.2021.100195

John, M. S., Nagoth, J. A., Ramasamy, K. P., Mancini, A., Giuli, G., Natalello, A., Ballarini, P., Miceli, C., & Pucciarelli, S. (2020). Synthesis of bioactive silver nanoparticles by a *Pseudomonas* strain associated with the Antarctic psychrophilic protozoon *Euplotes focardii*. *Marine Drugs*, *18*(1), 38. https://doi.org/10.3390/md18010038

Khane, Y., Benouis, K., Albukhaty, S., Sulaiman, G. M., Abomughaid, M. M., Ali, A. A., Aouf, D., Fenniche, F., Khane, S., Chaibi, W., Henni, A., Bouras, H. D., & Dizge, N. (2022). Green synthesis of silver nanoparticles using aqueous citrus limon zest extract: Characterization and evaluation of their antioxidant and antimicrobial properties. *Nanomaterials*, *12*(12), 2013. https://doi.org/10.3390/nano12122013

Kumari, S., Tehri, N., Gahlaut, A., & Hooda, V. (2021a). Actinomycetes mediated synthesis, characterization, and applications of metallic nanoparticles. *Inorganic and Nano-Metal Chemistry*, *51*(10), 1386–1395. https://doi.org/10.1080/24701556.2020.1835978

Kumari, S. C., Padma, P. N., & Anuradha, K. (2021b). Green silver nanoparticles embedded in cellulosic network for fresh food packaging. *Journal of Pure and Applied Microbiology*, *15*(3), 1236–1244. https://doi.org/10.22207/jpam.15.3.13

Li, B., Liu, G., Tang, X., Zhang, H., & Gao, X. (2023). Facile preparation of all cellulose composite with excellent mechanical and antibacterial properties via partial dissolution of corn-stalk biomass. *International Journal of Biological Macromolecules*, *228*, 89–98. https://doi.org/10.1016/j.ijbiomac.2022.12.212

Liu, J., Liu, Y., & Wang, X. (2023). Effects of bioactive compounds and pharmacological activities in medicinal fruits and vegetables by thermal processing. *Journal of Future Foods*, *3*(3), 252–262. https://doi.org/10.1016/j.jfutfo.2023.02.009

Lotfy, W. A., Alkersh, B. M., Sabry, S. A., & Ghozlan, H. A. (2021). Biosynthesis of silver nanoparticles by *Aspergillus terreus*: Characterization, optimization, and biological activities. *Frontiers in Bioengineering and Biotechnology*, *9*, 633468. https://doi.org/10.3389/fbioe.2021.633468

Mahmod, S. S., Takriff, M. S., Al-Rajabi, M. M., Abdul, P. M., Gunny, A. A. N., Silvamany, H., & Jahim, J. M. (2023). Water reclamation from palm oil mill effluent (POME): Recent technologies, by-product recovery, and challenges. *Journal of Water Process Engineering*, *52*, 103488. https://doi.org/10.1016/j.jwpe.2023.103488

Mohammad, S., Baidurah, S., Kobayashi, T., Ismail, N., & Leh, C. P. (2021). Palm oil mill effluent treatment processes – A review. *Processes*, *9*(5), 739. https://doi.org/10.3390/pr9050739

Mondal, A., Maity, S., Mondal, A., & Mondal, N. K. (2024). Antibacterial, antibiofilm and larvicidal activity of silver nanoparticles synthesized from spider silk protein. *International Journal of Biological Macromolecules*, *258*, 128775. https://doi.org/10.1016/j.ijbiomac.2023.128775

Mukherji, S., Bharti, S., Shukla, G., & Mukherji, S. (2019). Synthesis and characterization of size- and shape-controlled silver nanoparticles. *Physical Sciences Reviews*, *4*(1), 20170082. https://doi.org/10.1515/psr-2017-0082

Murugesan, S., Bhuvaneswari, S., & Sivamurugan, V. (2017). Green synthesis, characterization of silver nanoparticles of a marine red alga *spyridia fusiformis* and their antibacterial activity. *International Journal of Pharmacy and Pharmaceutical Sciences*, *9*(5), 192. https://doi.org/10.22159/ijpps.2017v9i5.17105

Nahar, K. N., Rahaman, M. H., Khan, G. A., Islam, M. K., & Al-Reza, S. (2021). Green synthesis of silver nanoparticles from *citrus sinensis* peel extract and its antibacterial potential. *Asian Journal of Green Chemistry*, *5*(1), 135–150. https://doi.org/10.22034/ajgc.2021.113966

Ng, W. K., Chow, W. S., & Ismail, H. (2021). Hybridization of 5-nitroisatin and silver nanoparticles for boosting the antimicrobial performance of poly(lactic acid)/nanocellulose nanocomposite films. *Food Packaging and Shelf Life*, *30*, 100763. https://doi.org/10.1016/j.fpsl.2021.100763

Phongtongpasuk, S., & Poadang, S. (2016). Green synthesis of silver nanoparticles using pomegranate peel extract. *Advanced Materials Research*, *1131*, 227–230. https://doi.org/10.4028/www.scientific.net/amr.1131.227

Rashid, S., Azeem, M., Khan, S. A., Shah, M. M., & Ahmad, R. (2019). Characterization and synergistic antibacterial potential of green synthesized silver nanoparticles using aqueous root extracts of important medicinal plants of Pakistan. *Colloids and Surfaces B Biointerfaces*, *179*, 317–325. https://doi.org/10.1016/j.colsurfb.2019.04.016

Savolainen, K., Alenius, H., Norppa, H., Pylkkänen, L., Tuomi, T., & Kasper, G. (2010). Risk assessment of engineered nanomaterials and nanotechnologies – A review. *Toxicology*, *269*(2-3), 92–104. https://doi.org/10.1016/j.tox.2010.01.013

Silva, L. S. C., Martim, S. R., Gomes, D. M. D., Prado, F. B., Marinho, N. M. V., De Amorim Silva, T., Castillo, T. A., De Arimatéia Rodrigues Do Rego, J., Seabra, A. B., Durán, N., & Teixeira, M. F. S. (2021). Amazonian tuber starch based films incorporated with silver nanoparticles for preservation of fruits. *Research Society and Development*, *10*(6), e23510615304. https://doi.org/10.33448/rsd-v10i6.15304

Srikhao, N., Kasemsiri, P., Ounkaew, A., Lorwanishpaisarn, N., Okhawilai, M., Pongsa, U., Hiziroglu, S., & Chindaprasirt, P. (2021). Bioactive nanocomposite film based on Cassava Starch/Polyvinyl alcohol containing green synthesized silver nanoparticles. *Journal of Polymers and the Environment*, *29*(2), 672–684. https://doi.org/10.1007/s10924-020-01909-2

Tang, M. T., Tan, K. T., & Wong, L. P. (2024). Palm oil mill effluent (POME) as a source of biofuels and value-added products via oil recovery: A review. *Journal of Oil Palm Research, 36*(2), 534–546. https://doi.org/10.21894/jopr.2023.0056

Tavakol, S., Hoveizi, E., Kharrazi, S., Tavakol, B., Karimi, S., & Sorkhabadi, S. M. R. (2017). Organelles and chromatin fragmentation of human umbilical vein endothelial cell influence by the effects of zeta potential and size of silver nanoparticles in different manners. *Artificial Cells Nanomedicine and Biotechnology*, *45*(4), 817–823. https://doi.org/10.1080/21691401.2016.1178132

Teo, S. L., Hussin, H., & Ahmad Zawawi, N. (2023). Study of green biosynthesized silver nanoparticles using banana peels on organic waste composting. *Journal of Materials in Life Sciences, 2*(2), 200–210.

Uzair, B., Liaqat, A., Iqbal, H., Menaa, B., Razzaq, A., Thiripuranathar, G., Rana, N. F., & Menaa, F. (2020). Green and cost-effective synthesis of metallic nanoparticles by algae: Safe methods for translational medicine. *Bioengineering*, *7*(4), 129. https://doi.org/10.3390/bioengineering7040129

Vadakkan, K., Rumjit, N. P., Ngangbam, A. K., Vijayanand, S., & Nedumpillil, N. K. (2024). Novel advancements in the sustainable green synthesis approach of silver nanoparticles (AgNPs) for antibacterial therapeutic applications. *Coordination Chemistry Reviews*, *499*, 215528. https://doi.org/10.1016/j.ccr.2023.215528

Vankudoth, S., Dharavath, S., Veera, S., Maduru, N., Chada, R., Chirumamilla, P., Gopu, C., & Taduri, S. (2022). Green synthesis, characterization, photoluminescence and biological studies of silver nanoparticles from the leaf extract of *Muntingia calabura*. *Biochemical and Biophysical Research Communications*, *630*, 143–150. https://doi.org/10.1016/j.bbrc.2022.09.054

Wasilewska, A., Klekotka, U., Zambrzycka, M., Zambrowski, G., Święcicka, I., & Kalska-Szostko, B. (2023). Physico-chemical properties and antimicrobial activity of silver nanoparticles fabricated by green synthesis. *Food Chemistry*, *400*, 133960. https://doi.org/10.1016/j.foodchem.2022.133960

Yahya, R., & Alharbi, N. M. (2023). Biosynthesized silver nanoparticles-capped chondroitin sulfate nanogel targeting microbial infections and biofilms for biomedical applications. *International Journal of Biological Macromolecules*, *253*, 127080. https://doi.org/10.1016/j.ijbiomac.2023.127080

Yusof, H. M., Rahman, N. A., Mohamad, R., & Zaidan, U. H. (2020). Microbial mediated synthesis of silver nanoparticles by *Lactobacillus plantarum* TA4 and its antibacterial and antioxidant activity. *Applied Sciences*, *10*(19), 6973. https://doi.org/10.3390/app10196973

Zahoor, M., Nazir, N., Iftikhar, M., Naz, S., Zekker, I., Burlakovs, J., Uddin, F., Kamran, A. W., Kallistova, A., Pimenov, N., & Khan, F. A. (2021). A review on silver nanoparticles: Classification, various methods of synthesis, and their potential roles in biomedical applications and water treatment. *Water*, *13*(16), 2216. https://doi.org/10.3390/w13162216

Zhang, H., Chen, S., Jia, X., Huang, Y., Ji, R., & Zhao, L. (2021). Comparation of the phytotoxicity between chemically and green synthesized silver nanoparticles. *The Science of the Total Environment*, *752*, 142264. https://doi.org/10.1016/j.scitotenv.2020.142264

Journal of Oil Palm Research Vol. 38 (3) September 2026 p. 509–518
DOI: https://doi.org/10.21894/jopr.2025.0046

SPRAY COVERAGE AND EFFECTIVENESS OF UNMANNED AERIAL VEHICLE POINT-TO-POINT SPRAYING TECHNOLOGY FOR THE CONTROL OF *Oryctes rhinoceros* IN IMMATURE OIL PALM

MEOR BADLI SHAH AHMAD RAFIE[1]* and SAMSUDIN AMIT[1]

ABSTRACT

The study aimed to elucidate the characteristics of spray coverage and the effect of spraying in controlling Oryctes rhinoceros *beetle (ORB) in immature oil palm using an unmanned aerial vehicle point-to-point (UAVPTP) sprayer. The UAVPTP sprayer was compared to the semi-mechanised FM ORYCT sprayer and the INTER knapsack sprayer. The water-sensitive paper was used as a sampler to determine spray coverage and droplet density and was statistically analysed. Spray volume per palm was determined via a special calibration method, and fresh damage incidences of ORB attack before and after treatment of cypermethrin insecticide using the UAVPTP were conducted to determine the effectiveness of the treatments. The results showed that the spray coverage of UAVPTP at the targeted spears and first spiral of fronds reached a satisfactory level of above 80%. No significant differences were observed in the fresh damage of ORB ($F_{5,6}$ = 0.85, p > 0.05(1st-year-flat); $F_{5,6}$ = 2.34, p > 0.05 (1st-yr-terrace); $F_{5,6}$ = 0.67, p > 0.05 (2nd-yr-flat); $F_{5,6}$ = 1.92, p > 0.05 (2nd-yr-terrace)) upon treatments of cypermethrin between the UAVPTP sprayer, FM ORYCT semi-mechanised sprayer or INTER knapsack sprayer after six rounds of spraying treatment at all types of field terrains. The study results provide the theoretical basis and technical support for decision-making in using the UAVPTP sprayer in immature oil palms.*

Keywords: cypermethrin, *Oryctes rhinoceros*, point-to-point spraying, spray coverage, unmanned aerial vehicle (UAV).

Received: 30 December 2023**; Accepted:** 26 May 2025**; Published online:** 2 September 2025.

INTRODUCTION

Oryctes rhinoceros beetle (ORB) is one of the major pests that attack immature oil palms. Adult ORB feeds on the cabbage and spear parts of the palms, causing damage to the growing points (Ho, 2010). Losses due to ORB have been reported to reach 53% in the first year of harvesting (Chung et al., 1999). In addition, Chung et al. (1999) also discovered that the beetle damage could cause an average crop loss of 40%–92% during the first year of harvesting. Adult ORBs can live for about 6–9 months. They feed on the immature palm tissue for up to 4 days before they move to another palm. This process leads to severe crop loss (Desmier & Kang, 2001). Due to beetle attacks, a reduction of >15% in canopy size had also been observed (Samsudin et al., 1993), which often result in reduced photosynthetic activity, delayed plant maturity, smaller fruit bunch size and an approximately 25% crop loss (Liau & Ahmad, 1991).

To effectively control ORB, one of the common treatments is via spraying using cypermethrin insecticide at the spear region and bole of the palm with a spray volume of 100–200 mL/palm. The targeted spear and the base of the first spiral of younger fronds must be wetted to ensure that effective control of ORB is achieved. Spraying is conducted at 14-day intervals as a regular treatment to prevent severe damage and provide

[1] R&D Crop Protection,
Plantation Research and Advisory Department,
SD Guthrie Research Sdn. Bhd.,
Km 10, Jalan Banting-Kelanang, P.O. Box 207,
42700 Banting, Selangor, Malaysia.

* *Corresponding author e-mail: meor.badli.shah@sdguthrie.com*

good protection for palms without delaying the immature period (Ho, 2010). Although there are other methods, e.g., cultural control via constructing the close ended conservation trenches (CECT), the establishment of legume cover crops (LCC) and the biological control methods using *Metarhizium* bioinsecticides, chemical control is still required in areas where ORB infestation is significant. The spraying of cypermethrin insecticide is currently being practised in major plantation estates at a dosage of 0.1% active ingredient (a.i.) concentration with the spray volume of between 100–200 mL to the spear, new fronds and spear bases when damage has been detected. Cypermethrin insecticide used for the control of ORB is non-systemic; it only remains on the exterior of the plant and must be in contact and absorbed through the body of the insect, and may also act as a poison in the insect's stomach. It attacks the nervous system and interacts with the sodium channel in the insects, thus affecting neuron function (Macbean, 2012). Currently, spraying is done manually using conventional knapsack sprayers (CKS) or semi-mechanised tractor-drawn power sprayers. The current method of spraying using CKS is highly labourious, with productivity between 2–4 ha/man-day depending on the field terrain. Lower productivity is observed in fields with terraces. Therefore, there is a need to seek alternatives to replace this laborious method, and the use of precision agriculture using an unmanned aerial vehicle via point-to-point (UAVPTP) autonomous sprayer could be a good technological solution to this problem.

Precision agriculture (PA) technology that embodies the advancement in crop yield optimisation and managerial decision-making through cutting-edge sensor technology and analytical tools is capable of elevating production rates, streamlining labour and optimising fertiliser, irrigation and pest management. PA presents a solution to this issue through the precise monitoring and forecasting of pests, which improves productivity and guarantees environmental sustainability (Kanwal et al., 2022; Mulla, 2013). Kanwal et al. (2022) postulated that various PA technologies have enabled farmers to monitor and manage pests, including remote sensing, the Internet of Things (IoT), geographical information systems, and artificial intelligence. In the aerial field of precision agriculture, unmanned aerial vehicles (UAV) operation stands out among automation machinery due to its high flexibility, ease of control, high adaptability to complex terrain and high efficiency (Liu & Li, 2023). Hilz and Vermeer (2013) reported that UAV have emerged as capable plant protectors. It has the advantages of high operational efficiency, high speed and low drift, but it is also affected by environmental factors; UAV spraying often produces droplet drift. The control effects of UAV spraying on cotton aphids and spider mites were 63.7% and 61.3%, respectively (Lou et al., 2018). Drones, when equipped with precision techniques and variable-rate nozzles, minimise the use of pesticides, resulting in cost savings on pesticide materials. This makes drones a well-suited tool for PA. Moreover, drones excel in situations involving hazardous chemicals like pesticides. By flying closely to the crop canopy, they ensure that pesticides directly reach the leaves, with minimal runoff to the soil. Drones also target only pest-affected areas, avoiding wasteful pesticide application across the entire field, making them highly efficient (Krishna, 2017).

An innovation of spraying using an UAVPTP spraying method on top of the palm canopy has recently been introduced to replace the existing spraying method. One of the inventions is the UAVPTP sprayer under the trade name of ORYCTES, produced by a Malaysian company, Aonic Sdn. Bhd. (Aonic) (formerly known as Poladrone Solutions Sdn. Bhd.) (*Figure 1*). The sprayer consists of an airframe with 6 propeller blades and a propulsion system, 16 L tanks with a spraying pump fitted with a TG-8 full cone nozzle and powered by a 12S lithium polymer battery. It is equipped with collision avoidance radar and an altimeter radar system to detect and conduct point-to-point spraying on the palms (Aonic, 2021). ORYCTES has been claimed to be capable of conducting point-to-point spraying over the top of the palm canopy, delivering precise dosage, flying autonomously and being able to spray palms in terraced and hilly areas. SD Guthrie Research Sdn. Bhd., under the R&D Crop Protection Section, Plantation Research & Advisory Department, collaborated with Aonic with the objectives to develop, optimise and study the UAVPTP sprayer on its spray coverage and spray effectiveness. It was hypothesised that the UAVPTP would be able to provide satisfactory spray coverage on the targeted spear base region of the immature palms and be able to effectively control the ORB in the immature palms. This article provides a detailed report and discussion of the study.

MATERIALS AND METHODS

Before the commencement of the research, R&D Crop Protection, SD Guthrie Research Sdn. Bhd., =had set a list of parameters for the UAVPTP evaluation, which is listed in *Table 1*.

Trial Location and Treatment List

A total of four trials were conducted for four types of immature palm fields located in SD Guthrie Berhad's oil palm plantation in Johor, Malaysia, based on the following (*Table 2*).

Figure 1. ORYCTES unmanned aerial vehicle point-to-point (UAVPTP) sprayer.

TABLE 1. PARAMETER REQUIREMENTS FOR SPRAYING ACTIVITY FOR *Oryctes rhinoceros* BEETLE (ORB) CONTROL IN IMMATURE OIL PALM

Parameter requirements	Description
Targeted spray area	Spear, spear base, and the first spiral of fronds
Spray coverage	>80% at the spear base
Spray droplet density	>70 droplets/cm^2
Spray volume	Palm age between 1–2 yr: 100–200 mL/palm Palm age between 2–4 yr: 200–400 mL/palm
UAVPTP sprayer movement	Point-to-point spraying on top of the palm canopy
UAVPTP automation	To spray autonomously
Bio efficacy	ORB fresh damage incidences to reach below 5% after treatments

Note: UAVPTP - unmanned aerial vehicle point-to-point.

TABLE 2. TRIAL LIST AND TYPE OF FIELD

Trial	Field	Palm age at first round of treatment	Terrain
A	1st yr immature planting	6 months (1st yr)	Flat
B	1st yr immature planting	6 months (1st yr)	Terrace
C	2nd yr immature planting	18 months (2nd yr)	Flat
D	2nd yr immature planting	18 months (2nd yr)	Terrace

Note: yr - year.

All trials were conducted with the treatment list as shown in *Table 3*.

The FM ORYCT semi-mechanised sprayer was invented by a plantation estate in SD Guthrie Berhad in the Southern Region, Johor, Malaysia. FM ORYCT consists of a semi-mechanised tractor that was modified and installed with a fibreglass tank, water pump, telescopic lance and fitted with a hollow cone nozzle. GOIZPER Group company from Spain, produces the INTER knapsack sprayer, which is currently being sold in Malaysia. The INTER knapsack sprayer has a tank capacity of 16 L, and a long lance fitted with very low volume (VLV) hollow cone nozzles. The sprayer is capable of operating between 1.5–3.0 bar operating pressure. This is the common knapsack sprayer used in many plantations for ORB control (Goizper Group, 2023).

Spraying Methodology

The spraying methodology for the UAVPTP is based on the use of a Global Navigation Satellite System (GNSS) and Real-Time Kinematic (RTK) System that is elaborated as follows:

Global Navigation Satellite System (GNSS) and Real-Time Kinetic (RTK) System. GNSS is a satellite navigation system that uses small satellites to pinpoint the geographic location of a user's receiver on Earth. The GNSS use a constellation of satellites and is based on the concept of trilateration (determining a position by knowing your distance from three known points). The UAVPTP sprayer uses the RTK system, which is a GNSS technique that can improve the accuracy of GNSS positioning up to 1–2 cm level. RTK-enabled drones can track their geolocation accurately (*Figure 2*).

For the UAVPTP sprayer, a pre-treatment flight path was created via digital mapping of the field, and each palm was geotagged at the centre of the canopy to ensure precise point-to-point spraying at the spear and first spiral of the frond conducted. The UAVPTP sprayer was calibrated to provide a similar spray volume application rate per palm at 150 mL. This was implemented by determining the nozzle's flow rate and setting the timing to

TABLE 3. TREATMENT LIST

Trial	Treatment Spray coverage studies (palm)	Replicate	Number of palms per replicate (Experimental unit)	Treatment Fresh damage studies (palm)	Replicate	Minimum number of palms per replicate (Experimental unit)
A	T1: UAV Point-to-Point Sprayer – ORYCTES (UAVPTP) T2: FM ORYCT – Semi-mechanised sprayer T3: INTER knapsack sprayer	3	1	T1: UAV Point-to-Point Sprayer – ORYCTES (UAVPTP) T2: FM ORYCT – Semi-mechanised sprayer T3: INTER knapsack sprayer T4: Untreated control	3	73
B	T1: UAV Point-to-Point Sprayer – ORYCTES (UAVPTP) T2: FM ORYCT – Semi-mechanised sprayer T3: INTER knapsack sprayer	3	1	T1: UAV Point-to-Point Sprayer – ORYCTES (UAVPTP) T2: FM ORYCT – Semi-mechanised sprayer T3: INTER knapsack sprayer T4: Untreated control	3	61
C	T1: UAV Point-to-Point Sprayer – ORYCTES (UAVPTP) T2: FM ORYCT – Semi-mechanised sprayer T3: INTER knapsack sprayer	3	1	T1: UAV Point-to-Point Sprayer – ORYCTES (UAVPTP) T2: FM ORYCT – Semi-mechanised sprayer T3: INTER knapsack sprayer T4: Untreated control	3	130
D	T1: UAV Point-to-Point Sprayer – ORYCTES (UAVPTP) T2: FM ORYCT – Semi-mechanised sprayer T3: INTER knapsack sprayer	3	1	T1: UAV Point-to-Point Sprayer – ORYCTES (UAVPTP) T2: FM ORYCT – Semi-mechanised sprayer T3: INTER knapsack sprayer T4: Untreated control	3	58

Note: UAVPTP - unmanned aerial vehicle point-to-point.

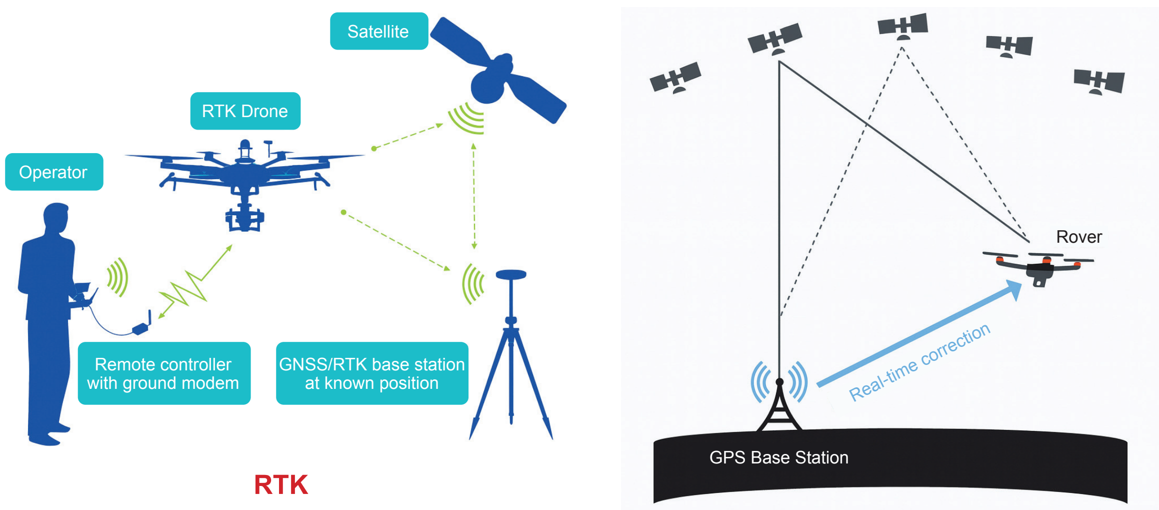

Source: Loosli (2020).

Figure 2. Global Navigation Satellite System (GNSS) and Real-Time Kinematic (RTK) system (trilateration concept).

spray per palm on each palm canopy. Spraying treatment was conducted using cypermethrin insecticide at a dosage of 0.1% a.i. with the spray volume of 150 mL, and the spraying time was set at 3 s/palm.

A base point was set at the highest point near the spraying area as a suitable location for the RTK base station. A Phantom 4 RTK drone was deployed to capture high-resolution aerial images with RTK-calibrated geospatial information. The aerial images were uploaded onto a software mapping platform that stitched the images into a cohesive map and generated a high-precision Digital Terrain Model (DTM). The software AI palm identification algorithm was used to pinpoint and tag individual palm crowns in the aerial map, and the GPS information of the detected palms was extracted for UAVPTP sprayer path planning. A path-planning algorithm was used to generate an optimal flight path for the UAVPTP sprayer that covers the plot within the shortest flight time. The generated flight path was visually reviewed in the software and then synced with the UAVPTP sprayer mobile app used to pilot the spraying drone.

During the spraying operation, the UAVPTP RTK base station was set up at the previously established base point, then the UAVPTP was turned on to establish a stable connection with the base station. The cypermethrin liquid insecticides were filled into UAVPTP at 14 L, and the pump system of the drone was checked to ensure smooth liquid flow through the nozzle. A pre-flight checklist (RTK signal strength, radar sensors, battery status, etc.) was run through to ensure the drone was ready for take-off. The pre-planned flight mission was reviewed for the final time on the UAVPTP mobile app, then the drone was launched in automatic mode to perform the pre-planned missions (*Figure 3*). During a drone flight, the pilot constantly monitored and ensured the drone flew along the correct paths and with a stable RTK connection. The UAVPTP mobile app captured all the data during the spraying for easy reporting (How & Ken, 2020). The temperature recorded was between 29°C–32°C with relative humidity between 65%–72%. The wind speed was recorded at 1–2 m/s, and the flight was set not to operate at 3 m/s and above.

For the INTER Knapsack Sprayer and FM ORYCT (*Figure 4*), the spraying treatment was conducted using cypermethrin insecticide at a dosage of 0.1% a.i. with the calibrated spray volume of 150 mL/palm. Calibration was conducted similarly to the UAVPTP via the determination of the average flow rate of the nozzles and setting the timing to spray per palm on each palm.

Spray Coverage and Spray Droplet Density Assessment

As displayed in *Table 3*, spray coverage studies related to all the machinery treatments (T1: UAV Point-to-Point Sprayer – ORYCTES (UAVPTP), T2: FM ORYCT – Semi-mechanised sprayer and T3: INTER knapsack sprayer) were conducted using water-sensitive paper (WSP) on three palms that represent three replicates (one palm per replicate) for the 1st, 2nd and 3rd rounds of spraying. The WSP was placed on the palm spears and at the base of the first spiral of the frond (6 points) (spear region). In addition, WSPs were placed on the 6 points at the lower, middle and upper fronds in the palm canopy surrounding the spears to study any drift of the spray droplets. As mentioned earlier, during the trial, the temperature recorded was between 29°C–32°C with relative humidity between 65%–72%. The wind speed was recorded at 1–2 m/s and flight was set not to operate at 3 m/s and above. The scoring of spray coverage was recorded based on the scale and weightage in *Table 4*. The droplet density for each WSP was analysed using the Syngenta Droplet Counting Aid to determine the number of droplets/cm^2.

Fresh Damage Assessment

Before the trial, the palms in all the fields were continuously treated with cypermethrin by the plantation estate every 14 days, and sprayings were

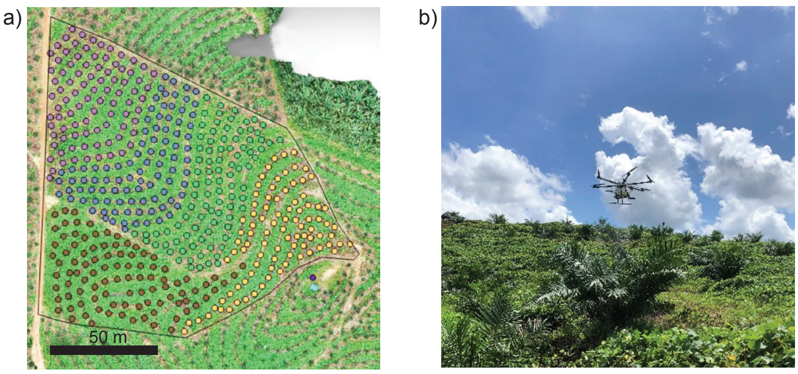

Figure 3. (a) Layout of mapping, flight path and geotagging of palms for the unmanned aerial vehicle point-to-point (UAVPTP) and (b) unmanned aerial vehicle point-to-point (UAVPTP) spraying on immature palms.

FM ORYCT semi-mechanised sprayer.

INTER knapsack sprayer.

Figure 4. FM ORYCT semi-mechanised sprayer and INTER knapsack sprayer.

TABLE 4. VISUAL SCORE RATING (VSR) OF WATER-SENSITIVE PAPER (WSP), SCORE WEIGHTAGE AND TOTAL SPRAY COVERAGE CALCULATION

Spray coverage description of each WSP	VSR (%)	Location of WSP	Score weightage for ORB control (%)	Calculation of spray coverage for each WSP point	Total spray coverage calculation
Full wetting	100	Spear Base 1 (SB1)	20	VSR x 20% = SCSB1	Total spray coverage = SCSB1+ SCSB2+ SCSB3+ SCSB4+ SCSM+ SCSE
Droplet covered 80%–99% of WSP	80–99	Spear Base 2 (SB2)	20	VSR x 20% = SCSB2	
Droplet covered 60%–79% of WSP	60–79	Spear Base 3 (SB3)	20	VSR x 20% = SCSB3	
Droplet covered 40%–59% of WSP	40–59	Spear Base 4 (SB4)	20	VSR x 20% = SCSB4	
Droplet covered 20%–39% of WSP	20–39	Spear Middle (SM)	10	VSR x 10 % = SCSM	
Droplet covered 1%–19% of WSP	1–19	Spear End (SE)	10	VSR x 10% = SCSE	
No droplet detected	0				

Note: ORB - *Oryctes rhinoceros* beetle.

stopped 21 days before the trial. Fresh damage of ORB assessment for all treatments in Trials A, B, C and D was conducted at pre-treatment and every seven days after each spraying treatment round (1st round until 6th round) to determine the spraying effectiveness. Fresh damage of ORB refers to spear snapping due to fresh chewing on the basal end, unopened spear dieback (easily pulled out), distinct chewing marks on the spear and spear cut-off and snapping of newly opened fronds. The assessment was conducted on all the palms in each replicate, and the percentage based on the number of damaged palms divided by the number of total palms in each replicate was reported as the data for fresh damage.

Experimental Design and Statistical Analysis

All the experiments were conducted in a randomized complete block design (RCBD) with three replications. All percentage data were subjected to analysis of variance (ANOVA) using the generalized linear model (GLM) to detect the differences between treatment effects, and means were compared using Tukey's HSD Test.

RESULTS AND DISCUSSION

Spray Coverage and Spray Droplet Density Assessment

Results from the spray coverage are tabulated in *Table 5*. In the first-year immature palms in flat terrain and the second-year immature palms in terrace terrain, the results showed that at the first to third round of treatment, INTER Knapsack and FM ORYCT showed significantly better spray coverage than the UAVPTP sprayer, this is understandable due to the ability of the workers to spray the whole spear shoot manually. Nevertheless, the results showed that the UAVPTP sprayer reached above 80% satisfactory spray coverage at the targeted area of the spear region for all the field terrains experimented with and for both first-year and second-year immature palms. Since the major targeted area is at the base of the spear region, the results proved that UAVPTP could reach the targeted area on the palms for all the fields, either flat or terraced.

As all the droplets at the spear region showed 100% wetting on the WSP due to the overlapping of spray droplets, the droplet density was declared as above 70 droplets/cm^2, which met the requirement set. All the treatments showed 100% wetting of the WSP, especially at the spear base region (*Figure 5*).

Fresh Damage Assessment

The fresh damage assessment results are tabulated in *Table 6*. The outcome of the trials showed that UAVPTP showed effective control of ORB in the one-year immature planting in a terrace field (Trial B in *Table 6*) compared to the untreated control, significantly after 1st round of treatment (A1STRT). These were observed significantly after the first, second, third and fifth rounds of treatment of UAVPTP against the untreated control plots in the 1st Year Immature Palms-Terrace Plot trial. However, during the trial, low pest pressure was observed in the one-year-old immature planting under flat terrain (Trial A) and two-year-old immature planting under both flat and terrace terrain (Trials A, C and D in *Table 6*) after the A1STRT. No significant differences in the level of control between the UAVPTP sprayer, FM ORYCT and the INTER knapsack sprayer for all the fields experimented after the 6th round of treatment. It was suspected that continuous cypermethrin treatment surrounding the untreated control plots had reduced the pest pressure in the fields.

Discussion

From the spray coverage, droplet density and bioefficacy results, UAVPTP showed good capability to replace the current spraying method of using the INTER knapsack sprayer as well as the FM ORYCT semi-mechanised sprayer for ORB control in immature palms. The geotagging and geopositioning via RTK-GNSS were accurate and aligned with the study conducted by Pérez-Ruiz et al. (2015), which reported that autonomous tractor systems showed good feasibility for extreme accuracy requirements.

TABLE 5. SPRAY COVERAGE (%) OF UNMANNED AERIAL VEHICLE POINT-TO-POINT (UAVPTP) SPRAYER VS. OTHER SPRAYERS

Palm age/ Terrain	Treatment	A1STRT		A2NDRT		A3RDRT	
1st yr immature palms/Flat (Trial A)	UAVPTP sprayer	85.00	c^z	81.67	b	85.00	b
	FM ORYCT semi-mech sprayer	90.00	b	93.33	a	93.33	a
	INTER knapsack sprayer	95.00	a	96.67	a	96.67	a
1st yr immature palms/Terrace (Trial B)	UAVPTP sprayer	83.33	c^z	83.33	a	83.33	a
	FM ORYCT semi-mech sprayer	90.00	b	88.33	a	88.33	a
	INTER knapsack sprayer	95.00	a	93.33	a	91.67	a
2nd yr immature palms/Flat (Trial C)	UAVPTP sprayer	86.67	a^z	83.33	b	83.33	a
	FM ORYCT semi-mech sprayer	93.33	a	91.67	ab	93.33	a
	INTER knapsack sprayer	95.00	a	95.00	a	93.33	a
2nd yr immature palms/Terrace (Trial D)	UAVPTP sprayer	81.67	b^z	83.33	b	83.33	b
	FM ORYCT semi-mech sprayer	91.67	a	93.33	a	93.33	a
	INTER knapsack sprayer	93.33	a	95.00	a	95.00	a

Note: A1STRT - At 1st round of treatment; A2NDRT - At 2nd round of treatment; A3RDRT - At 3rd round of treatment. ^{Z}Means within the same column followed by the same letter are not significantly different at *P* - 0.05 based on Tukey HSD for each of the trials. All data were transformed into arcsine for statistical analysis, and the original data were used for presentation.

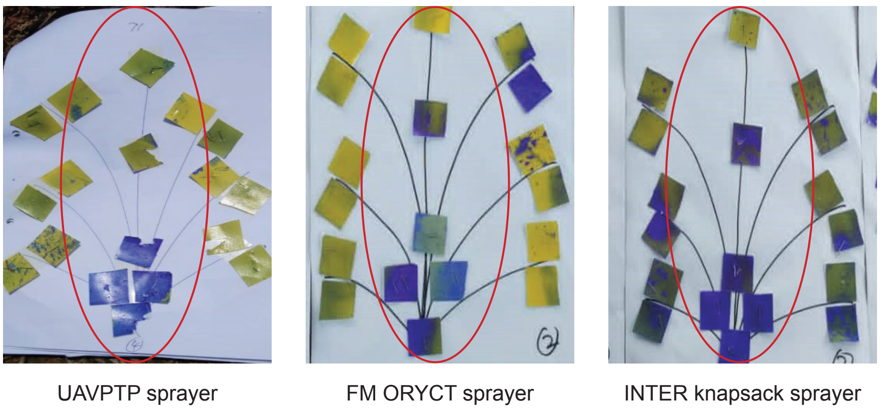

Figure 5. Spray coverage evaluation for all the sprayers.

TABLE 6. FRESH DAMAGE OF *Oryctes rhinoceros* BEETLE (ORB) ON IMMATURE PALMS AFTER TREATMENT OF CYPERMETHRIN

Palm age/Terrain	Treatment	Pre-treatment		A1STRT		A2NDRT		A3RDRT		A4THRT		A5THRT		A6THRT	
1st yr immature palms/ Flat (Trial A)	UAVPTP sprayer	0.00	a[z]	0.34	b	0.00	b	0.00	b	0.91	a	0.28	a	0.23	a
	FM ORYCT sprayer	0.00	a	0.65	a	0.31	a	0.39	a	0.97	a	0.26	a	0.26	a
	INTER knapsack sprayer	0.00	a	0.01	c	0.31	a	0.14	b	0.00	a	0.00	a	0.00	a
	Untreated control	0.00	a	0.46	ab	0.01	b	0.10	b	0.35	a	0.12	a	0.12	a
1st yr immature palms/ Terrace (Trial B)	UAVPTP sprayer	0.30	a[z]	**0.72**	**b**	0.00	c	0.41	b	0.52	a	0.00	b	0.00	a
	FM ORYCT sprayer	0.34	a	**0.12**	**b**	1.03	a	0.26	b	0.43	a	0.27	a	0.26	a
	INTER knapsack sprayer	0.00	a	**0.24**	**b**	0.34	bc	0.20	b	0.61	a	0.00	b	0.00	a
	Untreated control	0.35	a	**5.96**	**a**	0.65	b	0.95	a	0.95	a	0.32	a	0.32	a
2nd yr immature palms/ Flat (Trial C)	UAVPTP sprayer	0.35	a[z]	1.19	b	0.38	a	0.38	b	1.13	b	0.26	a	0.26	a
	FM ORYCT sprayer	0.34	a	0.96	b	0.37	a	5.99	a	6.18	a	0.19	a	0.19	a
	INTER knapsack sprayer	0.36	a	2.05	a	0.36	a	0.40	b	1.26	b	0.18	a	0.18	a
	Untreated control	0.26	a	1.20	b	0.26	a	1.82	b	0.09	b	0.26	a	0.28	a
2nd yr immature palms/ Terrace (Trial D)	UAVPTP sprayer	0.00	a[z]	1.92	ab	0.65	b	0.00	b	1.15	a	0.65	a	0.65	a
	FM ORYCT sprayer	0.00	a	1.12	b	1.15	b	2.43	a	1.50	a	0.19	a	0.19	a
	INTER knapsack sprayer	0.20	a	2.74	a	2.23	a	0.18	b	0.90	a	0.54	a	0.54	a
	Untreated control	0.13	a	1.44	b	1.57	ab	2.49	a	1.05	a	0.59	a	1.23	a

Note: A1STRT - 7 days after 1st round of treatment; A2NDRT - 7 days after 2nd round of treatment; A3RDRT - 7 days after 3rd round of treatment; A4THRT - 7 days after 4th round of treatment; A5THRT - 7 days after 5th round of treatment; A6THRT - 7 days after 6th round of treatment. [Z]Means within the same column followed by the same letter for each of the trials are not significantly different at *P* - 0.05 based on Tukey HSD. All data were transformed into arcsine for statistical analysis, and the original data were used for presentation.

The spray effectiveness of UAVPTP was satisfactory, even though some of the fields showed low pest pressure. The low pest pressure was observed in the untreated plots and was expected to occur due to the earlier continuous treatment of the plots before the trials. However, the UAVPTP showed the most significant control compared to the untreated control after the first round of treatment in the first-year immature palms with terrace terrain field (Trial B) and with no significant difference with FM ORYCT and INTER knapsack sprayer.

The spray coverage results were the most important finding in these studies, as UAVPTP spraying had reached the targeted spear base and the first spiral of fronds equally as the manual INTER knapsack sprayer and the mechanical FM ORYCT sprayer, as required and reported by Ho (2010). This has proven that UAVPTP could replace spraying using an INTER knapsack sprayer or the FM ORYCT mechanised sprayer. *Table 7* summarises the UAVPTP results that meet the parameter requirements set in *Table 1*.

The utilisation of UAVPTP demonstrated the capability to apply insecticides with precision, aligning with the principles of integrated pest management (IPM) to minimise insecticide usage (Barzman et al., 2015). The technology's efficiency, as corroborated by Krishna (2017), includes the ability to achieve accurate dosing and precise targeting of crop areas, thereby reducing insecticide drift and minimising losses. Furthermore, UAVPTP facilitates unmanned spraying over extensive areas, decreasing reliance on human labour for large-scale applications. This advancement offers potential cost reductions in workforce recruitment for plantation estates. These findings represent pioneering data that will serve as a reference for future unmanned application technologies in oil palm cultivation.

With the acute shortage of workers due to the restriction on importation of foreign workers caused by closed borders during the COVID-19 pandemic, the UAVPTP spraying method will be the best alternative to solve the ORB infestation issues in the plantation. However, additional requirements for obtaining a license to fly, meeting the safety requirements as well and higher costs will be the main obstacles to overcome in the use of the UAVPTP sprayer.

CONCLUSION

The UAVPTP sprayer achieved satisfactory spray coverage on the targeted area of the spear region in immature oil palm for the control of ORB. The UAVPTP showed effective control of ORB with no significant differences with the FM ORYCT semi-mechanised sprayer and INTER knapsack sprayer at the end of the trial, at first-year and second-year immature oil palm on both flat and terrace terrain fields. UAVPTP met all the requirements set for successful spraying activity in controlling ORB in immature palms.

ACKNOWLEDGEMENT

A special thank you to the Aonic Sdn. Bhd., team, SD Guthrie Berhad estates personnel, staff and workers of R&D Crop Protection, SD Guthrie Research Sdn. Bhd., who have contributed to the successful completion of the research project. The author would like to thank the management of SD Guthrie Research Sdn. Bhd., for the permission to publish this article. The authors declare no conflict of interest in conducting and completing the study.

TABLE 7. SUMMARY OF UAVPTP ACHIEVEMENT RESULTS ON THE PARAMETER REQUIREMENT FOR THE SPRAYING TREATMENT OF IMMATURE PALMS FOR THE CONTROL OF *Oryctes rhinoceros* BEETLE (ORB)

Parameters	Results	Conclusion
Targeted spray area	Spray droplets had reached the targeted spear, spear base and the first spiral of the frond region.	Meets the requirement
Spray coverage	Spray coverage: >80%.	Meets the requirement
Spray droplet density	The targeted area was fully wetted; therefore, it reached a droplet density above 70 droplets/cm^2.	Meets the requirement
Spray volume	Reached the targeted spray volume as follows: Palm age between 1–2 yr: Spray volume at 150 mL was sufficient to reach the targeted area (within 100–200 mL/palm target).	Meets the requirement
UAVPTP sprayer movement	Able to execute point-to-point spraying on top of the palm canopy.	Meets the requirement
UAVPTP automation	Able to spray autonomously.	Meets the requirement
Bio-efficacy (effectiveness of the pesticides in controlling the target pest)	Results – Equally effective with FM ORYCT semi-mechanised sprayer and INTER knapsack sprayer (reached below 5% after treatments).	Meets the requirement

Note: UAVPTP - unmanned aerial vehicle point-to-point.

REFERENCES

Aonic Sdn. Bhd. (2021). *ORYCTES Information Brochure*. Poladrone Solutions Sdn. Bhd.

Barzman, M., Bàrberi, P., Birch, A. N. E., Boonekamp, P., Dachbrodt-Saaydeh, S., Graf, B., Hommel, B., Jensen, J. E., Kiss, J., Kudsk, P., Lamichhane, J. R., Messéan, A., Moonen, A., Ratnadass, A., Ricci, P., Sarah, J., & Sattin, M. (2015). Eight principles of integrated pest management. *Agronomy for Sustainable Development, 35*, 1199–1215. https://doi.org/10.1007/s13593-015-0327-9

Chung, G. F., Sim, S. C., & Balasubramaniam, R. (1999). Effects of pest damage during the immature phase on the early yields of oil palm. In Y. Basiron, B. S. Jalani, & K. W. Chan (Eds.), *Proceedings of the PORIM International Palm Oil Congress: Emerging technologies and opportunities in the next millennium* (Vol. 1, pp. 454–476). Palm Oil Research Institute of Malaysia.

Desmier, D. C. R., & Kang, S. M. (2001). *Environmental-friendly approaches in the management of pests in young oil palm plantations* [Working paper]. Seminar on the Replanting of Oil Palm, Department of Agriculture, Sabah, Malaysia.

Goizper Group. (2023). *INTER sprayer website information*. https://www.intersprayer.com/en/evolution-164961.html

Hilz, E., & Vermeer, A.W. P. (2013). Spray drift review: The extent to which a formulation can contribute to spray drift reduction. *Crop Protection, 44*, 75–83. https://doi.org/10.1016/j.cropro.2012.10.020

Ho, C. T. (2010). *Pioneers and innovators of integrated pest management in oil palm*. Sime Darby Plantation Berhad.

How, Y. G., & Ken, K. (2020). *The accuracy of RTK spot spraying using Oryctes Dual and its application in oil palm plantations*. Poladrone Solutions Sdn. Bhd. https://www.poladrone.com

Kanwal, S., Khan, M. A., Saleem, S., Tahir, M. N., Muntaha, S. T., Samreen, T., Javed, S., Nazir, M., & Shahzad, B. (2022). Integration of precision agriculture techniques for pest management. *Environmental Sciences Proceedings, 23*(1), 19. https://doi.org/10.3390/environsciproc2022023019

Krishna, K. R. (2017). *Agricultural drones: A peaceful pursuit*. Apple Academic Press.

Liau, S. S., & Ahmad, A. (1991). The control of *Oryctes rhinoceros* by clean clearing and its effect on early yield in palm-to-palm replants. In *Proceedings of the 1991 PORIM International Palm Oil Development Conference: Module II – Agriculture* (pp. 396–406). Palm Oil Research Institute of Malaysia.

Liu, Z., & Li, J. (2023). Application of unmanned aerial vehicles in precision agriculture. *Agriculture, 13*(7), 1375. https://doi.org/10.3390/agriculture13071375

Loosli, E. (2020). *What's the difference between PPK and RTK drones, and which one is better?* Wingtra. https://wingtra.com/ppk-drones-vs-rtk-drones/

Lou, Z., Xin, F., Han, X., Lan, Y., Duan, T., & Fu, W. (2018). Effect of unmanned aerial vehicle flight height on droplet distribution, drift and control of cotton aphids and spider mites. *Agronomy*, *8*(9), 187. https://doi.org/10.3390/agronomy8090187

Macbean, C. (2012). Cypermethrin. In *The pesticide manual: A world compendium* (16th ed., pp. 274–275). British Crop Production Council.

Mulla, D. J. (2013). Twenty five years of remote sensing in precision agriculture: Key advances and remaining knowledge gaps. *Biosystems Engineering, 114*(4), 358–371. https://doi.org/10.1016/j.biosystemseng.2012.08.009

Pérez-Ruiz, M., Gonzalez-De-Santos, P., Ribeiro, A., Fernandez-Quintanilla, C., Peruzzi, A., Vieri, M., Tomic, S., & Agüera, J. (2015). Highlights and preliminary results for autonomous crop protection. *Computers and Electronics in Agriculture, 110*, 150–161. https://doi.org/10.1016/j.compag.2014.11.010

Samsudin, A., Chew, P. S., & Mohd, M. M. (1993). *Oryctes rhinoceros*: Breeding and damage on oil palm in an oil palm to oil palm replanting situation. *Planter, 69*(813), 583–591.

Journal of Oil Palm Research Vol. 38 (3) September 2026 p. 519–532
DOI: https://doi.org/10.21894/jopr.2025.0042

SSR MARKERS FACILITATE TESTING OF GENETIC PURITY AND PREDICTION OF BIOLOGICAL PARENTS FOR BREEDING CROSSES OF OIL PALM

NORHALIDA MOHAMED SERDARI[1,3]*; TING NGOOT-CHIN[1]; RAJINDER SINGH[1]; KANDHA SRITHARAN[2]; MARYAM MOHAMED REHAN[3]; JALANI BIN SUKAIMI[3] and MAIZURA ITHNIN[1]

ABSTRACT

The genetic purity of a controlled cross is essential for achieving the objectives of a breeding program for any crop. This study evaluated SSR markers for assessing the legitimacy of two oil palm interspecific BC_1 x BC_1 populations, namely, Populations 9 and 10. A total of 40 primer-pairs were screened, resulting in the identification of 19 and 20 informative markers for Populations 9 and 10, respectively. The markers revealed sufficient genetic variation in allele frequency, heterozygosity and polymorphic information content in both populations. The phylogenetic trees revealed three and 32 outliers in Populations 9 and 10, respectively. In addition, the palms originally recorded as parents to the crosses had numerous loci that were mismatched with the non-outlier offspring. We reconstructed the expected genotypes of the real parents based on the segregation profiles observed among the legitimate offspring in the two families, resulting in 100% parent-offspring assignment. This study discusses how the SSR genotypes of palms were examined to detect outliers and to predict the genotypes of the true parents in these interspecific hybrids, the first such report for oil palm. The information will be useful for various controlled crosses of oil palm interspecific hybrids and other outcrossing plant species.

Keywords: BC_1 x BC_1, genetic purity, interspecific hybrid, parental genotypes reconstruction.

Received: 17 October 2024; **Accepted:** 26 May 2025; **Published online:** 19 August 2025.

INTRODUCTION

The genus *Elaeis* (Arecaceae) consists of *E. guineensis*, which originated from Central and West Africa, and *E. oleifera* from Latin America. Both species produce versatile oil that has significant economic importance (Corley & Tinker, 2015; Rajanaidu et al., 2017). The two palm species exhibit contrasting growth characteristics where, *E. guineensis* grows 45–75 cm/yr (Barcelos et al., 2015) with an upright vascular stem that can reach over 12 m after 25 years, whereas *E. oleifera* is naturally shorter, as its trunk grows around 5–10 cm/yr (Corley & Tinker, 2015; Rajanaidu et al., 2017; Rivera et al., 2013). Their fruit morphology and oil composition are also very different. *E. guineensis* produces large fruitlets with thick mesocarp, coated with deep-violet/black colored skin when young and turns red when ripe. In contrast, *E. oleifera* produces much smaller fruitlets with a thinner layer of mesocarp, and the yellowish-green skin changes to ivory/orange when the fruits are ripe (Corley & Tinker, 2015). The distinctive change in color upon ripening is somewhat similar to virescens fruits observed in *E. guineensis* (Singh et al., 2014). The thick fleshy mesocarp is rich in oil, making *E. guineensis* the oil palm of commerce. *E. oleifera* is well-known for its natural high unsaturated oil, with the composition of oleic and linoleic acids comparable to that of olive and canola oils (Corley & Tinker, 2015; Mendoza et al., 2023).

[1] Malaysian Palm Oil Board,
6, Persiaran Institusi, Bandar Baru Bangi,
43000 Kajang, Selangor, Malaysia.

[2] United Plantation Berhad, Jendarata Estate,
36009 Teluk Intan, Perak, Malaysia.

[3] Universiti Sains Islam Malaysia, Bandar Baru Nilai,
71800 Nilai, Negeri Sembilan, Malaysia.

* *Corresponding author e-mail: norhalida@mpob.gov.my*

The two species of oil palm can crossbreed and generate fertile interspecific hybrids, which are tolerant to bud rot disease (also known as lethal decay), have a slower increment of height (Hormaza et al., 2012; Madon et al., 2018; Meléndez & Ponce, 2016) and produce oil with higher levels of unsaturated fatty acids than *E. guineensis* (Lieb et al., 2017; Mozzon et al., 2020). However, pollen viability, fruit sets and seed germination rates of the hybrids are relatively lower (Daza et al., 2020; Escobar & Chauza, 2018; Hardon & Tan, 1969; Hormaza et al., 2012; Mosquera et al., 2021; Romero et al., 2021; Socha et al., 2019). These could be due to incomplete chromosome-pairing and an increasing number of univalent chromosomes (Hardon & Tan, 1969; Sunilkumar et al., 2013). One way to overcome the constraints is to backcross the interspecific hybrids with a carefully selected *E. guineensis,* aiming to generate more viable and good-yielding backcross palms and yet possessing the desired traits of *E. oleifera* (Noh et al., 2012). The backcross-breeding strategy has also been successfully adopted in rice, where several disease resistance traits were introgressed from the wild species into the cultivated varieties (Collard & Mackill, 2008; Kannan et al., 2017; Sharma et al., 2012) as well as, for the improvement of grain quality, amylose content, aroma and seed weight traits (Bao, 2014; Cho et al., 2020; Miura et al., 2022). In *Elaeis*, repeating backcross to the recurrent parent (*E. guineensis*), aiming to eliminate undesirable traits of *E. oleifera*, could cumulatively reduce the genetic variability in subsequent generations. Nonetheless, genetic variability can be slightly increased by backcrossing to a different elite *E. guineensis*. Alternatively, intercrossing BC_1 individuals can help increase the genetic viability while stabilising the genetic background. This breeding strategy may also help combine desirable traits, particularly quantitative traits. Therefore, BC_1 x BC_1 crosses were initiated in this study with the long-term objectives of evaluating the levels of genetic heterozygosity in these crosses and the efficiency of trait introgression, particularly in comparison to the conventional interspecific backcross breeding programs of oil palm.

In oil palm breeding, potential parental palms are continuously evaluated through well-designed controlled crossing schemes and field experimental plots. The primary steps of this important activity include isolating pollen from selected male parents, bagging flowers on selected female palms and introducing the desired pollen onto the bagged flowers. Production of a low number male inflorescences coupled with the small quantity and poor viability of the pollen has been proven a major challenge in utilising interspecific hybrids as the pollen donor (Daza et al., 2020; Meléndez-Jácome et al., 2024; Meléndez & Ponce, 2016; Mosquera et al., 2021), making the interspecific breeding program a time-consuming process. The procedures involved in the breeding steps must be strictly complied with, to make sure that the offspring produced are free from illegitimates. In addition, great care is also undertaken during seed processing and germination, nursery development and field planting to prevent mix-up, which can significantly affect the quality and integrity of a breeding program (Budiman et al., 2019; Josia et al., 2021).

In recent years, DNA markers have been applied for genetic fingerprinting and identification of outliers and illegitimates in the controlled crosses involving pure *E. guineensis* (Corley, 2005; Okoye et al., 2020; Pomiès et al., 2019; Teh et al., 2019; Zolkafli et al., 2021). However, the use of DNA markers for accessing the genetic purity and parentage analysis in interspecific crosses has not been commonly reported. In other crops e.g., sunflower, maize, wild rye, cabbage and coconut, simple sequence repeat (SSR) panels ranging from 10 to 100 markers have been commonly used to screen for genetic purity in breeding trials and identification of true parental lines (Daniel et al., 2012; Liu et al., 2007; Pallavi et al., 2011; Rajesh et al., 2012; Saiful-Lazim et al., 2024; Shinde et al., 2021; Sudha et al., 2022; Wang et al., 2002). SSR markers have been applied in small-scale legitimacy assessment in oil palm due to their abundance in the genome, high reproducibility and polymorphism owing to their multi-allelic nature (Rosli et al., 2022; Singh et al., 2007). Furthermore, the genotype datasets are also useful for genetic diversity and lineage assessments, particularly, for the valuable materials owned by an organisation (Ahmad et al., 2018; Saiful-Lazim et al., 2024; Sudha et al., 2022). By leveraging DNA markers, the overall efficiency and precision of a breeding program can be enhanced, which, ultimately, can lead to the precise development of improved planting materials.

This study evaluates the efficiency of SSR markers in assessing the genetic purity in two interspecific BC_1 x BC_1 crosses as the prerequisite to ensure the integrity of the established breeding populations. The two-level check was performed, first to identify outliers among the offspring and subsequently, to validate their biological parents. Using the multi-allelic SSR markers, we demonstrated that it is also possible to reconstruct the genotypes of the biological parents of a family.

MATERIALS AND METHODS

Palm Samples

Two interspecific backcrosses of one intercrossing (BC_1 x BC_1) populations, namely, Population 9 (trial 6.6–9.0) and 10 (trial 6.6–10.0), were included in the present study. Population 9 (332/5.2–5.0 x 19/5.2–6.0) and 10 (438/5.2–5.0 x 19/5.2–6.0) consisting of 95 and 110 progeny palms, respectively (*Figure 1*), were created by crossing two sibs of the same family to a common paternal palm (19/5.2–6.0).

DNA Extraction

Young leaves were collected and preserved in the –80°C freezer while waiting for DNA extraction. The extraction of DNA was carried out using the modified CTAB method (Suzana et al., 2015). The quality of extracted DNA was checked by restriction enzymes (*Hae*III and *Eco*RI) digestion and gel electrophoresis (1.0% agarose). This was followed by measuring the optical density (OD) of DNA using the Multiskan Go spectrophotometer (Thermoscientific, USA) to determine their purity (A_{260}/A_{280} and A_{260}/A_{230}) and concentration (ng/µL). Good quality DNA samples with purity ≥1.8 were diluted to the 50 ng/µL working stocks for SSR analysis.

SSR Markers Screening and Genotyping

Screening was first carried out using 40 SSR primer-pairs (*Table 1*) in a subset of 28 samples (including the parents) to identify informative SSR markers. Subsequently, all samples in both populations were genotyped using the polymorphic SSR markers pre-selected from the screening experiment. The standard polymerase chain reaction (PCR) conditions as recommended by the manufacturer (Meridian Bioscience, USA), were applied in both screening and genotyping procedures. The PCR reaction for each sample contained 2.0 µL DNA (50 ng/µL), 0.03 µL M13-forward primer, 0.03 µL M13-flourescent dye, 0.03 µL reverse primer, 5.0 µL 2X myTaq™ master mix (Meridian Bioscience, USA) and 2.9 µL dH_2O. The Fluorescent Dye Set consisting of ROX, 6-FAM, VIC and NED was used for multiplexing and differentiating the SSR amplicons during fragment analysis (Applied Biosystems, USA). Sizing and calling the SSR alleles were carried out using GeneMapper™ v4.1 (Applied Biosystems, USA). Alleles observed were coded according to the bi-parental segregation configurations (Billotte et al., 2005; Ting et al., 2014).

SSR Data Analysis

The Neighbor-joining phylogenetic trees were constructed using DARwin 6.0 (Perrier & Jacquemoud-Collet, 2006). Allele frequency, simulation and parentage analyses were carried out using CERVUS 3.0.7 (Kalinowski et al., 2007, 2010; Marshall et al., 1998). For parentage assignments, the logarithm of the odds (LOD) at a 95.0% confidence level was determined through simulations performed on 100,000 samples, 1.0% typing error and 90.0% sampling proportion, executed separately for Populations 9 and 10. The first round of the parentage analysis was carried out to validate whether the candidate parents provided were the true parents. For comparison, a set of predicted genotype calls was also configured for each of the parents based on the genotypes observed among the legitimate progeny palms. The predicted parental genotypes were then included in the second round of parentage analysis (with parent sexes unknown).

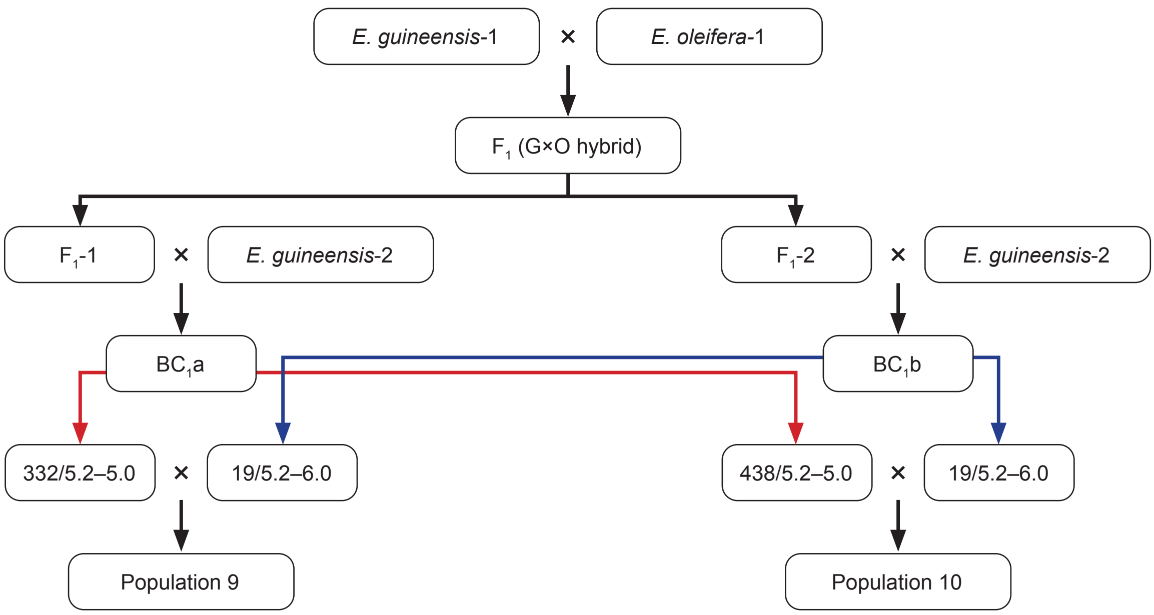

Figure 1. Pedigree of the interspecific BC_1 x BC_1 populations in this study.

TABLE 1. LIST OF 40 SSR PRIMER-PAIRS FOR SCREENING POPULATIONS 9 AND 10

No.	SSR marker	Forward sequence	TM (°C)	Reverse sequence	TM (°C)	TA (°C)	Expected fragment size (bp)	Observed fragment size (bp)	Reference
1	sEg00011*	GGAACCACGTTGGAGACTGT	60	TCCGACAAACTAGCAAAGCA	60	57	135	146–159	Low et al. (2008); Yaakub et al. (2020)
2	sEg00117*	GAGTGGTAGTGGCTATGGTCT	56	CCGTTGTATCTGTTCTCGTAGT	56	53	150	166–173	Low et al. (2008); Yaakub et al. (2020)
3	sMo00166*	CATAACATGCATTCACGGCT	60	AAGGGGCGGAAGGATTACTA	60	57	151	167–198	Yaakub et al. (2020); Ting et al. (2014)
4	Hght7_oSSR*	ATCCAACTTCCAACCAACCA	60	acgTGGGGATGTAGTTCCAA	60	58	203	176–204	Yaakub et al. (2020)
5	sMg00175*	TTTGTCTCCGTTTCCTTCTCT	58	CCCTAATCTCCTTCATCTCCTC	58	54	173	177–187	Ting et al. (2013); Yaakub et al. (2020)
6	sMo00132	ATAGCCAGAGGGCAAAACTGT	60	GCAACACACGGACTCAAAACTA	60	58	161	180–198	Yaakub et al. (2020); Zaki et al. (2010)
7	sEg00167*	AAAGAAAACACAACCACTGCC	59	AGGCTTATCGGAGATGGGAT	60	57	171	188–201	Low et al. (2008); Yaakub et al. (2020)
8	sMo00138*	AGGGTTGTCGCTCCAATTTAT	60	GGCATCTTTTTGACCTGTAGAAG	59	56	190	194–210	Yaakub et al. (2020); Zaki et al. (2010)
9	sEg00213*	TCCCCCAATACTCATCATGC	60	TGATCGACGGTTGTCACATT	60	57	178	200–209	Yaakub et al. (2020)
10	sMo00055*	GGCATTTCAGATAACGACAAA	58	GCACCCAAGTCTCTCTACCTC	58	54	202	205–216	Yaakub et al. (2020)
11	sMg00196*	CACAAACCAGGATAGCACACT	58	GTTGCTGGAGGTAGGGAAATA	58	56	200	208–230	Yaakub et al. (2020)
12	sEg00017	ATGGGTTGCTAATCTGTGGG	60	CATAAGAAGCAGAACCGTTGC	60	57	107	217–138	Low et al. (2008); Yaakub et al. (2020)
13	sPSc00488*	TTTCCTCGGAATGCTATTGG	60	TCCTCTCCCCAAAGGAAAAT	60	57	215	229–249	-
14	sEg00126*	CCGTCTCAAAAGCCCTAAAC	59	TTGTTGTCCCACTCCCTCTT	60	52	216	231–234	Yaakub et al. (2020); Ting et al. (2010)
15	sMo00027	TTACAGTTGAGGCAGTATGTCAAT	58	CTGTATGTCAAACCTTCTGCAC	57	50	209	235–252	Ting et al. (2013); Yaakub et al. (2020); Zaki et al. (2010)
16	sMg00051*	CCCTCCCTCTCCTTTTTATC	57	CCCTTCTCTCTCTCGTGTTAT	55	52	231	235–252	Ting et al. (2013); Yaakub et al. (2020)
17	sMg00011*	GTCCAAACCCTAACCCTAAC	55	GTCCTCGTAGTCCTCCTCTT	55	52	232	240–254	Yaakub et al. (2020)
18	sMo00246*	TGATGATGGAAAAGCTGCTG	56	TCCACCACAAATCAGGTCAG	60	53	220	241–249	Yaakub et al. (2020)
19	sMo00126*	AAGAGCAAGGGGAGAACTGACT	61	GTAAACACGCACACGGACAC	60	58	232	242–255	Yaakub et al. (2020)
20	sMg00235*	ATGGGAAGAGTACCAGTGCTT	58	CACCCTTTGCTTCAATTCAG	58	58	235	245–273	Ting et al. (2013); Yaakub et al. (2020)
21	sMg00168*	CGGGTAGGAACAAAAGAACC	59	GACGAGCAAGAGTCCAGAGAG	59	55	232	246–259	Ting et al. (2013); Zolkafli et al. (2021)

TABLE 1. LIST OF 40 SSR PRIMER-PAIRS FOR SCREENING POPULATIONS 9 AND 10 (continued)

No.	SSR marker	Forward sequence	TM (°C)	Reverse sequence	TM (°C)	TA (°C)	Expected fragment size (bp)	Observed fragment size (bp)	Reference
22	sMo00066	GTACAAGATGGAAAGGGAAAAA	57	TCAAGGGTCAGTTCATAAATCA	57	55	247	246–265	Yaakub et al. (2020)
23	sMo00222*	TCCACCCTTTGCTTCAATTC	60	AGAGTGGGGATGGGAAGAGT	60	57	236	255–285	Ting et al. (2013); Yaakub et al. (2020)
24	sEg00154*	TCCCCCAATACTCATCATGC	61	TGATCGACGGTTGTCACATT	60	57	238	257–268	Ting et al. (2013); Yaakub et al. (2020); Zolkafli et al. (2021)
25	sPSc00546*	GTCTAAATCCTATTCGATGGTGTT	58	CACAGCGTGGTTTCTCTGTT	59	56	241	258–264	Yaakub et al. (2020)
26	sMg00071*	CCAAATGTAAAAGGGGAAAATAA	58	GACGAGGAGAACGAAGGTAGA	59	54	272	270–284	Ting et al. (2013); Yaakub et al. (2020); Zolkafli et al. (2021)
27	sEg00019*	AGTGAAGCCCTTTCCCAAAT	60	CAGGCACCTGTAAGGGAAAA	60	57	261	271–281	Low et al. (2008); Yaakub et al. (2020)
28	sEg00146	TGTAGCAGCTGCAGAAGAGC	60	TCCTTTTTCTTGCTTTGCGT	60	57	210	245	Low et al. (2008); Yaakub et al. (2020)
29	sMg00030	AGCAAGGAATTTGAACTCTA	52	GATACCTCCCTTCTTGATGC	56	52	272	290	-
30	sMo00208	GCATGGCCAGTTTTCCTAGA	60	TAGCCCATATAGCACCCTGC	60	58	257	285	Ting et al. (2013); Yaakub et al. (2020)
31	sMg00093	CAATAACCTGAAACCCCTCTAATC	59	ATCTCCATCACCCTCTTCTTCTC	60	57	241	Not amplified	Yaakub et al. (2020)
32	sMg00066	TCTTGTTTCCGTTACTTGATGTT	58	AAGTTCTCGGCCTTCAAAAG	59	52	200	Not amplified	Ting et al. (2014); Yaakub et al. (2020)
33	sMo00023	TGACCCAATGATACCACCAC	59	GAGAACACAAACAGATGCACAC	58	53	243	Not amplified	Ting et al. (2013); Yaakub et al. (2020)
34	sPSc00481	TTTTCTGGATAAGTTGCTAAGATTT	57	CAACTCTCTTCCCTCCTCCTG	60	55	222	Not amplified	-
35	sMo00088	AGATACTGAGGGAAAGGTTAGG	56	TTCAAGACGAAACTGGTAAAA	55	54	204	Non-specific	Yaakub et al. (2020)
36	sMg00152	ATCGGACCAGCGCATATCTAA	62	CCTTGGGATTCTTATGGAACTTG	61	54	243	Non-specific	Ting et al. (2013); Yaakub et al. (2020)
37	sPSc00550	TAGATTCTTTCCGTGCGCTT	60	AAGAAGCTAAAAGGGCCCAC	60	57	185	Non-specific	-
38	sEg00072	TCTCTATGCAGCAGCCAAAT	59	ATAGACAACAGGCTTTTCATCA	57	54	136	Non-specific	Low et al. (2008); Yaakub et al. (2020)
39	sMg00016	GCGATTCCGGTTATCTTTAG	57	GAGTTTTTGCTGTGATGATTAG	54	52	274	Non-specific	Ting et al. (2014); Yaakub et al. (2020)
40	sMg00063	CACGAAAACGATAATAAAGTACA	54	ATGTGCCAGAACTTTTGTCTAT	56	52	209	Non-specific	Ting et al. (2014); Yaakub et al. (2020)

Note: *Informative marker; TM - melting temperature; TA - annealing temperature.

RESULTS AND DISCUSSION

Informative SSR Markers

Of the 40 SSR markers screened, a total of 19 and 20 polymorphic markers were identified following the analysis of selected palms from Populations 9 and 10, respectively. The remaining markers were either monomorphic, not amplifiable, or amplified with unspecific and ambiguous bands. The shortlisted informative SSR markers were then used to genotype all palms of the two populations, and the observed allelic information is summarised in *Figure 2*. For Population 9, the number of alleles (k) identified by the SSR markers ranged from two to six, where two alleles were observed in 31.6% of the markers, three to four segregating alleles were observed in 52.6% of the markers whereas the remaining 15.8% of the markers revealed five to six segregating alleles. For Population 10, 25.0% of the markers showed two alleles, 50.0% detected three to four segregating alleles and 25.0% showed five to six segregating alleles.

When the SSR markers were ranked from low to high in terms of the number of alleles (*Figure 2*), a clear pattern was also observed, where increased levels of observed heterozygosity (H_{Obs}), expected heterozygosity (H_{Exp}) and polymorphic information content (PIC) were detected. This trend was consistent for both populations where markers with a lower number of alleles (e.g., two and three) had on average lower H_{Obs} (0.41 and 0.48 for Population 9 and 0.33 and 0.46 for Population 10) and PIC (0.34 and 0.38 for Population 9 and 0.51 and 0.72 for Population 10) than markers with four to six segregating alleles. In this set of markers, the average of H_{Obs} and PIC ranged from 0.70 to 0.99 and 0.51 to 0.72 (for Population 9) and 0.67 to 0.73 and 0.52 to 0.60 (for Population 10). The present marker panel also included four to five markers that deviated from the Hardy-Weinberg equilibrium (HWE), and this is not uncommon for such a small population as Population 9 and 10. In general, the results indicated that the selected SSR markers are useful for assessing the genetic variation in the two interspecific backcross populations analysed.

Progeny Outliers

The neighbor-joining phylogenetic trees revealed three and 32 outliers among the offspring in Population 9 and 10, respectively (*Figure 3*). These outliers formed a separate sub-cluster in Population 9, whereas in Population 10, the outliers formed two sub-clusters. The two sub-clusters in Population 10 are likely to be closely related, possibly with one common parent. Further examination of their genotypes confirmed that the outliers in both populations were indeed illegitimates. For the three outliers in Population 9, different genotypes were observed in 14 SSR markers. For instance, in sMg00196, the outliers were called *dd* and *ae*, whereas, genotypes for other progeny palms were either *ab* or *bb*. In marker sMg00051, genotypes *cc* and *bd* were only observed in the three outliers, but the likely legitimate sibs had genotype calls *ab*, *ac*, *bb* and *bc*.

For Population 10, distinct genotypes in the outliers were also observed in 14 SSR markers, including the markers described in the two examples above. The two markers (sMg00196 and sMg00051) revealed a mixture of *aa*, *ab*, *ac* and *bc* genotypes in most of the progenies in Population 10. However, for the 32 outliers, distinct genotypes such as *ad*, *af*, *bb*, *cc*, *cf* and *de* were observed. As a result, the outliers were removed from further analysis and the number of justifiable legitimate offspring for Populations 9 and 10 was 92 and 78, respectively (*Figure 3b*).

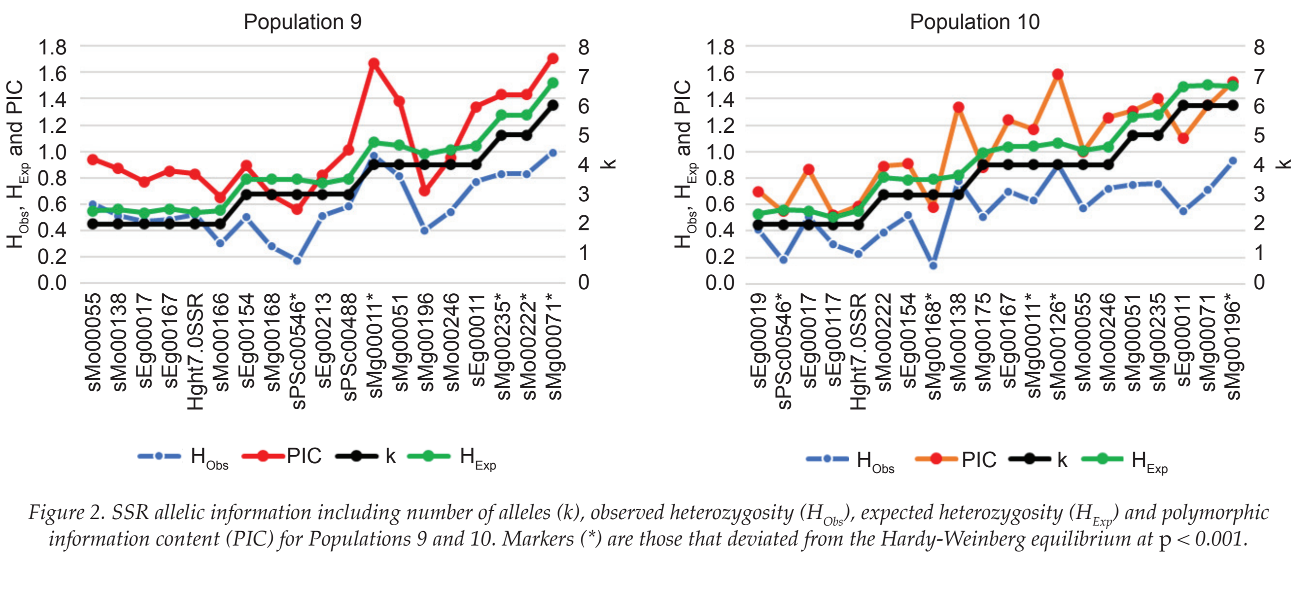

Figure 2. SSR allelic information including number of alleles (k), observed heterozygosity (H_{Obs}), expected heterozygosity (H_{Exp}) and polymorphic information content (PIC) for Populations 9 and 10. Markers (*) are those that deviated from the Hardy-Weinberg equilibrium at p *< 0.001.*

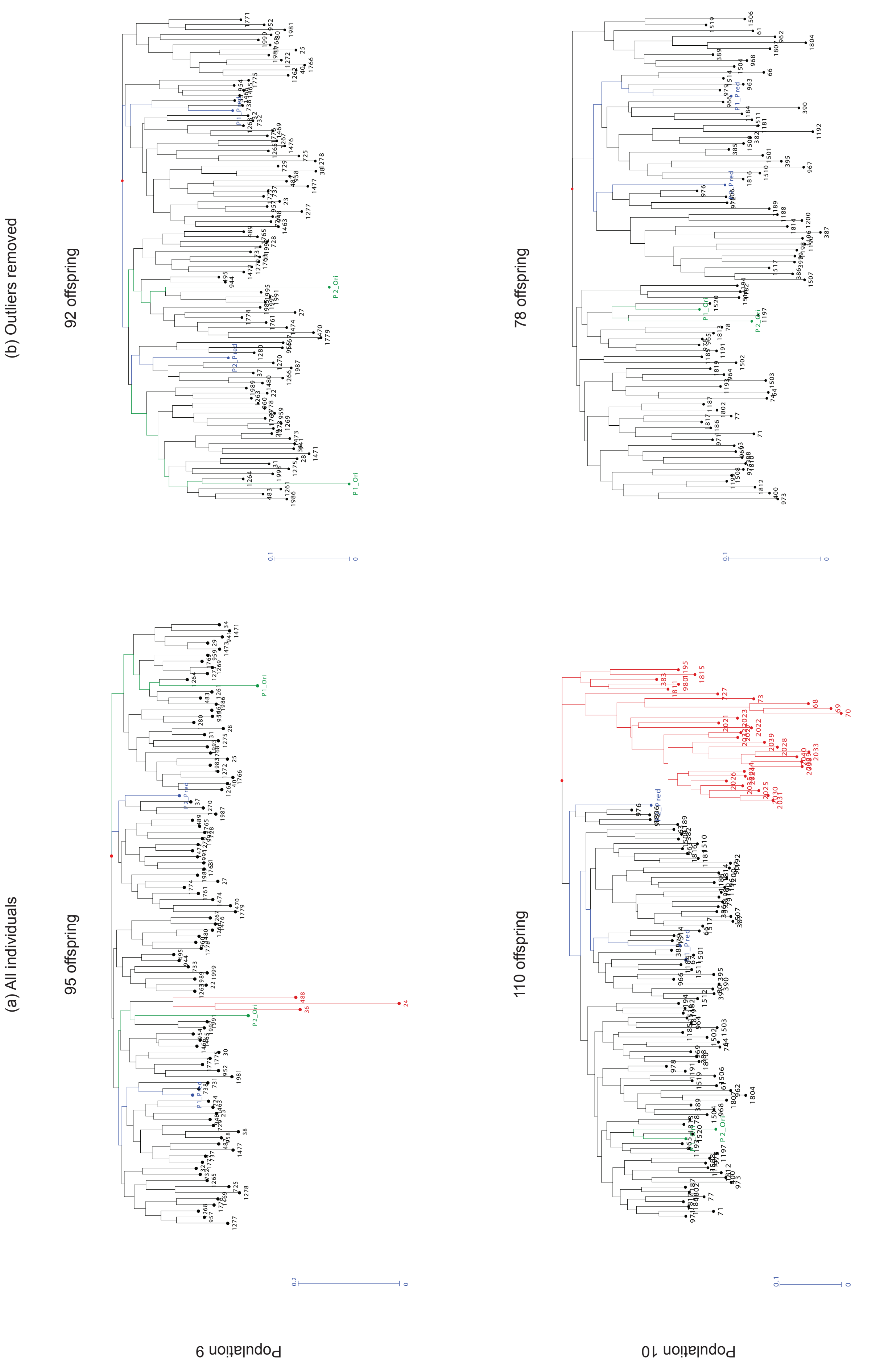

Figure 3. The neighbor-joining phylogenetic trees for Populations 9 and 10 show the original candidate parents in green (P1_ and P2_ori), the predicted parents in blue (P1_ and P2_pred), outliers in red and the legitimate offspring in black.

Missassignment of Parents for the Selected Crosses

The parentage analysis was first performed by including palms 332/5.2–5.0 and 19/5.2–6.0 (for Population 9) and 438/5.2–5.0 and 19/5.2–6.0 (for Population 10) as the parental candidates, based on earlier records. This analysis was conducted for the legitimate offspring after the removal of outliers. Unfortunately, no significant assignment was obtained, indicating that the candidate parents are not the true parents (*Figure 4*).

To verify this further, we re-examined the genotype calls of selected SSR markers. Markers sEg00117 and sEg00019 revealed heterozygous genotypes (of two and three alleles) in the two parental palms of Population 9, showing monomorphic genotypes (of single allele) among the offspring. Following the Mendelian inheritance, crossing of the two heterozygous alleles, e.g., *ab* x *ab* in the parents, was expected to recombine and produce the *aa*, *ab* and *bb* offspring. Similarly, crossing two parents with *ab* and *ac* heterozygous alleles (revealed by sEg00019) was expected to give rise to a mixture of *aa*, *ab*, *ac* and *bc* genotypes in their next generation instead of the monomorphic *cc* genotype that was observed throughout the offspring.

Unexpected genotypes in the parents of Population 9 were also observed for another six SSR markers (*Table 2*) (sEg00213, sMo00222, sMo00166, Hght7_oSSR, sMg00235 and sMo00132) where the maternal and paternal palms were genotyped as *aa* and *bb*, respectively. However, the progeny palms had *ac*, *cc*, *bb* and *bc* instead of the expected *ab* genotype. Among the six markers, sEg00213 revealed a similar scenario in Population 10, where the respective female and male parents were *aa* and *bb*, but the offspring exhibited up to four different genotypes.

Furthermore, the sMo00222, sMo00166 and Hght7_oSSR genotype data showed that both parental palms of Population 10 were homozygous (*aa*); however, their offspring were unexpectedly heterozygous, consisting of *ab*, *ac*, *bb* and *bc* genotypes (*Table 3*). In another example observed for Population 10, the parental genotypes for markers sMg00011, sMg00051, sMo00055, sMg00071, sEg00154 and sMg00235 were *ab*, which was expected to segregate and form three genotypes (*aa*, *ab* and *bb*) in their offspring. Instead, two to five different genotypes were observed among the progeny palms. These observations indicate that the candidate parents sampled for Population 9 and 10 may not be the true parents. Mislabeling or mix-up could have occurred, and these have been described as the potential causes of illegitimacy among oil palm progenies (Budiman et al., 2019; Corley, 2005; Hama-Ali et al., 2014; Thongtawee et al., 2010; Zolkafli et al., 2021).

Prediction of the Genotypes of the Biological Parents

To predict the genotypes of the actual biological parents, only genotype calls among legitimates were analysed while outliers were excluded. As an example, when genotypes *ac*, *bc*, *ad* and *bd* were observed in the offspring, the expected parental genotypes would be *ab* and *cd*. The predicted parental genotypes for all the informative markers (*Table 4*) were included as the new candidate parents for parentage analysis, resulting in 100% of the progeny palms in Population 9 and 10 being successfully assigned to the predicted parent-pairs at the 95% confidence threshold (*Table 5*).

Although the sexes for the two predicted parents were not known, parent pairs comparison (offspring-first parent and offspring-second parent) showed a perfect match across all the loci analysed. Similarly, for the trio comparison, the trio logarithm of the odds (LOD) scores ranging from 0.05 to 0.48 were observed in 98.0% offspring of Population 9, and LOD scores of 0.06 to 5.90 in 80.8% offspring of Population 10.

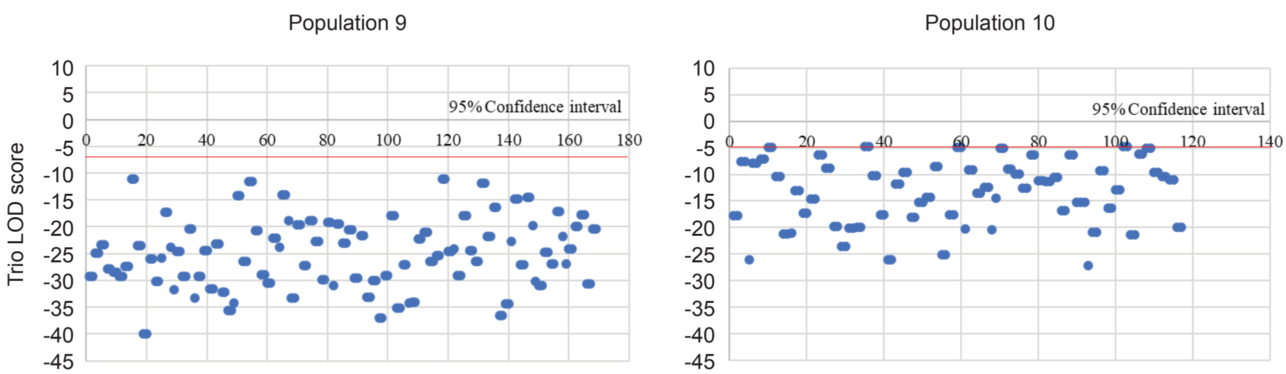

Figure 4. Distribution of trio logarithm of the odds (LOD) scores observed for Populations 9 and 10. No offspring were assigned to the sampled candidate parents.

TABLE 2. SUMMARY OF UNEXPECTED GENOTYPES OBSERVED IN POPULATION 9

SSR marker	Parental genotype		92 offspring genotype						
	332/5.2–5.0	19/5.2–6.0	*aa*	*ab*	*bb*	*cc*	*ac*	*bc*	missing
sEg00117	*ab*	*ab*	92	-	-	-	-	-	-
sEg00019	*ab*	*ac*	-	-	-	92	-	-	-
sEg00213	*aa*	*bb*	46	46	-	-	-	-	-
sMo00222	*aa*	*bb*	-	25	15	-	31	20	1
Hght7_oSSR	*aa*	*bb*	-	49	43	-	-	-	-
sMg00235	*aa*	*bb*	-	25	15	-	28	22	2
sMo00132	*aa*	*bb*	50	-	38	-	-	-	4

TABLE 3. SUMMARY OF UNEXPECTED GENOTYPES OBSERVED IN POPULATION 10

SSR marker	Parental genotype		78 offspring genotype						
	438/5.2–5.0	19/5.2–6.0	*aa*	*ab*	*bb*	*bc*	*ac*	*cc*	missing
sEg00213	*aa*	*bb*	1	24	12	-	16	12	15
sMo00222	*aa*	*aa*	43	21	14	-	-	-	2
sMo00166	*aa*	*aa*	58	-	-	-	-	-	22
Hght7_oSSR	*aa*	*aa*	25	18	20	-	-	-	17
sMg00011	*ab*	*ab*	11	50	19	-	-	-	-
sMg00051	*ab*	*ab*	18	26	1	8	17	-	10
sMo00055	*ab*	*ab*	39	40	-	-	-	-	1
sMg00071	*ab*	*ab*	-	25	31	15	9	-	-
sEg00154	*ab*	*ab*	9	38	33	-	-	-	-
sMg00235	*ab*	*ab*	20	23	-	15	22	-	-

TABLE 4. PREDICTED PARENTAL GENOTYPES BASED ON OBSERVED OFFSPRING GENOTYPES

Marker	Population 9		Population 10	
	Female parent	Male parent	Female parent	Male parent
sMg00011	*cd*	*ab*	*ab*	*ab*
sMg00051	*bc*	*ab*	*ac*	*ab*
sMo00055	*ac*	*aa*	*ab*	*aa*
sMo00246	*ab*	*ab*	*bd*	*ab*
sMg00168	*ab*	*ab*	*ab*	*ab*
sMg00071	*ae*	*bc*	*ab*	*bc*
sMg00196	*bb*	*ab*	*cc*	*ab*
sMo00138	*ab*	*ab*	*ac*	*ab*
sPSc00546	*ab*	*ab*	*ab*	*ab*
sEg00017	*ab*	*bb*	*ab*	*bb*
sEg00011	*ad*	*ab*	*ab*	*ab*
sEg00167	*ac*	*ac*	*ab*	*ac*
sEg00154	*ab*	*ab*	*ab*	*ab*
sMo00222	*bc*	*ab*	*ab*	*ab*
Hght7_oSSR	*bb*	*ab*	*ab*	*ab*
sMg00235	*bc*	*ab*	*ac*	*ab*
sPSc00488	*bc*	*bc*	-	*bc*
sMo00166	*ac*	*ac*	-	*ac*
sEg00213	*aa*	*ab*	-	*ab*
sMo00126	-	*cd*	*ab*	*cd*
sEg00117	-	*aa*	*ab*	*aa*
sMg00175	-	*bb*	*ab*	*bb*
sEg00019	-	*bb*	*ab*	*bb*

TABLE 5. ASSIGNMENTS OF THE PREDICTED PARENTS IN BC_1 x BC_1 POPULATIONS

Population	Number of legitimate offspring	Significance level (%)	Critical LOD	Parental assignment rate (%)
9	92	95.0	–1.84	100.0
10	78	95.0	–1.42	100.0

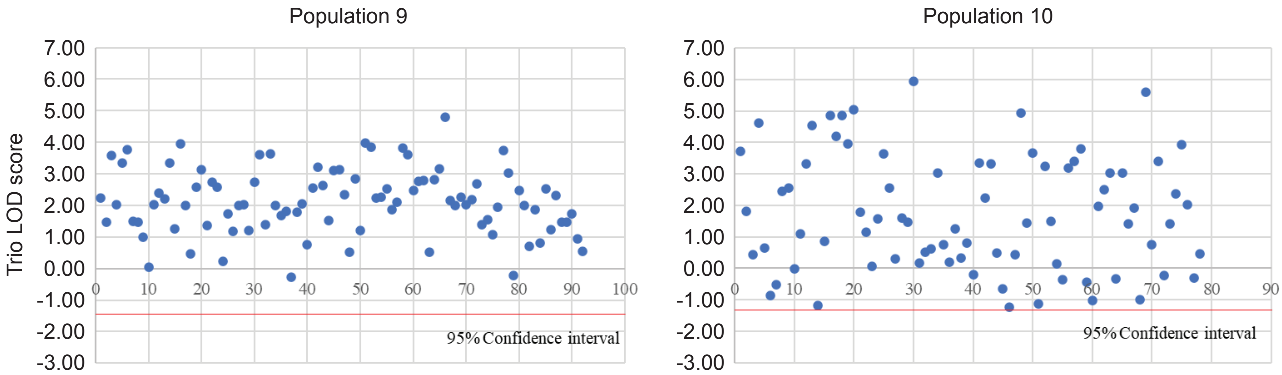

Figure 5. Distribution of trio logarithm of the odds (LOD) scores observed for Population 9 and 10. All the progeny palms were successfully assigned to the predicted parental-pairs at 95.0% confidence level.

A small number of offspring (two palms in Population 9 and 15 palms in Population 10) had slightly lower trio LOD scores ranging from –0.23 to –0.28 and –0.02 to –1.22, respectively (*Figure 5*), indicating that more markers are required for a better analysis of these samples.

As demonstrated in this study, the reconstruction of parental genotypes is possible by evaluating the segregation of genotypes among the offspring in a family, which is being demonstrated here for the first time for an interspecific hybrid cross of oil palm. This is particularly useful when the true parental information is unavailable either due to a mix-up or the original parental palm being not available before DNA analysis of the cross. In case of a mix-up, the predicted genotypes can be used as the reference to determine the actual parents in the seed garden. In general, the same approach can be applied for any species where the offspring share at least one parent (Jones et al., 2009) such as *Eucalyptus nitens* (Gea et al., 2007; Telfer et al., 2015). Reconstruction of parental genotypes has also been conducted for more complex breeding systems such as salamanders (Myers & Zamudio, 2004) and fish (Neff et al., 2001) where multiple paternity is involved.

CONCLUSION

This study reveals a set of SSR markers that effectively assess the genetic purity of two oil palm families where outliers have been identified among the progeny palms. More importantly, analysis using the selected SSR markers revealed that the available records did not reflect the true parentage, raising concerns about the legitimacy of the two families being true interspecific BC_1 x BC_1 hybrids. Nevertheless, the reconstruction of actual parental genotypes was successfully carried out. Although the number of informative markers reported in this study has allowed for an accurate assignment of offspring to the true parents, the inclusion of additional markers would further enhance the resolution of the parentage analysis.

ACKNOWLEDGEMENT

The authors would like to thank the Director-General of the Malaysian Palm Oil Board (MPOB) for permission to publish this article. This work was funded by MPOB (MOA/3(i)/ABBC/GENOMIK).

REFERENCES

Ahmad, A., Wang, J.-D., Pan, Y.-B., Sharif, R., & Gao, S.-J. (2018). Development and use of simple sequence repeats (SSRs) markers for sugarcane breeding and genetic studies. *Agronomy*, *8*(11), 260. https://doi.org/10.3390/agronomy8110260

Bao, J. (2014). Genes and QTLs for rice grain quality improvement. In Yan W., & Bao J. (Eds.), *Rice – Germplasm, genetic and improvement* (pp. 239–278). Intech. https://doi.org/10.5772/56621

Barcelos, E., De Almeida Rios, S., Cunha, R. N. V., Lopes, R., Motoike, S. Y., Babiychuk, E., Skirycz, A., & Kushnir, S. (2015). Oil palm natural diversity and the potential for yield improvement. *Frontiers in Plant Science, 6*, 190. https://doi.org/10.3389/fpls.2015.00190

Billotte, N., Marseillac, N., Risterucci, A.-M., Adon, B., Brottier, P., Baurens, F.-C., Singh, R., Herrán, A., Asmady, H., Billot, C., Amblard, P., Durand-Gasselin, T., Courtois, B., Asmono, D., Cheah, S. C., Rohde, W., Ritter, E., & Charrier, A. (2005). Microsatellite-based high density linkage map in oil palm (*Elaeis guineensis* Jacq.). *Theoretical and Applied Genetics*, *110*(4), 754–765. https://doi.org/10.1007/s00122-004-1901-8

Budiman, L. F., Apriyanto, A., Pancoro, A., & Sudarsono. (2019). Illegitimacy testing of *Elaeis guineensis* population based on simple sequence repeat markers. *Agrivita Journal of Agricultural Science, 41*(3), 512. https://doi.org/10.17503/agrivita.v41i3.1969

Cho, K. S., Kongsil, P., Wangsawang, T., & Sreewongchai, T. (2020). Marker-assisted pseudo-backcross breeding for improvement of amylose content and aroma in Myanmar rice cultivar Sinthukha. *ScienceAsia, 46*(5), 539–547. https://doi.org/10.2306/scienceasia1513-1874.2020.070

Collard, B. C. Y., & Mackill, D. J. (2008). Marker-assisted selection: An approach for precision plant breeding in the twenty-first century. *Philosophical Transactions of the Royal Society B Biological Sciences*, *363*(1491), 557–572. https://doi.org/10.1098/rstb.2007.2170

Corley, R. H. V. (2005). Illegitimacy in oil palm breeding – A review. *Journal of Oil Palm Research, 17*(2), 64–69.

Corley, R. H. V. & Tinker, P. B. (2015). *The oil palm* (5th ed.). Wiley Blackwell.

Daniel, I. O., Adetumbi, J. A., Oyelakin, O. O., Olakojo, S. A., Ajala, M. O., & Onagbesan, S. O. (2012). Application of SSR markers for genetic purity analysis of parental inbred lines and some commercial hybrid maize (*Zea mays* L.). *Journal of Experimental Agriculture International, 2*(4), 597–606. https://doi.org/10.9734/AJEA/2012/1579

Daza, E., Ayala-Díaz, I., Ruiz-Romero, R., & Romero, H. M. (2020). Effect of the application of plant hormones on the formation of parthenocarpic fruits and oil production in oil palm interspecific hybrids (*Elaeis oleifera* Cortes x *Elaeis guineensis* Jacq.). *Plant Production Science, 24*(3), 354–362. https://doi.org/10.1080/1343943x.2020.1862681

Escobar, H. C., & Chauza, J. J. D. (2018). Germinability and pollen viability of four improved cultivars of palm oil under laboratory conditions. *Revista Facultad Nacional de Agronomía Medellín*, *71*(1), 8395–8405. https://doi.org/10.15446/rfna.v71n1.69587

Gea, L. D., McConnochie, R., & Wynyard, S. (2007). Parental reconstruction for breeding, deployment and seed-orchard management of *Eucalyptus nitens*. *New Zealand Journal of Forestry Science*, *37*(1), 23–36.

Hama-Ali, E. O., Alwee, S. S. R. S., Tan, G. S., Panandam, J. M., Ling, H. C., Namasivayam, P., & Peng, H. B. (2014). Illegitimacy and sibship assignments in oil palm (*Elaeis guineensis* Jacq.) half-sib families using single locus DNA microsatellite markers. *Molecular Biology Reports*, *42*(5), 917–925. https://doi.org/10.1007/s11033-014-3829-7

Hardon, J. J., & Tan, G. Y. (1969). Interspecific hybrids in the genus *Elaeis* I. crossability, cytogenetics and fertility of F_1 hybrids of *E. guineensis* x *E. oleifera*. *Euphytica*, *18*(3), 372–379. https://doi.org/10.1007/BF00397784

Hormaza, P., Fuquen, E. M., & Romero, H. M. (2012). Phenology of the oil palm interspecific hybrid *Elaeis oleifera* x *Elaeis guineensis*. *Scientia Agricola*, *69*(4), 275–280. https://doi.org/10.1590/s0103-90162012000400007

Jones, A. G., Small, C. M., Paczolt, K. A., & Ratterman, N. L. (2009). A practical guide to methods of parentage analysis. *Molecular Ecology Resources*, *10*(1), 6–30. https://doi.org/10.1111/j.1755-0998.2009.02778.x

Josia, C., Mashingaidze, K., Amelework A. B., Kondwakwenda, A., Musvosvi, C., & Sibiya, J. (2021). SNP-based assessment of genetic purity and diversity in maize hybrid breeding. *PLoS ONE, 16*(8), e0249505. https://doi.org/10.1371/journal.pone.0249505

Kannan, P., Parameswari, C., Prasanyselvam, K., Sridevi, G., & Veluthambi, K. (2017). Introgression of sheath blight disease tolerance from the transgenic rice event Pusa Basmati-CG27 to the variety White Ponni through backcross breeding. *Indian Journal of Genetics and Plant Breeding, 77*(4), 501–507. https://doi.org/10.5958/0975-6906.2017.00066.9

Kalinowski, S. T., Taper, M. L., & Marshall, T. C. (2007). Revising how the computer program CERVUS accommodates genotyping error increases success in paternity assignment. *Molecular Ecology*, *16*(5), 1099–1106. https://doi.org/10.1111/j.1365-294X.2007.03089.x

Kalinowski, S. T., Taper, M. L., & Marshall, T. C. (2010.) Corrigendum. *Molecular Ecology, 19*(7), 1512. https://dx.doi.org/10.1111/j.1365-294X.2010.04544.x

Lieb, V. M., Kerfers, M. R., Kronmüller, A., Esquivel, P., Alvarado, A., Jiménez, V. M., Schmarr, H.-G., Carle, R., Schweiggert, R. M., & Steingass, C. B. (2017). Characterization of mesocarp and kernel lipid from *Elaeis guineensis* Jacq., *Elaeis oleifera* [Kunth] Cortés, and their interspecific hybrids. *Journal of Agricultural and Food Chemistry*, *65*(18), 3617–3626. https://doi.org/10.1021/acs.jafc.7b00604

Liu, L., Liu, G., Gong, Y., Dai, W., Wang, Y., Yu, F., & Ren, Y. (2007). Evaluation of genetic purity of F1 hybrid seeds in cabbage with RAPD, ISSR, SRAP and SSR markers. *HortScience*, *42*(3), 724–727. https://doi.org/10.21273/HORTSCI.42.3.724

Low, E.-T. L., Alias, H., Boon, S.-H., Shariff, E. M., Tan, C.-Y. A., Ooi, L. C. L., Cheah, S.-C., Raha, A.-R., Wan, K.-L., & Singh, R. (2008). Oil palm (*Elaeis guineensis* Jacq.) tissue culture ESTs: Identifying genes associated with callogenesis and embryogenesis. *BMC Plant Biology*, *8*, 62. https://doi.org/10.1186/1471-2229-8-62

Madon, M., Arulandoo, X., Sritharan, K., Nordiana, H. M. N., Muhammad Azwan, Z., & Mohd Zaki, N. (2018). Short communication: Genomic constitution of oil palm interspecific hybrid crosses monitored by genomic in situ hybridization (GISH). *Journal of Oil Palm Research, 30*(2), 338–344. https://doi.org/10.21894/jopr.2018.0027

Marshall, T. C., Slate, J., Kruuk, L. E. B., & Pemberton, J. M. (1998). Statistical confidence for likelihood-based paternity inference in natural populations. *Molecular Ecology*, *7*(5), 639–655. https://doi.org/10.1046/j.1365-294x.1998.00374.x

Meléndez-Jácome, M. R., Galvis-Correa, A. A., Mantilla-Valdivieso, E. M., Estefano-Tobar, F., Racines-Oliva, M. A., Jackson, T. A., & Vasquez-Castillo, W. (2024). Oil palm pollen compatibility with OxG hybrids in Ecuador. *Journal of Oil Palm Research*, *36*(2), 420–431. https://doi.org/10.21894/jopr.2023.0041

Meléndez, M. R., & Ponce, W. P. (2016). Pollination in the oil palms *Elaeis guineensis*, *E. oleifera* and their hybrids (OxG), in tropical America. *Pesquisa Agropecuaria Tropical, 46*(1), 102–110. http://doi.org/10.1590/1983-40632016v4638196

Mendoza, L., Barba, J., & Ligarreto, G. (2023). Bunch oil and fatty acid profile in *Elaeis oleifera* Taisha-Ecuador, *Elaeis guineensis* Jacq., interspecific hybrid and backcrosses. *Journal of Oil Palm Research, 35*(3), 504–516. https://doi.org/10.21894/jopr.2022.0057

Miura, S., Narita, M., Crofts, N., Itoh, Y., Hosaka, Y., Oitome, N. F., Abe, M., Takahashi, R., & Fujita, N. (2022). Improving agricultural traits while maintaining high resistant starch content in rice. *Rice*, *15*, 28. https://doi.org/10.1186/s12284-022-00573-5

Mosquera, D. J. C., Salinas, D. G. C., & Moreno, G. P. (2021). Pollen viability and germination in *Elaeis oleifera*, *Elaeis guineensis* and their interspecific hybrid. *Pesquisa Agropecuária Tropical*, *51*, e68076. https://doi.org/10.1590/1983-40632021v5168076

Mozzon, M., Foligni, R., & Mannozzi, C. (2020). Current knowledge on interspecific hybrid palm oils as food and food ingredient. *Foods, 9*(5), 631. https://doi.org/10.3390/foods9050631

Myers, E. M., & Zamudio, R. (2004). Multiple paternity in an aggregate breeding amphibian: The effect of reproductive skew on estimate of male reproductive success. *Molecular Ecology*, *13*(7), 1951–1963. https://doi.org/10.1111/j.1365-294X.2004.02208.x

Neff, B. D., Repka, J., & Gross, M. R. (2001). A Bayesian framework for parentage analysis: The value of genetic and other biological data. *Theoretical Population Biology*, *59*(4), 315–331. https://doi.org/10.1006/tpbi.2001.1520

Noh, A., Mohd Din, A., Marhalil, M., Rajanaidu, N., & Kushairi, A. (2012, September 21–24). *Performance of some Elaeis oleifera, interspecific hybrids and backcrosses* [Conference presentation]. International Seminar on Breeding for Oil Palm Disease Resistance and Field Visits, Bogotá, Colombia.

Okoye, M. N., Singh, R., Uguru, M. I., & Bakoumé, C. (2020). Application of microsatellite markers for hybrid verification and genetic analysis of oil palm (*Elaeis guineensis* Jacq.) *Nigerian Journal Biotechnology*, *37*(2), 1–12. https://doi.org/10.4314/njb.v37i2.1

Pallavi, H. M., Gowda, R., Shadakshari, Y. G., Bhanuprakash, K., & Vishwanath, K. (2011). Identification of SSR markers for hybridity and seed genetic purity testing in sunflower (*Helianthus annuus* L.) *HELIA*, *34*(54), 59–66. https://doi.org/10.2298/hel1154059p

Perrier, X., & Jacquemoud-Collet, J. P. (2006). *DARwin software*. https://darwin.cirad.fr/

Pomiès, V., Riou, V., Manez, A., Jacob, F., & Cochard, B. (2019, November). *Quality approach in oil palm selection and seed productivity by using ID checking test with 12 SSR markers* [Conference presentation]. International Palm Oil Congress and Exhibition (PIPOC 2019), Kuala Lumpur, Malaysia.

Rajanaidu, N., Kushairi, A., & Amiruddin, M. D. (2017). Oil palm genetic resources exploration. In *Oil palm genetic resources* (pp. 37–91). Perpustakaan Negara Malaysia.

Rajesh, M. K., Thomas, R. J., Rijith, J., Shareefa, M., & Jacob, P. M. (2012). Genetic purity assessment of DxT hybrids in coconut with SSR markers. *Indian Journal of Genetics and Plant Breeding, 72*(4), 472–474.

Rivera, Y. D., Cayón Salinas, D. G., & López M., J. E. (2013). Physiological and morphological characterization of American oil palms (*Elaeis oleifera* HBK Cortés) and their hybrids (*Elaeis oleifera* x *Elaeis guineensis*) on the Indupalma plantation. *Agronomia Colombiana*, *31*(3), 314–323.

Romero, H. M., Daza, E. S., Ayala-Diaz, I., & Ruiz-Romero, R. (2021). High-oleic palm oil (hopo) production from parthenocarpic fruits in oil palm interspecific hybrids using naphthalene acetic acid. *Agronomy*, *11*(2), 290. https://doi.org/10.3390/agronomy11020290

Rosli, R., Ab Halim, M. A., Ting, N.-C., Zaki, N. M., Jayanthi, N., Singh, R., Low, E.-T. L., & Mohamed-Hussein, Z.-A. (2022). Oil palm SSR resource interface (OPSRI) – Web-based bioinformatic analysis pipeline for SSR mining. *Journal of Oil Palm Research, 34*(4), 643–656. https://doi.org/10.21894/jopr.2022.0008

Saiful-Lazim, N. F., Rahmat, S. N., Mohd Fahmi, A. B., & Nur Fatihah, H. N. (2024). Identification of SSR markers for genetic purity testing in waxy corn F1 hybrid seeds. *Journal of Agrobiotechnology, 15*(S1), 25–33. https://doi.org/10.37231/jab.2024.15.s1.370

Sharma, T. R., Rai, A. K., Gupta, A. K., Vijayan, J., Devanna, B. N., & Ray, S. (2012). Rice blast management through host-plant resistance: Retrospect and prospects. *Agricultural Research*, *1*, 37–52. https://doi.org/10.1007/s40003-011-0003-5

Shinde, N. A., Bharose, A. A., Sarode, D. K., Swathi, R. S., Pimpale, P. A., & Shinde, S. S. (2021). Assessment of hybrid purity in Maize (*Zea mays* L.) using RAPD and SSR markers. *The Pharma Innovation Journal 2021, 10*(4), 870–874.

Singh, R., Jayanthi, N., Tan, S.-G., Panandam, J. M., & Cheah, S.-C. (2007). Development of simple sequence repeat (SSR) markers for oil palm and their application in genetic mapping and fingerprinting of tissue culture clones. *Asia-Pacific Journal of Molecular Biology and Biotechnology, 15*(3), 121–131.

Singh, R., Low, E.-T. L., Ooi, L. C., Ong-Abdullah, M., Nookiah, R., Ting, N.-C., Marjuni, M., Chan, P.-L., Ithnin, M., Abdul Manaf, M. A., Nagappan, J., Chan, K.-L., Rosli, R., Ab Halim, M. A., Azizi, N., Budiman, M. A., Lakey, N., Bacher, B., Van Brunt, A., ... Sambanthamurthi, R. (2014). The oil palm *VIRESCENS* gene controls fruit colour and encodes a R2R3MYB. *Nature Communications, 5*, 4106. https://doi.org/10.1038/ncomms5106

Socha, J., Cayón, D., Ligarreto, G., & Chaves, G. (2019). Effect of pollen doses on fruit formation and oil production in two hybrid palms genotypes (*Elaeis oleifera* H.B.K. Cortes x *Elaeis guineensis* Jacq.). *Agronomia Colombiana*, *37*(1), 12–17. https://doi.org/10.15446/agron.colomb.v37n1.75313

Sudha, R., Samsudeen, K., Rajesh, M. K., & Niral, V. (2022). Molecular marker assisted confirmation of hybrids in coconut (*Cocos nucifera* L.). *Indian Journal of Genetics and Plant Breeding*, *82*(3), 369–372. https://doi.org/10.31742/isgpb.82.3.15

Sunilkumar, K., Mathur, R., Sparjanbabu, D., & Reddy, A. (2013). Pollen viability and vigour in interspecific hybrids (*E. guineensis* x *E. oleifera*) of oil palm. *Journal of Plantation Crops*, *41*(1), 91–94.

Suzana, M., Rahimah, A. R., Maizura, I., & Singh, R. (2015). A simple and rapid protocol for isolation of genomic DNA from oil palm leaf tissue. *Journal of Oil Palm Research, 27*(3), 282–287.

Teh, C. K., Lee, H. L., Abidin, H., Ong, A. L., Mayes, S., Chew, F. T., & Appleton, D. (2019). A practical genome-enabled legitimacy assay for oil palm breeding and seed production. *BMC Plant Biology*, *19*(1), 470. https://doi.org/10.1186/s12870-019-2062-x

Telfer, E. J., Stovold, G. T., Li, Y., Silva-Junior, O. B., Grattapaglia, D. G., & Dungey, H. S. (2015). Parentage reconstruction in *Eucalyptus nitens* using SNPs and microsatellite markers: A comparative analysis of marker data power and robustness. *PLoS ONE, 10*(7), e0130601. https://doi.org/10.1371/journal.pone.0130601

Thongtawee, S., Tittinutchanon, P., & Volkaert, H. (2010). Microsatellites for parentage analysis in oil palm breeding population. *Thai Journal of Genetics*, *3*(2), 172–181. https://doi.org/10.14456/TJG.2010.1

Ting, N.-C., Jansen, J., Mayes, S., Massawe, F., Sambanthamurthi, R., Ooi, L. C. L., Chin, C. W., Arulandoo, X., Seng, T. Y., Alwee, S. S. R. S., Ithnin, M., & Singh, R. (2014). High density SNP and SSR-based genetic maps of two independent oil palm hybrids. *BMC Genomics*, *15*(1), 309. https://doi.org/10.1186/1471-2164-15-309

Ting, N.-C., Jansen, J., Nagappan, J., Ishak, Z., Chin, C.-W., Tan, S.-G., Cheah, S.-C., & Singh, R. (2013). Identification of QTLs associated with callogenesis and embryogenesis in oil palm using genetic linkage maps improved with SSR markers. *PLoS ONE*, *8*(1), e53076. https://doi.org/10.1371/journal.pone.0053076

Ting, N.-C., Zaki, N. M., Rosli, R., Low, E. T. L., Ithnin, M., Cheah, S. C., Tan, S. G., & Singh, R. (2010). SSR mining in oil palm EST database: Application in oil palm germplasm diversity studies. *Journal of Genetics*, *89*(2), 135–145. https://doi.org/10.1007/s12041-010-0053-7

Wang, J., Zhong, G. Y., Chin, E. C. L., Register III, J. C., Riley, R. D., Niebur, W. S., & Smith, J. S. C. (2002). Identification of parents of F1 hybrids through SSR profiling of maternal and hybrid tissue. *Euphytica*, *124*, 29–34. https://doi.org/10.1023/a:1015629600268

Yaakub, Z., Kamaruddin, K., Singh, R., Suzana, M., Marjuni, M., Ting, N.-C., Amiruddin, M. D., Low, E.-T. L., Ooi, L. C.-L., Sritharan, K., Rajanaidu, N., Jansen, J., & Abdullah, M. O. (2020). An integrated linkage map of interspecific backcross 2 (BC_2) populations reveals QTLs associated with fatty acid composition and vegetative parameters influencing compactness in oil palm. *BMC Plant Biology*, *20*, 356. https://doi.org/10.1186/s12870-020-02563-5

Zaki, N. M., Ismail, I., Rosli, R., Ting, N.-C., & Singh, R. (2010). Development and characterization of *Elaeis oleifera* microsatellite markers. *Sains Malaysiana*, *39*(6), 909–912.

Zolkafli, S. H., Ting, N.-C., Sanusi, N. S. N. M., Ithnin, M., Mayes, S., Massawe, F., Sambanthamurthi, R., Ismail, I., Abidin, M. I. Z., Roowi, S. H., Lee, Y. P., Hanafi, N. F. F., & Singh, R. (2021). Comparison of quantitative trait loci (QTLs) associated with yield components in two commercial *Dura* x *Pisifera* breeding crosses. *Euphytica*, *217*, 104. https://doi.org/10.1007/s10681-021-02825-9

Journal of Oil Palm Research Vol. 38 (3) September 2026 p. 533–544
DOI: https://doi.org/10.21894/jopr.2025.0039

THE GENETIC INFLUENCE ON OIL PALM PHENOLOGY-RELATED TRAIT INHERITANCE IN CAMEROON ACCESSIONS

TRININGSIH[1]*; SUJADI[1]; HERI ADRIWAN SIREGAR[1] and YURNA YENNI[1]

ABSTRACT

The characterisation of oil palms based on inflorescence phenology is vital for developing oil palm varieties with precocious traits. However, the study on genetic control for these traits still needs to be improved. This study evaluated the genetic variability at the inflorescence phase of 20 Cameroon accessions grown at Adolina Estate, North Sumatra, Indonesia. The analysis of variance for female and male inflorescence phenological traits showed significant differences between Cameroon accessions. This study revealed that genetic control for phenology phases is lower than the environmental control. Also, the heritability of the period from spear leaf to 70% open to ripening is about 23%, with a 5% genotypic coefficient of variance. Cluster analysis successfully grouped the accession into two major groups with no relationship between geographical origin and clustering pattern. This study gives insights into the genetic parameters and breeding potential of Cameroon accession in a way that allows accession selection based on inflorescence traits. A high environmental effect influences the observed phenotypes, so selection based on related traits will not be effective.

Keywords: BBCH, cluster analysis, coefficient variability, genetic variance.

Received: 10 May 2024**; Accepted:** 8 May 2025**; Published online:** 29 July 2025.

INTRODUCTION

The narrow genetic base of current commercial oil palm cultivars has encouraged oil palm breeders to pay more attention to improving genetic resources for sustainable oil palm breeding (Arias et al., 2013). According to Sayekti et al. (2015), the introduced germplasm is a promising genetic resource as breeding material to increase genetic diversity. One of the oil palm germplasm collections maintained by the Indonesian Oil Palm Research Institute (IOPRI) was introduced from Cameroon in 2008. Cameroon is one of the central origins of oil palm (*Elaeis guineensis* Jacq.) in Africa (Sarimana et al., 2017), and introducing these accessions can enrich the existing genetic diversity.

Germplasm collections are essential resources in plant breeding, mainly when accessions are described based on critical traits (Sujadi et al., 2019a). Therefore, selecting the best accession for future breeding programmes can be conducted through characterisation and evaluation based on these traits (Li-Hammed et al., 2015). Classical methods, which focus on agronomic performance or phenotype, are still efficient for understanding differences between accessions (Santosa et al., 2015). One of the morphological characterisations of oil palm is the inflorescence phase, known as phenology (Hernawati et al., 2022), which can help determine the precocious genotypes (Sujadi et al., 2019b). Trimanto et al. (2020) stated that phenology-related traits are particularly important as they relate to the initial stages of plant breeding. Therefore, studies on these traits, such as precocity, are valuable in germplasm collection breeding programmes.

Both genetic and environmental factors influence the phases of development and sex determination in oil palm inflorescence (Suresh et al., 2021). However, Corley and Tinker (2015) reported that determining the flowering pattern on oil palms may require more work due to the

[1] Indonesian Oil Palm Research Institute,
Jl. Brigjend Katamso No. 51,
20158, Medan, North Sumatra, Indonesia.

* *Corresponding author e-mail: Triningsih271@gmail.com*

different phases and periods of male and female flowering. Previous studies described the influence of the environment on oil palm inflorescence development, such as temperature (Pradiko et al., 2019), rainfall, soil water depth (Mubarok et al., 2022) and length of irradiation (Legros et al., 2009). The influence of genetics contributing to oil palm inflorescence has yet to be widely reported. Identifying oil palm genotypes with precocious traits in plant breeding supports yield improvement programmes (Maskromo et al., 2017). So, studying the genetic role in inheriting precocity traits should be a high concern.

Genetic parameters, such as genotype, phenotype, environment, genotype by environment (G×E) interaction, genetic diversity coefficient and heritability must be estimated before improving the trait (Lubis et al., 2014). Furthermore, the population's genetic variability and trait inheritance pattern are responsible for the success of plant improvement (Adhikari et al., 2018). Nevertheless, the information on genetic parameters based on phenology-related traits is still limited. Therefore, this study aims to evaluate the genetic variability and population structure of oil palm based on the inflorescence phases of Cameroon accession.

MATERIALS AND METHODS

Planting Materials

The open-pollinated palms were collected from seven sites (Nkong Biyen, Maloundou, Ballong I, Fapdolop, Bamese, Efok and Kola) in Cameroon. These palms were from IOPRI collection, labelled as CMR and was planted in the AD13S trial in 2010. The experiment was conducted at Adolina Estate, PT. Perkebunan Nusantara IV, Serdang Bedagai, North Sumatra, Indonesia. The climatic conditions at the study site included (1) temperature was around 25°C–28°C with an average of 27°C; (2) annual rainfall ranging from 1,718 to 2,130 mm/yr; (3) average daily humidity ranged at 75.0%–89.0%; and (4) average solar radiation at 15.6 MJ/m^2/day.

Data Collection

The phenology of inflorescence phases was recorded from January 2017 to June 2023. The duration of the phenological phase, starting from the opening of leaves to fruit development, was recorded for each leaf frond every 10 days based on the scale of *Biologische Bundesanstalt Bundessortenamt und Chemische Industrie* (BBCH) (Moreno & Romero, 2015). The number of leaf fronds was recorded as replication in this study. The number of inflorescences was calculated as the sex ratio (ISR) defined as the ratio of female flower (FF) to total inflorescences (Adam et al., 2011). The description of the observed traits in this study is presented in *Table 1*.

TABLE 1. INFLORESCENCE AND RELATED TRAITS DESCRIPTION IN THIS STUDY

BBCH code	Description
Female flowering	
159	Spear leaf 70.0% open
501	Emergence of 10.0% of the floral structure
601	Female pre-anthesis 1: The rachillae are tight toward the centre
607	Female anthesis: Opening of the stigma lobes
807	Fruit ripens
Male flowering	
159	Spear leaf 70.0% open
501	Emergence of 10.0% of the floral structure
601	Pre-anthesis
607	Anthesis
609	End of flowering
Flower production	
	Female flower
	Male flower
	Hermaphrodite
	Sex ratio

Note: BBCH - *Biologische Bundesanstalt Bundessortenamt und Chemische Industrie*.

Statistical Methods

The mixed linear model used in this study based on Henderson (1985) is as Equation (1):

$$y = X\beta + Z_a + e \quad (1)$$

where, y is the vector of observed traits, X is the design matrix of observed fixed effects, β is the vector of experimental effects (fixed effects), Z is the design matrix of observed random effects, a is the vector of accession palm effects (random effects), and e is the vector of residual effects.

Analysis of variance was conducted to part the source of variation following the model by Swaray et al. (2021). The analysis of variance is presented in *Table 2* and for the differences between treatments, the Duncan test ($P < 0.01$ and $P < 0.05$) was conducted using RStudio version 1.3-1 with the agricolae package (De Mendiburu, 2019).

The components of variances were estimated to determine the genetic variation, heritability and genotypic coefficients of variation among accession on phenology-related traits. Broad-sense heritability (h_b^2) is described as the proportion of the genotypic (σ_g^2) to the phenotypic variance (σ_p^2) estimated using the formula given by Hanson et al. (1956) [Equation (4)]. Johnson et al. (1955) categorised the broad-sense heritability (%) as low (<30%), moderate (30%–60%) and high (>60%). The genotypic coefficients of variation (GCV) were estimated from the following Equation (5) by Burton (1952), where a trait has a wide genotypic variability if the genotypic coefficient of variation (GCV) value is >20%, moderate 10%–20%, and low 0%–10% (Sivasubramaniam & Madhava Menon, 1973). The genetic variation is analysed by Restricted Maximum Likelihood (REML) using program RStudio version 4.3.1 lme4 package [Equation (2)]. PBSTAT-CL (https://apps.pbstat.com) is used for cluster analysis.

$$\text{Genetic variance } (\sigma_g^2) = \frac{(MSG\text{-}MSE)}{n_g} \quad (2)$$

$$\text{Error variance } (\sigma_e^2) = MSE \quad (3)$$

$$\text{Broad sense heritability } (h_b^2) = \frac{(\sigma_g^2)}{(\sigma_p^2)} \times 100 \quad (4)$$

$$GCV = \frac{\sqrt{\sigma_g^2}}{X} \times 100 \quad (5)$$

where, X is general mean for the characters.

RESULTS AND DISCUSSION

Performance of Inflorescence Phases

Analysis of variance shows highly significant differences among Cameroon accessions at each phase of female and male inflorescence (*Table 3*). The differences among the accessions also indicated a high genetic diversity in these populations (Maskromo et al., 2017). In addition, genetic diversity positively contributed to increasing the genetic base in oil palm populations for future oil palm breeding programmes (Swaray et al., 2021).

The female inflorescence period of 20 Cameroon accessions is presented in *Table 4*. The results show significant differences at 1.0% and 5.0% levels based on Duncan's multiple range test (DMRT). The period from the first leaf to visible inflorescence in the axil (BBCH 159–501) ranges from 266–362 days, with an average of about 315 days. Accession CMR075/24-14 has the shortest duration and significantly differed from the others, while CMR001/35-14 has the longest time. This result indicates a longer duration when compared to previous studies on other cultivars, such as Golden Hope (238 days), Dami (250 days), United

TABLE 2. ANALYSIS OF VARIANCE AND EXPECTED MEAN SQUARES OF OIL PALM PHENOLOGY TRAITS

Source of variation	Degree of freedom	Mean square	Expected mean square
Accession (g)	(g–1)	MSG	$\sigma_e^2 + n\sigma_r^2 + nr\sigma_g^2$
Replication (r)	(r–1)	MSR	$\sigma_e^2 + n\sigma_g^2 + nr\sigma_r^2$
Error (e)	(r–1) (g–1)	MSE	σ_e^2

Note: n - harmonic mean destined for accession palms/ replicate; MSG - mean square of genotype; MSR - mean square of replicate; MSE - mean square of error; σ_g^2 - genotypic variance; σ_e^2 - environmental variance; σ_r^2 - replication variance.

TABLE 3. ANALYSIS OF VARIANCE OF CAMEROON ACCESSION FOR FEMALE AND INFLORESCENCE DURATION (DAY)

Characters	MSG	MSR	MSE	CV (%)
Female inflorescence stage				
159–501	38,922.8**	150,911.9**	3,257.9	18.1
501–601	1.1**	1.5**	412.2	48.7
601–607	45.2*	73.4**	26.0	40.4
607–807	34.6**	135.1**	5.8	31.5
159–807	61.3**	118.1**	3.5	9.6
Male inflorescence stage				
159–501	57,465.0**	40,295.7**	6,572.5	28.2
501–601	1,296.9**	458.3^{ns}	443.0	53.1
601–607	68.0**	27.9^{ns}	24.5	38.8
607–609	15.2**	3.2^{ns}	5.9	22.2
159–609	46,714.1**	33,659.0**	6,794.2	24.2

Note: **- significant at α = 1%; *- significant at α = 5%; MSE - mean squares of environment; MSG - mean squares of genotype; MSR - mean squares of replicate; (159–501) - duration from spear leaf 70% open to inflorescence visible in axil; (501–601) - duration from inflorescence visible in axil to pre-anthesis; (601–607) - duration from pre-anthesis to anthesis; (607–807) - duration from anthesis to ripening of fruit; (159–807) - duration from Spear leaf 70.0% open to ripening of fruit; (607–609) - duration from anthesis to end of flowering; (159–607) - duration from Spear leaf 70.0% open to anthesis; CV - coefficient of variation.

Plantations (218 days) and Guthrie (242 days) (Forero et al., 2012), as well as on the commercial plant DxP Simalungun (227 days) (Pradiko et al., 2019). Cameroon accessions in this study are categorised as non-precocious genotypes.

In the inflorescence phase, from visible in axil to pre-anthesis (BBCH 501–601), the development of FF requires 42 days. Accession CMR102/33-16 has the shortest duration and was not significantly different from the other 14 accessions. The average duration range from pre-anthesis to anthesis (BBCH 601–607) is about 13 days. CMR075/24-14, which shows the shortest duration in the first leaf appearance, also shows the shortest duration in the anthesis phase at 11 days. These results show a shorter duration compared to the flowering of 8 varieties belonging to the IOPRI reported by Pradiko et al. (2019) on the duration from visible in axil to pre-anthesis (55–100 days) and from pre-anthesis to anthesis (12–20 days).

The required time from anthesis to ripening of fruit (BBCH 607–807) is 200–288 days, with an average of 243 days. Accession CMR075/24-14 has the shortest duration, followed by CMR023/25-16, CMR047/32-22, CMR073/30-11, CMR028/36-4, CMR103/34-23 and CMR102/36-21. Meanwhile, CMR075/28-19 and CMR074/32-14 has the longest time. In this phase, Cameroon accession palm shows longer duration compared to *Deli* x *Nigeria* (153–155 days) (Suresh et al., 2021) and Angola accessions (144–174 days) (Sujadi et al., 2017). The difference in duration from anthesis to fruit ripening is due to genetic and environmental factors. This phase involves complex biological processes from fruit formation and enlargement to oil synthesis in the kernel and mesocarp (Razali et al., 2012). Arifin et al. (2014) added that the oil synthesis phase in oil palm fruit at 17 weeks after anthesis was influenced mainly by climate such as temperature and rainfall.

The total time of female inflorescence, from spear leaf 70% open to ripening of fruit (BBCH 159–807), takes about 613 days on average, with a range of duration between 522 and 668 days. Accession CMR075/24-14 has the shortest female inflorescence emergence period while CMR001/35-14 has the longest time. Female inflorescence has a longer period compared to previous studies, such as in the DxP Marihat took 444 days (Mubarok et al., 2022), Angola accession (385–495 days) (Sujadi et al., 2019a) and 8 IOPRI varieties (452–484 days) (Pradiko et al., 2019). Comprehensive analyses with

TABLE 4. MEAN COMPARISON AND STANDARD ERROR (±) OF CAMEROON ACCESSION FOR FEMALE INFLORESCENCE DURATION

Accession	Female inflorescence stage				
	159–501	501–601	601–607	607–807	159–807
CMR001/29-16	$297.4^{f} \pm 7.5$	$42.4^{bcd} \pm 2.6$	$11.6^{bc} \pm 0.6$	$273.8^{abc} \pm 10.1$	$625.4^{cde} \pm 7.8$
CMR001/35-14	$362.3^{a} \pm 7.5$	$37.0^{cd} \pm 2.6$	$13.4^{abc} \pm 0.6$	$254.9^{b-e} \pm 10.1$	$667.8^{a} \pm 7.8$
CMR023/25-16	$313.1^{c-f} \pm 7.5$	$44.5^{abc} \pm 2.6$	$11.7^{bc} \pm 0.6$	$212.8^{fg} \pm 10.1$	$582.2^{fgh} \pm 7.8$
CMR023/26-14	$337.4^{bc} \pm 7.4$	$40.2^{bcd} \pm 2.6$	$13.3^{abc} \pm 0.6$	$238.3^{def} \pm 10.0$	$629.4^{bcd} \pm 7.7$
CMR028/31-18	$332.0^{bcd} \pm 7.6$	$40.1^{bcd} \pm 2.7$	$12.0^{bc} \pm 0.6$	$237.0^{def} \pm 10.3$	$621.2^{cde} \pm 7.9$
CMR028/36-04	$324.9^{b-e} \pm 8.1$	$37.8^{bcd} \pm 2.9$	$14.4^{a} \pm 0.7$	$226.8^{d-g} \pm 10.9$	$604.1^{d-g} \pm 8.4$
CMR032/30-24	$292.2^{f} \pm 8.2$	$38.0^{bcd} \pm 2.9$	$12.2^{abc} \pm 0.7$	$244.6^{c-f} \pm 11.0$	$587.1^{fgh} \pm 8.5$
CMR032/33-27	$296.6^{f} \pm 7.9$	$40.4^{bcd} \pm 2.8$	$12.2^{abc} \pm 0.7$	$246.4^{c-f} \pm 10.7$	$595.7^{fgh} \pm 8.2$
CMR047/27-26	$316.9^{b-f} \pm 7.1$	$52.5^{a} \pm 2.5$	$11.8^{bc} \pm 0.6$	$255.5^{b-e} \pm 9.7$	$636.8^{bc} \pm 7.4$
CMR047/32-22	$330.5^{bcd} \pm 8.3$	$42.2^{bcd} \pm 2.9$	$11.7^{bc} \pm 0.7$	$217.1^{fg} \pm 11.2$	$601.7^{e-h} \pm 8.6$
CMR073/30-11	$301.9^{ef} \pm 7.0$	$42.1^{bcd} \pm 2.4$	$12.3^{abc} \pm 0.6$	$221.0^{efg} \pm 9.4$	$577.5^{h} \pm 7.2$
CMR073/35-09	$325.0^{b-e} \pm 7.9$	$38.6^{bcd} \pm 2.8$	$12.3^{abc} \pm 0.7$	$257.7^{a-d} \pm 10.7$	$633.8^{bc} \pm 8.2$
CMR074/28-14	$339.4^{b} \pm 7.9$	$46.5^{ab} \pm 2.8$	$13.8^{ab} \pm 0.7$	$253.4^{b-e} \pm 10.6$	$653.2^{ab} \pm 8.2$
CMR074/32-14	$303.1^{ef} \pm 7.3$	$37.9^{bcd} \pm 2.6$	$13.4^{abc} \pm 0.6$	$288.2^{a} \pm 9.9$	$642.6^{bc} \pm 7.6$
CMR075/24-14	$266.9^{g} \pm 7.9$	$43.9^{abc} \pm 2.8$	$11.1^{c} \pm 0.7$	$200.4^{g} \pm 10.6$	$522.5^{i} \pm 8.2$
CMR075/28-19	$301.2^{ef} \pm 7.8$	$45.0^{abc} \pm 2.7$	$14.0^{ab} \pm 0.7$	$281.5^{ab} \pm 10.5$	$641.8^{bc} \pm 8.1$
CMR102/33-16	$323.5^{b-e} \pm 7.8$	$34.0^{d} \pm 2.7$	$13.3^{abc} \pm 0.7$	$253.6^{b-e} \pm 10.5$	$624.6^{cde} \pm 8.1$
CMR102/36-21	$340.2^{b} \pm 8.0$	$40.9^{bcd} \pm 2.8$	$12.0^{bc} \pm 0.7$	$232.1^{d-g} \pm 10.8$	$625.3^{cde} \pm 8.3$
CMR103/34-23	$293.5^{f} \pm 7.3$	$44.8^{abc} \pm 2.5$	$12.2^{abc} \pm 0.6$	$229.5^{d-g} \pm 9.8$	$580.2^{gh} \pm 7.5$
CMR103/36-14	$311.2^{def} \pm 7.8$	$41.6^{bcd} \pm 2.7$	$13.1^{abc} \pm 0.7$	$240.8^{c-f} \pm 10.5$	$606.8^{def} \pm 8.1$
Mean ± SE	315.5 ± 7.7	41.6 ± 2.8	12.6 ± 0.7	243.3 ± 10.4	613.0 ± 8.0

Note: 159–501 - duration from spear leaf 70% open to inflorescence visible in axil; 501–601 - duration from inflorescence visible in axil to pre-anthesis; 601–607 - duration from pre-anthesis to anthesis; 607–807 - duration from anthesis to ripening of fruit; 159–807 - duration from spear leaf 70% open to ripening of fruit; Means with the same letters of the alphabet within the same column are not significantly dissimilar at $p < 0.05$ with Duncan's new multiple range test (DNMRT); SE - standard error.

weather data need to be conducted to determine how weather factors influence the length of the inflorescence phase. However, for selection options on phenology characters, CMR075/24-14 can be selected as a precocious accession when compared to the other accessions and can prioritised in selection programmes aimed at enhancing early maturity.

Table 5 displays the male inflorescence period of 20 accessions. The duration ranges from 239–370 days for BBCH 159 to BBCH 501, with an average duration of about 290 days. Accession CMR023/25-16 has the shortest duration at 239 days. During the inflorescence phase, from visible in axil to pre-anthesis (BBCH 501–601), the development of male flowers (MF) requires 39 days and CMR001/29-16 has the shortest time. As seen in the previous female inflorescence results, the timing of MF and FF is different. Because of their different morphologies, the male and female inflorescences have different phase times (Yaakub et al., 2023). Corley and Tinker (2015) found that the male inflorescence rachis bears 100 and 300 spikelets, with each spikelet containing 400–1,500 flowers. Conversely, the female inflorescence comprises around 150 rachillas, each containing between five and 30 flowers.

The average time from pre-anthesis to anthesis (BBCH 601–607) was approximately 13 days, with accession CMR074/28-14 having the shortest duration. The phase from anthesis to the end of flowering (BBCH 607–609) had an average duration of 11 days across all Cameroon accessions. Accession CMR023/25-16 shows the shortest time, around 9 days, which is not significantly different from the other 12 accessions. The Cameroon accessions needed slightly longer time as Mubarok et al. (2022) found that the timeframe from anthesis to the conclusion of flowering was about eight days.

The phase duration from spear leaf 70.0% open to fruit ripening varied between and within individual accessions, as presented in *Figure 1*. There is high variability between 20 accessions, although some are from the exact origin, i.e., Accession CMR075/24-14 with CMR073/30-11, CMR075/28-19 and CMR074/32-14. The variability is also found within individual accession palms, as indicated by the extensive range of short and longer inflorescence phases. This variation is due to the Cameroon accessions derived from open-pollinated crosses, which account for the high genetic variability among individual palms. The result of this study is in line with those of

TABLE 5. MEAN COMPARISON AND STANDARD ERROR (±) OF CAMEROON ACCESSION FOR MALE INFLORESCENCE STAGE

Accession	Male inflorescence stage				
	159–501	501–601	601–607	607–609	159–609
CMR001/29-16	370.3^{a} ± 19.6	31.0^{c} ± 5.1	11.2^{cd} ± 1.2	13.4^{a} ± 0.5	412.6^{a} ± 19.9
CMR001/35-14	264.1^{cde} ± 13.9	53.4^{a} ± 3.6	15.2^{ab} ± 0.8	10.6^{cde} ± 0.4	332.7^{b-e} ± 14.1
CMR023/25-16	239.2^{e} ± 27.0	41.4^{abc} ± 7.0	11.7^{bcd} ± 1.6	9.2^{e} ± 0.8	292.4^{e} ± 27.4
CMR023/26-14	276.3^{b-e} ± 15.3	41.1^{abc} ± 3.9	12.7^{bcd} ± 0.9	11.4^{bcd} ± 0.4	330.2^{b-e} ± 15.5
CMR028/31-18	330.7^{ab} ± 21.6	33.1^{c} ± 5.6	13.5^{a-d} ± 1.3	10.2^{cde} ± 0.6	377.4^{ab} ± 22.0
CMR028/36-04	248.0^{e} ± 13.3	42.3^{abc} ± 3.4	14.0^{a-d} ± 0.8	10.6^{cde} ± 0.4	304.4^{de} ± 13.5
CMR032/30-24	254.7^{e} ± 17.2	40.1^{abc} ± 4.4	13.1^{a-d} ± 1.0	11.1^{bcd} ± 0.5	308.0^{cde} ± 17.5
CMR032/33-27	291.2^{b-e} ± 18.1	38.6^{abc} ± 4.7	13.3^{a-d} ± 1.1	11.1^{bcd} ± 0.5	343.1^{b-e} ± 18.4
CMR047/27-26	299.8^{b-e} ± 20.2	52.5^{ab} ± 5.2	11.5^{bcd} ± 1.2	10.7^{cde} ± 0.6	363.8^{a-d} ± 20.6
CMR047/32-22	290.3^{b-e} ± 21.6	37.5^{bc} ± 5.6	16.7^{a} ± 1.3	11.5^{bcd} ± 0.6	344.5^{b-e} ± 22.0
CMR073/30-11	322.8^{abc} ± 19.1	33.9^{c} ± 4.9	12.5^{bcd} ± 1.1	10.8^{cde} ± 0.5	369.3^{abc} ± 19.4
CMR073/35-09	272.5^{b-e} ± 17.2	32.2^{c} ± 4.4	13.0^{bcd} ± 1.0	12.7^{ab} ± 0.5	317.8^{b-e} ± 17.5
CMR074/28-14	316.8^{a-d} ± 17.6	39.7^{abc} ± 4.5	10.4^{d} ± 1.0	10.9^{cde} ± 0.5	367.0^{abc} ± 17.9
CMR074/32-14	324.4^{abc} ± 17.6	33.3^{c} ± 4.5	11.1^{cd} ± 1.0	12.0^{abc} ± 0.5	369.0^{abc} ± 17.9
CMR075/24-14	297.9^{b-e} ± 10.0	36.5^{c} ± 2.5	10.6^{d} ± 0.6	10.5^{cde} ± 0.3	345.0^{b-e} ± 10.1
CMR075/28-19	291.2^{b-e} ± 15.6	53.1^{ab} ± 4.0	12.5^{bcd} ± 0.9	11.0^{b-e} ± 0.4	356.8^{a-d} ± 15.8
CMR102/33-16	256.5^{de} ± 15.3	37.6^{bc} ± 3.9	14.6^{abc} ± 0.9	10.6^{cde} ± 0.4	308.7^{cde} ± 15.5
CMR102/36-21	268.9^{cde} ± 17.6	35.3^{c} ± 4.5	13.9^{a-d} ± 1.0	10.1^{de} ± 0.5	318.1^{b-e} ± 17.9
CMR103/34-23	257.0^{de} ± 19.1	38.0^{abc} ± 4.9	12.9^{bcd} ± 1.1	10.6^{cde} ± 0.5	308.0^{cde} ± 19.4
CMR103/36-14	325.1^{abc} ± 18.1	32.2^{c} ± 4.7	12.0^{bcd} ± 1.1	11.3^{bcd} ± 0.5	369.4^{abc} ± 18.4
Mean ± SE	289.9 ± 17.8	39.2 ± 4.6	12.9 ± 1.1	11.1 ± 0.5	342.0 ± 18.1

Note: 159–501 - duration from spear leaf 70.0% open to inflorescence visible in axil; 501–601 - duration from inflorescence visible in axil to pre-anthesis; 601–607 - duration from pre-anthesis to anthesis; 607–609 - duration from anthesis to end of flowering; 159–607 - duration from spear leaf 70.0% open to anthesis; Means with the same letters of the alphabet within the same column are not significantly dissimilar at $p < 0.05$ with Duncan's new multiple range test (DNMRT); SE - standard error.

Sarimana et al. (2017), which shows that about 26.0% of genetic variability between individuals and 74.0% within individuals derived from open pollination.

Genetic Performances of Inflorescence Phase

Variance components can be partitioned into phenotype, environment and genotype variances to obtain information on genetic variability (Lubis et al., 2014). Based on the variance components shown in *Table 6*, the environmental factors dominate all phases of oil palm inflorescence as indicated by the low broad-sense heritability values (<30.0%). The lowest heritability is found in BBCH 501–601 (3.1%) and BBCH 601–607 (1.3%). Meanwhile, the highest heritability is achieved in MF of BBCH 159–501 (29.3%). Considering the high influence of environmental effects, selection based on related traits will not be effective (Devesh et al., 2018). These results also in line with Paterson et al. (2015), who stated that oil palm phenology was related to climatic factors affecting each inflorescence phase. Climate factors that affect oil palm phenology have been reported, such as rainfall (Mubarok et al., 2022), growth degree days (Pradiko et al., 2019), length of irradiation and drought (Legros et al., 2009). A previous Pradiko et al. (2019) study reported that in the temperature range of 23ºC–34ºC, three varieties (DxP AVROS, DxP Dumpy and DxP PPKS 540) had shorter inflorescence.

Based on these criteria, the GCV value of Cameroon accessions in all female flowering phases was low (5.0%–9.5%), while the male flowering generally exhibited a moderate GCV. The results indicated that inflorescence in the 20 Cameroon accessions tested was more strongly influenced by the environment, especially in female flowering. A high genetic variability is required to improve or enhance the performance of these traits. Agronomic field improvements, such as selecting oil palm varieties based on suitable climatic conditions or implementing water management systems, were recommended to reduce the duration of inflorescence development. According to Sujadi et al. (2020), the Lame, Langkat, PPKS 540, and Simalungun varieties, which have longer fruit development phases, were predicted to be better suited for regions with low rainfall. Conversely, varieties with shorter fruit development phases, such as Dumpy, AVROS and PPKS 540, were expected to adapt more readily to rising air temperatures. Suharyanti et al. (2020) reported that water shortage affects inflorescence period, especially in the sex determination phase, so drought mitigation could have been pursued through proper water management. Therefore, it is imperative to conduct further study on the other genotypes/varieties to compare with this research and reassess at the phenology of these accessions under varying climatic conditions to gain deeper insight into environmental effects.

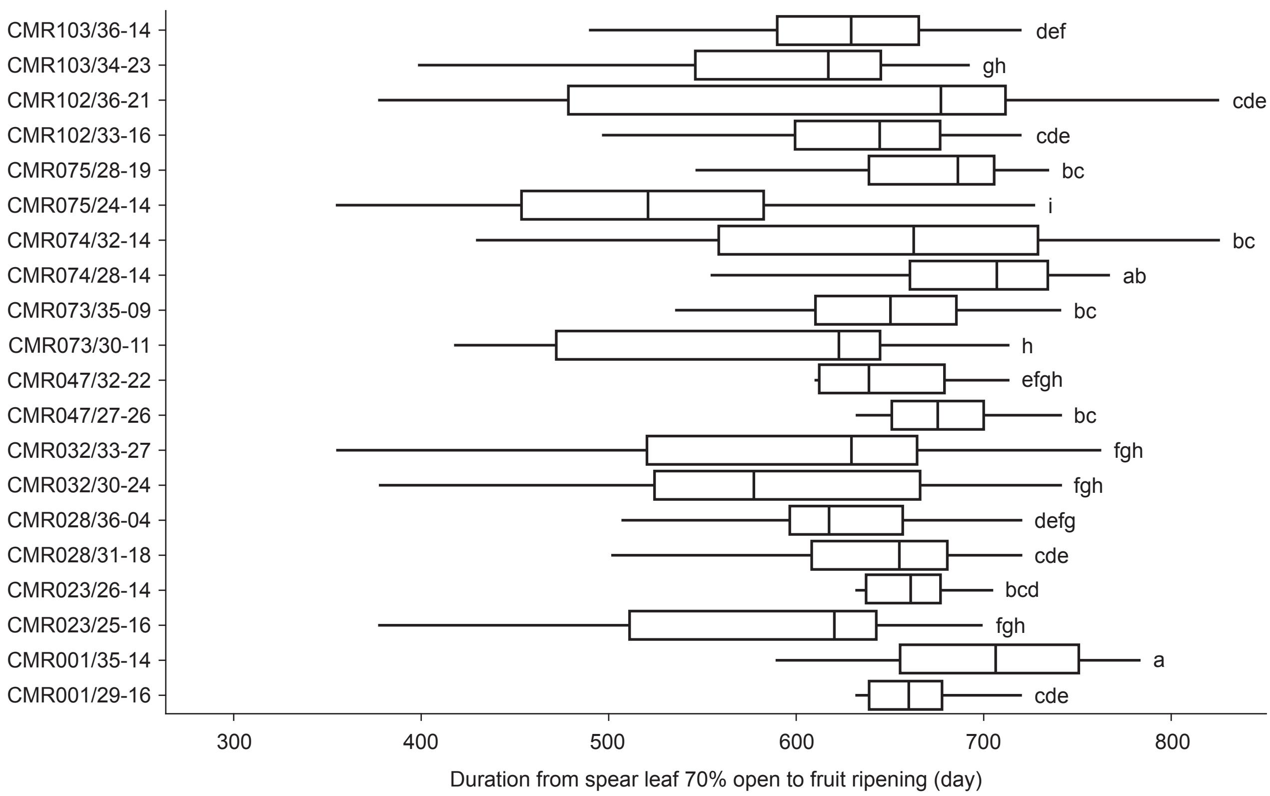

Figure 1. Box plot duration from spear leaf 70% open to the ripening of the fruit of 20 Cameroon accession palms. The same letters of the alphabet on the graph are not significantly dissimilar at $p < 0.05$ *with Duncan's multiple range test (DMRT).*

Performances of Female, Male Production and Sex Ratio

Analysis of variance among the 20 Cameroon accessions showed highly significant differences in MF, FF, hermaphrodite (HF) and ISR (*Table 7*). The results also showed significant differences among replication on all traits, indicating that accession performance was inconsistent. Corley and Tinker (2015) reported that the sexual phase pattern of oil palm is complex and cannot be determined due to the different phases and timing of male and female inflorescence, depending on environmental factors.

This study found that environmental effects highly influence FF, MF, HF and ISR traits. It was known from the low heritability value of the four traits (<30.0%), indicating that environmental effects play a more significant role in controlling these traits. This result was also in line with Swaray et al. (2021), who reported that the production of MF, FF and aborted flowers was more influenced by the environment, with a percentage of the environmental variance of more than 60% in 24 progeny-test experiments. Abdullah et al. (2017) reported that climatic factors, such as water availability and length of irradiation for MF and FF production, respectively, influence the sex differentiation of oil palms. This finding is also supported by Harahap and Lubis (2018), who stated that water dynamics affect the phases of oil palm flowering development in the formation of flower parts, sex differentiation, flower emergence and fruit ripening.

The performance of 20 Cameroon accessions on FF, MF, HF and ISR traits is shown in *Figure 2*. The results show MF production ranges from 2 and 13 (12.0%–59.0%) flowers/palm/yr. Accession CMR075/24-14 has the highest MF production. Meanwhile, ISR ranges from 41.0% to 88.0%, with an average of 64.0%. Over half (55.0%) of the 20 accessions palm shows an ISR of over 60.0%. Accessions CMR023/25-16 and CMR073/30-11 has the highest ISR, 88.0% and 80.0% respectively. It indicates that the ISR of the observed Cameroon accessions is still within a reasonable range. The optimal ISR was considered to be between 70.0% and 80.0%, as reported by Swaray et al. (2021). In line with a study by Sitepu et al. (2021), ISR in six PPKS varieties of eight years old palms ranged from 53.2% and 73.0%, indicating a sufficient availability of pollen for pollination.

TABLE 6. VARIANCE COMPONENT, HERITABILITY AND GENOTYPIC COEFFICIENT OF VARIATIONS FOR FEMALE AND MALE INFLORESCENE

Description	σ_g^2	σ_e^2	σ_p^2	h_b^2 (%)	GCV (%)
Female flowering phases					
(159–501) Spear leaf 70.0% open to inflorescence visible in axil	665.4	3,258.0	3,923.4	17.0	8.2
(501–601) Inflorescence visible in axil to pre-anthesis	12.9	412.1	425.1	3.1	8.6
(601–607) Pre-anthesis to anthesis	0.4	25.9	26.3	1.3	5.0
(607–807) Anthesis to ripening of fruit	539.3	5,885.4	6,424.7	8.4	9.5
(159–807) Spear leaf 70.0% open to ripening of fruit	1,053.0	3,498.0	4,551.0	23.1	5.3
Male flowering phases					
(159–501) Spear leaf 70% open to inflorescence visible in axil	2,723.0	6,576.0	9,299.0	29.3	18.0
(501–601) Inflorescence visible in axil to pre-anthesis	40.4	442.8	483.2	8.4	16.2
(601–607) Pre-anthesis to anthesis	1.9	24.5	26.5	7.4	10.9
(607–609) Anthesis to end of flowering	0.5	6.0	6.5	7.1	6.1
(159–607) Spear leaf 70.0% open to anthesis	2,129.0	6,799.0	8,928.0	23.8	13.5

Note: σ_g^2 - genotypic variance; σ_e^2 - error variance; σ_p^2 - phenotypic variance; h_b^2 - broad-sense heritability; GCV - genotypic coefficient of variation.

TABLE 7. ANALYSIS OF VARIANCE AND GENETIC COMPONENTS FOR INFLORESCENE PRODUCTION TRAIT AND SEX RATIO

Trait	Mean ± SE	MSG	MSR	MSE	σ_g^2	σ_e^2	σ_p^2	h_b^2 (%)
FF	13.0 ± 0.3	714.1**	183.2**	14.5	3.2	14.5	17.7	18.4
MF	7.4 ± 0.3	1,975.8**	89.8**	21.5	9.3	21.5	30.8	30.3
HF	0.2 ± 0.1	8.7**	2.5**	0.5	0.1	0.5	0.6	6.5
ISR	64.2 ± 2.8	289.5	61.3	3.3	1.3	3.5	4.6	29.2

Note: MF - male flower; FF - female flower; HF - hermaphrodite; ISR - sex ratio; MSG - mean square genotype; MSR - mean square replicate; MSE - mean square error; σ_g^2 - genotypic variance; σ_e^2 - error variance; σ_p^2 - phenotypic variance; h_b^2 - broad sense heritability.

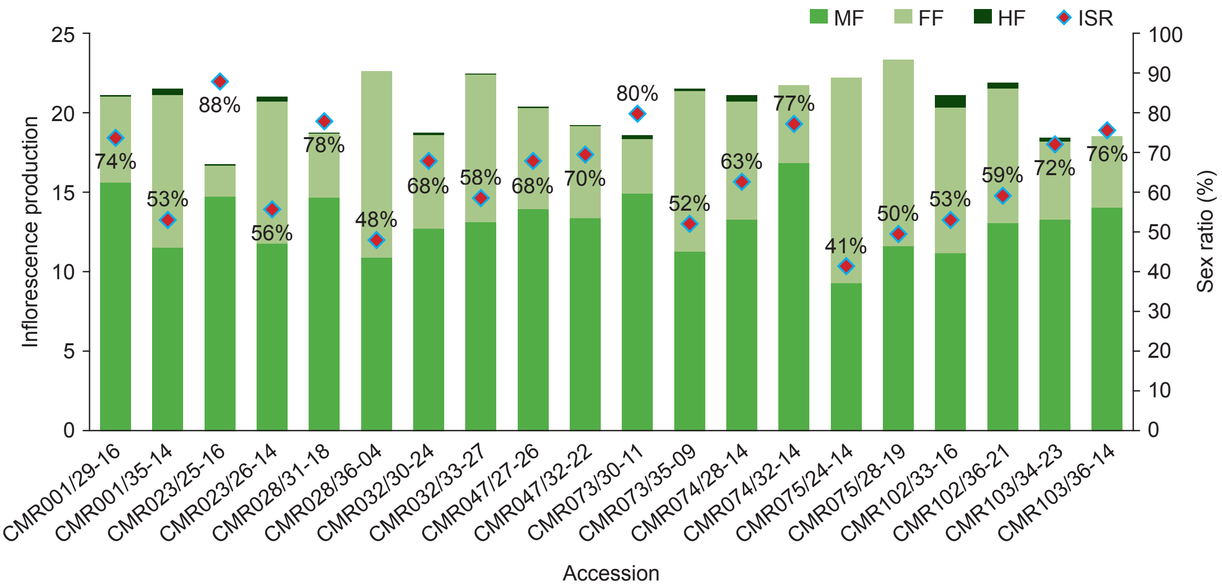

Figure 2. Performance of 20 Cameroon accession palms for female flower (FF), male flower (MF), hermaphrodite (HF) and sex ratio (ISR).

Genetic Distance Analysis on Flowering Phases and Flower Production Traits

Genetic distance and genetic variability analysis are the methods to understand the genetic characteristics of oil palm (Faizah et al., 2016). In this study, the evaluation of genotypic variability based on phenological traits was carried out through cluster analysis using Ward's coefficient and Gower's method. The results divided the twenty accessions from Cameroon into two main groups (*Figure 3*). Group 1 (green colour) comprises nine accessions that has a longer period of inflorescence except for CMR028/36-4 with a similarity of 13.0%–47.0%. The accessions in Group 2 (red colour) displays a relatively shorter period of inflorescence with a genetic similarity level of 10.0%–53.0%. The results of this study differ from a study conducted by (Sujadi et al., 2019b) on the same accessions using morphological traits, where the genetic distance was divided into three main groups with a degree of dissimilarity of 19.0%. Cluster analysis using molecular markers on Cameroon accessions (with different numbers of accessions) was also reported in several studies, with the results of genetic similarity ranging from 52.0% to 87.0% (Tasma & Arumsari, 2013) and 42.5% to 67.5% (Santosa et al., 2015). Information related to group analysis based on the inflorescence phase characteristics of oil palm is still limited. Therefore, the findings of this study provide a significant contribution to further understanding the genetic variability of oil palm, particularly in the context of the inflorescence phase.

Based on cluster analysis, it is known that accessions from different origins show neighbourhoods to other accessions (*Figure 3*). In both Group 1 and Group 2, accessions from different origins are represented, indicating that the same accession is not consistently assigned to a single group. In line with a study by Salim et al. (2023), Cameroon accessions palm clustering pattern differed based on geographical location, as populations from different locations are randomly distributed. Although the accessions have the same origin palm number, the accession palm are derived from different seeds, so they are assumed to be non-identical. It can be caused by the high level of genetic exchange through seed dispersal (Arias et al., 2013). Santosa et al. (2015) added the possibility that pollen carried by wind or insects comes from different palm, so they have different genomic structures. Therefore, the consideration of genotype selection with precocious characters should be based on individual palm among Cameroon accessions.

CONCLUSION

This study on genetic variability and distance analysis provides valuable insights into the genetic characteristics of oil palm accessions from Cameroon, particularly concerning phenological traits. The study indicated that Cameroon accessions are not precocious genotypes. Early developmental stages and fruit ripening suggest strong environmental influences, while genetic effects at specific stages indicate substantial diversity among accessions. However, there are traits with high h^2_b and GCV in the early stage of inflorescence that show strong genetic control and variability, making them ideal for selection. Agronomic field improvement is recommended to

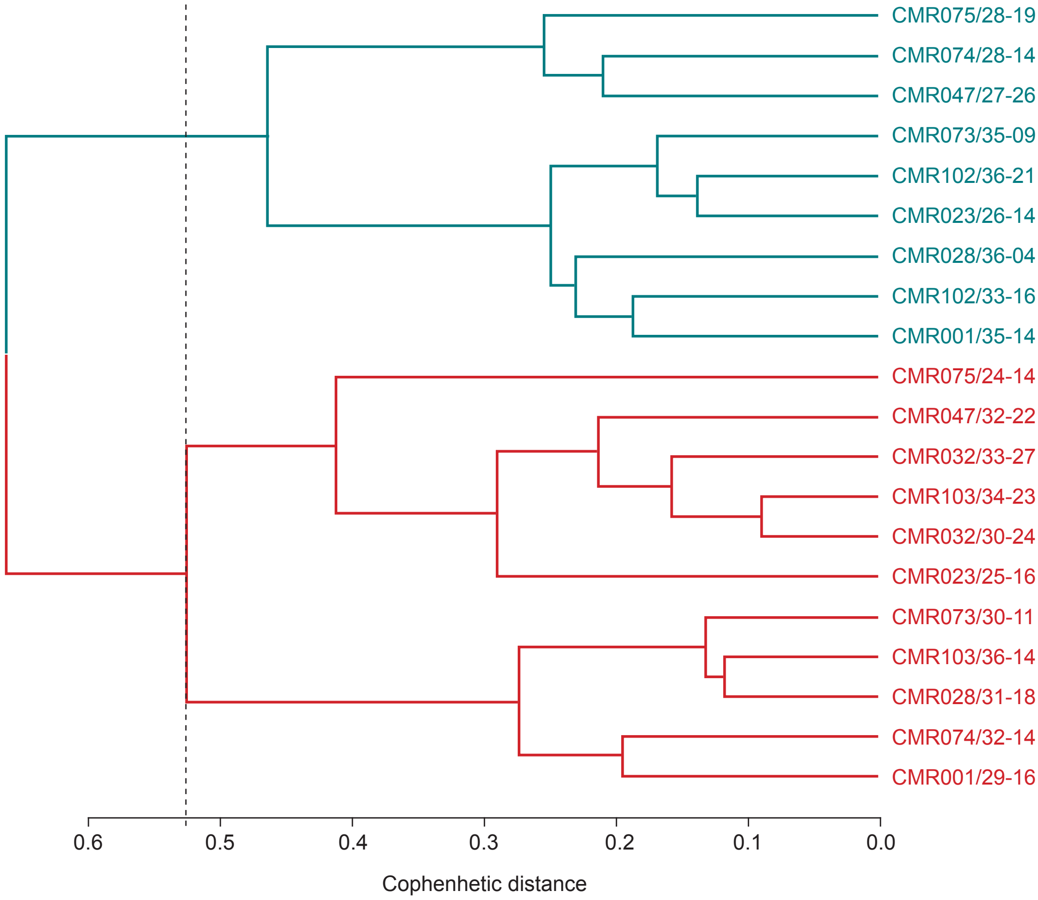

Figure 3. Genetic distance between 20 Cameroon accession palms according to Ward's coefficient.

improve the performance of these traits. Therefore, it is necessary to carry out further research on the other genotypes to compare with this research and investigate the phenology of these accessions on different climates conditions is essential to assess environmental impacts.

ACKNOWLEDGEMENT

The author wishes thank to the Indonesian Oil Palm Research Institute (IOPRI) for funding this research. We also thank all parties in helping to prepare the article.

REFERENCES

Abdullah, S. N. A., Azzeme, A. M., Ebrahimi, M., Ariff, E. A. K. E., & Hanifiah, F. H. A. (2017). Transcription factors associated with abiotic stress and fruit development in oil palm. In S. N. A. Abdullah, C. L. Ho, & C. Wagstaff, (Eds.), *Crop improvement: Sustainability through leading-edge technology* (pp. 71-99). Springer. https://doi.org/10.1007/978-3-319-65079-1_4

Adam, H., Collin, M., Richaud, F., Beulé, T., Cros, D., Omoré, A., Nodichao, L., Nouy, B., & Tregear, J. W. (2011). Environmental regulation of sex determination in oil palm: Current knowledge and insights from other species. *Annals of Botany*, *108*(8), 1529–1537. https://doi.org/10.1093/aob/mcr151

Adhikari, B. N., Shrestha, J., Dhakal, B., Joshi, B. P., & Bhatta, N. R. (2018). Agronomic performance and genotypic diversity for morphological traits among early maize genotypes. *International Journal of Applied Biology*, 2(2), 33–43. https://doi.org/10.20956/ijab.v2i2.5633

Arias, D., Montoya, C., & Romero, H. (2013). Molecular characterization of oil palm (*Elaeis guineensis* Jacq.) materials from Cameroon. *Plant Genetic Resources*, *11*(2), 140–148. https://doi.org/10.1017/s1479262112000482

Arifin, A. A., Foster, G. & Low, E. (2014). Maximising hydrolysis of sugar (gum/hemicellulose) that binds fruits to stalk and cell to cell; ensure greater detachment of fruits from stalk and very low viscosity pressed crude that enhances separation of oil during clarification.

Proceeding of International Oil Palm Conferences 2014, Bali, Indonesia.

Burton, G. W. (1952). Quantitative inheritance in grasses. *Proceeding of 6th International Grassland Congress, 1*, 277–283.

Corley, R. H. V., & Tinker, P. B. (2015). *The oil palm.* John Wiley & Sons. https://doi.org/10.1002/9781118953297

De Mendiburu, F. (2019). *Agricolae: Statistical procedures for agricultural research.* (R Package version 1.3-1) [Computer software].

Devesh, P., Moitra, P. K., Shukla, R. S., Shukla, S. S., Pandey, S., & Arya, G. (2018). Analysis of variability, heritability and genetic advance of yield, its components and quality traits in wheat. *International Journal of Agriculture Environment and Biotechnology*, *Special Issue*, 855–859.

Faizah, R., Wening, S., Rahmadi, H. Y., & Purba, A. R. (2016). Keragaman genetik populasi *E. oleifera* dan populasi *E. guineensis* x *E. oleifera* pada koleksi plasma nutfah PPKS. [Genetic variation of *E. oleifera* and *E. guineensis* x *E. oleifera* population of IOPRI's oil palm germplasm]. *Jurnal Penelitian Kelapa Sawit*, *24*(1), 13–22. https://doi.org/10.22302/iopri.jur.jpks.v24i1.3

Forero, D. C., Hormaza, P., & Romero, H. M. (2012). Phenological growth stages of African oil palm (*Elaeis guineensis*). *Annals of Applied Biology*, *160*(1), 56–65. https://doi.org/10.1111/j.1744-7348.2011.00520.x

Hanson, C. H., Robinson, H. F., & Comstock, R. E. (1956). Biometrical studies of yield in segregating populations of Korean lespedeza. *Agronomy Journal*, *48*(6), 268–272. https://doi.org/10.2134/agronj1956.00021962004800060008x

Harahap, I. Y., & Lubis, M. E. S. (2018). Dinamika air dan fase-fase perkembangan pembungaan penentu produktivitas kelapa sawit [Water dynamics and flowering phases that determines oil palm yield]. *Jurnal Penelitian Kelapa Sawit*, *26*(3), 101–112. https://doi.org/10.22302/iopri.jur.jpks.v26i3.64

Henderson, C. R. (1985). Best linear unbiased prediction of nonadditive genetic merits in noninbred populations. *Journal of Animal Science*, *60*(1), 111–117. https://doi.org/10.2527/jas1985.601111x

Hernawati, R., Wikantika, K., & Darmawan, S. (2022). Modeling of oil palm phenology based on remote sensing data: Opportunities and challenges. *Journal of Applied Remote Sensing*, *16*(02), 021501. https://doi.org/10.1117/1.jrs.16.021501

Johnson, H. W., Robinson, H. F., & Comstock, R. E. (1955). Estimates of genetic and environmental variability in soybeans. *Agronomy Journal*, *47*(7), 314–318. https://doi.org/10.2134/agronj1955.00021962004700070009x

Legros, S., Mialet-Serra, I., Caliman, J., Siregar, F. A., Clément-Vidal, A., & Dingkuhn, M. (2009). Phenology and growth adjustments of oil palm (*Elaeis guineensis*) to photoperiod and climate variability. *Annals of Botany*, *104*(6), 1171–1182. https://doi.org/10.1093/aob/mcp214

Li-Hammed, M. A., Kushairi, A., Rajanaidu, N., Mohd Sukri, H., Che Wan Zanariah, C. W. N., & Jalani, B. S. (2015). Multivariate analysis of vegetative and physiological traits in oil palm (*Elaies guineensis* Jacq.) germplasm. *Expert Opinion on Environmental Biology*, *4*(3), 1–5. https://doi.org/10.4172/2325-9655.1000120

Lubis, K., Sutjahjo, H. S., Syukur, M., & Trikoesoemaningtyas, (2014). Pendugaan parameter genetik dan seleksi karakter morfofisiologi galur jagung introduksi di lingkungan tanah masam. [Genetic parameter estimates and selection of morpho-physiological characters among introduced maize inbred lines on acid soil]. *Jurnal Penelitian Pertanian Tanaman Pangan*, *33*(2), 122–128.

Maskromo, I., Natawijaya, A., Djufry, F., & Syakir, D. M. (2017). Variabilitas genetik plasma nutfah kelapa sawit asal Angola dan seleksi genotipe berbasis famili dan individu untuk pembentukan breeding population baru. [Genetic variability of oil palm germplasm from Angola and genotype selection based on family and individual performance for formation a new breeding population]. *Buletin Palma*, *18*(1), 43–51.

Moreno, L. P., & Romero, H. M. (2015). Phenology of the reproductive development of *Elaeis oleifera* (Kunth) Cortes. *Agronomía Colombiana*, *33*(1), 36–42. https://doi.org/10.15446/agron.colomb.v33n1.47199

Mubarok, H., Ahmad, F., Tambusai, M. N., Hidayat, A. N., & Harahap, I. A. (2022). Fenologi kelapa sawit dan hubungannya dengan curah hujan dan kedalaman muka air di lahan gambut. [Oil palm phenology and its relationship to rainfall and water table depth in peatlands]. *Agrosains: Jurnal Penelitian Agronomi*, *24*(2), 111–118.

Paterson, R. R. M., Kumar, L., Taylor, S., & Lima, N. (2015). Future climate effects on suitability for growth of oil palms in Malaysia and Indonesia. *Scientific Reports*, *5*(1), 14457. https://doi.org/10.1038/srep14457

Pradiko, I., Sujadi, & Rahutomo, S. (2019). Pengamatan fenologi pada delapan varietas kelapa sawit (*Elaeis guineensis* Jacq.) menggunakan konsep thermal unit [Phenological observation on eight oil palm (*Elaeis guineensis* Jacq.) varieties using thermal unit concept]. *Jurnal Penelitian Kelapa Sawit*, *27*(1), 57–69. https://doi.org/10.22302/iopri.jur.jpks.v27i1.71

Razali, M. H., Somad, A., Halim, M. A., & Roslan, S. (2012). A review on crop plant production and ripeness forecasting. *International Journal of Agriculture and Crop Sciences*, *4*(2), 54–63.

Salim, W. N. S. T. M., Yaakub, Z., Mustaffa, S., Bakar, N. A. A., Nasir, F. M., Marjuni, M., Amiruddin, M. D., & Ong-Abdullah, M. (2023). Genetic variability of MPOB-Cameroon oil palm germplasm based on morphological traits using multivariate analysis. *Journal of Oil Palm Research*, *35*(3), 476–490. https://doi.org/10.21894/jopr.2022.0038

Santosa, B., Prasetiyono, J., Dadang, A., Pandin, D. S., Rachmadi, M., & Manambangtua, A. P. (2015). Analisis keragaman 35 aksesi kelapa sawit (*Elaeis guineensis* Jacq.) asal Kamerun berdasarkan karakter produksi awal menggunakan marka SSR [Diversity analysis of 35 oil palm accessions (*Elaeis guineensis* Jacq.) originated from Cameroon based on early production character by using SSR markers]. *Buletin Palma*, *16*(2), 183–194.

Sarimana, U., Pradipta, A., Herrero, J., Wendra, F., Zulhermana, S., & Asmono, D. (2017, October 2–3). *Genetic diversity of oil palm from Cameroon exploration at PT. Binasawit Makmur* [Poster presentation]. International and National Seminar of PERIPI (Indonesian Breeding Science Society), Bogor, Indonesia. https://doi.org/10.13140/RG.2.2.12048.87042

Sayekti, U., Widyastuti, U., & Toruan-Mathius, N. (2015). Keragaman genetik kelapa sawit (*Elaeis guineensis* Jacq.) asal Angola menggunakan marka SSR [Genetic diversity of the Angola-originated oil palm (*Elaeis guineensis* Jacq.) using SSR markers]. *Jurnal Agronomi Indonesia*, *43*(2), 140–146. https://doi.org/10.24831/jai.v43i2.10420

Sitepu, A., Yenni, Y., & Sujadi, N. (2021). Mengenal fenomena feminin pada kelapa sawit (*Elaeis guineensis* Jacq.) [Understanding the feminine phenomenon in oil palm (*Elaeis guineensis* Jacq.)]. *WARTA Pusat Penelitian Kelapa Sawit*, *26*(3), 154–161. https://doi.org/10.22302/iopri.war.warta.v26i3.65

Sivasubramaniam, S., & Madhava Menon, P. (1973). Genotypic and phenotypic variability in rice. *Madras Agricultural Journal*, *60*(9), 1093–1096.

Suharyanti, N. A., Mizuno, K., & Sodri, A. (2020). The effect of water deficit on inflorescence period at palm oil productivity on peatland. *E3S Web of Conferences*, *211*, 05005. https://doi.org/10.1051/e3sconf/202021105005

Sujadi, S., Pradiko, I., Rahutomo, S., & Farrasati, R. (2020). Prediksi kemampuan adaptasi delapan varietas kelapa sawit pada cekaman abiotik akibat perubahan iklim global [Prediction of adaptability of eight oil palm varieties under abiotic stresses as impact of global climate change]. *Jurnal Tanah dan Iklim*, *44*(2), 129–139.

Sujadi, S., Supena, N., & Lubis, M. I. (2017). Karakter pemuliaan penting pada 35 Aksesi Angola di kebun koleksi plasma nutfah Pusat Penelitian Kelapa Sawit [Important breeding characteristic of 35 Angola accession in Indonesian Oil Palm Research Institute]. In B. Waluyo & D. Saptadi (Eds.), *Prosiding Seminar Nasional Peripi Komda Jatim 2017*. Fakultas Pertanian Universitas Brawijaya.

Sujadi, S., Supena, N., & Suprianto, E. (2019a). Karakteristik perkembangan bunga dan buah 35 aksesi Angola koleksi Pusat Penelitian Kelapa Sawit di Kebun Adolina PT Perkebunan Nusantara IV [Characteristics of flower and fruit development of 35 Angola accessions of Indonesian Oil Palm Research Institute's collection at Adolina Estate of PT Perkebunan Nusantara IV]. *Jurnal Penelitian Kelapa Sawit*, *27*(2), 97–114. https://doi.org/10.22302/iopri.jur.jpks.v27i2.76

Sujadi, S., Wandita, T. S., Supena, N., & Yenni, Y. (2019b). Jarak genetik 47 aksesi plasma nutfah kelapa sawit (*Elaeis guineensis* Jacq.) asal Kamerun berdasarkan karakter morfologi [Genetic distance of 47 accessions of oil palm (*Elaeis guineensis* Jacq.) germplasm from Cameroon based on morphological character]. *Jurnal Penelitian Kelapa Sawit*, *27*(1), 25–40. https://doi.org/10.22302/iopri.jur.jpks.v27i1.70

Suresh, K., Behera, S. K., Manorama, K., & Mathur, R. K. (2021). Phenological stages and degree days of oil palm crosses grown under irrigation in tropical conditions. *Annals of Applied Biology*, *178*(1), 121–128. https://doi.org/10.1111/aab.12641

Swaray, S., Rafii, M. Y., Amiruddin, M. D., Ismail, M. F., Jamian, S., Marjuni, M., & Mohamad, M. M. (2021). Study on yield variability in oil palm progenies and their genetic origins. *Biology and Life Sciences Forum*, *4*(1), 68.

Tasma, I. M., & Arumsari, S. (2013). *A*nalisis diversitas genetik aksesi kelapa sawit Kamerun berdasarkan marka SSR [Genetic diversity analysis of the Cameroon-originated oil palm accessions assessed with SSR markers]. *Jurnal Littri*, *19*(4), 194–202.

Trimanto; Pitaloka, D. A., & Metusala, D. (2020). Karakterisasi morfologi dan fenologi pembungaan dua aksesi *Kopsia pauciflora* Hook.f. bunga putih dan merah muda di Kebun Raya Purwodadi, Jawa Timur [Morphological and phenological characterization of two accessions of white and pink flowers of *Kopsia pauciflora* Hook.f. in Purwodadi Botanic Garden, East Java]. *Buletin Plasma Nutfah*, *26*(2), 77–88.

Yaakub, N. Z. Z., Shaipulah, N. F. M., Mohamed, N. Z., & Idrus, A. M. (2023). Flower development of male and female inflorescence of oil palm, *Elaeis guineensis* Jacq. *Universiti Malaysia Terengganu Journal of Undergraduate Research*, *5*(4), 89–97. https://doi.org/10.46754/umtjur.v5i4.440

Journal of Oil Palm Research Vol. 38 (3) September 2026 p. 545–558
DOI: https://doi.org/10.21894/jopr.2025.0040

CONSERVED TRANSCRIPTIONAL RESPONSES TO SALT AND WATER STRESS IN OIL PALM (*Elaeis guineensis* Jacq.) LEAF TISSUES

FERNANDA FERREIRA SALGADO[1]; THALLITON LUIZ CARVALHO DA SILVA[1]; ANDRÉ PEREIRA LEÃO[2]; ROBERTO COITI TOGAWA[3]; CARLOS ANTÔNIO FERREIRA DE SOUSA[4]; PRISCILA GRYNBERG[3] and MANOEL TEIXEIRA SOUZA JÚNIOR[1,2,*]

ABSTRACT

*Abiotic stresses negatively impact oil palm (*Elaeis guineensis *Jacq.) cultivation. Transcription factors (TFs) are essential proteins regulating gene expression in plants. While numerous TF gene families are implicated in plant responses to abiotic stress, their specific roles in oil palm's drought and salinity responses remain largely unexplored. This study aimed to get insights into the TFs' involvement in the oil palm's response to these stresses. Twenty TF genes, classified into four families (MYB, HD-ZIP, NF-Y and HSFF) and exhibiting strong co-expression under both salinity and drought conditions, were selected for in-depth analysis. Such behaviour suggests a shared regulatory mechanism for abiotic stress responses. Promoter analysis revealed the presence of known stress-responsive *cis*-regulatory elements, while sequence homology analysis indicated functional conservation with stress-tolerance genes in other plants. Quantitative real-time PCR (qRT-PCR) validated RNA-Seq expression profiles for 19 of the 20 selected genes. While these findings offer promising avenues for genetic modification, a cautious approach is necessary. Understanding the complex regulatory networks of these TFs and their potential side effects is crucial to avoid unintended consequences. Future study should focus on the functional validation of these TFs and integrate this knowledge with potential inherent tolerance mechanisms to develop resilient oil palm cultivars.*

Keywords: abiotic stress, drought, salinity, tolerance, transcriptome.

Received: 27 May 2024**; Accepted:** 8 May 2025**; Published online:** 11 August 2025.

INTRODUCTION

Palm oil reigns supreme as the world's leading vegetable oil, with consumption in 2022–2023 reaching a staggering 85 million tonnes. This dwarfs the output of soybean (60.0 million tonnes), rapeseed (31.0 million tonnes) and sunflower seed oil (18.5 million tonnes) (Statista, 2024). Despite possessing millions of hectares suitable for oil palm (*Elaeis guineensis* Jacq.) cultivation, Brazil's 2022 harvest only reached around 200,000 ha, ranking it 10th globally and contributing less than 1% of the world's production (Foreign Agricultural Services [FAS], 2024). A whopping 93% of its plantations are concentrated within the Legal Amazon Area, primarily in the Northeastern region of the Pará State (Instituto Brasileiro de Georgrafia e Estatistica [IBGE], 2024). Expanding oil palm cultivation in Brazil presents a dilemma: Continue operating within the Amazon Biome, with its abundant year-round rainfall, or venture into drier climates that present significant challenges.

Oil palm thrives in constant moisture, but Brazil's Midwest and Northeast regions experience

[1] Graduate Program of Plant Biotechnology, Federal University of Lavras (UFLA), Lavras, Minas Gerais (MG), Brazil.

[2] Embrapa Agroenergy, Brasília, Distrito Federal (DF), Brazil.

[3] Embrapa Genetic Resources and Biotechnology, Brasília, Distrito Federal (DF), Brazil.

[4] Embrapa Mid-North, Teresina, Piauí (PI), Brazil.

* *Corresponding author e-mail: manoel.souza@embrapa.br*

extended droughts. Therefore, irrigation is required for oil palm to succeed in these regions. These trees require around 2,000 mm of water annually and become vulnerable after just 90 days without water (Corley et al., 2018). The Cerrado Savanna in Brazil's Midwest have dry winters, and the Northeast is semi-arid, leading to water scarcity and a concerning trend: Soil salinisation. As water evaporates, salts accumulate in the soil, harming plants and threatening sustainability. This is not unique to Brazil; globally, 30% of irrigated land suffers from salinity, with projections reaching over 50% by 2050 (Ivushkin et al., 2019; Machado & Serralheiro, 2017; Shahid et al., 2018; Zaman et al., 2018).

Plants exhibit remarkable adaptive capabilities in response to abiotic stresses such as drought and salinity, primarily mediated by the intricate gene regulatory networks operating at the transcriptional and post-transcriptional levels (Angon et al., 2022; Wang et al., 2022). Transcription factors (TFs), constituting a substantial portion of the plant genome (7%–10%) (Wang et al., 2019), function as pivotal regulators in orchestrating plant stress responses (Zhang et al., 2022). These proteins, organised into diverse families, regulate the expression of downstream genes to enhance stress tolerance (Javed et al., 2020; Wang et al., 2022). Specifically, stress-inducible transcription factors from the MYB, WRKY, bZIP and AP2/ERF families are known to be pivotal for plant resilience against various environmental stresses (Chaudhari et al., 2023; Hajyzadeh et al., 2015; He et al., 2018). Notably, the HD-Zip family, a large and plant-specific group of TFs, has been implicated in both plant growth and stress responses (Belamkar et al., 2014; Bhattacharjee et al., 2016; Gong et al., 2019; Sharif et al., 2021). Overexpression of HD-Zip TFs has been shown to enhance drought tolerance (Dezar et al., 2005; Gong et al., 2019; Jiao et al., 2022) and confer resistance to combined drought and salt stress conditions (Zhao et al., 2014).

Building on the work of Vieira et al. (2020) and Salgado et al. (2021, 2022), this study further investigates the transcriptomic response of young oil palms to abiotic stresses. Their large-scale analyses using miRNA and RNA-Seq elucidated responses to high salinity and water deprivation, respectively. This study focuses on the crucial role of TF in early stress responses. By comprehensively analysing all differentially expressed TF genes, not just those targeted by miRNAs, it expands on these prior works. This approach provides a more complete understanding of TF families and their constituent genes commonly affected by both stresses. Twenty TF genes representing distinct families were chosen for structural and functional annotation, along with their promoter sequences. Subsequent qRT-PCR analysis validates their expression patterns under both salinity and water deficit conditions.

MATERIALS AND METHODS

RNA-Seq Data Generation

The raw RNA sequencing (RNA-Seq) data used in this study are publicly available in the Sequence Read Archive (SRA) database at the National Center for Biotechnology Information (NCBI) under BioProject ID PRJNA573093 and BioSample ID SAMN12799239.

For details on plant material, growth conditions and stress treatments, refer to Bittencourt et al. (2022), Leão et al. (2022), Salgado et al. (2021, 2022) and Vieira et al. (2020). In brief, experiments were conducted in a greenhouse at Embrapa Agroenergia, Brasília, Brazil (15° 43′ 55.2″ S, 47° 54′ 00.0″ W). Young bifid saplings received the treatments. Oil palm clones, regenerated from embryogenic callus derived from adult AM33 genotype leaves, were used. Apical leaves from control and stressed plants were collected after 12 days of salinity stress or 14 days of drought stress. Salinity treatments included a control (0.0 g NaCl/100 g substrate) and a stressed group (2.0 g NaCl/100 g substrate). Drought treatments consisted of a control (field capacity) and a stressed group (water withheld). Three replicates were collected per treatment. Plant tissue was immediately frozen in liquid nitrogen and stored at –80°C until RNA extraction, library preparation, and sequencing. Total RNA isolation, quality and quantity analysis followed the methods described by Salgado et al. (2021, 2022). RNA sequencing (RNA-Seq) was outsourced to GenOne Company (Brazil) using an Illumina HiSeq platform with a paired-end strategy.

RNA-Seq Data Analysis

RNA-Seq analyses, performed using OmicsBox version 1.3, are detailed in Salgado et al. (2021, 2022). Briefly, high-quality RNA-Seq reads were mapped to the oil palm reference genome (Singh et al., 2013) downloaded from NCBI (BioProject PRJNA192219; BioSample SAMN02981535) in March and October 2020. The mapping used the default settings of STAR software (Dobin et al., 2013) within OmicsBox version 1.3. Gene expression levels were quantified using HTSeq v0.9.0 (Anders et al., 2015) with default parameters within OmicsBox v1.3. Differential expression analysis between control and stressed samples was performed using edgeR v3.28.0 (Robinson et al., 2010). This study employed a simple experimental design with an exact statistical test in edgeR. No filters for low-count genes were applied.

Genes Selection and Annotation

This study unveils TF potentially critical for stress response in young oil palm. Building upon the work of Salgado et al. (2021, 2022) who identified differentially expressed genes (DEGs) through functional annotation using GhostKOALA (Kanehisa et al., 2016), this study employed a multi-step approach to pinpoint TF potentially involved in the young oil palm's stress response: a) Relevant scientific literature was reviewed to identify key plant transcription factor families associated with stress responses; b) the DEGs were filtered to retain only those belonging to the pre-selected TF families; c) this list was further refined by selecting DEGs that exhibited differential expression under both salinity and drought stress conditions; and d) finally, genes displaying the most significant positive or negative regulation in response to stress were prioritised for further analysis.

Intron and exon data were retrieved from National Center for Biotechnology Information (NCBI) (Sayers et al., 2022). Promoter sequences (1,432 bp upstream of ATG) for each gene were extracted from the oil palm reference genome (Singh et al., 2013). The PlantCARE database (Lescot, 2002) identified known *cis*-elements with a significance threshold (Score ≤ 5). Additionally, MEME software (Bailey et al., 2015) identified potential TF binding motifs within promoters, retaining only those with a statistically significant E-value ≤ 0.05.

Protein sequences were retrieved from the oil palm reference genome (Singh et al., 2013). Only statistically significant domains (E-value ≤ 1) were retained after analysis using NCBI Conserved Domain Search. Functional annotation was performed using EggNOG (Huerta-Cepas et al., 2019). Multiple sequence alignments (protein and promoter regions) were generated with Clustal W (Thompson et al., 1994). Phylogenetic trees were constructed using the maximum likelihood method with 1,000 bootstrap replicates in MEGA11 (Tamura et al., 2021). DNA Features Viewer (Zulkower & Rosser, 2020) generated figures for *cis*-element analysis results (motifs), protein domains and intron/exon regions.

RNA Extraction, Reverse Transcriptase-PCR and Quantitative Real-Time PCR Analyses

Total RNA isolation, quality and quantity analyses were performed as described by Salgado et al. (2021, 2022). Following quantification, the isolated RNA was used as a template for cDNA synthesis using the SuperScript® IV Reverse Transcriptase kit (Invitrogen, USA) according to the manufacturer's instructions. The positive control gene was *EgEfMPOB00119*, encoding the constitutive 40S ribosomal protein S23 mRNA in *E. guineensis*.

FASTA sequences for the selected genes were downloaded from NCBI and imported into PerlPrimer software for primer design. qRT-PCR reactions were performed in 96-well plates on a 7,500 real-time PCR system (Applied Biosystems, USA) using PowerUp™ SYBR™ Green Master Mix (Thermo Fisher Scientific, USA) according to the manufacturer's protocol. The reaction conditions were: 50°C for 2 min, 95°C for 2 min, followed by 40 cycles of 95°C for 5 s and 60°C for 30 s. A melting curve analysis was performed to confirm amplicon specificity. Three biological replicates were performed for each sample. The expression level of the untreated control sample was set to 1 for normalisation. The qRT-PCR data analysis was done using the $2^{-\Delta\Delta CT}$ method (Rao et al., 2013).

Pair-by-Pair Comparison and Correlation Analysis

A pairwise correlation analysis was performed to compare gene expression changes identified by RNA-Seq and qRT-PCR for DEGs under both salinity and drought stress conditions. Log_2 (fold change) values from each method were used as input data for the analysis.

RESULTS AND DISCUSSION

Although roots are the primary sensors of salinity and drought stress, this study prioritised leaf tissue for molecular analysis due to the challenges associated with root sample preparation and the initial focus on morphophysiological parameters. Despite the potential for distinct responses in roots, the presented findings offer valuable insights into the molecular mechanisms underlying leaf adaptation to these abiotic stresses.

Selection of Putative Transcription Factors Responsive to Drought and Salinity Stresses

Employing the GhostKOALA annotation platform (Kanehisa et al., 2016), the current study identified 36 and 19 TF families exhibiting differential expression in response to drought and salinity stress, respectively. Eighteen of these families were commonly affected by both stress conditions (data not shown). Building on previous identification of stress-responsive miRNAs potentially regulating TFs (Salgado et al., 2021, 2022), as well as in the transcriptome profiles of oil palm under both stresses (Bittencourt et al., 2022; Leão et al., 2022), a subset of 20 DEGs from four TF families was selected for further analysis (*Table 1*).

TABLE 1. PROFILE OF TRANSCRIPTION FACTOR (TF) GENES FROM THE LEAF OF OIL PALM PLANTS DIFFERENTIALLY EXPRESSED UNDER SALT AND WATER STRESS ACCORDINGLY TO RNA-Seq AND qPCR ANALYSES, FOLD CHANGE (FC), LOG_2 (FC) AND FALSE DISCOVERY RATE (FDR)

Gene #	Gene ID	Protein ID	TF family	Salt stress			Drought stress		
				RNA-Seq		qPCR	RNA-Seq		qPCR
				Log_2 (FC)	FDR	Log_2 (FC)	Log_2 (FC)	FDR	Log_2 (FC)
01	LOC105032141	XP_010904805.1	MYB	2.064	0.000	1.895	5.650	0.000	3.113
02	LOC105033230	XP_010906239.1	MYB	–3.259	0.000	–5.059	–4.404	0.000	–5.059
03	LOC105038205	XP_010912232.1	HSF	–2.665	0.000	–1.184	–2.762	0.000	–0.971
04	LOC105039680	NP_001306836.1	NFY-C	2.121	0.000	–0.943	4.228	0.000	–1.690
05	LOC105040563	XP_010915439.1	HSF	1.213	0.000	1.459	3.530	0.000	1.803
06	LOC105040719	XP_010915677.1	MYB	–3.141	0.000	–1.358	–2.490	0.000	–2.059
07	LOC105041192	XP_010916352.1	MYB	–2.226	0.000	–2.556	–1.629	0.000	–1.152
08	LOC105044046	XP_010920127.1	MYB	–2.454	0.000	–3.322	–2.430	0.000	–2.322
09	LOC105048425	XP_010926024.1	MYB	2.817	0.000	3.276	4.536	0.000	2.759
10	LOC105048648	XP_010926338.1	HD-ZIP	–0.832	0.016	–0.737	–3.068	0.000	–2.396
11	LOC105048799	XP_010926549.1	MYB	0.831	0.029	1.485	3.214	0.000	2.373
12	LOC105053150	XP_019708739.1	HD-ZIP	1.405	0.027	1.070	–1.798	0.007	–1.690
13	LOC105053200	XP_010932583.1	MYB	1.823	0.001	1.844	–1.552	0.001	–1.737
14	LOC105053827	XP_010933430.1	MYB	1.455	0.022	0.774	3.319	0.000	0.748
15	LOC105053827	XP_010933626.2	HD-ZIP	1.127	0.024	1.736	2.140	0.000	1.118
16	LOC105055678	XP_010935898.1	MYB	3.378	0.000	2.134	3.974	0.000	1.915
17	LOC105056442	XP_010936941.1	MYB	–4.104	0.000	–5.059	–2.942	0.000	–4.059
18	LOC105056443	XP_010936942.1	MYB	–1.926	0.002	–2.252	–2.513	0.000	–3.644
19	LOC105058320	XP_010939500.1	MYB	1.904	0.000	1.220	2.387	0.000	1.480
20	LOC105058124	XP_010939223.1	NFY-B	–0.746	0.002	–0.059	–0.908	0.000	–0.644

Note: Protein (Super)Families: MYB - Myb transcription factor, plants (IPR015495); HD-ZIP - Homeobox-leucine zipper protein, class I, plant (IPR045224); NFY - Histone Fold (IPR009072) - Transcription factor CBF/NF-Y/archaeal histone domain (IPR003958); HSF - Heat Shock Transcrition Factor (PTHR10015).

This subset comprised 13 MYB (Ambawat et al., 2013), three HD-ZIP (Chen et al., 2014), two HSFs (Guo et al., 2016), two NF-Y from Histone Fold Motif family (IPR009072) members (Stephenson et al., 2007). Salinity stress significantly upregulated eleven genes and downregulated nine, while drought stress upregulated nine genes and downregulated eleven (*Table 1*). A total of 18 of the 20 genes exhibited similar qualitative responses to both stresses. However, gene 13 and 14 displayed contrasting qualitative responses, being upregulated under salt stress and downregulated under drought stress.

Soil salinity and water deficit, imposing severe constraints on crop growth, constitute significant environmental challenges (Qin et al., 2011). In response, plants activate intricate signalling cascades, encompassing both abscisic acid (ABA)-dependent and -independent pathways (Yamaguchi-Shinozaki et al., 2007). Transcription factors serve as pivotal regulators within these pathways, modulating stress tolerance. These proteins orchestrate the expression of genes involved in osmotic homeostasis, ionic balance and other stress mitigation processes, thereby contributing to overall plant resilience (Ni et al., 2013; Xu et al., 2015).

Differential Expression and Correlation Analyses

To further characterise the response of the 20 selected genes to abiotic stress, their expression levels were quantified using qRT-PCR. Primer sequences are provided in *Table 2*. qRT-PCR analysis revealed significant upregulation of gene 1, 5, 9 and 11 under water deprivation stress, with the remaining genes showing downregulation (*Figure 1*). Similarly, under salt stress, genes 1, 5, 9, 11–16 and 19 exhibited upregulation, while genes 2–4, 6–8, 10, 17, 18 and 20 displayed downregulation (*Figure 1*).

Gene expression patterns showed a high correlation ($R^2 = 0.7317$) between salt and drought stress (*Figure 2*), indicating similar responses for most genes. However, gene 12 and 13 displayed contrasting regulation. These findings align with prior studies (Hazzouri et al., 2020; Li et al., 2019;

TABLE 2. PAIRS OF PRIMERS USED FOR DIFFERENTIAL EXPRESSION ANALYSIS USING THE qRT-PCR TECHNIQUE OF THE 20 PROSPECTED GENES

Gene #	Forward primer	Reverse primer
01	5′-GATAAGAATGGTCTGAAGAAGGG-3′	5′-CAATTGCTGACCACTTGTTCC-3′
02	5′-GGAGGACCAGAAACTTGTAGAC-3′	5′-ATTAGAGACCATCTGTTGCCC-3′
03	5′-TTTTCGCAAGATTGATGCTG-3′	5′-TCATGAGATGCTCCTGTTGC-3′
04	5′-GGTAGACCTCTCTGCATCG-3′	5′-CCTACCACCAGCTGAAAATACC-3′
05	5′-GCTCAACACCTATGGGTTTCG-3′	5′-ACCTTCTCTTCGATCTTCCTCTG-3′
06	5′-CACCACTTAAGATCCGTTGCC-3′	5′-GCTATCAAATCCCACCTGTCAC-3′
07	5′-ACGAGAAGCTCATTAACTACATCC-3′	5′-CTATCAATGACCACCGATTGCC-3′
08	5′-GGACCAAGGAGGAAGATGAC-3′	5′-AGAGACCATTTGTTGCCGAG-3′
09	5′-CTAAGTGCTCAGGCTTGAAGAG-3′	5′-GTCCTCCAGTAGTTCTTTATCTCG-3′
10	5′-TCGAGCGTGGTGTTTAATG-3′	5′-CGGAGCAGTACCAAGAGAGG-3′
11	5′-TTTAGGCAATAGGTGGGCAG-3′	5′-TATTGAGCTTCTCCACAGACAG-3′
12	5′-AGTCACAGTTCACAAGAGCAC-3′	5′-CATTCAGAGCACGAAGGAGAG-3′
13	5′-AGCTAGCAGGATTGCTTAGG-3′	5′-CTGGTCAACAGTTTCAGCG-3′
14	5′-CAAGGGTTCATGGACACCAG-3′	5′-TTCGACCATTTGTTTCCAAGC-3′
15	5′-GACACAAGCCATGATTGAAG-3′	5′-TAGCGAGCAACCCTTTTATCTC-3′
16	5′-CAAGCAAGCTGGTCTATTGAGG-3′	5′-CGGCTGGTTTGGATTCACTC-3′
17	5′-CTTCACTCTAGCGATATCTACCG-3′	5′-AACGTTTCAACCCTGCTCTC-3′
18	5′-CCATGTTGTTCAAAGGAGGG-3′	5′-GCAATTAGAGACCATCTGTTTCC-3′
19	5′-CCTACTAATACTGGGCTGATGAG-3′	5′-GGTGTTCCAATAGTTCTTGATGTC-3′
20	5′-GGTGGGAATTCTTCCTCTTC-3′	5′-TAATTCAGAGACCAACCCAACC-3′
ICG	5′-CCAGGGTTCAGCTGATTAAG-3′	5′-TCGTCCAAATCCAGCAATC-3′

Note: ICG - Internal control gene: *EgEfMPOB00119*.

Rasmussen et al., 2013; Zhu, 2002) suggesting a core set of genes involved in early responses to both stresses in oil palm.

Gene expression profiles (*Figure 3*) largely agreed between RNA-Seq and qRT-PCR, with one exception: Gene 4 showed positive regulation under both stresses in RNA-Seq but negative in qRT-PCR. This discrepancy highlights potential technique-specific variations. Further analysis using alternative methods or replicates may be needed to confirm gene 4's expression pattern under stress.

Annotation of the Promoter Region from the Genes Coding for the Putative TFs

Phylogenetic analysis based on the 1,432-nucleotide promoter sequences upstream of the start codon for each gene revealed four distinct groups among the 20 TFs (data not shown). However, these groupings did not correlate with the expression profiles of the genes under drought and salinity stress (*Table 1*). MEME analysis identified three conserved promoter motifs present in all 20 genes. Similar to the phylogenetic analysis, the distribution of these motifs did not exhibit any significant pattern within the four previously identified phylogenetic groups.

Analysis of the promoter regions using the PlantCARE database revealed the presence of seven putative *cis*-acting elements potentially associated with stress responses in the 20 selected TF genes. These elements included the ABA-responsive element (ABRE), stress-responsive element (STRE), motifs responsive to methyl jasmonate (MeJA) signalling (CGTCA-motif and TGACG-motif), the core promoter elements TATA-box and CAAT-box and the salicylic acid and auxin-responsive element as-1.

Consistent with their regulatory role, all 20 TF gene promoters contained key *cis*-elements. Notably, both CAAT-box and TATA-box elements were ubiquitous, suggesting their potential role in stress response. The CAAT-box, known for enhancing promoter activity, might contribute to increased expression under stress (Song et al., 2018). The TATA-box, often found in stress-responsive genes (Roelofs et al., 2010), could facilitate rapid and variable regulation under stress conditions (Yu et al., 2012).

Despite ubiquitous CAAT-box and TATA-box elements, TF promoters exhibited variation. Notably, *HSF* genes (3 & 5) possessed ABRE, as-1, and stress-related motifs (CGTCA, TGACG) alongside core elements. Interestingly, genes 2, 6–10 displayed all identified *cis*-elements (ABRE, STRE, as-1, CGTCA,

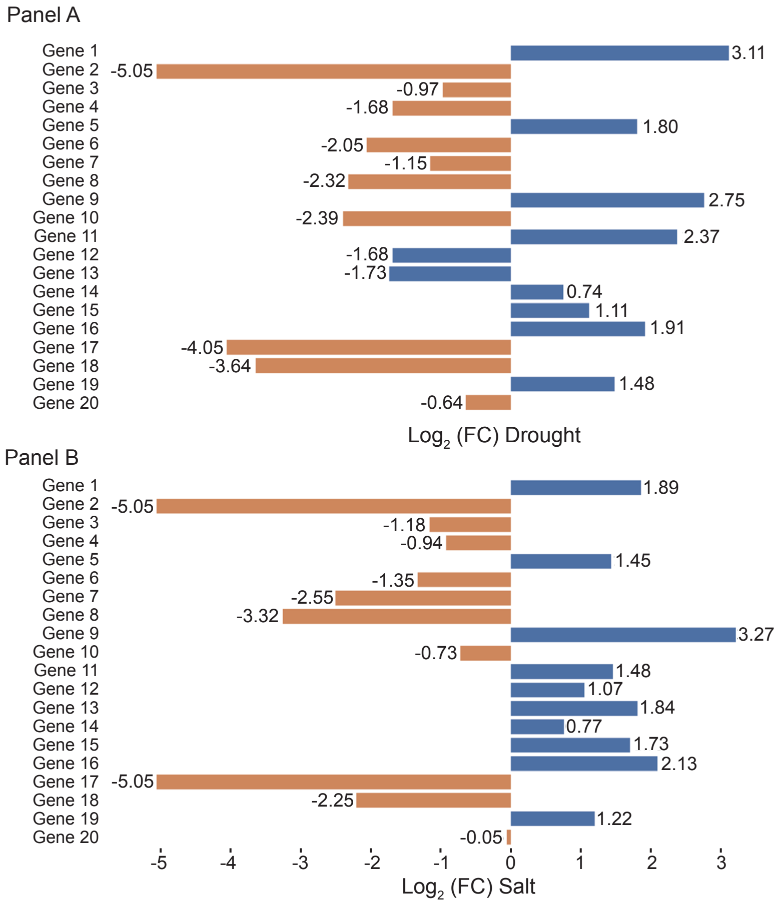

Figure 1. Log_2 (FC) in transcript abundance of 20 selected genes measured using qRT-PCR. Panel A depicts the results for young oil palm plants exposed to drought stress and panel B shows the results for plants exposed to saline stress. FC denotes fold change.

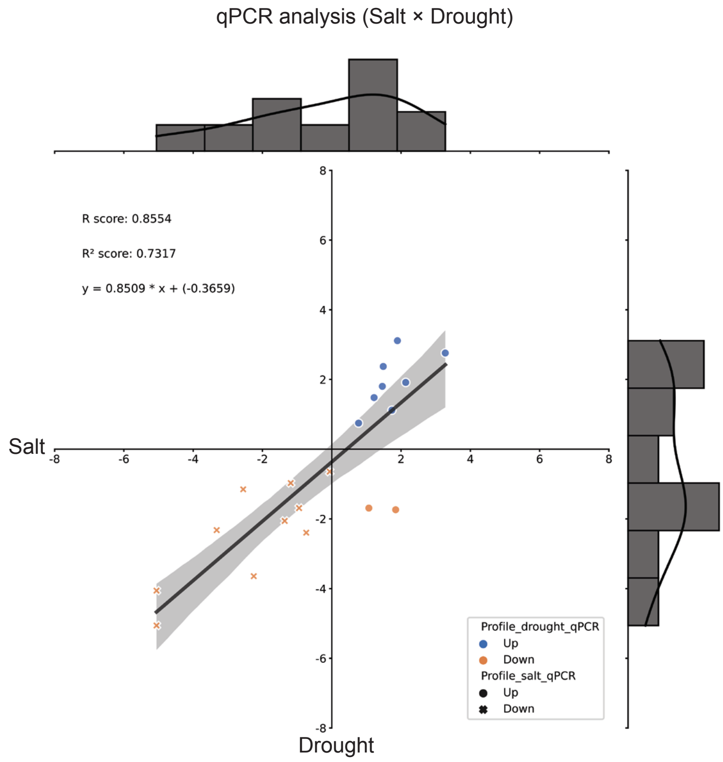

Figure 2. Log_2 (FC) correlation analysis of transcript abundance changes for the 20 selected genes identified through qRT-PCR. The analysis compares gene expression profiles under saline stress ("salt") and water stress ("drought"). FC denotes fold change.

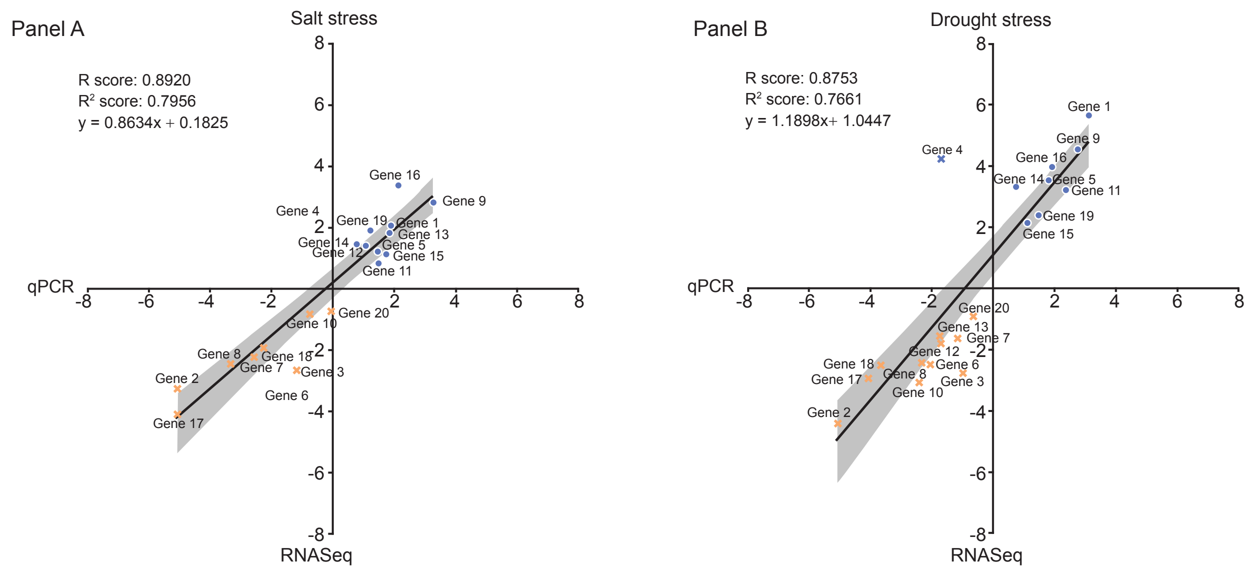

Figure 3. Correlation analysis of the Log_2(FC) for the 20 selected genes. Panel A compares FC in gene expression under saline stress and panel B compares under drought stress, as measured by qRT-PCR and RNA-Seq. FC denotes fold change.

TGACG) associated with ABA, heat/osmotic, salicylic acid and methyl jasmonate responses. While 18/20 genes showed similar expression under both stresses (validated by RNA-Seq and qRT-PCR), no correlation between *cis*-element number/position and expression patterns was observed.

Structural and Functional Annotation of the Coding Region of the Putative TFs

The 20 TF genes displayed coding sequence lengths varying up to 7,500 nucleotides (Gene 4) and intron numbers ranging from zero (Gene 20) to nine (Gene 12), with distinct intron-exon patterns for each TF family - egMYB: 2 introns; egHSFF: 1 intron; egNFY: 0-1 introns; egHD-ZIP: 2-9 introns (data not shown). Phylogenetic analysis based on protein sequences identified three clades (*Figure 4a*), with Gene 9 (*MYB*) forming a solitary clade, eight MYB proteins in a second clade and the remaining proteins from all TF families clustering within the third clade.

Arabidopsis studies revealed contrasting stress responses upon HSFA4A activation (tolerance) vs. inactivation (hypersensitivity) under salt stress (Pérez-Salamó et al., 2014). Similarly, over-expression of lily *HSFA3* genes in *Arabidopsis* led to salt hypersensitivity (Wu et al., 2018). The present study found a *HSFA3* (Gene 3) was negatively-regulated, while *HSFC2b* (Gene 5) was positively-regulated under drought and salinity stresses. This suggests potentially distinct roles for these HSFs in oil palm stress responses.

Analysis of conserved protein domains revealed 23 distinct types among the 19 stress-responsive proteins (excluding gene 6). Notably, PLN03091 and PLN03212 domains were consistently present in all *MYB TFs* (Genes 1, 2, 7-9, 11, 13, 14, 16-19; *Figure 4b*). REB1, Myb and SANT domains were also identified within these MYB proteins, but their distribution varied.

Analysis of conserved protein domains in the coding regions revealed distinct domain compositions for the identified stress-responsive proteins (*Figure 4b*). HSF proteins (Gene 3 & 5) possess HSF and DNA-binding domains, suggesting roles in heat stress response and gene activation. Proteins from Gene 4, 10, 12, 15 and 20 exhibited domains HOX, homeodomain, homeodomain superfamily, Homeobox, HHT1, HALZ, and H4, suggesting a potential role in developmental regulation. Additionally, the presence of domains like Histone superfamily, START, HAP5, HD-ZIP_N, START_Argleabra2_like and CBFD_NFYB_HMF highlights potential interactions with chromatin remodelling and other transcription factors. Notably, the HD-ZIP_N domain suggests membership in the HD-Zip family.

MEME analysis revealed seven motifs (8-50 amino acids) in 18/20 proteins (*Figure 4c*). The number of motifs per protein varied between one and five, with the proteins from genes 11 and 19 exhibiting the highest number of motifs. Motif 1, 2 and 4 consistently occurred within PLN03091/PLN03212 domains (Gene 1, 2, 7-9, etc.). Motif 5 was unique to HSFF proteins (Gene 3 & 5), while motif 6 was specific to potential HD-Zip family members (Gene 10, 12 & 15). Motif 3 had the broadest presence (9 proteins), while motif 7 was identified in only 3 (Gene 10, 11 & 19).

Analysis of conserved domains and motifs (*Figure 4b, 4c*) aligned with GhostKOALA's functional predictions (KO0300 – Transcription Factor group). Proteins within the same TF family

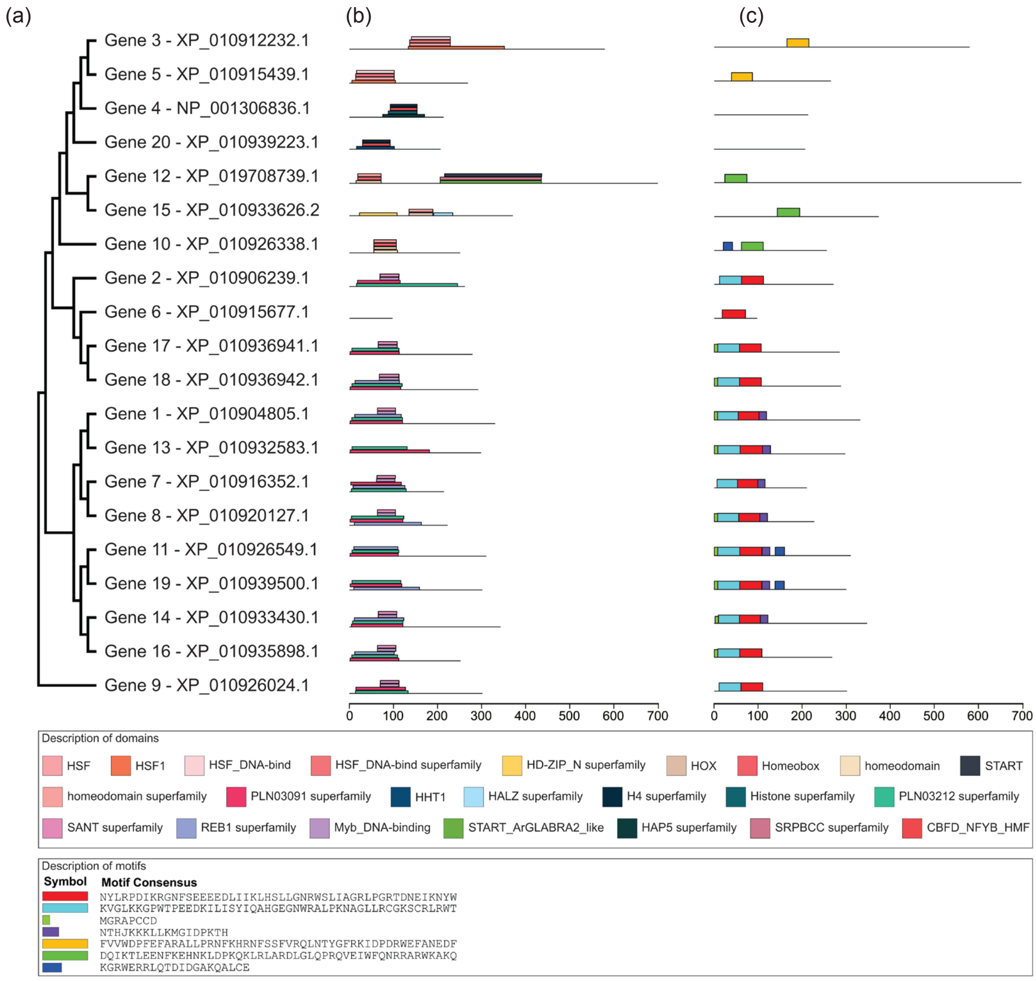

Note: HSF - Heat Shock Transcrition Factor; HD-ZIP_N - Homeodomain-leucine zipper; HOX - homeobox; START - StAR-related Lipid Transfer; HALZ - Homeobox associated leucine zipper; SANT - SWI3, ADA2, N-CoR and TFIIIB; REB1 - RNA polymerase I Enhancer Binding protein; HAP5 - Heme Activator Protein 5 subunit; SRPBCC - START/RHO_alpha_C/PITP/Bet_v1/CoxG/CalC; CBFD_NFYB_HMF - Histone-like transcription factor (CBF/NF-Y) and archaeal histone.

Figure 4. In silico *Analysis of Stress-Responsive Protein Sequences. (a) Phylogenetic tree constructed using MEGA11 software. (b) Protein domain architecture. (c) Conserved motifs were identified within the amino acid sequences. Different colours represent distinct domains or motifs.*

shared similar domain architectures and motif compositions. This consistency reinforces the *in-silico* annotation and suggests family-specific sequence features relevant to their regulatory roles.

GO term enrichment analysis revealed diverse functions for the 20 identified TFs. The associated GO terms spanned biological processes (87 terms), molecular functions (nine terms), and cellular components (four terms). Notably, some TFs had more assigned GO terms, suggesting greater functional complexity (e.g., gene 14: 29 terms, Genes 9, 11, 19: 23 terms each). This highlights the potential for varied roles of these TFs in the oil palm's stress response.

Thirteen DEGs encode MYB TFs, known for diverse stress responses (Dubos et al., 2010; Roy, 2016; Wang et al., 2021). *MYB20* (Gene 13) showed contrasting expression: Salinity-induced (positive) vs. drought-repressed (negative). Gao et al. (2014) reported AtMYB20's negative role in ABA-mediated drought response, while Wang et al. (2021) linked its salinity tolerance to MYB TFs repressing ABA repressors (PP2Cs). *MYB30* (Gene 16) exhibited increased expression under both stresses. This TF regulates salt tolerance via AOX1s (mitochondrial alternative oxidase) and wax synthesis genes for cuticle reinforcement, protecting leaves from stress (Gong et al., 2020; Lee & Suh, 2015; Wang et al., 2021).

Two DEGs encode NF-Y family members. These hetero-trimeric TFs (NF-YA, NF-YB, NF-YC) bind to CCAAT boxes in promoters, regulating gene expression (Nelson et al., 2007). Studies link NF-Y to abiotic stress responses (Leyva-González et al., 2012; Li et al., 2013; Kumar, 2014; Zhao et al., 2014). Notably, NF-YA, a target of miR169, enhances salt tolerance in *Arabidopsis* (Li et al., 2013).

The present study revealed differential expression of *NF-Y* subunit genes (NF-YB3, NF-YC2) under both stresses. *NF-YB3* (Gene 20) showed negative regulation, while *NF-YC2* (Gene 4) displayed positive regulation. Our prior work linked miR169 to NF-Y regulation in oil palms under stress (Salgado et al., 2021, 2022). miR169 was down-regulated, while NF-YA protein increased only under salinity stress.

Leyva-González et al. (2012) proposed a model for NF-Y regulation under stress, postulating that stress induces NF-YA activation while concurrently decreasing miR169 levels. The findings of Salgado et al. (2021), demonstrating negative regulation of miR169 and positive regulation of NF-YA protein in oil palm leaves under salinity stress, align with this proposed model. Elevated NF-YA might form inactive complexes with NF-YB/YC subunits, potentially repressing stress response genes and acting as a negative feedback loop during prolonged stress. However, this model seems salinity-specific. Drought stress also reduces miR169 (Salgado et al., 2022) but lacks the NF-YA protein increase, suggesting additional drought-specific regulatory mechanisms requiring further investigation.

Previous studies have indicated stress-specific functions for NF-Y subunits. *At*NF-YB1 in *Arabidopsis* and its maize orthologous *Zm*NF-YB2 have been shown to enhance drought tolerance (Nelson et al., 2007), establishing them as potential markers for stress resilience. The present study revealed the upregulation of *NF-YC2* (Gene 4) under both salinity and drought conditions. This expression pattern aligns with the overexpression of *Pw*HAP5 (NF-YC2 homologue) in *Picea wilsonii*, which has been associated with increased stress tolerance (Li et al., 2013), suggesting a potential positive role for NF-YC2 in oil palm stress responses.

Three DEGs (10, 12 and 15) encode HD-Zip TFs in the present study. HD-Zip TFs belong to a diverse plant superfamily involved in development and stress responses (Belamkar et al., 2014; Gong et al., 2019; Li et al., 2022; Sharif et al., 2021). These Genes displayed contrasting expression: Gene 15 (positive under both stresses), Gene 10 (negative under both) and Gene 12 (positive under salinity, negative under drought). This suggests potential subfamily- or gene-specific roles for HD-Zip TFs in oil palm's abiotic stress responses.

Class I HD-Zip TFs are known for their positive roles in plant stress responses (Dezar et al., 2005; Gong et al., 2019; Jiao et al., 2022; Zhao et al., 2014). This study identified three DEGs from distinct subfamilies: HD-Zip I (Gene 10), HD-Zip II (Gene 15) and HD-Zip IV (Gene 12). Their contrasting expression patterns (Gene 10: Negative under both stresses, Gene 15: Positive under both, Gene 12: Positive under salinity, negative under drought) suggest potential subfamily-specific roles in oil palm's abiotic stress responses.

Two DEGs encode HSFs, key regulators in plant stress responses (Guo et al., 2016). They induce heat-shock proteins (HSPs) and activate stress-responsive genes (Ohama et al., 2017). HSFs respond to various stresses, including heat, drought, cold and salt (Li et al., 2019). There are three HSF classes: A (activators), B (repressors) and C (unknown function) (Ohama et al., 2017; Wu et al., 2018).

At last, understanding a gene's regulatory influence is crucial. For example, consider Gene 15, an oil palm HD-Zip II gene was positively regulated under both stresses, which silencing using techniques like RNAi or CRISPR-Cas9 could be a promising strategy for engineering tolerance. Does it have a widespread regulatory role, affecting dozens or hundreds of genes under stress conditions, or is its influence limited to just a few target genes? Additionally, how many regulatory factors control Gene 15 itself? These questions are vital because manipulating genes with extensive regulatory roles carries a higher risk of unintended consequences. Future research should focus on functionally validating these TFs and identifying those that enhance stress tolerance without disrupting other crucial plant functions. Integrating these findings with existing knowledge of inherent tolerance mechanisms will be vital for developing robust stress-tolerant oil palm cultivars.

A Gene Regulatory Network (GRN), named EG-Net was constructed for *Elaeis guineensis* to address some of the aforementioned questions. EG-Net, a GRN derived from 428 oil palm transcriptomes (comprising 21,852 target genes and 3,069 regulators), indicates that this oil palm HD-Zip II gene regulates 3,925 genes (235 downregulated and 165 upregulated by both salinity and drought stresses). Conversely, it is regulated by 58 regulators, including 49 transcription factors, seven long non-coding RNAs (lncRNAs) and two epigenetic regulators (EpRs). Based on these findings, silencing this gene could directly impact 400 genes exhibiting similar qualitative responses to both abiotic stresses. Notably, 25 of these genes encode transcription factors that, in turn, regulate a substantial number of genes.

CONCLUSION

The present study investigated the potential for engineering stress-tolerant oil palm cultivars by identifying TFs involved in the response to salinity and drought stress. To the best of our knowledge, there were no prior reports to suggest inherent tolerance in oil palms to such stresses. Transcriptome data was collected from young oil palm leaves subjected to severe stress (high salinity and water deprivation) for two weeks (this study, Salgado et al. 2021, 2022). This induced visible signs of stress, such as browning and wilting. The data reflects the plants' responses to these extreme conditions, rather than their inherent tolerance mechanisms. It's important to note that prolonged exposure to such severe stress would likely be detrimental to the plants.

This study identified 20 TFs from four distinct families that appear to play a crucial role in the response to both salinity and drought stress. The consistency observed in the behaviour of these TFs suggests the existence of shared molecular pathways. This overlap presents a valuable opportunity to pinpoint genes capable of conferring tolerance to both stresses. However, further consideration is required before selecting candidate TF genes for genetic engineering or editing.

Stress-responsive TFs offer significant potential for engineering plants with enhanced stress tolerance. A systematic approach involving the identification, characterisation and functional validation of TFs can accelerate the development of stress-resilient crops. While TF research has been extensive, it often neglects the broader context of GRNs. The development and incorporation of such GRN analysis into this process might, as shown for an oil palm HD-Zip II gene in the present study, certainly provide valuable insights into the complex regulatory mechanisms underlying stress responses, leading to more effective and targeted genetic engineering strategies.

ACKNOWLEDGEMENT

The authors acknowledge funding to F.F.S. and T.L.C.S. by the Coordination for the Improvement of Higher Education Personnel (CAPES). The author(s) disclosed receipt of the following financial support for the study, authorship and/or publication of this article: The grant (01.13.0315.00 DendêPalm Project) for this study was awarded by the Brazilian Innovation Agency (FINEP). The authors confirm that FINEP did not influence the study design, the content of the article, or the selection of this journal. Authors APL, RCT, CAFdS, PB and MTSJ were employed by the company Embrapa. The remaining authors declare that the research was conducted in the absence of any commercial or financial relationships that could be construed as a potential conflict of interest.

REFERENCES

Ambawat, S., Sharma, P., Yadav, N. R., & Yadav, R. C. (2013). MYB transcription factor genes as regulators for plant responses: An overview. *Physiology and Molecular Biology of Plants*, *19*(3), 307–321. https://doi.org/10.1007/s12298-013-0179-1

Anders, S., Pyl, P. T., & Huber, W. (2015). HTSeq–A Python framework to work with high–throughput sequencing data. *Bioinformatics*, *31*(2), 166–169. https://doi.org/10.1093/bioinformatics/btu638

Angon, P. B., Tahjib-Ul-Arif, M., Samin, S. I., Habiba, U., Hossain, M. A., & Brestic, M. (2022). How do plants respond to combined drought and salinity stress – A systematic review. *Plants*, *11*(21), 2884. https://doi.org/10.3390/plants11212884

Bailey, T. L., Johnson, J., Grant, C. E., & Noble, W. S. (2015). The MEME Suite. *Nucleic Acids Research*, *43*(W1), W39–W49. https://doi.org/10.1093/nar/gkv416

Belamkar, V., Weeks, N. T., Bharti, A. K., Farmer, A. D., Graham, M. A., & Cannon, S. B. (2014). Comprehensive characterization and RNA-Seq profiling of the HD-Zip transcription factor family in soybean (*Glycine max*) during dehydration and salt stress. *BMC Genomics*, *15*, 950. https://doi.org/10.1186/1471-2164-15-950

Bhattacharjee, A., Khurana, J. P., & Jain, M. (2016). Characterization of rice homeobox genes, *oshox22* and *oshox24*, and over-expression of *oshox24* in transgenic *Arabidopsis* suggest their role in abiotic stress response. *Frontiers in Plant Science*, *7*, 627. https://doi.org/10.3389/fpls.2016.00627

Bittencourt, C. B., Carvalho da Silva, T. L., Rodrigues Neto, J. C., Vieira, L. R., Leão, A. P., De Aquino Ribeiro, J. A., Abdelnur, P. V., De Sousa, C. A. F., & Souza, M. T., Jr. (2022). Insights from a multi-omics integration (MOI) study in oil palm (*Elaeis guineensis* Jacq.) response to abiotic stresses: Part one – Salinity. *Plants*, *11*(13), 1755. https://doi.org/10.3390/plants11131755

Chaudhari, R. S., Jangale, B. L., Krishna, B., & Sane, P. V. (2023). Improved abiotic stress tolerance in *Arabidopsis* by constitutive active form of a banana DREB2 type transcription factor, *MaDREB20.CA*, than its native form, *MaDREB20*. *Protoplasma*, *260*(3), 671–690. https://doi.org/10.1007/s00709-022-01805-7

Chen, X., Chen, Z., Zhao, H., Zhao, Y., Cheng, B., & Xiang, Y. (2014). Genome-wide analysis of soybean HD-Zip gene family and expression profiling under salinity and drought treatments. *PLoS ONE*, *9*(2), e87156. https://doi.org/10.1371/journal.pone.0087156

Corley, R. H. V., Rao, V., Palat, T., & Praiwan, T. (2018). Breeding for drought tolerance in oil palm. *Journal of Oil Palm Research*, *30*, 26–35.

Dezar, C. A., Gago, G. M., González, D. H., & Chan, R. L. (2005). *Hahb-4*, a sunflower homeobox-leucine zipper gene, is a developmental regulator and confers drought tolerance to *Arabidopsis thaliana* plants. *Transgenic Research*, *14*(4), 429–440. https://doi.org/10.1007/s11248-005-5076-0

Dobin, A., Davis, C. A., Schlesinger, F., Drenkow, J., Zaleski, C., Jha, S., Batut, P., Chaisson, M., & Gingeras, T. R. (2013). STAR: Ultrafast universal RNA-seq aligner. *Bioinformatics*, *29*(1), 15–21. https://doi.org/10.1093/bioinformatics/bts635

Dubos, C., Stracke, R., Grotewold, E., Weisshaar, B., Martin, C., & Lepiniec, L. (2010). MYB transcription factors in *Arabidopsis*. *Trends in Plant Science*, *15*(10), 573–581. https://doi.org/10.1016/j.tplants.2010.06.005

Foreign Agricultural Services. (2024). *PSD online custom query*. U.S. Department of Agriculture. Retrieved April 10, 2024, from https://apps.fas.usda.gov/psdonline/app/index.html#/app/downloads

Gao, S., Zhang, Y. L., Yang, L., Song, J. B., & Yang, Z. M. (2014). *AtMYB20* is negatively involved in plant adaptive response to drought stress. *Plant and Soil*, *376*(1–2), 433–443. https://doi.org/10.1007/s11104-013-1992-6

Gong, Q., Li, S., Zheng, Y., Duan, H., Xiao, F., Zhuang, Y., He, J., Wu, G., Zhao, S., Zhou, H., & Lin, H. (2020). SUMOylation of *MYB30* enhances salt tolerance by elevating alternative respiration via transcriptionally upregulating *AOX1a* in *Arabidopsis*. *The Plant Journal*, *102*(6), 1157–1171. https://doi.org/10.1111/tpj.14689

Gong, S., Ding, Y., Hu, S., Ding, L., Chen, Z., & Zhu, C. (2019). The role of HD-Zip class I transcription factors in plant response to abiotic stresses. *Physiologia Plantarum*, *167*(4), 516–525. https://doi.org/10.1111/ppl.12965

Guo, M., Liu, J.-H., Ma, X., Luo, D.-X., Gong, Z.-H., & Lu, M.-H. (2016). The plant heat stress transcription factors (Hsfs): Structure, regulation, and function in response to abiotic stresses. *Frontiers in Plant Science*, *7*, 114. https://doi.org/10.3389/fpls.2016.00114

Hajyzadeh, M., Turktas, M., Khawar, K. M., & Unver, T. (2015). *miR408* overexpression causes increased drought tolerance in chickpea. *Gene*, *555*(2), 186–193. https://doi.org/10.1016/j.gene.2014.11.002

Hazzouri, K. M., Flowers, J. M., Nelson, D., Lemansour, A., Masmoudi, K., & Amiri, K. M. A. (2020). Prospects for the study and improvement of abiotic stress tolerance in date palms in the post-genomics era. *Frontiers in Plant Science*, *11*, 293. https://doi.org/10.3389/fpls.2020.00293

He, M., He, C.-Q., & Ding, N.-Z. (2018). Abiotic stresses: General defenses of land plants and chances for engineering multistress tolerance. *Frontiers in Plant Science*, *9*, 1771. https://doi.org/10.3389/fpls.2018.01771

Huerta-Cepas, J., Szklarczyk, D., Heller, D., Hernández-Plaza, A., Forslund, S. K., Cook, H., Mende, D. R., Letunic, I., Rattei, T., Jensen, L. J., von Mering, C., & Bork, P. (2019). eggNOG 5.0: A hierarchical, functionally and phylogenetically annotated orthology resource based on 5090 organisms and 2502 viruses. *Nucleic Acids Research*, *47*(D1), D309–D314. https://doi.org/10.1093/nar/gky1085

Instituto Brasileiro de Geografia e Estatística. (2024). *Produção agropecuária: Dendê*. Retrieved April 10, 2024, from https://www.ibge.gov.br/explica/producao-agropecuaria/dende/br

Ivushkin, K., Bartholomeus, H., Bregt, A. K., Pulatov, A., Kempen, B., & De Sousa, L. (2019). Global mapping of soil salinity change. *Remote Sensing of Environment*, *231*, 111260. https://doi.org/10.1016/j.rse.2019.111260

Javed, T., Shabbir, R., Ali, A., Afzal, I., Zaheer, U., & Gao, S.-J. (2020). Transcription factors in plant stress responses: Challenges and potential for sugarcane improvement. *Plants*, *9*(4), 491. https://doi.org/10.3390/plants9040491

Jiao, P., Jiang, Z., Wei, X., Liu, S., Qu, J., Guan, S., & Ma, Y. (2022). Overexpression of the homeobox-leucine zipper protein *ATHB-6* improves the drought tolerance of maize (*Zea mays* L.). *Plant Science*, *316*, 111159. https://doi.org/10.1016/j.plantsci.2021.111159

Kanehisa, M., Sato, Y., & Morishima, K. (2016). BlastKOALA and GhostKOALA: KEGG tools for functional characterization of genome and metagenome sequences. *Journal of Molecular Biology*, *428*(4), 726–731. https://doi.org/10.1016/j.jmb.2015.11.006

Leão, A. P., Bittencourt, C. B., Carvalho Da Silva, T. L., Rodrigues Neto, J. C., Braga, Í. O., Vieira, L. R., De Aquino Ribeiro, J. A., Abdelnur, P. V., De Sousa, C. A. F., & Souza Júnior, M. T. (2022). Insights from a multi-omics integration (MOI) study in oil palm (*Elaeis guineensis* Jacq.) response to abiotic stresses: Part two–Drought. *Plants*, *11*(20), 2786. https://doi.org/10.3390/plants11202786

Lee, S. B., & Suh, M. C. (2015). Advances in the understanding of cuticular waxes in *Arabidopsis thaliana* and crop species. *Plant Cell Reports*, *34*(4), 557–572. https://doi.org/10.1007/s00299-015-1772-2

Lescot, M. (2002). PlantCARE, a database of plant *cis*-acting regulatory elements and a portal to tools for *in silico* analysis of promoter sequences. *Nucleic Acids Research*, *30*(1), 325–327. https://doi.org/10.1093/nar/30.1.325

Leyva-González, M. A., Ibarra-Laclette, E., Cruz-Ramírez, A., & Herrera-Estrella, L. (2012). Functional and transcriptome analysis reveals an acclimatization strategy for abiotic stress tolerance mediated by *Arabidopsis* NF-YA family members. *PLoS ONE*, *7*(10), e48138. https://doi.org/10.1371/journal.pone.0048138

Li, L., Yu, Y., Wei, J., Huang, G., Zhang, D., Liu, Y., & Zhang, L. (2013). Homologous HAP5 subunit from *Picea wilsonii* improved tolerance to salt and decreased sensitivity to ABA in transformed *Arabidopsis*. *Planta*, *238*(2), 345–356. https://doi.org/10.1007/s00425-013-1894-0

Li, W., Wan, X.-L., Yu, J.-Y., Wang, K.-L., & Zhang, J. (2019). Genome-wide identification, classification, and expression analysis of the Hsf gene family in carnation (*Dianthus caryophyllus*). *International Journal of Molecular Sciences*, *20*(20), 5233. https://doi.org/10.3390/ijms20205233

Li, Y., Yang, Z., Zhang, Y., Guo, J., Liu, L., Wang, C., Wang, B., & Han, G. (2022). The roles of HD-ZIP proteins in plant abiotic stress tolerance. *Frontiers in Plant Science*, *13*, 1027071. https://doi.org/10.3389/fpls.2022.1027071

Machado, R., & Serralheiro, R. (2017). Soil salinity: Effect on vegetable crop growth. Management practices to prevent and mitigate soil salinization. *Horticulturae*, *3*(2), 30. https://doi.org/10.3390/horticulturae3020030

Nelson, D. E., Repetti, P. P., Adams, T. R., Creelman, R. A., Wu, J., Warner, D. C., Anstrom, D. C., Bensen, R. J., Castiglioni, P. P., Donnarummo, M. G., Hinchey, B. S., Kumimoto, R. W., Maszle, D. R., Canales, R. D., Krolikowski, K. A., Dotson, S. B., Gutterson, N., Ratcliffe, O. J., & Heard, J. E. (2007). Plant nuclear factor Y (NF-Y) B subunits confer drought tolerance and lead to improved corn yields on water-limited acres. *Proceedings of the National Academy of Sciences*, *104*(42), 16450–16455. https://doi.org/10.1073/pnas.0707193104

Ni, Z., Hu, Z., Jiang, Q., & Zhang, H. (2013). *GmNFYA3*, a target gene of miR169, is a positive regulator of plant tolerance to drought stress. *Plant Molecular Biology*, *82*(1–2), 113–129. https://doi.org/10.1007/s11103-013-0040-5

Ohama, N., Sato, H., Shinozaki, K., & Yamaguchi-Shinozaki, K. (2017). Transcriptional regulatory network of plant heat stress response. *Trends in Plant Science*, *22*(1), 53–65. https://doi.org/10.1016/j.tplants.2016.08.015

Pérez-Salamó, I., Papdi, C., Rigó, G., Zsigmond, L., Vilela, B., Lumbreras, V., Nagy, I., Horváth, B., Domoki, M., Darula, Z., Medzihradszky, K., Bögre, L., Koncz, C., & Szabados, L. (2014). The heat shock factor A4A confers salt tolerance and is regulated by oxidative stress and the mitogen-activated protein kinases MPK3 and MPK6. *Plant Physiology*, *165*(1), 319–334. https://doi.org/10.1104/pp.114.237891

Qin, F., Shinozaki, K., & Yamaguchi-Shinozaki, K. (2011). Achievements and challenges in understanding plant abiotic stress responses and tolerance. *Plant and Cell Physiology*, *52*(9), 1569–1582. https://doi.org/10.1093/pcp/pcr106

Rao, X., Huang, X., Zhou, Z., & Lin, X. (2013). An improvement of the 2^(-ΔΔCT) method for quantitative real-time polymerase chain reaction data analysis. *Biostatistics, Bioinformatics and Biomathematics*, *3*(3), 71–85.

Rasmussen, S., Barah, P., Suarez-Rodriguez, M. C., Bressendorff, S., Friis, P., Costantino, P., Bones, A. M., Nielsen, H. B., & Mundy, J. (2013). Transcriptome responses to combinations of stresses in *Arabidopsis*. *Plant Physiology*, *161*(4), 1783–1794. https://doi.org/10.1104/pp.112.210773

Roelofs, D., Morgan, J., & Stürzenbaum, S. (2010). The significance of genome-wide transcriptional regulation in the evolution of stress tolerance. *Evolutionary Ecology*, *24*(3), 527–539. https://doi.org/10.1007/s10682-009-9345-x

Roy, S. (2016). Function of MYB domain transcription factors in abiotic stress and epigenetic control of stress response in plant genome. *Plant Signaling & Behavior*, *11*(1), e1117723. https://doi.org/10.1080/15592324.2015.1117723

Salgado, F. F., Vieira, L. R., Silva, V. N. B., Leão, A. P., Grynberg, P., Do Carmo Costa, M. M., Togawa, R. C., De Sousa, C. A. F., & Souza Júnior, M. T. (2021). Expression analysis of miRNAs and their putative target genes confirm a preponderant role of transcription factors in the early response of oil palm plants to salinity stress. *BMC Plant Biology*, *21*(1), 518. https://doi.org/10.1186/s12870-021-03296-9

Salgado, F. F., da Silva, T. L. C., Vieira, L. R., Silva, V. N. B., Leão, A. P., Costa, M. M. D. C., Togawa, R. C., De Sousa, C. A. F., Grynberg, P., & Souza Júnior, M. T. (2022). The early response of oil palm (*Elaeis guineensis* Jacq.) plants to water deprivation: Expression analysis of miRNAs and their putative target genes, and similarities with the response to salinity stress. *Frontiers in Plant Science*, *13*, 970113. https://doi.org/10.3389/fpls.2022.970113

Sayers, E. W., Bolton, E. E., Brister, J. R., Canese, K., Chan, J., Comeau, D. C., Connor, R., Funk, K., Kelly, C., Kim, S., Madej, T., Marchler-Bauer, A., Lanczycki, C., Lathrop, S., Lu, Z., Thibaud-Nissen, F., Murphy, T., Phan, L., Skripchenko, Y., . . . Sherry, S. T. (2022). Database resources of the national center for biotechnology information. *Nucleic Acids Research*, *50*(D1), D20–D26. https://doi.org/10.1093/nar/gkab1112

Shahid, S. A., Zaman, M., & Heng, L. (2018). Soil salinity: Historical perspectives and a world overview of the problem. In M. Zaman, S. A. Shahid, & L. Heng (Eds.), *Guideline for salinity assessment, mitigation and adaptation using nuclear and related techniques* (pp. 43–53). Springer International Publishing. https://doi.org/10.1007/978-3-319-96190-3_2

Sharif, R., Raza, A., Chen, P., Li, Y., El-Ballat, E. M., Rauf, A., Hano, C., & El-Esawi, M. A. (2021). HD-ZIP gene family: Potential roles in improving plant growth and regulating stress-responsive mechanisms in plants. *Genes*, *12*(8), 1256. https://doi.org/10.3390/genes12081256

Singh, R., Ong-Abdullah, M., Low, E.-T. L., Manaf, M. A. A., Rosli, R., Nookiah, R., Ooi, L. C.-L., Ooi, S., Chan, K.-L., Halim, M. A., Azizi, N., Nagappan, J., Bacher, B., Lakey, N., Smith, S. W., He, D., Hogan, M., Budiman, M. A., Lee, E. K., … Sambanthamurthi, R. (2013). Oil palm genome sequence reveals divergence of interfertile species in Old and New Worlds. *Nature*, *500*(7462), 335–339. https://doi.org/10.1038/nature12309

Song, S., Xu, Y., Huang, D., Miao, H., Liu, J., Jia, C., Hu, W., Valarezo, A. V., Xu, B., & Jin, Z. (2018). Identification of a novel promoter from banana aquaporin family gene (*MaTIP1;2*) which responds to drought and salt-stress in transgenic *Arabidopsis thaliana*. *Plant Physiology and Biochemistry*, *128*, 163–169. https://doi.org/10.1016/j.plaphy.2018.05.003

Statista. (2024). *Consumption of vegetable oils worldwide from 2013/14 to 2023/24, by oil type*. Retrieved April 10, 2024, from https://www.statista.com/statistics/263937/vegetable-oils-global-consumption/

Stephenson, T. J., McIntyre, C. L., Collet, C., & Xue, G.-P. (2007). Genome-wide identification and expression analysis of the NF-Y family of transcription factors in *Triticum aestivum*. *Plant Molecular Biology*, *65*(1–2), 77–92. https://doi.org/10.1007/s11103-007-9200-9

Tamura, K., Stecher, G., & Kumar, S. (2021). MEGA11: Molecular evolutionary genetics analysis version 11. *Molecular Biology and Evolution*, *38*(7), 3022–3027. https://doi.org/10.1093/molbev/msab120

Thompson, J. D., Higgins, D. G., & Gibson, T. J. (1994). CLUSTAL W: Improving the sensitivity of progressive multiple sequence alignment through sequence weighting, position-specific gap penalties and weight matrix choice. *Nucleic Acids Research*, *22*(22), 4673–4680. https://doi.org/10.1093/nar/22.22.4673

Vieira, L. R., Silva, V. N. B., Casari, R. A. D. C. N., Carmona, P. A. O., Sousa, C. A. F. D., & Souza Junior, M. T. (2020). Morphophysiological responses of young oil palm plants to salinity stress. *Pesquisa Agropecuária Brasileira*, *55*, e01835. https://doi.org/10.1590/S1678-3921.pab2020.v55.01835

Wang, J., Ye, Y., Xu, M., Feng, L., & Xu, L. (2019). Roles of the *SPL* gene family and miR156 in the salt stress responses of tamarisk (*Tamarix chinensis*). *BMC Plant Biology*, *19*(1), 370. https://doi.org/10.1186/s12870-019-1977-6

Wang, W., Pang, J., Zhang, F., Sun, L., Yang, L., Fu, T., Guo, L., & Siddique, K. H. M. (2022). Saltresponsive transcriptome analysis of canola roots reveals candidate genes involved in the key metabolic pathway in response to salt stress. *Scientific Reports*, *12*(1), 1666. https://doi.org/10.1038/s41598-022-05700-2

Wang, X., Niu, Y., & Zheng, Y. (2021). Multiple functions of MYB transcription factors in abiotic stress responses. *International Journal of Molecular Sciences, 22*(11), 6125. https://doi.org/10.3390/ijms22116125

Wu, Z., Liang, J., Wang, C., Zhao, X., Zhong, X., Cao, X., Li, G., He, J., & Yi, M. (2018). Overexpression of lily HsfA3s in *Arabidopsis* confers increased thermotolerance and salt sensitivity via alterations in proline catabolism. *Journal of Experimental Botany, 69*(8), 2005–2021. https://doi.org/10.1093/jxb/ery035

Xu, Z., Gongbuzhaxi, Wang, C., Xue, F., Zhang, H., & Ji, W. (2015). Wheat NAC transcription factor *TaNAC29* is involved in response to salt stress. *Plant Physiology and Biochemistry*, *96*, 356–363. https://doi.org/10.1016/j.plaphy.2015.08.013

Yamaguchi-Shinozaki, K., & Shinozaki, K. (2007). Improving plant drought, salt and freezing tolerance by gene transfer of a single stress-inducible transcription factor. In J. A. Goode & D. Chadwick (Eds.), *Rice biotechnology: Improving yield, stress tolerance and grain quality* (pp. 142–153). Wiley. https://doi.org/10.1002/9780470515778.ch13

Yu, Y., Xu, W., Wang, J., Wang, L., Yao, W., Xu, Y., Ding, J., & Wang, Y. (2012). A core functional region of the RFP1 promoter from Chinese wild grapevine is activated by powdery mildew pathogen and heat stress. *Planta, 237*(1), 293–303. https://doi.org/10.1007/s00425-012-1769-9

Zaman, M., Shahid, S. A., & Heng, L. (2018). *Guideline for salinity assessment, mitigation and adaptation using nuclear and related techniques*. Springer International Publishing. https://doi.org/10.1007/978-3-319-96190-3

Zhang, H., Zhu, J., Gong, Z., & Zhu, J.-K. (2022). Abiotic stress responses in plants. *Nature Reviews Genetics*, *23*(2), 104–119. https://doi.org/10.1038/s41576-021-00413-0

Zhao, Y., Ma, Q., Jin, X., Peng, X., Liu, J., Deng, L., Yan, H., Sheng, L., Jiang, H., & Cheng, B. (2014). A novel maize homeodomain–leucine zipper (HD-ZIP) I gene, *Zmhdz10*, positively regulates drought and salt tolerance in both rice and *Arabidopsis*. *Plant and Cell Physiology*, *55*(6), 1142–1156. https://doi.org/10.1093/pcp/pcu054

Zhu, J.-K. (2002). Salt and drought stress signal transduction in plants. *Annual Review of Plant Biology*, *53*(1), 247–273. https://doi.org/10.1146/annurev.arplant.53.091401.143329

Zulkower, V., & Rosser, S. (2020). DNA Features Viewer: A sequence annotation formatting and plotting library for Python. *Bioinformatics*, *36*(15), 4350–4352. https://doi.org/10.1093/bioinformatics/btaa213

Journal of Oil Palm Research Vol. 38 (3) September 2026 p. 559–571
DOI: https://doi.org/10.21894/jopr.2025.0024

OPTIMISATION OF BOMBARDMENT PARAMETERS IN OIL PALM EMBRYOGENIC CALLI BASED ON TRANSIENT EXPRESSION OF RFP GENE

A RAHMAN NURFAHISZA[1]*; MAT YUNUS ABDUL MASANI[1]*; SUBHI SITI MASURA[1]; MD PIJI MOHD AL AKMARUL FIZREE[1]; OMAR ABD RASID[1] and GHULAM KADIR AHMAD PARVEEZ[1]

ABSTRACT

Particle bombardment is a transformation method that uses a mechanical injury mechanism to deliver deoxyribonucleic acid (DNA) into plant cells. In early studies, a few aspects influencing the efficiency of DNA delivery through biolistic have been determined. However, the developed protocol yields low transformation efficiency, which requires further improvement. Re-evaluation of bombardment parameters by monitoring the expression of reporter genes for a longer duration post-bombardment will provide more conclusive results on stable expression than the previous two-day evaluation. Several bombardment parameters were evaluated; helium pressure, distance between the stopping screen and tissues, size of gold, DNA quantity and the bombardment number. Each parameter was assessed by monitoring the expression of red fluorescent protein (RFP) transiently in oil palm embryogenic calli (EC). The optimal parameters were determined based on the highest RFP signals retained in the EC after three months of bombardment. The optimal parameters were obtained when EC were bombarded three times at 2,000 psi pressure using 1.0 µm of gold particles coated with 1.0 µg of DNA and the distance between the stopping screen and tissues was fixed at 6 cm. The optimal parameters could improve DNA delivery through bombardment and lead to the production of edited oil palm at high efficiency.

Keywords: oil palm, optimal parameters, particle bombardment, red fluorescent protein, transient expression.

Received: 21 December 2023**; Accepted:** 13 February 2025**; Published online:** 11 April 2025.

INTRODUCTION

Malaysia is the world's major producer and exporter of palm oil. It is one of the sectors contributing to Malaysia's economic growth (Parveez et al., 2022). Furthermore, palm oil also contributes to the world's oil and fat supply and demand has increased over the years. The challenges such as climate change, disease and the limitations of arable farmland have affected palm oil production. Study on genetic enhancements is likely to be the potential solution for achieving maximum yields (Masani et al., 2018; Parveez et al., 2015). Genetic enhancements through genome editing, such as CRISPR/Cas9 technology, could provide opportunities for plant improvement by precisely targeting gene modification at a specific site. Recently, genome editing studies have been initiated to edit the oil palm genome precisely (Bahariah et al., 2023; Jamaludin et al., 2023; Yeap et al., 2021) which will lead to the production of improved planting materials and subsequently fulfil palm oil supply in the future.

One factor affecting genome editing efficiency is the success of deoxyribonucleic acid (DNA) delivery into oil palm tissues. A few DNA delivery systems have been developed for oil palm, such as particle bombardment or biolistic (Parveez, 2000; Parveez et al., 2015), *Agrobacterium*-mediated transformation (Izawati et al., 2009, 2015), polyethylene glycol-mediated transfection and DNA microinjection

[1] Malaysian Palm Oil Board,
6, Persiaran Institusi, Bandar Baru Bangi,
43000 Kajang, Selangor, Malaysia.

* *Corresponding authors e-mail: fahisza@mpob.gov.my; masani@mpob.gov.my*

(Masani et al., 2014, 2022). The transformation efficiency of oil palm is relatively low (0.7%–1.5%), with the highest at 1.5% obtained from DNA delivery using the bombardment method (Parveez et al., 2015). In contrast, other crops, such as wheat, have reported a transformation efficiency of up to 12.9% (Miroshnichenko et al., 2020). Thus, the transformation efficiency in oil palm must be improved by optimising bombardment parameters.

Particle bombardment is a mechanical injury technique that delivers the foreign gene into the cells. It delivers rapid DNA and can transfer multiple genes in one shot (Ramkumar et al., 2020). Since this system has no biological or host limitations, it can target various plant species and tissues (Lacroix & Citovsky, 2020). Particle bombardment as an efficient DNA delivery method has been applied in many plant species, such as soybean (Khalafalla et al., 2005), rice (Zhao et al., 2011) and wheat (Melchiorre et al., 2002). For oil palm, the bombardment protocol was established by Parveez (2000). The protocol has been applied to transform and regenerate transgenic oil palms. However, molecular analyses revealed that most regenerated oil palms were escapes and chimeric (Nurfahisza et al., 2014). To overcome these problems, the protocol must be re-established to increase DNA delivery efficiency and produce more transformants. In addition, Parveez (2000) might have used different oil palm clones, influencing the established bombardment protocol. Therefore, using the same clone to optimise bombardment parameters is also important.

Since oil palm requires a long regeneration time, stable transformation results cannot be obtained quickly (Masani et al., 2018). Therefore, optimal bombardment parameters were determined through transient expression studies. This approach allows an easy and rapid assay and serves as a reliable indicator for stable transformation. In plant studies, the most commonly utilised reporter gene expression systems include β-glucuronidase (GUS) (Xiong et al., 2011), green fluorescent protein (GFP) (Parveez & Majid, 2018; Stewart, 2001), red fluorescent protein (RFP) (Okwuonu et al., 2015; Sun et al., 2018) and luciferase (LUC) (Hastings & Morin, 2006). The bombardment protocol reported by Parveez (2000) was based on the optimal parameters obtained from the GUS transient assay. Although GUS can be easily observed by staining with a substrate, its assay is laborious, disruptive, and very toxic to the cells; subsequently, monitoring of expression along with cell development is almost impossible.

In contrast, RFP, GFP and LUC expression can be visualised and monitored in real-time in living tissues. More importantly, gene expression can be observed along with plant development (Hastings & Morin, 2006; Stewart, 2001). RFP, such as the Discosoma Red Fluorescent Protein (*DsRED*) gene, derived from coral (*Discosoma* sp.), was chosen as a visual reporter gene in our study due to the advantage of RFP expression that could be monitored in all stages of plant development. Moreover, Fizree et al. (2019) reported that *DsRED* produced distinct bright RFP signals compared to the pale background in the non-transformed samples and showed improved signal retention in oil palm embryogenic calli (EC). *DsRED* has a much higher extinction coefficient and fluorescence quantum yield as compared to GFP (Baird et al., 2000), which showed no abnormalities in the regenerated transgenic plants (Jach et al., 2001) and is much easier to detect *DsRED* expression in green tissues compared to GFP (Jach et al., 2001). Due to this characteristic, *DsRED* has been used widely in plant transformation, such as in soybeans (Cho et al., 2022), wheat (Tanaka et al., 2022) and walnuts (Zhang et al., 2015).

In this study, we used a visual reporter gene (*DsRED*) and performed assessment times longer than those previously developed by Parveez (2000). Transient expression occurs almost immediately after gene transfer, where non-integrated DNA is eventually degraded by nucleases. Thus, the highest signal retained over a longer duration may have a higher possibility of integration into the plant genome, leading to a stable transformation. This study presents the current optimal bombardment protocol utilising *DsRED* as a reporter gene, which is potentially reliable for producing stable transgenic palms with higher efficiency.

MATERIALS AND METHODS

Plant Materials

Oil palm friable calluses derived from cabbage of P164 clones were obtained from the Clonal Propagation Group of the Malaysian Palm Oil Board (MPOB). The friable calluses formed after being cultured for one to three months were then induced to suspension calli using liquid induction media [MS salts (Murashige & Skoog, 1962), Y3 vitamins (Eeuwens, 1976), 0.1 g/L myo-inositol and L-glutamine, 3% sucrose, 5 µM 2,4-dichlorophenoxyacetic acid (2, 4-D)] and incubated in the dark at 28ºC for six months. The EC formed were collected and cultured on Y3A-4 solid media (Masani et al., 2014, 2022) and incubated at 28°C for a week before bombardment.

Particle Bombardment Transformation

This study used a construct, namely pAMDsRED (Fizree et al., 2019), carrying the *DsRED* gene driven by the CaMV35S promoter as a plasmid

DNA for precipitation with gold particles. High concentration (>2.0 µg/µL) and good quality plasmid DNA (an A260/280 ratio between 1.8 and 2.0) was isolated from bacterial culture using NucleoBond PC 500, Maxi kit (Macherey Nagel) following the manufacturer's instructions. The precipitation procedure to bind gold particles with DNA was performed according to Nurfahisza et al. (2020).

The bombardment was performed according to the method described by Parveez (2000). Five parameters (*Table 1*) were examined independently during the bombardment. Standard parameters that were optimised by Parveez (2000) (marked with * in *Table 1*) were used as a control for comparison. Four replicates (each containing about 0.5 g of EC per plate) were carried out for each tested parameter. The bombarded calli were then incubated at 28°C in dark conditions and subcultured on fresh Y3A-4 solid media (Masani et al., 2014, 2022) without selection for every four weeks.

TABLE 1. FIVE BOMBARDMENT PARAMETERS WERE EXAMINED INDEPENDENTLY

Parameters	Treatments
Helium pressure (psi)	650, 900, 1,100*, 1,350, 1,550, 1,800, 2,000
Distance from stopping screen to tissue (cm)	6.0, 7.5*, 9.0, 10.5, 12.0
Number of bombardments	1*, 2, 3
Size of gold (µm)	0.6, 1.0*, 1.6
DNA quantity (µg)	1.0, 1.5*, 2.0

Note: The asterisk mark (*) represents the standard conditions (Parveez, 2000) used as control during the bombardment.

RFP Monitoring and Transient Assessment

RFP signals were observed through a Nikon AZ100 fluorescence microscope paired with an ET-mcCherry, Texas Red® filter set (Chroma, USA). An imaging system, QICAM-12bit (QImaging, Canada), was also attached to a fluorescence microscope to capture the image in real time. The RFP signals from four replicates of each treatment were observed and scored at a week, a month, two months and three months after the bombardment. Then, the average number of RFP signals and the standard error were calculated based on three months of observation data from four replicate plates of each treatment. The significant differences among the treatments were analysed using Duncan's multiple range test (DMRT) with $p \leq 0.05$. In addition, a graph was plotted to identify the optimal parameter based on the highest average number of RFP signals retained after three months of bombardment.

RESULTS AND DISCUSSION

To efficiently transfer gene constructs through bombardment, it is necessary to determine specific parameters that affect the efficiency of DNA delivery. A brief overview of the optimised parameters is illustrated in *Figure 1*. Five parameters that affect DNA delivery were systematically evaluated. Since the efficiency of particle bombardment in most plants is species- and genotype-dependent, all the samples used as explants in this study were from a similar genetic background. This study was carried out using EC from the P164 clonal palm. P164 is a high-yielding hybrid resulting from crosses between the *Dura* and *Pisifera* varieties (Amanina et al., 2022). Using biological samples from a similar P164 genetic background could reduce experimental variation and improve data precision. The efficiency of bombardment parameters was evaluated by monitoring and counting the red fluorescing spots or RFP signals optically for a week, a month and up to three months after bombardment. Usually, none or, most likely, very few RFP signals will be observed after three months of bombardment. This occurred possibly due to the inevitable loss of vector DNA after several cell replication cycles. After three months of bombardment, the RFP signals may have a higher potential for stable DNA integration into the plant genome. Thus, the optimal parameter was identified based on the highest average number of RFP signals retained three months after bombardment, since the scores imply the number of successful DNA that might be integrated into the targeted tissues.

Effect of Helium Pressure

The pressurised helium gas accelerated the DNA-gold particles to penetrate through different cell layers of tissues. The strength of acceleration may influence the depth of penetration and distribution of gold-DNA particles into the target tissues (Mahdavi et al., 2014). In the first week after bombardment, the highest average number of RFP signals was observed when EC was bombarded at 650 psi (367.75 spots). This was followed by 1,100 psi (289.50 spots), 2,000 psi (252.25 spots), 1,800 psi (198.00 spots), 1,350 psi (181.25 spots) and the least using 900 psi (121.25 spots) (*Figure 2*). Meanwhile, bombardment using 1,550 psi only showed 29.50 spots of RFP signals. After a month and two months of bombardment, a pressure of 650 psi maintains the highest average number of RFP signals among the tested pressures. However, after three months of bombardment, the average number of RFP signals dropped about five-folds for 650 psi (from 33.25 to 6.50 spots) compared to two-folds for 2,000 psi (from 14.00 to 7.75 spots). Since the pressure at 2,000 psi

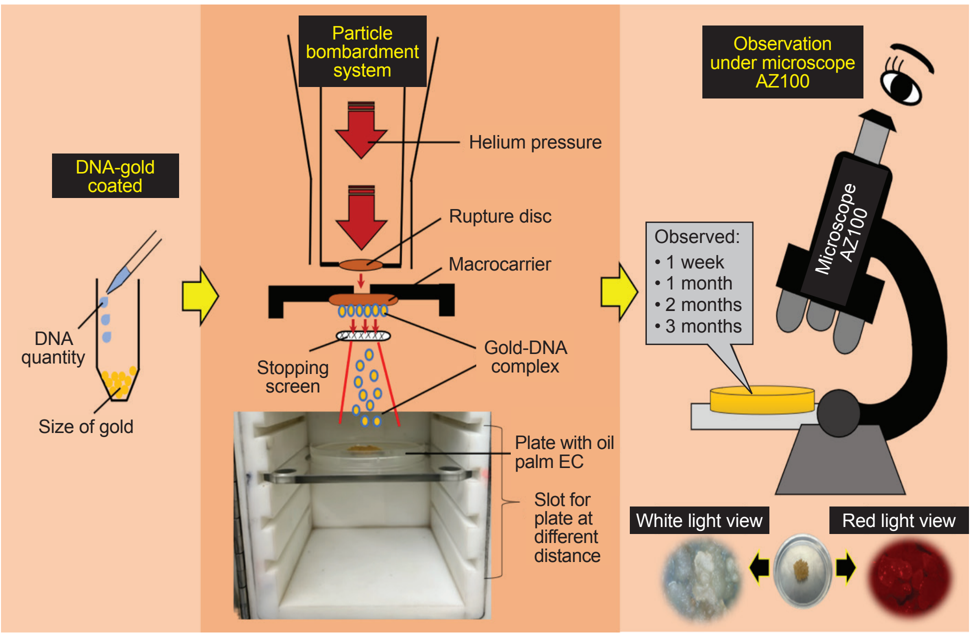

Figure 1. A brief overview for optimisation of bombardment parameters affecting the transient expression of discosoma red fluorescent protein (DsRED) *gene in oil palm embryogenic calli (EC).*

could retain the highest average number of RFP signals after three months, this parameter was chosen as the optimal helium pressure for oil palm bombardment.

The result contrasted with the studies reported by Liu et al. (2024) in Chinese cabbage microspore, Mahdavi et al. (2014) in male banana flowers, and Mousavi et al. (2009) in date palm EC, which showed that helium pressure at 1,100 psi is the most optimal pressure to penetrate the target tissues. Previous studies in oil palm EC also showed 1,100 psi as the optimal pressure (Nurfahisza et al., 2020; Parveez, 2000). The contrasted results may be attributed to different biological materials for bombardment and various durations for evaluating transgene expression. This present study used EC derived from the cabbage of the P164 clone, while Parveez (2000) used EC derived from various clones and tissues, such as immature embryos, leaflets and roots. Meanwhile, the optimal pressure at 1,100 psi evaluated by Nurfahisza et al. (2020) was based on the number of putative transgenic shoots generated. A study on tobacco showed the best pressure at 1,350 psi (Davlekamova et al., 2023). Moreover, a study by Tee and Maziah (2005) showed the different optimal pressures obtained from the same species, *Dendrobium* Sonia 17, which were 1,100 and 650 psi for type-A and type-B calli, respectively. Our result showed that 2,000 psi was the best pressure to penetrate through oil palm P164 clonal EC. Using low-pressure bombardment may cause low penetration of gold-DNA into target tissues (Mousavi et al., 2009; Parveez, 2000).

Effect of Distance from Stopping Screen to Tissue

The distance between the stopping screen and the tissue can be adjusted according to the slot provided in the biolistic device, which is a distance of 6.0, 9.0 and 12.0 cm. The distance at 7.5 and 10.5 cm can be adjusted when an extra plate is put on stages at 9.0 and 12.0 cm slots, respectively. It is necessary to determine the optimal distance to distribute the DNA-gold particles evenly to the target tissue without causing severe tissue damage (Chernobrovkina et al., 2007).

At a week of bombardment, the highest average number of RFP signals (789.75 spots) with significant differences ($p < 0.05$) were obtained when using 6 cm. The average number of RFP signals observed in EC that were bombarded using a distance of 6 cm was continually maintained as the highest number (compared with other tested distances) for a month (141.25 spots), two months (132.25 spots) and three months (11.50 spots) after bombardment, even though the signal count has reduced throughout observation period (*Figure 3*). The second and third highest average number of RFP signals were recorded at a distance of 7.5 and 9.0 cm, respectively. Meanwhile, 10.5 and 12.0 cm showed very low signal counts from the first to the last observation.

Significant differences in RFP signal numbers were observed between the shortest (6 cm) and longest (12 cm) distances. The distance between the stopping screen and the target tissues possibly influences the number of RFP signals obtained. If the distance is too far, the DNA may not reach and

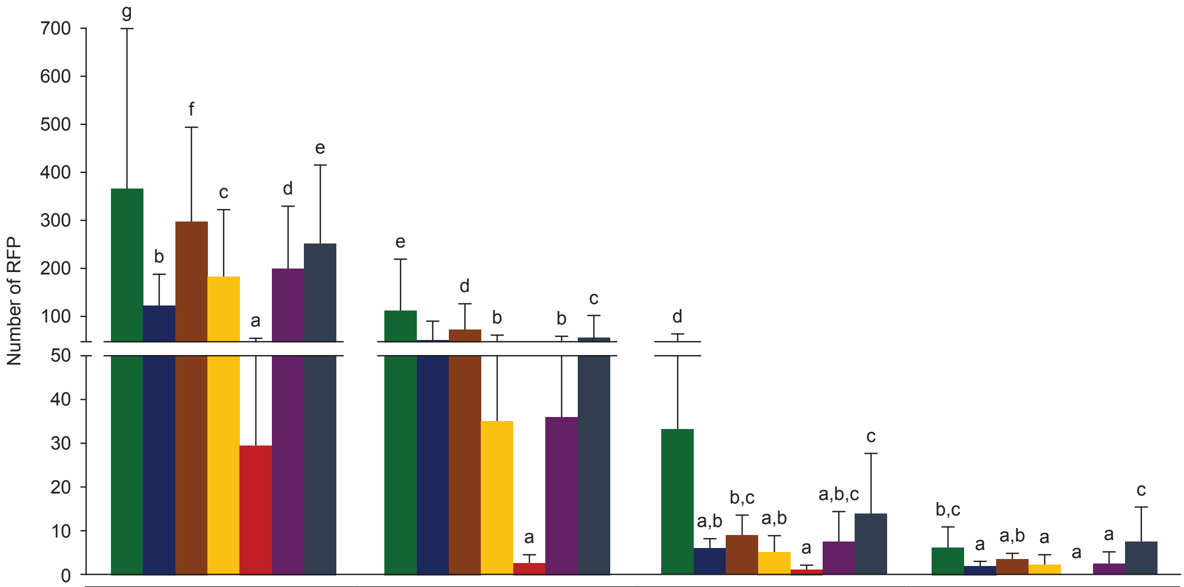

	1 week	1 month	2 months	3 months
650 psi	367.75	112.50	33.25	6.50
900 psi	121.25	51.00	6.25	2.25
1,100 psi	298.50	72.00	9.25	3.75
1,350 psi	181.25	35.00	5.50	2.50
1,550 psi	29.50	3.00	1.50	0.00
1,800 psi	198.00	36.00	7.75	2.75
2,000 psi	252.25	56.00	14.00	7.75

Figure 2. Effects of helium pressure on discosoma red fluorescent protein (DsRED) *expression in oil palm embryogenic calli (EC).*

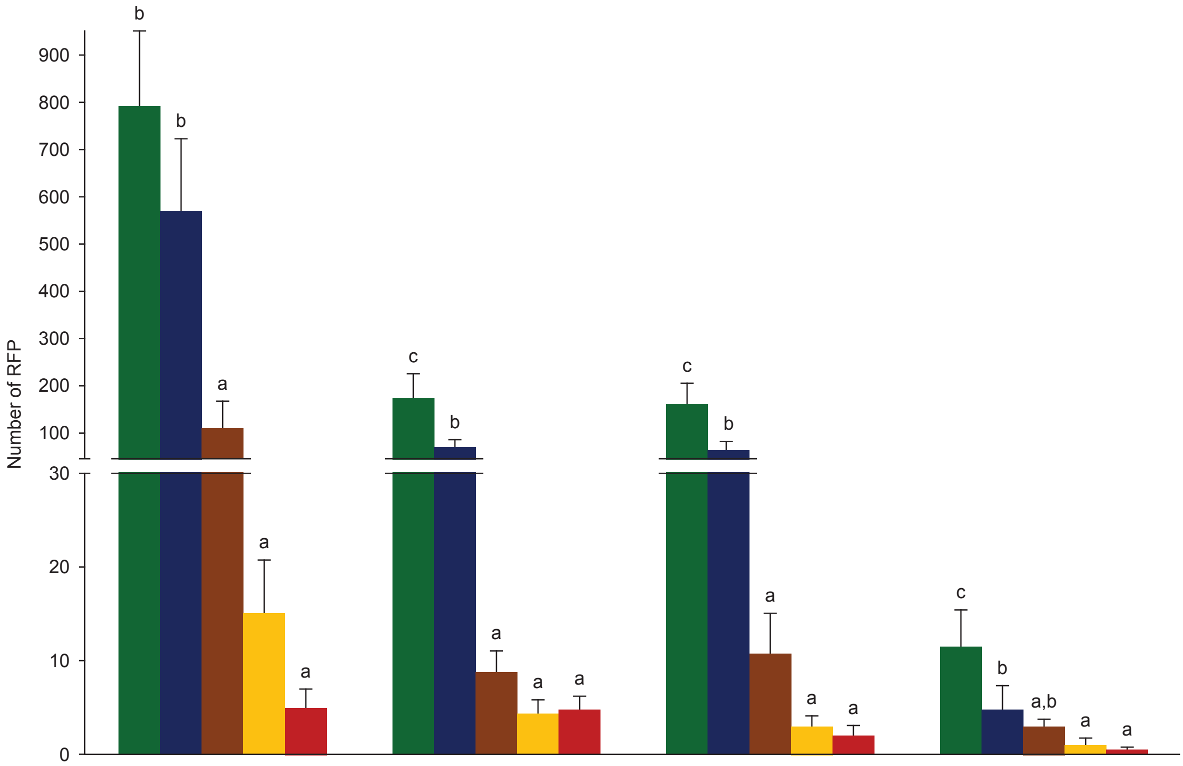

	1 week	1 month	2 months	3 months
6.0 cm	789.75	141.25	132.25	11.50
7.5 cm	569.25	41.25	41.00	4.75
9.0 cm	107.25	8.75	10.75	3.00
10.5 cm	15.00	4.25	3.00	1.00
12.0 cm	5.00	4.75	2.00	0.50

Figure 3. Effects of distance from stopping screen to tissue on discosoma red fluorescent protein (DsRED) *expression in oil palm embryogenic calli (EC).*

penetrate the target tissue efficiently (Nurfahisza et al., 2020). Moreover, the gold-DNA acceleration through the tissue may reduce across the distance (Parveez et al., 1997). This study showed that 6 cm was the optimal distance, whereby the RFP signals were consistently the highest during the period of observation. The result was in agreement with other studies conducted on soybeans (Khalafalla et al., 2005), bananas (Mahdavi et al., 2014) and Chinese cabbage (Liu et al., 2024), which showed 6 cm from the stopping screen to the tissue as the optimal distance for bombardment.

Effect of Number of Bombardments

Generally, three-times bombardments may deliver a high amount of DNA into tissue as more DNA is being penetrated into tissue. However, multiple bombardments tended to create severe injury and cause the cell not to be able to survive for tissue development. The injured cells may cause the delivered gene not to be expressed (Dhir et al., 2010; Mahdavi et al., 2014). Furthermore, the capacity of cell damage may also depend on the target tissue type. During the first week of observation, there was no significant difference in the number of bombardments tested on oil palm EC (*Figure 4*). The average numbers of RFP signals for one, two and three-times bombardment were 587.5, 611.0 and 594.5 spots, respectively. After three months of observation, the RFP signals were reduced for each treatment, but the lowest average of RFP signals was observed when EC was treated with a one-time bombardment (14.0 spots). Meanwhile, the highest average of RFP signals was observed when EC was bombarded three times (27.5 spots).

Multiple bombardments might cause the target tissue to undergo severe injury and subsequently reduce its ability to generate shoots. Studies in oil palm (Nurfahisza et al., 2020; Parveez et al., 1997), medical plant (*Erigeron breviscapus*) (Zhao et al., 2023) and banana (Sreeramanan et al., 2005) showed one-time bombardment was enough for high transgene expression. Contrary, studies in soybean (Khalafalla et al., 2005), Indian mulberry (Bhatnagar et al., 2002), *Centella asiatica* (Lai et al., 2011) and orchid (Da Silva & Tanaka, 2009) revealed that the highest transgene expressions were obtained when the samples were bombarded two-times compared to one or three-times of bombardment. These studies agree that multiple bombardments increase the transformation efficiency but may cause low tissue survivability when bombarded three times. However, our results showed that three-time bombardments gave much better RFP signals than one-time bombardments. Bombardment for more than one time might produce higher RFP signals as the coverage area of bombardment increases. Besides that, multiple bombardments may improve penetration through compensation from misfires caused by faulty or improper rupture disk

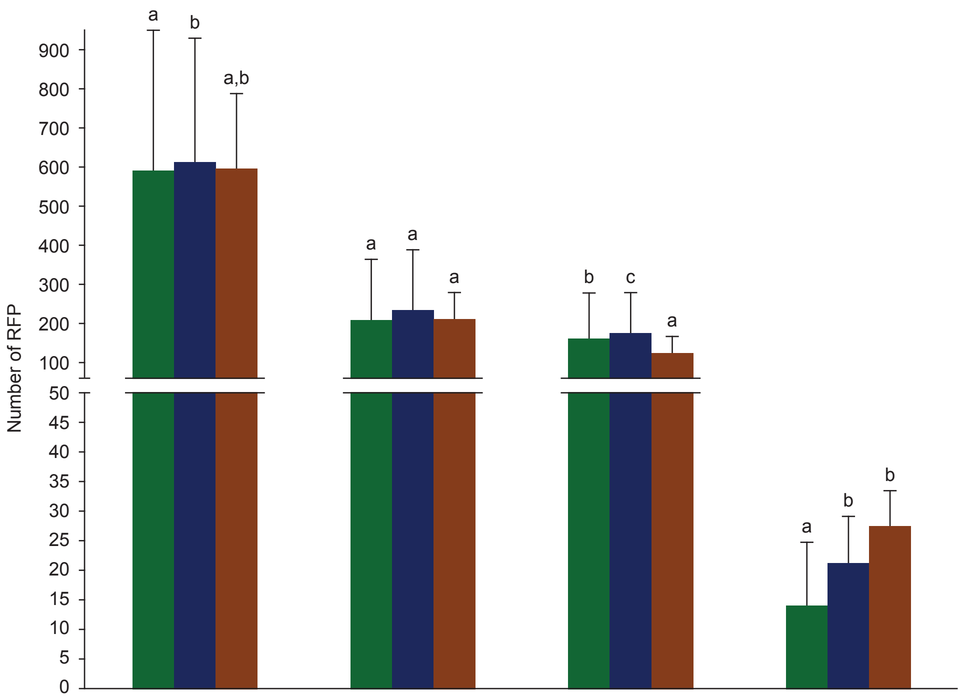

	1 week	1 month	2 months	3 months
1x	587.50	207.25	156.50	14.00
2x	611.00	232.50	172.75	21.25
3x	594.50	209.25	120.00	27.50

Figure 4. Effects of bombardment number on discosoma red fluorescent protein (DsRED) *expression in oil palm embryogenic calli (EC).*

set-up. Fitch et al. (1990), Kuehnle and Sugii (1992), and Zhao et al. (2018), also showed three-times bombardments as efficient transformations for liana, orchid and papaya, respectively. These types of plants belong to woody plants, which are related to the degree of lignification of the tissues that cause less injury (Zhao et al., 2018). Similarly, three-times bombardments were seen as the optimal number of bombardments to improve penetration and increase the transformation efficiency of oil palm. Higher signal expression at three times bombardment demonstrated the ability of oil palm EC to survive and subsequently regenerate into plants.

Effect of Size of Gold Particles

Gold particles act as a microcarrier to assist the DNA in penetrating target tissues. Even though gold particles are expensive, they are uniform in size and biologically inert (Bhatnagar et al., 2002; Dhir et al., 2010). The different sizes of gold particles (0.6, 1.0 and 1.6 µm) may affect the number of DNA carried into the target tissue and it also affects the capacity for tissue damage. The highest average number of RFP signals was obtained at 1.0 µm followed by 1.6 and 0.6 µm at all observation periods (*Figure* 5). The 1.0 µm is the medium size of gold particles which showed better penetration into oil palm tissues compared to the smallest (0.6 µm) and largest (1.6 µm) sizes tested. Since a significant difference was observed among the treatments, the results conclusively indicated that the treatment with 1.0 µm size scored the highest number of RFP signals retained until three months (*Figure 6e-h*) compared to treatments with 0.6 µm (*Figure 6a-d*) and 1.6 µm of gold particles (*Figure 6i-l*).

Several studies showed that the smallest size of gold particles (0.6 µm) gave efficient DNA penetration into explants, such as in soybean (Khalafalla et al., 2005), sorghum (Wang et al., 2021) and maize (Sreenu et al., 2016). At the same time, studies in date palm (Mousavi et al., 2009) and sunflower (Mohamed et al., 2006) were in contrast to our findings as the highest gene expressions were obtained when the DNA was precipitated using 1.6 µm of gold particles. However, most studies in plants such as rice (Mukhtar & Hasnain, 2018), banana (Mahdavi et al., 2014) and giant reed (Dhir et al., 2010) have documented that 1.0 µm is the suitable size of gold particles for bombardment. Theoretically, the large size of gold particles may carry a higher amount of DNA, which may increase the expression of the transgene. However, factors such as tissue types could have different impacts. A study by Ma et al. (2013) showed that hard tissues like stems needed 1.6 µm gold particles compared to calli, which only required 1.0 µm gold particles for better penetration.

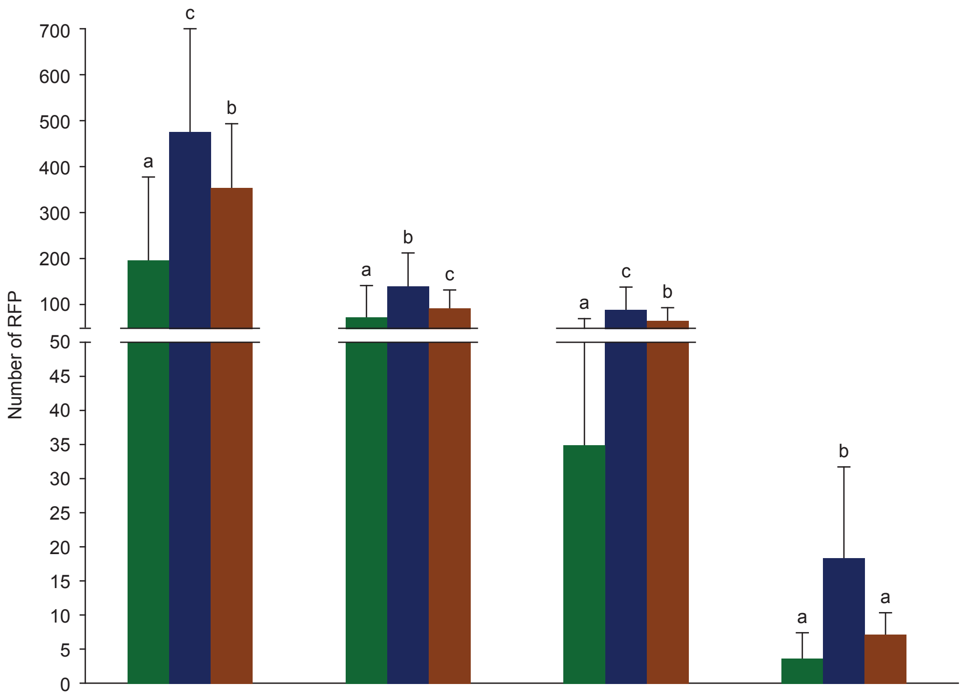

	1 week	1 month	2 months	3 months
0.6 µm	196.50	72.75	35.00	3.75
1.0 µm	480.00	141.50	89.75	18.50
1.6 µm	356.75	92.00	66.25	7.25

Figure 5. Effects of gold particle sizes on discosoma red fluorescent protein (DsRED) *expression in oil palm embryogenic calli (EC).*

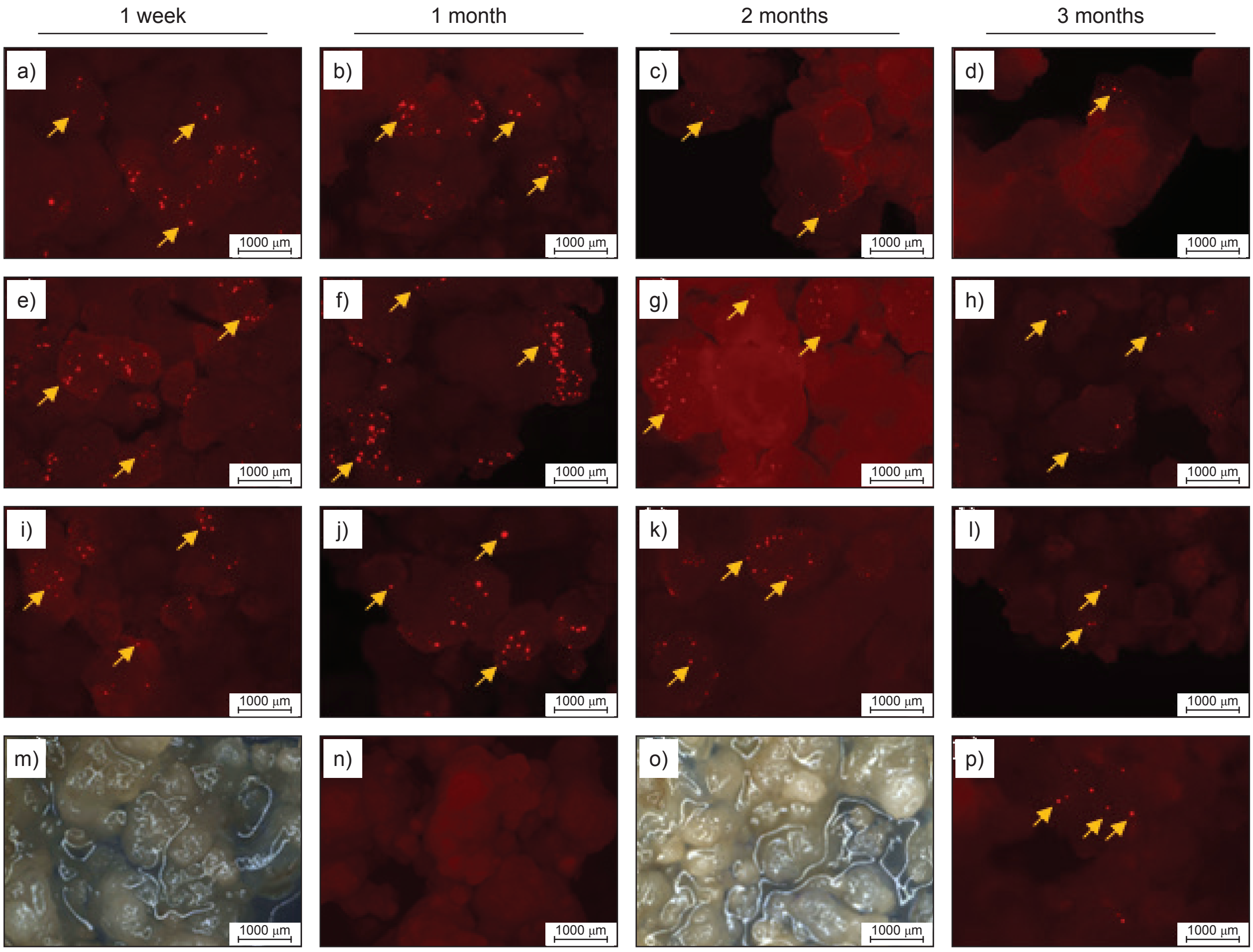

Figure 6. Red fluorescent protein (RFP) spots observed in oil palm embryogenic calli (EC) bombarded with gold particles, at size (a-d) 0.6, (e-h) 1.0 and (i-l) 1.6 µm. No RFP spots were observed for non-bombardment control, (m) under white light and (n) red light. No RFP spots were observed for bombarded calli, (o) under white light but the spots were observed under (p) red light. The yellow arrow indicated RFP spots in EC.

Effect of DNA Quantity

Gold particles could coat the appropriate amount of DNA for efficient delivery of DNA into tissue (Mookkan, 2018). The concern is choosing the right amount of DNA to avoid using a high concentration of DNA that may cause large aggregation. The large aggregation may cause inefficient DNA delivery. Thus, three different DNA quantities were evaluated: 1.0, 1.5 and 2.0 µg. In this study, RFP signals observed in the first week up to three months showed bombardment with 1 µg of DNA, resulting in the highest average number of RFP signals compared to 1.5 and 2.0 µg of DNA (*Figure 7*). The results contrasted with our expectations, as the lowest DNA quantity consistently showed the highest RFP signals throughout the observation.

Generally, the transgene expression may reduce when less DNA is transferred into the targeted tissues. The results may be due to several factors, such as the ratio of gold-DNA precipitation to form aggregates, which might affect the DNA transfer. Our results demonstrated that 1.0 µg of DNA was the appropriate ratio of DNA to bind with gold particles. It was noticeable that the RFP signals reduced when the DNA quantity increased, indicating an amount greater than 1.0 µg may cause improper DNA coating. This may contribute to improper particle aggregation, resulting in inefficient DNA delivery. A study by Mahdavi et al. (2014) on bananas showed that 1.5 µg of DNA per bombardment was the optimal DNA quantity. They also concluded that transient gene expression was reduced at lower (less than 1.5 µg) and higher (more than 1.5 µg) DNA quantities due to insufficient DNA-microcarrier binding and poor cell penetration efficiency, respectively.

Optimal Bombardment Parameters of Oil Palm EC

In this study, the efficient bombardment transformation system was determined by studying the effect of different bombardment parameters. Simultaneously, we are systematically evaluating the amenability of the P164 clone for oil palm transformation. The optimal parameters were identified based on the highest number of RFP

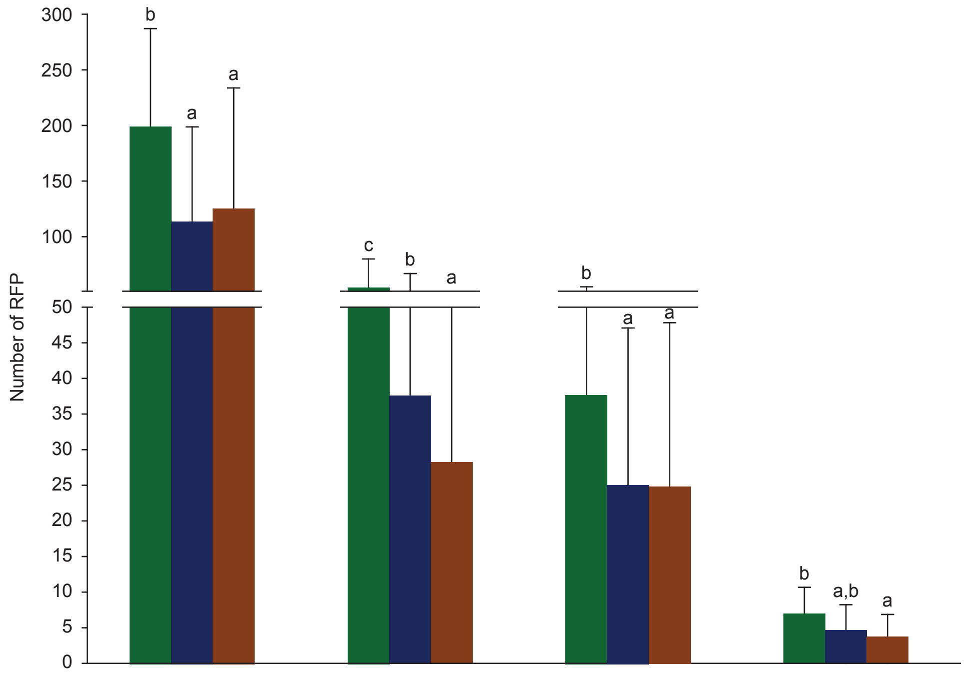

	1 week	1 month	2 months	3 months
1.0 µg	199.25	55.25	37.75	6.75
1.5 µg	114.25	37.50	25.00	4.50
2.0 µg	126.50	28.00	24.75	3.50

Figure 7. Effects of DNA quantity per bombardment on discosoma red fluorescent protein (DsRED) *expression in oil palm embryogenic calli (EC).*

signals retained after three months of bombardment. This study revealed that, except for gold particle sizes for bombardment, the optimal parameters differed from those identified by Parveez et al. (1997, 1998). The differences in penetration impact during bombardment may relate to genotype and target tissue types. Parveez et al. (1997, 1998) used EC from diverse genetic backgrounds, whereas this study focused solely on P164 clone calli, potentially explaining the optimal parameter discrepancy. Additionally, Parveez et al. (1998) showed varying GUS expression in EC derived from different tissue types, with calli from immature embryos exhibiting the highest GUS expression compared to those from leaflets or roots. However, most researchers will prefer using leaflets for the successful initiation of EC (Yarra et al., 2019). Therefore, using biological materials from the same genetic background in empirical studies is preferable for generating precise data with fewer variables.

On the other hand, in previous studies by Parveez et al. (1997, 1998), the transient GUS expressions were monitored after two days of bombardment, contrary to our data which monitored for a longer time, three months after the bombardment. The signals of expression remaining at a longer period showed the stability of transformation compared to the shortened time. Besides that, the highest signals observed at the early observation did not exactly remain high after a long time. For example, in helium pressure and the number of bombardment studies, the high signals observed in the first week were scored at 650 psi and two times bombardment, respectively. Later observation at three months after bombardment showed the highest signal for helium pressure, and the number of bombardments was at 2,000 psi and three times of bombardment, respectively. The reduced number of signals over the period may be because of the DNA not integrated into the plant genome or the foreign DNA being degraded in the cytoplasm. Thus, it is not too speculative to suggest that data obtained over a longer time of monitoring is much more convincing as it reflects the reliability of stable transformation.

CONCLUSION

Further improvement of DNA delivery into the oil palm through bombardment is necessary since the developed protocol produced a low transformation efficiency. Modification of transient expression involving a longer duration of assessment using *DsRED* as a reporter gene gave a more definitive conclusion on stable expression over the previous two-day evaluation using the GUS destructive assay. By monitoring the highest *DsRED* expression that was retained in plant cells for up to three months and using sample from the same genetic background, a new optimal protocol was determined. The 2,000 psi helium pressure, the 6 cm distance of stopping screen to tissue, three-times bombardment, using 1 µm of gold and 1.0 µg of DNA per bombardment were identified as optimal parameters for oil palm transformation. These optimal parameters could lead to further improvements in oil palm transformation, leading to the production of transgenic or edited palms at a higher efficiency in the future.

ACKNOWLEDGEMENT

The authors would like to thank the management of MPOB for permission to publish this article. We also thank the Clonal Propagation Group (CPG) of MPOB for providing EC. Finally, we would like to acknowledge all Transgenic Technology Group (TTG) members for their kind assistance.

REFERENCES

Amanina, N. S., Linatoc, A. C., Haniff, M. H., & Roslan, M. N. (2022). Growth and development of oil palm clone P164 exposed to long-term carbon dioxide enrichment in open top chamber. *Journal of Oil Palm Research*, *34*(1), 56–67. https://doi.org/10.21894/jopr.2021.0030

Bahariah, B., Masani, M. Y. A., Fizree, M. P. M. A. A., Rasid, O. A., & Parveez, G. K. A. (2023). Multiplex CRISPR/Cas9 gene-editing platform in oil palm targeting mutations in *EgFAD2* and *EgPAT* genes. *Journal of Genetic Engineering and Biotechnology*, *21*(1), 3. https://doi.org/10.1186/s43141-022-00459-5

Baird, G. S., Zacharias, D. A., & Tsien, R. Y. (2000). Biochemistry, mutagenesis, and oligomerization of *DsRed*, a red fluorescent protein from coral. *Proceedings of the National Academy of Sciences*, *97*(22), 11984–11989. https://doi.org/10.1073/pnas.97.22.11984

Bhatnagar, S., Kapur, A., & Khurana, P. (2002). Evaluation of parameters for high efficiency gene transfer via particle bombardment in Indian mulberry. *Indian Journal of Experimental Biology*, *40*(12), 1387–1392. https://pubmed.ncbi.nlm.nih.gov/12974402

Chernobrovkina, M. A., Sidorov, E. A., Baranov, I. A., Kharchenko, P. N., & Dolgov, S. V. (2007). The effect of the parameters of biolistic transformation of spring barley (*Hordeum vulgare* L.) on the level of transient expression of GFP reporter gene. *Biology Bulletin*, *34*, 558–563. https://doi.org/10.1134/s1062359007060040

Cho, H., Moy, Y., Rudnick, N. A., Klein, T. M., Yin, J., Bolar, J., Hendrick, C., Beatty, M., Castañeda, L., Kinney, A. J., Jones, T. J., & Chilcoat, N. D. (2022). Development of an efficient marker-free soybean transformation method using the novel bacterium *Ochrobactrum haywardense* H1. *Plant Biotechnology Journal*, *20*(5), 977–990. https://doi.org/10.1111/pbi.13777

Davlekamova, A. A., Zubritsky, A. V., Timofeeva, T. A., Yakovleva, I. V., & Kamionskaya, A. M. (2023). Optimization of biolistic transformation parameters for *Nicotiana tabacum*. *Applied Biochemistry and Microbiology*, *59*, 368–372. https://doi.org/10.1134/s0003683823030055

Da Silva, J. A. T., & Tanaka, M. (2009). Optimization of particle bombardment conditions for hybrid *Cymbidium*. *Transgenic Plant Journal*, *3*(1), 119–122. https://www.academia.edu/24931975/Optimization_of_Particle_Bombardment_Conditions_for_Hybrid_Cymbidium

Dhir, S., Knowles, K., Pagan, C., & Mann, J. (2010). Optimization and transformation of *Arundo donax* L. using particle bombardment. *African Journal of Biotechnology*, *9*(39), 6460–6469.

Eeuwens, C. J. (1976). Mineral requirements for growth and callus initiation of tissue explants excised from mature coconut palms (*Cocos nucifera*) cultured *in vitro*. *Physiologia Plantarum*, *36*, 23–28. https://doi.org/10.1111/j.1399-3054.1976.tb05022.x

Fitch, M., Manshardt, R., Gonsalves, D., Slightom, J., & Sanford, J. (1990). Stable transformation of papaya via microprojectile bombardment. *Plant Cell Reports*, *9*, 189–194. https://doi.org/10.1007/bf00232177

Fizree, M. P. M. A. A., Shaharuddin, N. A., Ho, C. L., Masura, S. S., Manaf, M. A. A., Parveez, G. K. A., & Masani, M. Y. A. (2019). Evaluation of transient *DsRED* gene expression in oil palm embryogenic calli. *Scientia Horticulturae*, *257*, 108679. https://doi.org/10.1016/j.scienta.2019.108679

Hastings, J., & Morin, J. G. (2006). Photons for reporting molecular events: Green fluorescent protein four luciferase systems. In M. Chalfie & S. R. Kain (Eds.) *Green fluorescent protein: Properties, applications, and protocols* (pp. 15–38). John Wiley & Sons. https://doi.org/10.1002/0471739499.ch2

Izawati, A. M. D., Masani, M. Y. A., Ismanizan, I., & Parveez, G. K. A. (2015). Evaluation on the effectiveness of 2-deoxyglucose-6-phosphatephosphatase (*DOG^{R}1*) gene as a selectable marker for oil palm (*Elaeis guineensis* Jacq.) embryogenic calli transformation mediated by *Agrobacterium tumefaciens*. *Frontiers in Plant Science, 6*(727), 1–10. https://doi.org/10.3389/fpls.2015.00727

Izawati, A. M. D., Parveez, G. K. A., & Masani, M. Y. A. (2009). Transformation of oil palm using *Agrobacterium tumefaciens*. *Journal of Oil Palm Research, 21*, 643–652.

Jach, G., Binot, E., Frings, S., Luxa, K., & Schell, J. (2001). Use of red fluorescent protein from *Discosoma* sp. (*DsRED*) as a reporter for plant gene expression. *The Plant Journal, 28*, 483–491. https://doi.org/10.1046/j.1365-313x.2001.01153.x

Jamaludin, N., Bahariah, B., Shaharuddin, N. A., Ho, C. L., Rasid, O. A., Parveez, G. K. A., & Masani, M. Y. A. (2023). Designing gRNAs targeting oil palm phytoene desaturase (*EgPDS*) gene and construction of vectors for oil palm CRISPR/Cas9 study. *Journal of Oil Palm Research, 35*(1), 133–146. https://doi.org/10.21894/jopr.2022.0032

Khalafalla, M. M., Rahman, S. M., El-Shemy, H. A., Nakamoto, Y., Wakasa, K., & Ishimoto, M. (2005). Optimization of particle bombardment condition by monitoring of transient sGFP(S65T) expression in transformed soybean. *Breeding Science, 55*, 257–263. https://doi.org/10.1270/jsbbs.55.257

Kuehnle, A., & Sugii, N. (1992). Transformation of *Dendrobium* orchid using particle bombardment of protocorms. *Plant Cell Reports, 11*, 484–488. https://doi.org/10.1007/bf00232696

Lacroix, B., & Citovsky, V. (2020). Biolistic approach of transient gene expression studies in plants. Biolistic DNA delivery in plants. In S. Rustagi & H. Luo (Eds.), *Methods in molecular biology* (pp. 125–139). Humana. https://doi.org/10.1007/978-1-0716-0356-7_6

Lai, K., Abdullah, P., Yusoff, K., & Mahmood, M. (2011). An efficient protocol for particle bombardment-mediated transformation of *Centella asiatica* callus. *Acta Physiologiae Plantarum, 33*, 2547–2552. https://doi.org/10.1007/s11738-011-0786-9

Liu, Y., Zhang, S., Zhang, S., Zhang, H., Li, G., Sun, R., & Li, F. (2024). Efficient transformation of the isolated microspores of Chinese cabbage (*Brassica rapa* L. *ssp. pekinensis*) by particle bombardment. *Plant Methods, 20*(1), 17. https://doi.org/10.1186/s13007-024-01134-1

Ma, N. L., Cha, T. S., Maziah, M., & Aziz, A. (2013). Comparison of particle bombardment-transformation parameters between stem and calli explants of *Aglaonema simplex*. *Journal of Fisheries and Aquatic Science, 8*(4), 544–552. https://doi.org/10.3923/jfas.2013.544.552

Mahdavi, F., Mahmood, M., & Noor, N. M. (2014). Optimization of particle bombardment parameters for DNA delivery into the male flowers of banana. *Biologia: Section Cellular and Molecular Biology, 69*(7), 888–894. https://doi.org/10.2478/s11756-014-0391-7

Masani, M. Y. A., Izawati, A. M. D., Rasid, O. A., & Parveez, G. K. A. (2018). Biotechnology of oil palm: Current status of oil palm genetic transformation. *Biocatalysis and Agricultural Biotechnology, 15*, 335–347. https://doi.org/10.1016/j.bcab.2018.07.008

Masani, M. Y. A., Noll, G. A., Parveez, G. K. A., Sambanthamurthi, R., & Prüfer, D. (2014). Efficient transformation of oil palm protoplasts by PEG-mediated transfection and DNA microinjection. *PLoS ONE, 9*(5), e96831. https://doi.org/10.1371/journal.pone.0096831

Masani, M. Y. A., Parveez, G. K. A., Noll, G., Fizree, M. P. M. A. A., Sambanthamurthi, R., & Pruefer, D. (2022). Protoplast isolation and transformation in oil palm. In K. Wang & F. Zhang (Eds.), *Methods in molecular biology* (pp. 187–202). Humana. https://doi.org/10.1007/978-1-0716-2164-6_14

Melchiorre, M. N., Lascano, H. R., & Trippi, V. S. (2002). Transgenic wheat plants resistant to herbicide Basta obtained by microprojectile bombardment. *Biocell, 26*(2), 217–223. https://doi.org/10.32604/biocell.2002.26.217

Miroshnichenko, D., Klementyeva, A., Pushin, A., & Dolgov, S. (2020). A competence of embryo-derived tissues of tetraploid cultivated wheat species *Triticum dicoccum* and *Triticum timopheevii* for efficient and stable transgenesis mediated by particle inflow gun. *BMC Plant Biology, 20*, 442. https://doi.org/10.1186/s12870-020-02580-4

Mohamed, S., Boehm, R., & Schnabl, H. (2006). Particle bombardment as a strategy for the production of transgenic high oleic sunflower (*Helianthus annuus* L.). *Journal of Applied Botany and Food Quality, 80*(2), 171–178.

Mookkan, M. (2018). Particle bombardment-mediated gene transfer and GFP transient expression in *Seteria viridis*. *Plant Signaling and Behaviour*, *13*(4), e1441657. https://doi.org/10.1080/15592324.2018.1441657

Mousavi, M., Mousavi, A., Habashi, A. A., & Arzani, K. (2009). Optimization of physical and biological parameters for transient expression of *uidA* gene in embryogenic callus of date palm (*Phoenix dactylifera* L.) via particle bombardment. *African Journal of Biotechnology, 8*(16), 3721–3730. https://doi.org/10.4314/ajb.v8i16.61923

Mukhtar, Z., & Hasnain, S. (2018). Optimization of particle bombardment conditions for rice (*Oryza sativa* L.) transformation. *Pakistan Journal of Agricultural Sciences, 55*(02), 271–278. https://doi.org/10.21162/pakjas/18.3678

Murashige, T., & Skoog, F. (1962). A revised medium for rapid growth and bio assays with tobacco tissue cultures. *Physiologia Plantarum*, *15*(3), 473–497. https://doi.org/10.1111/j.1399-3054.1962.tb08052.x

Nurfahisza, A. R., Parveez, G. K. A., Rasid, O. A., & Masani, M. Y. A. (2020). Optimisation of bombardment parameters for transformation and regeneration of stable oil palm transformants. *Journal of Oil Palm Research*, *32*(4), 696–704. https://doi.org/10.21894/jopr.2020.0060

Nurfahisza, A. R., Rafiqah, M. A., Masani, M. Y. A., Hanin, A. N., Rasid, O. A., Parveez, G. K. A., & Ismail, I. (2014). Molecular analysis of transgenic oil palm to detect the presence of transgenes. *Journal of Oil Palm Research, 26*(1), 96–103.

Okwuonu, I. C., Achi, O. K., Egesi, C. N., & Taylor, N. J. (2015). Evaluation of red fluorescent protein (*DsRED*) as alternative visual marker of genetic transformation in cassava (*Manihot esculenta* Crantz). In Vitro *Cellular & Developmental Biology – Plant, 51*(5), 571–579. https://doi.org/10.1007/s11627-015-9718-5

Parveez, G. K. A. (2000). Production of transgenic oil palm (*Elaeis guineensis* Jacq.) using biolistic techniques. In S. M. Jain & S. C. Minocha (Eds.), *Molecular biology of woody plants* (pp. 327–350) Kluwer Academic Publishers. https://doi.org/10.1007/978-94-017-2313-8_15

Parveez, G. K. A., & Majid, N. A. (2018). Green fluorescent protein as a visual selection marker for oil palm transformation. *Industrial Crops and Products, 115*, 134–145. https://doi.org/10.1016/j.indcrop.2018.02.016

Parveez, G. K. A., Chowdhury, M. K. U., & Saleh, N. M. (1997). Physical parameters affecting transient GUS gene expression in oil palm (*Elaeis guineensis* Jacq.) using the biolistic device. *Industrial Crops and Products*, *6*(1), 41–50. https://doi.org/10.1016/s0926-6690(96)00204-x

Parveez, G. K. A., Chowdhury, M. K. U., & Saleh, N. M. (1998). Biological parameters affecting transient GUS gene expression in oil palm (*Elaeis guineensis* Jacq.) embryogenic calli via microprojectile bombardment. *Industrial Crops and Products*, *8*(1), 17–27. https://doi.org/10.1016/s0926-6690(97)00077-0

Parveez, G. K. A., Kamil, N. N., Zawawi, N. Z., Ong-Abdullah, M., Rasuddin, R., Loh, S. K., Selvaduray, K. R., Hoong, S. S., & Idris, Z. (2022). Oil palm economic performance in Malaysia and R&D progress in 2021. *Journal of Oil Palm Research*, *34*(2), 185–218. https://doi.org/10.21894/jopr.2022.0036

Parveez, G. K. A., Rasid, O. A., Masani, M. Y. A., & Sambanthamurthi, R. (2015). Biotechnology of oil palm: Strategies towards manipulation of lipid content and composition. *Plant Cell Reports, 34*(4), 533–543. https://doi.org/10.1007/s00299-014-1722-4

Ramkumar, T. R., Lenka, S. K., Arya, S. S., & Bansal, K. C. (2020). A short history and perspectives on plant genetic transformation. In S. Rustgi & H. Luo (Eds.), *Biolistic DNA delivery in plants: Method in molecular biology* (pp. 39–68). Humana. https://doi.org/10.1007/978-1-0716-0356-7_3

Sreenu, P., Sridevi, M., Satesh Kumar, P., Reddy, M. K., Sailaja, D., & Pavan Kumar, G. (2016). Optimization of some influential factors in maize genetic transformation through microprojectile bombardment. *International Journal of Recent Scientific Research*, *7*(4), 10517–10522.

Sreeramanan, S., Maziah, M., Abdullah, M. P., Sariah, M., Xavier, R., & Nor'Aini, M. F. (2005). Physical and biological parameters affecting transient GUS and GFP expression in banana via particle bombardment. *Asia Pacific Journal of Molecular Biology and Biotechnology, 13*(1), 35–57.

Stewart, C. N. (2001). The utility of green fluorescent protein in transgenic plants. *Plant Cell Reports, 20(5)*, 376–382. https://doi.org/10.1007/s002990100346

Sun, L., Alariqi, M., Zhu, Y., Li, J., Li, Z., Wang, Q., Li, Y., Rui, H., Zhang, X., & Jin, S. (2018). Red fluorescent protein (*DsRED2*), an ideal reporter for cotton genetic transformation and molecular breeding. *The Crop Journal*, *6*(4), 366–376. https://doi.org/10.1016/j.cj.2018.05.002

Tanaka, J., Minkenberg, B., Poddar, S., Staskawicz, B., & Cho, M. J. (2022). Improvement of gene delivery and mutation efficiency in the CRISPR-Cas9 wheat (*Triticum aestivum* L.) genomics system via biolistics. *Genes*, *13*(7), 1180. https://doi.org/10.3390/genes13071180

Tee, C. S., & Maziah, M. (2005). Optimization of biolistic bombardment parameters for *Dendrobium* Sonia 17 calluses using GFP and GUS as the reporter system. *Plant Cell, Tissue and Organ Culture*, *80*(1), 77–89. https://doi.org/10.1007/s11240-004-9144-6

Wang, L., Gao, L., Liu, G., Meng, R., Liu, Y., & Li, J. (2021). An efficient sorghum transformation system using embryogenic calli derived from mature seeds. *PeerJ, 9*, e11849. https://doi.org/10.7717/peerj.11849

Xiong, A., Peng, R., Zhuang, J., Chen, J., Zhang, B., Zhang, J., & Yao, Q. H. (2011). A thermostable β-glucuronidase obtained by directed evolution as a reporter gene in transgenic plants. *PLoS ONE, 6*(11), e26773. https://doi.org/10.1371/journal.pone.0026773

Yarra, R., Jin, L., Zhao, Z., & Cao, H. (2019). Progress in tissue culture and genetic transformation of oil palm: An overview. *International Journal of Molecular Sciences*, *20*(21), 5353. https://doi.org/10.3390/ijms20215353

Yeap, W-C., Khan, C. M. K., Janalludin. N., Muad, M. R., Appleton, D. R., & Kulaveerasingam, H. (2021). An efficient Clustered Regularly Interspaced Short Palindromic Repeat (CRISPR)/CRISPR-associated protein 9 mutagenesis system for oil palm (*Elaeis guineensis*). *Frontiers in Plant Science*, *12*, 773656. https://doi.org/10.3389/fpls.2021.773656

Zhang, Q., Walawage, S. L., Tricoli, D. M., Dandekar, A. M., & Leslie, C. A. (2015). A red fluorescent protein (*DsRED*) from *Discosoma sp*. as a reporter for gene expression in walnut somatic embryos. *Plant Cell Reports, 34*(5), 861–869. https://doi.org/10.1007/s00299-015-1749-1

Zhao, Y., Guo, L., Wang, H., & Huang, D. (2011). Integration and expression stability of transgenes in hybriding transmission of transgenic rice plants produced by particle bombardment. *Molecular Plant Breeding*, *2*, 48–59. https://doi.org/10.5376/mpb.2011.02.0008

Zhao, Y., Yu, Y., Guo, J., Zhang, Y., & Huang, L. (2023). Rapid and efficient optimization method for a genetic transformation system of medicinal plants *Erigeron breviscapus*. *International Journal of Molecular Sciences, 24*, 5611. https://doi.org/10.3390/ijms24065611

Zhao, Y., Zhang, Y., Su, P., Yang, J., Huang, L., & Gao, W. (2018). Genetic transformation system for woody plant *Tripterygium wilfordii* and its application to product natural celastrol. *Frontiers in Plant Science, 8*, 2221. https://doi.org/10.3389/fpls.2017.02221

Journal of Oil Palm Research Vol. 38 (3) September 2026 p. 572–581
DOI: https://doi.org/10.21894/jopr.2025.0029

POSTPRANDIAL INVESTIGATION ON PLANT AND ANIMAL DERIVED PALMITIC ACID VERSUS OLEIC ACID-RICH HIGH FAT DIETS ON ENDOTHELIAL DYSFUNCTION BIOMARKERS IN HEALTHY MEN: A PILOT STUDY

GOWRI NAGAPAN[1]* and TENG KIM-TIU[1]

ABSTRACT

Prolonged postprandial lipemia has been associated with endothelial dysfunction and an increased risk of cardiovascular disease. While the effect of dietary fatty acids on postprandial lipemia is well recognised, less is known about their effects on endothelial dysfunction biomarkers. We investigated the effects of palmitic acid rich high-fat diets from either plant (palm olein) or animal (lard) compared with an oleic acid-rich high-fat diet (virgin olive oil) on endothelial dysfunction biomarkers in healthy young men. This pilot study employed a randomised crossover design involving 10 healthy men. Each subject consumed 50 g of test fat incorporated in a diet. The diets were consumed on three different days, with blood samples collected at baseline and hourly over 4 hr post-meal. Plasma concentrations of monocyte chemoattractant protein-1 (MCP-1), E-selectin, soluble vascular cell adhesion molecule-1 (sVCAM-1), soluble CD40 ligand (sCD40L) and plasminogen activator inhibitor-1 (PAI-1) were analysed. All types of fat consumption were linked with a significant decrease in plasma PAI-1 and sCD40L throughout 4 hr, but did not influence other pro-inflammatory markers measured during the postprandial state. In conclusion, palmitic acid-rich high-fat diets from different sources had limited effects on endothelial dysfunction biomarkers in the postprandial state, underscoring the need for further investigation in larger cohorts.

Keywords: endothelial function, oleic acid, palmitic acid, postprandial lipemia, saturated fat.

Received: 5 July 2024**; Accepted:** 13 April 2025**; Published online:** 13 June 2025.

INTRODUCTION

Prolonged postprandial lipemia has been associated with endothelial dysfunction and increased cardiovascular risk (Zhao et al., 2021). While numerous studies have explored how saturated fats (SFA) influence the magnitude of postprandial lipemia, less is known about their effects on endothelial markers in the postprandial state (Berry et al., 2007; Masson & Mensink, 2011; Sanders et al., 2011; Teng et al., 2011, 2015, 2017; Tholstrup et al., 2011).

Animal fats and vegetable oils, such as lard and palm oil, are rich sources of palmitic acid (16:0), a dietary SFA known for its cholesterol-raising effects. However, the cholesterol response to palm oil containing 44% palmitic acid does not align with predictions made by Mensink's equations (Mensink et al., 2003). This may be due to the differences in the positional distribution of palmitic acid within triacylglycerol (TAG) molecules. In palm oil, palmitic acid is mainly positioned at the outer *sn*-1 and *sn*-3 positions, whereas in lard, it is predominantly at the *sn*-2 position. Study suggests that fats containing *sn*-2 fatty acids are efficiently absorbed as monoglycerides and transported to the liver, where they may influence cholesterol homeostasis differently compared to when occupying the *sn*-1,3 positions (Hunter et al., 2001; Kritchevsky, 2000; Kritchevsky et al., 2000).

The quantity and quality of dietary fats have a substantial influence on the postprandial lipemia (Kdekian et al., 2020). Monounsaturated fatty acids

[1] Malaysian Palm Oil Board,
6, Persiaran Institusi, Bandar Baru Bangi,
43000 Kajang, Selangor, Malaysia.

* *Corresponding author e-mail: gowri@mpob.gov.my*

(MUFA) and polyunsaturated fatty acids (PUFA) have been shown to reduce postprandial lipemia compared to SFA in both healthy individuals and those with metabolic syndrome (Dror et al., 2017; Margioris, 2009; Masson & Mensink, 2011; Telle-Hansen et al., 2017). However, some findings are contradictory. Sciarrillo et al. (2019) reported higher postprandial lipemia with MUFA and PUFA than with SFA. Notably, a study found lower TAG responses after consuming SFA-rich lard compared to palm olein (Teng et al., 2011).

Postprandial lipemia has been associated with low-grade-systemic inflammation and endothelial dysfunction (Zhao et al., 2021). Endothelial dysfunction is characterised by increased permeability, allowing low-density lipoprotein (LDL) infiltration and oxidation. Oxidised LDL promotes pro-inflammatory responses by stimulating the release of cytokines like TNF-α and IL-6. These cytokines increased endothelial adhesion molecule expression (e.g., ICAM-1 and sVCAM-1) and the secretion of chemokines such as MCP-1, fostering immune cell adhesion and migration, which accelerates the development of endothelial dysfunction and atherosclerosis (Badimon & Vilahur, 2014; Fritsche, 2015; Meessen et al., 2020; Wang et al., 2017; Zhao et al., 2021). Epidemiological evidence linked SFAs with increased markers of inflammation (Fernández-Real et al., 2003; Klein-Platat et al., 2005). This was also supported by human trials (Baer et al., 2004; Dumas et al., 2016; López-Moreno et al., 2017). However, the findings were inconsistent, with some studies reporting no significant effects (Dehghan et al., 2017; Siri-Tarino et al., 2010). Conversely, PUFA- and MUFA-rich meals have been shown to lower postprandial inflammatory markers at 4–6 hr compared to SFA-rich meals (Cruz-Teno et al., 2012; Masson & Mensink, 2011; Rathnayake et al., 2018).

Despite having similar fatty acid content, the distinct physical properties of fats from different sources, such as palm olein (plant-based) and lard (animal-based), may result in varying effects on postprandial endothelial function. To address the limited understanding of these divergent impacts, this study aimed to investigate the postprandial responses of endothelial dysfunction biomarkers after consuming SFA-rich high-fat meals derived from different sources, compared to meals rich in MUFA (oleic acid), in healthy individuals.

MATERIALS AND METHODS

Subjects

Ten healthy males with a body mass index (BMI) between 18.5–30.0 kg/m^2 and a mean age of 21.9 ± 0.7 yr were recruited. A history of cardiovascular disease, diabetes, hypertension, plasma cholesterol levels more than 5.2 mmol/L, TAG levels more than 1.7 mmol/L, intake of medication and smoking were among the exclusion criteria. Prior to the enrolment, all potential participants attended a screening session for medical evaluation and blood collection for further determination of their health and fitness. In the end, 10 eligible participants met the inclusion criteria. All participants gave informed written consent. This study protocol was approved by the University Malaya Medical Centre Research Ethics Committee, Reference number 732.22 and was registered at ClinicalTrials.gov under the identifier NCT01124487. *Table 1* presents the baseline characteristics of study participants.

TABLE 1. BASELINE CHARACTERISTICS OF THE STUDY PARTICIPANTS

Variables	Mean ± SD
Male (n)	10
Age (yr)	21.9 ± 0.7
BMI (kg/m^2)	21.0 ± 1.6
Systolic BP (mmHG)	126.8 ± 8.6
Diastolic BP (mmHG)	71.3 ± 4.9
Waist (cm)	79.5 ± 6.2
Total cholesterol (mmol/L)	4.8 ± 0.7
TAG (mmol/L)	0.9 ± 0.7
LDL cholesterol (mmol/L)	2.6 ± 0.8
HDL cholesterol (mmol/L)	1.6 ± 0.4

Note: BP - blood pressure.; BMI - body mass index; TAG - triacylglycerol; LDL - low-density lipoprotein; HDL - high-density lipoprotein

Experimental Procedures

Study design. This study employed a single-blind, randomised crossover design, with all subjects receiving three experimental meals in a random order. A three days wash out period was given after each meal. Subjects were instructed to avoid consuming high-fat meals, caffeinated drinks and alcohol. Additionally, they were asked to refrain from strenuous physical activities a day before the study visit. A regular low-fat dinner (containing less than 10 g of fat) was also given to the subjects the night before their postprandial testing. Subjects reported to the study centre at 7.30 am after a 10 hr overnight fast and baseline blood samples were collected. Subjects finished their meals within 15 min and blood samples were obtained hourly for 4 hr. Drinking water *ad libitum* was permitted.

Test meals. The meals were made at the study centre. The test meals comprised 60 g of mashed potato incorporated with 50 g test fat (virgin olive oil, palm oil, or lard); baked beans (180 g), skimmed milk (50 mL) and orange juice (200 mL). The meals provided a total energy of 754 kcal. *Table 2* presents the nutrient compositions of the test meals. Unilever Best Foods Italia s.r.l., Italy, supplied the olive oil. Wilmar International Limited, Singapore, provided the palm olein. Sainsbury's in the United Kingdom provided the lard.

TABLE 2. NUTRIENT COMPOSITION OF TEST MEALS

Nutrient composition	Olive oil	Palm olein	Lard
Total calorie (kcal)	754	754	754
Energy (%)			
Carbohydrates	33.0	33.0	33.0
Protein	7.0	7.0	7.0
Fat	60.0	60.0	60.0
SFAs	9.2	39.7	44.1
MUFAs	44.6	27.7	27.8
PUFAs	6.2	8.6	5.9
Fatty acid composition (mol %)			
Palmitic acid ($C_{16:0}$)	12.4	33.7	25.4
Stearic acid ($C_{18:0}$)	2.7	3.7	17.0
Oleic acid ($C_{18:1}$)	72.1	46.1	42.2
Linoleic acid ($C_{18:2}$)	10.1	13.8	9.1
Linolenic acid ($C_{18:3}$)	0.6	0.3	0.6
Others	2.1	2.4	5.8

Note: Values are means of double determinations; SFAs - saturated fatty acids; MUFAs - monounsaturated fatty acids; PUFAs - polyunsaturated fatty acids.

Laboratory Procedures

Blood sampling. Blood samples were drawn into K2 EDTA vacutainers (Becton Dickinson, USA) and centrifuged at 1,300xg for 15 min at 4°C. Plasma samples were stored at –80°C until they were analysed.

Endothelial biomarkers. Plasma endothelial biomarkers (sVCAM-1, MCP-1, PAI-1, E-selectin and sCD40L) were analysed with the (Panomics Inc. USA) Procarta® Cytokine Assay Kit (Panomic Inc. USA). Multiple protein targets were detected and quantified simultaneously using xMAP® technology and multi-analyte profiling beads. Intra-assay values were 4.4% for sVCAM (n = 20), 9.3% for MCP-1 (n = 20), 7.8% for E-selectin (n = 16), 8.3% for PAI-1 (n = 20) and 6.5% for sCD40L (n = 20).

Statistical Analysis

All data were corrected with baseline values and a general linear model for repeated measures was used for statistical analysis. GraphPad Prism 5.03 for Windows and PASW Statistics 18.0 from Chicago, USA were used for all analyses.

RESULTS AND DISCUSSION

The primary findings of the present study revealed that ingesting a high-fat meal, irrespective of the fat type, is linked to a significant decrease in plasma PAI-1 and sCD40L concentrations (time effect, $P_{sCD40L} = 0.007$; $P_{PAI-1} = 0.041$) over time up to 4 hr as shown in *Figure 1a-1b*. This observation was consistent with other studies that have also reported a decreased response in PAI-1 level in a postprandial setting due to diurnal variation (Teng et al., 2015; Tholstrup et al., 2003). SFA has a tendency to decrease PAI-1 antigens 8 hr after ingestion when compared to the unsaturated fatty acids (Tholstrup et al., 2003). Elevated plasma free fatty acids (FFAs) levels have been shown to further elevate endothelial injury via endothelial activation with an increase in plasma TNF-a, IL-6, sICAM-1 and sVCAM-1 after an intake of a high-fat meal (Nappo et al., 2002). We previously reported that FFA decreased after a post-meal period and displayed a transient increase after 1 hr. Notably, lard resulted in a smaller increase in plasma FFAs at 2 and 3 hr compared to olive oil and palm olein (Teng et al., 2011). However, this observation was not consistent with the plasma PAI-1 levels. Lack of response of PAI-1 levels indicated that healthy and lean subjects were included in the trial. Intake of stearic, oleic and linoleic acids for 5 weeks had similar effects on thrombotic factors in healthy subjects (Thijssen et al., 2005). Similarly, Delgado-Lista et al. (2008) also found that dietary SFAs, MUFAs, and carbohydrate intake did not show significant differences in PAI-1 levels after 4 weeks in healthy subjects.

Elevated sCD40L levels were reported in obese people (Unek et al., 2010) but decreased after weight loss. Higher waist circumferences, which indicate higher visceral fat, are associated with elevated sCD40L concentrations. Our finding suggests that individuals with a healthier body composition, as indicated by normal BMI and waist circumference, may exhibit different sCD40L responses compared to obese individuals with larger waist circumferences. Understanding the role of sCD40L and its relationship with body composition may provide valuable insights into metabolic and cardiovascular health.

No apparent changes were noted in plasma MCP-1, sVCAM-1 and E-selectin (*Figure 1c-1e*) measured to identify inflammatory responses related to atherosclerosis. Corroborating with our data, De Souza et al. (2022) and Rubin et al. (2008) have observed no alterations in these biomarkers after high-fat meals in healthy and obese individuals. Another study has also reported that dietary fats in meals had varying effects on acute inflammation and endothelial activation in overweight and obese individuals. PUFA has activated the inflammatory factor, nuclear factor-Kappa B (NF-κB) with no response in sICAM-1. Whereas SFA induced sICAM-1 and sVCAM-1 are slightly reduced following all meals in these individuals (Peairs et al., 2011). In a different study with lean and obese men there was a decrease of sICAM-1 and sVCAM-1 after consuming milkshakes rich in SFA, MUFA and PUFA, although postprandial TAG responses were increased in MUFA compared to SFA and PUFA (Esser et al., 2013). Similarly, other studies have reported a lack of response of sVCAM-1 and E-selectin after high-fat meals (Cortés et al., 2006; Tsai et al., 2004). In contrast with ours and others, a postprandial study has reported significant elevation in adhesion molecules for 4 hr after a high-fat meal compared to a high-carbohydrate meal in both healthy and type 2 diabetes mellitus individuals (Nappo et al., 2002). Fuentes et al. (2008) have reported that chronic ingestion of SFA-rich diet increased the plasma levels of sVCAM-1 in the postprandial state versus MUFA-rich meals. The effects were also more pronounced in patients with type 2 diabetes mellitus when a high-fat meal and glucose were combined and prolonged.

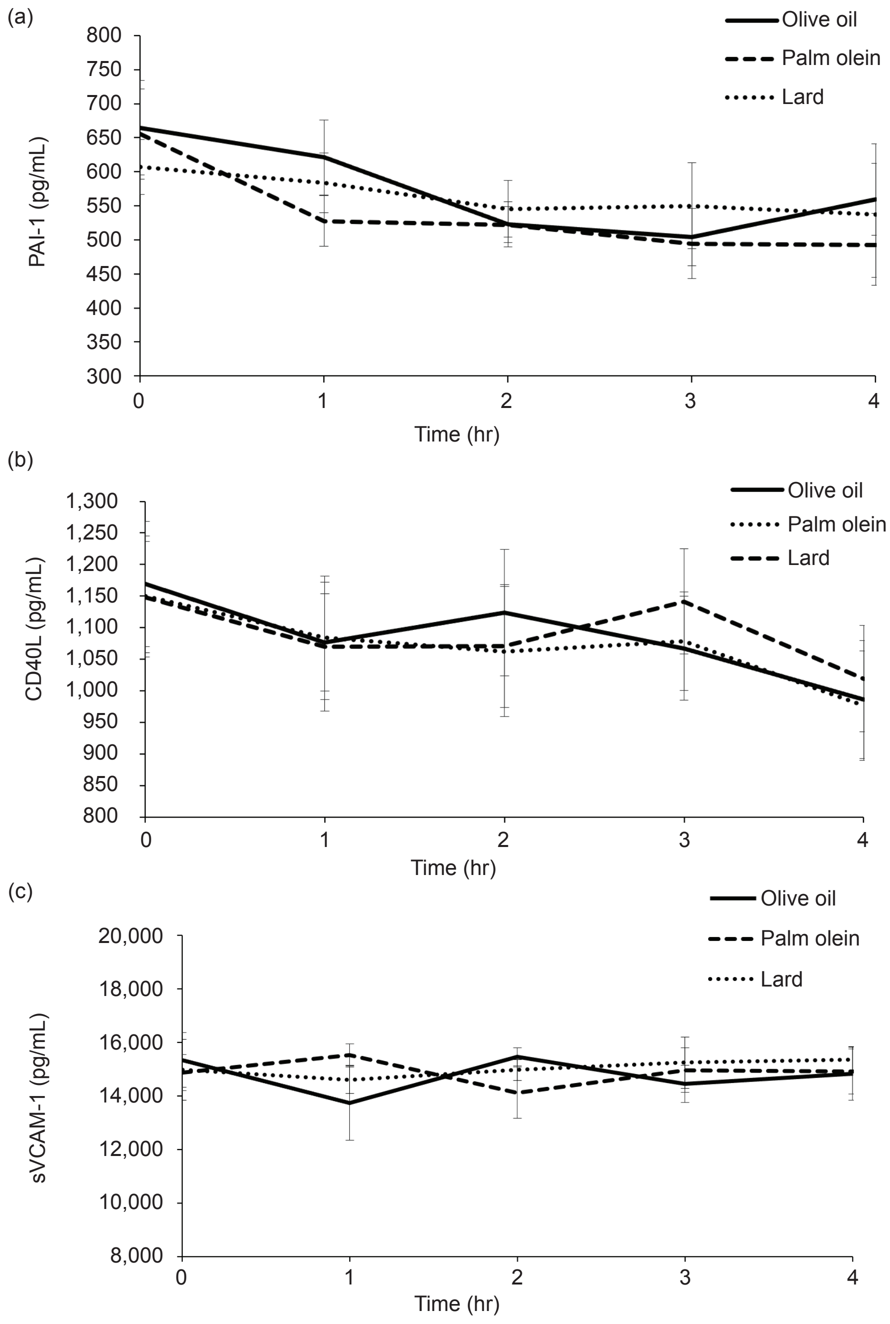

(d)

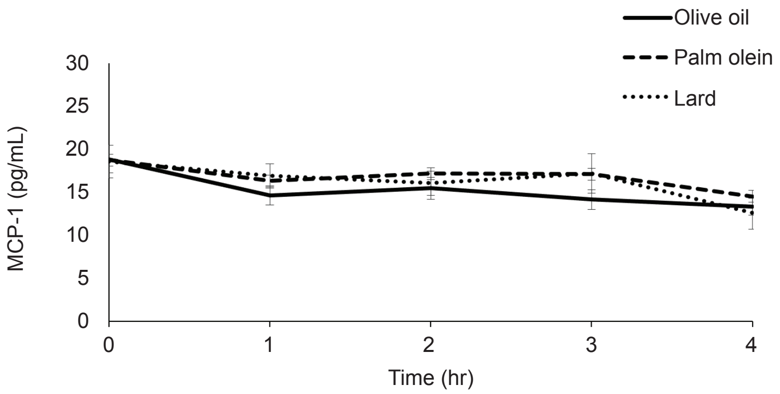

(e)

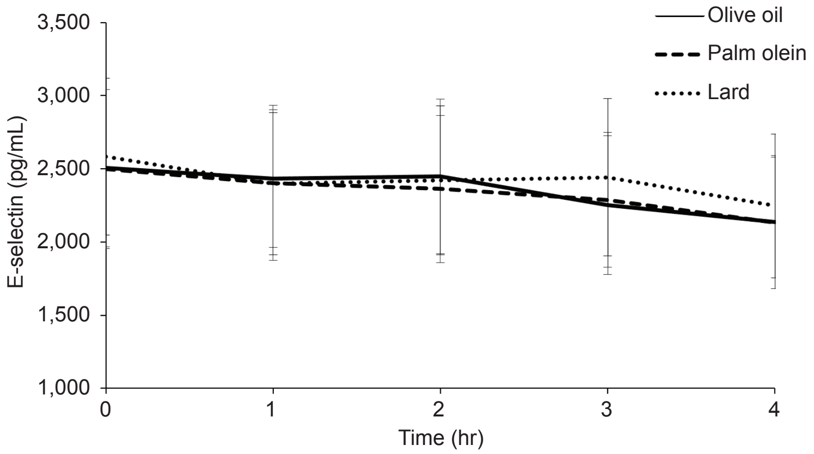

Figure 1. Mean changes for endothelial markers (a) PAI-1, (b) sCD40L, (c) sVCAM-1, (d) MCP-1 and (e) E-selectin after high- fat meals containing palm olein or lard or olive oil. Data are mean ± SEM (n = 10). Changes from baseline values were assessed using repeated-measures ANOVA, with Bonferroni's multiple comparison tests used to compare the three test meals across the time points (0-4 hr). No significant differences were observed for type test meals, but a significant time effect was observed for sCD40L, (P = 0.007) PAI-1, (P = 0.041) over time up to 4 hr.

The Diet-Body-Brain (DietBB) postprandial study was carried out with older adults at risk for cardiometabolic diseases revealed that consuming an energy-rich Mediterranean diet compared to two types of Western diets [approximately 4,300 kilojoules (kJ)] resulted in significant increases in glycemia, lipemia and inflammatory responses. Notably, the Mediterranean diet exhibited more favourable effects on these postprandial responses compared to the Western diets (Diekmann et al., 2019; Schönknecht et al., 2020). In the secondary data analysis of the DietBB study, which examined the changes in inflammatory response to meal intake over a 5 hr periods, the magnitude of the inflammatory response was similar between subjects with pro-inflammatory markers and those without for all meals. In other words, individuals who exhibited proinflammatory markers prior to the meal showed a comparable inflammatory response to the meal as those without such markers. This suggests that the presence of pre-existing proinflammatory markers did not significantly influence the acute inflammatory response to the meal in this group of older individuals with metabolic syndrome traits (Schönknecht et al., 2020, 2022).

Limitations of This Study

Some limitations of our study should be noted. Firstly, the ideal postprandial period should have been extended from 4 to 6 hr, as recommended in previous literature (De Souza et al., 2022). However, due to the discomfort it would inflict on the participants, performing sequential blood sampling for more than 4 hr would be challenging. In our study, the high-fat meal used might not have been high enough to induce significant endothelial damage and inflammatory response. Obtaining different results might have been possible by including higher proportions of SFA and extending the testing period to at least 4 hr or observing the effects after the meals throughout the day. It is worth noting that while SFA levels were comparable between the two palmitic acid-rich fats, other types of fatty acids such as MUFA and PUFA were present in the test fats as well. These fatty acids could still contribute to the different metabolic responses despite the similar SFA content between the two tested palmitic acid-rich diets.

It is crucial to note that this study was conducted on healthy male subjects, which means that the interpretation of the data may not be directly applicable to other populations, including women. Gender differences can significantly influence postprandial lipemia and inflammation (Kolovou et al., 2006; Manning et al., 2008; Orem et al., 2018; Schillaci et al., 2001). Men and women have distinct physiological and biological characteristics that can affect metabolic outcomes, including the regulation of lipid metabolism, which can vary due to hormonal factors (Lee et al., 2016; Lindegaard et al., 2018). In women, protective hormones such as estrogen play a crucial role in maintaining vascular health and metabolic stability (Schillaci et al., 2001). These hormones help regulate lipid profiles, reduce inflammation and improve overall cardiovascular function. However, following menopause, the protective effects of female sex hormones diminish, leading to a narrowing of the gender disparity in risk for cardio-metabolic diseases (Lee et al., 2016). This shift suggests that estrogen and possibly other sex hormones are significant contributors to the differential risk profiles between men and women for conditions such as cardiovascular disease and metabolic syndrome (Henstridge et al., 2019; Lindegaard et al., 2018).

It should also be noted that the small sample size in this pilot study may limit the ability to detect significant changes acutely following a high-fat meal. While this study provides valuable preliminary insights, a future study involving a larger cohort, including patients with metabolic syndrome, would be necessary to observe meaningful changes in plasma endothelial biomarkers and better understand the broader implications for gender-specific metabolic responses.

CONCLUSION

In summary, this pilot work indicates that the acute consumption of high-fat meals containing lard and palm olein, both rich in palmitic acid, does not have a significant effect on endothelial dysfunction biomarkers. The specific mechanisms underlying this outcome remain unclear based on these findings. Moreover, in-depth investigations are required to assess the long-term health implications of consuming different quantities and types of dietary fats in larger cohorts.

ACKNOWLEDGEMENT

We extend our gratitude to our colleagues Ms. Che Hui Ling, Ms. Fatmawati and Wong Weng Yew from the Malaysian Palm Oil Board (MPOB) for their technical assistance. This study received funding from the MPOB.

REFERENCES

Badimon, L., & Vilahur, G. (2014). Thrombosis formation on atherosclerotic lesions and plaque rupture. *Journal of Internal Medicine*, *276*(6), 618–632. https://doi.org/10.1111/joim.12296

Baer, D. J., Judd, J. T., Clevidence, B. A., & Tracy, R. P. (2004). Dietary fatty acids affect plasma markers of inflammation in healthy men fed controlled diets: A randomized crossover study. *American Journal of Clinical Nutrition*, *79*(6), 969–973. https://doi.org/10.1093/ajcn/79.6.969

Berry, S. E., Miller, G. J., & Sanders, T. A. (2007). The solid fat content of stearic acid-rich fats determines their postprandial effects. *American Journal of Clinical Nutrition*, *85*(6), 1486–1494. https://doi.org/10.1093/ajcn/85.6.1486

Cortés, B., Núñez, I., Cofán, M., Gilabert, R., Pérez-Heras, A., Casals, E., Deulofeu, R., & Ros, E. (2006). Acute effects of high-fat meals enriched with walnuts or olive oil on postprandial endothelial function. *Journal of the American College of Cardiology*, *48*(8), 1666–1671. https://doi.org/10.1016/j.jacc.2006.06.057

Cruz-Teno, C., Pérez-Martínez, P., Delgado-Lista, J., Yubero-Serrano, E. M., García-Ríos, A., Marín, C., Gómez, P., Jiménez-Gómez, Y., Camargo, A., Rodríguez-Cantalejo, F., Malagón, M. M., Pérez-Jiménez, F., Roche, H. M., & López-Miranda, J. (2012). Dietary fat modifies the postprandial inflammatory state in subjects with metabolic syndrome: The LIPGENE study. *Molecular Nutrition & Food Research*, *56*(6), 854–865. https://doi.org/10.1002/mnfr.201200096

De Souza, M. D. G. C., Maranhão, P. A., Panazzolo, D. G., Neto, J. F. N., Bouskela, E., & Kraemer-Aguiar, L. G. (2022). Effects of a high-fat meal on inflammatory and endothelial injury biomarkers in accordance with adiposity status: A cross-sectional study. *Nutrition Journal*, *21*(1), 65. https://doi.org/10.1186/s12937-022-00819-4

Dehghan, M., Mente, A., Zhang, X., Swaminathan, S., Li, W., Mohan, V., Iqbal, R., Kumar, R., Wentzel-Viljoen, E., Rosengren, A., Amma, L. I., Avezum, A., Chifamba, J., Diaz, R., Khatib, R., Lear, S., Lopez-Jaramillo, P., Liu, X., Gupta, R., Mohammadiford, N., ... Mapanga, R. (2017). Associations of fats and carbohydrate intake with cardiovascular disease and mortality in 18 countries from five continents (PURE): A prospective cohort study. *The Lancet*, *390*(10107), 2050–2062. https://doi.org/10.1016/s0140-6736(17)32252-3

Delgado-Lista, J., Lopez-Miranda, J., Cortés, B., Perez-Martinez, P., Lozano, A., Gomez-Luna, R., Gomez, P., Gomez, M. J., Criado, J., Fuentes, F., & Perez-Jimenez, F. (2008). Chronic dietary fat intake modifies the postprandial response of hemostatic markers to a single fatty test meal. *American Journal of Clinical Nutrition, 87(2)*, 317–322. https://doi.org/10.1093/ajcn/87.2.317

Diekmann, C., Huber, H., Preuß, M., Preuß, P., Predel, H., Stoffel-Wagner, B., Fimmers, R., Stehle, P., & Egert, S. (2019). Moderate postmeal walking has no beneficial effects over resting on postprandial lipemia, glycemia, insulinemia, and selected oxidative and inflammatory parameters in older adults with a cardiovascular disease risk phenotype: A randomized crossover trial. *Journal of Nutrition*, *149*(11), 1930–1941. https://doi.org/10.1093/jn/nxz148

Dror, E., Dalmas, E., Meier, D. T., Wueest, S., Thévenet, J., Thienel, C., Timper, K., Nordmann, T. M., Traub, S., Schulze, F., Item, F., Vallois, D., Pattou, F., Kerr-Conte, J., Lavallard, V., Berney, T., Thorens, B., Konrad, D., Böni-Schnetzler, M., & Donath, M. Y. (2017). Postprandial macrophage-derived IL-1β stimulates insulin, and both synergistically promote glucose disposal and inflammation. *Nature Immunology*, *18*(3), 283–292. https://doi.org/10.1038/ni.3659

Dumas, J. A., Bunn, J. Y., Nickerson, J., Crain, K. I., Ebenstein, D. B., Tarleton, E. K., Makarewicz, J., Poynter, M. E., & Kien, C. L. (2016). Dietary saturated fat and monounsaturated fat have reversible effects on brain function and the secretion of pro-inflammatory cytokines in young women. *Metabolism*, *65*(10), 1582–1588. https://doi.org/10.1016/j.metabol.2016.08.003

Esser, D., Van Dijk, S. J., Oosterink, E., Müller, M., & Afman, L. A. (2013). A high-fat SFA, MUFA, or n3 PUFA challenge affects the vascular response and initiates an activated state of cellular adherence in lean and obese middle-aged men. *Journal of Nutrition*, *143*(6), 843–851. https://doi.org/10.3945/jn.113.174540

Fernández-Real, J., Broch, M., Vendrell, J., & Ricart, W. (2003). Insulin resistance, inflammation, and serum fatty acid composition. *Diabetes Care*, *26*(5), 1362–1368. https://doi.org/10.2337/diacare.26.5.1362

Fritsche, K. L. (2015). The science of fatty acids and inflammation. *Advances in Nutrition*, *6*(3), 293S–301S. https://doi.org/10.3945/an.114.006940

Fuentes, F., López-Miranda, J., Pérez-Martínez, P., Jiménez, Y., Marín, C., Gómez, P., Fernández, J. M., Caballero, J., Delgado-Lista, J., & Pérez-Jiménez, F. (2008). Chronic effects of a high-fat diet enriched with virgin olive oil and a low-fat diet enriched with α-linolenic acid on postprandial endothelial function in healthy men. *British Journal of Nutrition*, *100*(1), 159–165. https://doi.org/10.1017/s0007114508888708

Henstridge, D. C., Abildgaard, J., Lindegaard, B., & Febbraio, M. A. (2019). Metabolic control and sex: A focus on inflammatory-linked mediators. *British Journal of Pharmacology*, *176*(21), 4193–4207. https://doi.org/10.1111/bph.14642

Hunter, K. A., Crosbie, L. C., Horgan, G. W., Miller, G. J., & Dutta-Roy, A. K. (2001). Effect of diets rich in oleic acid, stearic acid and linoleic acid on postprandial haemostatic factors in young healthy men. *British Journal of Nutrition*, *86*(2), 207–215. https://pubmed.ncbi.nlm.nih.gov/11502234

Kdekian, A., Alssema, M., Van Der Beek, E. M., Greyling, A., Vermeer, M. A., Mela, D. J., & Trautwein, E. A. (2020). Impact of isocaloric exchanges of carbohydrate for fat on postprandial glucose, insulin, triglycerides, and free fatty acid responses – A systematic review and meta-analysis. *European Journal of Clinical Nutrition*, *74*(1), 1–8. https://doi.org/10.1038/s41430-019-0534-6

Klein-Platat, C., Drai, J., Oujaa, M., Schlienger, J., & Simon, C. (2005). Plasma fatty acid composition is associated with the metabolic syndrome and low-grade inflammation in overweight adolescents. *American Journal of Clinical Nutrition*, *82*(6), 1178–1184. https://doi.org/10.1093/ajcn/82.6.1178

Kolovou, G. D., Anagnostopoulou, K. K., Pavlidis, A. N., Salpea, K. D., Iraklianou, S. A., Hoursalas, I. S., Mikhailidis, D. P., & Cokkinos, D. V. (2006). Metabolic syndrome and gender differences in postprandial lipaemia. *European Journal of Cardiovascular Prevention & Rehabilitation*, *13*(4), 661–664. https://doi.org/10.1097/01.hjr.0000224490.10845.26

Kritchevsky, D. (2000). Overview: Dietary fat and atherosclerosis. *Asia Pacific Journal of Clinical Nutrition*, *9*(2), 141–145. https://doi.org/10.1046/j.1440-6047.2000.00140.x

Kritchevsky, D., Tepper, S. A., Kuksis, A., Wright, S., & Czarnecki, S. K. (2000). Cholesterol vehicle in experimental atherosclerosis. 22. Refined, bleached, deodorized (RBD) palm oil, randomized palm oil and red palm oil.

Nutrition Research, *20*(6), 887–892. https://doi.org/10.1016/s0271-5317(00)00166-4

Lee, S., Ko, Y., Kwak, C., & Yim, E. (2016). Gender differences in metabolic syndrome components among the Korean 66-year-old population with metabolic syndrome. *BMC Geriatrics*, *16*(1), 27. https://doi.org/10.1186/s12877-016-0202-9

Lindegaard, B., Abildgaard, J., Heywood, S. E., Pedersen, B. K., & Febbraio, M. A. (2018). Female sex hormones are necessary for the metabolic effects mediated by loss of Interleukin 18 signaling. *Molecular Metabolism*, *12*, 89–97. https://doi.org/10.1016/j.molmet.2018.04.005

López-Moreno, J., García-Carpintero, S., Jimenez-Lucena, R., Haro, C., Rangel-Zúñiga, O. A., Blanco-Rojo, R., Yubero-Serrano, E. M., Tinahones, F. J., Delgado-Lista, J., Pérez-Martínez, P., Roche, H. M., López-Miranda, J., & Camargo, A. (2017). Effect of dietary lipids on endotoxemia influences postprandial inflammatory response. *Journal of Agricultural and Food Chemistry*, *65*(35), 7756–7763. https://doi.org/10.1021/acs.jafc.7b01909

Manning, P. J., Sutherland, W. H., McGrath, M. M., De Jong, S. A., Walker, R. J., & Williams, M. J. (2008). Postprandial cytokine concentrations and meal composition in obese and lean women. *Obesity*, *16*(9), 2046–2052. https://doi.org/10.1038/oby.2008.334

Margioris, A. N. (2009). Fatty acids and postprandial inflammation. *Current Opinion in Clinical Nutrition & Metabolic Care*, *12*(2), 129–137. https://doi.org/10.1097/mco.0b013e3283232a11

Masson, C. J., & Mensink, R. P. (2011). Exchanging saturated fatty acids for (n-6) polyunsaturated fatty acids in a mixed meal may decrease postprandial lipemia and markers of inflammation and endothelial activity in overweight men[1–3]. *Journal of Nutrition*, *141*(5), 816–821. https://doi.org/10.3945/jn.110.136432

Meessen, E. C. E., Sips, F. L. P., Eggink, H. M., Koehorst, M., Romijn, J. A., Groen, A. K., Riel, N. A. W., & Soeters, M. R. (2020). Model-based data analysis of individual human postprandial plasma bile acid responses indicates a major role for the gallbladder and intestine. *Physiological Reports*, *8*(5), e14358. https://doi.org/10.14814/phy2.14358

Mensink, R. P., Zock, P. L., Kester, A. D., & Katan, M. B. (2003). Effects of dietary fatty acids and carbohydrates on the ratio of serum total to HDL cholesterol and on serum lipids and apolipoproteins: A meta-analysis of 60 controlled trials. *American Journal of Clinical Nutrition*, *77*(5), 1146–1155. https://doi.org/10.1093/ajcn/77.5.1146

Nappo, F., Esposito, K., Cioffi, M., Giugliano, G., Molinari, A. M., Paolisso, G., Marfella, R., & Giugliano, D. (2002). Postprandial endothelial activation in healthy subjects and in type 2 diabetic patients: Role of fat and carbohydrate meals. *Journal of the American College of Cardiology*, *39*(7), 1145–1150. https://doi.org/10.1016/s0735-1097(02)01741-2

Orem, A., Yaman, S. O., Altinkaynak, B., Kural, B. V., Yucesan, F. B., Altinkaynak, Y., & Orem, C. (2018). Relationship between postprandial lipemia and atherogenic factors in healthy subjects by considering gender differences. *Clinica Chimica Acta*, *480*, 34–40. https://doi.org/10.1016/j.cca.2018.01.038

Peairs, A. D., Rankin, J. W., & Lee, Y. W. (2011). Effects of acute ingestion of different fats on oxidative stress and inflammation in overweight and obese adults. *Nutrition Journal*, *10*(1), 122. https://doi.org/10.1186/1475-2891-10-122

Rathnayake, K. M., Weech, M., Jackson, K. G., & Lovegrove, J. A. (2018). Meal fatty acids have differential effects on postprandial blood pressure and biomarkers of endothelial function but not vascular reactivity in postmenopausal women in the randomized controlled dietary intervention and VAScular function (DIVAS)-2 study. *Journal of Nutrition*, *148*(3), 348–357. https://doi.org/10.1093/jn/nxx042

Rubin, D., Helwig, U., Nothnagel, M., Lemke, N., Schreiber, S., Fölsch, U. R., Döring, F., & Schrezenmeir, J. (2008). Postprandial plasma adiponectin decreases after glucose and high fat meal and is independently associated with postprandial triacylglycerols but not with − 11388 promoter polymorphism. *British Journal of Nutrition*, *99*(1), 76–82. https://doi.org/10.1017/s0007114507791857

Sanders, T. A., Filippou, A., Berry, S. E., Baumgartner, S., & Mensink, R. P. (2011). Palmitic acid in the *sn*-2 position of triacylglycerols acutely influences postprandial lipid metabolism. *American Journal of Clinical Nutrition*, *94*(6), 1433–1441. https://doi.org/10.3945/ajcn.111.017459

Schillaci, G., Marchesi, S., Siepi, D., Lupattelli, G., Vaudo, G., Pasqualini, L., & Mannarino, E. (2001). Gender differences in postprandial endothelial function. *The American Journal of Cardiology*, *87*(11), 1323–1325. https://doi.org/10.1016/s0002-9149(01)01535-1

Schönknecht, Y. B., Crommen, S., Stoffel-Wagner, B., Coenen, M., Fimmers, R., Holst, J. J., Simon, M., Stehle, P., & Egert, S. (2020). Acute effects of three different meal patterns on postprandial metabolism in older individuals with a risk phenotype for cardiometabolic diseases: A randomized controlled crossover trial. *Molecular Nutrition & Food Research*, *64*(9), 1901035. https://doi.org/10.1002/mnfr.201901035

Schönknecht, Y. B., Crommen, S., Stoffel-Wagner, B., Coenen, M., Fimmers, R., Stehle, P., & Egert, S. (2022). Influence of a proinflammatory state on postprandial outcomes in elderly subjects with a risk phenotype for cardiometabolic diseases. *European Journal of Nutrition*, *61*(6), 3077–3083. https://doi.org/10.1007/s00394-022-02870-7

Sciarrillo, C. M., Koemel, N. A., Tomko, P. M., Bode, K. B., & Emerson, S. R. (2019). Postprandial lipemic responses to various sources of saturated and monounsaturated fat in adults. *Nutrients*, *11*(5), 1089. https://doi.org/10.3390/nu11051089

Siri-Tarino, P. W., Sun, Q., Hu, F. B., & Krauss, R. M. (2010). Meta-analysis of prospective cohort studies evaluating the association of saturated fat with cardiovascular disease. *American Journal of Clinical Nutrition*, *91*(3), 535–546. https://doi.org/10.3945/ajcn.2009.27725

Telle-Hansen, V. H., Christensen, J. J., Ulven, S. M., & Holven, K. B. (2017). Does dietary fat affect inflammatory markers in overweight and obese individuals? – A review of randomized controlled trials from 2010 to 2016. *Genes & Nutrition*, *12*(1), 26. https://doi.org/10.1186/s12263-017-0580-4

Teng, K., Chang, C., Kanthimathi, M. S., Tan, A. T. B., & Nesaretnam, K. (2015). Effects of amount and type of dietary fats on postprandial lipemia and thrombogenic markers in individuals with metabolic syndrome. *Atherosclerosis*, *242*(1), 281–287. https://doi.org/10.1016/j.atherosclerosis.2015.07.003

Teng, K., Chang, L. F., Vethakkan, S. R., Nesaretnam, K., & Sanders, T. A. (2017). Effects of exchanging carbohydrate or monounsaturated fat with saturated fat on inflammatory and thrombogenic responses in subjects with abdominal obesity: A randomized controlled trial. *Clinical Nutrition*, *36*(5), 1250–1258. https://doi.org/10.1016/j.clnu.2016.08.026

Teng, K., Nagapan, G., Cheng, H. M., & Nesaretnam, K. (2011). Palm olein and olive oil cause a higher increase in postprandial lipemia compared with lard but had no effect on plasma glucose, insulin and adipocytokines. *Lipids*, *46*(4), 381–388. https://doi.org/10.1007/s11745-010-3516-y

Thijssen, M. A., Hornstra, G., & Mensink, R. P. (2005). Stearic, oleic, and linoleic acids have comparable effects on markers of thrombotic tendency in healthy human subjects. *Journal of Nutrition*, *135*(12), 2805–2811. https://doi.org/10.1093/jn/135.12.2805

Tholstrup, T., Miller, G. J., Bysted, A., & Sandström, B. (2003). Effect of individual dietary fatty acids on postprandial activation of blood coagulation factor VII and fibrinolysis in healthy young men. *American Journal of Clinical Nutrition*, *77*(5), 1125–1132. https://doi.org/10.1093/ajcn/77.5.1125

Tholstrup, T., Teng, K., & Raff, M. (2011). Dietary cocoa butter or refined olive oil does not alter postprandial HSCRP and IL-6 concentrations in healthy women. *Lipids*, *46*(4), 365–370. https://doi.org/10.1007/s11745-011-3526-4

Tsai, W., Li, Y., Lin, C., Chao, T., & Chen, J. (2004). Effects of oxidative stress on endothelial function after a high-fat meal. *Clinical Science*, *106*(3), 315–319. https://doi.org/10.1042/cs20030227

Unek, I. T., Bayraktar, F., Solmaz, D., Ellidokuz, H., Sisman, A. R., Yuksel, F., & Yesil, S. (2010). The levels of soluble CD40 ligand and C-Reactive protein in normal weight, overweight and obese people. *Clinical Medicine & Research*, *8*(2), 89–95. https://doi.org/10.3121/cmr.2010.889

Wang, D., Wang, Z., Zhang, L., & Wang, Y. (2017). Roles of cells from the arterial vessel wall in atherosclerosis. *Mediators of Inflammation*, *2017*, 1–9. https://doi.org/10.1155/2017/8135934

Zhao, Y., Liu, L., Yang, S., Liu, G., Pan, L., Gu, C., Wang, Y., Li, D., Zhao, R., & Wu, M. (2021). Mechanisms of atherosclerosis induced by postprandial lipemia. *Frontiers in Cardiovascular Medicine*, *8*, 636947. https://doi.org/10.3389/fcvm.2021.636947.

Journal of Oil Palm Research Vol. 38 (3) September 2026 p. 581–592
DOI: https://doi.org/10.21894/jopr.2025.0030

MIXTURE DESIGN OPTIMISATION OF RED PALM OIL IN CANDY: EFFECTS ON HARDNESS AND FRIABILITY

TECK-KIM TANG[1]*; NORAZURA AILA MOHD HASSIM[1]; SOON-SEN LEOW[1]; SIVARUBY KANAGARATNAM[1]; RADHIKA LOGANATHAN[1]; HAZRATI WAZIR[1]; NUR HAQIM ISMAIL[1] and MEI-HUEY SAW[1]

ABSTRACT

Although red palm oil (RPO) is rich in carotenes (500–800 ppm) and vitamin E (800 ppm), its unique flavour may not be appealing to some consumers. Incorporating RPO in candy not only toning down the flavour but also serves as a convenient delivery system and increases its market acceptability. In this study, direct compression was chosen for preparing candy, as it generates minimal heat, thereby preserving most of the carotenes and vitamin E. The primary objective of this study was to optimise the formulation of RPO candy to achieve desirable responses: Hardness and friability. The process began with the screening of raw materials. Screening results indicated that erythritol with the highest sweetness-to-calorie ratio was a good candidate with a mesh size of 80–100, exhibited fair flow properties and good homogeneity. Gum arabic was selected among the three tested binders due to its highest binding ability. The mixture design was employed to examine the interaction of the three components: Erythritol, RPO powder (RPOP) and gum arabic on the responses. Through the optimisation process, the formulation consisting of 50.0% erythritol, 10.0% RPOP and 33.5% gum arabic was successful in producing intact RPO candy.

Keywords: candy, carotenes, red palm oil, vitamin E.

Received: 1 August 2024**; Accepted:** 13 April 2025**; Published online:** 13 June 2025.

INTRODUCTION

Red palm oil (RPO) is a type of refined palm oil rich in carotenes (500–800 ppm) and vitamin E (800 ppm). The carotenes in RPO function not only as pro-vitamin A, which is essential for eye health, but also act as a strong antioxidant with several health effects (Bohn, 2019; Parveez et al., 2023; Tan et al., 2021). In addition, the vitamin E in RPO is predominantly composed of tocotrienols, which exhibit higher antioxidant properties compared to the commonly recognised form of vitamin E – i.e., tocopherols (Szewczyk et al., 2021).

[1] Malaysian Palm Oil Board,
6, Persiaran Institusi, Bandar Baru Bangi,
43000 Kajang, Selangor, Malaysia.

* *Corresponding author e-mail: teck.kim@mpob.gov.my*

Studies conducted on RPO have revealed several promising health benefits. A meta-analysis conducted by Dong et al. (2017) demonstrated that RPO effectively addresses vitamin A deficiency in both adults and children. Furthermore, RPO may help reduce cholesterol and triglycerides supported by evidence from both human and animal studies. Its antiatherogenic properties contribute to improved cardiovascular health (Loganathan et al., 2017). Due to its antioxidant-rich composition, RPO could improve oxidative status by reducing oxidative stress in patients with cardiovascular disease, cancer and other chronic diseases. Subsequently, lowering the risk of atherosclerosis and supporting overall wellbeing (Oguntibeju et al., 2009).

In animal models, RPO shows potential in preventing neurodegenerative diseases like Alzheimer's disease. It improved cognitive function, increased levels of dopamine and antioxidant biomarkers and enhanced the spatial memory of treated rats. These effects are attributed to RPO's rich antioxidant profile, which helps mitigate neuron, mitochondrial, protein and DNA damage caused by aging-related oxidative stress (Zubaidi et al., 2021).

Despite RPO numerous health benefits, its distinct flavour may be unappealing to some individuals. Moreover, the commercially available RPO is typically in liquid form and is heat sensitive. Therefore, incorporating RPO into the food matrix could increase its acceptability and ease of consumption while preserving its nutrient profile. For instance, candy provides a ready-to-eat option that requires no additional preparation, making it a practical and desirable alternative for delivering RPO.

Candy is generally well-accepted due to its sweet taste, appealing flavour, ease of consumption, no additional preparation required during consumption and most importantly ability to mask RPO's distinct flavour. However, the use of sugar (usually sucrose) in conventional candy making has drawbacks. For example, the candy must be heated to melt and the mixing process with other ingredients is conducted at high temperatures. In view that carotenes are heat sensitive, they start to degrade at temperatures of 65°C (Demiray & Tulek, 2017). Thus, using the conventional candy-making process can lead to a significant loss of carotenes as well as other heat-sensitive vitamins during the process.

Besides that, high sugar content in candy can pose health issues such as tooth decay and type 2 diabetes if consumed excessively (Jayadevan et al., 2019; Qin et al., 2020). While sugar substitutes are widely used to replace sugar to avoid these problems, some of them, particularly artificial sweeteners such as aspartame possess side effects, including being harmful to individuals with phenylketonuria and possibly carcinogenic (Czarnecka et al., 2021). The existing evidence is inconclusive regarding the potential heightened risk of certain cancers with extended and frequent use of artificial sweeteners (Mishra et al., 2015). Nevertheless, this uncertainty contributes to consumer apprehension about the use of artificial sweeteners.

Although being natural does not necessarily mean that a product is safe, it is important to consider consumer preferences in product development. Natural sweeteners, such as sugar alcohols, are gaining prominence in recent years due to their safety guarantees, low calorie content and absence of oral issues (Mazi & Stanhope, 2023). They have gained interest as good candidates as sugar replacers with fewer side effects and possess the added benefit of providing bulkiness (better texture or mouthfeel) to the product.

Another important ingredient in candy making is the binder. Gum arabic is a good candidate due to its good binding effects, film-forming capability and can improve texture while preventing sugar crystallisation, making it beneficial for soft candies and gummy products (Afoakwah et al., 2023). Microcrystalline cellulose is also used as a binder. It enhances texture and stability in candy formulations by acting as a filler, disintegrant, lubricant and glidant (Bordoloi et al., 2021; Zhao et al., 2022). Additionally, staple food ingredients like rice flour, especially glutinous rice, have a higher oil-binding ability when heat-treated (Tabara et al., 2015).

Binders play a crucial role in candy making especially in processes like direct compression which involves minimal heat. For candy-making process, direct compression is one of the best methods for preparing candies that contain heat-sensitive compounds. Under short compression, the heat generated is minimal, allowing for the preservation of carotenes and vitamins in RPO. However, incorporating RPO into candy via direct compression may impose several challenges. Firstly, the addition of oil can reduce the flowability of the premix powder, causing clumping. A flowable powder is crucial to ensure smooth candy production during the feeding process of direct compression. Additionally, the presence of oil can interrupt the binder function of ingredients, causing a reduction in candy hardness and an increase in friability. Therefore, the main objective of this study is to determine the optimal composition for producing RPO candy, specifically addressing challenges related to flowability, hardness and friability of the product.

MATERIALS AND METHODS

Materials

RPO powder (RPOP, 70% w/w oil content) was procured from Lipidchem Sdn. Bhd., Johor, Malaysia and stored at –20°C prior to use. Erythritol, gum arabic, microcrystalline cellulose and other food ingredients used in the candy-making process were of food grade. The RPO used in this study contained 874.4 ppm carotenes and 503.1 ppm vitamin E.

Experimental Design

A screening was performed to select sugar alcohol types and the mesh size of the sugar alcohol with the highest sweetness to calorie ratio, binder types and RPOP range. Following the screening process, the selected ingredients were incorporated into the mixture design to study their interactions in terms of powdered mix flowability, hardness and friability of the produced candy.

Sugar Alcohol Selection and Evaluation

The sweetness level and calories of various sugar alcohols were evaluated through a literature search. The ratio of sweetness per calorie was calculated, and the sugar alcohol with the lowest calorie was chosen.

Mesh Size Selection of Selected Sugar Alcohol Based on Granular Separation and Flowability

Two sets of chosen sugar alcohols with different mesh sizes (40–60 and 80–100 mesh sizes) were tested for granular separation and flowability after being thoroughly mixed with other candy making ingredients. For homogeneity, the mixtures were tapped 700 times using a tap density tester (Electrolab, India). The colour distribution within the mixture was used as an indicator to determine the granular separation of the sample. Non-granular separation showed uniform yellow colour distribution whereas granular separation displayed non-uniform yellow colour distribution. The mixtures' flowability was then tested using an angle of repose. The test method involved carefully pouring 100 g of powdered mix into a funnel with a 10 mm nozzle to build a cone, with the height of the funnel to the base being 100 mm (Mat Dian et al., 2019). The diameter and the height of the built cone were measured, and the angle of repose was calculated using the following Equation (1):

$$\text{Angle of repose} = \tan^{-1}\left(\frac{2 \text{ x height}}{\text{diameter}}\right) \quad (1)$$

The mesh size of sugar alcohol that was able to form a homogenous candy mixture and able to flow without aid (as determined by angle of repose) was chosen.

Binder Selection and RPOP Range

Four different binders, namely gum arabic, microcrystalline cellulose (MCC), glutinous rice flour (GRF) and cooked GRF, were evaluated for their binding abilities based on the intactness of candy produced. The screening process began with the mixing of ingredients. The amount of sugar alcohol, glidant and lubricant was kept constant, while the amount of binder and RPOP were varied. The process started with 10% RPOP and 33% binder to give a total composition of 43% while other ingredients were kept constant, then progressed to 15% RPOP with 28% binder, and continued in 5% intervals up to a maximum of 30% RPOP. The mixtures were then used to produce candy using an automatic tableting machine, Model EP200 (Elizabeth Parle, India). During this process, the integrity of the produced candies was observed. A candy was deemed intact if it remained unbroken upon release from the mould. Binders capable of producing intact candy with higher amounts of RPOP were chosen and this value was used to set the upper limit of RPOP in the mixture design.

Optimisation of RPO Candy

Design of experiment. Mixture design is commonly used when the responses depend on the proportions of the different ingredients rather than the absolute amount. Unlike factorial and response surface methodology, where the ingredients are treated independently, this method is suitable in formulation studies as the total amount of the overall composition remains constant despite changes in the formulation. Therefore, in this study, a Mixture Design-Optimal (Custom) Design was generated by Design-Expert® v13 software (Stat-Ease Inc., USA) and used to study the formulation of the candy ingredients. The selection of ingredients/components and the lower and upper constraints of each component were based on the screening results and literature reviews. Three major components comprising chosen sugar alcohol, RPOP and binder, and the responses of flowability of powdered mix, hardness and friability of the candy, were studied. The ranges for erythritol (A), RPOP (B) and gum arabic (C) in the candy formulation were set from 50.0%–73.5%, 10.0%–20.0%, 10.0%–33.5%, respectively and their combination was 93.5% of the formulation. Other additives constituted the remaining 6.5% were kept constant. A total of 16 runs (formulations) were generated by the software.

Preparation of powdered mix and candy. All ingredients were sieved and thoroughly mixed to create the powdered mix. The flowability of the powdered mix was assessed by angle of repose. Subsequently, the powdered mix was used to produce candy using an automatic tableting machine, Model EP200. The hardness and friability of the resulting candy were analysed.

Data Analysis, Model Fitting and Evaluation of Mixture Design

The software was used to analyse experimental data and create the models to define the relationship between components and responses. All responses were fitted to linear, quadratic, special cubic and cubic models. Statistical analyses were performed using analysis of variance (ANOVA). The model selection was based on the *p*-value of the model (must be lower than 0.05), coefficient of determination (R^2), adjusted R^2, predicted R^2, predicted residual sum of squares (PRESS) and lack of fix (*p*-value must be higher than or equal to 0.05).

Subsequently, the data were checked for normality and homogeneity using Box-Cox plots to determine if transformation was needed. Cook's distance was used to identify any outliers.

Optimisation of Candy Formulation

Based on the well fitted model obtained, optimisation was conducted to achieve the acceptable flowability and maximum value of hardness, while minimising friability of the candy with maximum RPOP content.

Flowability of powdered mix. The flowability of the ingredients was determined using the angle of repose as described previously.

Hardness of candy. Hardness of the candies was measured using a Texture Analyser, model TA.XTplusC (Stable Micro System, United Kingdom) according to Nakhon et al. (2023) with slight modification. A 30 kg load cell weight and a cylinder probe p35 were used. Five samples were compressed with a trigger distance of 1.6 mm and a force of 100 g. The maximum force recorded was defined as the hardness of the candies.

Friability of candy. Friability of the candy was determined using a friabilitor, model PI-FTV-01 (Pharmag Instruments, India). The test was conducted at a rotation speed of 25 rpm for 100 cycles. Initially, 10 tablets (candies) were weighed and placed in the friabilitor. After completing 100 cycles, the tablets (candies) were weighed again to determine the final weight. The weight loss was calculated by subtracting the final weight from the initial weight. The weight loss percentage, friability was determined as Equation (2) (Osei-Yeboah & Sun, 2015).

$$\text{Friability} = \left[\frac{(\text{Weight}_{\text{initial}} - \text{Weight}_{\text{final}})}{\text{Weight}_{\text{initial}}}\right] \times 100 \qquad (2)$$

Data Analysis

All experiments were performed in triplicate unless otherwise stated. Results are expressed as means ± standard deviations.

RESULTS AND DISCUSSION

Selection of Sugar Alcohol and Its Mesh Size

There are several types of sugar alcohols available in the market, such as erythritol, xylitol, sorbitol, maltitol and mannitol. Although many of these are claimed as zero calories, they do contain some calories. The results of the literature review and the calculated sweetness per calorie ratios are presented in *Table 1*. Most of the sugar alcohols exhibit lower sweetness compared to sucrose. However, erythritol has a high sweetness per calorie ratio of 2.5–3.5. This suggests that erythritol has lower calories while providing acceptable sweetness, making it a suitable ingredient for lower-calorie products while providing sufficient sweetness, particularly useful in products such as confectionery, beverages and baked goods (Li et al., 2023). Considering that obesity is a significant health issue in many countries, creating low-calorie products could be an effective approach to address this problem (Nogueira-de-Almeida & Filho, 2021). Besides, consumption of erythritol does not raise the blood sugar level and may help in preventing diabetes. It is also a good alternative for diabetic patients, allowing for controlled consumption without impacting blood sugar levels. Furthermore, candy made with erythritol does not pose the oral health problem, since it is not metabolised by oral bacteria that cause tooth decay. Therefore, in this study, erythritol with the highest sweetness per calorie ratio was selected for the development of the RPO candy.

Particle size significantly influences the flowability of ingredients. Generally, the granulated form (smaller mesh size) of the same ingredients exhibits better flowability than powdered forms (larger mesh size), as granulated ingredients have lesser interactions between particles (Mullarney et al., 2003). Although a small mesh size (big particles) offers better flow properties, it may cause granular separation when mixed with other fine particles. This phenomenon occurs when the larger particles tend to concentrate at the top and smaller particles settle at the bottom during shaking or vibration (Porion et al., 2004).

TABLE 1. SUGAR ALCOHOLS' SWEETNESS AND CALORIE CONTENT

Sugar alcohol	Relative sweetness to sucrose	Calorie (kcal/g)	Ratio (sweetness/ calorie)
Erythritol	0.5–0.7	0.2	2.50–3.50
Xylitol	1.0	3.0	0.33
Sorbitol	0.5–0.7	2.6	0.19–0.27
Maltitol	0.9	3.0	0.30
Mannitol	0.5–0.7	1.6	0.31–0.44
Sucrose (as reference)	1.0	4.0	0.25

Source: Health Canada (2005).

In this study, the flowability and granular separation effect of two common mesh sizes of erythritol (40–60 and 80–100 mesh sizes) were assessed after mixing with other candy-making ingredients to form the powdered mix. The powdered mix with 40–60 mesh erythritol exhibited higher flowability (good range); however, granular separation was observed after 700 taps. This indicates that the powdered mix using this mesh size of erythritol can cause a non-homogeneous sample during candy production. In contrast, the flowability of the powdered mix containing 80–100 mesh erythritol fell within the fair range, but no granular separation was observed after 700 taps. This suggests that the mix could flow freely during the feeding process of candy production while maintaining homogeneity with other ingredients. Flowable raw materials are essential in direct compression, as the materials must be able to flow and properly fill the mould. Raw materials that do not flow freely can form arches or ratholes in the hopper leading to production stoppage. Nevertheless, flowability can be improved using various tools such as vibratory feeders and stirring devices (Hörmann-Kincses et al., 2022). Therefore, erythritol with an 80–100 mesh size that ensures homogeneity and consistency was chosen for the production of RPO candy.

Screening of Binder and RPOP Range

In the candy production, binders play an important role in holding ingredients together. Binders are crucial as they determine the texture and structural integrity of the candy, such as its softness, or hardness, which ultimately affects the mouthfeel of the final product. The ability of various binders to form an intact candy with different amounts of RPOP is shown in *Table 2*. Powdered mixes using gum arabic and MCC as binders successfully formed intact candy with up to 20% of RPOP. However, when GRF and cooked GRF were used, the powdered mixes failed to form intact candy even at the lowest amount of RPOP (10%), indicating poor binding properties. Gum arabic not only demonstrated superior binding properties compared to other binders, but it also did not possess the dry mouthfeel effect associated with MCC. Therefore, gum arabic was chosen for the subsequent mixture design study, with the maximum range of RPOP set at 20%, beyond which intact candies could not be formed.

The following parameters, determined through screening, were incorporated into the mixture design: Erythritol (sweetener), 80–100 mesh erythritol, gum arabic (binder) and RPOP (maximum 20%).

Evaluation of Mixture Design

Modelling fitting of the responses. The flowability of the powdered mix, hardness and friability of the produced candy, were determined and are presented in *Table 3*. None of the models fitted well with the flowability of the powdered mix, as *p*-values of the models were higher than 0.05, indicating non-significance in the models (data not shown). The observed variation in flowability, represented by the angle of repose, ranged between 36.94 and 40.58 (*Table 3*), indicating a narrow range. This suggested that the flowability of the powdered mix was not significantly influenced by the three components within the designed range. Generally, the flowability of the powder is greatly influenced by the oil content and the particle size of the ingredients.

Given that the powdered mix was made from erythritol with the same mesh size (80–100) and a narrow range of RPOP, the lack of statistical significance in the models was anticipated. Nevertheless, the angle of repose of the powdered mixes remained within the free-flow range (36–40) and none of the samples within 16 runs formed arches or ratholes in the hopper during the candy making process (Mat Dian et al., 2019). Even though no model could be built for flowability, it still fulfilled our objective. Widening the range of RPOP to more than 20% or below 10% to allow a model to be built, could lead to the production of broken candy for RPOP above 20%, while using less than 10% RPOP would compromise the purpose of making RPO candy.

Statistical analysis suggested that the best model for hardness was the quadratic model with a *p*-value of 0.0011 (significant), while for friability the best model was linear with a *p*-value of less than 0.0001 (*Table 4*). Model validation was assessed

TABLE 2. BINDER EFFECTIVENESS WITH DIFFERENT RED PALM OIL POWDER (RPOP) PERCENTAGES

Binder	RPOP % (w/w)				
	10	15	20	25	30
Gum arabic	O	O	O	X	X
Microcrystalline cellulose (MCC)	O	O	O	X	X
Glutinous rice flour (GRF)	X	X	X	X	X
Cooked GRF	X	X	X	X	X

Note: O - intact, X - not intact.

TABLE 3. COMPOSITION OF RED PALM OIL (RPO) CANDY (16 RUNS) AND THE RESPONSES

Run	Component			Responses		
	A (%)	B (%)	C (%)	Angle of repose (N/A)	Hardness of candy (N)	Friability (%)
13	62.4	20.0	11.1	39.73 ± 0.35	6.22 ± 0.50	28.64 ± 2.95
3	57.5	20.0	16.0	38.28 ± 0.62	8.45 ± 0.80	19.65 ± 6.48
11	67.6	15.9	10.0	38.67 ± 0.56	8.74 ± 0.51	19.30 ± 5.92
16	53.0	19.2	21.3	38.54 ± 0.25	8.83 ± 0.73	11.45 ± 3.02
14	63.6	14.5	15.4	39.50 ± 0.45	9.77 ± 0.51	12.27 ± 2.03
7	67.6	15.9	10.0	38.68 ± 0.32	9.85 ± 0.39	10.13 ± 3.70
12	50.0	16.4	27.1	38.83 ± 0.24	10.42 ± 0.74	4.64 ± 1.40
8	63.6	14.5	15.4	39.57 ± 0.29	11.75 ± 0.66	11.88 ± 2.97
2	50.0	16.4	27.1	37.70 ± 0.50	12.29 ± 0.69	8.66 ± 2.77
15	60.8	11.8	20.9	39.76 ± 0.25	16.27 ± 0.68	7.87 ± 5.08
4	60.8	11.8	20.9	36.94 ± 0.55	18.43 ± 1.35	6.16 ± 1.15
9	73.5	10.0	10.0	40.58 ± 0.38	18.44 ± 1.33	4.30 ± 0.56
6	60.8	11.8	20.9	38.52 ± 0.31	20.95 ± 1.47	4.81 ± 1.62
1	68.4	10.0	15.1	37.32 ± 0.29	22.70 ± 1.10	5.59 ± 3.85
5	56.0	10.0	27.5	37.65 ± 0.59	29.43 ± 1.16	3.46 ± 0.29
10	50.0	10.0	33.5	39.11 ± 0.37	31.30 ± 1.47	3.37 ± 1.23

Note: Mean value ± standard deviation; N - Newton; N/A - not applicable; A - erythritol; B - red palm oil powder (RPOP); C - gum arabic.

using indicators such as lack of fit, R^2 and other relevant metrics, as detailed below: The lack-of-fit was insignificant for both of the models, indicating a good fit to the data, with *p*-values of 0.6748 and 0.7107 for hardness and friability respectively. The hardness model also demonstrated a high R^2 of 0.9714, adjusted R^2 of 0.9571 and predicted R^2 of 0.9229, indicating a good fit and strong predictive power. The model's adequate precision of 24.56 (greater than 4) suggests a good signal-to-noise ratio (Kumar, 2020). For friability, the R^2, adjusted R^2 and predicted R^2 values were 0.8289, 0.8025 and 0.7207, respectively, indicating a good fit to the data with slightly lower predictive power. The adequate precision of the friability model was 16.88, which was also higher than 4. Cook's distance showed no outliers in the data for either response. The Box-Cox plot suggested that no data transformation was needed for hardness, while a log transformation of the data was needed for friability. Coded Equations (3) and (4) of the models are shown as follows:

$$\text{Hardness} = 19.28A + 47.30B + 31.66C - 95.96AB - 1.61AC - 123.08BC \quad (3)$$

$$\text{Log}_{10}\ \text{friability} = 0.831A + 2.12B + 0.44C \quad (4)$$

where, A is erythritol, B is RPOP and C is gum arabic.

Table 5 presents the coefficients along with the corresponding variance inflation factors (VIF) of the equation. The coefficients in the equation quantify the change in response for a one-unit change in the component, assuming all remaining components are held constant. A positive value indicates a positive effect, while a negative value indicates a negative effect on the response. VIF measures the multi-collinearity of the coefficients. If the value is 1, there is no correlation between the components. A VIF greater than 1 indicates multicollinearity. The greater the VIF, the more severe the correlation of factors.

Hardness of candy. The coefficients in *Table 5* indicate that gum arabic has a greater positive effect on the hardness of candy, with a coefficient of 31.66, compared to erythritol's coefficient of 19.28. The low VIF for both gum arabic (2.91) and erythritol (3.47) shows that their coefficients are less correlated with other ingredients, or higher accuracy towards the prediction of the hardness of the candy. Since both components positively affect the hardness of candy, it was anticipated that their interaction should produce a synergistic effect. However, the negative coefficient of erythritol and gum arabic combinations (AC), indicated that both ingredients counteract each other, resulting in a reduction in candy hardness. Fortunately, the antagonistic effect is just minor, with a coefficient of –1.61. Overall, the results suggest that an increase in these two components can help to improve the hardness of the candy but gum arabic has a more prominent effect due to its high coefficient value (31.66) and low VIF value (2.91). In order to improve the hardness of the candy one must increase the amount of gum arabic rather than erythritol.

TABLE 4. FIT SUMMARY OF THE MODELS

Suggested model	Source	Sequential *p*-value	Lack of fit *p*-value	R^2	Adjusted R^2	Predicted R^2	Adequate precision
Hardness	Quadratic	0.0011	0.6748	0.9714	0.9571	0.9229	24.56
Friability	Linear	<0.0001	0.7107	0.8289	0.8025	0.7207	16.88

Note: R^2 - coefficient of determination.

TABLE 5. COEFFICIENTS IN TERMS OF CODED FACTORS

Component	Coefficient			
	Hardness	VIF	Log_{10} friability	VIF
A	19.28	3.47	0.8296	1.47
B	47.30	62.83	2.1200	1.72
C	31.66	2.91	0.4448	1.35
AB	-95.96	33.63	-	-
AC	-1.61	2.58	-	-
BC	-123.08	24.47	-	-

Note: VIF - variance inflation factor; A - erythritol; B - RPOP; C - gum arabic; AB - erythritol + RPOP; AC - erythritol + gum arabic; BC - RPOP + gum arabic.

Meanwhile, the RPOP which had the highest coefficient (47.30), reflects the greatest positive effect on the hardness of candy. However, the high VIF value (62.83) indicated that its coefficient was highly correlated with other components in the formulation. This is evident from RPOP's interaction with erythritol (AB), which had a negative coefficient value of –95.96, and interaction with gum arabic (BC), which had a negative value of –123.08. The result indicated that increasing the amount of RPOP in the formulation will have a substantial negative effect on the hardness of the candy. Similar results have been observed in hard candies, where an increase in liquid components (such as water or oil content) led to a reduction in hardness (Souiy et al., 2023). Overall, in order to maximise the RPOP, the gum arabic amount should be increased to counterbalance the negative impact and the amount of erythritol must be reduced.

The interaction plot of two component mixes (AB, BC and AC) and a contour plot of three components on the hardness of candy are illustrated in *Figure 1*. The two component mixes in *Figure 1a–1b* revealed the non-linear interaction of RPOP with erythritol and gum arabic toward the hardness of the candy. When the percentage of RPOP reduced linearly (and other components increased linearly), the hardness of the candy increased exponentially. This shows a strong inverse relationship between RPOP content and candy hardness. In other words, the hardness of the candy was significantly influenced by the RPOP content, as a linear increase in RPOP can trigger a substantial exponential reduction in hardness (*Figure 1b*). To resemble a soft chewable tablet, the hardness of the candy should be above 1.5 kp (around 15 N) and should not exceed 12.0 kp (117 N) (Robinson et al., 2006; U.S. Food and Drug Administration [FDA], 2018). This implies that RPOP has to be kept low in the formulation to maintain the hardness of the candy within the soft chewable range. It can be deduced from *Figure 1b* that the maximum RPOP is approximately 12.5%.

Apart from this, the two-component mix plot of AC (*Figure 1c*) revealed that the linear interaction of erythritol and gum arabic blending on the hardness of candy, with gum arabic having a dominating effect on improving hardness (indicated by the increase of hardness when its amount increases). The contour plot (*Figure 1d*) summarises the effects of three components on the hardness of the candy. The colour transitions from dark blue through green to red, indicating an increase in hardness from low to high values. The plot also illustrated that the maximum hardness of the candy (~31 N) can be achieved with the lowest amount of RPOP and erythritol, with the maximum amount of gum arabic. Maximising RPOP in a candy production using direct compression while maintaining its hardness was a challenge nevertheless through adjustment of gum arabic content and sugar amount, the desired sweetness and hardness can be achieved.

Friability of candy. Friability is another criterion in tablet making. It describes the tendency of candy to break, chip and crumble under mechanical stress, such as handling, packaging and transportation. It can also be applied in candy making to determine how susceptible a candy is to mechanical stress (Zhao et al., 2022). High friability suggests that a candy is likely to break easily. Referring to Equation (4), RPOP (B) had a higher coefficient of 2.12, indicating a significant positive effect on friability of the candy,

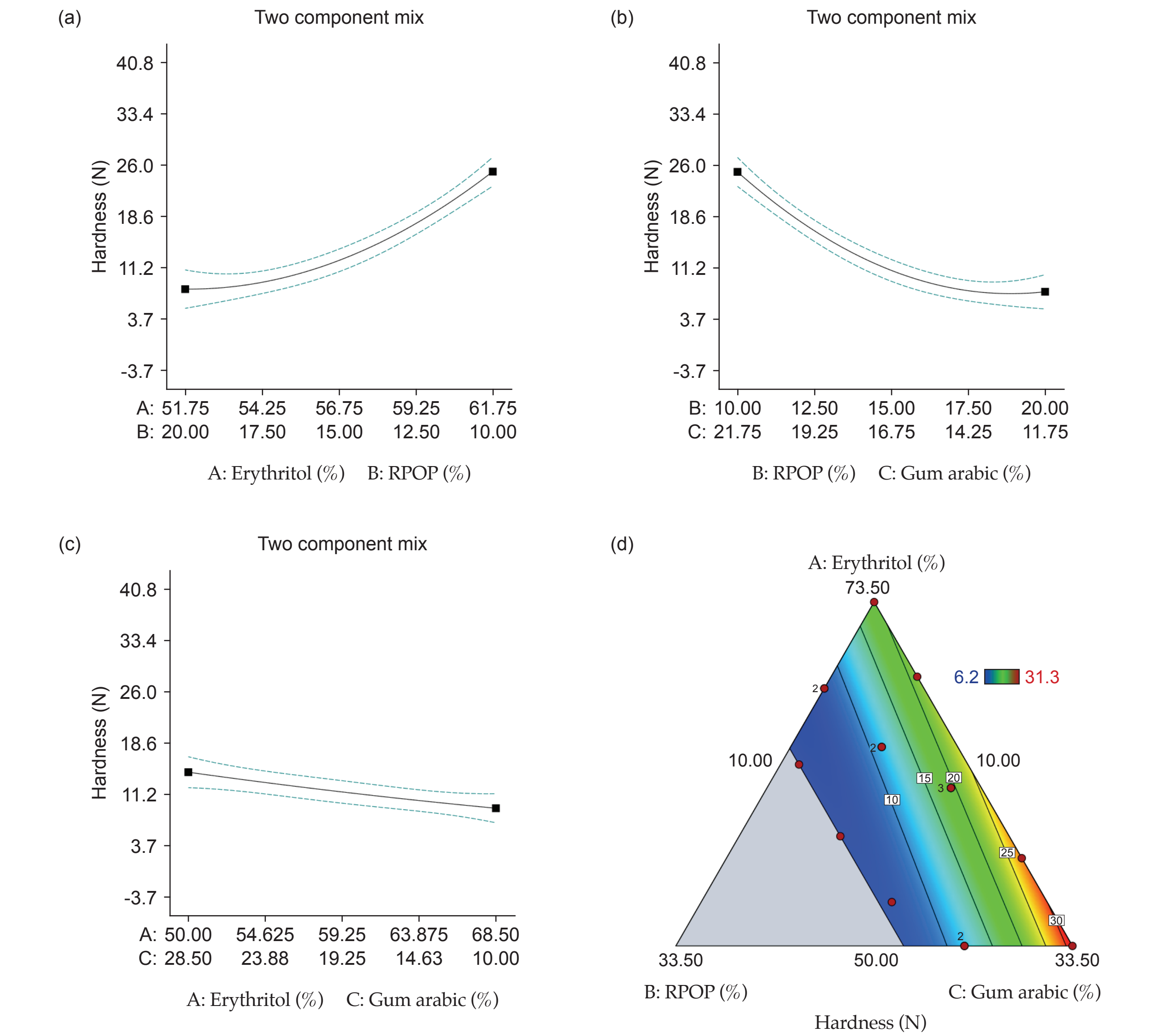

Note: The X-axis across the bottom of the two-component plot represents two variables. For instance, plot (a) the component associated with the X1 axis (A: Erythritol) increases in value from left to right in the top row, while the component associated with the X2 axis [B: Red palm oil powder (RPOP)] decreases in value from left to right in the bottom row. Dashed lines represent the 95.00% confidence interval. In the contour plots, colour represents the hardness of the candy, with values transitioning from low (blue) to high (red). The three values, A, B and C, are placed on the sides of the triangle, representing the maximum of each component for instance on the right side the 33.50 means 33.50% of gum arabic. The value at the middle of the triangle 50, 10, 10 represents the minimum value of opposite angle components, for example 50 indicates the minimum value of the erythritol in the design is 50.00%.

Figure 1. (a, b and c) Two component mix plots and (d) contour plots for the hardness of candy.

which is undesirable. In contrast, erythritol had a lower coefficient (0.8296), showing a moderate contribution to the friability of the candy. Gum arabic with the lowest coefficient value (0.4448), demonstrated that it can help reduce friability. With VIF values closer to 1 (as shown in *Table 5*), all the coefficients in the friability model can be considered to have a low correlation. This indicates that multicollinearity is not a concern in this model. Overall, the result suggests that an increase of RPOP in the candy could make it easier to break, while increase of gum arabic and erythritol improves this. Therefore, in order to maximise RPOP content in candy, it is unavoidable erythritol amount needs to be reduced, as gum arabic has a more prominent effect in reducing the friability.

The interaction plots of two-component mixes (AB, BC, AC) and a contour plot of three components on the friability of candy are illustrated in *Figure 2*. The two-component mix plots revealed that RPOP had a linear interaction with erythritol and gum arabic on the friability of the candy when its percentages was close to 10%. An increase in RPOP in the formulation (while other components were reduced) caused an increase in friability. This suggests that the initial increase in RPOP is consistent and could predict friability, as evidenced by the closer 95% confidence interval (CI) bands (represented by the dashed line) in *Figure 2a–2b*. In contrast, as the RPOP percentages approach its maximum (20%) the friability tends to increase exponentially and becomes harder to predict, as illustrated by the wider 95% CI bands. This can be observed in the screening results, whereby the RPOP content increased by just 5% from 20% to 25%, the candies broke down into pieces during production even without mechanical stress, indicating that the friability was 100% since the candies were not intact. Meanwhile, for the two-component plot of erythritol and gum arabic (*Figure 2c*), their effects towards the friability were linear with an increase in gum arabic reducing friability. The contour plot (*Figure 2d*) illustrates that gum arabic was the key component to maintain the low friability of candy, with erythritol having a similar but slightly lower effect. Low friability is important as it helps maintain the integrity of the candy.

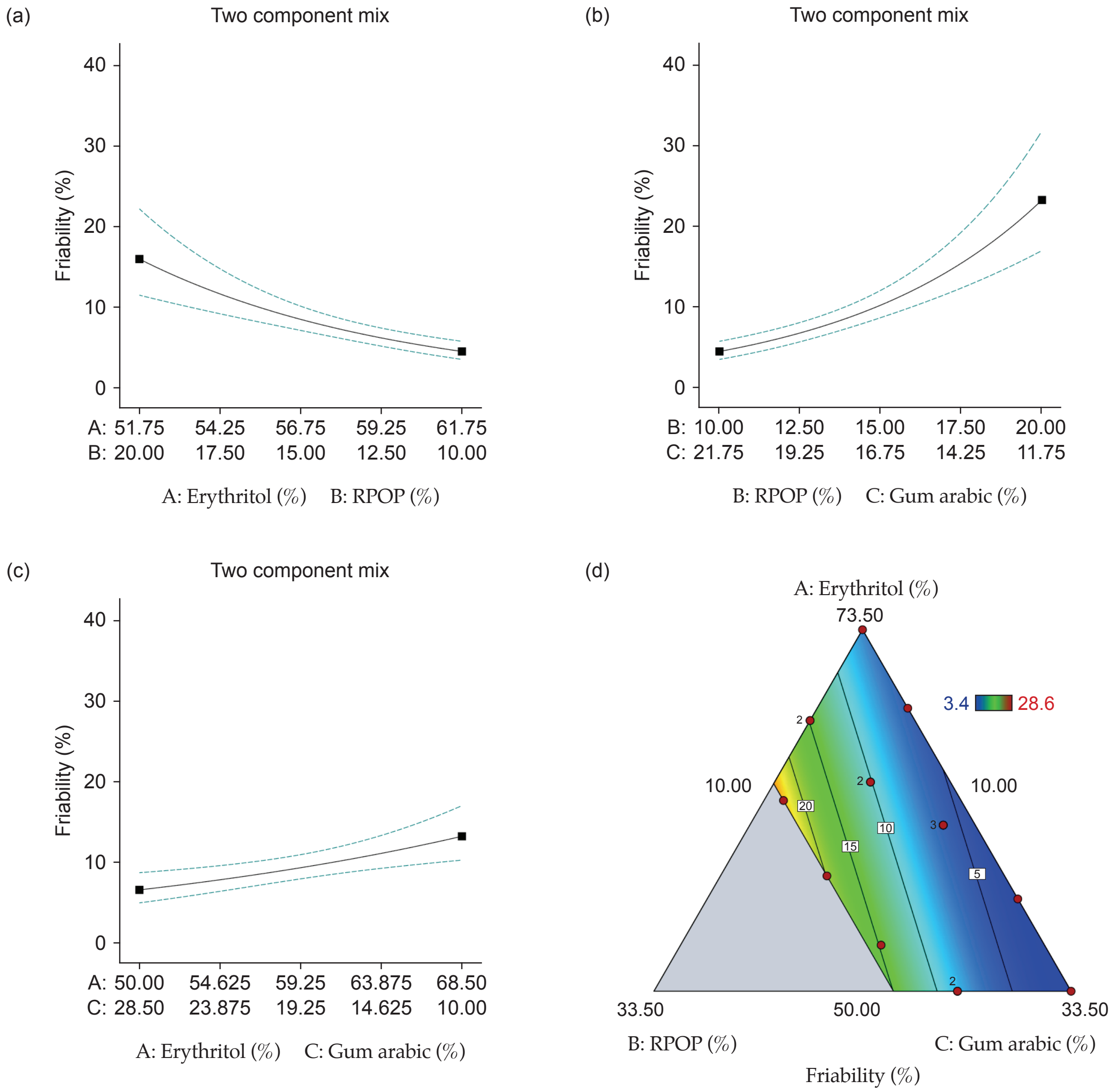

Note: The X-axis across the bottom of the two-component plot represents two variables. For instance, plot (a) the component associated with the X1 axis (A: Erythritol) increases in value from left to right in the top row, while the component associated with the X2 axis [B: Red palm oil powder (RPOP)] decreases in value from left to right in the bottom row. Dashed lines represent the 95.00% confidence interval. In the contour plots, colour represents the friability of the candy, with values transitioning from low (blue) to high (red). The three values, A, B and C, placed on the sides of the triangle, represent the maximum of each component for instance on the right side the 33.50 means 33.50% of gum arabic. The value at the middle of the triangle 50, 10, 10 represents the minimum value of opposite angle components, For example 50 indicates the minimum value of the erythritol in the design is 50.00%.

Figure 2. (a, b and c) Two-component mix plot and (d) contour plot for the friability of the candy.

In pharmaceuticals, polyvinylpyrrolidone and similar types of binders are used to improve or reduce friability (Kurakula & Rao, 2020). Although these binders are effective in direct compression formulations, they have seldom been used in food products due to concerns regarding their safety and regulatory status. In this study, we demonstrate that achieving lower friability is feasible by adjusting the content in the formulation.

Optimisation of Red Palm Oil Powder

Higher RPOP content in candy is desirable and preferable since it offers optimal health benefits. Unfortunately, it also compromises the candy's resistance to mechanical stress and reduces its hardness. Therefore, optimisation should consider maximising the RPOP and the hardness of the candy while minimising friability. In the optimisation procedure, the goal of RPOP and hardness was set to maximum; while friability was set to minimum. However, the suggested formulation had a very low desirability score of 0.448. Therefore, the goal was adjusted to set the RPOP in range given the significant impact of RPOP on the hardness and friability of the candy. The new optimum formulation of the candy as suggested by the mixture design comprised 50.00% erythritol, 10.00% RPOP and 33.50% gum arabic, with an acceptable desirability of 0.834. The experimental values for the candy's hardness (29.61 ± 2.09 N) and friability (3.87 ± 0.84%) fell within the 95.00% prediction intervals.

CONCLUSION

Erythritol, with a high sweetness-to-calorie ratio of 2.5–3.5, emerged as an ideal sweetener for RPO candy production. Its mesh size (80–100) played an important role in the homogeneity of the powdered mix. Together with the most effective binder, gum arabic helped improve candy hardness and reduce friability, which were negatively affected by the oily ingredient RPOP. The optimisation result showed that the desirable amounts of erythritol, RPOP and gum arabic in RPO candy production were 50.00%, 10.00% and 33.50%, respectively. The resulting candy had moderate hardness (around 30 N) and low friability (3.87%) fell within 95.00% of the predicted interval, indicating that the optimised formulations met the desired quality standards. This formulation can serve as a healthier confectionery product and a convenient means of delivering RPO to consumers. This product aligns with the current market trend toward healthier options for those seeking to reduce sugar intake as well as enjoy the health benefits of RPO without compromising on taste. The success will motivate RPO manufacturers to look into another food segment such as snacks and ready-to-eat products. Lastly, future studies such as sensory studies and large-scale products should be conducted to further understand consumer preferences and challenges regarding scalability.

ACKNOWLEDGEMENT

The authors acknowledge Dr. Lee Yee Ying from Monash University Malaysia, School of Science for her valuable assistance with the mixture design study.

REFERENCES

Afoakwah, N. A., Komla, M. G., S. Ahmad & A. Ali (Eds.), (2023). Extraction, structural properties, and applications of gum arabic. In *Natural gums.* (pp. 347–371). Elsevier. https://doi.org/10.1016/b978-0-323-99468-2.00013-9

Bohn, T. (2019). Carotenoids and markers of oxidative stress in human observational studies and intervention trials: Implications for chronic diseases. *Antioxidants*, *8*(6), 179. https://doi.org/10.3390/antiox8060179

Bordoloi, S. S., Chakraborty, T., Das, A., Islam, J., Rynjah, D., & Baishya, B. (2021). The applicability of palm trees in pharmaceuticals as excipients with a special emphasis on palm sugar: A review. *World Journal of Pharmaceutical Research, 10*(6), 1778–1792.

Czarnecka, K., Pilarz, A., Rogut, A., Maj, P., Szymańska, J., Olejnik, Ł., & Szymański, P. (2021). Aspartame – True or false? Narrative review of safety analysis of general use in products. *Nutrients*, *13*(6), 1957. https://doi.org/10.3390/nu13061957

Demiray, E., & Tulek, Y. (2017). Degradation kinetics of β-carotene in carrot slices during convective drying. *International Journal of Food Properties*, *20*(1), 151–156. https://doi.org/10.1080/10942912.2016.1147460

Dong, S., Xia, H., Wang, F., & Sun, G. (2017). The effect of red palm oil on vitamin A deficiency: A meta-analysis of randomized controlled trials. *Nutrients*, *9*(12), 1281. https://doi.org/10.3390/nu9121281

Health Canada. (2005). *Sugar alcohols (polyols) and polydextrose used as sweeteners in foods – Food safety*. https://www.hc-sc.gc.ca/fn-an/securit/addit/sweeten-edulcor/polyols_polydextose_factsheet-polyols_polydextose_fiche-eng.php

Hörmann-Kincses, T. R., Beretta, M., Kruisz, J., Stauffer, F., Birk, G., Piccione, P. M., Holman, J., & Khinast, J. G. (2022). Predicting powder feedability: A workflow for assessing the risk of flow stagnation and defining the operating space for different powder-feeder combinations. *International Journal of Pharmaceutics*, *629*, 122364. https://doi.org/10.1016/j.ijpharm.2022.122364

Jayadevan, A., Chakravarthy, D., Padmaraj, S. N., VijayaRaja, S., Bal, L., & Dimple, N. (2019). Dental caries and sugar substitutes: A review. *IOSR Journal of Dental and Medical Sciences, 18*(5, Ser. 8), 13–23. https://doi.org/10.9790/0853-1805081323

Kumar, R. (2020). Modified mix design and statistical modelling of lightweight concrete with high volume micro fines waste additive via the Box-Behnken design approach. *Cement and Concrete Composites*, *113*, 103706. https://doi.org/10.1016/j.cemconcomp.2020.103706

Kurakula, M., & Rao, G. K. (2020). Pharmaceutical assessment of polyvinylpyrrolidone (PVP): As excipient from conventional to controlled delivery systems with a spotlight on COVID-19 inhibition. *Journal of Drug Delivery Science and Technology*, *60*, 102046. https://doi.org/10.1016/j.jddst.2020.102046

Li, J., Dai, Q., Zhu, Y., Xu, W., Zhang, W., Chen, Y., & Mu, W. (2023). Low-calorie bulk sweeteners: Recent advances in physical benefits, applications, and bioproduction. *Critical Reviews in Food Science and Nutrition*, *64*(19), 6581–6595. https://doi.org/10.1080/10408398.2023.2171362

Loganathan, R., Subramaniam, K. M., Radhakrishnan, A. K., Choo, Y., & Teng, K. (2017). Health-promoting effects of red palm oil: Evidence from animal and human studies. *Nutrition Reviews*, *75*(2), 98–113. https://doi.org/10.1093/nutrit/nuw054

Mat Dian, N. L. H., Wan, S. Y., Ju Yen, F., Meganathan, P., Nik Ibrahim, N. M. A., Mohd Hassim, N. A., Wasoh, H., & Lai, O. M. (2019). Palm-based vitamin E (tocotrienol-rich fraction) has excellent stability in chewable tablet after one-year of storage at ambient temperature. *Journal of Oil Palm Research, 31*(4), 662–669. https://doi.org/10.21894/jopr.2019.0023

Mazi, T. A., & Stanhope, K. L. (2023). Erythritol: An in-depth discussion of its potential to be a beneficial dietary component. *Nutrients*, *15*(1), 204. https://doi.org/10.3390/nu15010204

Mishra, A., Ahmed, K., Froghi, S., & Dasgupta, P. (2015). Systematic review of the relationship between artificial sweetener consumption and cancer in humans: Analysis of 599,741 participants. *International Journal of Clinical Practice*, *69*(12), 1418–1426. https://doi.org/10.1111/ijcp.12703

Mullarney, M. P., Hancock, B. C., Carlson, G. T., Ladipo, D. D., & Langdon, B. A. (2003). The powder flow and compact mechanical properties of sucrose and three high-intensity sweeteners used in chewable tablets. *International Journal of Pharmaceutics*, *257*(1–2), 227–236. https://doi.org/10.1016/s0378-5173(03)00144-3

Nakhon, P. P. N. S., Aimkaew, M., Leesuksawat, W., & Tongsai, S. (2023). Optimization of sorbitol, fructooligosaccharides and sugar levels in the syrup based on physicochemical properties and sensory acceptance of healthy, sweet egg yolk drop (a traditional egg-based dessert) using response surface methodology. *International Journal of Food Properties*, *26*(1), 2229-2242. https://doi.org/10.1080/10942912.2023.2245581

Nogueira-de-Almeida, C. A., & Filho, D. R. (2021). Positioning on the use of polyols as table sweeteners. *International Journal of Nutrology*, *14*(02), e71–e80. https://doi.org/10.1055/s-0041-1733907

Oguntibeju, O. O., Esterhuyse, A. J., & Truter, E. J. (2009). Red palm oil: Nutritional, physiological and therapeutic roles in improving human wellbeing and quality of life. *British Journal of Biomedical Science*, *66*(4), 216–222. https://doi.org/10.1080/09674845.2009.11730279

Osei-Yeboah, F., & Sun, C. C. (2015). Validation and applications of an expedited tablet friability method. *International Journal of Pharmaceutics*, *484*(1–2), 146–155. https://doi.org/10.1016/j.ijpharm.2015.02.061

Parveez, G. K. A., Rasid, O. A., Ahmad, M. N., Taib, H. M., Bakri, M. A. M., Hafid, S. R. A., Ismail, T. N. M. T., Loh, S. K., Abdullah, M. O., Zakaria, K., & Idris, Z. (2023). Oil palm economic performance in Malaysia and R&D progress in 2022. *Journal of Oil Palm Research, 35*(2), 193–216. https://doi.org/10.21894/jopr.2023.0028

Porion, P., Sommier, N., Faugère, A., & Evesque, P. (2004). Dynamics of size segregation and mixing of granular materials in a 3D-blender by NMR imaging investigation. *Powder Technology*, *141*(1–2), 55–68. https://doi.org/10.1016/j.powtec.2004.02.015

Qin, P., Li, Q., Zhao, Y., Chen, Q., Sun, X., Liu, Y., Li, H., Wang, T., Chen, X., Zhou, Q., Guo, C., Zhang, D., Tian, G., Liu, D., Qie, R., Han, M., Huang, S., Wu, X., Li, Y., . . . Zhang, M. (2020). Sugar and artificially sweetened beverages and risk of obesity, type 2 diabetes mellitus, hypertension, and all-cause mortality: A dose-response meta-analysis of prospective cohort studies. *European Journal of Epidemiology*, *35*(7), 655–671. https://doi.org/10.1007/s10654-020-00655-y

Robinson, R. L., Damon, J. R., Mossop, J. R., & Palmer, M. D. (2006). *Soft chewable tablets* (U.S. Patent No. US7029699B2). United States Patent and Trademark Office. https://patents.google.com/patent/US7029699B2/en

Souiy, Z., Amri, Z., Sharif, H., Souiy, A., Cheraief, I., Hamden, K., & Hammami, M. (2023). The use of D-Optimal mixture design in optimizing formulation of a nutraceutical hard candy. *International Journal of Food Science*, *2023*(1), 7510452. https://doi.org/10.1155/2023/7510452

Szewczyk, K., Chojnacka, A., & Górnicka, M. (2021). Tocopherols and tocotrienols-bioactive dietary compounds; what is certain, what is doubt? *International Journal of Molecular Sciences*, *22*(12), 6222. https://doi.org/10.3390/ijms22126222

Tabara, A., Nakagawa, M., Ushijima, Y., Matsunaga, K., & Seguchi, M. (2015). Effects of heat treatment on oil-binding ability of rice flour. *Bioscience, Biotechnology and Biochemistry*, *79*(10), 1629–1634. https://doi.org/10.1080/09168451.2015.1039479

Tan, C. H., Lee, C. J., Tan, S. N., Poon, D. T. S., Chong, C. Y. E., & Pui, L. P. (2021). Red palm oil: A review on processing, health benefits and its application in food. *Journal of Oleo Science*, *70*(9), 1201–1210. https://doi.org/10.5650/jos.ess21108

U.S. Food and Drug Administration. (2018). *Quality attribute considerations for chewable tablets: Guidance for industry*. https://www.fda.gov/files/drugs/published/Quality-Attribute-Considerations-for-Chewable-Tablets-Guidance-for-Industry.pdf

Zhao, H., Yu, Y., Ni, N., Zhao, L., Lin, X., Wang, Y., Du, R., & Shen, L. (2022). A new parameter for characterization of tablet friability based on a systematical study of five excipients. *International Journal of Pharmaceutics*, *611*, 121339. https://doi.org/10.1016/j.ijpharm.2021.121339

Zubaidi, S. N. C. M., Halim, S., Mohd Kasini, Z., Fazleen, N. E., Thiruselvam, V., & Rajagopal, V. (2021). Red palm oil prevents congestive impairment in a rat model of D-galactose-induced aging. *Journal of Cellular & Molecular Anesthesia, 6*(4), 294–305. https://doi.org/10.22037/jcma.v6i4.36213

JOURNAL OF OIL PALM RESEARCH

GUIDE FOR AUTHORS

(for more details, kindly visit http://jopr.mpob.gov.my)

Type of Articles

1. **Regular Article**
   Full-length original empirical investigations, consisting of introduction, materials and methods, results and discussion, conclusions. Original work must provide references and an explanation on research findings that contain new and significant findings. Conclusion should be brief and focus on the research output, should not be in point form. These papers should not exceed 6,000 words of text (including tables, figures and references) and generally not more than a total of 10 figures and tables. After peer-review, the article word count limit can be extended to a maximum of 8,000 words to better address the reviewers' and editors' comments. Any additional figures or tables can be included in the supplementary data. Please note that papers submitted to JOPR will be sent back to authors because of poor figure resolution or exceeding the number of figures permitted.

2. **Short Communication**
   Significant new information to readers of the Journal in a short but complete form. Preferably not exceeding 3,000 words (including tables, figures and references), and is intended for rapid publication. They are not intended for publishing preliminary results or to be a reduced version of regular article.

3. **Review Article**
   Critical evaluation of materials about current research that have already been published by organising, integrating, and evaluating previously published materials. Re-analyses as meta-analysis and systemic reviews are encouraged. Review articles provide systemic overview, evaluation and interpretation of research in a given field. They should not exceed 12,000 words (including references) and should contain no more than a total of 20 figures and tables. Any additional figures or tables can be included in the supplementary data. Please note that papers submitted to JOPR will be sent back to authors because of poor figure resolution or exceeding the number of figures permitted. The same information should not be repeated in a figure and a table.

Language

Please write your text in good English (US or UK). We do not accept mixture of US and UK English in one manuscript. All spelling must be checked carefully.

JOPR's Template

JOPR's template, which is a standard format that facilitates the manuscript writing and copyediting process. This template is created to provide a detail and clear house style of JOPR. The template is drafted according to JOPR's house style, but in standard word version format. When writing a paper, authors need to format their papers to fit into the journal's house style. To make this easier, Word templates are available for many of other established journals, ready for them to download and apply to their research paper format. It is crucial for author to write a research paper while considering formatting. Each journal has its own guidelines for formatting; hence, the template defines how an article will look when it is published online or in print.

JOPR's Aims & Scope

This is established to provide a detail and clear aims and scope for author reference. Authors should declare in the cover letter how the research fits the aims and scope of JOPR.

JOPR's House Style

A detail listing of JOPR's house style for authors and a checklist to facilitate the copyediting process and standardise the copyediting process. The JOPR's house style remains the same and is drafted into a detail version for author's reference.

Manuscript Submission

- Manuscripts should be submitted via: https://www.editorialmanager.com/jopres.defult.aspx
- JOPR does not permit dual submission, publication and/or any archive platform (preprint) in violation of journal ethical practices.

For more details and to download the JOPR's House Style and Template, kindly visit http://jopr.mpob.gov.my

Contents of the Coming Issue

Journal of Oil Palm Research

Vol. 38 (4) December 2026*

Note: * Subject to change.